Indian and Northern Affairs Canada
Affaires indiennes et du Nord Canada

YUKON GEOLOGY

Volume 3

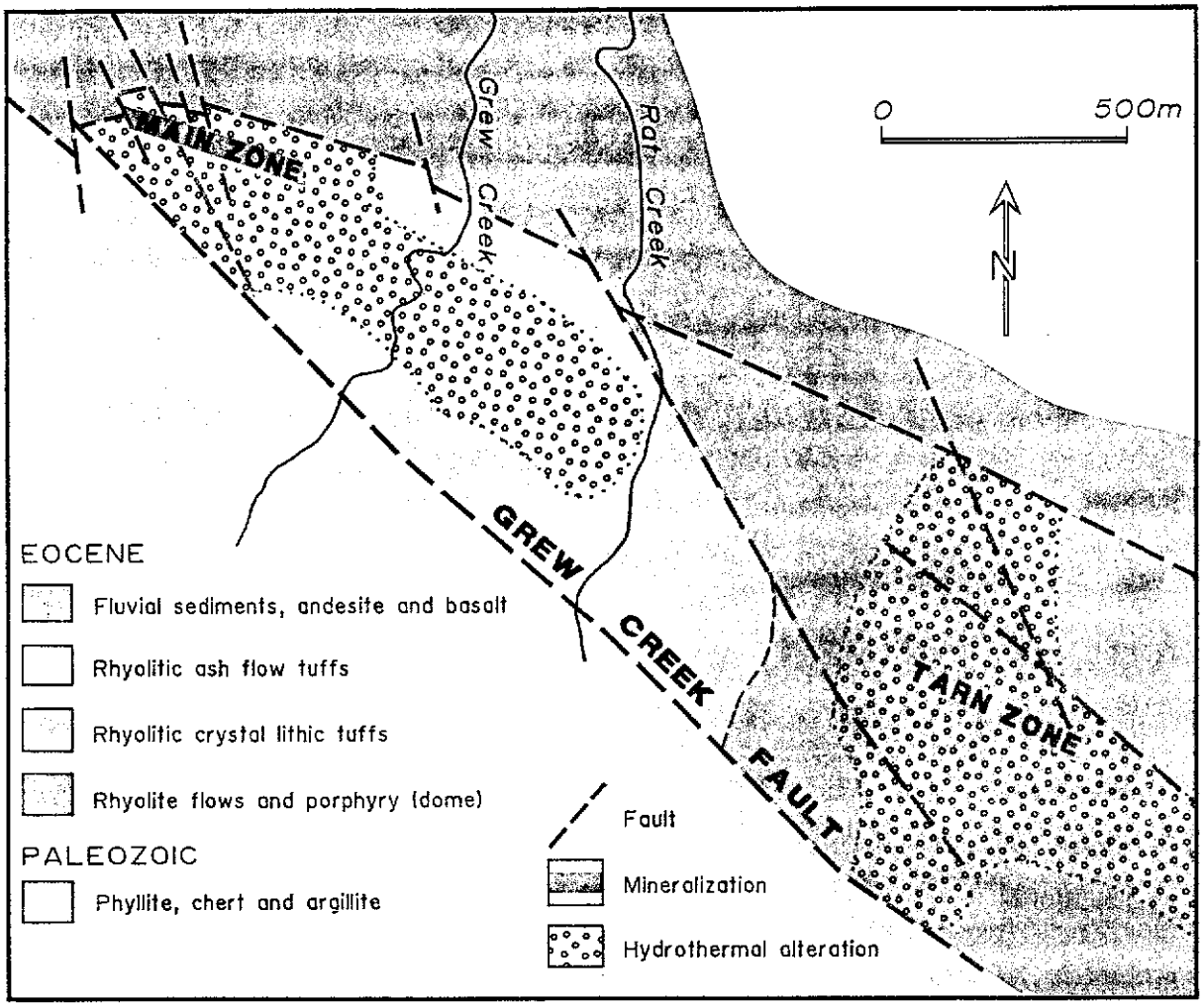

Canada

COVER: The GREW CREEK deposit, discovered by Al Carlos in 1983, is hosted by Eocene felsic volcanic tuffs and sedimentary rocks. The epithermal gold-silver deposit is located in a pull-apart basin within the Tintina Fault zone. Geological reserves are estimated to be 772,012 tonnes grading 8.9 g/t Au and 33.6 g/t Ag with a cut-off grade of 0.2 g/t Au.

Exploration and Geological Services Division of Northern Affairs Program, Yukon Region, invites readers to write and inform us of their language preference with respect to Yukon Exploration and Yukon Geology Reports, and other geotechnical reports prepared by the Division. Please write to:

Exploration and Geological Services Division
Northern Affairs Program
200 Range Road
Whitehorse, Yukon
Y1A 3V1

La Division de l'éxploration et des services géologiques du Programme des Affairs du Nord, dans la région du Yukon, invite ses lectuers à lui écrire ét à lui communiquer dans quelle langue ils préfèreraient recevoir les rapports sur l'exploration et la géologie du Yukon, et les autres rapports géotechniques préparés par la Division.
Vueillez vous adresser à:

la Divisioin de l'exploration et des
services géologiques
Programme des Affaires du Nord
Affaires indiennes et du Nord Canada
200 Range Road
Whitehorse, Yukon
Y1A 3V1

YUKON GEOLOGY

Volume 3

Exploration and Geological Services Division
Mineral Resources Directorate
Northern Affairs Program, Yukon
Indian and Northern Affairs Canada

Edited by T.J. Bremner,
Mineral Deposit Geologist

Published under the authority of the
Hon. Tom Siddon, P.C., M.P.,
Minister of Indian Affairs and
Northern Development
Whitehorse, 1992

QS-Y082-000-EE-A1

Available in Canada through
Associated Bookstores
and Other booksellers

Primarily available from
Exploration and Geological Services
Indian and Northern Affairs Canada
200 Range Road, Whitehorse
Yukon, Canada, Y1A 3V1

or by mail from
Canadian Government Publishing Centre
Supply and Services Canada
Ottawa, Canada K1A 0S9

Catalogue no. R71-40/3E
ISBN 0-662-19598-1

It is recommended that reference to this report be made in the following form:

INAC, (1992). Yukon Geology Volume 3, 1992; Exploration and Geological Services Division, Yukon, Indian and Northern Affairs Canada.

PREFACE

This third volume of Yukon Geology represents the culmination of approximately five years of geoscientific research sponsored and funded by Exploration and Geological Services Division (EGSD), Northern Affairs Program, Yukon Region. Under the Northern Mineral Policy, Indian and Northern Affairs Canada has the responsibility to develop and maintain the geoscientific database in Yukon Territory. In support of this policy, EGSD has assisted the authors through direct funding or by logistical support during the field season. Although the papers in this volume cover a wide range of topics, the majority have direct implications for mineral exploration in Yukon.

We sincerely thank the authors for their contributions and a final note of thanks is personally directed to Trevor Bremner, Mineral Deposit Geologist, EGSD, for his tremendous effort in bringing this publication together.

S.R. Morison
Chief Geologist
Exploration and Geological Services Division
Northern Affairs Program
Yukon Region

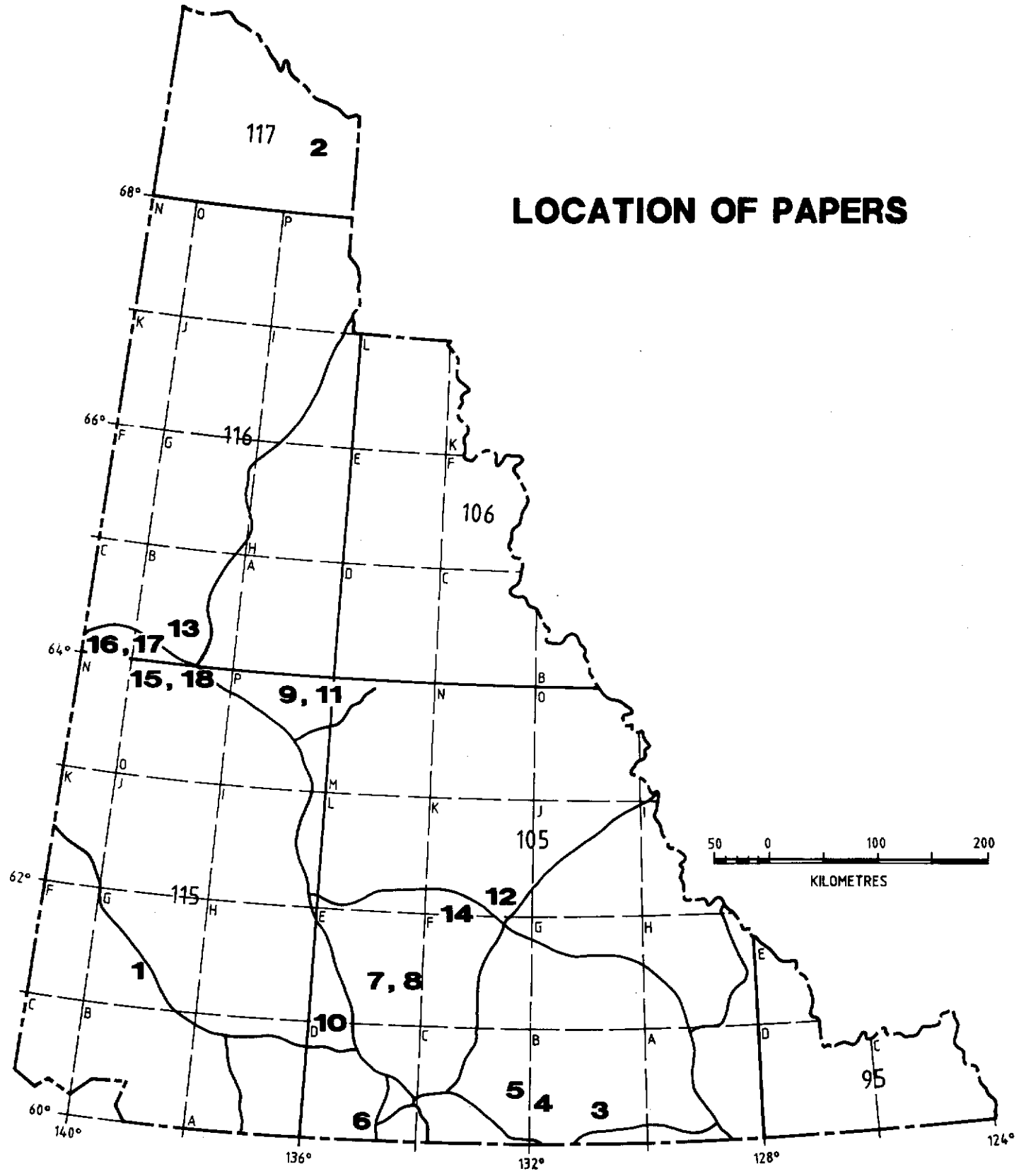
LOCATION OF PAPERS
117
2
116
106
105
115
95
16, 17
13
15, 18
9, 11
12
14
1
7, 8
10
5
4
3
6
68°
66°
64°
62°
60°
140°
136°
132°
128°
124°
50 0 100 200
KILOMETRES

CONTENTS

CENOZOIC SYNTECTONIC SEDIMENTATION AND STRIKE-SLIP BASIN DEVELOPMENT ALONG THE DENALI FAULT SYSTEM, YUKON TERRITORY

K.D. Ridgway and P.G. DeCelles,
Dept. of Geological Sciences,
University of Rochester,
Rochester, New York
14627

and

A.R. Cameron and A.R. Sweet
Geological Survey of Canada
Institute of Sedimentary and Petroleum Geology
3303-33rd St, NW
Calgary, Alberta
T2A 2L7

RIDGWAY, K.D., DE CELLES, P.G., CAMERON, A.R., and SWEET, A.R., 1992. Cenozoic syntectonic sedimentation and strike-slip basin development along the Denali fault system, Yukon Territory. In: Yukon Geology, Vol. 3; Exploration and Geological Services Division, Yukon, Indian and Northern Affairs Canada, p.1-26

ABSTRACT

This is a multidisciplinary study which combines sedimentology and sedimentary petrology, palynology, organic petrology and structural analysis of the middle Cenozoic Amphitheatre Formation in the St. Elias Mountains, and documents syntectonic deposition in strike-slip basins along the Denali fault system. The outcrops of the Amphitheatre Formation can be divided into two discrete basins: the northern Burwash basin and the southern Bates Lake basin.

Sedimentological analysis of the Burwash basin identified fault-controlled depocenters which allowed the development of several different types of non-marine depositional environments in close proximity. Palynology and organic petrology data indicate that the Amphitheatre Formation is diachronous and spans the Eocene-Oligocene boundary.

Light-mineral provenance studies of sandstones, clast-counts in conglomerates and paleocurrent analyses suggest that the Wrangellia and Yukon Crystalline Terranes were sources for the Amphitheatre Formation in the Burwash basin. In contrast, preliminary work suggests that Wrangellia and possibly the Gravina-Nutzotin Terrane may have been important sources for the Amphitheatre Formation in the Bates Lake basin.

Structural data combined with geologic mapping indicate a predominance of strike-slip deformation during and after deposition of the Amphitheatre Formation in the Burwash basin. The presence of syndepositional faults with subhorizontal slickensides indicates that strike-slip deformation occurred during deposition of the Amphitheatre sediments. The Burwash basin contains structures indicative of both contractional and strike-slip deformation, whereas the Bates Lake basin contains structures indicative of both extensional and strike-slip deformation. The change in structural style between the two basins suggests that the Amphitheatre Formation may have been deposited in transpressional as well as transtensional tectonic settings along individual segments of the Denali fault system during the middle Cenozoic.

RÉSUMÉ

Cette étude multidisciplinaire combine la sédimentologie, la pétrologie sédimentaire, la palynologie, la pétrologie organique et l'analyse structurale de la formation d'Amphitheatre du Cénozoïque moyen dans les monts St. Elias et on y documente le dépôt syntectonique dans les bassins de décrochement le long du système de Denali. Les affleurements de la formation d'Amphitheatre peuvent être répartis comme appartenant à deux bassins discrets : le bassin septentrional de Burwash et le bassin méridional du Lac Bates.

L'analyse sédimentologique du bassin de Burwash a permis d'identifier les dépocentres limités par des failles où ont pu se former en étroite proximité plusieurs types différents de milieux de sédimentation non marins. Les données palynologiques et de pétrologie oprganique indiquent que la formation d'Amphitheatre est diachrone et chevauche la limite Éocène-Oligocène.

Des études de la provenance des minéraux clairs des grès, des dénombrements des fragments dans les conglomérats et des analyses des paléocourants suggèrent que les terranes Wrangellia et Cristallin du Yukon constituaient les sources pour la formation d'Amphitheatre dans le bassin de Burwash. Par contraste, des travaux préliminaires suggèrent que la Wrangellia et le terrane de Gravina-Nutzotin ont pu constituer des sources importantes pour la formation d'Amphitheatre dans le bassin du Lac Bates.

Les données structurales combinées aux données de la cartographie géologique indiquent une prédominance de déformations de décrochement pendant et après le dépôt de la formation d'Amphitheatre dans le bassin de Burwash. La présence de failles contemporaines de la sédimentation avec surfaces de friction subhorizontales indique que la déformation par décrochement s'est produite pendant le dépôt des sédiments de la formation d'Amphitheatre. Le bassin de Burwash renferme des structures indicatives de déformations par contraction et par décrochement alors que le bassin du Lac Bates renferme des structures indicatives de déformations par extension et par décrochement. Le changement de style structural d'un bassin à l'autre suggère que la formation d'Amphitheatre peut avoir été mise en place dans des cadres tectoniques de transpression ainsi que de transtension le long de segments individuels du système de Denali au Cénozoïque moyen.

INTRODUCTION

Middle Cenozoic coarse-grained sedimentary rocks, collectively referred to as the Amphitheatre Formation, were deposited in several small basins along or near the Shakwak-Dalton and Duke River segments of the Denali fault system in the eastern St. Elias Mountains (Fig. 1). The Amphitheatre Formation forms a narrow, discontinuous belt approximately 350 km long, following the southwest side of the Shakwak-Dalton fault (Campbell and Dodds, 1982a, 1982b). Because of their age, textural and compositional immaturity and proximity to the fault, it is possible that sedimentary rocks of the Amphitheatre Formation record much of the Cenozoic tectonic history of the eastern St Elias Mountains and the Denali fault system. Our ongoing study, combined with observations by Eisbacher and Hopkins (1977), strongly suggests that Amphitheatre sedimentation was coeval with movement on the Denali fault system. In addition, later folding and faulting of the Amphitheatre Formation indicates post-Amphitheatre deformation along the strike-slip system. The Amphitheatre Formation consists of 350 - 1100 m of conglomerate, sandstone, shale and coal (Read and Monger, 1976) and is considered an overlap assemblage because it was deposited across several juxtaposed, accreted terranes which comprise the eastern St. Elias Mountains (Fig. 1). The Amphitheatre Formation thus contains the only sedimentary record of middle Cenozoic movement on the Denali fault system, as well as the post-accretionary history of the terranes in southwest Yukon.

SEDIMENTOLOGY

The outcrops of the Amphitheatre Formation that we have studied can be divided into two discrete areas with contrasting petrofacies, structures and sedimentological characteristics. Each area represents the remnant of a separate basin. We refer to the northern area as the Burwash basin and the southern area as the Bates Lake basin.

Sedimentological data indicate that the Amphitheatre Formation is characterized by (1) abrupt and localized facies changes both laterally and vertically; (2) markedly different lithostratigraphies within the Burwash basin, suggesting the existence of small (10's km), discrete, fault-controlled depocenters; (3) abrupt changes in local paleocurrent direction within fault-controlled depocenters; and (4) ample evidence of syndepositional tectonism, including intraformational unconformities, syndepositional faults, angular scree deposits and boulder conglomerates (Ridgway et al., 1989; Cole et al., 1989; Eisbacher and Hopkins, 1977). These characteristics are common in strike-slip tectonic settings, where multiple source areas are tectonically transported along the basin margins and sedimentation is synchronous with deformation of the basin.

Northern Area - Burwash Basin

The Burwash basin is approximately 35 km long (Fig. 2) and can be differentiated into three depocenters which are

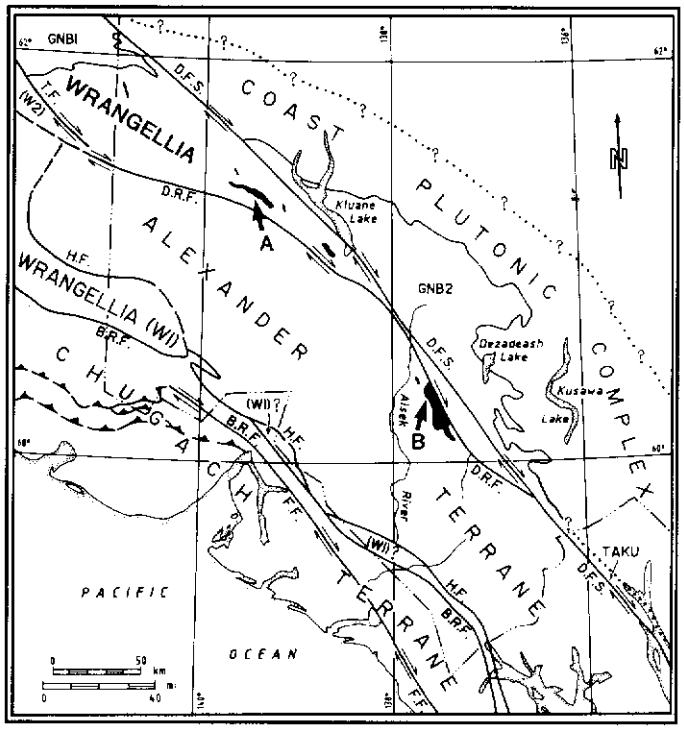

Figure 1: Regional geologic setting of the Amphitheatre Formation (black areas) in the Yukon Territory. The Amphitheatre Formation was deposited in several small basins along or near the Denali fault system in the eastern St. Elias Mountains. The Amphitheatre Formation, an overlap assemblage, overlies the Wrangellia Terrane in the northern part of the study area and the Alexander Terrane in the southern area. A - Burwash basin, B- Bates Lake basin, DRF - Duke River Fault, DFS - Denali Fault, GNB - Gravina-Nutzotin Belt, BRF - Border Range Fault, HF - Hubbard Fault, FF - Fairweather Fault. Modified from Campbell and Dodds, 1982a; 1982b.

defined by unique lithostratigraphies and distinctive depositional sequences. The unique stratigraphies representing individual depocenters cannot be correlated across major faults within the basin and are best exposed at the Mount Hoge, Amphitheatre Mountain and Cement Creek measured section localities (Fig. 2) (Ridgway et al., 1989).

Mount Hoge Depocenter

The Mount Hoge depocenter is the southernmost depocenter in the Burwash basin. It is located on the north flank of Mount Hoge at the southwest basin margin, and is characterized by proximal gravel-dominated fluvial deposits with poorly developed overbank facies. At Mt Hoge, the Amphitheatre Formation consists of sheet-like packages of clast-supported conglomerate 30-40 m thick, separated by 8 to 10-m thick units of interbedded sandstone and coal (Fig. 3-4). Conglomerate clast sizes range from pebble to cobble. Conglomerate lithofacies are established on the basis of trough and planar cross-stratification, crude horizontal stratification, and imbrication. Laterally extensive, sheet-form conglomerates showing sharp vertical separations between overbank and channelized facies suggest deposition on wet alluvial fans (Ethridge, 1985; Fraser and Suttner, 1986). Paleocurrent data indicate paleodrainage toward the west-northwest (Fig. 2).

Amphitheatre Mountain Depocenter

The next depocenter north of the Mount Hoge depocenter is the Amphitheatre Mountain depocenter (Fig. 2). It is characterized by proximal gravel-dominated fluvial deposits with well-developed overbank facies. At Amphitheatre Mountain, the basin fill consists of lenticular conglomerate packages 40 m thick, separated by well-developed sandstone, mudstone and coal packages ranging in thickness from 30 to 40 m (Fig. 5). In addition, the conglomerate packages grade laterally into finer-grained overbank facies (Fig. 6). The lack of extensive channel scouring, the well-developed channel-bar deposits (Fig. 7), and thick channel deposits that are laterally equivalent to coal deposits suggest deposition on a broad braidplain with well-established channel systems and perennial flow. This fluvial system may have been the central trunk stream into which more proximal, basin-margin streams discharged. Paleocurrent data indicate paleodrainage toward the west.

Cement Creek Depocenter

The Cement Creek depocenter is the northernmost depocenter in the Burwash basin (Fig. 2). Distal sandstone-dominated braided stream, lacustrine/fan-delta, and meandering stream deposits predominate. The stratigraphic sequence is characterized by three lower, 100 m thick, trough cross-bedded, conglomerate and coarse sandstone units which are overlain by 40m of mudstone and very fine-grained sandstone (probably lacustrine). These grade upward into laterally persistent (200 to 250 m wide) fine to medium-grained sandstone units of fan-delta affinity. This package is in turn overlain by a 50m thick unit of upward-fining, coarse to conglomeratic sandstone packages which were probably deposited by meandering streams (Fig. 8-9). Paleocurrent data indicate paleodrainage toward the south.

Southern Area - Bates Lake Basin

Initial work in the Bates Lake basin (Fig. 10) indicates that these sediments are characterized by abrupt changes in facies. However, confinement of depositional systems to specific fault-bounded depocenters, as is typical of the Burwash basin, has not been documented to date. Outcrops studied along the eastern basin margin (Fig. 11-12) (e.g. BL1 and BL2 on Fig. 10) consist of approximately 1,000 m of coarse, proximal alluvial-fan deposits which form an overall upward-fining sequence. Paleodrainage was toward the south-

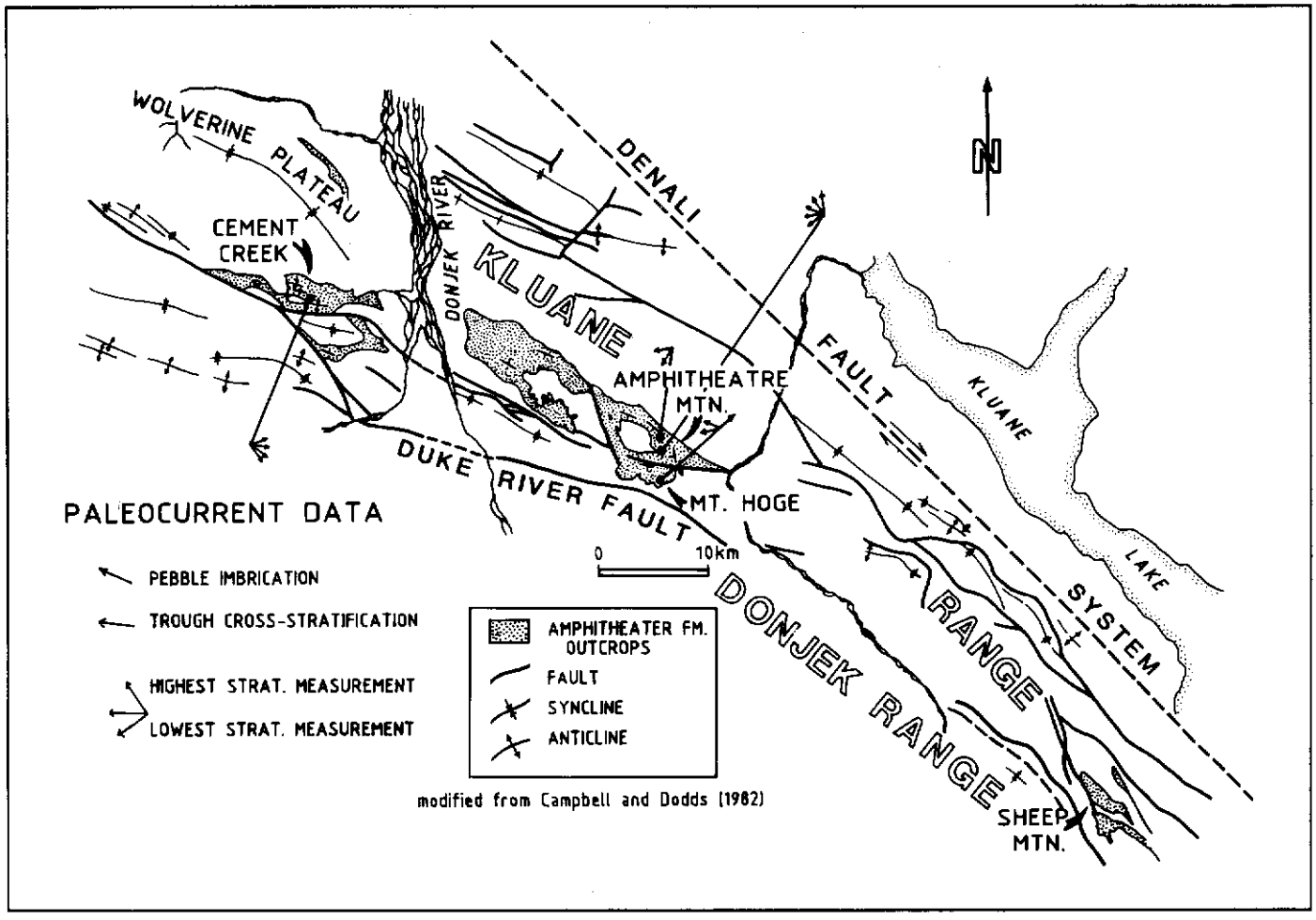

Figure 2: Location of stratigraphic sections measured in the Burwash basin. Map shows major folds and faults and outcrops of the Amphitheatre Formation based on Campbell and Dodds' (1982a; 1982b) maps. Leader lines connect clusters of paleocurrent arrows (from trough cross-strata and pebble imbrications) to their respective localities.

southwest. Outcrops along the southwest basin margin (Fig. 13)(e.g. WC2 on Fig. 10) consist predominantly of lenticular, coarse to medium-grained sandstones, encased in mudstones and siltstones which were probably deposited in a distal, axial fluvial system.

PALYNOLOGY AND ORGANIC PETROGRAPHY

Ongoing palynology and coal petrography studies document diachronous filling of the Burwash basin, spanning the Eocene-Oligocene boundary (Ridgway et al., 1989). The palynology and coal petrography support the model of localized fault-controlled depocenters within the Burwash basin. Owing to the structural complexities in ancient strike-slip basins, it becomes important to document the chronology and distribution of sediment packages in different parts of individual basins to understand the history of basin development. Our current interpretation of specific fault-bounded depocenters in the Burwash basin and the documentation of specific pollen and coal-type domains within these depocenters indicates the sediment packages become younger toward the basin center. This in turn suggests that the Burwash basin closely resembles the pull-apart model of strike-slip basin development (Crowell, 1974; Aydin and Nur, 1982; Mann et al., 1983). The pull-apart model constrains the oldest sediment to the perimeter of the basin, with sediments becoming progressively younger toward the center of the basin owing to structural enlargement of the basin with time. Studies of pollen types and coals in the Bates Lake basin are in progress.

Palynology

Palynological data indicate that the Amphitheatre Formation in the Burwash basin spans the Eocene-Oligocene boundary, which is marked by a global temperature decline. The global temperature decline resulted in a shift from angiosperm-dominated to gymnosperm-dominated forest types.

In the Burwash basin, the change in forest character is documented by an angiosperm-dominated temperate deciduous

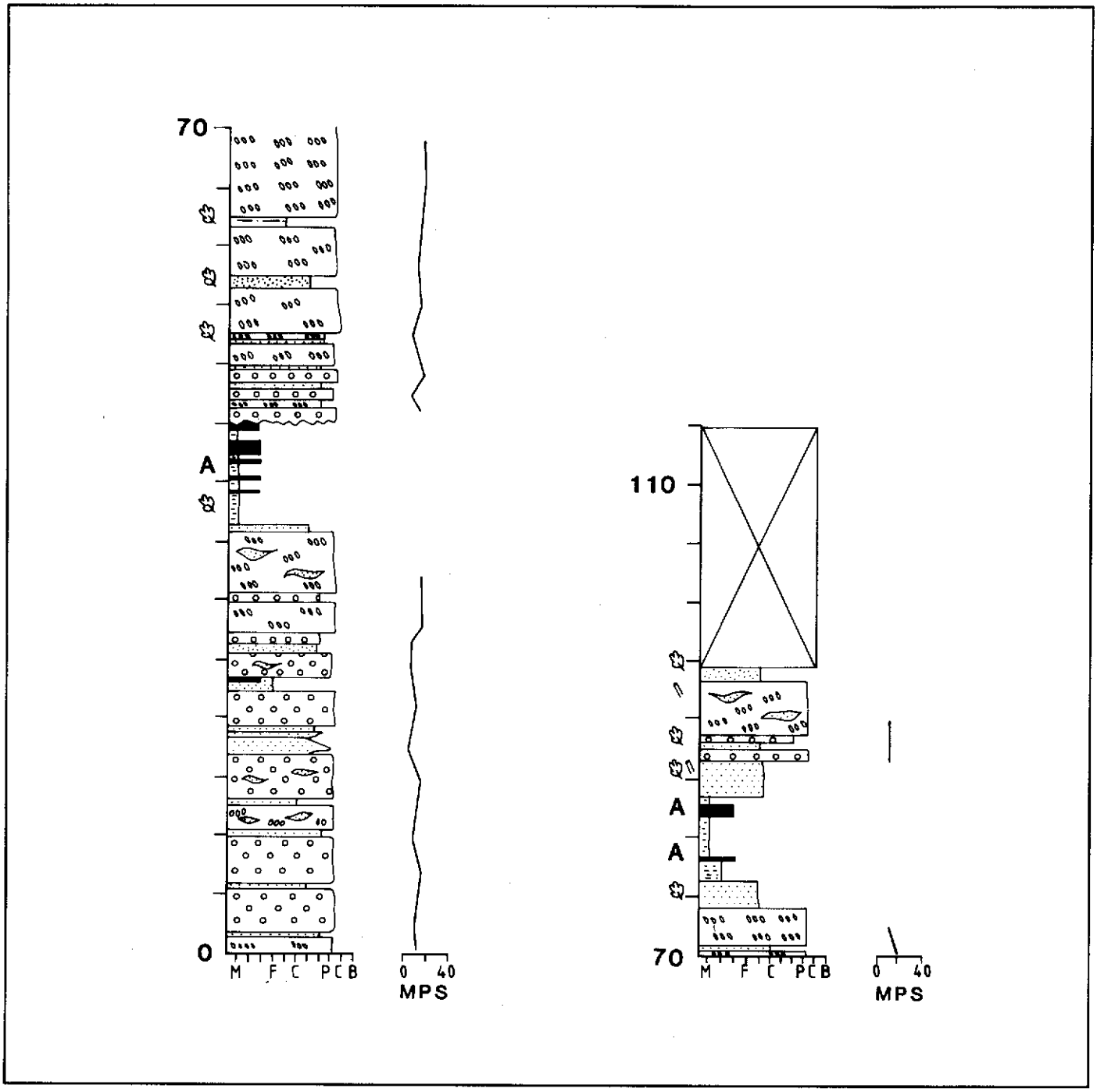

Figure 3: Measured stratigraphic section of the Amphitheatre Formation near Mount Hoge. Columns stack from left to right. Scale in meters on all measured sections. See Table 1 for explanation of lithofacies codes. Grain sizes: F - fine sand; M - medium sand; C - coarse sand; VC - very coarse sand; P - pebble; C - cobble; B - boulder. MPS = maximum particle size in cm.

pollen spectrum at the Mount Hoge and Cement Creek depocenters (Fig. 14) (see Fig. 2 for map locations), which contrasts with subtemperate, dominantly coniferous, forest pollen at the Amphitheatre Mountain depocenter (Fig. 14).

The difference in pollen dominances and the inferred forest character between depocenters suggest that Mount Hoge and Cement Creek localities on the perimeter of the basin are slightly older than the Amphitheatre Mountain locality in the more central part of the basin.

The oldest distinctive genus documented to date is Platycarya from the Cement Creek depocenter. In North America, Platycarya has mostly been found in Eocene rocks

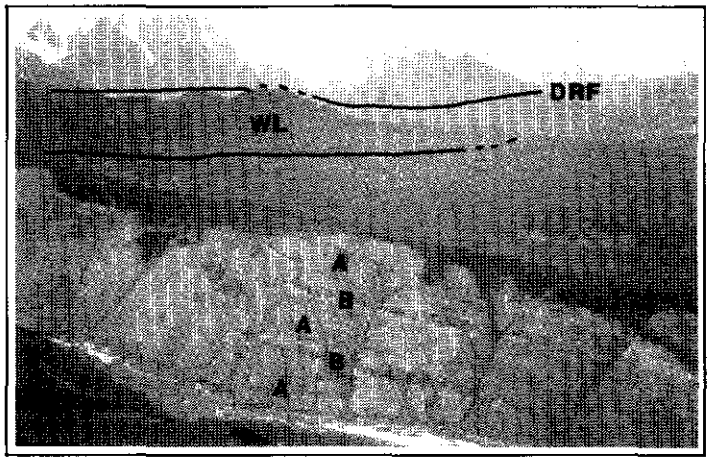

Figure 4: Typical exposures of the Mount Hoge depocenter consist of 30 to 40 m thick units of highly scoured, clast-supported conglomerate (A) that are separated by 8 to 10 m thick units of interbedded sandstone and coal (B). Two-man tent (arrow) for scale. DRF: Duke River Fault, WL: Wrangell Lavas.

(Tschudy and Scott, 1969, p.350), but Frederiksen and Christopher (1978) have recorded this genus in the upper Paleocene of South Carolina. The youngest distinctive genus is Carophyllaceae from the upper 10 meters of exposure at Amphitheatre Mountain. The oldest documentation of Carophyllaceae is from the middle Oligocene of New Zealand (Muller, 1981). Wiggins (1976) has also recognized Carophyllaceae in the well-dated middle Oligocene rocks of Cook Inlet, Alaska.

Organic Petrography

Petrographic studies of coal document the same change in the character of plant communities as recorded in the palynology studies, corresponding to the global temperature decline across the Eocene-Oligocene boundary. Petrographically, the coals of the three depocenters have low inertinite macerals (<6%) and most have high percentages of huminite macerals (>85%) (Fig.15). The huminite occurs in two distinctive populations correlated with the two different types of forest vegetation (Fig. 16). Coals at Mount Hoge (MINFILE 115G 011) and Cement Creek (MINFILE 115G 028) have more eu-ulminite B relative to eu-ulminite A, whereas the trend is reversed at the Amphitheatre Mountain depocenter (MINFILE 115G 012)(Fig. 16). Eu-ulminite A macerals are typical of subtemperate, conifer-dominated coal swamps (e.g. Amphitheatre Mountain), whereas eu-ulminite B and densinite are more typical of temperate, angiosperm-dominated coal swamps (e.g. Mount Hoge, Cement Creek). This change from temperate to subtemperate coal swamps with time probably resulted from the temperature decline across the Eocene-Oligocene boundary.

PROVENANCE

An ongoing objective of this study is to develop a better understanding of the relationship between the terranes comprising the eastern St. Elias Mountains, the Yukon Crystalline Terrane to the east, and the displacement history of individual segments of the Denali fault system which separate these terranes. The immature petrographic composition of the Amphitheatre Formation, combined with paleodrainage analysis, should be a very sensitive recorder of the relationship between the timing of fault movement and resultant sedimentation.

Several terranes are possible source areas for the Amphitheatre Formation (Fig. 1). The Wrangellia Terrane, which composes the Kluane Range, is a late Paleozoic terrane consisting of submarine volcanic-arc rocks, overlain by Triassic subaerial and submarine mafic volcanic rocks and shallow marine sedimentary rocks (Read and Monger, 1976; Campbell and Dodds, 1982a). The Alexander Terrane, which underlies the Icefield Ranges, is an early Paleozoic terrane consisting of carbonate, pelitic and volcanic rocks that are complexly deformed and metamorphosed to greenschist facies (Campbell and Dodds, 1982a). The Gravina-Nutzotin Terrane is an Upper Jurassic to Lower Cretaceous flysch basin composed of interbedded sandstone and shale (Eisbacher, 1976). The Yukon Crystalline Terrane, in the northern part of the study area, consists of high-grade metamorphosed Paleozoic rocks (Tempelman-Kluit, 1976; Mortensen and Jilson, 1985). All of these terranes are locally intruded by younger granitic rocks.

Sandstone Petrology

The detrital compositions of sandstones are directly related to the tectonic setting of the source area. Dickinson and Suczek (1979) used ternary diagrams to demonstrate the distinctiveness of detritus derived from different tectonic settings. In strike-slip settings, where source-area terranes of different rock types are juxtaposed along the basin margins, it may be informative to plot variables that characterize specific terranes. For example, the high-grade metamorphic rocks of the Yukon Crystalline Terrane would be the nearest "high-volume" source of polycrystalline quartz, whereas the volcanic rocks of the Wrangellia Terrane would be the nearest "high-volume" source of plagioclase and lithic volcanic and sedimentary rock fragments.

This "high-volume" sediment source characterization is not entirely satisfactory because of geological complexities at the local scale. For example, a local Cretaceous diorite intrusion within the volcanic-rich Wrangellia Terrane could easily have sourced part of the Amphitheatre Formation. To avoid misinterpretations due to local anomalous sources, we are collecting and analyzing sandstone samples on a basin-wide scale. A basin-wide data base should homogenize local source influences within the dominant source signature. Another complication is the possible former presence of supracrustal rocks above the metamorphic core of the Yukon Crystalline

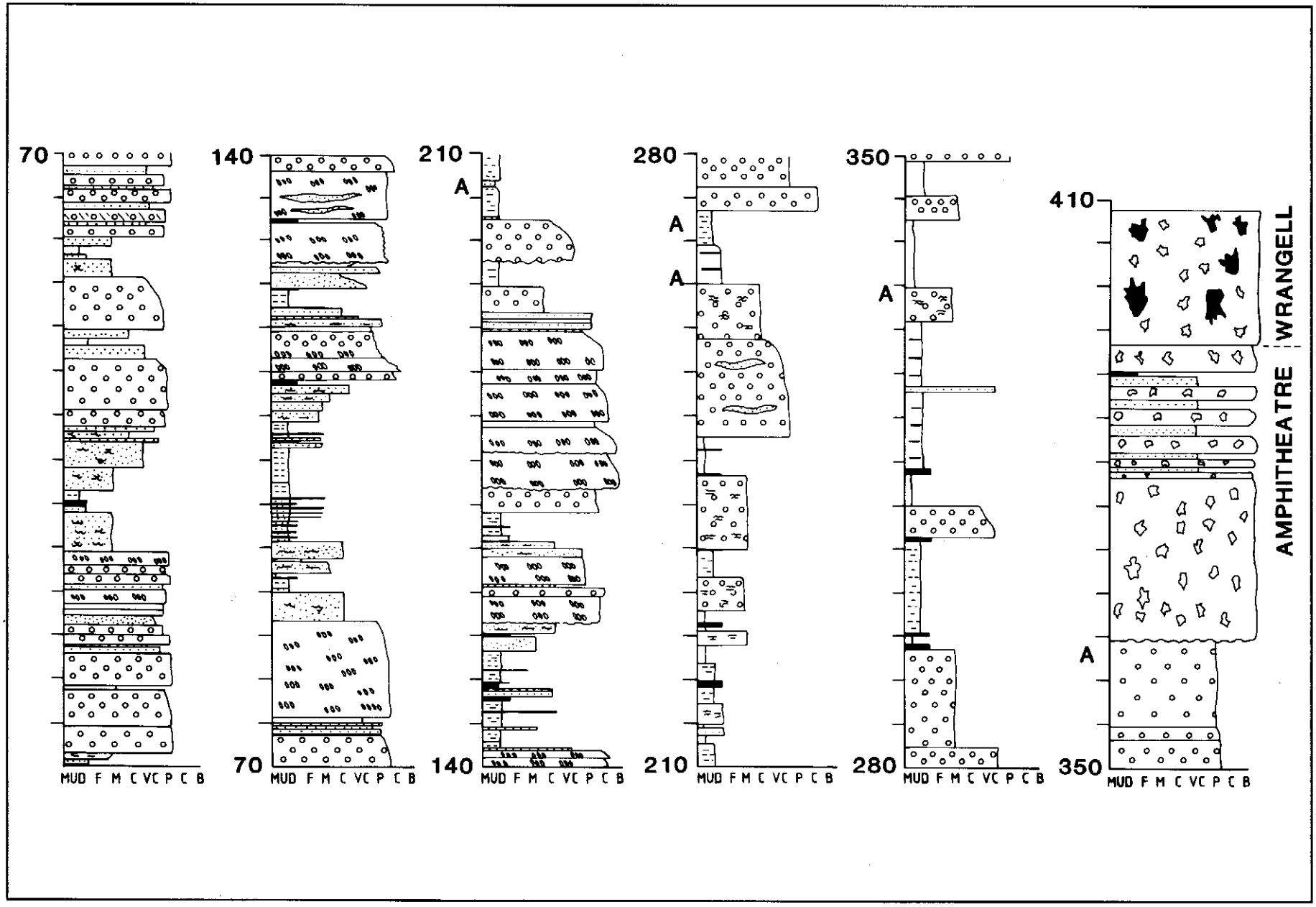

Figure 5: Measured stratigraphic section of the Amphitheatre Formation near Amphitheatre Mountain. Columns stack from left to right. See Table 1 and Figure 3 for explanation of lithofacies codes and grain sizes.

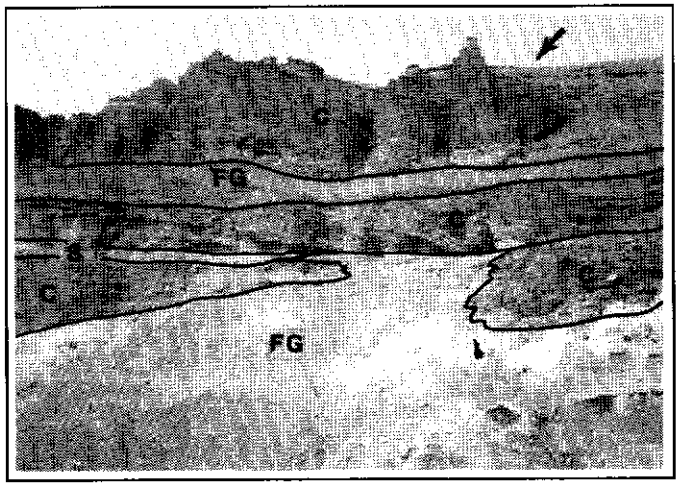

Figure 6: Individual amalgamated channels within channel complex interbedded with finer-grained facies at the Amphitheatre Mountain depocenter. Dall sheep (arrow) for scale. C - coarse, channel conglomerate; S - trough, cross-bedded sandstone; FG - finer-grained overbank deposits.

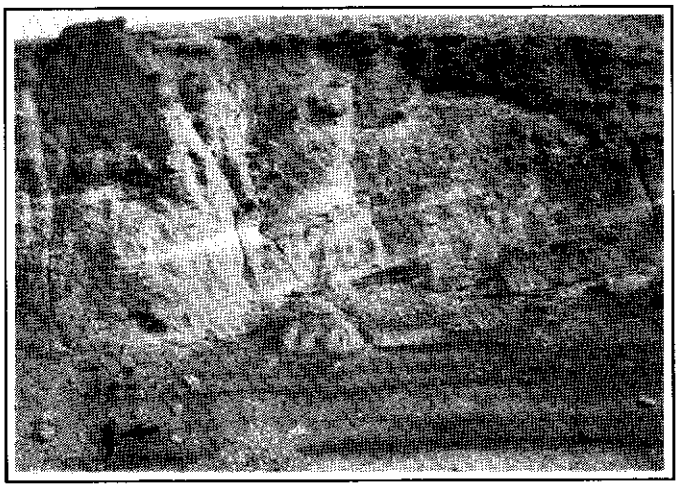

Figure 7: Well-developed foresets in channel-bar complex exposed at the Amphitheatre Mountain depocenter. Person (arrow) for scale.

Terrane and the Coast Plutonic Complex. These hypothetical supracrustal rocks are now completely eroded, but may have supplied sediment to the structural basins associated with the Denali fault system during the middle Cenozoic. If this is the case, any sediment contributed to the structural basins by the "supracrustals" should have contained a large component of metamorphic grains (e.g. Qp; Lm) by Eocene time based on studies (Tempelman-Kluit, 1976, p.1355; Mortensen and Jilson, 1985) which indicate that by the Late Triassic the entire eugeoclinal assemblage in the Yukon Crystalline Terrane (including the allochthonous Permian and older rocks) had undergone strong deformation and metamorphism. Therefore, any possible sediment contributed by the former supracrustal rocks would resemble the schists, gneisses, quartzites, and granitic rocks presently being eroded in the Yukon Crystalline Terrane and should not result in any gross misinterpretation.

Several trends are apparent in our preliminary sandstone petrology data. On QFL diagrams (Fig. 17a) sandstone compositions suggest mixing of continental block detritus (from sources rich in Q and F) and arc orogen detritus (from sources rich in F and L) in the Burwash basin. Together with paleocurrent data (Fig. 2) the petrologic data suggest that the most likely source for this particular sandstone composition is a mixture of sediments derived from Wrangellia and the Yukon Crystalline Terranes. Sandstones from the Bates Lake basin have QFL compositions that suggest a predominantly arc-orogen source (Fig. 17b). Combined with the south-southwestward paleocurrent data (Fig. 10), the Bates Lake petrologic data indicate derivation from Wrangellia and possibly the Gravina-Nutzotin Terrane.

On QpPK diagrams, sandstone compositions in both the Burwash and Bates Lake basins show marked enrichment in plagioclase (Fig. 18a,b) which, combined with paleocurrent data, suggests that the plagioclase-rich volcanic rocks of Wrangellia may have been the dominant source terrane during the filling of these basins.

Conglomerate Clast-Count Data

The identification of clast types in conglomerates within the Amphitheatre basins is an important tool for recognizing possible source areas. Because conglomerates are deposited in environments close to the source area, they accurately record source-area compositions. Clast-count data from the Amphitheatre conglomerates exposed in the Burwash basin indicate a predominance of local sources within the Wrangellia Terrane (Fig. 19). The conglomerates are dominated by meta-basalts (Fig. 20), meta-pelites and meta-tuffs (Fig. 21). We have field inspected and identified several potential source rocks in the Kluane Range (Wrangellia Terrane), including the Hasen Creek and Station Creek Formations (Pennsylvanian-Permian), the Nikolai volcanics (Triassic), and the Kluane Range intrusions (Cretaceous). Eisbacher and Hopkins (1977) suggested that the volcanic clasts in the Amphitheatre conglomerates were derived from Tertiary volcanic rocks (e.g. Mount Nansen - Eocene) which overlie parts of the metamorphic core of the Yukon Crystalline Terrane. At this stage in this study, we cannot rule out Eisbacher and Hopkins' interpretation. However, the coarseness of the conglomerates, abundant evidence for syndepositional faulting and syntectonic unconformities (see Structural Geology section), and the close proximity of the Wrangellia Terrane, finger the Wrangellia Terrane as a more likely source for the high volume of volcanic clasts in the Amphitheatre conglomerates. Future geochemical analysis of the volcanic clasts in the conglomerates may help to pinpoint their source rocks.

The relative abundance of high-grade metamorphic clasts in conglomerate in the Cement Creek depocenter parallels the greater abundance of polycrystalline quartz in the sandstones from Cement Creek. Both trends indicate that a minor

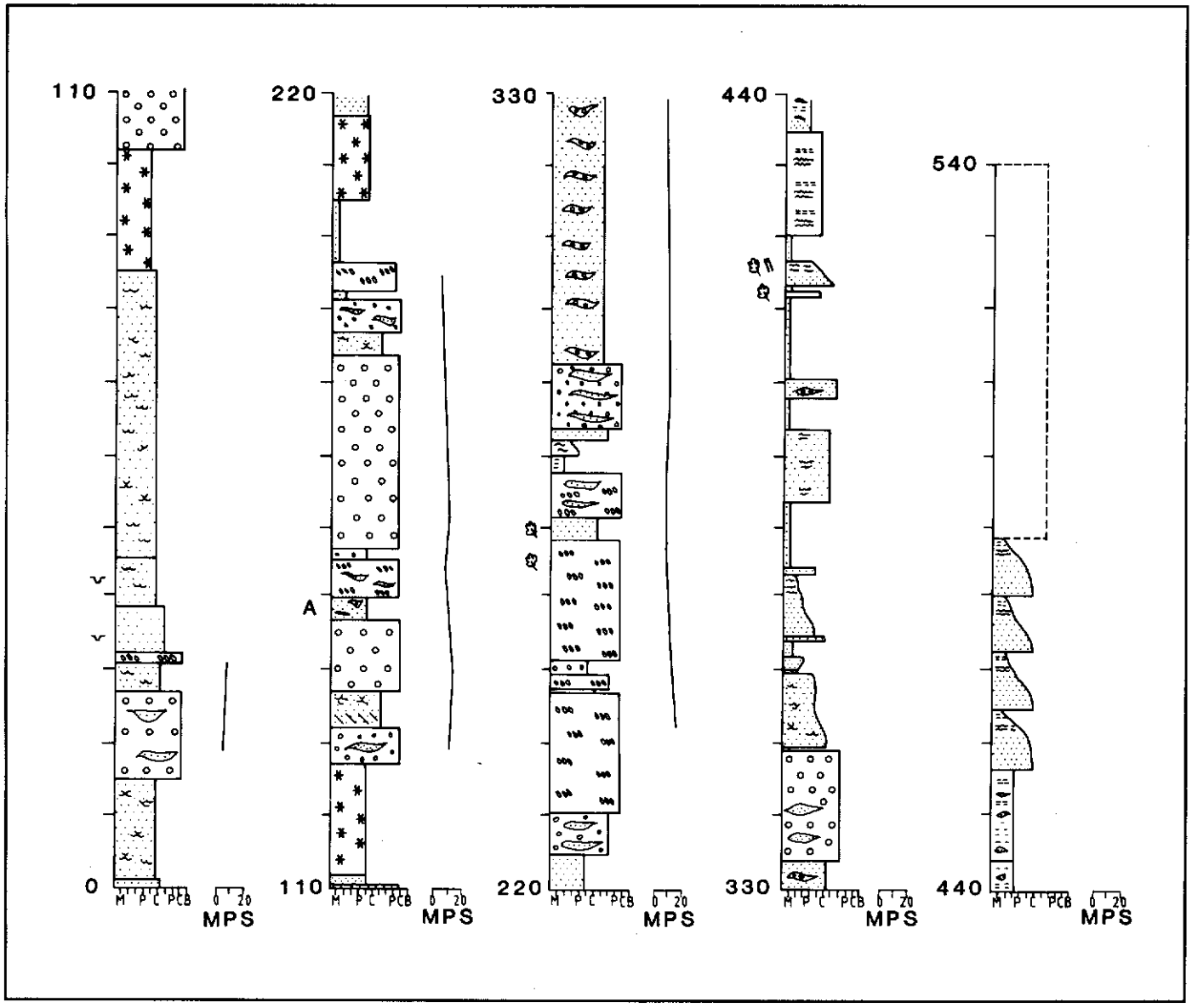

Figure 8: Measured stratigraphic section of the Amphitheatre Formation near Cement Creek. Columns stack from left to right. See Table 1 and Figure 3 for explanation of lithofacies codes and grain sizes.

component of the sediments deposited in the Cement Creek area was sourced from the high-grade metamorphic rocks of the Yukon Crystalline Terrane.

STRUCTURAL GEOLOGY AND BASIN DEVELOPMENT

A salient problem addressed by this study concerns the displacement histories of the Shakwak-Dalton and Duke River faults during and after Amphitheatre deposition. Most regional studies of the Denali fault system in the Yukon Territory and adjacent Alaska (Forbes et al., 1973a, 1973b, 1974; Eisbacher, 1976; Lanphere, 1978; Clague, 1979; Stout and Chase, 1980; Nokleberg et al., 1985; Plafker et al., 1989) indicate 300 - 400 km of displacement within a vaguely constrained time interval from Late Cretaceous to Recent.

Regional mapping in the study area by Campbell and Dodds (1978, 1982) and Read and Monger (1976) suggests that the major displacement was probably younger than early Late Cretaceous but older than Miocene. It appears certain that the Amphitheatre Formation was deposited during, and later deformed by, movements along these major strike-slip faults. Moreover, steeply-dipping slivers of Amphitheatre Formation rocks occur along the Shakwak-Dalton fault zone, indicating that further movement occurred during or after Amphitheatre deposition (Read and Monger, 1976).

In order to sort out the complicated relationships between the various fault systems and the Amphitheatre Formation, we are mapping the Amphitheatre Formation at a scale of 1:20,000. Detailed mapping of the Amphitheatre Formation

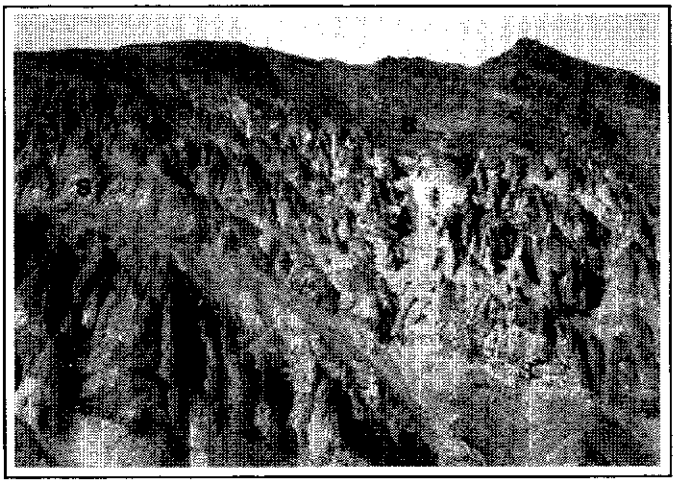

Figure 9: The stratigraphic succession at Cement Creek is characterized by three lower, 100 m thick conglomerate and coarse sandstone units (A), overlain by a 40 m-thick mudstone unit (B) which grades upward into laterally persistent fine to medium-grained sandstones (C). Exposure in photo is approximately 300 meters thick. Numerous sills (S) have intruded the lower part of the section.

is addressing the following questions: (1) What is the trend of deformation within the Amphitheatre in different parts of the basin(s) and how does it relate to the major regional strike-slip faults? (2) Are the present faulted Amphitheatre basin margins artefacts of post-Amphitheatre deformation or did these faulted margins actively control Amphitheatre sedimentation? This facet of the study is improving current understanding of fault movements between Late Cretaceous and Pliocene time, and indicates controls on basin development along the Denali fault system. Results to date indicate that obvious structural differences exist between the Burwash and Bates Lake basins.

Burwash Basin

The Burwash basin is characterized by: (1) fault-bounded margins which strike at oblique angles to the major strike-slip faults in the area; (2) right-stepping en echelon folds (Cement Creek area); (3) steeply dipping strata in local areas; and (4) intraformational unconformities (Sheep Creek area) and syndepositional faults (Amphitheatre Mountain area). These characteristics commonly are associated with basins developed in transpressional strike-slip settings (Lowell, 1972; Wilcox et al., 1973; Christie-Blick and Biddle, 1985).

Figure 22 is a geologic sketch map, completed during the summer of 1989, of the Amphitheatre Formation along the southern margin of the Burwash basin. This part of the basin displays contractional deformation. The southwest basin margin is an eastward trending asymmetric anticline, exposed along transect A-A'. The south limb is very gentle, whereas the north limb dips steeply and is truncated by a fault.

Several different structural styles are present in the small part of the basin mapped in Figure 22. A three-fold hierarchy of faults is present in this part of the Burwash basin; regional first-order faults, intra-basinal second-order faults, and syndepositional third-order faults. For example, at location B the "basement" rocks for this particular basin (e.g. Pv) have been juxtaposed against the Amphitheatre Formation along a set of conjugate high-angle NW-SE striking second-order faults (Fig. 23). In contrast, the structural style at location C is dominated by high-angle, NE-SW third-order syndepositional faults (Fig. 24). Slickenside orientation data (Figs. 25-26) indicate that at least the latest movements on the faults at both locations B and C have been primarily horizontal. Additional evidence that the basins were proximal to areas of active deformation includes boulder conglomerate deposits at Amphitheatre Mountain (Fig. 27) and Sheep Creek.

Comparison between the dominant NNW dip of bedding south of the major fault which parallels Granite Creek (a first-order fault, taken from Campbell and Dodds, 1982a) and the dominant SW dip of bedding north of the major fault suggests that fault-bounded segments of the basin may have acted as independent blocks and undergone different deformational histories. These contrasting structural histories should be identifiable as unique structural domains by field mapping.

Bates Lake Basin

In contrast to the Burwash basin, the Bates Lake basin is characterized by: (1) predominantly flat-lying strata; (2) little evidence of folding; (3) depositional onlap of the basin margins; and (4) numerous NE-SW striking faults which do not appear to rotate bedding. Initial work in the Bates Lake basin suggests that this basin has many of the characteristics of transtensional strike-slip basins, such as extensional structures (mainly normal faults) and a lack of en echelon folds (Wilcox et al., 1973; Harding et al., 1985; Christie-Blick and Biddle, 1985).

Figure 28 is a geologic sketch map of the southwest margin of the Bates Lake basin, located at the south end of Bates Lake (Fig. 10). The map demonstrates the extensional nature of this part of the basin. Note that the Amphitheatre Formation is exposed in two small graben within older "basement" rocks (e.g. locations A and B). The individual graben appear to have been rotated differentially, the rocks in the northernmost graben having a northeast dip and the rocks in the southwest graben having west-southwest dips. Clearly, this structural configuration of the Bates Lake basin is much different from that of the Burwash basin.

SUMMARY

Several lines of evidence indicate that deposition of middle Cenozoic coarse-grained sediments in small basins along or near the Shakwak-Dalton and Duke River segments of the Denali fault system was coeval with movement on the Denali fault system. This ongoing multi-disciplinary study of the Amphitheatre Formation is the first comprehensive study of

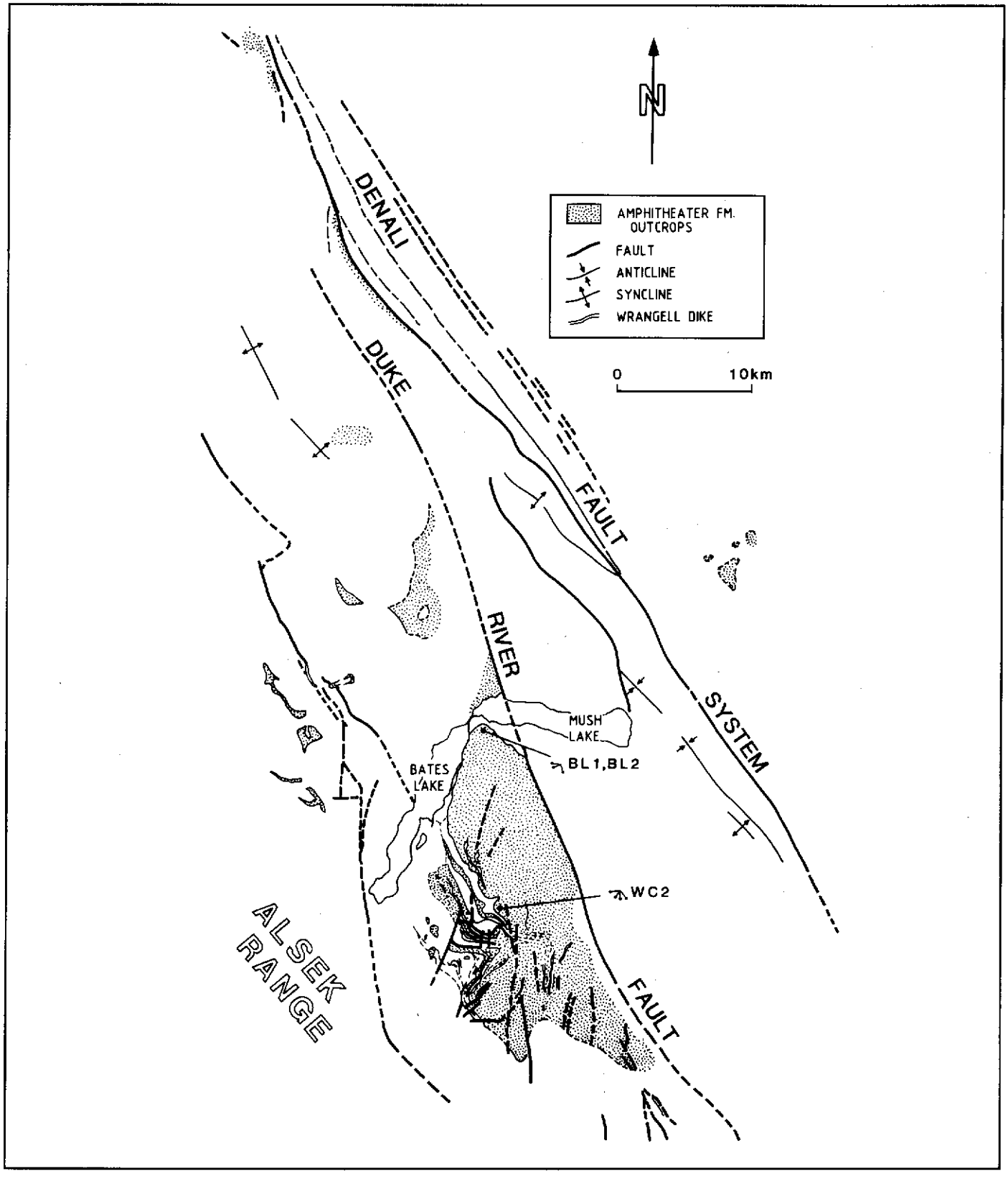

Figure 10: Location of stratigraphic sections studied in the Bates Lake basin. Map shows major folds and faults and outcrops of Amphitheatre Formation based on Campbell and Dodds' (1982a; 1982b) maps. Leader lines connect clusters of paleocurrent arrows (from trough cross-stratification and pebble imbrication) to their respective localities.

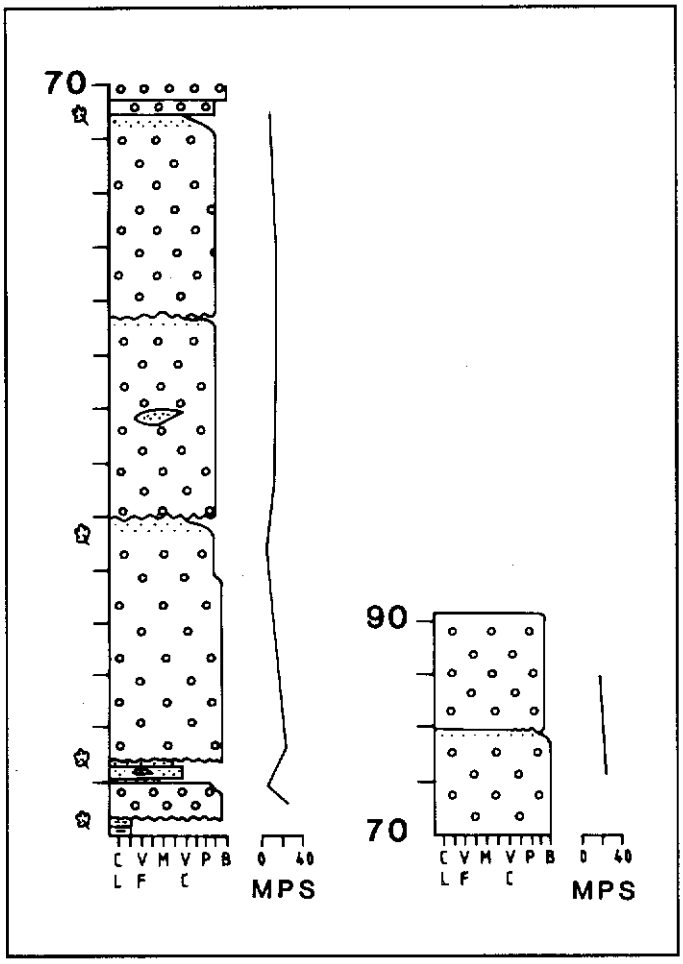

Figure 11: Measured stratigraphic section of the lower Amphitheatre Formation near the eastern margin of the Bates Lake basin. The section is dominated by 20 to 25 m thick units of pebble to boulder conglomerate. Columns stack from left to right. See Table 1 and Figure 3 for explanation of lithofacies codes and grain sizes.

these basins and sheds new light on the middle Cenozoic history of the eastern St Elias Mountains and the Denali fault system.

Sedimentological analysis of the Amphitheatre basins documents characteristics common to nonmarine strike-slip basins such as: (1) fault-controlled depocenters; (2) abrupt and localized facies changes; and (3) abrupt changes in local paleocurrent directions within each depocenter. The fault-controlled depocenters allowed several different types of depositional environments to exist in close proximity to each other within individual basins. Braided stream, wet alluvial fan, fan-delta, lacustrine and meandering stream deposits all occur within the Burwash basin, which is only 35 km in length and 5 km wide (Ridgway et al., 1989; Cole et al., 1989). The recognition and further documentation of wet alluvial-fan deposits may help clarify the depositional enigmas pointed out by Eisbacher (1978), Eisbacher and Hopkins (1977), and Long (1981) in Cenozoic rocks within the Canadian Cordillera intermontane basins. The intimate association of coarse clastics and coals, the lack of proximal alluvial-fan facies, and the non-conformity of the fluvial conglomerates to documented modern braided-stream deposits may be explained by a wet alluvial-fan depositional model.

Palynology and coal petrography document diachronous filling of the Burwash basin, which spanned the Eocene-Oligocene boundary. The global temperature decline at the Eocene-Oligocene boundary resulted in a change in forest character from temperate, angiosperm-dominated to subtemperate, gymnosperm (mainly coniferous)-dominated. Distinctive pollen and coal type domains within individual fault-bounded depocenters support the current interpretation of a pull-apart basin model for the Burwash basin.

Light-mineral provenance studies of sandstones and clast-types in conglomerates, combined with paleocurrent analyses, are helping to identify the possible source terranes for the Amphitheatre sediments. Our data suggest mixed continental block and arc-orogen sources of sand and gravel for the Burwash basin. The most likely candidates are the Wrangellia Terrane (for the volcanic lithic grains) and the Yukon Crystalline Terrane (for the high-grade metamorphic lithic grains). Meta-basalt, meta-pelite and meta-tuff are the most common conglomerate clast types in the Burwash basin and, combined with paleocurrent analyses, suggest local sources within the Wrangellia Terrane. The presence of local uplifted sources along the fault-bounded Amphitheatre basin margins, and evidence for syndepositional tectonism, supports a strike-slip origin for these basins.

Structural data indicate a predominance of strike-slip deformation during and after deposition of the Amphitheatre Formation in the Burwash basin. We have mapped high-angle faults of several orders including syndepositional faults which indicate strike-slip deformation during deposition of the Amphitheatre sediments. Second-order faults form a conjugate set of high-angle faults with subhorizontal slickensides indicating a predominance of oblique strike-slip fault movement.

The Burwash basin contains structures indicative of both contractional and strike-slip deformation, which is characteristic of basins developed in transpressional strike-slip settings.

Initial structural mapping in the Bates Lake basin indicates a graben and horst structural configuration along the basin margin, suggesting a major component of extensional deformation. The Amphitheatre Formation is exposed in small, fault-bounded graben bordered by older basement rocks along the Bates Lake basin margin. The Bates Lake basin has structures indicative of both extensional and strike-slip deformation, which is characteristic of basins developed in transtensional strike-slip settings.

ACKNOWLEDGEMENTS

Initial reconnaissance and logistical support for this study were provided by Indian and Northern Affairs Canada

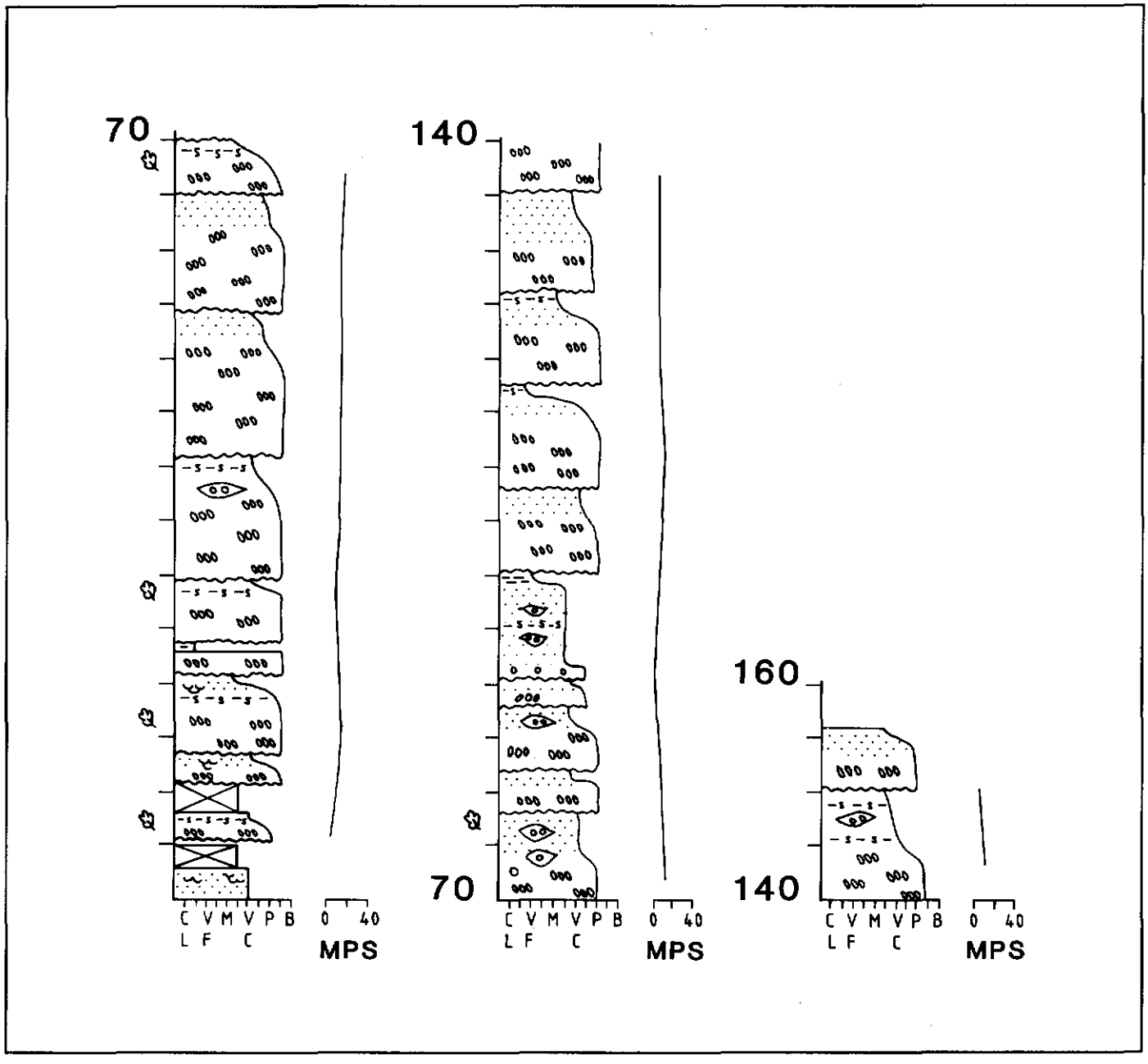

Figure 12: Measured stratigraphic section of the upper Amphitheatre Formation near the eastern margin of the Bates Lake basin. The section is dominated by 10 m thick units of pebble conglomerate which fine-upward. Columns stack from left to right. See Table 1 and Figure 3 for explanation of lithofacies codes and grain sizes.

(DIAND). A grant from the American Chemical Society-Petroleum Research Fund #23279-AC8-C to PGD provided continued support for the research. Additional partial funding for KDR was provided by the American Association of Petroleum Geologists, American Geological Institute Minority Participation Program, American Indian Science and Engineering Society, Geological Society of America, Antoinette Lierman Medlin Scholarship Award (G.S.A.-Coal Division) and Sigma Xi. Tomasz Jerzykiewicz (Geological Survey of Canada) first called our attention to the strike-slip basins of the Denali Fault. We especially thank Trevor Bremner and Steve Morison (DIAND) for their interest in the project and valuable assistance during the reconnaissance stages of the study. Parks Canada (Kluane National Park) allowed us access to the exposures in the Bates Lake Basin. Archer, Cathro & Associates (1981) Ltd, on behalf of All-North Resources Ltd, provided KDR with shelter and many warm meals at their Wellgreen camp during the rainy 1988 field season. We thank Grant Smith (GSC) for reviewing the manuscript.

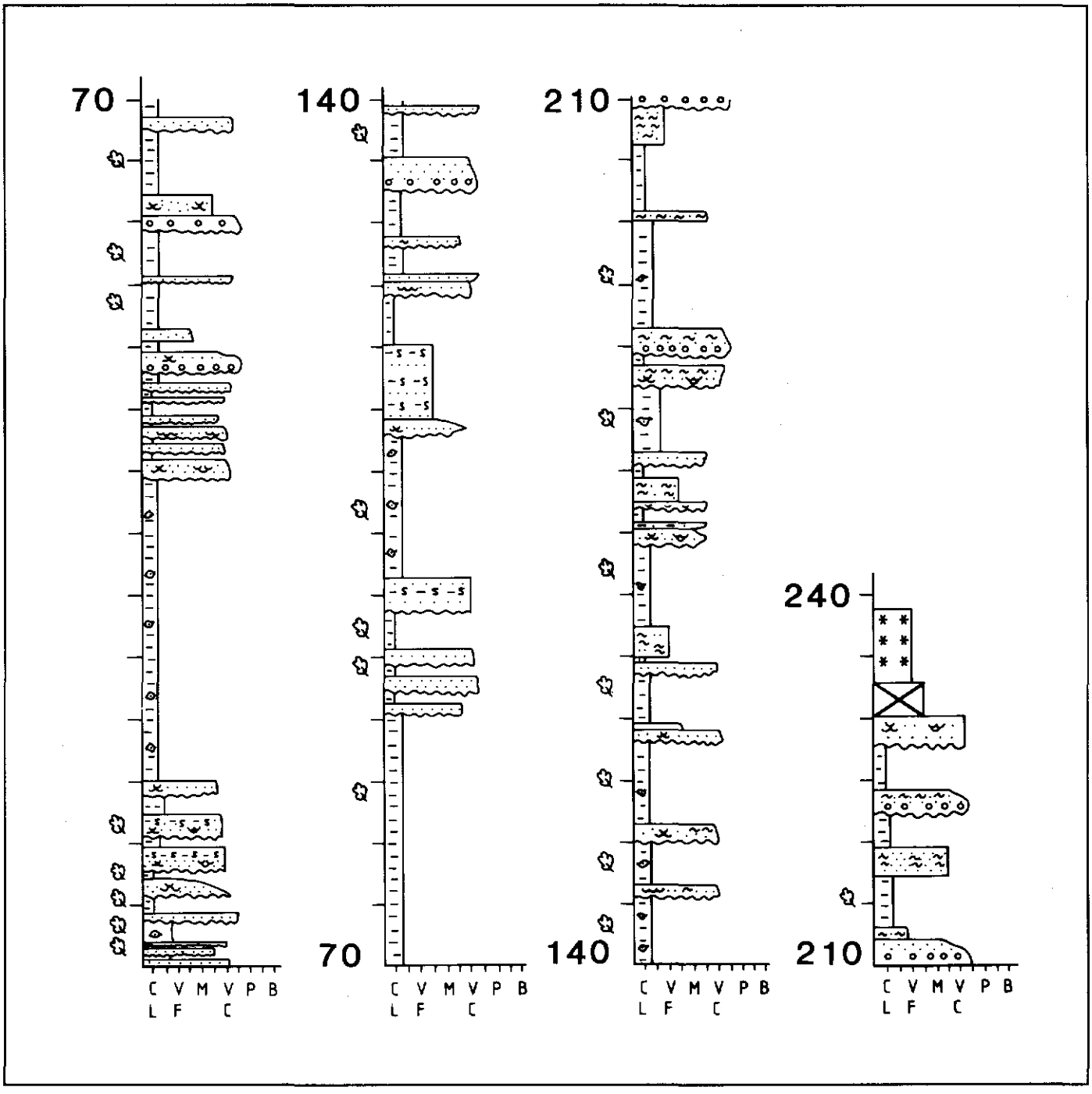

Figure 13: Measured stratigraphic section of the Amphitheatre Formation near the southwestern margin of the Bates Lake basin near Wolverine Creek. Columns stack from left to right. The section is dominated by sandstone lenses 2 to 3 m thick, which fine upward and are encased in mudstones. See Table 1 and Figure 3 for explanation of lithofacies codes and grain sizes.

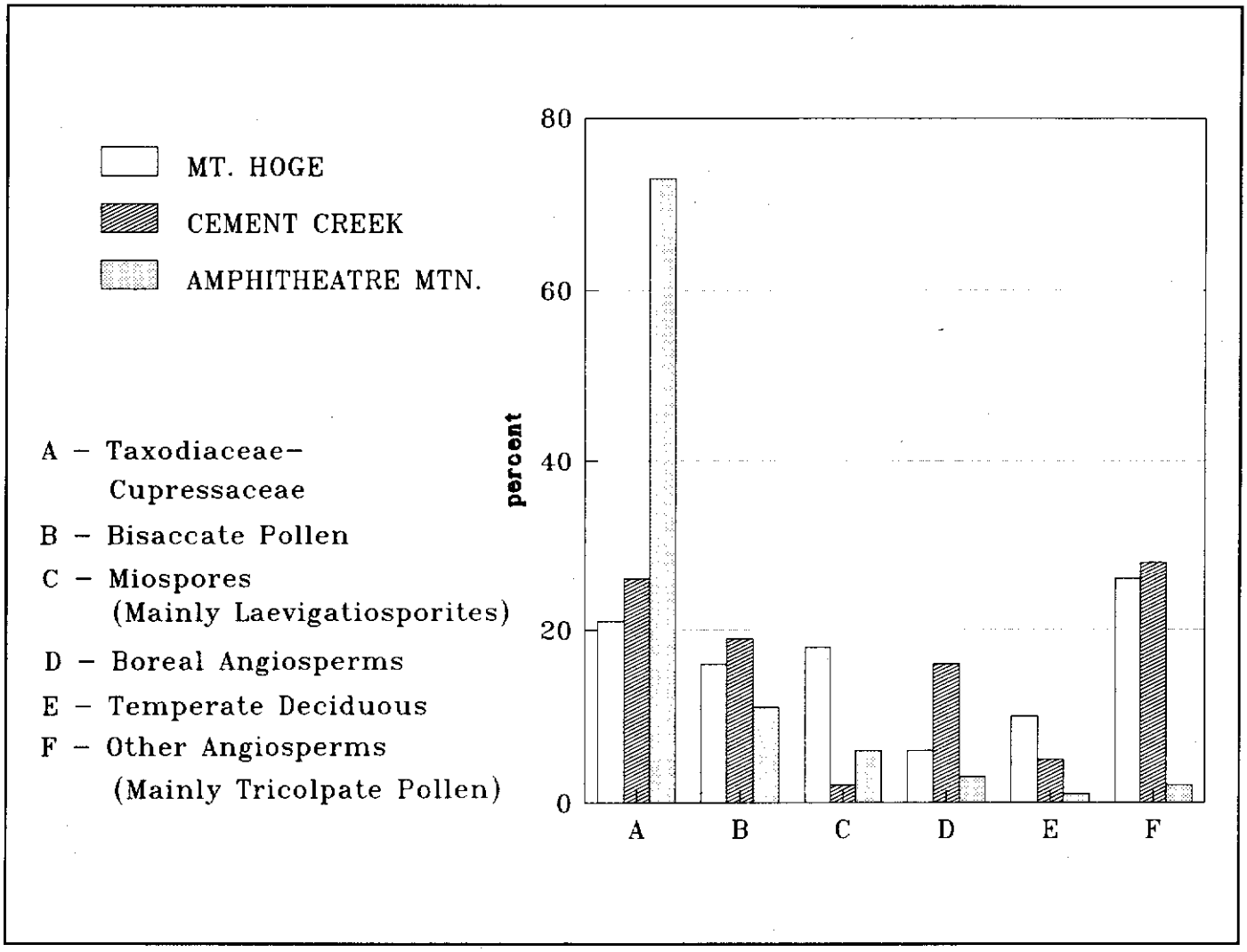

Figure 14: Histogram of the entire pollen spectrum documented for the Burwash basin. Percentages of coniferous pollen types are represented in columns A and B. Percentages of angiosperm pollen types are represented in columns D, E and F. Note the dramatic increase in coniferous pollen types at the Amphitheatre Mountain section relative to the Mount Hoge and the Cement Creek sections. Plots represent analysis of 23 fine-grained samples.

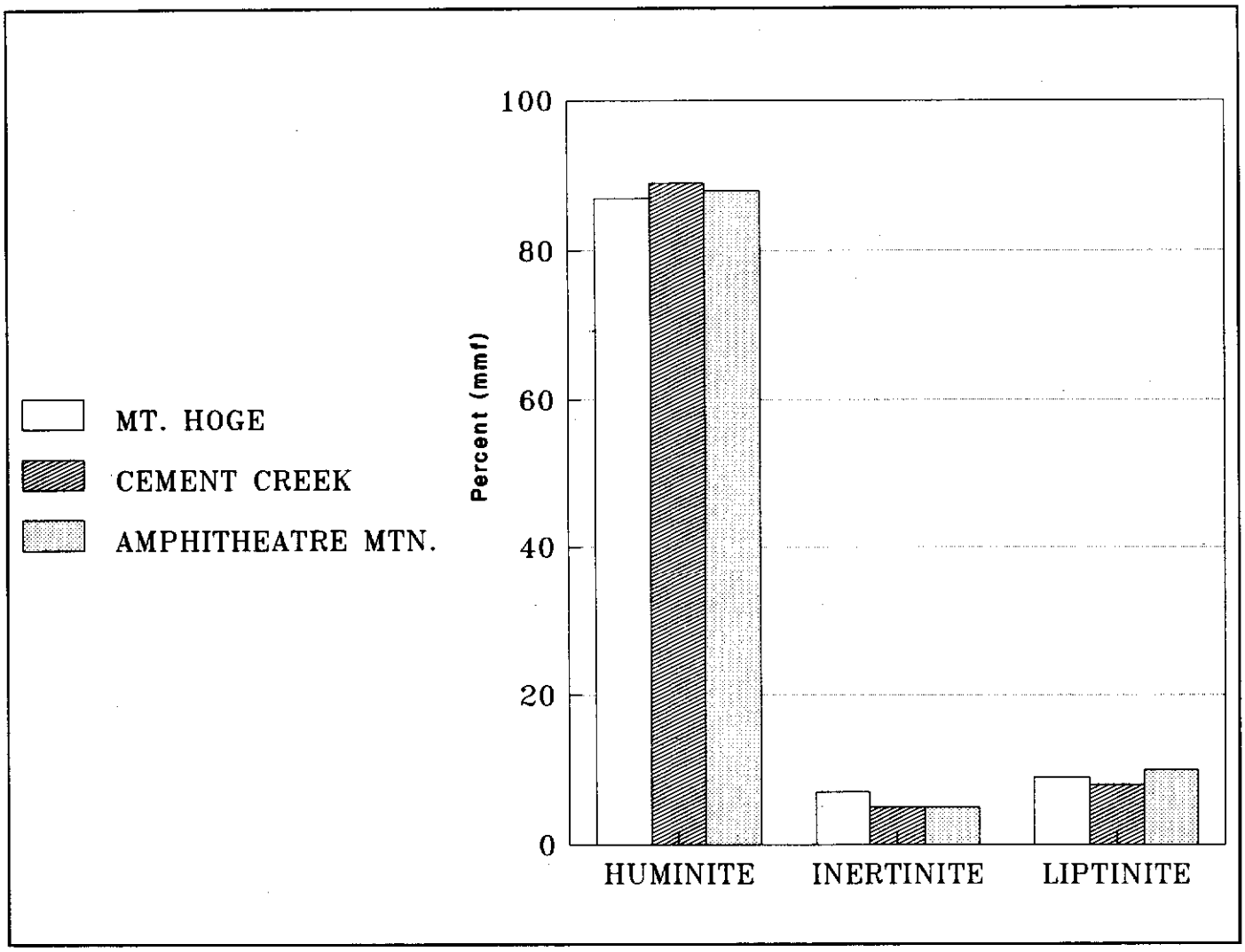

Figure 15: Histogram of maceral types in coal (lignite) from the Burwash basin.

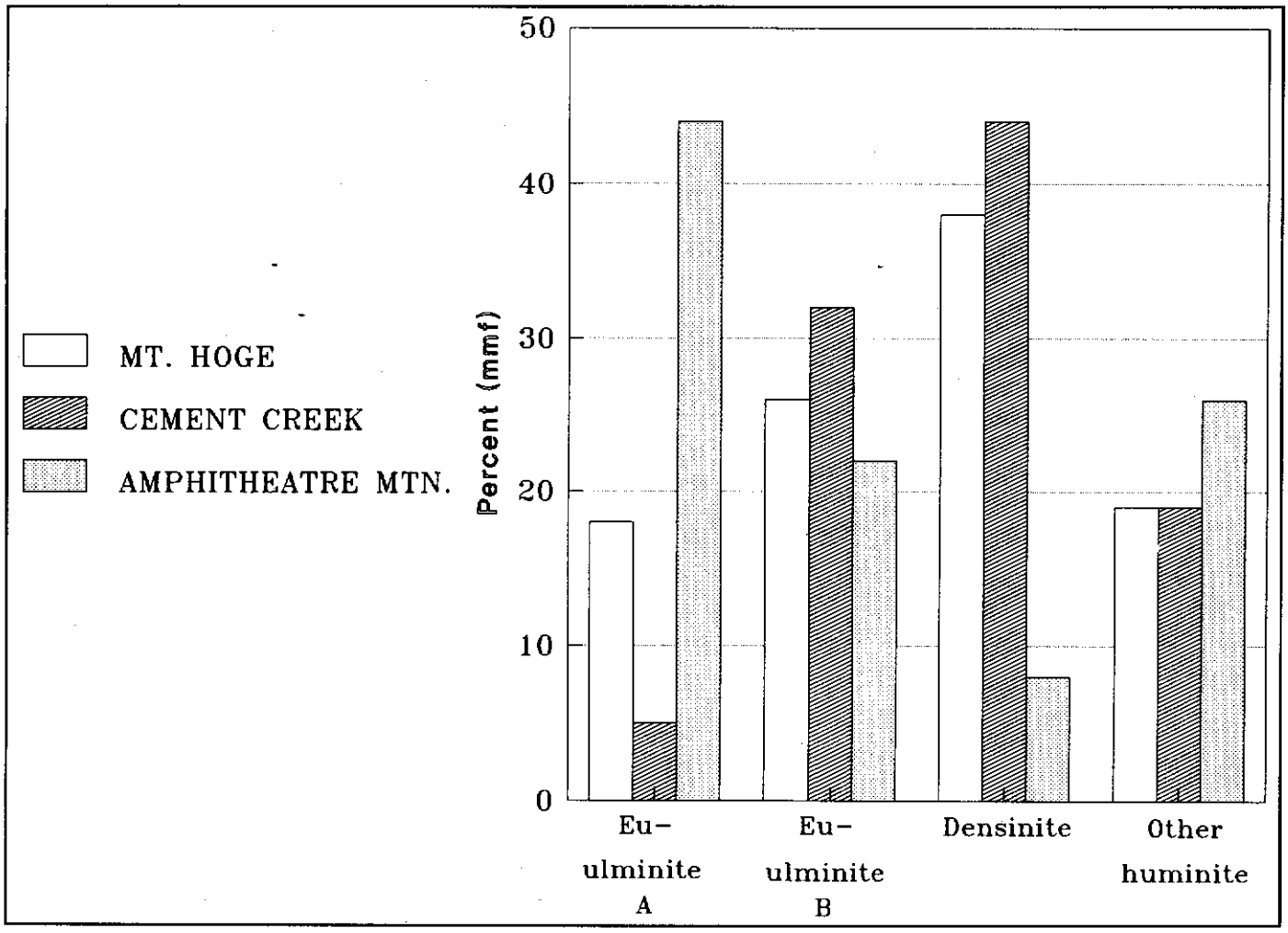

Figure 16: Histograms of individual components of the huminite maceral group for each section in the Burwash basin. Eu-ulminite A is believed to be the decomposition product of conifer wood whose cell walls are commonly impregnated with resin, wax and/or tannins. Eu-ulminite B is the decomposition product of non-coniferous angiosperm wood whose cell walls lack abundant impregnating substances. Densinite is the decomposition product of plants low in lignin and rich in cellulose, a characteristic of the angiosperm woods. Note the enrichment of eu-ulminite A, suggesting conifer-rich coal swamps at the Amphitheatre Mountain section, relative to eu-ulminite B and densinite rich coals located at the Mount Hoge and Cement Creek measured sections, correlating with angiosperm-rich palynomorph assemblages.

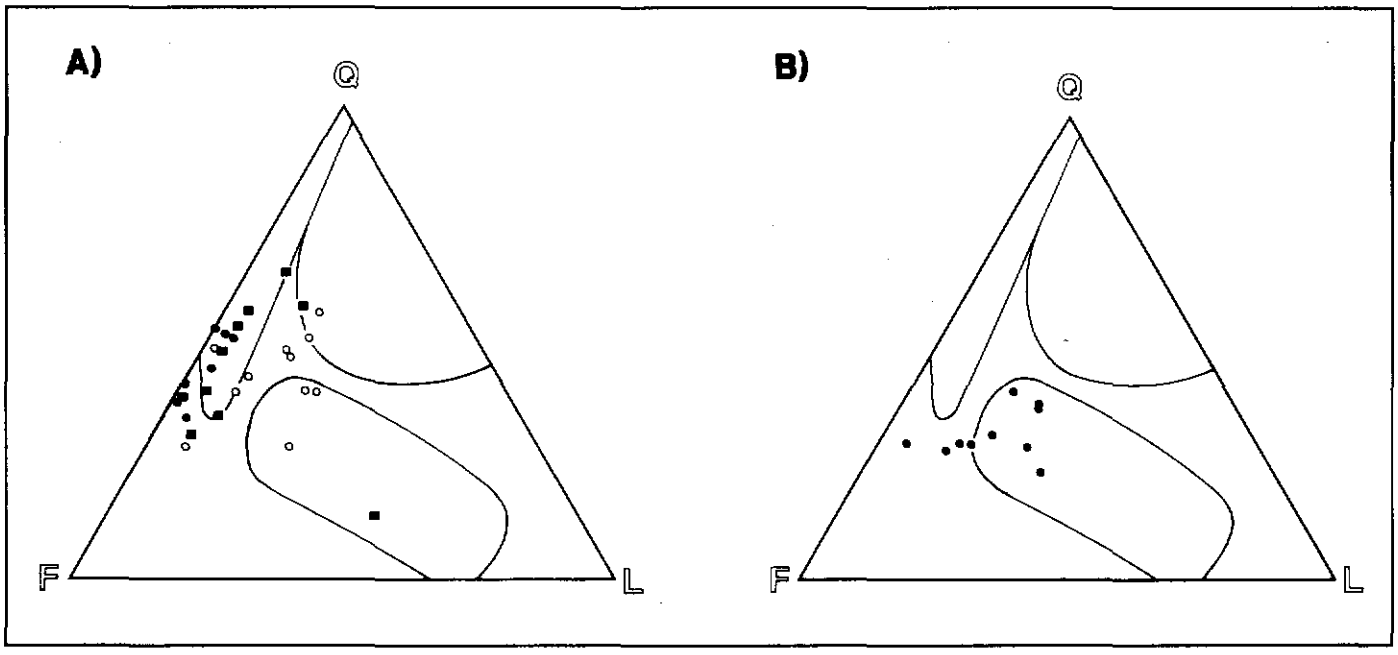

Figure 17: Ternary diagrams showing petrographic modal compositions of sandstones from the Amphitheatre Formation. A) Burwash basin; ● = Mount Hoge, ○ = Amphitheatre Mountain, ■ = Cement Creek; B) Bates Lake basin; Q = total quartz (including chert); F = total feldspar (including plagioclase and K-spar); L = unstable lithic fragments. See Figure 2 and Figure 10 for specific locations. Each point represents a modal analysis based on 450 counts per slide.

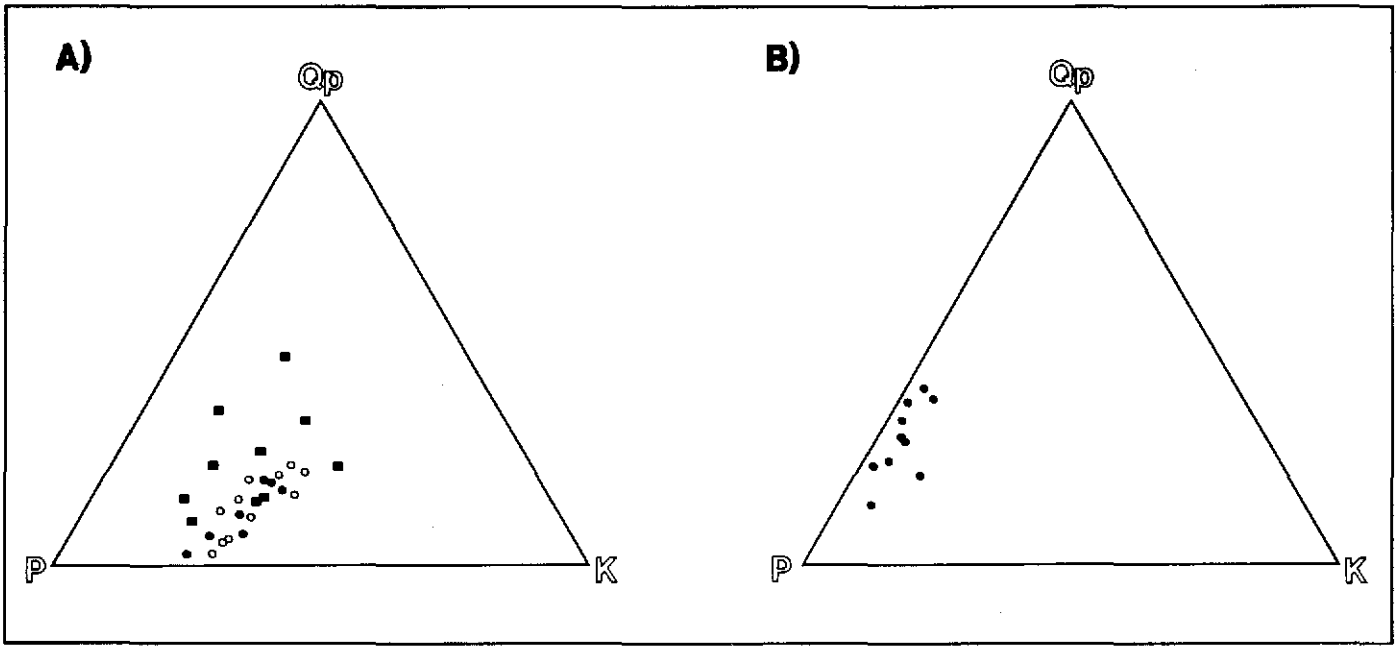

Figure 18: Ternary diagrams showing petrographic modal compositions of sandstones from the Amphitheatre Formation. A) Burwash basin; ○ = Amphitheatre Mountain, ■ = Cement Creek, ● = Mount Hoge; B) Bates Lake basin; Qp = polycrystalline quartz; P = plagioclase; K = potassium feldspar. See Figure 2 and Figure 10 for specific locations. Each point represents a modal analysis based on 450 counts per slide.

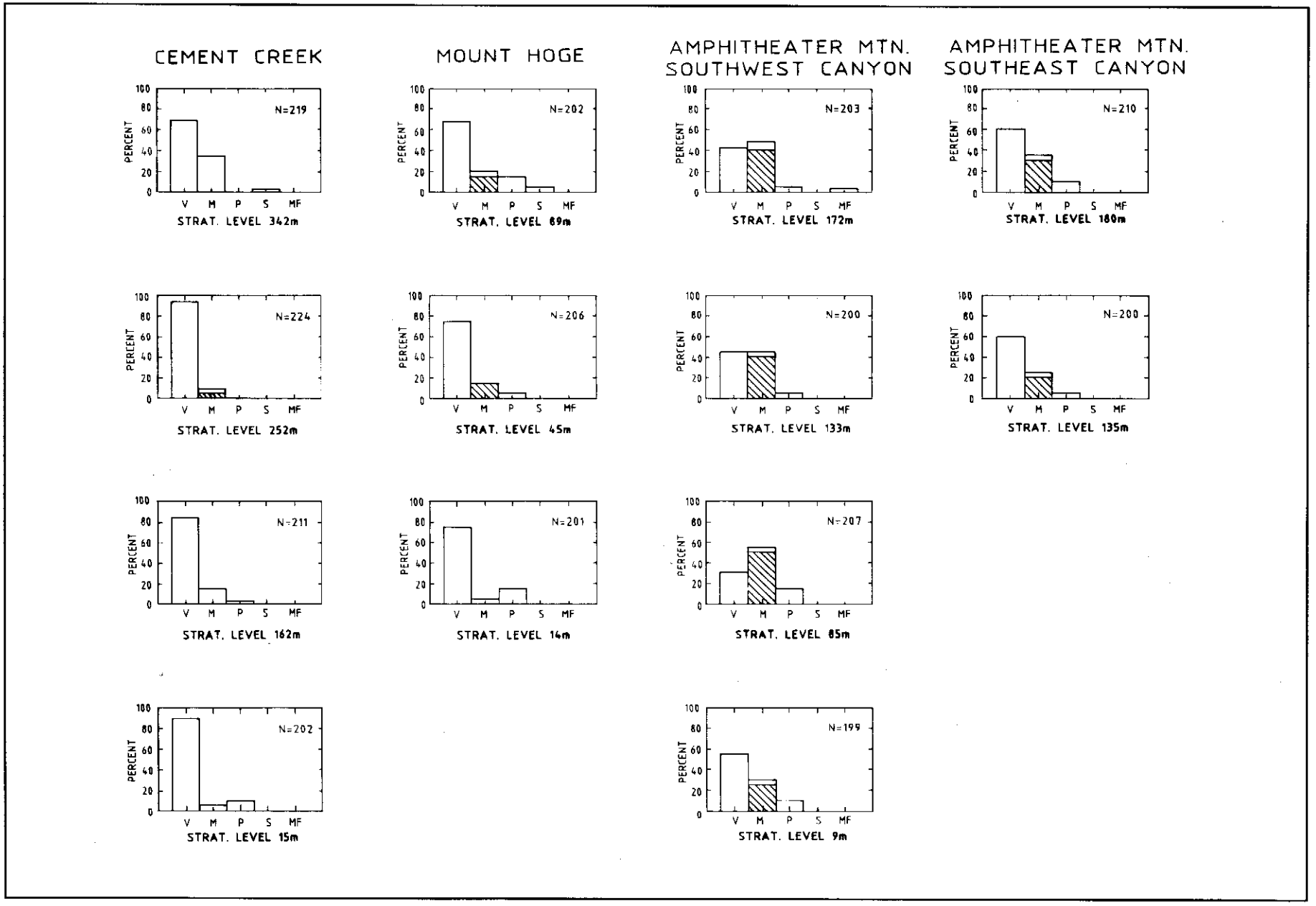

Figure 19: Clast-count data from the Amphitheatre Formation at four sections in the Burwash basin. n = number of clasts counted; STRAT.LEVEL = location of clast count on measured section; V = volcanic clast; M = metamorphic clast (cross-hatched = meta-sedimentary)(blank = high-grade metamorphic); P = plutonic clast; S = sedimentary clast; MF = fine-grained mafic clast. See text for discussion.

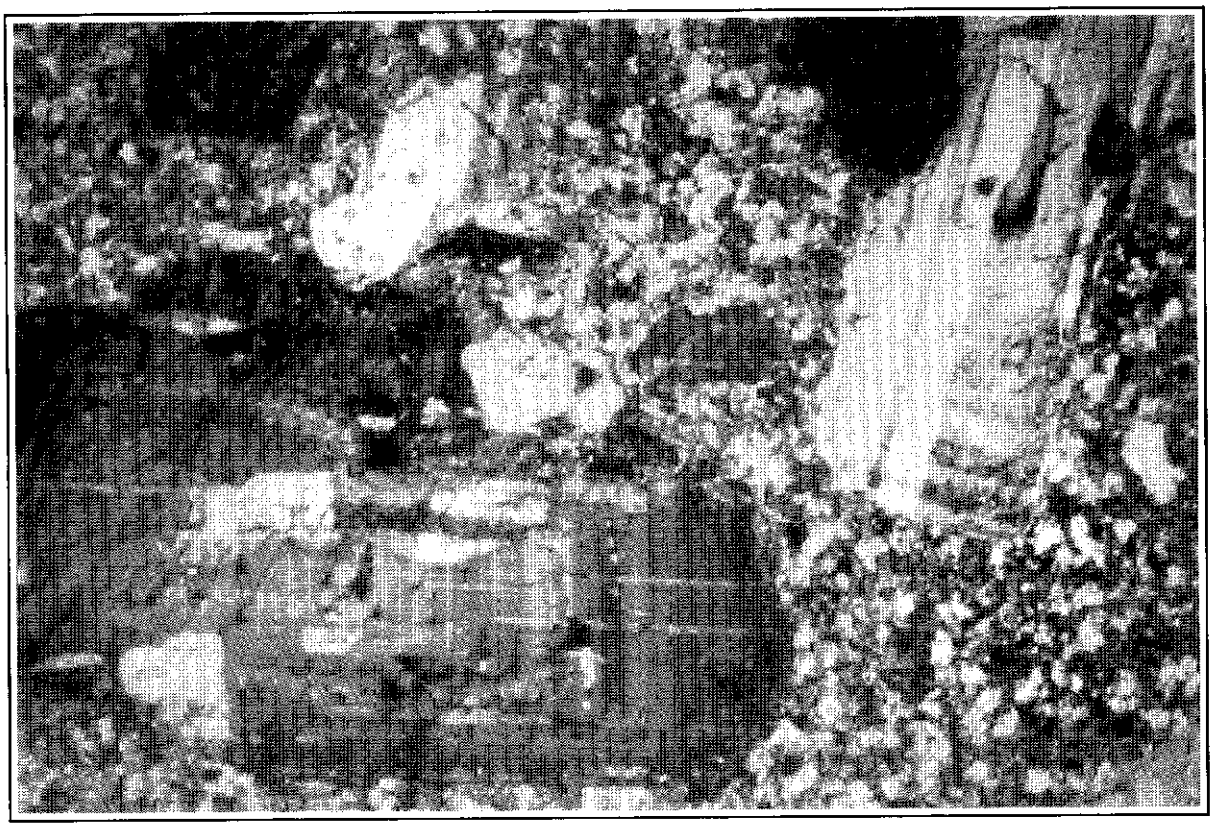

Figure 20: Photomicrograph of a typical meta-basalt conglomerate clast of the Amphitheatre Formation from the Burwash basin. Field of view is 2 mm.

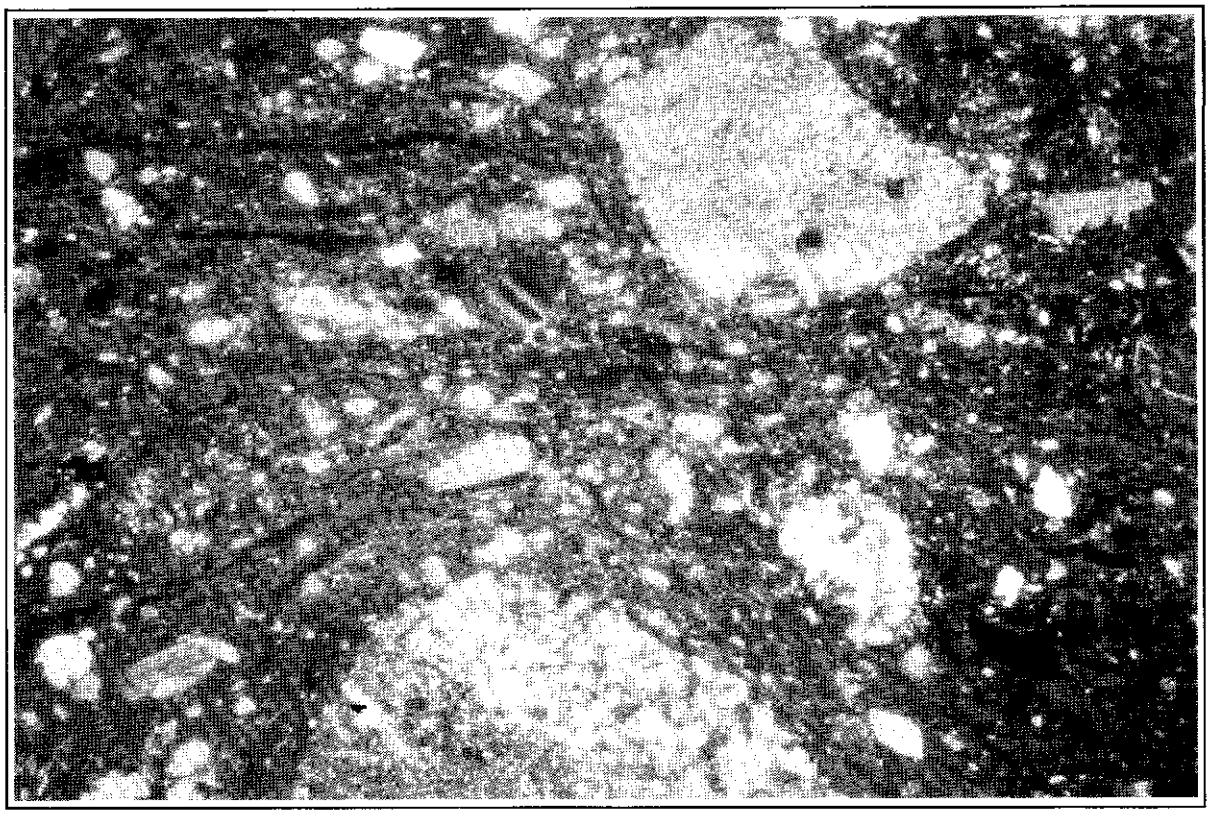

Figure 21: Photomicrograph of a typical welded-tuff conglomerate clast of the Amphitheatre Formation from the Burwash basin. Field of view is 2 mm.

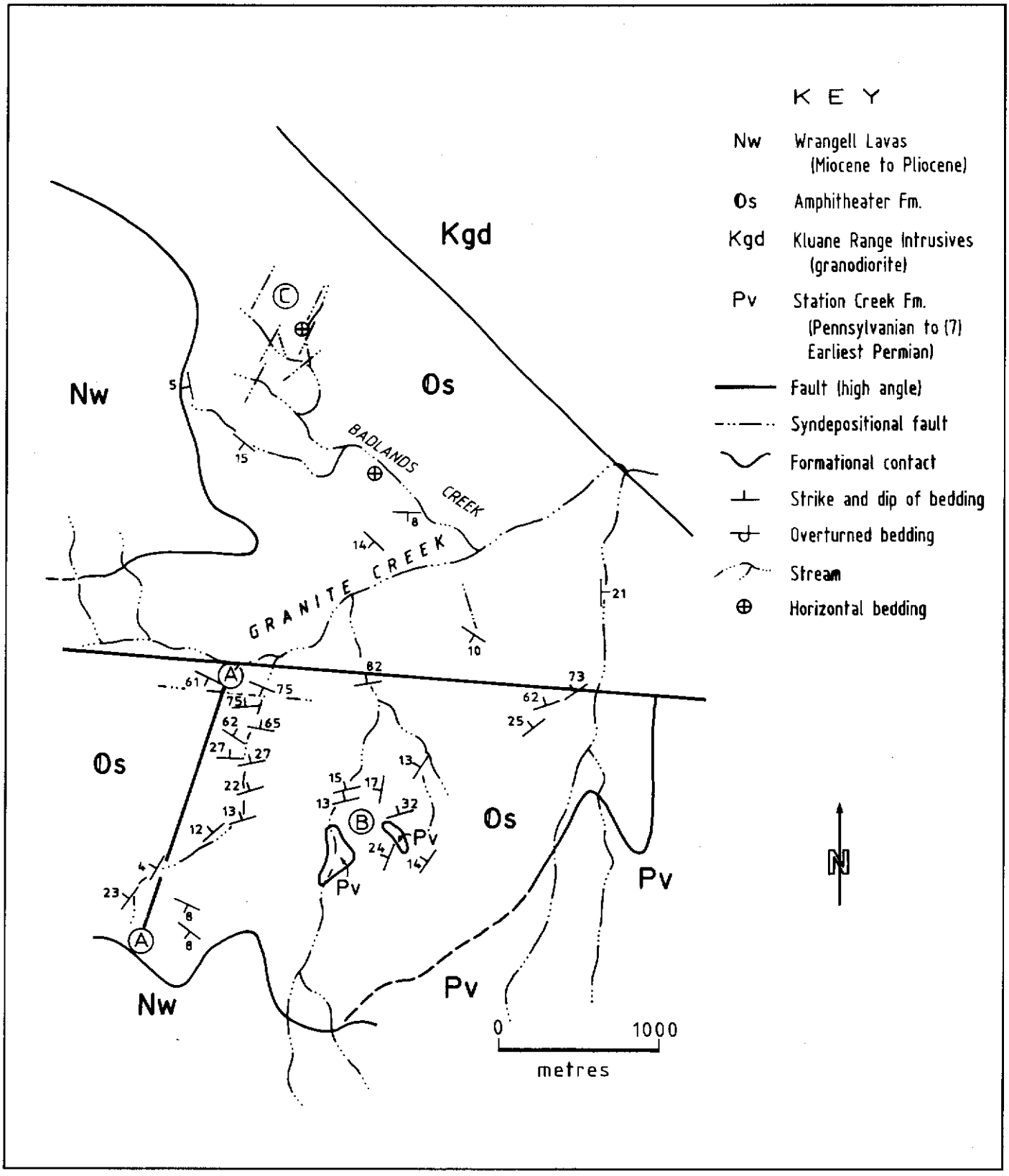

Figure 22: Geologic sketch map of the Amphitheatre Formation along the southern margin of the Burwash basin. See text for explanation.

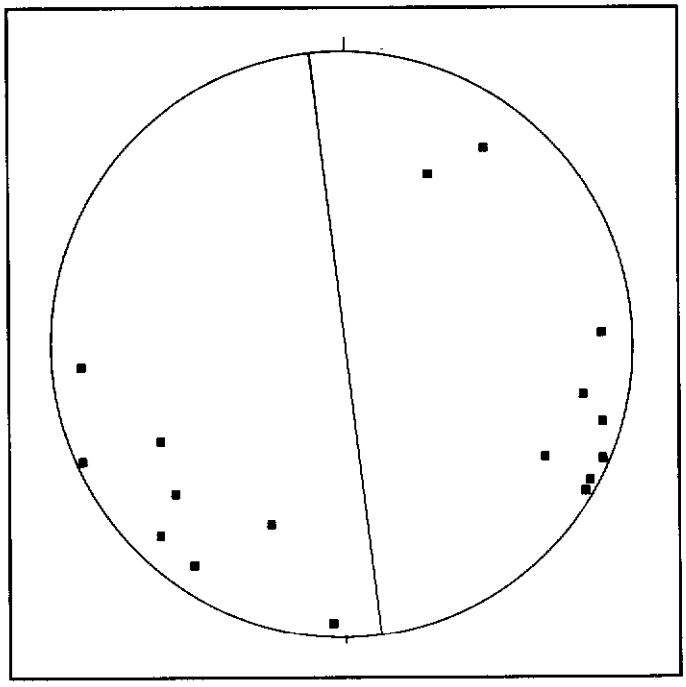

Figure 23: Equal-area projection of poles to 2° faults in the Burwash basin. The steeply dipping faults trend NW-SE. The dark line is the acute bisector of the two conjugate fault populations.

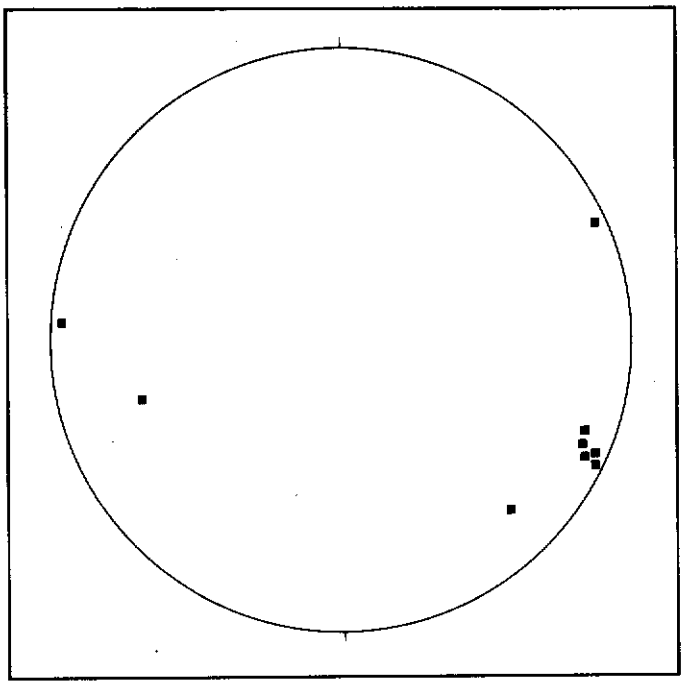

Figure 24: Equal-area projection of poles to 3° syndepositional faults in the Burwash basin. The steeply dipping faults trend northeast-southwest.

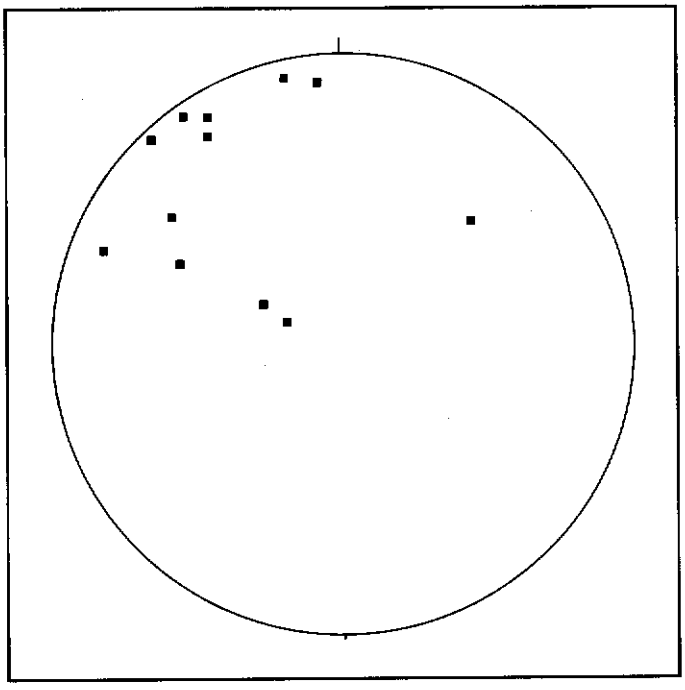

Figure 25: Equal-area projection of slickenside orientations from 2° faults in the Burwash basin. This array demonstrates a large component of horizontal displacement as well as a smaller component of vertical displacement.

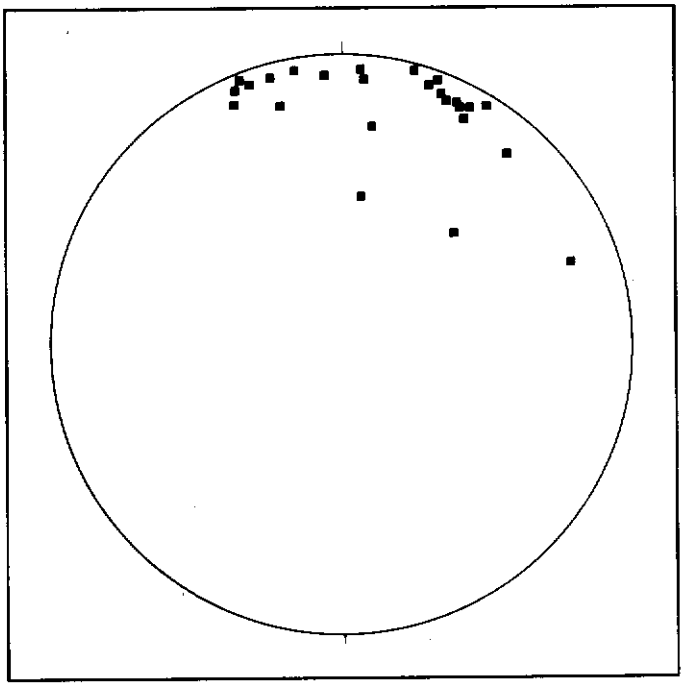

Figure 26: Equal-area projection of slickenside orientations on 3° syndepositional faults in the Burwash basin. This array indicates a large component of sub-horizontal displacement.

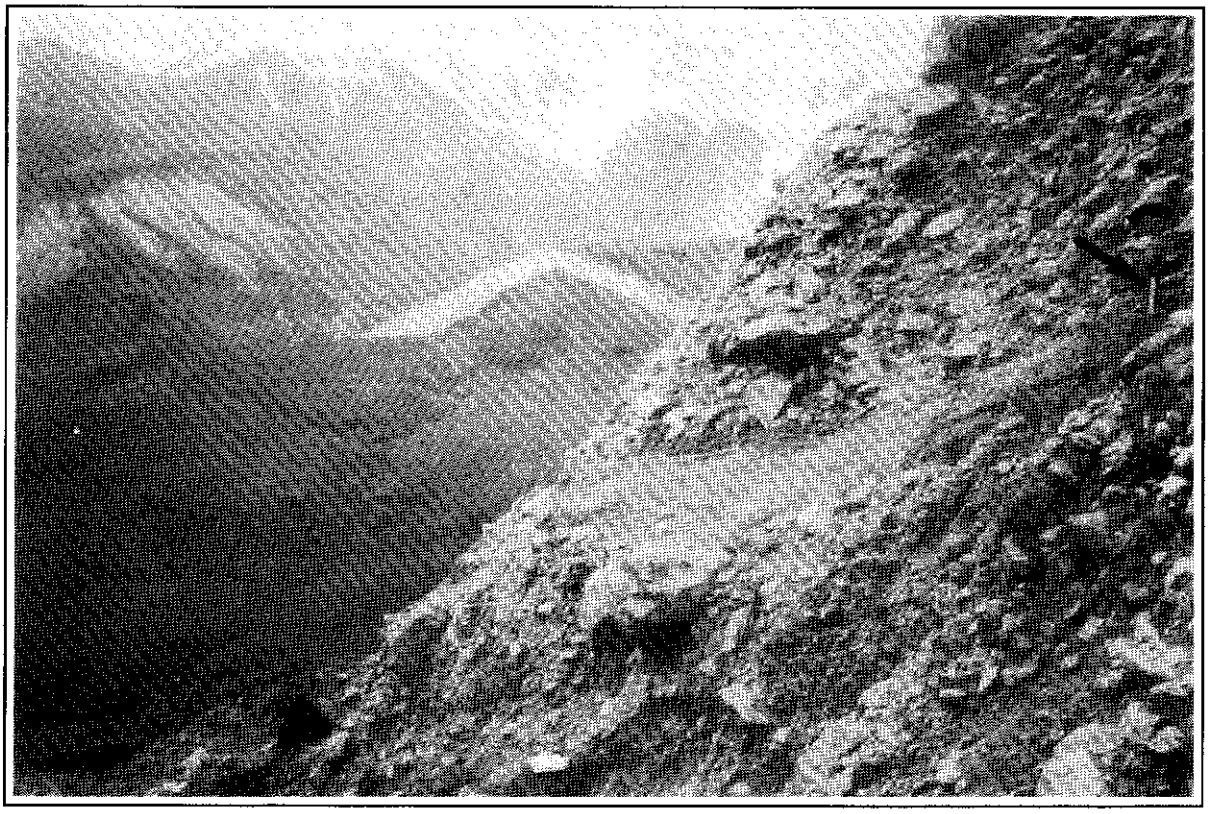

Figure 27: 30-m-thick monomictic boulder conglomerate composed of granodiorite clasts, some of which are up to 5 meters in diameter, exposed in the Burwash basin. Granodiorite clasts are uncommon in conglomerates lower in the section, indicating that a granodioritic source terrane was rapidly exposed along the Burwash basin. Hammer (arrow) for scale.

TABLE 1

Gch	Gravel, clast-supported, horizontal stratification		Granodiorite / basalt breccia
Gcmi	Gravel, clast-supported, massive, imbrication		Coal
Gcp	Gravel, clast-supported, planar cross-stratification	A	Volcanic-ash rich layer
St	Sand, trough cross-stratification		Conglomerate lenses
Sr	Sand, ripple stratification		Sandstone lenses
Sm	Sand, massive		Plant fragments
Sh	Sand, horizontal stratification		Covered
Fsm	Silt, mud - massive		Volcanic sill
	Granodiorite breccia		Logs
			Burrows
			Siltstone Drape

Table 1: Lithofacies code for measured sections in the Amphitheatre Formation, Yukon Territory.

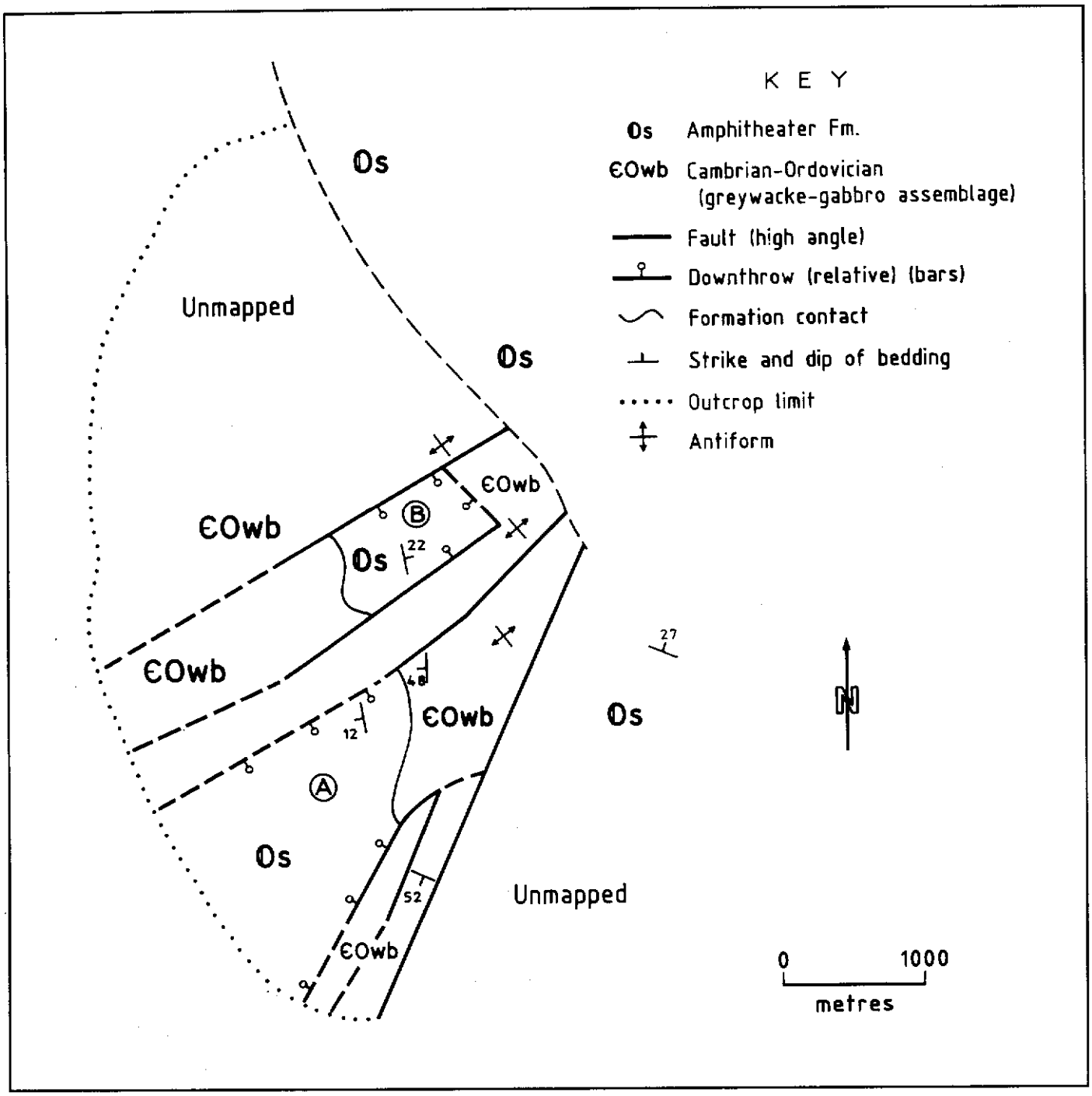

Figure 28: Geologic sketch map of the southwest margin of the Bates Lake basin demonstrating the extensional nature of this part of the basin. See text for explanation.

REFERENCES

AYDIN, A. and NUR. A., 1982. Evolution of pull-apart basins and their scale dependence. Tectonics, vol. 1, p. 91-105.

CAMPBELL, R.B. and DODDS, C.J., 1978. Operation St. Elias, Yukon Territory. Geological Survey of Canada, Paper 78-1A, p. 35-41.

CAMPBELL, R.B. and DODDS, C.J., 1982a. Geology of southwest Kluane Lake map area, Yukon Territory (115G&F, E½), 1:125,000. Geological Survey of Canada, Open File 829.

CAMPBELL, R.B. and DODDS, C.J., 1982b. Geology of the southwest Dezadeash map area, Yukon Territory (115A), 1:125,000. Geological Survey of Canada, Open File 831.

CHRISTIE-BLICK, N. and BIDDLE, K.T. (eds.), 1985. Strike-slip deformation, basin formation, and sedimentation. Society of Economic Paleontologists and Mineralogists, Special Publication No. 37, p. 127-141.

CLAGUE, J.J., 1979. The Denali fault system in southwest Yukon Territory - a geologic hazard? Geological Survey of Canada Paper 79-1A, p. 169-178.

COLE, R.B., RIDGWAY, K.D. and DeCELLES, P.G., 1989. Late stage deposition within a Cenozoic strike-slip basin: fluvial/basalt/pyroclastic transitions, St. Elias Mountains, Yukon Territory, Canada. Geological Society of America Abstracts with Programs, p. A128.

CROWELL, J.C., 1974. Origin of late Cenozoic basins in southern California. In: Tectonics and Sedimentation; Society of Economic Paleontologists and Mineralogists, Special Publication No. 22, p. 190-204.

DICKINSON, W.R. and SUCZEK, C.A., 1979. Plate tectonics and sandstone compositions. American Association of Petroleum Geologists Bulletin, Vol. 63, p. 2164-2182.

EISBACHER, G.H., 1976. Sedimentology of the Dezadeash flysch and its implications for strike-slip faulting along the Denali Fault, Yukon Territory and Alaska. Canadian Journal of Earth Sciences, Vol. 13, p. 1495-1513.

EISBACHER, G.H., 1978. Vertical accretion during high-gradient progradation of fluvial systems. In: Fluvial Sedimentology, A.D. Miall, (ed.); Canadian Society of Petroleum Geologists, Memoir No.10, p. 850.

EISBACHER, G.H. and HOPKINS, S.L., 1977. Mid-Cenozoic paleogeomorphology and tectonic setting of the St. Elias Mountains, Yukon Territory. Geological Survey of Canada, Paper 77-1B, p. 319-335.

ETHRIDGE, F.G., 1985. Modern alluvial fans and fan deltas. In: Recognition of Fluvial Depositional Systems and their Resource Potential. SEPM Short Course No. 19, p. 101-126.

FORBES, R.B., TURNER, D.L., STOUT, J.H. and SMITH, T.E., 1973a. Cenozoic offset along the Denali Fault. EOS abstracts, 54, p. 495.

FORBES, R.B., TURNER, D.L., SMITH, T.E., STOUT, J.H. and WEBER, F.R., 1973b. The Denali fault offset problem. In: United States Geological Survey Alaskan program, 1973; U.S. Geological Survey Circular 683, p. 46.

FORBES, R.B., SMITH. T.E. and TURNER, D.L., 1974. Comparative petrology and structure of the Maclaren, Ruby Range and Coast Range belts: implications for offset along the Denali Fault. Geological Society of America, Abstracts with Programs, Vol. 6, p. 176.

FRASER, G.S. and SUTTNER, L.J., 1986. Alluvial fans and fan deltas - a guide to exploration for oil and gas. International Human Resources Development Corp., Boston, 199 p.

FREDERIKSEN, N.O. and CHRISTOPHER, R.A., 1978. Taxonomy and biostratigraphy of late Cretaceous and Paleogene triatriate pollen from South Carolina. Palynology, Vol. 2, p. 113-145.

HARDING, T.P., VIERBUCHEN, R.C. and CHRISTIE-BLICK, N., 1985. Structural styles, plate-tectonic settings, and hydrocarbon traps of divergent (transitional) wrench faults. In: Strike-Slip Deformation, Basin Formation, and Sedimentation, K.T. Biddle and N. Christie-Blick (eds.); Society of Economic Paleontologists and Mineralogists, Special Publication No.37, p. 51-77.

LANPHERE, M.L., 1978. Displacement history of the Denali fault system, Alaska and Canada. Canadian Journal of Earth Sciences, Vol. 15, p. 815-822.

LONG, D.J.F., 1981. Dextral strike-slip faults in the Canadian Cordillera and depositional environments of related fresh-water intermontane coal basins. In: Sedimentation and Tectonics in Alluvial Basins, A.D. Miall, (ed.); Geological Association of Canada Special Paper 23, p. 154-186.

LOWELL, J.D., 1972. Spitsbergen Tertiary orogenic belt and the Spitsbergen fracture zone. Geological Society of America Bulletin, Vol. 83, p. 3091-3102.

MANN, P., HEMPTON, M.R., BRADLEY, D.C. and BURKE, K., 1983. Development of pull-apart basins. Journal of Geology, Vol. 91, p. 529-554.

MORTENSEN, J.K. and JILSON, G.A., 1985. Evolution of the Yukon-Tanana terrane: evidence from southeastern Yukon Territory. Geology, Vol. 13, p. 806-810.

MULLER, J., 1981. Fossil pollen records of extant angiosperms. The Botanical Review, v.47, p.1-47.

NOKLEBERG, W.J., JONES, D.L. and SILBERLING, N.J., 1985. Origin and tectonic evolution of the Maclaren and Wrangellia terranes, Eastern Alaska Range, Alaska. Geological Society of America Bulletin, Vol. 96, p. 1251-1270.

PLAFKER, G., BLOME, C.D. and SILBERLING, N.J., 1989. Reinterpretation of lower Mesozoic rocks on the Chilkut Peninsula, Alaska, as a displaced fragment of Wrangellia. Geology, Vol. 17, p. 3-6.

READ, P.B. and MONGER, J.W.H., 1976. Pre-Cenozoic volcanic assemblages of the Kluane and Alsek Ranges, southwestern Yukon Territory. Geological Survey of Canada, Open File 381, 97 p.

RIDGWAY, K.D., CAMERON, A.R., SWEET, A.R. and DeCELLES, P.G., 1989. Evolution of a strike-slip basin as defined by sedimentology, palynology, and organic petrology, St. Elias Mountains, Yukon Territory, Canada. Geological Society of America, Abstracts with Programs, p. A50.

STOUT, J.H., and CHASE, C.G., 1980. Plate kinematics of the Denali fault system. Canadian Journal of Earth Sciences, Vol. 17, p. 1527-1537.

TEMPELMAN-KLUIT, D.J., 1976. The Yukon Crystalline Terrane: enigma in the Canadian Cordillera. Geological Society of America Bulletin, Vol. 87, p. 1343-1357.

TSCHUDY, R.H., and SCOTT, R.A.,(eds.), 1969. Aspects of Palynology, John Wiley and Sons, New York, 510 p.

WIGGINS, V.D., 1976. Fossil oculata pollen from Alaska. Geoscience and Man, Vol. 15, p. 51-76.

WILCOX, R.E., HARDING, T.P., and SEELY, D.R., 1973. Basic wrench tectonics. American Association of Petroleum Geologists Bulletin, Vol. 57, p. 74-96.

PHOSPHORITES, IRONSTONES, AND SECONDARY PHOSPHATES IN MID-CRETACEOUS FLYSCH OF THE BLOW TROUGH, NORTHERN YUKON

Gary M. Yeo
Geology Department,
Acadia University,
Wolfville, Nova Scotia
B0P 1X0

YEO, G.M., 1992. Phosphorites, ironstones and secondary phosphates in mid-Cretaceous Flysch of the Blow Trough, Northern Yukon. In: Yukon Geology, Vol.3; Exploration and Geological Services Division, Yukon, Indian and Northern Affairs Canada, p.27-36

ABSTRACT

The Blow River Formation was deposited in the Blow Trough, a north-trending, middle Cretaceous downwarp near the junction of the Western Canada Seaway and the Brooks and Sverdrup Basins. At Rapid Creek, the Blow River Formation comprises a 380 m cyclic succession of thick, silty, siderite-phosphate pellet packstone and intraformational boulder-pebble conglomerate lenses interbedded with grey, laminated siltstone and sideritic siltstone. These rocks rest conformably on grey shale with thin ferruginous siltstone beds, and are overlain conformably by grey siltstone with chert pebbles and siderite concretions. To the west, the formation thickens dramatically, as the ironstone-bearing member interfingers with and overlies dark grey shales and thin sandstones. To the east, it thins, passing into 160 m of interbedded shale and sideritic shale at Boundary Creek. Facies changes indicate a clastic source to the west. Early Albian ammonites and charcoal fragments are locally common. The widespread iron and phosphorous-rich hemipelagic sequence is an important regional marker, and is best known for the variety of secondary phosphate minerals (MINFILE 117A 027)found as nodules or along fractures related to Eocene folding.

The Blow River formation contains about 7 x 10^8 tonnes of P_2O_5. This major deposit (MINFILE 117A 027) falls between the peak global episodes of phosphogenesis in the Callovian and Campanian, and, like them, corresponds to the late stage of a global anoxia. Unlike most phosphorites, this is a high latitude deposit.

RÉSUMÉ

La formation de Blow River a été déposée dans la dépression de Blow, un fléchissement du Crétacé moyen d'orientation nord près de la jonction du passage marin de l'Ouest canadien et des bassins de Brooks et de Sverdrup. Au ruisseau Rapid, la formation de Blow River se compose d'une succession cyclique de packstone à granules de sidérite et phosphate, épais et silteux avec lentilles intraformationnelles de conglomérat de blocs et de galets, interstratifiées de siltstone feuilleté et de siltstone sidéritique gris d'une épaisseur de 380 m. Ces roches reposent en concordance sur le shale gris avec minces couches de siltstone ferrugineux et sont recouvertes en concordance par un siltstone gris à galets de chert et à concrétions de sidérite. À l'ouest, la formation s'épaissit de manière saisissante alors que le membre renfermant les roches sédimentaires ferrugineuses forme des interdigitations avec des shales gris foncé et des grès minces qu'il recouvre également. À l'est, elle s'amincit pour passer à 160 m de shale et de shale sidéritique interstratifiés au ruisseau Boundary. Le changement de faciès indique la présence d'une source de matériaux clastiques à l'ouest. Par endroits les ammonites et les fragments de charbon de bois de l'Albien précoce sont communs. La séquence hémipélagique riche en fer et en phosphore répandue constitue un important repère régional et est des mieux connues pour la grande variété de ses minéraux phosphatés secondaires présents sous forme de nodules ou le long de fractures associées au plissement de l'Éocène.

La formation de Blow River renferme environ 7 x 10^8 tonnes de P_2O_5. Ce dépôt majeur se situe entre les épisodes de pointe globaux de phosphogenèse au Callovien et au Campanien, et comme ceux-ci, il correspond au dernier stade d'anoxie globale. À l'opposé de la plupart des dépôts de phosphorites, celui-ci constitue un dépôt de hautes latitudes.

INTRODUCTION

The rocks described in this report are part of a thick flyschoid sedimentary package deposited in the northern Yukon in middle Cretaceous time. The ironstone-phosphorite bearing unit is informally called the Blow River formation. It is preserved in a north-trending lowland area which lies between the Richardson and Barn Mountains and links the Old Crow Basin with the Mackenzie Bay area of the Beaufort Shelf. This area was the site of a major, north-trending tectonic depression developed during the Columbian Orogeny, known as the Blow Trough (Young et al., 1976) or Rapid Depression (Norris and Yorath, 1981). The regional geology has been described by Young (1972; 1977), Young and others (1976), and Norris and Yorath (1981). The secondary minerals in the Blow River Formation (MINFILE 117A 027)(Robertson, 1982) have attracted considerable attention from mineralogists and collectors. Locally common invertebrate fossils, including the pelecypod Inoceramus ex gr. I. anglicus-cadottensis and the ammonite ?Sonneratia sp., indicate that the Blow River formation is early Albian or younger (J.A. Jeletzky in Young, 1977).

The Blow River formation is unusual in many respects. (1) Phosphorites and ironstones are not commonly closely associated with each other. (2) Most phosphorites are believed to accumulate in tectonically stable settings in low latitudes, but this deposit accumulated in a tectonically active depression at high latitudes. (3) Although the secondary minerals are clearly related to their host rocks, the conditions under which they formed are not clear. In an attempt to resolve these problems, H.G. Ansell of the Geological Survey of Canada, and the writer, visited well-known exposures of the Blow River formation in July, 1988. The two exposures are located on Cross Cut Creek, a tributary of Rapid Creek (Fig. 1), and on the Big Fish River.

GEOLOGICAL SETTING OF THE BLOW RIVER FORMATION

Tectonics

Blow Trough (Young et al., 1976) is a structurally controlled mid-Cretaceous depression that developed near the junction of the Western Canada Intracratonic Seaway and the southern margin of the Amerasian Basin. It lies between Cache Creek High and the Romanzoff Uplift-Keele-Old Crow Landmass, the easternmost elements of the Brooks Range fold and thrust belt. It links the southwest-trending Keele-Kandik Trough and the southeast-trending Peel Trough with the Beaufort Shelf.

Blow Trough (Rapid Depression) developed in response to late Mesozoic dextral movement on the Kaltag-Porcupine Fault System (Norris and Yorath, 1981), in turn accomodating dextral transcurrent movement on the Tintina-Kaltag Fault system, and resulting ultimately from an increased spreading rate at the mid-ocean ridge separating the Pacific and Farallon plates. This movement also resulted in north-directed thrusting and uplift of the Brooks Range. This tectonic activity in the northern Cordillera was accompanied by the deposition of clastic sediments in the foredeep of Colville Basin to the north and Blow Trough to the east.

Structure

The chief structural feature of northern Porcupine Plateau is the Rapid Fault Array, a family of steeply dipping, anastomosing northwest to northeast-trending faults which fan northward from the two major faults of northern Yukon, the dextral Kaltag-Porcupine Fault and the Yukon thrust fault (Norris, 1974 in Young, 1977; Norris and Yorath, 1981). Recent mapping by Lane (1988) indicates that the faults are predominantly west-directed thrust faults, rather than normal faults as interpreted by earlier workers. These faults cut Paleocene strata (Reindeer Formation) and hence were active in early Tertiary time (Norris and Yorath, 1981, Lane, 1988). Mid-Cretaceous facies changes between adjacent fault blocks of the Rapid Fault Array, and consistency of stratigraphy within each block (Young, 1977) indicate that many of the faults of the Rapid Fault Array are re-activated Cretaceous structures. Within the blocks of the Rapid Fault Array, strata as young as the early Paleocene upper Moose Channel formation are folded about north- trending axes. (Folding affects rocks as young as Norris' (1981) map unit Tmc3, but not Tak. The younger unit Tak is faulted, but not folded.)

Hence, the latest deformation event recorded in the Rapid Depression is east-west compression which occurred during Paleocene to Eocene time (Lane, 1988). The northerly orientation of the early Tertiary structures is most likely controlled by early Cretaceous extensional(?) features which also controlled Cretaceous sedimentation patterns in Blow Trough. Offset of the Shaktolik Formation and granitic intrusions of the Koyukuk Basin of Alaska suggests up to 130 km of dextral displacement on the Kaltag-Porcupine Fault system during the Late Cretaceous or Early Tertiary. In the Rapid Depression, this movement was accomodated by the east-west folding and thrusting outlined above.

Stratigraphy

During the Jurassic and Early Cretaceous (to early Neocomian), widespread epicontinental mudrocks of the Kingak and Husky formations and sandstones and siltstones of the Bug Creek Group and Porcupine River Formations were shed north and west across the area. These rocks are up to 1600m thick in the Richardson Mountains-Mackenzie delta area (Young et al, 1976). They lie disconformably on older strata.

The Jurassic-Early Cretaceous rocks are overlain conformably to disconformably (Norris, 1983) by transgressive, late Neocomian marine mudstones of the Martin Creek Formation and Unit Kmc (Norris, 1981; equivalent to the "upper shale-siltstone division" which Young et al (1976) interpreted to be Barremian). Lithofacies distributions (Young

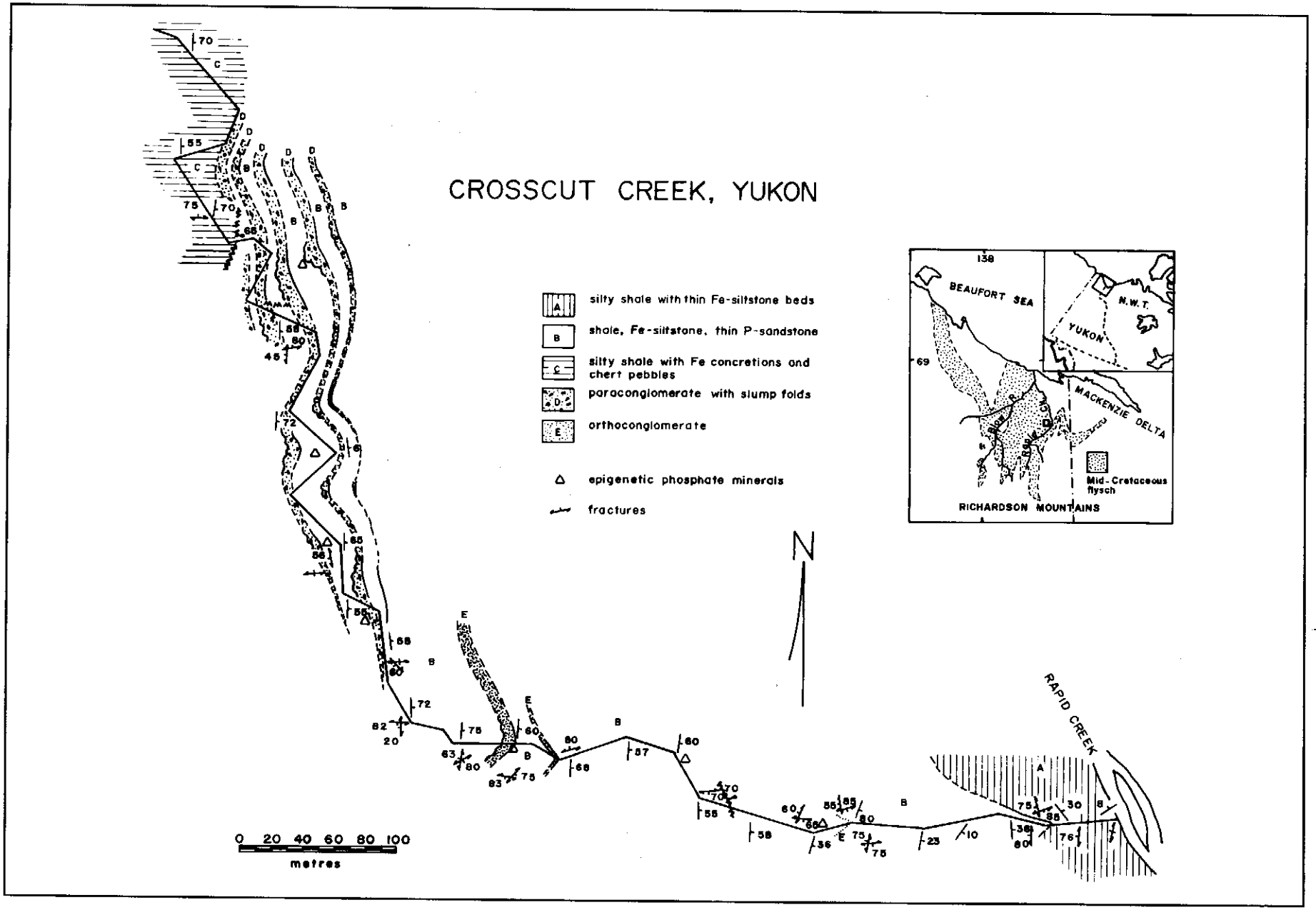

Figure 1. Map of Crosscut Creek, a tributary of Rapid Creek, where phosphate minerals were first found in 1962. Of thirty-two phosphate minerals recognized in these rocks, Rapid Creek is the type locality for seven.

et al, 1976) indicate that these clastics were also shed northwesterly. By this time, Blow Trough was an actively subsiding feature.

Regressive, coarse-grained marine clastics of the Aptian Mt Goodenough Formation ("lower shale" and "upper sandstone" divisions of Young, 1977) conformably to disconformably overlie unit Kmc and Martin Creek Formation rocks (Norris, 1983). Lithofacies distributions (Young et al, 1976) and limited sediment dispersal data (Young, 1973) suggest that these sediments were mostly shed westward from the North American craton. In the upper part of this interval, an increase in lithic fragments and a shift in sediment dispersal from an easterly to a westerly source marks a transition from epicontinental to flyschoid sedimentation (Young, 1973; Norris and Yorath, 1981).

The Mt Goodenough Formation is overlain unconformably (Norris and Yorath, 1981, Fig. 7) to conformably (Norris, 1983) by a sequence of flyschoid Albian mudstones, sandstones and conglomerates, here called the Rapid Creek Group. These rocks are described below.

The Rapid Creek Group is disconformably overlain (Norris, 1983) by transgressive Cenomanian mudstones of the Boundary Creek Formation.

The Boundary Creek Formation is disconformably overlain by a wedge of Maestrichtian, molassoid sandstones and siltstones, the Moose Channel Formation (Norris, 1983). This unit thickens northward, and marks a major, non-marine progradation (Norris and Yorath, 1981).

The Moose Channel Formation is conformably overlain by non-marine, coal-bearing Paleocene mudstones of the Reindeer Formation (Young et al, 1976; Norris, 1983).

Rapid Creek Group

The name Rapid Creek Group is here proposed for the thick sequence of flyschoid clastics between the mudrocks of the Mt Goodenough Formation (Upper sandstone and upper siltstone divison of Jeletzky, 1971; Young 1972, 1974 and others) and the Boundary Creek Formation in northern Richardson Mountains. These strata have been variously called the upper Aptian to lower Albian flysch (Jeletzky, 1971), the Aptian-Albian flysch sequence (Young, 1972), the Albian flyschoid phase (Young, 1973; Norris and Yorath, 1981), or the Aptian-Albian flysch division (Young et al, 1976). Robertson (1980, 1982) proposed the name Rapid Creek Formation for this succession, but Young (1977) and Norris (1981, 1983) have shown that at least three units of formation rank can be recognized within it.

The Rapid Creek Group includes three map units, Ksr, Krr and Kbr distinguished by Norris (1981). The unit of chief interest here is unit Kbr, informally called the Blow River Formation. The other two are described briefly.

The Rapid Creek Group is correlative to the south with the Sans Sault Formation and Fort St John Group in the northern part of the Interior Seaway (Mannville and Blairmore equivalents). To the northwest it correaltes with the Fortress Mountain, Torok, Oumalik and Topagarok Formations of Colville Basin, north of the Brooks Range Uplift. It also correlates to the northeast with the Christopher Formation of the Sverdrup Basin. All of these middle Cretaceous strata were deposited during a period of global transgression (e.g. Haq et al. 1987).

Unit Ksr

Norris' (1981) map unit Ksr, informally called Skull Ridge Formation, corresponds lithologically to subunit A of Young's (1977) map unit K4b. It is best exposed at Skull Ridge, where polymictic orthoconglomerates overlain by sandstones form impressive cliffs. Clast compositions suggest a source to the southwest (Lane, 1988). According to Young (1977), this unit is about 550m thick. The Skull Ridge Formation is restricted to the west side of Blow Trough. It rests conformably on extensive grey-black shale with quartz sandstone and ironstone, chert pebble orthoconglomerate, and diamictite of the Mount Goodenough Formation (Unit K4a of Young, 1977).

Unit Krr

Norris' (1981) map unit Krr, informally called Rat River Formation, corresponds lithologically to subunit B of Young's (1977) Unit K4b. It comprises mainly grey sandstones and siltstones, the fine-grained distal facies equivalents of the Skull Ridge Formation on the east side of Blow Trough. Like the latter, the Rat River Formation conformably overlies shales of the Mount Goodenough Formation.

Blow River Formation

Norris' (1981) map unit Krb, informally called Blow River Formation, corresponds lithologically to Young's (1977) Units K4c and K4d. It comprises interbedded siderite ironstone and shale with sandstone and conglomerate. Found throughout Blow Trough, it overlies and interfingers westward with the Skull Ridge and Rat River Formations. It is overlain disconformably by grey shales of the Boundary Creek Formation. The easternmost exposures of the Blow River Formation, in the Big Fish River area, are relatively thin and comprise pelagic clay shale and siderite ironstone. Exposures of the Blow River Formation on Cross Cut Creek, the best known of several phosphate mineral locations in this unit, are described below.

CROSS CUT CREEK

Stratigraphy

On Cross Cut Creek the Blow River Formation is represented by 358m of interbedded dark grey silty shale, sideritic siltstone and phosphorite granule sandstone (Robertson, 1982). Beds of intraformational para- and orthoconglomerate are common in the lower part of the

ironstone- and phosphorite-bearing interval. Both sandstones and conglomerates are lenticular (Fig. 1). These rocks overlie a thick unit of pale grey silty shale with siderite concretions and scattered black chert pebbles, interpreted to be the Mt Goodenough Formation.They are overlain by light grey silty shale with thin, rusty weathering, sideritic siltstone beds. Robertson (1980) interpreted these to belong to the Boundary Creek Formation. Alternately, they may be a shaly upper member of the Blow River Formation, as suggested by Norris (1981).

A detailed section through the lower part of the succession on Cross Cut Creek (Fig. 2) shows that deposition of massive and laminated siltstones interbedded with massive, planar and ripple-laminated sandstones was interrupted episodically by scouring and deposition of silty pebble-boulder paraconglomerates. Internally deformed, laminated, intraformational siltstone blocks in the conglomerate are up to 6m across. These conglomerates also contain rounded grey chert pebbles, possibly derived from the underlying Mt Goodenough Formation. Some of the paraconglomerates pinch out laterally over a few hundred metres and infill channels up to 14 m deep in the rhythmically deposited clastic sequence. Ripple lamination in sandstone beds suggests local northwesterly sediment transport, but slump folds overturned towards the east indicate an easterly paleoslope.

Well preserved fossils are rare in the Blow River Formation. Ammonite impressions ?Sonneratia were observed locally, and fragments of charcoal were found in the lower part of the unit.

Structure

The style of deformation observed on Rapid Creek is consistent with that described farther west in Blow Trough by Lane (1988). In the vicinity of its tributary, Cross Cut Creek, Rapid Creek flows northward along the hinge of a north plunging syncline. Bedding at Cross Cut Creek is gently folded about north-trending axes. A minor, east-dipping reverse fault is exposed about 250m upstream on Cross Cut Creek. A comparable fault is exposed immediately upstream from the phosphate showings. Small-scale synthetic and antithetic duplex thrusts are common. Two sets of steeply dipping fractures are developed. North-trending fractures which lie subparallel to regional fold axes are generally not mineralized. East-trending fractures which lie normal to local fold axes commonly contain secondary phosphate minerals (Fig. 3).

Secondary Mineralization

The Blow River Formation is best known for the secondary minerals, chiefly phosphates, found as veins and breccia fillings in the Rapid Creek area (MINFILE 117A 027)(Fig. 1), and as nodules further east at Big Fish River (Robertson, 1982). Thirty-two phosphate minerals have been identified, and of these, about half a dozen are unique to the Blow River Formation. The best known is lazulite, Yukon's

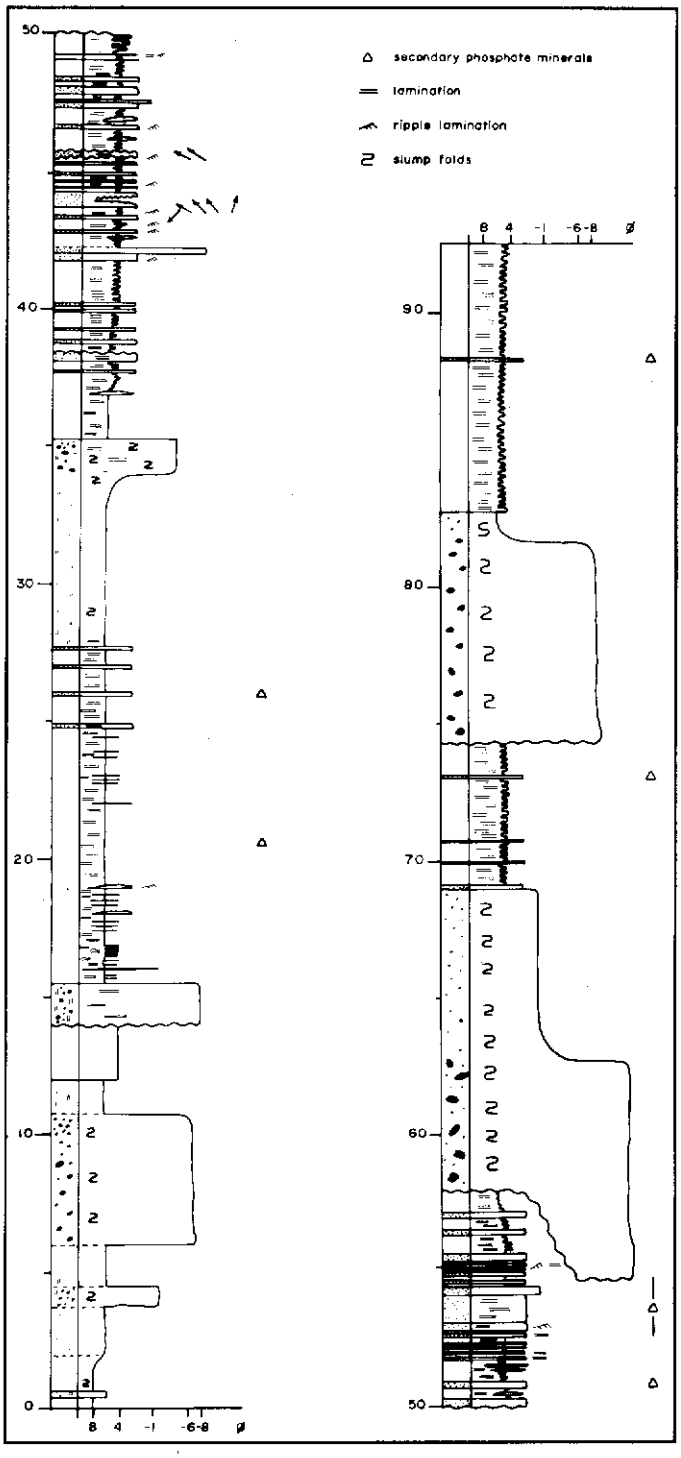

Figure 2. Graphic log of a section through the lower (western) part of the Crosscut Creek exposure of the Blow River formation. Thin to medium-bedded dark grey shale, phosphatic sandstone and siderite ironstone alternate with paraconglomerates containing slump folds and reworked intraformational fragments. The shales, sandstones and ironstones are interpreted as starved basin deposits; the paraconglomerates are inferred to be base-of-slope slump deposits.

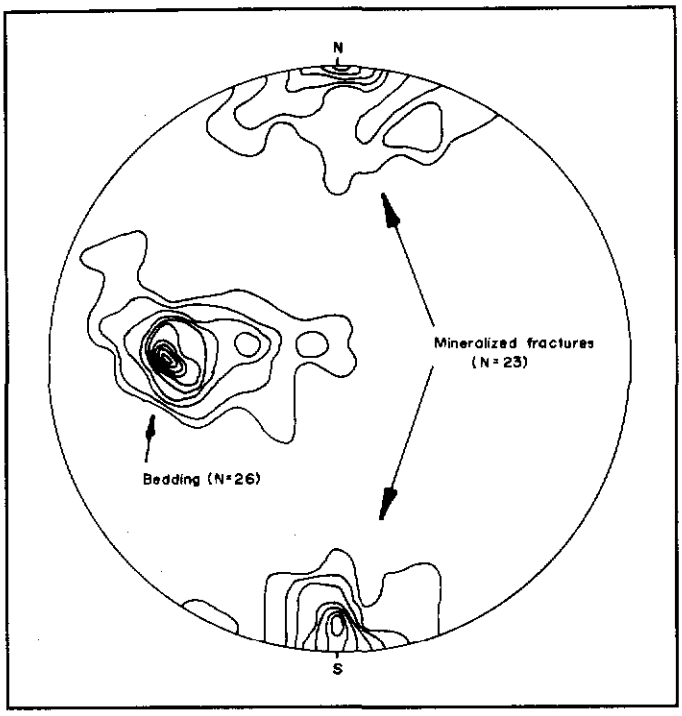

Figure 3. Contoured lower hemisphere stereonet plots of poles to bedding, and fractures containing phosphate minerals at the Crosscut Creek location. Contour interval is 1%. The plot indicates that the mineralized fractures are perpendicular to the poles to bedding, and were probably formed during Early Tertiary regional folding.

official gemstone.

Most of the work on the Blow River Formation has focused on the secondary phosphate minerals (Campbell, 1962; Coleman and Robertson, 1981; Mandarino and Sturman, 1976; Mandarino, Sturman and Corlett, 1971; 1978; Robertson, 1980; 1982; Sturman and Mandarino, 1976; Sturman, Mandarino and Corlett, 1977; Sturman, Mandarino, Mrose and Dunn, 1981; Sturman, Peacor and Dunn, 1981). Of these authors, only Robertson (1980; 1981; 1982) paid much attention to the host rocks and the controls on the secondary mineralization.

DISCUSSION

Depositional Setting of the Cross Cut Creek Member

Robertson (1980; 1982) inferred the Blow River Formation to be a shallow marine deposit, based on what he interpreted as coarsening-upward cycles at Cross Cut Creek. However, only the basal contacts of the conglomeratic beds are scoured, and the cycles fine rather than coarsen upward (Figures 1 and 2). There is no other evidence for a shallow water setting. The predominance of mudrock, scarcity of current structures, fossils, or trace fossils, all suggest that the Blow River Formation is a deep water deposit, as Young (1973; 1977), Young and others (1976) have argued.

The Blow River beds on Cross Cut Creek can be interpreted according to Mutti and Ricci Lucchi's (1972; 1975) turbidite facies classification as Facies D (base-cut-out Bouma sandstones), Facies F (chaotic slump deposits), and Facies G (pelagic muds). This assemblage is probably a slope facies association (Mutti and Ricci Lucchi, 1972; 1975) deposited on or near the base of an east-facing submarine slope. The existence of such submarine bathymetric relief is consistent with active subsidence of Blow Trough during the middle Cretaceous.

Robertson (1980; 1982) interpreted the clastic sediments to have been derived from the east. Although local ripple lamination lends some support to this interpretation, regional easterly thinning of the Rapid Creek clastics, east-verging slump folds at Cross Cut Creek and elsewhere, (Young, 1977), sparse regional paleocurrent data (Young, 1973), and facies changes, especially the eastward-increasing proportion of chemical sediment, all indicate a source to the west or southwest.

Deposition of the Phosphorite Beds

It is widely believed phosphorites result from upwelling of nutrient-rich waters along basin margins in middle to low latitudes, an interpretation first developed by Kazakov (1937 in Gulbrandsen, 1969). Although most known phosphorites were deposited in low latitudes (Cook and McElhinny, 1979), there is no compelling reason why upwelling should be restricted by latitude. Investigations of global paleocirculation patterns (Curtis and Parrish, 1982) show that in the mid-Cretaceous, as at present, a high pressure cell was centred over the North Pole and the prevailing winds were easterly, parallel to the coastline. Under such conditions, surface waters will flow offshore, due to Ekman transport. Hence, the Blow River Trough, a re-entrant on the southern margin of the Arctic Basin, was a potential upwelling area in the mid-Cretaceous (Fig. 4).

The phosphorite beds at Cross Cut Creek are allochthonous phosphate granule sands. The phosphate granules most likely formed diagenetically in a shelf environment further west in Blow Trough and were mechanically concentrated and carried down slope by turbidity currents.

Phosphorite preservation should be favoured by anoxic conditions since in well-oxygenated waters, phosphate-rich organic matter is swiftly decomposed and the phosphorus is rapidly recycled. Although it has been argued that anoxic conditions are not necessary for phosphogenesis (Arthur and Jenkyns, 1981)) there is a striking temporal correspondence between phosphogenesis and anoxic events (Fig. 5). Arthur and Jenkyns' argument was based on the fact that no major phosphorite deposit was known to correspond with the global Aptian-Albian anoxic event. The Blow River phosphorite was deposited during this interval, however, and it is a substantial

accumulation, containing roughly 7 billion tonnes of P_2O_5 according to data of Young (1977).

The relationship between anoxia and phosphogenesis may be a "chicken and egg" problem. Anoxic conditions would inhibit decomposers and recycling of phosphorus in the marine system, thus favouring preservation of phosphatic organic-rich sediments. Upwelling of phosphorus would result in dramatically increased biological productivity near the surface (e.g. present-day offshore Peru). A well known effect of increased organic productivity is increased biological oxygen demand in the water column, and expansion of the oxygen minimum zone. This might lead to the onset of an oceanic anoxic event. Reduced phosphorus upwelling due to the burial and removal of phospate sediment from the system, active circulation under anoxic conditions, or perhaps a change in ocean circulation patterns (e.g. El Nino), could have resulted in a decrease in biological productivity, decreased biological oxygen demand, contraction of the oxygen minimum, and the end of an oceanic anoxic event.

Deposition of the Ironstone

As the Rapid Creek Group thins eastward, the proportion of ironstone increases, reaching a maximum in the Big Fish River area (Young et al, 1976). Such an accumulation of chemical sediment is typical of clastic-starved basins. Precipitation of primary siderite requires low Eh, high P_{CO2},and low S (Berner, 1971). While anoxic conditions would result in reducing, CO_2-enriched waters, the concentration of dissolved iron in sea water is typically very low, and organic-rich sediments should generate quantities of H_2S. With sufficient dissolved iron, pyrite precipitation is favoured. However, siderite precipitation is common under diagenetic conditions. Abundant pyritic nodules in shale in the Big Fish River area indicate that diagenetic conditions there favoured pyrite, as opposed to siderite. Hence it is unlikely that the siderite ironstone beds formed diagenetically in that part of the basin. Like the phosphorite beds, siderite must have formed diagenetically elsewhere in the basin, and was reworked into the beds in which it is now found. The high P_{CO2} and low Eh conditions of anoxia should have favoured such siderite precipitation.

Phosphorites and sideritic ironstones rarely occur together, because the conditions under which siderite and phosphate minerals form are incompatible. In the presence of dissolved calcium, a major constituent of phosphate minerals, calcite rather than siderite should precipitate (Berner, 1971). Both minerals could precipitate sequentially, however. Resedimentation of authigenic siderite and phosphate grains, formed under different diagenetic conditions in the same part of the basin, probably accounts for the association between siderite ironstone and phosphorite beds in the Blow River Formation.

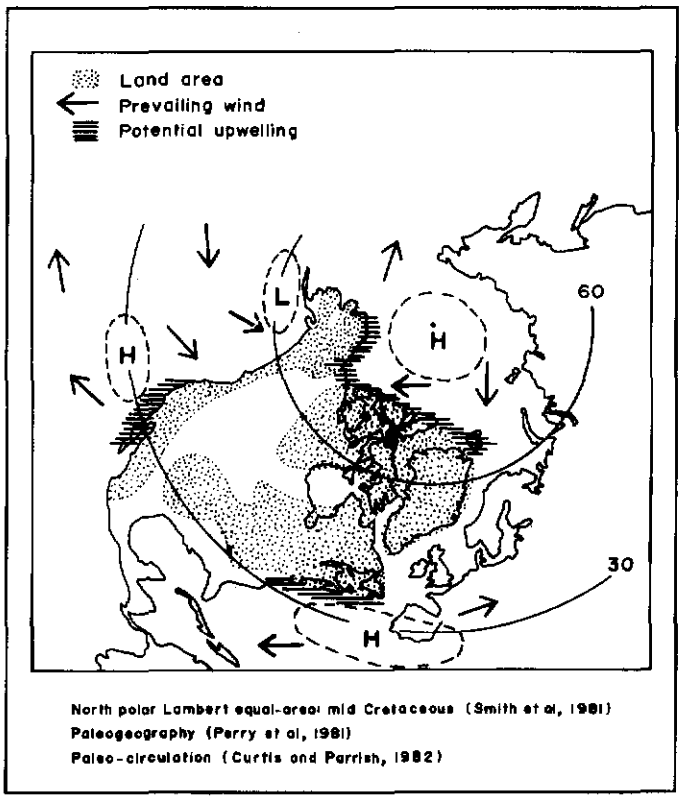

Figure 4. Unlike the Blow River Formation, most known phosphorites were deposited in low latitudes, probably in response to upwelling of nutrient-rich waters and increased biotic productivity. This figure shows there is no reason why phosphorite deposition should should be restricted to low latitudes, as the rim of the Arctic Basin was a potential area of upwelling during the mid-Cretaceous.

Emplacement of the Secondary Minerals

The epigenetic phosphates and associated minerals are clearly related to their unusual host rocks. Robertson (1982) identified four phosphate mineral assemblages, each associated with a particular host rock type. Veins are most common in the more competent phosphorite beds. Poles to mineralized fractures are perpendicular to the domain of poles to gently folded bedding, indicating that the fractures are extensional cross-fractures related to regional folding (Fig. 3) which, as pointed out above, affects rocks as young as Eocene (Lane, 1988). This Early Tertiary compression probably also mobilized the relatively low temperature fluids which precipitated the secondary minerals (Robertson, 1982).

CONCLUSIONS

(a) The Blow River ironstones and phosphorites are distal, deep water deposits, not shallow water deposits.

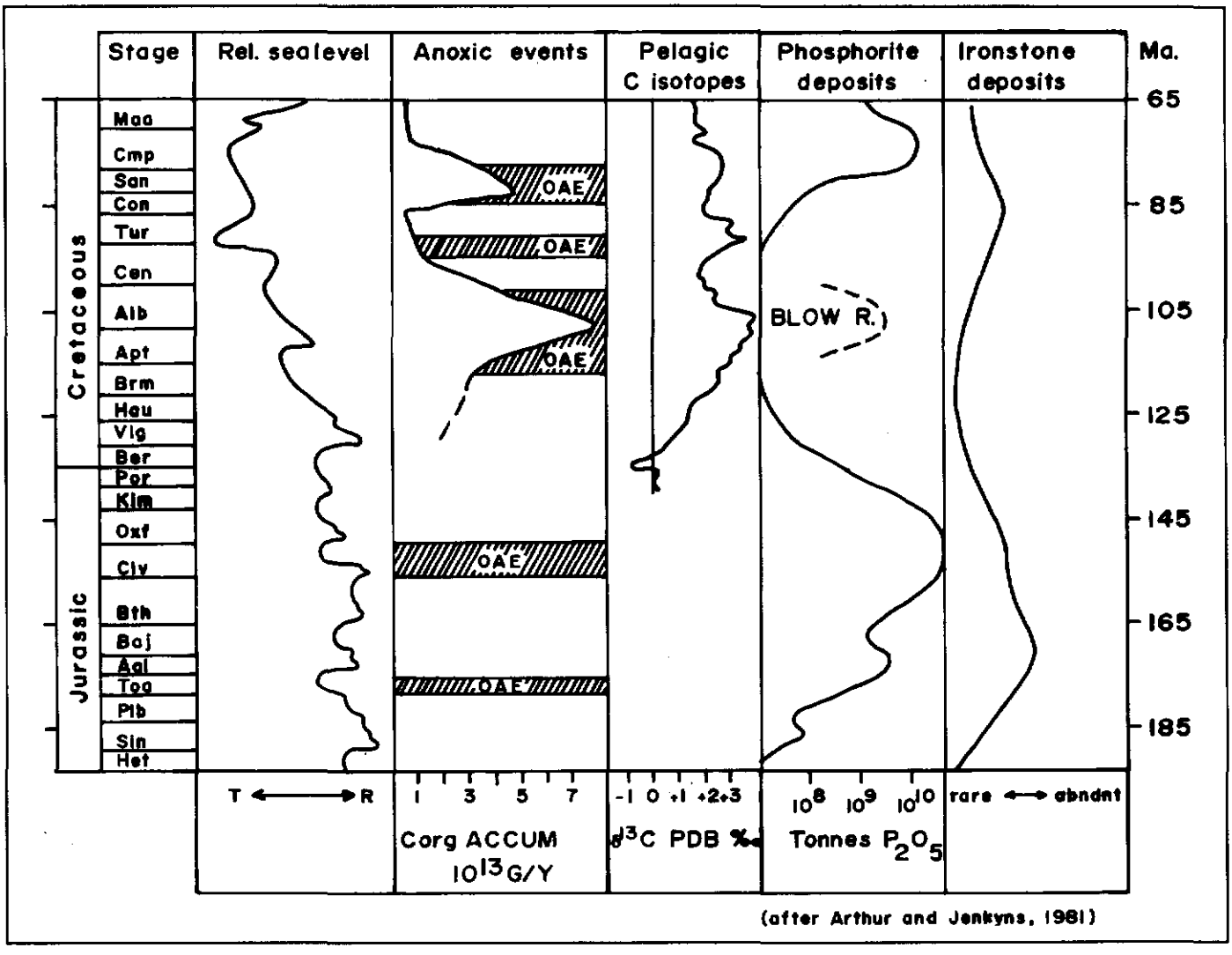

Figure 5. Strongly reducing conditions such as the Oceanic Anoxic Events (OAE's) which occurred repeatedly throughout the Mesozoic, favour accumulation and preservation of organo-sedimentary deposits including phosphorites. Major phosphorite deposits including the Blow River Formation appear to be associated with such anoxic events. There is no clear association with sea level changes.

(b) Penecontemporaneous reworking of deep water sediments suggests continued tectonism in Blow Trough during the early Albian.

(c) Anoxic conditions, as well as upwelling, favoured deposition of the phosphorites in Blow Trough.

(d) The precipitation of phosphate minerals at Cross Cut Creek was controlled by the composition and competence of the host rocks and by early Cenozoic folding.

ACKNOWLEDGEMENTS

This investigation was suggested by I. Jonasson, and carried out jointly with Gary Ansell of the Geological Survey of Canada, Ottawa. Field work for this project was supported by the Exploration and Geological Services Division, Indian and Northern Affairs Canada, in Whitehorse. Field support was provided by L. Lane, Institute for Sedimentary and Petroleum Geology, Calgary.

REFERENCES

ARTHUR, M.A. and JENKYNS, H.C., 1981. Phosphorites and paleooceanography. Oceanologica Acta, 1981; Proceedings of the 26th International Geological Congress, Geology of Oceans Symposium, Paris, July 7 - 17, 1980, p. 83-96.

BERNER, R.A., 1971. Principles of Chemical Sedimentology. McGraw-Hill, 223 p.

CAMPBELL, F.A., 1962. Lazulite from Yukon, Canada. American Mineralogist, Vol.47, p. 157-160.

COLEMAN, L.C. and ROBERTSON, B.T., 1981. Nahpoite, Na_2HPO_4, a new mineral from the Big Fish River area, Yukon Territory. Canadian Mineralogist, Vol. 19, p. 373-376.

COOK, P.J. and McELHINNY, M.W., 1979. A re-evaluation of the spatial and temporal distribution of sedimentary phosphate deposits in the light of plate tectonics. Economic Geology, Vol. 74, p. 315-330.

GULBRANDSEN, R.A., 1969. Physical and chemical factors in the formation of marine apatite. Economic Geology, Vol. 64, p. 365-382.

HAQ, B.U., HARDENBOL, J. and VAIL, P.R., 1987. Chronology of fluctuating sea levels since the Triassic. Science, Vol. 235, p. 1156-1167.

JELETZKY, J.A., 1971. Stratigraphy, facies and paleogeography of Mesozoic rocks of northern and west-central Yukon. In: Report of Activities, 1970, Part A; Geological Survey of Canada Paper 71-1A, p.203-221.

LANE, L.S., 1988. The Rapid Fault Array: a foldbelt in Arctic Yukon. In Current Research, Part D, Geological Survey of Canada, Paper 88-1D, p. 95-98.

MANDARINO, J.A. and STURMAN, B.D., 1976. Kulanite, a new barium iron aluminum phosphate from the Yukon Territory, Canada. Canadian Mineralogist, Vol. 14, p. 127-131.

MANDARINO, J.A., STURMAN, B.D., and CORLETT, M.I., 1977. Penikisite, the magnesium analogue of kulanite, from Yukon Territory. Canadian Mineralogist, Vol. 15, p. 396-398.

MANDARINO, J.A., STURMAN, B.D., and CORLETT, 1978. Satterlyite, a new hydroxyl-bearing ferrous phosphate from the Big Fish River area, Yukon Territory. Canadian Mineralogist, Vol. 16, p. 127-131.

MUTTI, E., and RICCI LUCCHI, F., 1975. Turbidites and facies associations. In: Examples of Turbidite Facies and Facies Associations from Selected Formations of the Northern Appenines. Field Trip Guidebook A-11; International Sedimentological Congress IX, Nice, p. 21-36.

NORRIS, D.K., 1981. Blow River and Davidson Mountains. Geological Survey of Canada, Map 1516A.

NORRIS, D.K., 1983. Geotectonic Correlation Chart 1532A - Operation Porcupine Area.

NORRIS, D.K., and YORATH, C.J., 1981. The North American Plate from the Arctic Archipelago to the Romanzoff Mountains. In: The Ocean Basins and Margins, Vol. 5. The Arctic Ocean, A.E.M Nairn, M. Churkin and G.G. Stehli, (eds); Plenum Press, New York and London, p. 37-103.

PARRISH, J.T., and CURTIS, R.L., 1982. Atmospheric circulation, upwelling, and organic-rich rocks in the Mesozoic and Cenozoic eras. Paleogeography, Paleoclimatology, Paleoecology, Vol. 40, p. 31-66.

ROBERTSON, B.T., 1980. Stratigraphic setting of some new and rare phosphate minerals in the Yukon Territory. Unpublished M.Sc. thesis, University of Saskatchewan, Saskatoon.

ROBERTSON, B.T., 1981. The geology of the Rapid Creek-Big Fish River phosphatic iron formation, northern Richardson Mountains, Yukon. In: Yukon Geology and Exploration 1979-80, Exploration and Geological Services Division, Yukon, Indian and Northern Affairs Canada, p. 115.

ROBERTSON, B.T., 1982. Occurrence of epigenetic phosphate minerals in a phosphatic iron-formation, Yukon Territory. Canadian Mineralogist, Vol. 20, p. 177-187.

STURMAN, B.D., and MANDARINO, J.A., 1976. Baricite, the magnesium analogue of vivianite, from Yukon Territory, Canada. Canadian Mineralogist, Vol. 14, p. 403-406.

STURMAN, B.D., MANDARINO, J.A., and CORLETT, M.I., 1977. Maricite, a sodium iron phosphate from the Big Fish River area, Yukon Territory, Canada. Canadian Mineralogist, Vol. 15, p. 396-398.

STURMAN, B.D., MANDARINO, J.A., ROSE, M.E., and DUNN, P.J., 1981. Gormanite, $Fe^{2+}{}_3Al_4(PO_4)_4(OH)_6{,}2H_2O$, the ferrous analogue of souzalite, and new data for souzalite. Canadian Mineralogist, Vol. 19, p. 381-387.

STURMAN, B.D., PEACOR, D.R., and DUNN, P.J., 1981. Wicksite, a new mineral from northeastern Yukon Territory. Canadian Mineralogist, Vol. 19, p. 377-380.

YOUNG, F.G., 1972. Cretaceous stratigraphy between Blow and Fish Rivers, Yukon Territory. Report of Activities, Part A; Geological Survey of Canada Paper 72-1A, p. 229-235.

YOUNG, F.G., 1973. Mesozoic epicontinental, flyschoid and molassoid depositional phases of Yukon's North Slope. In: Canadian Arctic Geology, J.D. Aitkin and D.J. Glass (eds); Proceedings of the Geological Association of Canada-Canadian Society of Petroleum Geologists Symposium on Geology of the Canadian Arctic, Saskatoon, p. 181-202.

YOUNG, F.G., 1977. The mid-Cretaceous flysch and phosphatic ironstone sequence, northern Richardson Mountains, Yukon Territory. In: Report of Activities, 1977, Part C; Geological Survey of Canada, Paper 77-1C, p. 67-74.

YOUNG. G.G., MYHR, D.W., and YORATH, C.J., 1976. Geology of the Beaufort-Mackenzie Basin. Geological Survey of Canada, Paper 76-11.

ORE MINERALOGY AND FORMATION CONDITIONS OF VEIN AND REPLACEMENT-TYPE PB-ZN-AG-OCCURRENCES, LOGAN AND YP PROPERTIES, RANCHERIA DISTRICT YUKON, CANADA

Albrecht Germann
Gunther Friedrich,
and Robert Schattner

Institute of Mineralogy and Economic Geology
Aachen University of Technology
Wüllnerstr. 2, 5100 Aachen
Aachen, Germany

GERMANN, A., FRIEDRICH, G., and SCHATTNER, R., 1992. Ore mineralogy and formation conditions of vein and replacement-type Pb-Zn-Ag occurrences, Logan and YP properties, Rancheria District, Yukon. In: Yukon Geology, Vol. 3; Exploration and Geological Services Division, Yukon, Indian and Northern Affairs Canada, p.37-44

ABSTRACT

The Logan (MINFILE 105B 099) and YP (MINFILE 105B 001) zinc-lead-silver deposits are located in the Rancheria District, Yukon Territory. These deposits and numerous other occurrences occur in veins and breccia zones which cut clastic sedimentary rocks of Proterozoic and Palaeozoic age, along fracture zones cross-cutting Cretaceous granites and Eocene volcanic dykes of mafic and felsic composition, and form replacement bodies in Palaeozoic carbonates. At the Logan and YP deposits, four phases of mineralization can be distinguished. The main sulphide minerals are sphalerite, galena, pyrrhotite, pyrite, chalcopyrite and arsenopyrite. Silver is mostly confined to galena, but also occurs in tennantite-freibergite group minerals, stannite, Pb-Ag-Bi-sulphosalts of the matildite-galena series and lillianite homologues.

Arsenopyrite geothermometry using the method of Kretschmar and Scott (1976) returned maximum formation temperatures of 465° - 490°C at YP and 335° - 385°C at Logan. Microthermometric investigations of fluid inclusions in quartz associated with the YP mineralization showed formation pressures corresponding to a depth of 2500 m.

Fluid inclusion data from quartz suggest that mineralization at YP and Logan is caused by a mixture of magmatic and metamorphic fluids. The fluid inclusions have low salinities of 3-4 weight per cent NaCl equivalent, an unusually low value for fluids which have separated from acid magmas. The metamorphic fluids may have been derived from metamorphic dewatering of Palaeozoic sediments.

RÉSUMÉ

Les gisements Logan et YP de plomb, zinc et argent sont situés dans le district de Rancheria (territoire du Yukon). Ces gisements et de nombreux autres indices minéralisés prennent la forme de zones de veines et de brèche recoupant des roches sédimentaires clastiques du Protérozoïque et du Paléozoïque le long de zones de fractures recoupant des granites du Crétacé et des dykes mafiques et felsiques de l'Éocène, et forment des masses de remplacement dans des carbonates paléozoïques. Aux gisements Logan et YP, quatre phases de minéralisation peuvent être distinguées. Les principaux minéraux sulfurés sont la sphalérite, la galène, la pyrrhotine, la pyrite, la chalcopyrite et l'arsénopyrite. L'argent n'est pas confiné à la galène, mais est également présent dans les minéraux du groupe tennantite-freibergite, dans la stannite, dans les sulfosels de Pb-Ag-Bi de la série matildite-galène et dans les homologues de la lillianite.

l'étude géothermométrique de l'arsénopyrite par la méthode de Kretschmar et Scott (1976) a indiqué des températures maximales de formation comprises entre 465 et 490 °C au YP et entre 335 et 385 °C au Logan. Les études microthermométriques des inclusions fluides dans le quartz associé à la minéralisation YP ont indiqué des pressions de formation correspondant à une profondeur de 2500 m.

Les données sur les inclusions fluides dans le quartz suggèrent qu'aux gisements YP et Logan la minéralisation a été causée par un mélange de fluides magmatiques et métamorphiques. Les inclusions fluides présentent de faibles salinités de 3 à 4 pourcent d'équivalent de NaCl en poids, des valeurs inhabituellement faibles pour des fluides s'étant séparés de magmas acides. Les fluides métamorphiques peuvent avoir été dérivés de l'assèchement métamorphique des sédiments paléozoïques.

INTRODUCTION

This work follows several studies initiated by Indian and Northern Affairs Canada in the Rancheria area (e.g., Abbott, 1984; Amukun & Lowey, 1987; Lowey & Lowey, 1986). The present study focuses on the mineralogy of the Logan (105B 099) and YP (105B 001) lead-zinc-silver occurrences, and its genetic implications.

GEOLOGICAL SETTING

The Cassiar Platform and the Slide Mountain Terrane are the two main tectonic units in the Rancheria District (Tempelman-Kluit, 1979, 1981; Wheeler, 1987; Fig. 1). The Logan and YP occurrences occur within the Cassiar Platform, which includes slightly metamorphosed and folded Proterozoic and Palaeozoic siliciclastic and carbonate rocks. The sedimentary rocks which host the Pb-Zn-Ag mineralization belong to the Atan Group, deposited during the Cambrian in a continental margin setting (Tempelman-Kluit, 1979). The lower part of the Atan Group consists of quartzite, sandstone and phyllite (Boya Formation), and the upper part consists of massive marble (Rosella Formation; Fritz, 1980). During the Late Jurassic and Early Cretaceous, the Slide Mountain and other terranes, representing ancient island arcs, back-arcs and fore-arcs, drifted against the North American continent from the west, and were obducted over the autochthonous strata of the continental margin.

The subduction and obduction processes resulted in partial melting and the emplacement of widespread granitic and granodioritic plutons. The Cassiar and Marker Lake Batholiths are the most important of these in the study area (Fig. 1).

Continued transpressive subduction caused major northwest-southeast trending dextral strike-slip faults during the late Cretaceous and early Tertiary and led to the development of an east-west joint system (Lowey & Lowey, 1986; Abbott, 1984). Mafic and felsic dykes which intrude Cretaceous plutonic rocks or Proterozoic and Palaeozoic sedimentary rocks are probably related to strike-slip faulting and jointing.

Lowey & Lowey (1986) and Abbott (1984) suggested that the Pb-Zn-Ag mineralization is genetically related to fluorite-bearing felsic porphyry dykes. Sinclair (1987) distinguished two types of porphyries. Type I porphyries are characterized by varying amounts of fluorite and sericite while type II porphyries contain up to 5 vol. % of primary topaz and tourmaline. The chemical composition of these intrusive rocks resembles that of A-type granites which are the product of final magmatism in orogenic belts or of magmatism at rift zones within shield areas (Pitcher, 1982). Abbott (1984) and Sinclair (1987) considered the Tertiary volcanism to be genetically related to deep-reaching Cretaceous and Tertiary shift faults. Quaternary basalts of the Rancheria Valley are younger than the mineralization.

LOGAN PROPERTY (MINFILE 105B 099)

The Logan deposits occur in a fault zone which strike about 060° and dips about 70° NW. Mineralization occurs as massive veins up to several metres thick, as impregnations in tectonic breccias, and as stockworks in highly brecciated zones. Four phases of mineralization have been identified:

Phase I minerals include sphalerite 1, pyrrhotite and arsenopyrite 1 (Figs 2 & 3). The sphalerite 1 contains traces of Sn.

Phase II is characterized by Cu-bearing minerals such as chalcopyrite, stannite, fahlore (tetrahedrite) and galena, Pb-Ag-Bi-sulphosalts and pyrrhotite. Chalcopyrite occurs along fractures in phase I minerals and as minute inclusions in sphalerite 1 ("chalcopyrite disease" after Barton, 1978), which are most abundant near chalcopyrite veinlets.

Phase II galena is significantly enriched in silver and bismuth (up to 4.25 wt. % Ag and 9.18 wt. % Bi); mean values are 1.3 wt. % Ag and 2.74 wt. % Bi. Pb-Ag-Bi-sulphosalts of the matildite-galena solid solution series or lillianite homologues (Fig. 4) occur as exsolutions in galena. They are also found along cracks in other minerals, especially sphalerite (Fig. 5), or along grain boundaries (Fig. 6). Sulphosalt minerals contain up to 9 wt % Ag and are therefore important Ag carriers at Logan. Stannite (0.7 wt. % Ag), chalcopyrite (0.15 wt. % Ag) and minor fahlore of the freibergite-tennantite solid solution series also contain elevated levels of silver. Stannite occurs mainly along cracks within sphalerite 1 (Fig. 5).

Phase III is characterized by Sb-bearing minerals such as jamesonite and galena with maximum Sb-values of 0.8 %. Galena of phase III has average Sb/Bi ratios of 0.235, compared to galena of phase II which has a Sb/Bi ratio of 0.0056. Minor emplectite ($CuBiS_2$) and sulphosalts are the Bi-bearing minerals. Cubanite exsolved from chalcopyrite during cooling, in the form of lamellae or as xenomorphic crystals. Phase III also saw the continued formation of stannite and fahlore and the onset of precipitation of iron-poor sphalerite, marcasite, second generation pyrite and arsenopyrite.

Phase IV probably reflects mobilization and cataclasis of pre-existing minerals. Pyrrhotite has been altered to pyrite and marcasite as described by Ramdohr (1975) in other localities. Galena formed during phase IV is poor in silver and bismuth, and sphalerite is Fe-poor. Arsenopyrite 2 occurs as idiomorphic crystals which replace the earlier formed ore minerals. Siderite is restricted to phase IV mineralization and occurs mainly near mafic dykes. Minor amounts of chalcocite also formed during phase IV. Chalcocite, limonite, bornite, digenite and covellite are primarily supergene products.

The Logan deposit shows a distinct vertical mineral zonation. In the upper mineralized levels, pyrite 1 occurs instead of pyrrhotite. Chalcopyrite and arsenopyrite increase with depth. These changes reflect a downward increase in the temperature of mineralization.

Amukun & Lowey (1987) mentioned the occurrence of colourless cassiterite in a brecciated felsic dyke. This mineral was not found during our present study.

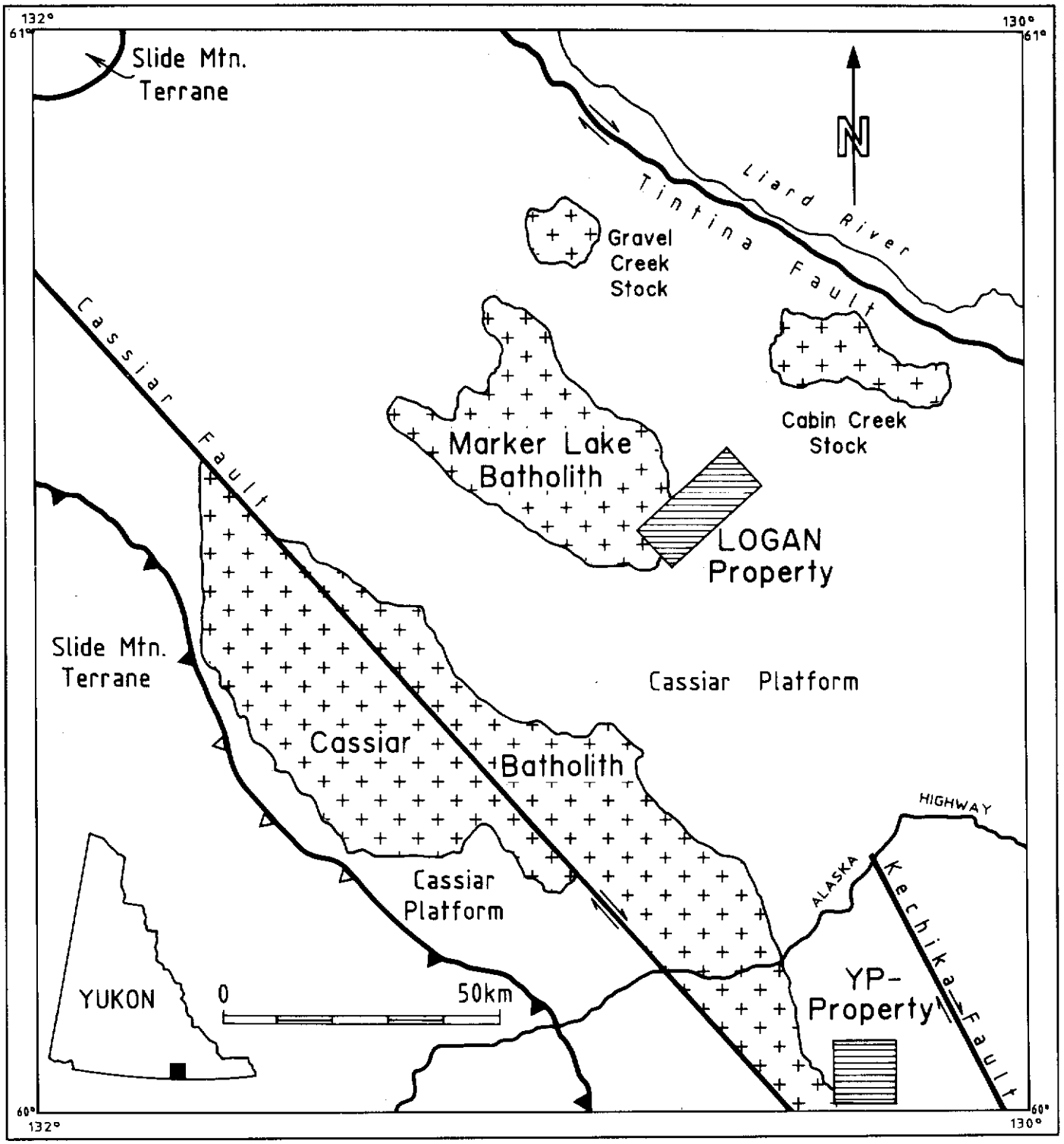

Figure 1. Rancheria District: Location of Logan and YP areas and reconnaissance geology (after Wheeler, 1987).

YP (LORD) PROPERTY (MINFILE 105B 001)

On the YP property, veins, breccia zones and replacement bodies in limestone are associated with a north-trending zone of steeply dipping quartz-feldspar-porphyries dated at 52 ± 3 Ma (Abbott, 1984; Sinclair, 1987). Mineralization at YP also consists of four phases:

Phase I is dominated by sphalerite 1 (Fig. 7), arsenopyrite 1 and pyrrhotite. Pyrite 1 is restricted to the upper levels, pyrrhotite to the lower levels.

Phase II is characterized by an increase of copper causing the already described "chalcopyrite disease" (Barton, 1978)

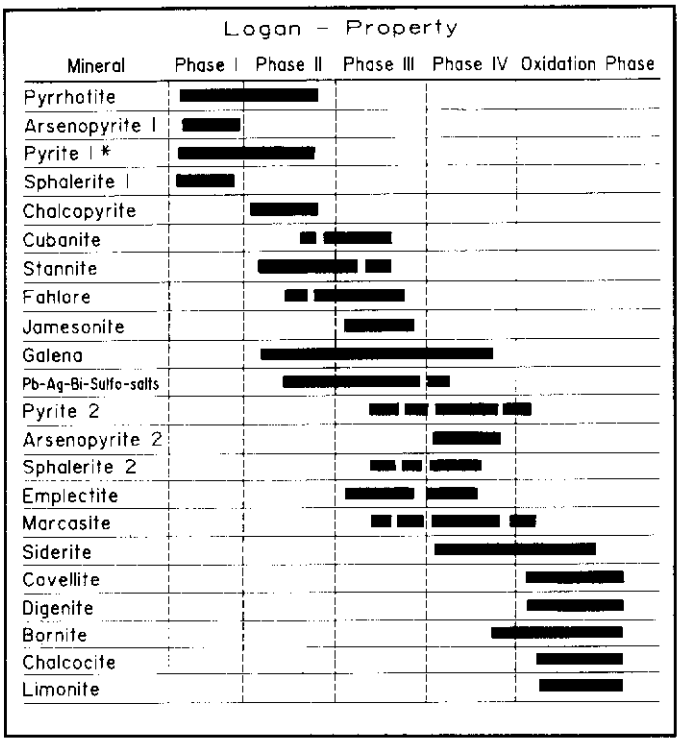

Figure 2. Diagram showing precipitation sequence of ore-minerals at Logan; (* pyrite occurs instead of pyrrhotite in the upper levels).

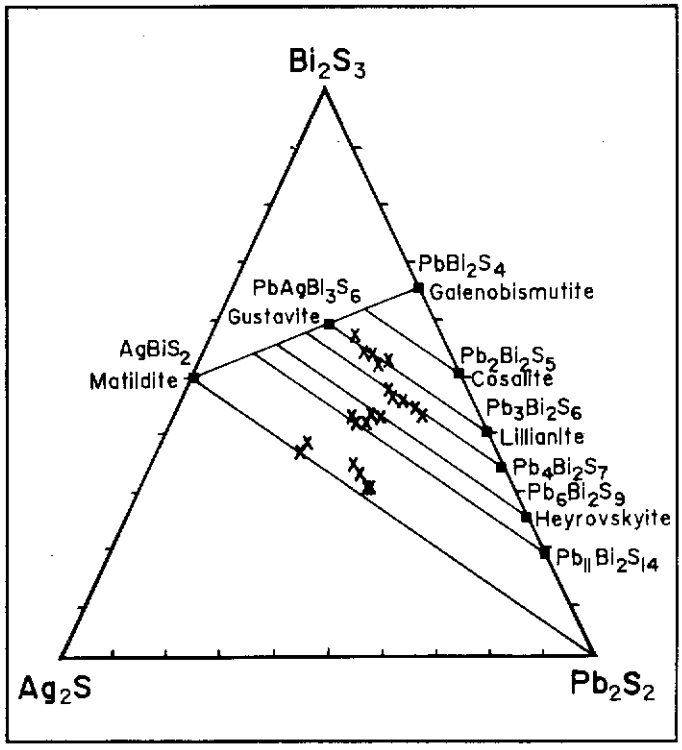

Figure 4. Position of the Logan area sulphosalts of Logan in the system Ag_2S-Bi_2S_3-Pb_2S_2 (Craig, 1967).

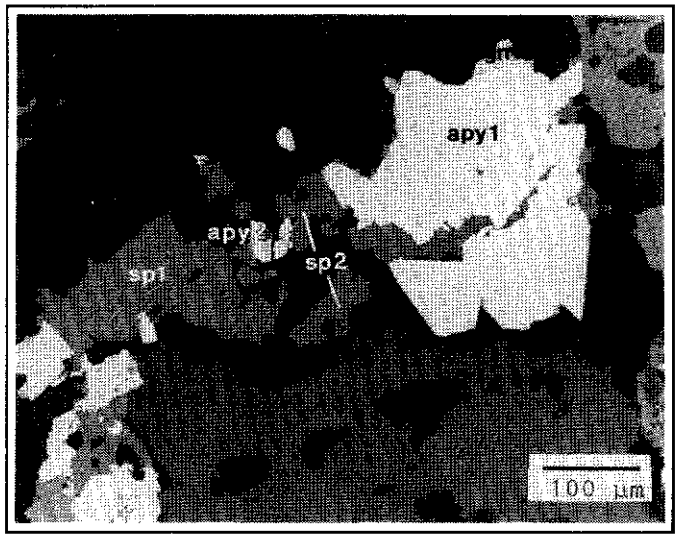

Figure 3. Intergrowth of sphalerite 1 (spl, with chalcopyrite disease) arsenopyrite 1 (apy1) and galena (gn); sphalerite 2 (sp2) as fissure filling in arsenopyrite 1 (apy1) is partly replaced by arsenopyrite 2 (apy2); (plane polarized light).

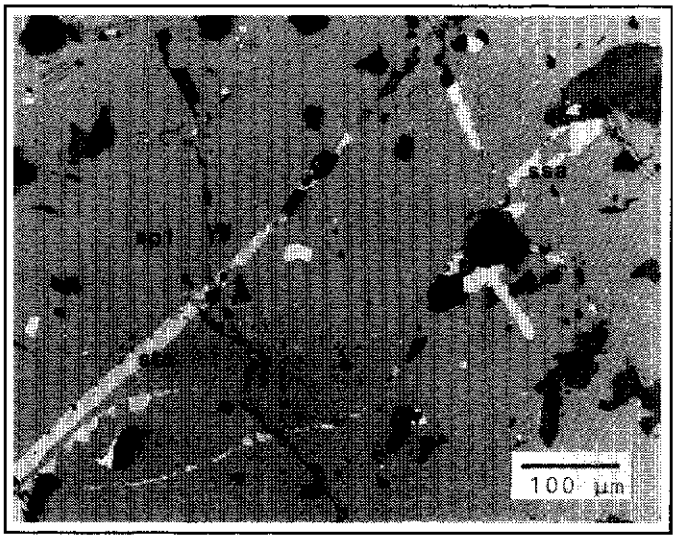

Figure 5. Stannite (sta) and sulphosalts (ssa) as fissure fillings in sphalerite 1; (x nicols).

which grades in the upper levels of the mineralization into a "pyrrhotite disease". Its intensity increases in the vicinity of pyrrhotite veinlets, indicating formation by replacement. Larger chalcopyrite grains of phase 2 contain small star-shaped sphalerite exsolutions (Fig. 8). Stannite, galena, fahlore of the freibergite-tennantite solid solution series, bismuthinite and native bismuth also crystallized during phase II. Sulphosalts of the matildite-galena solid solution series or lillianite homologues frequently observed in the Logan deposit, were not identified. Silver values in galena of the YP

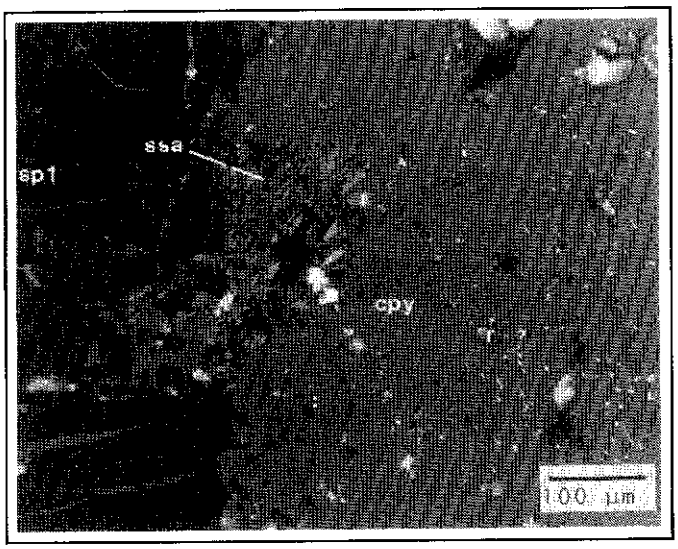

Figure 6. Sulphosalts (ssa) replacing chalcopyrite (cpy) on cracks in sphalerite 1 (sp1) (x nicols).

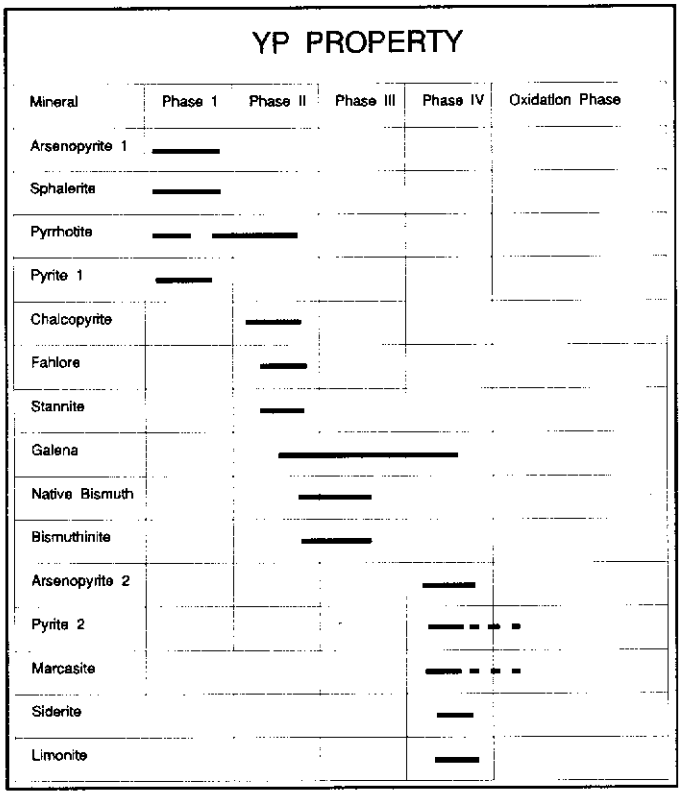

Figure 7. Diagram showing precipitation sequence of ore-minerals in YP; (* pyrite occurs instead of pyrrhotite in the upper levels).

occurrence reach a maximum of 2.8 weight per cent Ag, which is lower than at Logan. The highest Bi content is 15.84 weight per cent. A characteristic feature of phase II mineralization in the YP deposit is the presence of native Bi at grain boundaries or as inclusions in other ore minerals, preferentially in galena and chalcopyrite (Fig. 8).

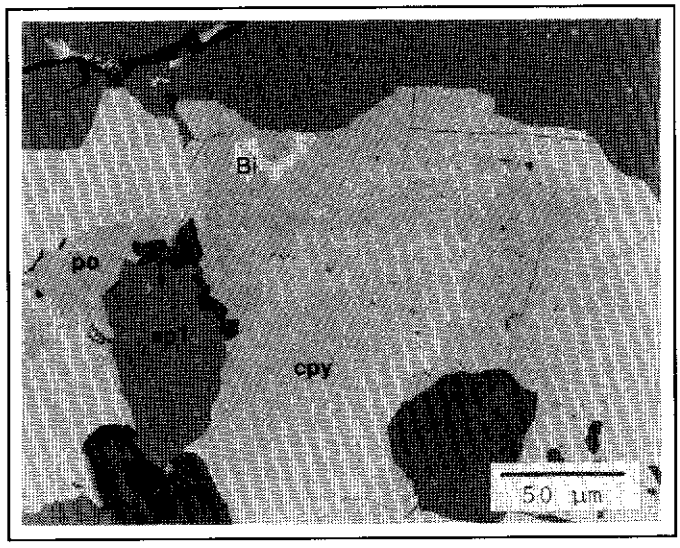

Figure 8. Galena (gn) with inclusions of native bismuth (Bi) intergrown with chalcopyrite (cpy, with star-shaped sphalerite), pyrrhotite (po) and sphalerite 1 (sp1), (plane polarized light).

During Phase III the precipitation of galena and native Bi continued. The existence of different generations of galena is indicated by differing Sb/Bi ratios in galena. While galena crystals of Phase II have Sb/Bi ratios near 0.004, galena of Phase III has ratios of 0.41.

As at Logan, Phase IV resulted from mobilization of pre-existing minerals. Idiomorphic arsenopyrite 2, pyrite 2, marcasite, galena and siderite belong to this phase. Marcasite and pyrite form the fine-grained alteration products of pyrrhotite ("intermediate product" after Ramdohr, 1975), and also occur as larger crystals along fissures. Idiomorphic pyrite 2 sometimes replaces the "intermediate product", and is thus the youngest sulphide mineral.

Limonite was the only weathering product observed. Furneaux & White (1983) reported gold concentrations up to 15.26 ppm in drill core. Native gold and gold-bearing minerals were not found in the present study. Microprobe data obtained from arsenopyrite, pyrrhotite and pyrite were below the detection limit of 0.1-0.15 weight per cent Au. The distribution of gold is assumed to be very erratic.

TEMPERATURE AND PRESSURE CONDITIONS DURING MINERALIZATION AT LOGAN AND YP

Temperature determinations using the arsenopyrite geothermometer (after Kretschmar & Scott (1976)) indicate that formation temperatures at YP differ from those at Logan. At Logan, Phase 1 mineralization formed at temperatures between 385°C and 435°C; at YP, between 465°C and 490°C (Fig. 9). The high temperatures of hydrothermal mineralization at YP reflect the presence of the quartz-feldspar porphyry nearby.

The chalcopyrite disease of sphalerite 1, typical of phase II mineralization at Logan and YP, forms at temperatures of

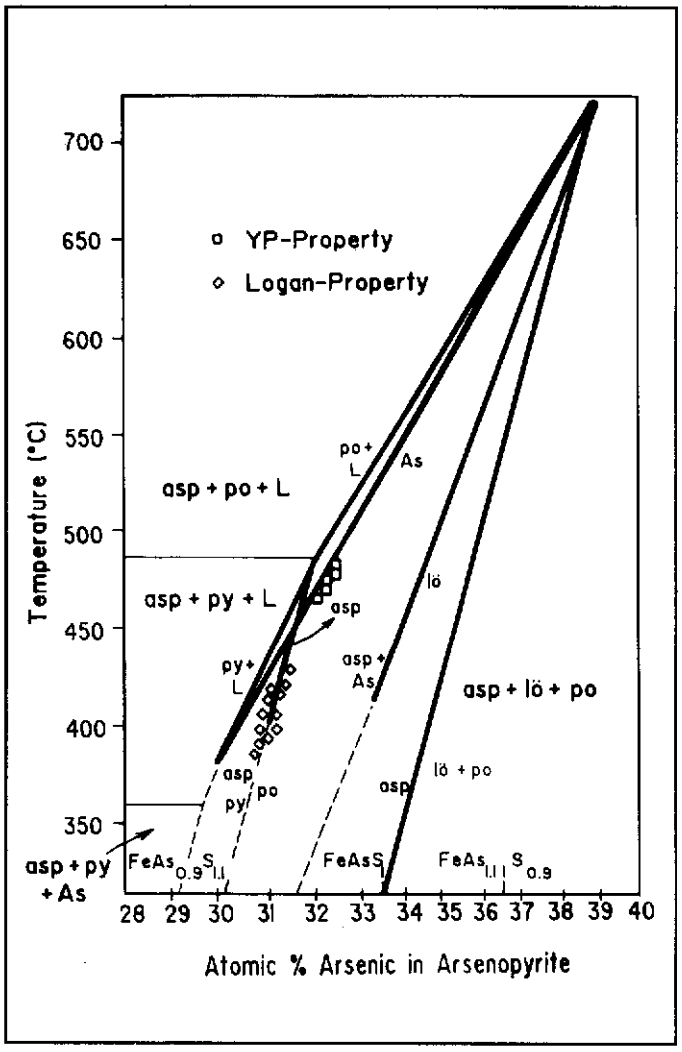

Figure 9. Formation temperature of arsenopyrite 1 from Logan and YP properties, using the arsenopyrite thermometer (after Kretschmar and Scott (1976)).

200° - 400°C (Barton, 1987). The star-shaped sphalerite crystals in chalcopyrite, which have been observed only in samples from the YP deposit, indicate that the chalcopyrite formed at temperatures higher than 400°C (Sugaki, 1985). Chalcopyrite can exsolve such a considerable amount of Zn only at these temperatures. Therefore temperatures in YP appear to have been higher than 400°C during Phase II. Formation temperatures during phase II, obtained from microthermometric investigations of fluid inclusions in quartz, were also higher than 400°C.

Solid solution in the system PbS-$AgBiS_2$ is complete at temperatures above 215°C (Van Hook, 1960; Craig, 1967). The common association of matildite and galena, which is also present at Logan and YP, is believed to represent exsolution at a solvus with a crest of 215±15°C (Craig, 1967). According to Malakhov (1969) the ratio Sb/Bi based on the weight per cent of both elements in galena principally reflects the temperature of crystallization of the galena. Very low ratios of less than 0.6 Sb/Bi are characteristic of high temperature galena which formed at 200° - 300°C. At Logan the Sb/Bi ratios of Phase II galena are around 0.0056, while at YP they are around 0.0042, indicating that in both study areas, the lower temperature limit of Phase II was between 200° and 215°C.

The Sb/Bi ratio in galena of Phase III and IV indicates a formation temperature between 140° and 220°C (Malakhov, 1969). At Logan, cubanite was found in one Phase III sample. According to Borchert (1938) chalcopyrite exsolves cubanite at temperatures between 250° and 300°. This indicates an upper temperature limit of about 250°C for Phase III mineralization.

Fluid inclusion data from quartz at YP indicate mineral precipitation at pressures of 800 to 1000 bar. This corresponds to a depth of about 2500 m. According to Malakhov (1969) the bismuth content of galena increases with depth. Galena from Logan generally has a lower Bi content than galena from YP, indicating that mineralization at Logan precipitated at a shallower level and/or at lower temperatures.

DISCUSSION AND CONCLUSIONS

The high formation temperatures of the YP and Logan Pb-Zn-Ag occurrences and cataclastic deformation of the ore minerals suggest a close relationship to faulting and magmatism. Tectonic movements opened percolation pathways for hydrothermal fluids. Fractures, joint systems and breccia zones controlled the distribution of the different occurrences, and the size and shape of each deposit depends largely on the composition of the surrounding rocks. At Logan the host rock consists of granite, which deformed in a brittle manner, resulting in the opening of wide vein or breccia structures favorable for ore precipitation. In incompetent phyllite or schist, plastic deformation dominates and fracture zones are too small to contain larger ore bodies of economic value. Fracture-controlled dykes can sometimes act as barriers for the hydrothermal solutions, leading to major ore accumulations adjacent to the dykes.

At the YP deposit, the surrounding rock includes different types of carbonates, which were replaced by acid hydrothermal solutions thus forming sulphide accumulations.

At both YP and Logan, four separate phases of mineralization can be distinguished. The first consists of sphalerite, arsenopyrite and Fe-sulfides, the second of chalcopyrite, fahlore, stannite, galena and Pb-Ag-Bi-sulphosalts, the third includes different Bi-bearing minerals and galena and the fourth includes siderite, galena and other sulfides which formed by remobilization of earlier-formed minerals.

The chalcopyrite disease of sphalerite is common in both deposits. Between 200° and 400°C, iron in sphalerite reacts with the copper ions of percolating hydrothermal fluids and forms chalcopyrite which replaces sphalerite in form of minute inclusions. During this process the iron content in sphalerite decreases. In areas of less intense chalcopyrite disease as at

YP, the iron content of sphalerite may reach 17 weight per cent. At Logan where sphalerite 1 is frequently replaced by chalcopyrite, the iron content of the sphalerite decreases to 5 weight per cent. The fact that the chalcopyrite disease is most intense in the vicinity of chalcopyrite veinlets, indicates it is formed by replacement and not by exsolution.

The antimony content of sulphides from Logan and YP is very low, while bismuth is a major constituent especially in galena and sulphosalts. According to Malakhov (1968), elevated bismuth values in galena are typical of deposits which formed at high temperatures.

Pure galena can contain a maximum of 0.6 mole % Ag_2S at 600°C (Van Hook, 1960). At room temperature the solubility of silver in galena is almost negligible. Nevertheless the Ag-solubility in galena can be strongly increased by the presence of bismuth and/or antimony (Van Hook, 1960; Hoda & Chang, 1975; Amcoff, 1976). According to Van Hook (1960) solubility in the system PbS-$AgBiS_2$ is complete above 215°C. Even at room temperature it is about 8 mole %. The reason for the good solubility of $AgBiS_2$ in PbS is the easily performed six-fold co-ordination of bismuth (Povarennykh, 1971). With decreasing temperature, sulphosalts of the system Ag-Pb-Bi-(Cu)-S can exsolve from galena. This has been observed in galena from the Logan property. At YP where the Ag-content is generally lower, silver appears to be completely dissolved in galena together with bismuth, yielding no sulphosalts on cooling. Excess bismuth has been exsolved as native bismuth.

While the precipitation sequence of the ore minerals and the formation temperature has been determined, the origin of the metals is still uncertain. Sinclair (1987) proposed that the mafic dykes and fluorite and topaz-bearing quartz-feldspar-porphyries which are contemporaneous with the mineralization at YP are evidence of a magmatic origin. As already mentioned, cassiterite was found in a brecciated felsite dyke on the Logan property. Nevertheless no fluorite has been found in the gangue of the mineral deposits, and low-salinity fluids occur as inclusions in quartz which is cogenetic with the sulphides. These fluid inclusions are not consistent with a magmatic origin. The increased heat flow related to the intrusion of the dykes may have formed major convective systems extending outward into the Palaeozoic sedimentary rocks, which include black shales rich in sulfides. The extent to which these rocks are involved in mobilization and ore formation is still an open problem. Sulphur isotopic analysis is expected provide further evidence about the mineralization process.

The Rancheria area deposits show significantly higher formation temperatures than those at Keno Hill, 354 km north of Whitehorse, where structurally and mineralogically similar Pb-Zn-Ag occurrences occur (Keno Hill: 250° - 310°C, Lynch, 1989; Logan: 385°-435°C; YP: 465°-490°C). This higher formation temperature led to higher bismuth and lower antimony contents in the Rancheria occurrences. Distinct lateral zonation, which is typical of the Keno Hill area, was not observed at Rancheria. On the other hand vertical zoning, less developed at Keno Hill, is typical for YP and Logan.

ACKNOWLEDGEMENTS

The mineralogical studies of selected Ag-Zn-Pb deposits of the Rancheria District were carried out under the Canada/Germany Science and Technology Exchange Agreement, which was organized by the Geological Survey of Canada (GSC) and the Federal Institute for Geosciences and Mineral Resources (BGR). Thanks are due to the German Ministry of Research and Technology for financial support and to the German Research Foundation (DFG) for sponsoring our research projects in the Yukon. We also wish to thank the Department of Indian and Northern Affairs, Whitehorse, Yukon for scientific help and logistic assistance, and Cordilleran Engineering who provided ore-samples from the Logan occurrence and gave the permission to visit their prospects. Many thanks are due to M. Stammers for his hospitality and for sharing much information about the geology and mineralization during our stay on the Logan property. Finally we gratefully acknowledge very valuable discussions of D. Sinclair (GSC) and P. Herzig (RWTH Aachen).

REFERENCES

ABBOTT, G., 1984. Silver bearing veins and replacement deposits of the Rancheria District. In: Yukon Exploration and Geology 1983; Exploration and Geological Services Division, Yukon, Indian and Northern Affairs Canada, p. 34-41.

AMCOFF, O., 1976. The solubility of silver and antimony in galena. Neues Jahrbuch fur Mineralogie, Monatshefte, p. 247-261.

AMUKUN, S.E. and LOWEY, G.W., 1987. Geology of the Sab Lake (105 B 7) and Meister Lake (105 B 8) map-areas, Rancheria District, southeast Yukon, Canada. Exploration and Geological Services Division, Yukon, Indian and Northern Affairs Canada, Open File Report 1987-1.

BARTON, P.B., 1987. Some ore textures involving sphalerite from the Furutobe mine, Akita Prefecture, Japan. Mining Geology, Vol. 28, p. 293-300.

BORCHERT, H., 1934. Uber Entmischungen im System Cu-Fe-S und ihre Bedeutung als geologisches Thermometer. Chemie der Erde, Vol. 9, p. 145-172.

CRAIG, J.R., 1967. Phase relations and mineral assemblages in the Ag-Bi-Pb-S system. Mineralium Deposita, Vol. 1, p. 278-306.

FURNEAUX, B. and WHITE G.E., 1983. Assessment Report 091501. Unpublished assessment report on YP claims for Butler Mountain Minerals Corp. (data published in LOWEY & LOWEY, 1986).

FRITZ, W.H., 1980. Two new formations in the Lower Cambrian Atan Group, Cassiar Mountains, north-central British Columbia. In: Current Research, Part B; Geological Survey of Canada, Paper 80-1B, p. 217-225.

HODA, S.N. and CHANG, L.L.Y., 1975. Phase relations in the systems PbS-Ag_2S-Sb_2S_3 and PbS-Ag_2S-Bi_2S_3. American Mineralogist, Vol. 60, p. 621-633.

KLEPACKI, D.W., 1983. Stratigraphic and structural relations of the Milford, Kaslo and Slocan Groups, Goat Range, Lardeau and Nelson map-areas, British Columbia. In: Current Research, Part A, Geological Survey of Canada, Paper 83-1A, p. 229-233.

KRETSCHMAR, U. and SCOTT, S.D., 1976. Phase relations involving arsenopyrite in the system Fe-As-S and their application. Canadian Mineralogist, Vol. 14, p. 364-386.

LOWEY, G.W. and LOWEY, J.F., 1986. Geology of Spencer Creek (105 B 1) and Daughney Lake (105 B 2) map areas, Rancheria District, southeast Yukon, Canada. Exploration and Geological Services Division, Yukon, Indian and Northern Affairs Canada, Open File Report 1986-1, 110 p.

LYNCH, J.V.G., 1989. Large scale hydrothermal zoning reflected in the tetrahedrite-freibergite solid solution, Keno Hill Ag-Pb-Zn District, Yukon. Canadian Mineralogist, Vol. 27, p. 383-400.

MALAKHOV, A.A., 1968. Bismuth and antimony in galenas as indicators of some conditions of ore formation. Geochemistry International, Vol. 5, p. 1055-1068.

NEDACHI, M., TAKEUCHI, T., YAMAOKA, K. and TANIGUCHI, M., 1973. Bi-Ag-Pb-S minerals from Agenosawa mine, Akita Prefecture, northeastern Japan. Tohoku University, Scientific Reports, Third Series, Vol. 12/I, p. 69-80.

PITCHER, W.S., 1982. Granite type and tectonic environment. In: Hsu, K.J., Mountain Building Processes; London, New York, Academic press.

POVARENNYKH, A.A., 1971. Crystallography of complex sulfides of arsenic, antimony and bismuth. Society of Mining Geologists of Japan, Special Issue, Vol. 2, p. 42-46.

RAMDOHR, P., 1975. Die Erzmineralien und ihre Verwachsungen. Akademie Verlag, Berlin, 1277 p.

SINCLAIR, W.D., 1987. A compilation of K-Ar-ages. In: Radiogenic age and Isotopic Studies, Hunt, P.A. and Roddick, J.C., 1987,(eds); Geological Survey of Canada, Paper 87-2, p. 185.

SUGAKI, A., KITAKAZE, A.and KOJIMA, S., 1987. Bulk compositions of intimate intergrowths of chalcopyrite and sphalerite and their genetic implications. Mineralium Deposita, Vol. 22, p. 26-32.

TEMPELMAN-KLUIT, D.J., 1979. Transported cataclasite, ophiolite and granodiorite in Yukon: evidence of arc-continent collision. Geological Survey of Canada, Paper 79-14, 27 p.

TEMPELMAN-KLUIT, D.J., 1981. Geology and mineral deposits of southern Yukon. In: Yukon Geology and Exploration, 1979-1980; Exploration and Geological Services Division, Yukon, Indian and Northern Affairs Canada, p. 7-31.

VAN HOOK, H.J., 1960. The ternary system Ag_2S-Bi_2S_3-PbS. Economic Geology, Vol. 55, p. 759-788.

WHEELER, J.O., 1987. Tectonic assemblage map of the Canadian Cordillera and adjacent parts of the USA. Geological Survey of Canada, Open File 1565.

TRACE AMMONIUM IN GRANITES OF THE SOUTHERN YUKON AND ITS PETROGENETIC SIGNIFICANCE

A. Hall and T. Liverton
Department of Geology,
Royal Holloway and Bedford New College,
University of London,
Egham, Surrey, U.K.
TW20 0EX

HALL, A. and LIVERTON, T., 1992. Trace ammonium in granites of the southern Yukon and its petrogenetic significance. In: Yukon Geology; Vol. 3, Exploration and Geological Services Division, Yukon, Indian and Northern Affairs Canada, p. 45-51

ABSTRACT

This reconnaissance study compares the ammonium content of some granites from the southern Yukon with granites in other regions. Analyses show a slight variation in ammonium content between individual intrusions, but there appears to be no correlation between NH_4 content and granite type.

All analysed specimens showed low ammonium contents when compared with granites from other regions. This ammonium deficiency in the original magma is taken as evidence that magma was uncontaminated by sedimentary wall rocks at the level of emplacement.

RÉSUMÉ

Dans cette étude de reconnaissance la teneur en ammonium de certains granites du Yukon méridional est comparée à celle de granites d'autres régions. Les analyses montrent une légère variation de la teneur en ammonium entre diverses intrusions individuelles, mais il ne semble exister aucune corrélation entre la teneur en NH_4 et le type de granite.

Tous les échantillons analysés présentaient de faibles teneurs en ammonium comparativement à celles de granites provenant d'autres régions. Cet appauvrissement en ammonium du magma original indique que le magma n'était pas contaminé par des roches sédimentaires encaissantes au niveau de l'emplacement.

INTRODUCTION

The ammonium ion occurs as a trace constituent of many rocks and minerals. In fresh granites it occurs as a constituent of feldspars and micas, in isomorphous substitution for potassium. In weathered or hydrothermally altered granites, it may also be present in secondary phyllosilicate alteration products.

The ultimate source of primary ammonium is believed to be the nitrogenous organic matter originally present in sediments. Nitrogen from this source can be retained throughout diagenesis and metamorphism, and can be incorporated in granitic magma by anatexis or assimilation. The possibility therefore exists that nitrogen (i.e. the ammonium ion) in granites could be useful as a tracer to indicate the degree of sedimentary involvement in granite petrogenesis. The evidence on this point has up to now been rather equivocal. Hall (1987) found that in the Caledonian granites of the northern British Isles there is no correlation between NH_4 contents and the $^{87}Sr/^{86}Sr$ initial ratios of different intrusions. In contrast, the Variscan granites of southern Britain show quite a good correlation between NH_4 content, initial $^{87}Sr/^{86}Sr$ ratio and the peraluminosity of the granites in different intrusions (Hall, 1988). Analytical data are available for only a few other granites, mostly in Europe and Japan, and wide variations in ammonium content have been found, from zero to more than 100 parts per million. This study was therefore carried out to see what level of ammonium was present in the granites of an area in northwest Canada, and whether the NH_4 contents in that area showed any significant variation.

The plutons examined for this reconnaissance study are currently receiving attention as part of a study of tin/tungsten skarn-type mineralization in the Thirtymile Range (Liverton, work in progress). Figure 1 shows the various bodies and sample locations. Table 2 gives the precise location of the samples in UTM 1000-metre grid coordinates.

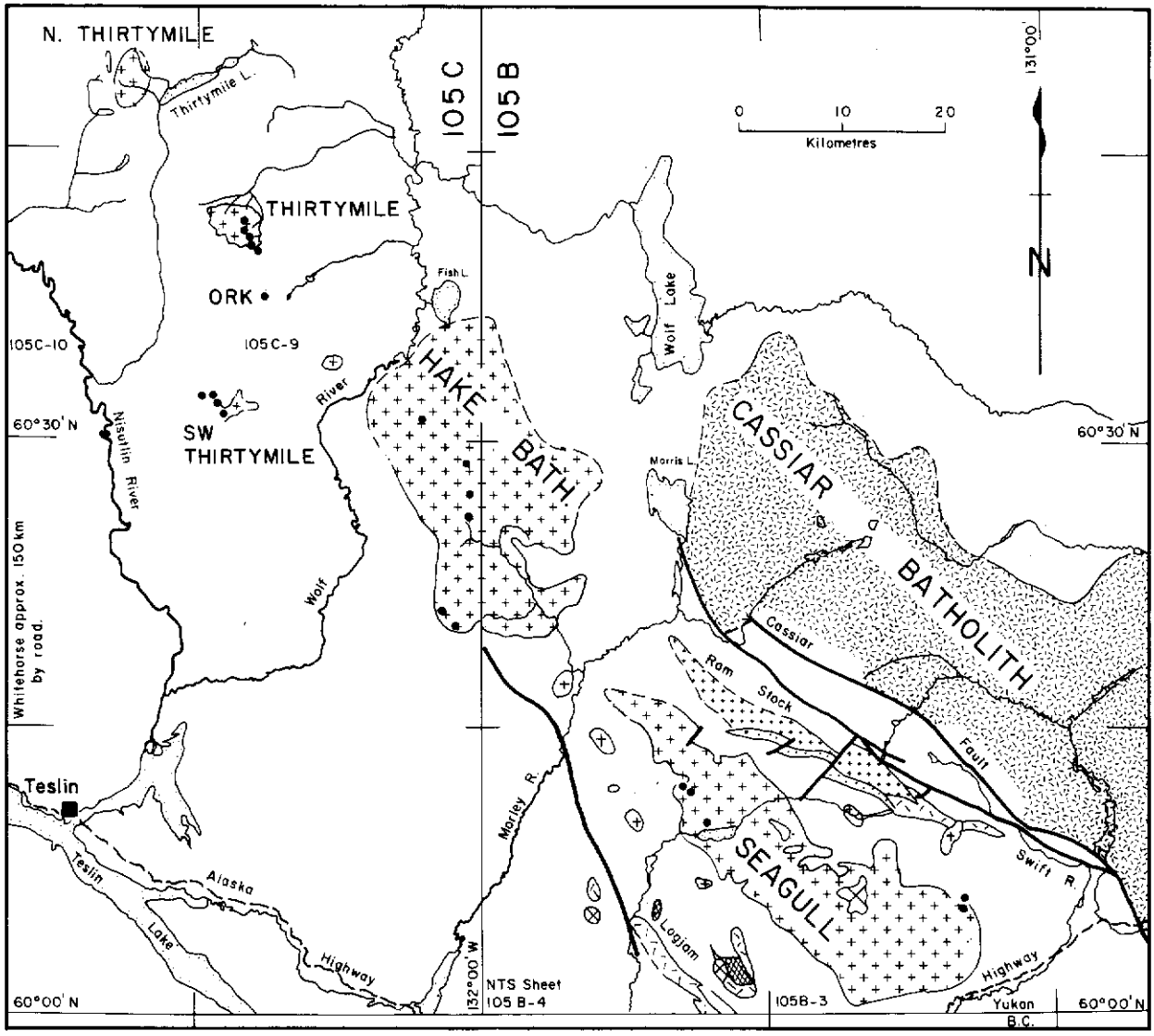

LEGEND

CRETACEOUS

- Cassiar Batholith: Quartz monzonite
- Seagull & Hake batholiths, Thirtymile and Ork stocks: granite.
- Southwest & Northwest Thirtymile stocks: gabbro to hornblende granodiorite

JURASSIC

- Diorite
- Quartz monzonite
- Gabbro & ultrabasics

PALAEOZOIC to MESOZOIC

- Foliated diorite to granodiorite
- Quartz monzonite and granodiorite

Geology after Poole, Roddick & Green (1960), Mulligan (1963) & Abbott (1981)

Sample localities are shown as dots & faults as heavy lines.

THE SEAGULL - THIRTYMILE PLUTONIC SUITE, CASSIAR BATHOLITH & DIORITES.

Figure 1.

THE INTRUSIONS STUDIED: SUMMARY OF MINERALOGY AND GEOCHEMISTRY

The Seagull and Hake batholiths are NW-SE elongated plutons with an outcrop length of 85 km. The Thirtymile and Southwest Thirtymile stocks are intrusions of under 8 km length, which outcrop 20 km further to the NW. These plutons intrude a tectonically imbricated, mainly siliciclastic platformal sequence of Middle Paleozoic age. These sedimentary rocks form part of the Yukon Cataclastic Complex, which represents the western edge of the Omineca Belt in the Northern Cordillera. Metamorphic rocks of the Teslin suture zone outcrop immediately west of the SW Thirtymile stock (Fig. 1).

The Seagull batholith, Hake batholith and Thirtymile stock show linear major and trace element trends in whole-rock composition, and a regular progression in mica composition through the various plutonic facies, from biotite in the least evolved granites to zinnwaldite in quartz-rich leucogranites. A 101 ± 4.6 Ma whole-rock Sr-isotopic age determined from the Thirtymile stock (Liverton, unpublished data) is comparable to published ages for the Seagull batholith (Gabrielse et al., 1980; Sinclair, 1978), supporting the hypothesis that these intrusions comprise a single intrusive suite. The Thirtymile and Ork stocks have received the most attention because of their close spatial relationship to Sn/W mineralization (MINFILE 105C 038,054).

The Southwest Thirtymile (SWTM) stock, which is comparatively mafic and contains gabbro, diorite and hornblende granodiorite, was also included in the study. It is considered to be part of a different plutonic suite and may be older than the Seagull-Thirtymile biotite granites, i.e. related to other Jurassic-Cretaceous diorites of the southern Yukon, although tectonic considerations would place the undeformed stocks at no older than Early Cretaceous. A brief description of each pluton follows:

Thirtymile Stock:

The roughly elliptical 7 km long Thirtymile stock exhibits four texturally recognizable facies:

Porphyry:

This exists as isolated bodies up to 1 km in length, enclosed in either even-grained or megacrystic facies. It has prominent phenocrysts of euhedral oscillatory-zoned plagioclase, microperthite (sometimes rapakivi textured and up to 25 mm long) and euhedral hornblende with round or subhedral quartz (up to 5 mm) in a fine-grained quartz-2 feldspar-biotite groundmass. Modal hornblende content is 0.8% and modal biotite ranges up to 6.5%.

Even-grained and megacrystic facies:

These are granites of similar composition, the principal difference being the presence of perthite megacrysts. Biotite is the principal mafic mineral present and only rare secondary muscovite has been observed. An $^{87}Sr/^{86}Sr$ ratio of 0.707 has been calculated using measured whole rock isotopic ratios for the megacrystic facies (work in progress).

Li-mica topaz leucogranite:

This is a marginal facies of the Thirtymile stock. It also exists as dykes and sills in the surrounding country-rocks and crops out again as the barely exposed Ork stock 4.5 kilometres tc the south. The rock has a higher plagioclase content than the biotite granites and a texture dominated by large round quartz phenocrysts. Zinnwaldite is the mica in this facies. Interstitial fluorite is common. The extreme Rb/Sr ratio of the Li-mica leucogranite and its depleted Ba content are obvious from the data summarized. This facies is considered to be the result of extreme fractionation in a cupola above a buried portion of the batholith, and its high F content is apparently responsible for observed F metasomatism in the nearby skarn deposits. Opaque minerals are not plentiful in any of these granites: the few tenths of 1% present in the first three facies are mainly ilmenite with little magnetite, although occasional pyrite is seen.

Hake Batholith:

The Hake batholith consists of very coarse-grained biotite granite with a grain size sometimes exceeding 10 mm, which often displays mantled (rapakivi) perthitic feldspar. Some specimens are porphyritic, with centimetre-sized aggregates of potash and plagioclase feldspars containing smaller aggregates of fine biotite. Large round quartz grains are found in this variety.

Seagull Batholith:

The granite of this pluton is much finer grained and is comparatively even-grained. Round quartz phenocrysts dominate the texture of some specimens. Biotite is the only mafic mineral present and slight alteration to Li-mica is occasionally visible. Tourmaline and fluorite are common accessory minerals. In the eastern region of the batholith granophyre is present, with occasional zones containing prominent quartz- and topaz-bearing miarolitic cavities.

Southwest Thirtymile:

This stock has two principal components recognizable in outcrop. A mafic body which is barely exposed at surface forms the southeast part of the stock consists mostly of diorite containing up to 21% modal hornblende. Minor gabbro containing pyroxene variably altered to hornblende and biotite occurs at its northwest extremity. The western part of the stock is a well-exposed body of quartz-diorite to granodiorite which contains centimetre-sized enclaves of the gabbro.

Average analyses, with selected trace element contents and CIPW normative corundum are presented in Table 1 for each of the plutons. The granites of the Seagull-Thirtymile suite as a whole are characterized by a very slightly peraluminous composition, relatively high sodium (often $>3.5\%$ Na_2O), and

biotite alone as the most usual ferromagnesian constituent.

COUNTRY ROCKS:

The Ork stock intrudes white to grey calcitic and dolomitic marble. The Southwest Thirtymile stock intrudes quartzite, grey slate and phyllonite. The Hake batholith intrudes siliciclastic lithologies and one major marble unit, and the Seagull batholith intrudes mostly siliceous sediments. No lithologies with significant organic content were noted within 3 km of any of these intrusions. The Thirtymile stock intrudes chert, black slaty mylonite and quartzite. Some organic matter (or graphite) is possibly present in the slaty mylonite: where mineral veins cut pelitic rocks which overlie skarn at the nearby Mindy prospect, a distinct bleached selvedge is produced in otherwise unaltered rock, indicating the presence of a readily oxidized phase.

ANALYTICAL METHOD

The method of analysis consisted of three stages: (1) cold digestion in HF for 7 days; (2) separation of ammonia by distillation after the addition of excess KOH; and (3) colorimetric measurement of the separated ammonia as the indophenol blue complex (Mann, 1963). At the low levels of ammonium present in the analysed rocks, the reproducibility of the results is rather poor, being approximately $\pm 25\%$ of the amount stated.

RESULTS OF ANALYSIS FOR AMMONIUM

The analytical results are presented in Table 2. The average ammonium content varies from pluton to pluton, but the differences are small compared to the internal variation, so one cannot necessarily infer a different ammonium content for the parent magma of each pluton.

The normal (i.e. biotite-bearing) facies of the Thirtymile pluton has the lowest ammonium content of all, with an average of only 1.2 ppm, but higher levels occur in two of the Li-mica bearing samples (3.1 and 8.5 ppm). There is no consistency, however, since a third Li-mica-bearing sample has low ammonium content, not much different from the biotite-granites (1.8 ppm). It seems possible that hydrothermal processes may have played a part in the development of the Li-mica facies, in which case the ammonium content of two of the samples may be due to its hydrothermal redistribution, and the low values of the biotite-bearing facies may be more representative of the original magma composition.

Biotite granite of the Hake batholith, with a mean ammonium content of 3.5 ppm, is consistently richer in ammonium than that of the Thirtymile stock, and it seems reasonable to infer in this case that the Hake magma was more ammonium-rich. Biotite granite of the Seagull batholith is also relatively ammonium-rich compared to that of the Thirtymile stock, but the values are also much more variable. It should be noted that the Seagull samples were collected mainly from locations near the border of the batholith, in contrast to the Hake samples which came from the interior. The Southwest Thirtymile stock has an ammonium content in the same range as the other granitic rocks, despite its more mafic composition.

The mean ammonium content of all the analysed rocks is 3.1 parts per million. If the three mafic samples are excluded, the average for the granites alone is 3.0 parts per million.

DISCUSSION

Table 3 shows the average ammonium content of granites from various other parts of the world. The Yukon granites have a far lower ammonium content than any other granites which has yet been analysed. The ammonium ion is expected to be more variable than other trace element constituents of granitic magmas, since it is ultimately derived from sedimentary organic matter which is very unevenly distributed in the crust. However, a level of approximately 30 ppm NH_4 seems to be typical of granites, and levels much above or below this must be considered unusual.

The ammonium content of any particular granite is determined initially by the ammonium content of the material in the magmatic source region, and can subsequently be modified by processes occurring during and after emplacement of the granite. The nature of the source material is the major variable which determines the ammonium content. For an S-type granite (i.e. one with predominantly sedimentary source material), an organic component in the source material is both feasible and likely, since ammonium resulting from the decay of organic matter in sediments is readily incorporated in silicate minerals during diagenesis and metamorphism. For an I-type granite (i.e. one with predominantly igneous source material), an organic source component is less likely but not impossible. If, as proposed by many authors, the calc-alkaline magma suite was derived from the partial melting of subducted oceanic crust, a small sedimentary component can be envisaged. In fact, subducted sediment is not the only possible source of nitrogen, because ammonium has been shown to be present in spilitized basalts and diabases (Hall, 1989), and subducted ocean-floor igneous rocks could play a significant part in the recycling of nitrogen.

In terms of the S- and I-type classification, the status of the granites studied here is rather ambiguous. There are no muscovite granites, which are normally characteristic of an S-type paragenesis, but high levels of B, Li and F inferred from the mineralogy of some of the contact facies and minor intrusions tend to be characteristic of S-type granites elsewhere. The initial $^{87}Sr/^{86}Sr$ ratio of 0.707 for the megacrystic facies of the Thirtymile stock is too high for an entirely I-type magma, but not as high as those of undisputed S-type granites. It would be most reasonable to infer a mixed source. If the ammonium contents of these magmas had been high, there would be no problem about postulating the existence of N-rich lithologies within a mixed protolith, but a low ammonium content is not evidence that sedimentary material was absent in the source region. A magma source region in the lower crust containing sediments of sufficiently

great age or of sufficiently high metamorphic grade might have contained very little ammonium even though its lithologies were predominantly sedimentary.

In addition to the NH_4 content of the magmas and their source region, one must also take account of the various possibilities for ammonium gain or loss at the level of intrusion. These include contamination of the magma by country rocks during emplacement, loss of magma volatiles if emplacement was near enough to the surface, and postmagmatic hydrothermal activity.

There is no field or petrographic evidence for large scale contamination, and without such contamination it would be difficult to cause a large change in the ammonium content of a magma body. However, small scale contamination could have increased the ammonium content if the contaminants included organic-rich sedimentary rocks. Both the low ammonium contents of the granites and the scarcity of suitable country rocks suggest that contamination was not a factor in determining the ammonium content of these intrusions. Loss of magma volatiles is more difficult to evaluate. There is no direct evidence for emplacement of the granites at a very shallow depth, and the they lack intrusive features such as ring dykes which would indicaate near-surface emplacement. The Seagull Batholith does contain miarolitic cavities, but closed miarolitic cavities would not necessarily have permitted ammonium to be lost. In a previous study (Hall and Neiva, 1990), pegmatites which presumably formed by water exsolution from granitic magmas were found to have NH_4/K ratios very similar to those of coexisting aplites and granites, suggesting that the exsolution of magmatic water was not sufficient to cause ammonium loss.

Hydrothermal activity is the process most likely to modify the ammonium content of granitic rocks, and elsewhere it has been observed to cause large increases (Hall, 1988; Bencini and Hall, 1988). Among the Yukon granites described here, the most likely to have been affected by hydrothermal activity are those of the Thirtymile stock, and the highest ammonium content recorded here is indeed in a topaz-rich Li-mica granite. Even so, the concentration is still low compared to hydrothermally altered granites from other regions - for example the greisenized granites from Cornwall contain up to 300 ppm of ammonium (Hall, 1988) - and ammonium anomalies do not appear to be a reliable indicator of hydrothermal mineralization in these granites.

REFERENCES:

BENCINI, A. and HALL, A., 1988. A reconnaissance study of ammonium content in rocks of the Tuscan granitic province. Periodico di Mineralogia, Vol. 57, p. 671-674.

GABRIELSE, H., TEMPELMAN-KLUIT, D.J., BLUSSON, S.L. and CAMPBELL, R.B., 1980. MacMillan River. Geological Survey of Canada, Map 1398A.

HALL, A., 1987. The ammonium content of Caledonian granites. Journal of the Geological Society of London, Vol. 144, p. 671-674.

HALL, A., 1988. The distribution of ammonium in the granites of south-west England. Journal of the Geological Society of London, Vol. 144, p. 37-41.

HALL, A., 1989. Ammonium in spilitized basalts of southwest England and its implications for the recycling of nitrogen. Geochemical Journal, Vol. 23, p. 19-23.

HALL, A. and NEIVA, A.M.R., 1990. Distribution of the ammonium ion in pegmatites, aplites and their minerals from central northern Portugal. Mineralogical Magazine, Vol. 54, p. 455-461.

JUNGE, F., SELTMANN, R. and STIEHL, G., 1989. Nitrogen isotope characteristics of breccias, granitoids and greisens from eastern Erzgebirge tin ore deposits (Sadisdorf: Altenberg), G.D.R. Proceedings of the 5th Working Meeting "Isotopes in Nature", Leipzig, p. 321-332.

MANN, L.T., 1963. Spectrophotometric determination of nitrogen in total micro-Kjeldahl digests. Analytical Chemistry, Vol. 35, p. 2179-2182.

SINCLAIR, W.D., 1978. Molybdenum, tungsten and tin deposits and associated granitoid intrusions in the northern Canadian Cordillera and adjacent parts of Alaska. In: Mineral deposits of the northern Cordillera; J. Morin (ed.); Canadian Institute of Mining and Metallurgy, Special Volume 37, p. 216-233.

URANO, H., 1971. Geochemical and petrological study on the origins of metamorphic rocks and granitic rocks by determination of fixed ammoniacal nitrogen. Journal of Earth Sciences, Nagoya University, Vol. 19, p. 1-24.

Table 1. Analyses. Mean values for the Seagull-Thirtymile granites, and selected specimens from the SW Thirtymile stock.

Pluton	Thirtymile	Thirtymile	Thirtymile	Thirtymile	Batholiths	Batholiths	SW Thirtymile	SW Thirtymile	SW Thirtymile	SW Thirtymile
Facies or Sample	Mean of Porphyry (7)	Mean of Mega-crystic (8)	Mean of Even-grained (11)	Mean of Li-mica (5)	Mean of Hake (11)	Mean of Seagull (10)	08/18-3 (Diorite)	08/20-4 (Diorite)	08/20-6 (Gabbro)	08/20-2 (Gabbro)
SiO_2	72.70	75.19	76.97	75.61	76.04	76.50	60.61	59.39	50.93	54.22
Al_2O_3	13.66	13.00	12.49	14.21	12.57	12.45	16.22	16.36	13.18	14.07
Fe_2O_3	2.63	1.78	1.28	0.59	1.76	1.53	6.66	6.36	11.40	9.46
MgO	0.41	0.23	0.07	0.01	0.23	0.08	2.90	2.70	7.83	5.93
CaO	1.17	0.92	0.06	0.12	0.71	0.56	5.90	4.86	9.78	7.96
Na_2O	3.50	3.68	3.67	5.12	3.10	3.23	3.48	4.15	2.54	3.01
K_2O	5.35	4.89	4.83	4.07	5.07	5.03	2.81	4.30	2.76	3.81
TiO_2	0.40	0.24	0.12	0.01	0.20	0.12	0.64	0.48	0.88	0.75
MnO	0.05	0.04	0.03	0.06	0.03	0.12	0.10	0.11	0.18	0.15
P_2O_5	0.10	0.07	0.03	0.01	0.05	0.03	0.26	0.29	0.48	0.40
TOTAL	99.57	100.04	100.09	99.80	99.76	99.65	99.56	99.03	99.97	99.76
LOI							1.15	0.69	2.20	0.85
Sr	123	71	21	1	46	16	598	961	615	627
Rb	304	391	497	2087	424	499	55	102	70	80
Sb	771	318	90	15	192	123	1643	1499	1146	1066
Zr	270	163	129	49	160	191	91	87	31	44
Nb	54	59	72	77	63	70	6	6	3	4
CIPW COR	0.22	0.15	0.21	1.19	0.81	0.75	0.00	0.00	0.00	0.00

CIPW COR = Normative corundum.

TABLE 2. Ammonium contents of granites and related rocks.

Specimen	NTS map sheet	UTM coordinates	NH_4+ (ppm)	Petrographic comments
Thirtymile pluton				
HPG	105C-9	407309	1.1	Porphyry
97/29-1	105C-9	415286	1.1	Even-grained facies
TOR	105C-9	408303	2.0	Megacrystic facies
97/28-5	105C-9	411292	0.7	Megacrystic facies
97-26-3	105C-9	419280	1.4	Li-mica border facies
97/26-3 (repeat)	105C-9	419280	1.8	Li-mica border facies
97/28-4	105C-9	420279	8.5	Li-mica facies sill
78/23-1	105C-9	429235	3.1	Li-mica facies, Ork stock
Hake batholith				
08/17-1	105C-9	589123	2.5	Granite porphyry
08/17-2	105C-8	638030	2.3	Granite, coarse-grained
08/17-3	105C-8	636055	5.2	Granophyre
08/17-5	105C-8	634084	3.1	Granite, coarse-grained
08/21-3	105C-8	630925	2.7	Granite, coarse-grained
08/21-14	105C-8	614938	4.3	Granite, coarse-grained
Seagull batholith				
07/21-2	105B-3	800042	5.5	Granophyre, near contact
08/21-2	105B-3	800630	2.9	Microgranite
07/30-1	105B-4	534765	3.5	Microgranite
07/30-4	105B-4	539759	1.9	Microgranite
08/02-1	105B-4	557728	1.9	Granite, porphyry
Southwest Thirtymile Stock				
08/18-3	105C-9	396119	4.3	Diorite, fine-grained
08/20-4	105C-10	371138	3.5	Diorite, coarse-grained
08/20-2	105C-9	388131	2.4	Gabbro, fine-grained

TABLE 3. Ammonium content of Yukon granites compared to those of other regions.

Region	Mean NH_4+ (ppm)	No. of specimens	Reference
Yukon	3	18	This paper
Elba, Italy	13	15	Bencini & Hall, 1988
Germany	29	9	Junge et al., 1989
Japan	31	20	Urano, 1971
British Isles	33	35	Hall, 1987
N. Portugal	159	10	Hall & Neiva, 1990

TIN-BEARING SKARNS OF THE THIRTYMILE RANGE, N.T.S. SHEET 105 C 9: A PROGRESS REPORT

Tim Liverton
Royal Holloway and Bedford New College,
University of London,
Egham, Surrey,
U.K. TW20 OEX

LIVERTON, T., 1990. Tin-bearing skarns of the Thirtymile Range: a progress report. In: Yukon Geology, Vol. 3, Exploration and Geological Services Division, Yukon, Indian and Northern Affairs Canada, p.52-70

ABSTRACT

This report summarizes the results of geological mapping of the Thirtymile Range, Sheet 105 C 9, and an investigation of tin skarns at the Mindy (MINFILE 105C 054) and Ork (MINFILE 105C 038) prospects. The Thirtymile range is a tectonic mélange of Upper Palaeozoic and (3) siliciclastic and carbonate sediments, the more competent members of which survive as sheared and brecciated disrupted units or phacoids surrounded by highly foliated ultramylonite of slaty appearance. These have been deformed by later low angle thrusting, moderate angle faulting and extensional faulting and have been intruded by Mid Cretaceous granitic plutons. Tin-tungsten-boron-fluorine-bearing skarns have formed in the aureoles of the granites. A granitic stock about 6 km in diameter which occurs north of the Thirtymile Range, a smaller granite at the Ork prospect further south, and the fluorine-boron mineralized skarns at the Ork and Mindy prospects were mapped in detail. Initial petrographic and analytical work shows that the Mindy skarn horizons are predominantly pure diopside-andradite or diopside-actinolite ± pyrrhotite/arsenopyrite assemblages, with complex retrograde assemblages containing magnetite, magnesium borate/fluoride and cassiterite/tin borate mineralization. The Ork showing contains abundant fluorite and axinite but little metallic mineralization. Mapping indicates that extensional faulting played an important role in control of the tin-tungsten mineralization at the Mindy prospect.

RÉSUMÉ

Ce rapport résume les résultats de la cartographie géologique de la chaîne Thirtymile sur la feuille 105 C 9 et d'une étude des skarns stannifères dans les zones d'intérêt Mindy et Ork. La chaîne Thirtymile est un mélange tectonique de sédiments du Paléozoïque supérieur, de sédiments siliciclastiques (3) et de sédiments carbonatés dont les membres les plus compétents persistent sous forme d'unités perturbées ou phacoïdes cisaillées et bréchifiées entourées d'ultramylonite très feuilletée d'apparence ardoiseuse. Elles ont été déformées par un ultérieur charriage à faible angle d'incidence, par la formation de failles à un angle modéré et par la formation de failles de distension en plus d'avoir été pénétrées par des plutons granitiques au Crétacé moyen. Des skarns renfermant de l'étain, du tungstène, du bore et du fluor se sont formés dans les auréoles des granites. Un petit massif intrusif de granite d'un diamètre d'environ 6 km situé au nord de la chaîne Thirtymile, une masse de granite plus petite dans la zone d'intérêt Ork plus loin au sud et les skarns minéralisés en fluor et en bore des zones Ork et Mindy ont fait l'objet d'une cartographie détaillée. Les travaux pétrographiques et analytiques initiaux indiquent que les horizons skarnifiés de la zone Mindy sont des assemblages principalement purs de diopside et andradite ou de diopside et actinolite ± pyrrhotine et arsénopyrite avec des assemblages rétrogrades complexes renfermant des minéralisations en magnétite, en borate/fluorure de magnésium et en cassitérite/borate d'étain. L'indice minéralisé Ork renferme en abondance de la fluorine et de l'axinite mais peu de minéralisation métallique. La cartographie indique que la formation de failles de distension a joué un rôle important dans la détermination de la minéralisation en étain et en tungstène dans la zone Mindy.

INTRODUCTION

The Thirtymile Range is located between the Wolf and Nisutlin Rivers 25 miles (40 km) northeast of Teslin and is found on the west half of Yukon NTS map 105 C 9. This study is based on 13 weeks of fieldwork in the central and northern parts of the Thirtymile Range, between 1987 and 1989. The work focused on areas around the Ork (MINFILE 105C 038) and Mindy (MINFILE 105C 054) prospects and the granitic stock 9 km to the north (Fig. 1). It forms part of a larger study of regional geology, tectonics and metallogeny of the Thirtymile Range: in particular the petrology and geochemistry of the Cretaceous granitic intrusions, differentiates and "specialized" fluorine-rich facies, their metamorphic aureoles and the tin-tungsten or base metal prospects within them. Distinctly anomalous amounts of boron and fluorine minerals were noted in the assessment work filed by various companies working on prospects in the area (Mindy, Mindy 3 and Ork). The distribution of these elements and their relation to the tin mineralization is an important part of the present study.

This paper describes field geology and the limited petrographic and analytical data obtained to date. Detailed coordinates are given for the localities discussed, based on the 1000 m Universal Transverse Mercator grid covering map sheets 105 C 9 and 10.

REGIONAL GEOLOGY

The Thirtymile Range encompasses an unstudied area of Paleozoic metasedimentary rocks (Englishman's Group) which are intruded by Mesozoic granitoids similar to those of the Hake and Seagull Batholiths to the SE (a significant tin province). The region lies immediately east of the Teslin Suture Zone (Fig. 2), the boundary between the Intermontane Belt (Mesozoic volcanic and sedimentary rocks) and the Omineca Crystalline Belt (Paleozoic metasedimentary rocks intruded by Mesozoic to Cenozoic intermediate to felsic plutons). The Teslin Suture is the root zone for nappe structures thrust to the NE. The Englishman's Group rocks are probably derived from the Teslin Suture Zone.

The Englishman's Group is a tectonic mélange according to the definition of Raymond (1984). It consists of Upper Paleozoic and (?)Mesozoic siliciclastic and carbonate cataclasites, which lie between the Teslin Suture Zone and sedimentary rocks of the Cassiar Platform. Disruption of the sediments forming the cataclasites prevents the tracing of individual lithologic units along strike for more than 5 km.

Tempelman-Kluit (1979, p. 20) considered that cataclasis in the Teslin Suture Zone occurred between the Late Triassic and Early Jurassic and involved blocks from both the Stikine Terrane and North America, while transport of allochthons took place during the late Early Cretaceous. In the case of the Englishman's Group, low angle thrust faulting, probably during the Early Cretaceous, juxtaposed different allochthonous units; then the thrust planes were gently folded, either by compression or as a result of non-planar thrust geometry.

Later steep, east and ENE-trending extensional faults caused relatively minor vertical displacements within the mylonitic sequence. These faults are believed to have controlled the emplacement of mid-Cretaceous granitic plutons (Armstrong, 1988; Sinclair, 1983). The stocks of the Thirtymile Range form the NW limit of the tin district, which also includes the Seagull and Hake batholiths.

Mulligan (1963) divided the Englishman's Group metasediments into a lower carbonate unit and an upper unit (the cataclasites of this study) of "slate, quartzite and chert with minor arkose and conglomerates", the cataclastic nature of the allochthon not being recognized at that time. Lithologies range from highly sheared quartzite/arkose and marble, to phyllonite, mylonite and ultramylonite. Middle Mississippian macrofossils are reported from the lower carbonate unit (Mulligan, 1963), but the exact structural relationship between this and the adjacent cataclasites is unknown - they could be separated by either high angle reverse or low angle thrust faults.

Regional correlation is problematic; the Englishman's Group could still be part of the Omineca Crystalline Belt. Two interpretations have been suggested:

(a) The clastic sequence generally resembles the Devono-Mississippian sequence mapped by Gordey (1982) in the Indigo Lake map sheet to the northeast, although some units of the mylonitic sequence (the phyllonites) are more easily correlated with the Klondike Schist of Gordey's allochthon. The phyllonites could represent tectonic slices or inclusions as described by Raymond (1984).

(b) Templeman-Kluit (1979) suggested that arkoses of the Englishman's Group might be the protolith for the mylonites found in the McNeil Klippe, which lies 60 km to the NE. The present work recognizes the Englishman's Group as a totally disrupted mylonitic sequence and suggests a direct correlation with the McNeil Klippe.

Where limestone occurs in the aureoles around the granitic plutons it is metamorphosed to skarn and marble which at some localities carry significant tin-tungsten-arsenic mineralization.

GEOLOGY OF THE THIRTYMILE RANGE

During this study, the mylonitic siliciclastic sequence which represents the upper part of Mulligan's (1963) Unit 3, was mapped, along with two of five granitic stocks of the Thirtymile Range (Fig. 3). Coordinates given pertain to the 1000 metre UTM grid shown on 1:50,000 scale map sheets 105 C 9, 10. The following map units were identified (see sketch of mylonite stratigraphy, Fig. 5 and cross section, Fig. 4):

Unit A. The topographically lowest unit consists of quartzite which forms outcrops and felsenmeer on ridges east of the Mindy prospect. Like all quartzite (phacoid) units within the

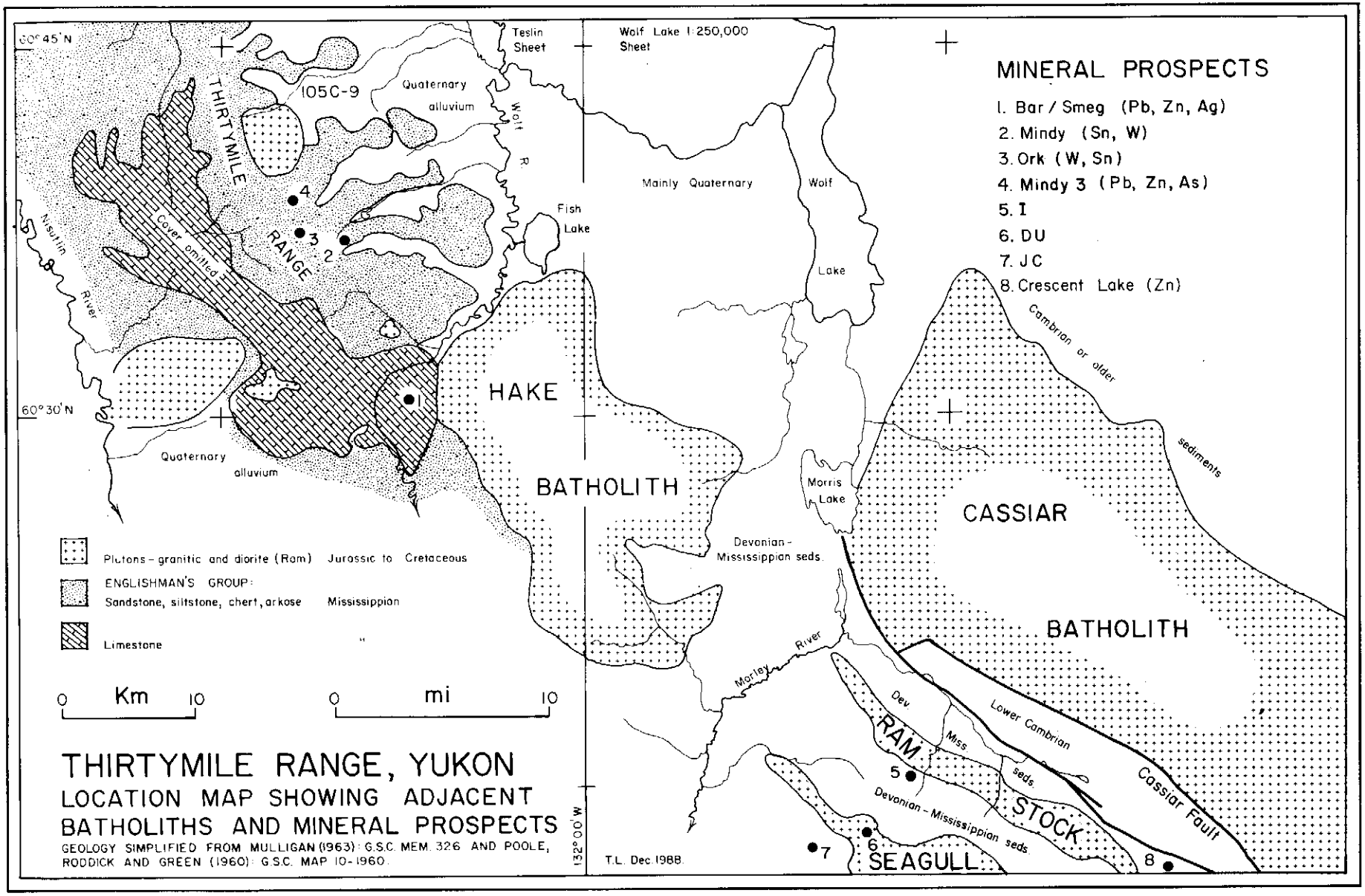

Figure 1. Location map and regional geology.

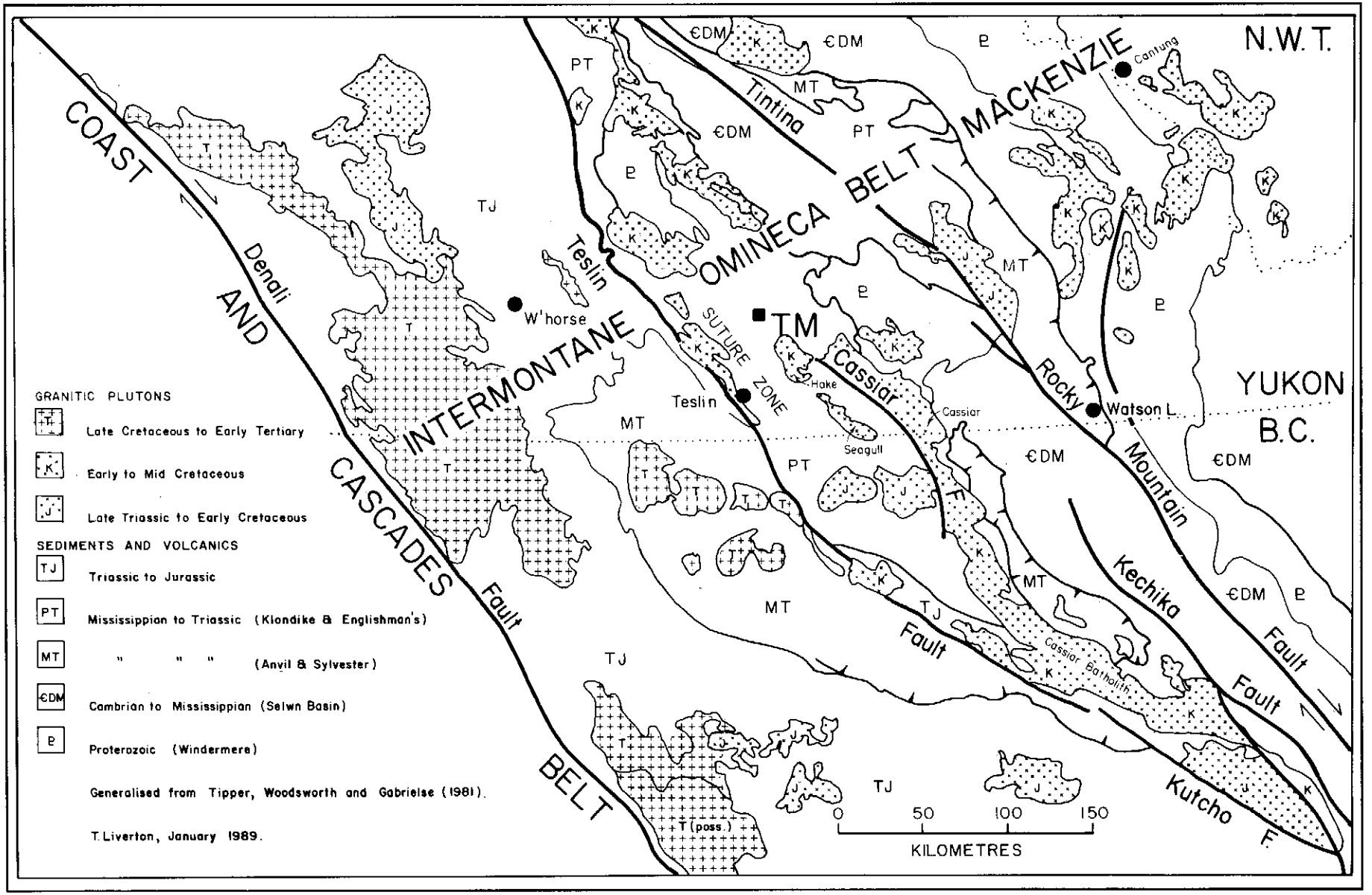

Figure 2. Tectonic setting.

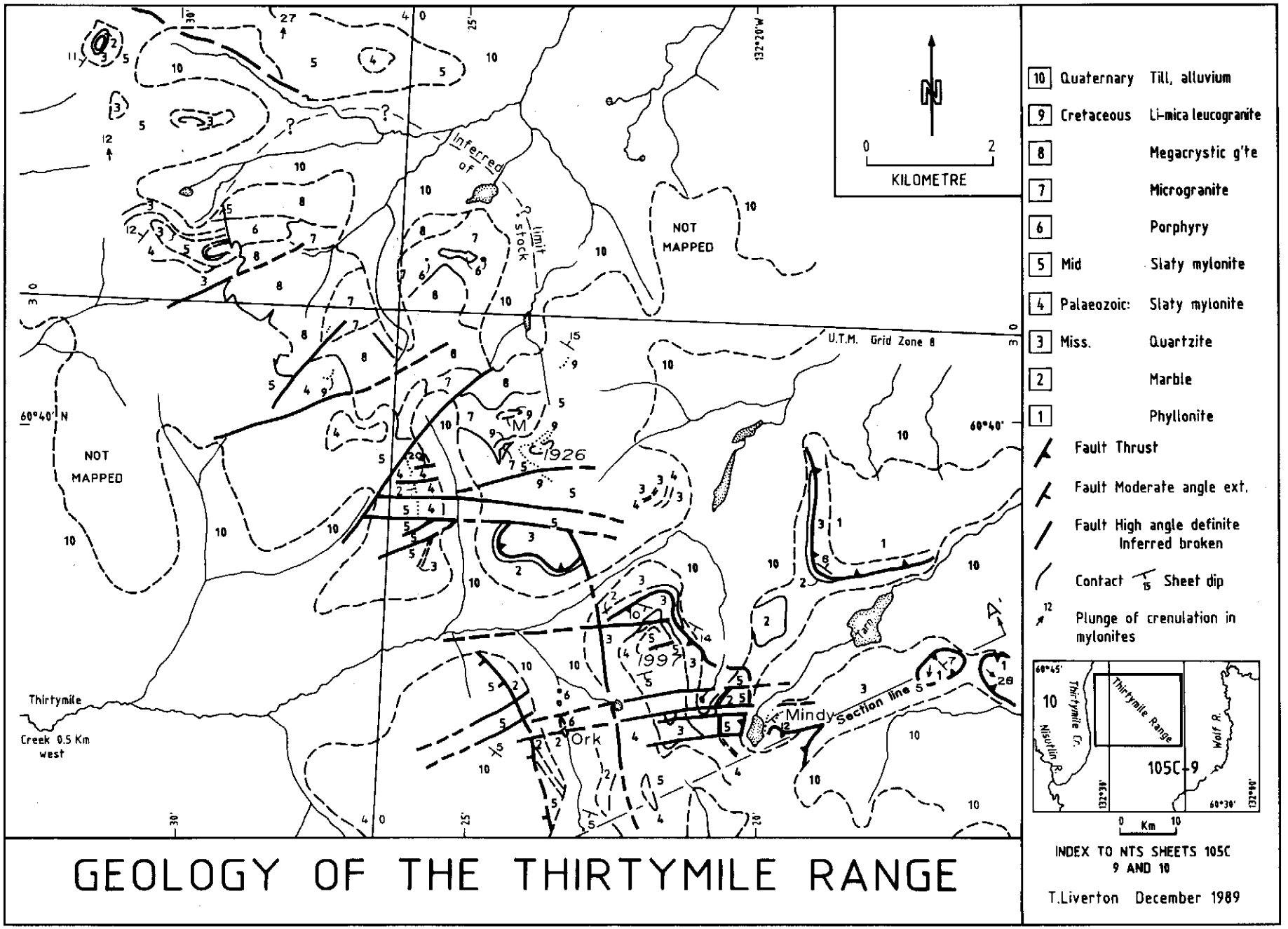

Figure 3. Geology of the Thirtymile Range.

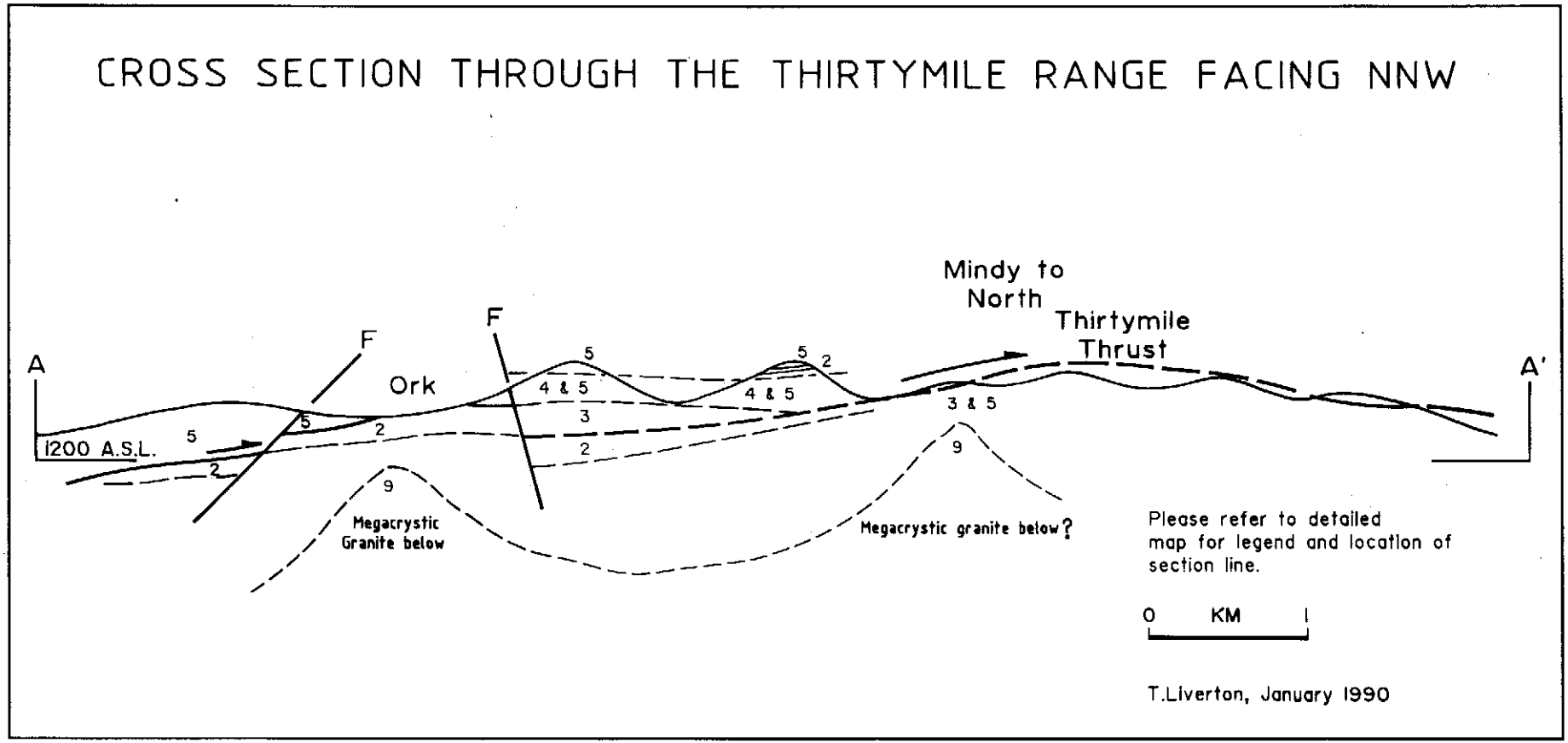

Figure 4. Cross section through the Thirtymile Range.

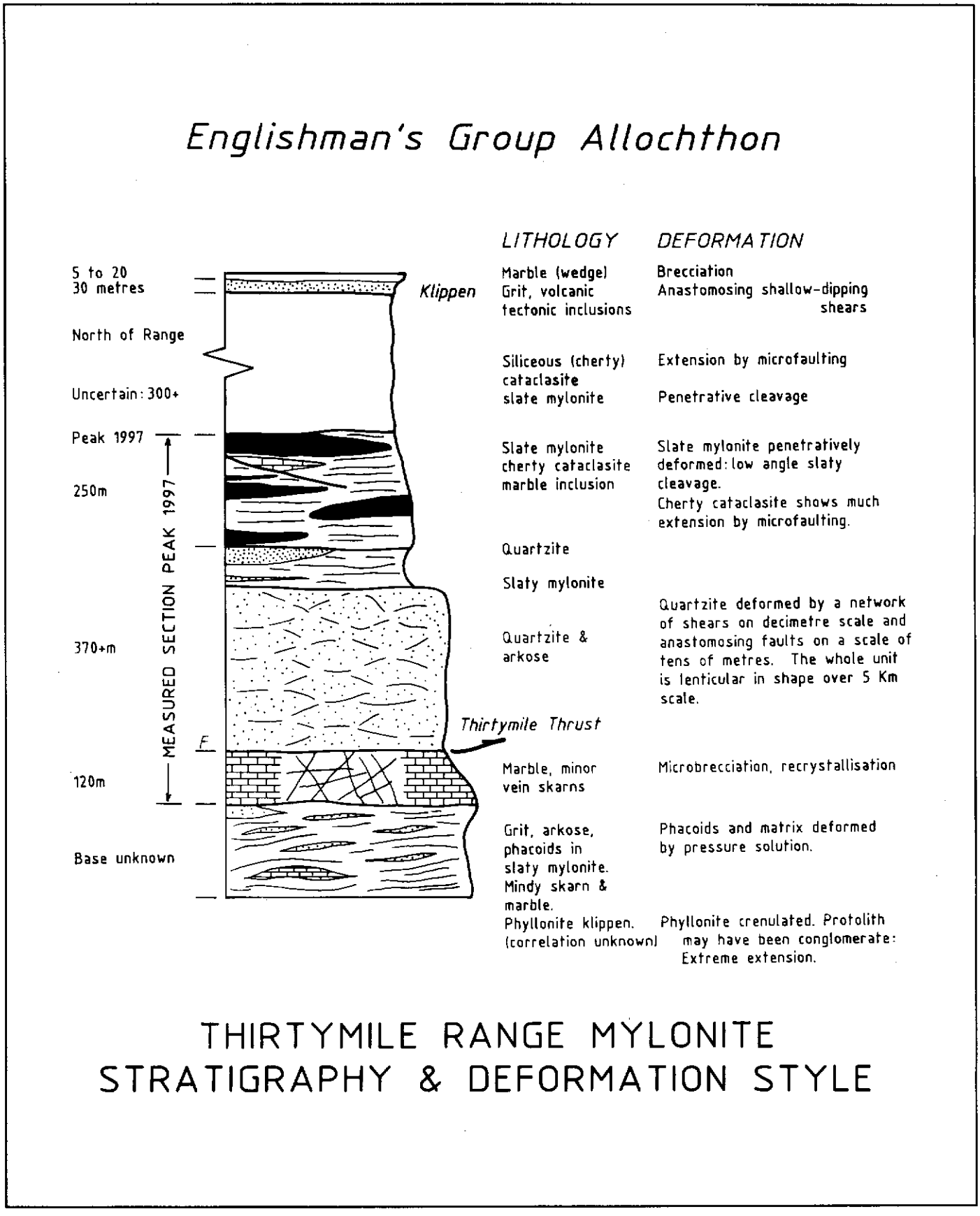

Figure 5. Thirtymile Range cataclasite stratigraphy.

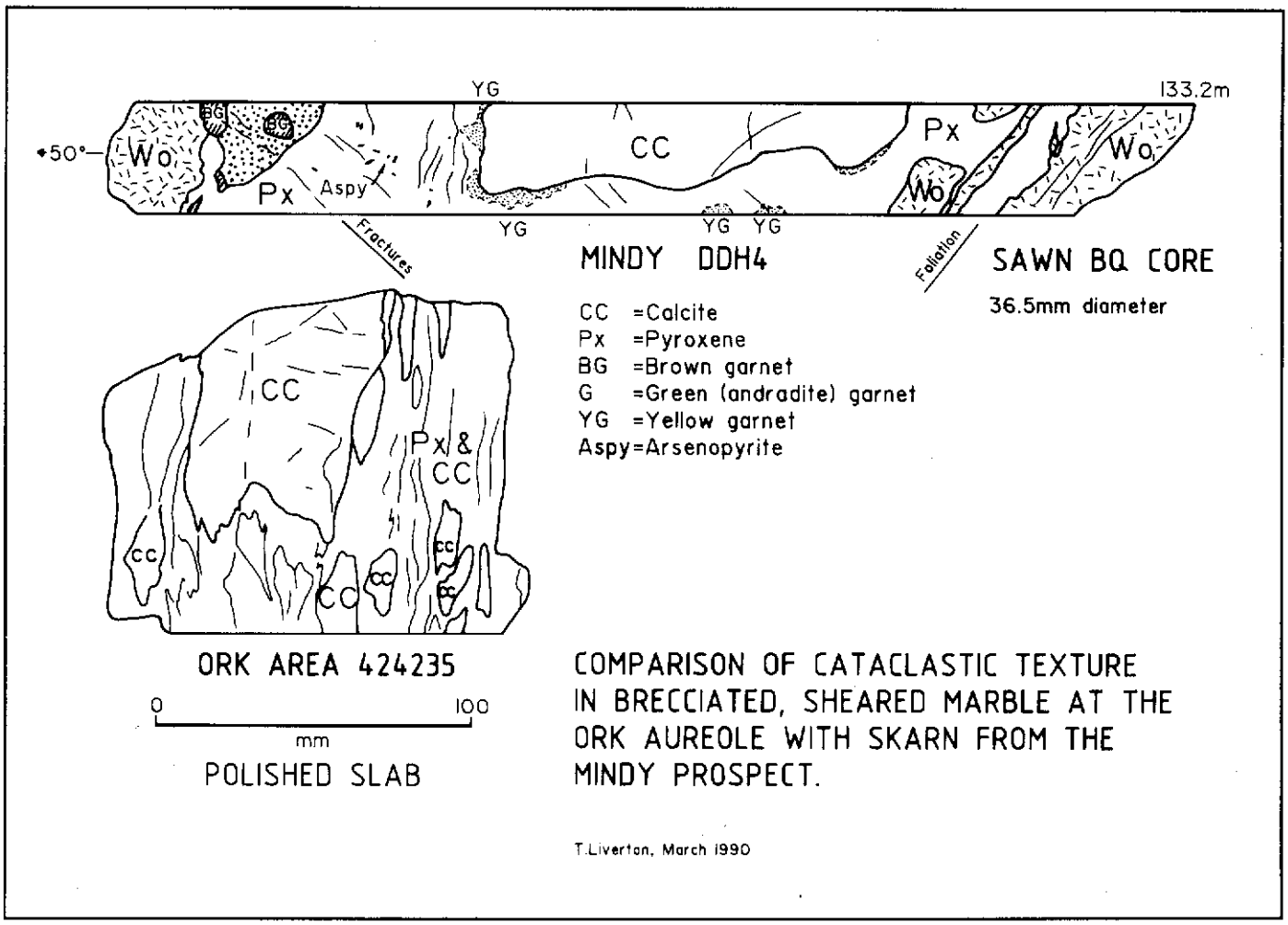

Figure 6. Cataclastic texture in marble, Ork and Mindy Showings.

mylonites, this one shows considerable small-scale shearing. A low angle pressure solution (PS) cleavage is visible in places.

Unit B. This sequence adjacent to the Mindy prospect consists of mylonitic, silty metasediments containing clasts and phacoids of quartzite and arkose from a few centimetres to several metres across. In outcrop, the dominant foliation is a metamorphic pressure-solution cleavage which dips at a shallow angle. The only evidence of bedding is grading in the disrupted sandy layers, which is recognizable in thin section and oriented at a few degrees to the PS cleavage. One major and several minor marble/skarn layers occur in Unit B at the Mindy prospect. The main mineralized (lower) skarn varies considerably in thickness along strike, as indicated by diamond drill hole intersections, and appears boudinaged on a scale of several hundred metres. This marble may not correlate with either the major carbonate unit to the northwest or the minor marble unit found about 750 m to the west.

Unit C. Below Peak 1997 in the main range (UTM Coordinates 443248), quartzite which possibly correlates with unit (A) is overlain by thick white calcite marble. The marble consists of totally recrystallized calcite grains 2 to 5 mm in size, and lacks sedimentary structures. A section measured down the northeast spur of this peak traversed a true thickness of 120 metres. Cliff exposures on the north side of the peak reveal that the marble is extensively brecciated down to a centimetre scale. Exposures west of the Ork prospect show a striking cataclastic texture (Fig. 6). Minor wollastonite-veined skarns are developed within the unit. The cliff exposure north of Peak 1997 shows a strong, nearly horizontal foliation developed in a 3 m thick diopside-rich zone at the top of the marble, and chevron folding in the lowest metre or two of overlying quartzite. These features are inferred to indicate a thrust faulted contact which postdates the main cataclasis of the Englishman's Group. To the west, a fault truncates the top of the marble at a moderate angle and the marble thins rapidly toward the south.

Unit D. This consists of 290 m of massive quartzite, overlain by 80 m of intercalated quartzite and slate mylonite. The quartzite is brecciated and cut by small shears spaced every few decimetres throughout the succession. The slaty rocks are

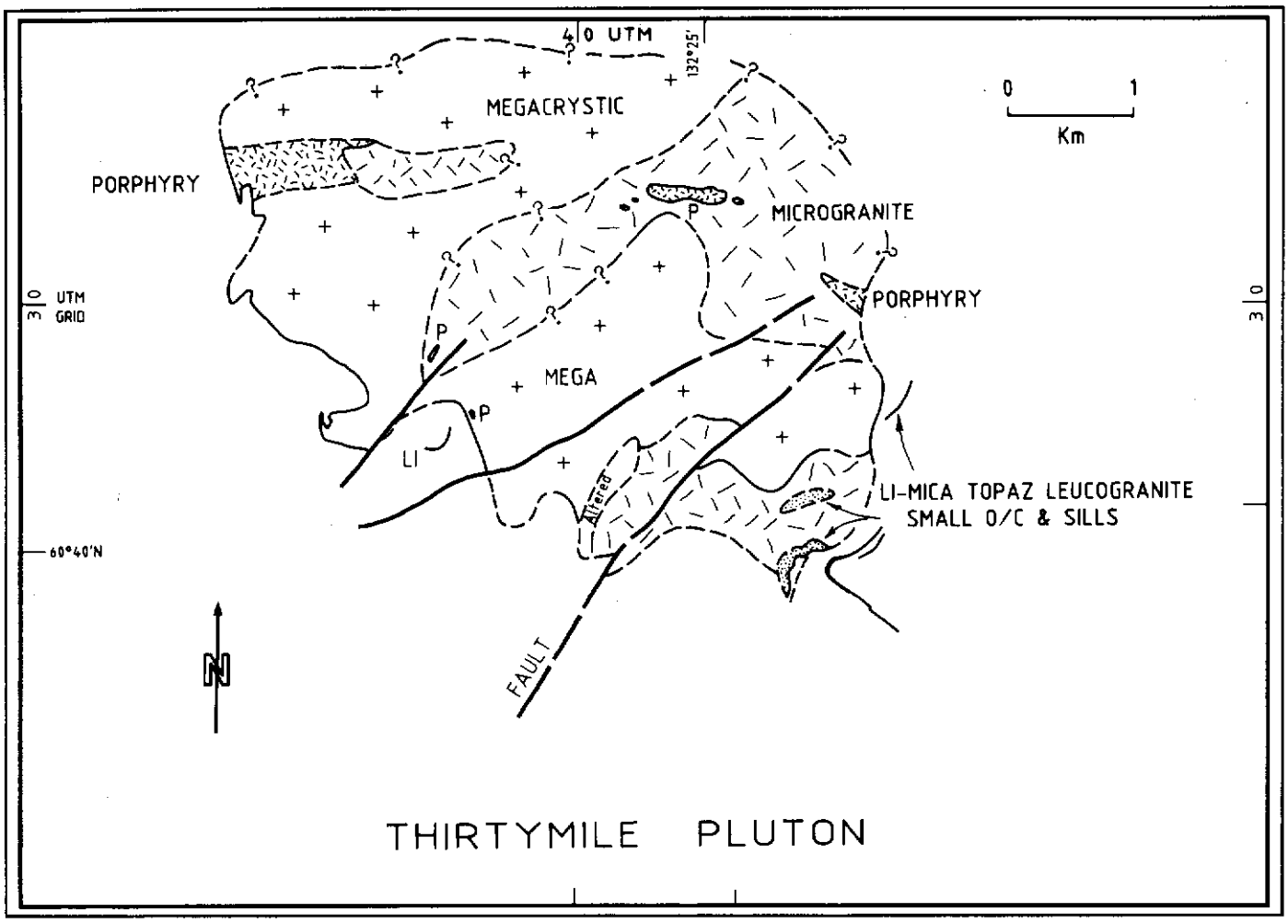

Figure 7. Facies map of the Thirtymile stock.

mylonitic and have a chaotic cleavage or foliation which shows abrupt variations in dip up to 30°. The attitude of this foliation is not reflected in the sheet dip of the lithologic units: the tectonic cleavage is likely deflected around phacoids of more competent rock, which are on a scale of tens of metres.

Unit E. Above unit D, some 240 m of intercalated massive chert, cherty mylonite and slate mylonite are exposed on the northeast spur of Peak 1997. A five-metre thick tectonic slice of marble exposed on the spur 80 metres northeast of the peak is also assigned to this unit. On the northwest spur, the thickness of individual "chert" units varies from 10 to 105 metres. A marble/calc-silicate hornfels unit 4.5 km northwest of the peak occurs in a possibly equivalent chert/mylonite sequence.

Unit F. In the northwest part of the map area (360330), slaty mylonite is overlain by a grit unit. Whether this represents a separate clastic unit structurally and stratigraphically higher than unit B is uncertain. At UTM 365329, sheared intermediate volcanic rocks form a tectonic inclusion within this grit at (365329).

Unit G. At location 350340, a thin marble overlies the grit and rapidly thickens toward the NE, from 5 m to over 20 m. East of the Mindy showing (UTM 475266 & 490247), highly deformed phyllonites overlie the Unit A quartzite. These show many open disharmonic folds on a decimetre scale, with sheet dips varying from 8° SW to 30°E between individual exposures. They are lithologically similar to the thick phyllonite sequence that outcrops west of Thirtymile Lake (105 C 15, UTM 270420) and might represent tectonic inclusions of Big Salmon Complex metamorphic rocks within the Mississippian sequence; however their position within the general mylonite stratigraphy is uncertain.

INTRUSIONS

Two granite intrusions have been mapped in the Thirtymile Range: a small poorly exposed leucogranite at the Ork prospect, and the Thirtymile Pluton, a roughly elliptical exposure 8 km across (Fig. 7). A low angle dip at the western contact of the Thirtymile Pluton suggests that the present exposures on the centre ridge may be within 400 vertical metres of the original roof. The Thirtymile Pluton is

considered to be an apophysis of a large batholith that may underlie the whole range. In order of emplacement, the various facies which make up the Thirtymile Pluton are:

(a) Porphyry mingled with tonalite or diorite, which exists as isolated remnants within microgranite.

(b) Microgranite (equigranular).

(c) Megacrystic granite, which forms more than half of the exposed pluton.

(d) Leucocratic topaz and fluorite-bearing microgranite, which occurs as a marginal facies in the main stock, as adjacent sills in the overlying metasediments, and forms a stock and dykes at the Ork prospect to the south (UTM 429236, 435248, 438237).

Porphyry

At the west limit of exposure in the map-area (UTM 407309) the predominant lithology is porphyritic. The texture is frequently dominated by euhedral to subhedral equant quartz phenocrysts, some with their margins intergrown with the grains of the groundmass. Anhedral to euhedral single-twinned perthite phenocrysts 4 to 10 mm long often occur in clusters with very little quartz between (a cumulus texture) and occasionally show rapakivi texture. Plagioclase is finer grained (2 to 4 mm), subhedral to rarely euhedral, and often shows both albite and carlsbad-albite twinning and oscillatory zoning. Rare subhedral hornblende xenocrysts, often altered to biotite and chlorite, are up to 3 mm long. Deep brown biotite, often chloritized and very ragged, forms phenocrysts up to 2 mm in size, and smaller (0.5 mm) grains in the groundmass. The micas contain some euhedral zircon inclusions and are occasionally intergrown with anhedral monazite. Occasional clusters of biotite, very fragmented hornblende (0.5 mm), monazite, pyrite and apatite are seen. Monazite is common in the groundmass as anhedral grains up to 0.8 mm, and allanite is also common, forming subhedral to euhedral crystals up to 1 mm long. Quartz and K-feldspar form the bulk of the groundmass. Quartz is the most common mineral in the groundmass, forming grains of approximately 0.5 mm across which poikilitically enclose the feldspar. The porphyry frequently contains rounded enclaves of dark grey fine grained tonalitic rock up to 0.5 metres across, which in turn enclose centimetre-sized darker rounded dioritic enclaves. Similar enclaves have been interpreted as clear evidence of magma mixing (Chandra Kumar, 1988; Vernon, 1983; Vernon, Etheridge and Wall, 1988).

East of this exposure the intrusion consists entirely of tonalite. Enclaves of tonalite are found in both the microgranite and megacrystic granite at widely separated locations, so the porphyry-tonalite body is considered to be the earliest intrusion.

Microgranite

The microgranite consists of perthite (30-40%), plagioclase (10-15%) and quartz (40-55%). The texture varies from fine grained (0.2 to 0.5 mm) to more coarse-grained and porphyritic. Chloritized, dark biotite occurs in small amounts, generally 1% or less and rarely up to 5%. Accessory minerals include occasional fluorite, monazite, zircon, allanite and pyrite. At the southern contact, the equigranular microgranite is red due to alteration, the feldspars are extensively sericitized and kaolinized and the micas are altered to sericite and opaque minerals. Blocks of microgranite occur in megacrystic granite near their contact.

Megacrystic Granite

This is a coarse grained facies with 6-15 mm potash feldspar megacrysts. The megacrysts are subhedral, micro-perthitic and often zoned, some zones being altered to a red sericite-iron oxide mixture. Plagioclase feldspars are finer grained (1 to 8 mm), and show normal zoning and frequently cloudy cores. Zoning is optically distinct, and microprobe analysis indicates compositions of An_5 in the groundmass and a variation from An_{47} in the cores of quartz phenocrysts to An_{28} in the rims. Quartz is usually anhedral and occurs in phenocrysts up to 5 mm across. Deep red-brown biotite flakes up to 2 mm across have very ragged margins and often contain numerous apatite inclusions and very fine grained zircons surrounded by pleochroic halos up to 0.05 mm across. Biotite forms occasional pseudomorphs after hornblende also occurs as clusters up to 4 mm diameter. Groundmass crystals 0.5-1 mm in size make up less than 50% of the rock. Accessory minerals include apatite, monazite, zircon, allanite (occasional 2 mm euhedral crystals) and, less commonly, pyrite and interstitial topaz or fluorite. Alteration is ubiquitous, but is limited to slight kaolinization of feldspars, particularly perthite. Mineral proportions vary from: perthite 30-40%; plagioclase 20-10%; quartz 40-45% and micas <1 to 5%. Occasional centimetre-sized miarolitic cavities containing quartz and tourmaline occur close to the margins of the pluton.

Leucocratic zinnwaldite-topaz-fluorite bearing microgranite

This rock has a striking texture: equant quartz phenocrysts 2 to 4 mm across occur in a groundmass dominated by 1 mm subhedral to euhedral plagioclase. Some plagioclase crystals are poikilitically enclosed in quartz. At some localities, perthite feldspar predominates in the groundmass. Between 1 and 15% of the rock consists of pale lithium mica, which is present as anhedral, often skeletal phenocrysts 1 to 4 mm across. Accessory minerals are rarely included in this mica. Proportions of the other minerals vary greatly between localities (K feldspar 10 to 50%, plagioclase 60 to 30%). Topaz is a common interstitial mineral and may constitute 3% of the rock by volume. Fluorite is also common in this facies. Schorl, apatite and allanite are occasional accessories.

Surprisingly, the K-feldspar is the only mineral showing slight alteration. Where they form sills, (as at 421279), rocks of this facies show a preferred orientation of plagioclase laths (flow banding). Although no intrusive rocks are evident on the east side of the Thirtymile Range at the Mindy prospect, rocks of this facies are the probable source of the fluorine in the skarns.

Greisens, miarolitic cavities

At the southeast corner of the Thirtymile stock the microgranite is cut by greisen veins up to 1 cm wide and spaced about 10 cm apart. The greisen veins consist of topaz, quartz and zinnwaldite. Miarolitic cavities up to 0.5 metres long were observed in the adjacent small body of leucocratic microgranite.

Lamprophyres

One hornblende lamprophyre dyke a few metres wide cuts hornfels at the southwest contact of the main stock (392290).

Ork Stock

The intrusion in this region resembles the leucocratic topaz-bearing microgranite of the Thirtymile Stock to the north. Four exposures were sampled between the contact and a point 250 metres to the north. The northernmost exposure shows a texture characterized by subhedral equidimensional quartz phenocrysts of 2-4 mm across, and finer (0.5 mm) albite which makes up about 40% of the rock by volume. Ragged anhedral grains of pale (lithium?) mica enclose the smaller feldspars and make up less than 2% of the rock.

Closer to the contact the intrusion is slightly finer grained (1 - 3 mm) and contains less quartz (30%). Both potash feldspar (45%) and albite (25%) are evident, but only occasional mica phenocrysts are present. A few crystals of topaz were noted in a specimen taken from the contact. The contact with the calc-silicates is very sharp and can be seen on the scale of a thin section. Both potash feldspar (50%) and albite (40%) are found within 3 cm of the calc-silicate contact.

In the contact zone, fine-grained untwinned plagioclase feldspar with fluorite occurs both interstitial to and included in the feldspars over a 2 cm width, forming a possible endoskarn. Zircon is present as occasional tiny euhedral crystals. Included in the fluorite are nordenskioldine (?) and tiny, high relief inclusions producing brilliant purple haloes. Titanite was identified in thin section in the fluorite zone. The presence of crystals which fluoresce under ultraviolet light suggests that some of the titanite is be the malayaite variety. Massive vesuvianite occurs in 10 mm long crystals which include some fluorite. A few millimetres of fibrous cebollite (normally an alteration product of melilite) mark the transition to coarse marble (8 mm grain size), occuring within half a metre of the contact. Also found at the contact are two-metre wide pegmatite dykes consisting of 20 cm green orthoclase microperthite with coarse violet mica (zinnwaldite?) and quartz.

West of the exposed granite is a cliff exposure of two cataclastic marble layers separated by aphanitic calc-silicate hornfels. The hornfels has abundant vertical fractures filled with axinite crystals up to 20 mm long. The upper carbonate is a sheared breccia with grey calcite phacoids with carbonate pressure shadows surrounded by diopside marble. In the lower marble unit, epidote and axinite have developed around many of the calcite clasts.

Three smaller topaz-bearing aplite bodies occur northeast and east of the "Ork" contact. Based on limited outcrop, these appear to be dykes 5 to 10 metres wide. The easternmost dyke lies immediately above (north of) tin-tungsten soil anomalies reported by the JC Syndicate.

STRUCTURE

(1) Thrust Faults.

The upper surface of marble unit (C) is at least partly bounded by a low-angle thrust fault. This structure may be gently warped and correspond to a fault underlying a klippe of phyllonite at location UTM 475266. Many other low angle faults probably exist, but the mylonite stratigraphy does not permit these to be traced.

(2) Extensional faults.

Figure 3 shows steep east to northeast-trending faults, probably extensional, which cut the entire sequence but usually show vertical displacements of less than 50 metres. Good field evidence exists for many of the faults shown, the remainder being inferred from airphoto interpretation. Only one fault noticeably offsets the granite facies, and some are traceable as zones of close-spaced joints extending into the intrusion. It is suggested that the faulting immediately preceded intrusion of the granite.

Where the southernmost of two east-west faults is exposed immediately northwest of the Mindy showing (UTM 459240) is exposed, carbonate breccia is locally converted to diopside-pyrrhotite-(scheelite) skarn, indicating that the fault zone has acted as a conduit for hydrothermal fluids.

The thick marble unit (C) is partly or completely bounded to the west by a fault dipping about 45°SW (UTM425232). The north-south faults are probably related to granite emplacement.

At the Mindy prospect, micro-faulting abounds: near-vertical normal faults cut the upper skarn every few metres. Most of the faults are downthrown to the west a few centimetres to a metre.

(3) Fields

The outcrop pattern of the major lithologic units indicates a gentle warping of the mylonitic sequence with sheet dips of up to ten degrees. Small-scale structures suggestive of later folding are not evident.

MINERALIZATION

The Mindy Prospect, UTM 463237 (MINFILE 105C 054)

Although granite is not exposed at surface, it probably occurs at a shallow depth below the Mindy showing. An exotic skarn mineralogy is present. Fig. 8 shows the outcrop geology of the Mindy prospect, and a longitudinal section through it. Two skarn/marble horizons occur in outcrop. An upper unit of calc-silicate hornfels and skarn about 2 m thick is exposed in a cliff. The hornfels shows alternating bands of birefringent, sector-twinned red grossular garnet and diopside grading to a central skarn of massive garnet with coarse vesuvianite. The coarse skarn contains scheelite crystals up to 5 mm across (visual estimate $<0.3\%$ WO_3). The exposures show abundant metre-spaced, small-scale, extensional faults with 10-50 cm of movement, downthrown to the southwest. Thin sections show fracturing normal to the layering and some re-crystallization of the fracture cleavage fabric is evident. The upper horizon is considerably more aluminous than the pure calcite marble of the lower horizon (maximum values of 0.13% MgO, 0.65% FeO and 3.30% MnO were obtained from microprobe analyses of calcite from the lower layer). Kwak (1987) classified such skarns as bimetasomatic, implying transfer of Al and Si from surrounding pelite, and Ca in the opposite direction, across an original limestone/pelite contact.

The lower skarn-marble horizon is up to 15 metres thick in surface exposures and can be traced discontinuously along strike in exposures and float for 1100 metres (see Fig. 8). From south to north the skarn mineralogy changes as follows:

(1) Diopside-actinolite-humite-fluorite-pyrrhotite (surface exposure).

(2) Massive marble with vein skarns of pale brown garnet-arsenopyrite and green (pure andrandite) garnet-diopside-fluoborite. In diamond drill core the marble is tectonically thickened to 80 metres and contains prograde vein skarns up to a metre thick. The massive marble consists of wollastonite $\pm$ garnet and the vein skarns consist mainly of andradite-arsenopyrite.

3) Massive magnetite-diopside-vesuvianite-garnet-epidote-cassiterite-pyrrhotite-chalcopyrite skarn, with highly variable proportions of the above minerals. This skarn contains several rare borates:

vonsenite - a $Fe^{+3}(Fe^{+3},Sn^{+4})O_2BO_3$ to $Mg_2(Fe^{+3},Sn^{+4})O_2.BO_3$ series,
hulsite - a $Mg_2(Fe^{+3},Sn^{+4})BO_4$ to $Fe^{+2}(Fe^{+2},Sn^{+4})BO_5$ series, and
fluoborite - $Mg_3BO_3(F,OH)_3$.

Other borate minerals have yet to be positively identified. (Surface exposure and diamond drill core: see Fig. 9).

4) Impure marble with bands of diopside-pistacite-clinozoisite-scapolite (surface exposures).

The skarns comprise prograde pyroxene-andradite or calcite-scapolite rich assemblages which have been replaced by actinolite, then later by phlogopite- or epidote/chlorite-rich retrograde skarn containing significant tin.
The mineralized assemblages show successive replacement by magnetite, fluorite, cassiterite, vonsenite and hulsite then fluoborite. Magnetite-rich sections have a very low sulphide content.

Between and below the skarns, a succession of metre-sized phacoids of grit and subarkose occur in a pelitic matrix, intercalated with cherty cataclasite. In outcrop, bedding is obliterated by pressure solution cleavage, but can it be recognized in thin section from grading, and lies at a low angle to the flat-lying cleavage. Cleavages in some of the sandy layers show some recrystallization, indicating that the cleaveage formed prior to thermal metamorphism. Cordierite is developed in pelitic layers.

Two types of significant microstructures are recognized: pervasive pressure solution stripes in the pelite and quartzite, which cut the shallow-dipping (up to 15°) lithologic contacts at a low angle, and less common, steeply-dipping fractures containing fluorite and tourmaline which cut brecciated quartzite below the lowest skarn. The low-angle cleavage is related to regional mylonite formation (c.f. Byrne, 1984: S2). The steeply-dipping fractures are believed to be related to the high-angle east-west extensional faults, which probably formed the conduit for metasomatizing and mineralizing fluids at the Mindy prospect.

In Australia, Kwak and Askins (1981) demonstrated that quartz-cassiterite lodes may exist beneath skarn tin deposits, provided there is adequate vertical separation between the granite contact and the skarn. There appears to be good potential for drill targets of this type beneath the Mindy prospect. Newmont's drill logs from the Mindy prospect (Nebocat and Oneschuck, 1981) described several "bleached zones" in silty mylonite above the lower skarn, and bleaching can still be seen around fractures in surviving remnants of the core. Kwak (1987) attributed such bleaching of graphite-bearing sediments above skarns to oxidation of the sediment by rising $CaCl_2$ rich solutions associated with skarn formation.

Diamond drill core (hole 4) shows a phacoid of calcite marble surrounded by diopside skarn, and massive andradite where the foliation curves around it. Away from the phacoid, wollastonite layers define the foliation. A strikingly similar texture is seen in sheared, brecciated marble at the Ork aureole, where calcite-rich phacoids occur in a more magnesian matrix (UTM 425234)(Fig. 6). The textural evidence suggests that at least some of the magnesian skarns at Mindy may reflect the chemistry of the marble after the layers were dismembered and redistributed by cataclasistic processes. Formation of the main skarn minerals then required only the addition of silica, and in places iron.

Table 1 shows that prograde skarn pyroxenes have variable MgO/FeO ratios but are predominantly diopside.

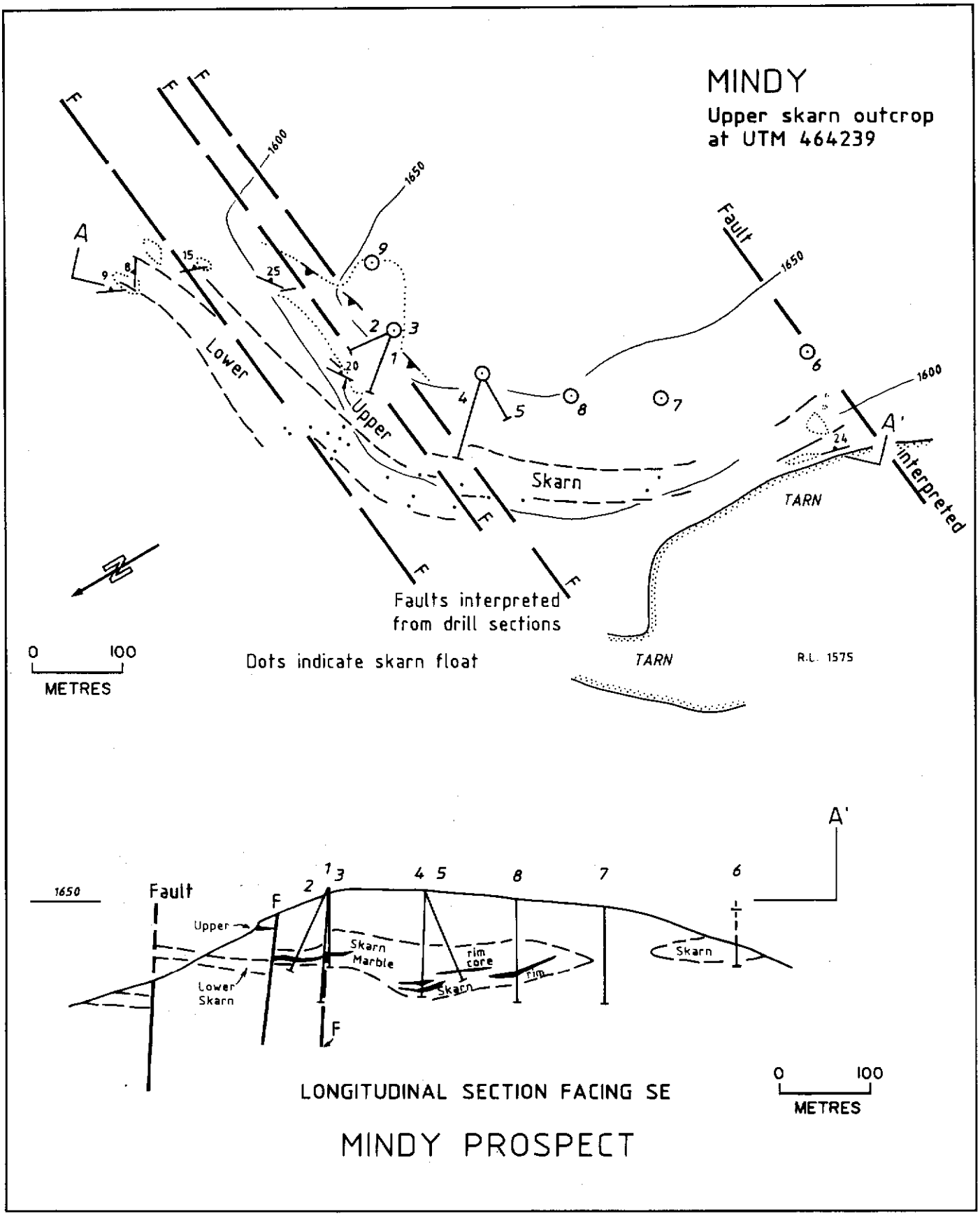

Figure 8. Geology of the Mindy prospect.

Mineralized skarns have erratic MgO/FeO ratios on a centimetre scale, and pyroxene compositions range from diopside to ferrosalite, reflecting iron introduction during mineralization. Garnets (table 2) are andradite and vary only in iron and manganese content. No significant amounts of MgO or Al_2O_3 were noted. Skarn mineral paragenesis is summarized in Table 3.

DISCUSSION:

Granites

Four granitic facies were observed: porphyry/diorite, even-grained microgranite, megacrystic biotite granite and highly leucocratic topaz-fluorite granite. The globular mafic enclaves noted in the porphyry facies are considered clear evidence of magma mixing early in the intrusion process. The porphyry could represent remnants of a linear intrusion controlled by an east-west extensional fault that preceded the main granite emplacement. The model for tin granites proposed by Plimer (1987) involves passive introduction of water-poor magma in regional extensional shear zones, and the formation of a pressure-quenched carapace which allows internal crystallization of the intrusion. Fluid release by hydro-fracturing and repeated hydrothermal activity introduces mineralization to the aureole and causes the development of porphyritic textures and oscillatory zoning of feldspars in the outermost phase of the pluton. Such features are characteristic of the Thirtymile stock.

The low angle of the intrusive contacts around the Thirtymile stock indicates that roof of the pluton may lie less than a few hundred metres below the central ridge of the Thirtymile Range. The leucocratic facies may therefore represent a highly differentiated facies in the roof of a cupola.

A metasomatic subsolidus origin was proposed by Stone and Exley (1985) for fluorine-rich granite in the Cornubian Batholith. However, such a concentration of fluorine in Thirtymile Stock can be explained by extreme differentiation. This would be consistent with the occurrence of the fluorine-rich facies as frequent small sills and dykes. The occurrence of biotite mostly as interstitial grains, as in the microgranite and megacrystic facies, is cited by Plimer (1987) as evidence of high fluorine fugacity. Future research will investigate whole rock major and trace-element chemistry, and the mica chemistry of the various facies, particularly with regard to the elements Mg, Li, Fe^{2+}, Fe^{3+}, Cl, F, and Sn. The degree of specialization of the facies and the tin content in the granite will also be examined (see Henderson and Martin, 1989; Scott, 1988).

Skarn Mineralogy

The classification of Sn and W skarns by Kwak (1987) can be applied to the skarns in the Thirtymile Range. The following features of Kwak's type II-2a skarns are relevant to the Mindy skarns:

(a) Tin skarns can be both magnetite and silicate-rich if associated with high B and F.

(b) Tungsten and most tin skarns have high pyrrhotite to pyrite ratios.

(c) There is no correlation between the tin content of skarns and the magnetite or sulphide content. However, if a magnetite-rich assemblage does occur, it hosts 75% of the tin.

(d) Tin and tunsten show an inverse relationship. The upper skarn at the Mindy deposit contains scheelite but no tin minerals and would conform to Kwak's magnesian bimetasomatism type (type II) as it grades from massive vesuvianite skarn through garnet to calc-silicate hornfels and pelite. Kwak also noted that the type of Fe-bearing skarn minerals formed varies with oxygen fugacity. Where an early, oxygen-rich fluid, presumably derived from a magnetite series granite interacts with graphite-free marble, an andradite garnet skarn is the result. If oxygen fugacity is low due to reduction of the fluid by graphite, a Ca-Fe pyroxene and either grossularite or anorthitic plagioclase is formed. In the main carbonate/skarn section of the Mindy prospect, where the original carbonate was mostly pure calcite, prograde andradite (vein) skarns are found. At the northern limit of exposure, where relict carbonates are almost black, a more varied mineralogy has resulted. Kwak (1987) also noted that if the original sediments contain graphite, the reduction of fluids released during skarn formation produces bleached zones. In the upper Mindy skarn, where thin carbonate layers are tectonically interlayered with pelitic cataclasites, bleaching occurs adjacent to cross-cutting veins, indicating oxidation by fluids exhausted by the metasomatism.

Based on Kwak's table of mineral assemblages (Kwak, 1987: table 8.2) the Mindy deposit belongs to the oxidized magnetite type. The retrograde borate-rich skarn assemblages of the mineralized lower horizon possibly reflect a magnesian marble protolith in that limited area.

Extensional Faulting

The Mindy prospect lies immediately south of an east-west fault. This fault probably controlled the mineralization by providing a conduit for fluid rising from the buried pluton. Continued tectonism during contact metamorphism probably allowed the operation of a continuous crack-seal mechanism described by Bucher-Nurminen (1989), and minerals were deposited along small-scale fractures. This hypothesis is supported by the following evidence:

(a) An exposure of the east-west fault on the ridge 750 m west of Mindy tarn shows a calcite breccia partly replaced by pyroxene and mineralized with pyrrhotite and

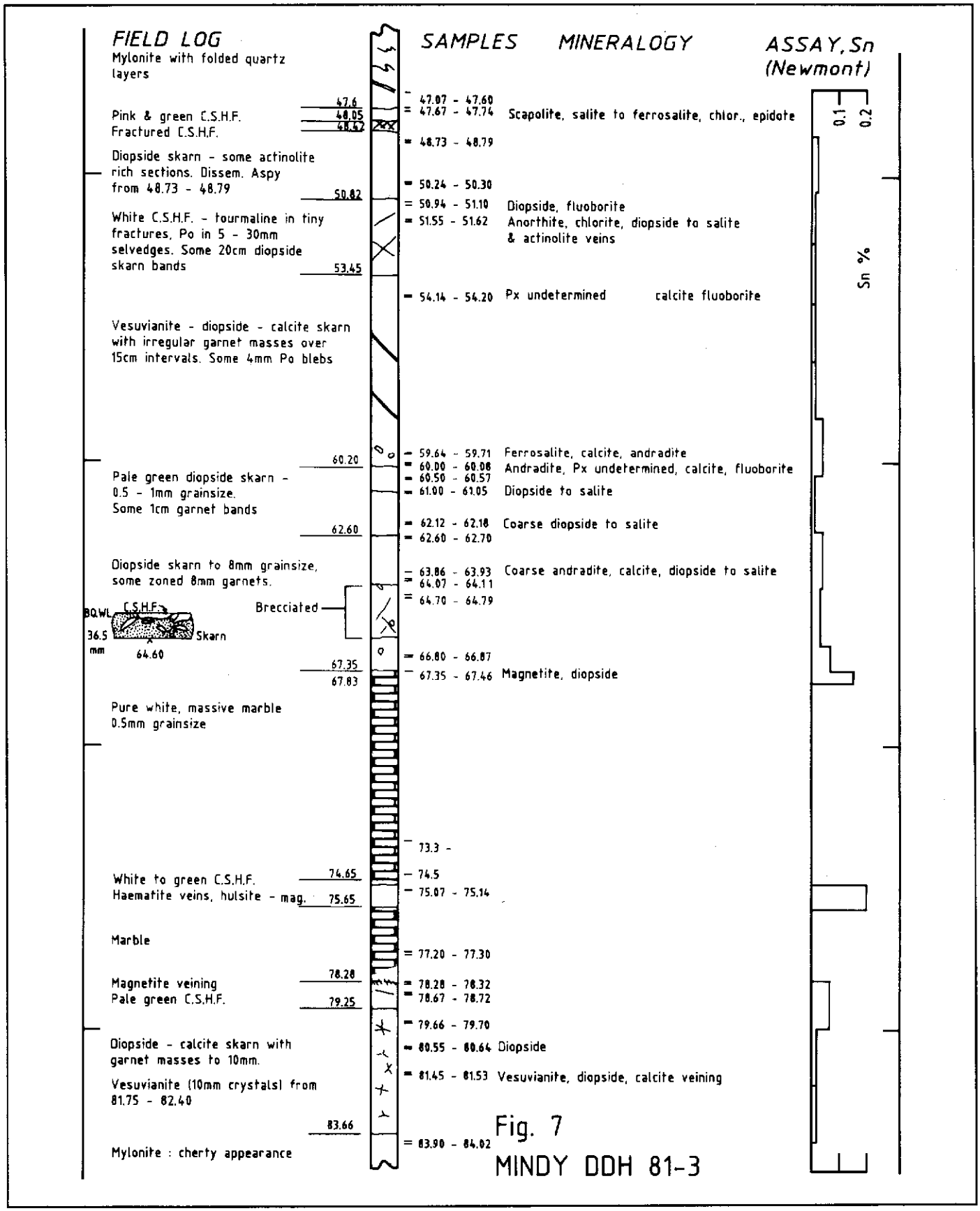

Figure 9. Field and drill section through the Mindy prospect.

scheelite, indicating fluid transfer up the fault to a level some hundreds of metres higher than the Mindy.

(b) Cherty mylonite in the deepest drill core from Mindy shows fractures mineralized with pyrrhotite or tourmaline and fluorite, which cut the near horizontal pressure solution fabric at a steep angle.

(c) The garnet-vesuvianite skarn is highly fractured in places, indicating hydraulic fracturing probably followed primary skarn development.

(d) Many small, zoned retrograde skarn veins are developed along fractures in the marble.

CONCLUSIONS

The Thirtymile Range consists of cataclasites derived from Middle Palaeozoic to Mesozoic siliciclastic and carbonate sediments which have been deformed by:

(1) cataclasis and transposition in broad shear zones.

(2) low angle thrust faulting, the full extent of which is unknown.

(3) high-angle extensional faults striking east-west, which predate the emplacement of mid-Cretaceous granitic plutons. Some movement appears to have continued during emplacement of the granite.

(4) moderate-angle normal faults striking north-south, which appear to be contemporaneous with granite emplacement.

Skarns formed in the aureoles of the granites contain tin-tungsten-boron-fluorine mineralization. Carbonate units (mega-boudins) in the cataclasite sequence formed a stratigraphic control on the location of mineralization.

Extensional tectonics are believed to have controlled the granite emplacement and provided the conduits for movement of tin- and tungsten-mineralizing fluids in the overlying sediments. Small-scale movement on the faults continued during mineralization, allowing successive mineralization of steeply dipping veins in carbonate megaboudins by a fracture-reaction-seal mechanism. Tin and tungsten-bearing stockworks may well exist within the extensional fault systems.

On the east side of the Range, at the Mindy prospect (MINFILE 105C 054), very coarse skarn is developed with a highly variable mineralogy. Boron and fluorine are associated with the later stages of mineralization. Scheelite is confined to the upper (bimetasomatic) skarn unit, and the first retrograde skarn assemblage at the southwest limit of the main skarn, where no tin is evident. There is clearly an inverse relationship between the occurrence of W and the occurrence of Sn.

On the west side of the range, hornfels more than 100 m thick is sporadically developed in cataclastic dolomite but coarse skarn is absent. At the Ork prospect (MINFILE 105C 38), boron occurs as axinite along micro-fractures in the hornfels, and fluorine occurs as fluorite at the granite contact. The JC syndicate documented, but did not adequately test, geochemical anomalies in the Ork area. The 100 metre thick carbonate section which overlies the "specialized" granitic stock is mostly covered by glacial drift and appears to have excellent exploration potential for tin and tungsten deposits.

ACKNOWLEDGEMENTS

The Exploration and Geological Services Division of the Department of Indian Affairs and Northern Development provided the majority of helicopter time and other support for this fieldwork. Encouragement and useful discussion were provided by J.G. Abbott, S.R. Morison, T. Bremner and J.A. Morin. Supervision has been provided by Dr Ken McClay and Dr D.H.M. Alderton. Much assistance was given by Dr A. Hall, Dr G. Marriner, Ian Gill and Grahame Lawes at the Royal Holloway and Bedford New College, University of London.

REFERENCES

ARMSTRONG, R.L., 1988. Mesozoic and early Cenozoic magmatic evolution of the Canadian Cordillera. In: Clark, S.P., Burchfiel, B., and Suppe, J., (eds), Processes in continental lithospheric deformation. Geological Society of America Special Paper 218.

BUCHER-NURMINEN, K., 1989. Reaction veins in marbles formed by a fracture-reaction-seal mechanism. Eur. Journal of Mineralogy, Vol. 1, p. 701-714.

BYRNE, T., 1984. Early deformation in melange terranes of the Ghost Rocks formation, Kodiak Islands, Alaska. In: Raymond, L.A. (ed.), Melanges: their nature, origin and significance. Geological society of America, Special Paper 198, p. 21-51.

CHANDRA KUMAR, S., 1988. Microgranular enclaves in granitoids: agents of magma mixing. Journal of Southeast Asian Earth Sciences, Vol. 2, p. 109-121.

CHAPPELL, B.W., WHITE, A.J.R. and WYBORN, D., 1987. The importance of residual source material (restite) in granite petrogenesis. Journal of Petrology, Vol. 28, p. 1111-1138.

DAWSON, K.M. and DICK, L.A., 1978. Regional metallogeny of the Northern Cordillera: tungsten and base-metal bearing skarns in southeastern Yukon and southwestern MacKenzie. In: Current Research, Part A; Geological Survey of Canada, Paper 78-1A, p. 287-292.

DIDIER, J., 1987. Contribution of enclave studies to the understanding of origin and evolution of granitic magmas. Geologische Rundschau, Vol. 76, p. 41-50.

GORDEY, S.P., 1981. Stratigraphy, structure and tectonic evolution of Southern Pelly Mountains in the Indigo Lake area, Yukon Territory. Geological Survey of Canada; Bulletin 318, 44 p.

HENDERSON, C.M.B. and MARTIN, J.S., 1989. Compositional relations in Li-micas from S.W. England and France: an ion- and electron- microprobe study. Mineral Magazine, Vol. 53, p. 427-449.

KWAK, T.A.P., 1987. W-Sn skarn deposits and related granitoids. Developments in Economic Geology, Vol. 24, Elsevier, 451 p.

KWAK, T.A.P. and ASKINS, P.W., 1981. Geology and genesis of the F-Sn-W (-Be-Zn) skarn (wrigglite) at Moina, Tasmania. Economic Geology, Vol. 76, p. 439-467.

KWAK, T.A.P. and NICHOLSON, M., 1988. Szaibelyite and fluoborite from the St. Dizier Sn-borate skarn deposit, NW Tasmania, Australia. Mineral Magazine, Vol. 52, p. 713-716.

KWAK, T.A.P. and TAN, T.H., 1981. The geochemistry of zoning in skarn minerals at the King Island (Dolphin) mine. Economic Geology, Vol. 76, p. 468-497.

MULLIGAN, R., 1963. Geology of Teslin map area, Yukon Territory. Geological Survey of Canada Memoir 326, 96 p.

NEBOCAT, J., 1981. Unpublished drill logs and assessment report, Newmont Exploration of Canada Limited.

PLIMER, F.R., 1987. Fundamental parameters for the formation of granite-related tin deposits. Geologische Rundschau, vol. 76, p. 23-40.

RAYMOND, L.R., 1984. Melanges: their nature, origin and significance. Geological Society of America, Special Paper 198, 170 p.

SCOTT, K.M., 1988. Phyllosilicate and rutile compositions as indicators of Sn specialization in some southeastern Australian granites. Mineralium Deposita, Vol. 23, p. 159-165.

STONE, M. and EXLEY, C.S., 1985. High heat production granites of southwest England and their associated mineralization: a review. In: High heat production (HHP) granites, hydrothermal circulation and ore genesis; Institute of Mining and Metallurgy, London, p. 571-593.

TEMPELMAN-KLUIT, D.J., 1979. Transported cataclasite, ophiolite and granodiorite in Yukon: evidence of arc-continent collision. Geological Survey of Canada, Paper 79-14, 27 p.

VERNON, R.H., 1983. Restite, xenoliths and microgranitoid enclaves in granites. Journal and Proceedings of the Royal Society of New South Wales, Vol. 116, p. 77-103.

VERNON, R.H., ETHERIDGE, M.A. and WALL, J.V., 1988. Shape and microstructure of microgranitoid enclaves: indicators of magma mingling and flow. Lithos, Vol. 22, p. 1-11.

TABLE 1: PYROXENE ANALYSES (Microprobe).

The range shown is for the lowest and highest silica analyzed in the one thin section. The number of analyses per section is shown in brackets.

(1) Pyroxene-dominated skarns with little or no mineralization:

DIOPSIDE TO SALITE PYROXENE:

SAMPLE		SiO_2	CaO	MgO	FeO	MnO	
50.94 (4)		From	55.4	26.3	16.5	1.8	0.5
		to	55.1	25.6	15.7	2.2	0.2
61.00 (6)		From	55.9	26.5	15.8	2.5	0.3
		to	52.4	25.4	9.1	12.6	1.3
62.12 (8)		From	55.8	26.7	15.7	1.9	0.3
		to	53.0	25.3	9.5	11.4	1.5
67.35 (4)		From	55.9	26.3	15.7	1.8	0.5
		to	54.6	26.7	15.4	2.8	0.6
80.55 (13)	From		56.4	26.7	16.2	1.2	0.2
		to	54.9	26.5	15.2	2.7	0.4
81.45 (16)	From	56.7	27.2	16.3		-	
		to	55.3	26.9	16.3	1.1	0.2

(2) Skarns with mostly garnet or retrograde assemblages and significant mineralization:

SALITE TO FERROSALITE PYROXENE:

47.67 (4)		From	52.8	24.7	10.2	9.8	1.0
		to	51.5	24.1	6.6	17.0	1.2
51.55 (4)		From	56.1	26.1	15.9	1.5	0.4
		to	54.6	25.9	12.3	6.7	0.6
52.05 (1)			51.9	22.7	9.1	15.0	1.1
59.64 (2)		From	52.1	24.3	6.5	15.5	2.5
		to	51.0	24.5	6.1	16.9	2.2
63.86 (7)		From	54.9	27.1	14.8	2.6	0.4
		to	53.4	25.1	12.0	7.5	1.8

TABLE 2: GARNET ANALYSES (Microprobe)

ANDRADITE:

59.64 (2)		From	38.1	35.4	0.0	17.1	1.4
		to	38.1	35.1	-	17.2	1.2
60.00 (11)	From	38.0	34.7	-	21.7	1.3	
		to	37.0	34.7	-	22.6	0.8
63.86 (1)			37.0	34.1	-	25.9	0.7

TABLE 3: SKARN MINERAL PARAGENESIS

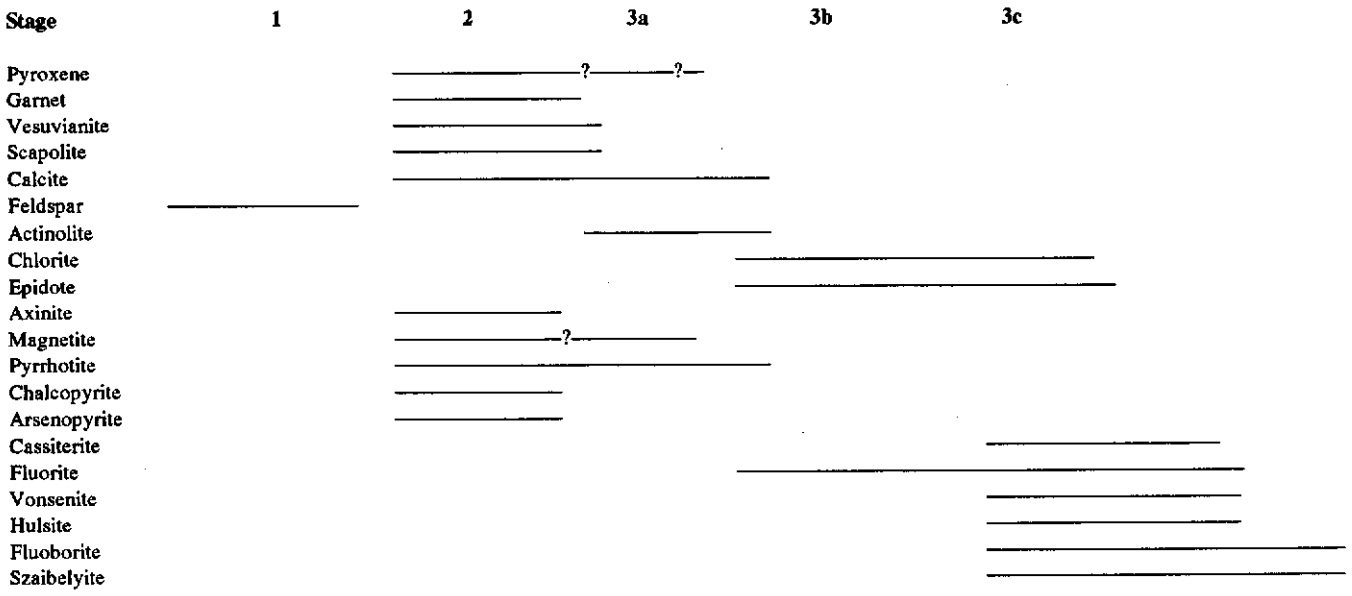

1 = Primary (prograde) skarn, including vein skarns.
2 = First retrograde skarn
3a = Hydrous retrograde alteration
3b = Main tin mineralization
3c = Late fluorine mineralization

A PLIENSBACHIAN SUBMARINE SLOPE AND CONGLOMERATIC GULLY-FILL SUCCESSION: RICHTHOFEN TO CONGLOMERATE FORMATION TRANSITION (LABERGE GROUP), BRUTE MOUNTAIN, YUKON

John R. Dickie
Centre for Marine Geology,
Dalhousie University
Halifax, Nova Scotia
B3H 3J5

and

Frances J. Hein
Geology Department
University of Calgary
Calgary, Alberta
T2N 1N4

DICKIE, J.R., and HEIN, F.J., 1992. A Pliensbachian submarine slope and conglomeratic gully-fill succession: Richthofen to Conglomerate Formation transition (Laberge Group), Brute Mountain, Yukon. In: Yukon Geology, Vol. 3; Exploration and Geological Services Division, Indian and Northern Affairs Canada, p.71-86

ABSTRACT

The diachronous Richthofen-Conglomerate Formation transition separates lithostratigraphic subunits of the Jurassic Laberge Group, Whitehorse Trough. The contact is superbly exposed on the west flank of Brute Mountain, south-central Yukon. This succession of Pliensbachian marine shales, sandstones and conglomerates records submarine gully and slope apron progradation. Distal prodelta shales and sandstones, conglomeratic chute/gully fill sequences, slope shales and slope conglomerates were deposited from the Middle Pliensbachian to the Early Toarcian.

Submarine chutes fed coarse clastic detritus past the shelf-break and across the slope. Ponding of coarse-grained mass flows built an onlap wedge against the slope, followed by deposition of mud turbidites and pelagic sediments. A rise in relative sea level continued during the deposition of the entire succession, suggesting the intercalated sequence formed as a result of variations in the rate of clastic input. The Brute Mountain succession is entirely of deep marine origin, typical of Laberge Group exposures elsewhere in the Whitehorse Trough.

Collision between the allochthonous Lewes River Arc and the cratonic margin of North America occurred during the Late Triassic. The final stages of convergence led to closure of the Whitehorse Trough seaway in the Middle Jurassic. Laberge Group strata record this closure. Brute Mountain exposures of late Early Jurassic age indicate that deep basin conditions existed at least into the Toarcian. Slope turbidite and pelagic sedimentary rocks place additional constraints on the timing of arc-continent collision. Significant shoaling of the Whitehorse Trough seaway apparently did not occur until after deposition of the Brute Mountain sequences.

RÉSUMÉ

La transition diachrone de la formation de Richtofen à la formation de Conglomerate sépare des sous-unités lithostratigraphiques du groupe jurassique de Laberge dans la dépression de Whitehorse. Le contact est magnifiquement mis à nu sur le flanc occidental du mont Brute dans la partie méridionale centrale du Yukon. Cette succession de shales, de grès et de conglomérats marins du Pliensbachien révèle la progradation sous-marine de ravins et d'une plaine alluviale. Des shales et des grès prodeltaïques distaux, des séquences de comblement conglomératique d'entailles et de ravins, des shales de talus et des conglomérats de talus ont été déposés du Pliensbachien moyen au Toarcien précoce.

Des entailles sous-marines acheminaient des débris clastiques au-delà de la rupture de pente et sur le talus. L'accumulation d'écoulements en masse de granulométrie grossière a construit un biseau d'aggradation contre le talus après quoi il y a eu dépôt de turbidites vaseuses et de sédiments pélagiques. Une élévation du niveau relatif des mers s'est poursuivie pendant le dépôt de toute la succession, ce qui suggère que la séquence intercalée doit sa formation à des variations des taux d'apport en matériaux détritiques.

Le succession du mont Brute, entièrement d'origine marine profonde, est caractéristique des affleurements du groupe de Laberge ailleurs dans la dépression de Whitehorse. Les unités intercalées consistent en séquences superposées de conglomérat et de shale.

La collision de l'allochtone de l'arche de Lewes River et de la marge cratonique de l'Amérique du Nord s'est produite au Trias tardif. Les derniers stades de convergence ont mené à la fermeture du passage marin de la dépression de Whitehorse au Jurassique moyen. Cette fermeture est documentée dans les couches du groupe de Laberge. Les affleurements datant de la fin du Jurassique précoce au mont Brute indiquent que des conditions de bassin profond se sont prolongées au moins jusqu'au Toarcien. Des turbidites de talus et des roches sédimentaires pélagiques limitent davantage dans le temps la collision arc-continent. Il n'y a apparemment eu diminution importante de la profondeur dans le passage marin de la répression de Whitehorse qu'après le dépôt des séquences du mont Brute.

INTRODUCTION

Brute Mountain is situated approximately 9 km south of Carcross and 4 km east of Bennett Lake in Carcross map area (105D-2), southern Yukon. The Brute Mountain locality lies north of the southern extremity of the Whitehorse Trough in Yukon (Fig. 1). It exhibits excellent outcrop exposure of the contact between two Lower Jurassic formations of the Hettangian to Bajocian Laberge Group within the Whitehorse Trough. This Pliensbachian to Toarcian succession consists of (1) a basal 80+ m thick argillaceous unit consisting of finely interbedded greywacke and grey-black silty mudstone; (2) 208 m of thick, massive, polymictic pebble to cobble conglomerate, grading laterally to volcanic litharenite and epiclastic (tuffaceous) greywacke that interdigitates with Unit (1) along-strike; (3) an upper, 80 m thick argillaceous succession of very finely laminated, very fine-grained sandstone and silty mudstone couplets associated with internally graded cherty mudstone; and (4) an overlying, laterally extensive sequence of massive pebble-cobble conglomerate 180 m thick (Figs. 2; 3).

An Early Jurassic age was determined from ammonite biochronozones. This, combined with its sedimentologic character, identified the Brute Mountain section as part of the Jurassic Laberge Group. In particular, the Richthofen and Conglomerate Formations of Tempelman-Kluit (1985) are represented. As part of a sedimentologic analysis of the Laberge conglomerates (e.g. Dickie and Hein, 1988; Dickie, 1989), the Brute Mountain study serves to (1) document diachroneity across the contact separating the Richthofen and Conglomerate Formations of the Laberge Group; (2) describe Jurassic deep-sea sediment mobilization and transport dynamics in terms of process and depositional environment; and (3) provide evidence for a deep Anvil Ocean (i.e. seaway between the Lewes River Arc and the Jurassic North American passive margin) prior to Middle Jurassic overriding of the cratonic margin by a volcanic arc terrane (Tempelman-Kluit, 1979).

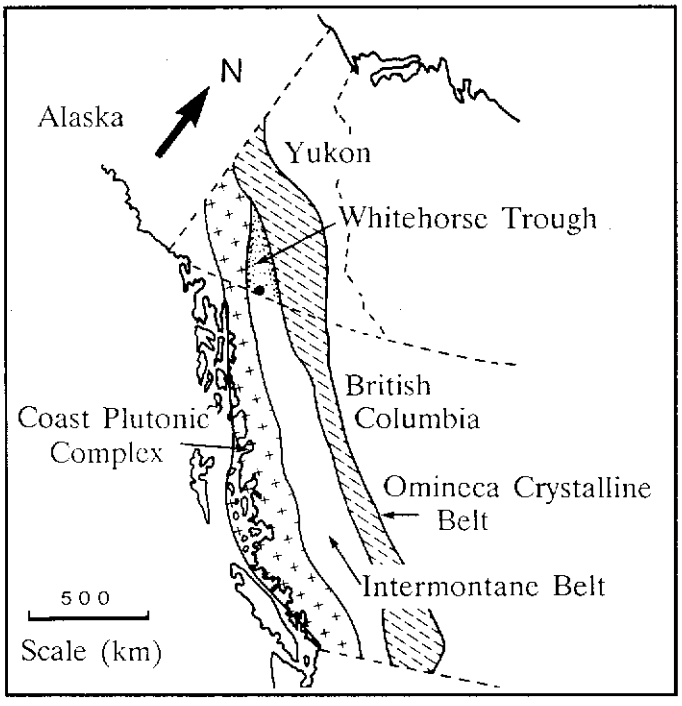

Figure 1. Location of Brute Mountain within the Whitehorse Trough. The Omineca Crystalline Belt, Intermontane Belt and Coast Plutonic Complex are depicted.

Brute Mountain stratigraphy and sedimentology was studied through detailed (bed-by-bed) and regional reconnaissance mapping. Facies stacking trends were tested by Harper's (1984) modified Markov Chain Analysis, involving statistical weighting of high probability facies transitions. The results were subsequently tested by the iterative proportional fitting method of Turk (1979). High probability facies sequences, thus determined, were interpreted in terms of flow mechanisms and environment. Maximum

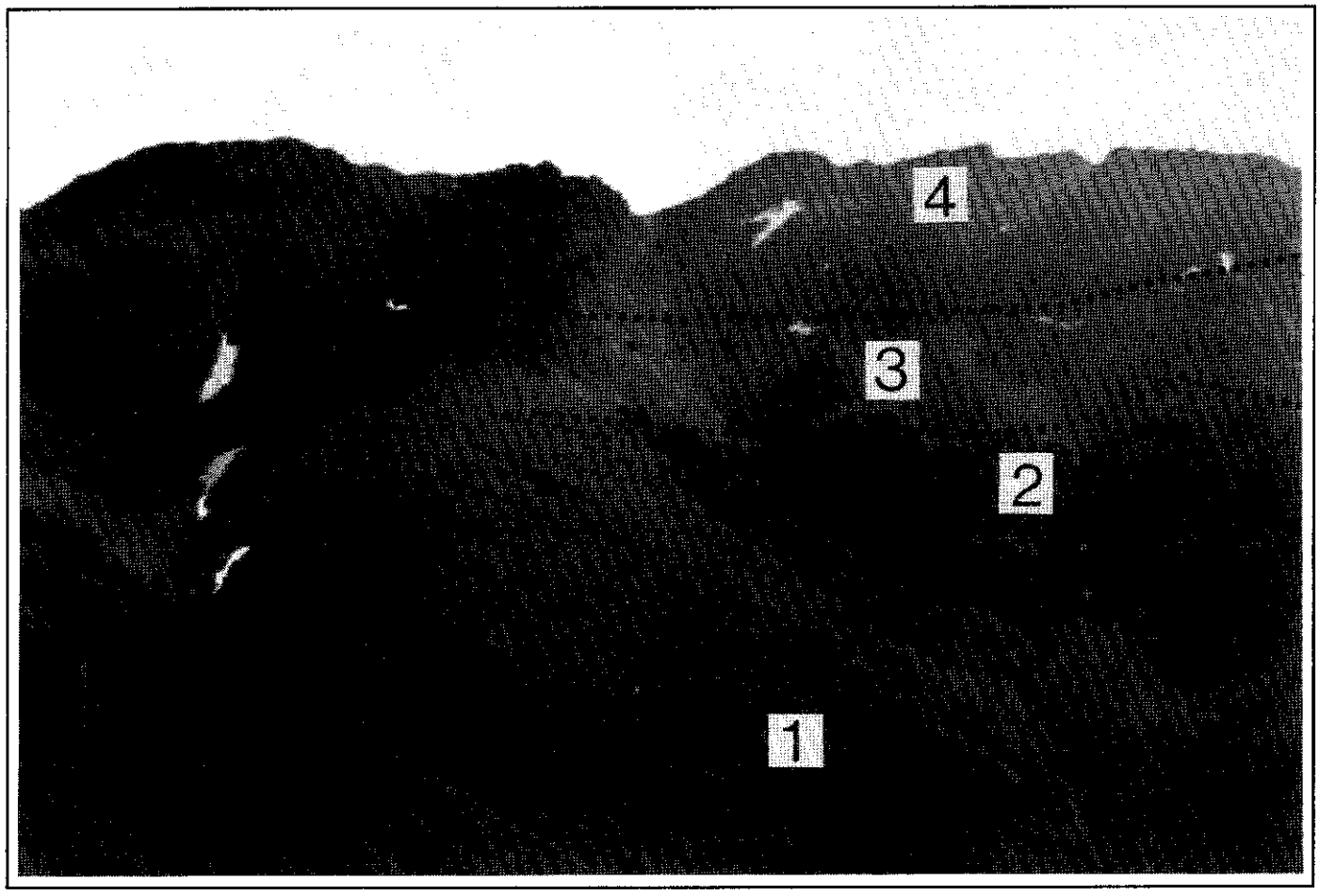

Figure 2. Brute Mountain exposure of the Laberge Group. Units 1-4 are depicted, as is the intercalated margin of Unit (2) where it fines laterally from conglomerate to sandstone. Units 1 and 3 are part of the Richthofen Formation, whereas Units 2 and 4 represent the Conglomerate Formation.

particle size (MPS) and bed thickness (Bth) trends, plotted against stratigraphic height, revealed how sequences fit within larger successions (megasequences) depicting temporal flow competence variations. Moving averages of MPS and Bth data assisted in separating large (i.e. sequence and megasequence) progradation/regression trends from bed-scale perturbations.

JURASSIC WHITEHORSE TROUGH EVOLUTION

The Mesozoic Whitehorse Trough is a northwest-trending, asymmetric, remnant forearc basin (Tempelman-Kluit, 1979; Morrison, 1981; Hansen, 1987; 1988). This basin extends from northern British Columbia into south-central Yukon. Situated between the Omineca Crystalline Belt to the east and Coast Plutonic Complex to the west, the Whitehorse Trough delimits the northern extent of the Intermontane Belt of the Canadian Cordillera. Whitehorse Trough strata and allochthonous terranes to the west are separated from autochthonous North American lithotectonic assemblages in the east by the Teslin Suture Zone (Fig. 4).

Coarse-grained conglomerates and associated facies of the Early Jurassic Laberge Group record forearc evolution during the final stages of arc-continent collision. The Lewes River volcanic arc (northern Stikine Terrane?) appears to have collided initially in the Latest Triassic (e.g. Monger et al., 1982). Basin fill characteristics of the Whitehorse Trough western belt (Wheeler, 1961) support a probable Rhaetian-Hettangian collision (Dickie, 1989). Convergence between the arc terrane and the miogeoclinal edge of North America was oblique (Hansen, 1987; 1988), typical of most plate collisions (Fitch, 1972). Tectonic transport of forearc slivers proceeded in the direction of the transverse component of oblique convergence (c.f. Fitch, 1972; Beck, 1983). The resulting arcward-stepping, dextral transpressive faults (Hansen, 1987; 1988) suggest that the accretionary complex abutted the continental margin, overriding the subduction trench in the process. Mechanical flexure of the basin between colliding blocks contributed to the development of the basin and long-term subsidence of the forearc.

Arc-continent collision led to tectonic incision and exhumation (uplift) of the arc plutons. Laberge conglomerate

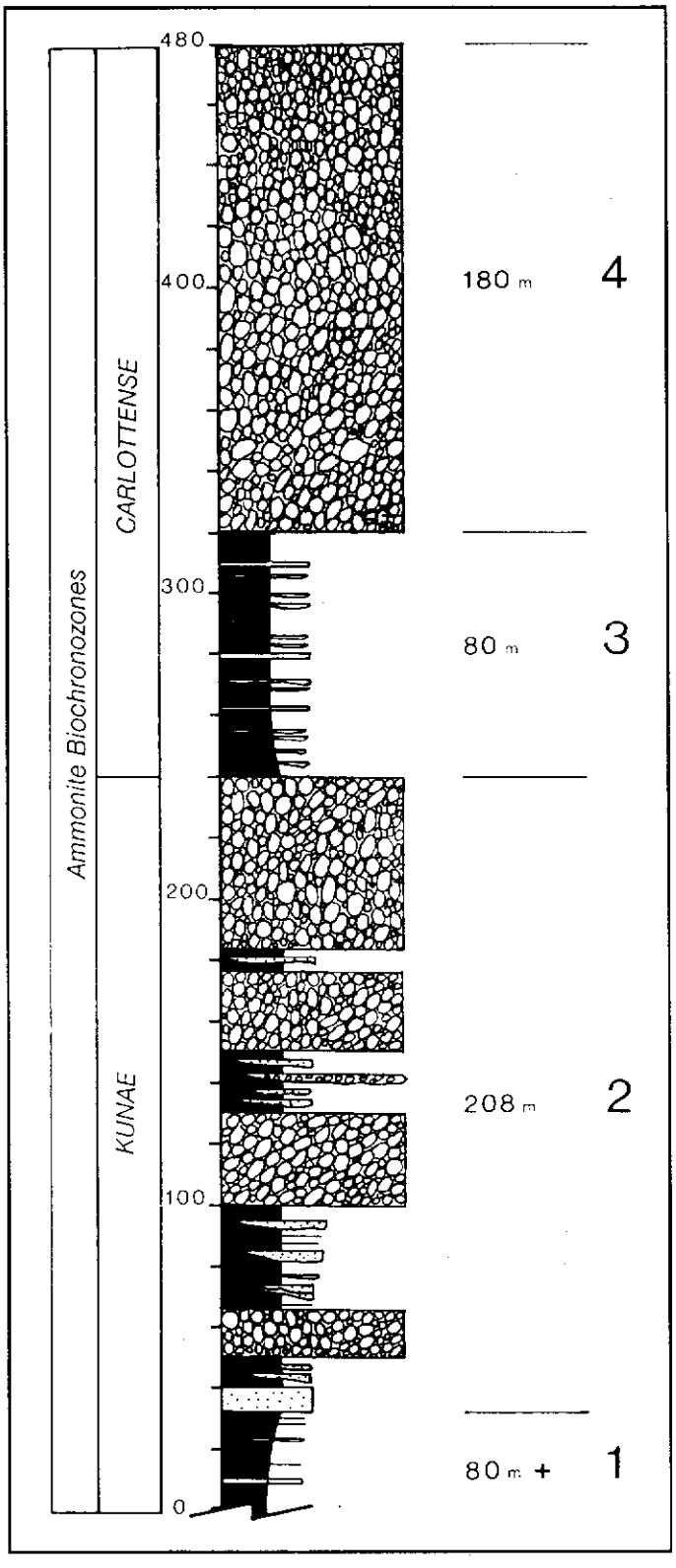

Figure 3. Generalized stratigraphy of the Brute Mountain section. Units 1-4 are shown (refer to Fig. 2). Ammonite biochronozones, defined from collections taken from organic shales, were used to define relative ages of strata.

petrographic evolution documents a progressive unroofing and dissection of the arc through a vertical decrease in volcanic clasts (e.g. basalt-andesite; saussurite; augite porphyry; agglomerate) and a concomitant increase in arc-derived plutonic clasts (e.g. megacrystic, lightly to non-foliated hornblende-biotite granodiorite; pink, megacrystic quartz monzonite; quartz diorite; leucogranite) (Dickie, 1989).

SEDIMENTOLOGY OF THE BRUTE MOUNTAIN SUCCESSION

Unit (1): Lower Argillite

Argillaceous strata, consisting of non-graded sandstone-mudstone couplets (Figs 5a-b; facies 4.1) and subordinate graded sequences (facies 4.2), reflect cyclic alterations of fine-grained bedload (distal, lower regime hyperpycnal flows) and suspension fallout of silt and clay. Graded beds display partial Bouma (1962) sequences (Fig. 5c). T^a and T^{ab} sequences are abundant, while truncated T^b and T^{bc} sequences are less common. Graded sandstone beds are capped by either T^e division mudstones or hemipelagite (rarely siliceous mudstone). Graded sandstones are the product of medium concentration, sandy turbidity currents. Synsedimentary compressional faults and folds are typical of steep-gradient systems. Downslope slip caused deformation of unconsolidated to semi-consolidated interbedded sand and mud.

Ammonites collected by the first author (identified by H. Tipper, Geological Survey of Canada) from Unit (1) shale (GSC Loc. No. C-117413) include Amaltheus c.f. stokesi, Fucinoceras sp., and Protogrammoceras (?). This collection places these strata in the Lower Kunae Zone of the late Middle Pliensbachian (Tipper, 1989, pers. comm.). Preserved organic debris occurs with authigenic pyrite horizons. Zoophycos trace fossils indicate poorly oxygenated, organic-rich bottom sediments. Unidentified, subvertical tubular burrows were formed as suspension feeders burrowed through unconsolidated turbidite sand.

Non-graded, variably stratified very fine-grained sandstones occur interbedded with organic-rich mudstones. Facies, sequences and Zoophycos trace fossils categorize this shale unit as being of distal prodelta/shelfbreak to upper slope origin (Frey and Pemberton, 1984). Submarine mass-flow beds and slide deformation suggest a fairly steep gradient system. These features are commonly associated with steeper gradients typical of continental slopes. Unit (1) shales were likely deposited in a distal prodelta-upper slope environment.

Unit (2): Lower Conglomerate

Unit (2), dominated by polymictic pebble-cobble (to boulder) conglomerate (Fig. 5d), overlies and laterally interfingers with Unit (1) shales. Graded-stratified (Fig. 6), clast-supported (ungraded), matrix-supported (coarse-tail) normally graded, and matrix-supported (coarse-tail) inversely

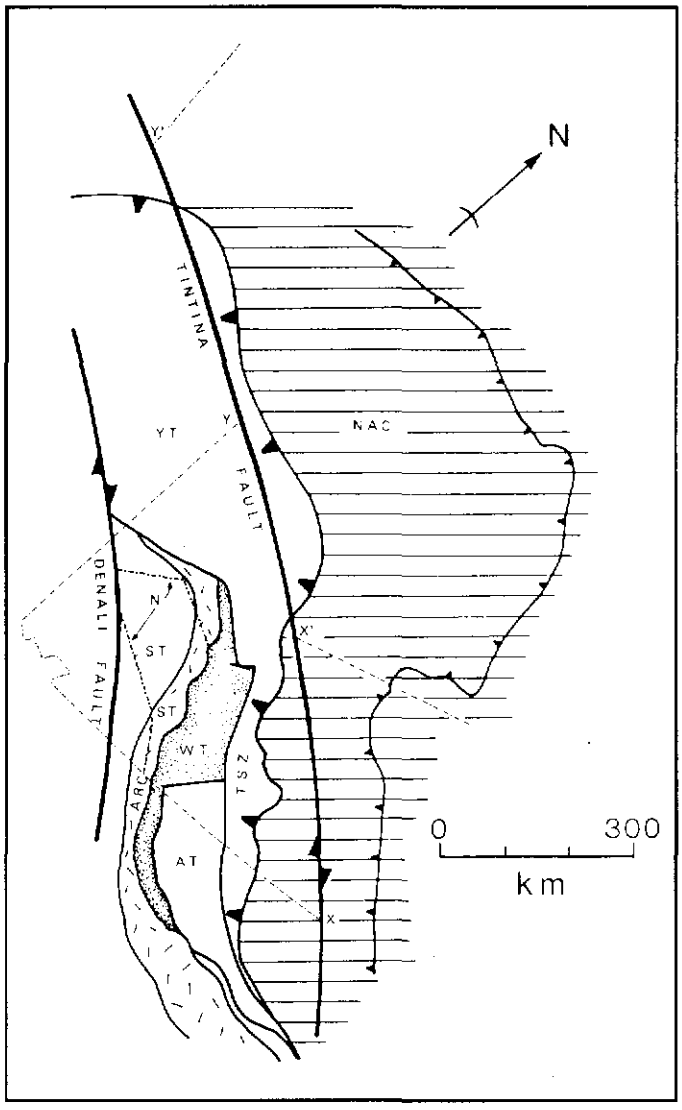

Figure 4. Northern Cordilleran terranes prior to 450 km of dextral strike-slip along the Tintina Fault (after Tempelman-Kluit, 1979). Reconstruction to present conditions may be reached by matching X-X' and Y-Y'. Terranes are depicted as: YT-Yukon Tanana Terrane; ST-Stikine Terrane (subdivided into Lewes River Arc (arc) and possible northern Stikinia; N-known exposures of Nisling Terrane; NAC-North American Craton; TSZ-Teslin Suture Zone. Hachures represent (small) present eastern extent of Cordilleran deformation and (large) Mesozoic deformation belt.

graded conglomerate form the dominant facies (facies 9.1, 10.2, 11.1 and 11.2, respectively). Unit (2) also contains lesser pebbly sandstone (facies 8.1), massive sandstone (facies 6.1), upper regime plane bed sandstone (facies 5.1), and combined-flow origin wavy stratified sandstone (facies 5.3).

Unit (2) coarse-grained facies are almost invariably of mass-flow origin, primarily representing cohesive and cohesionless debris flow sediment transport mechanisms. Graded-stratified conglomerate (facies 9.1) formed during velocity fluctuations in high-concentration, turbulent flows. Flows expanded laterally from cohesionless gravel dispersions and experienced frictional effects from the bounding chute walls. Internal organization of conglomerate beds extends from a disorganized core to graded-stratified (organized) margins.

Markov Chain Analysis (Harper, 1984) revealed two high-probability facies sequences. These consist of (1) turbidite sandstone-cohesionless debris flow conglomerate-hyperconcentrated flow pebbly sandstone (Figs. 7; 8), and (2) ungraded sandstone/mudstone-upper plane bed sandstone-wavy stratified sandstone-ungraded sandstone/mudstone (cyclic relationship). Sequence-scale trends (i.e. 10's m thick), observed in MPS and Bth plots, (Fig. 9) are representative of prograding mass flows.

Sequence 1 sandy turbidites preceded cohesionless debris plugs, perhaps being a product of flow dilution and gravitational bedload separation. Subsequent cohesive flows, possibly due to chute side-wall collapse, followed existing bathymetric contours (slide scars), yet true channelization is not evident. Mudstone rip-up clasts, which exhibit an a-b plane-parallel (relative to bedding) fabric, suggest erosion by turbulent flows. Orientation of clasts and their positions within beds indicates that slowing flows lost erosive energy, leaving clasts suspended above the bed by a combination of turbulence and dispersive pressure. Oriented clasts within cohesive flows may have experienced migration away from the high shear stresses generated along the base of the flow. Sequence 2 exhibits a predominance of bedload transport over mass transport. Storm waves modified suspended sediment during frictional freezing of thin, short periodicity turbidity flows. Storm surge entrainment of sand preceded cyclic resedimentation to a deeper water zone near storm wavebase. Wavy stratified sandstone is a product of combined flow (oscillatory storm currents and unidirectional mass-flow) and serves as an estimate of storm wavebase. Storm-generated structures in deep-water facies imply a fetch sufficiently large that larger storm waves (i.e. lowered wavebase) can be generated before impinging the coast.

Megasequence characteristics (Fig. 9) document the aggradation of mass-flow conglomerate sequences. These grade northwestward into sandstones and, eventually, into Unit (1) shales. To the southeast, conglomerate forms a monotonous stacked succession lacking shale interbeds. Channels are not evident; scouring of the substrate was minimal. The succession represents stacked mass-flow chute or gully fill sequences, combined to form a slope onlap wedge.

Unit (3): Upper Argillite

Unit (3) contains rare ungraded sandstone/mudstones (facies 4.1). Graded successions containing truncated turbidite

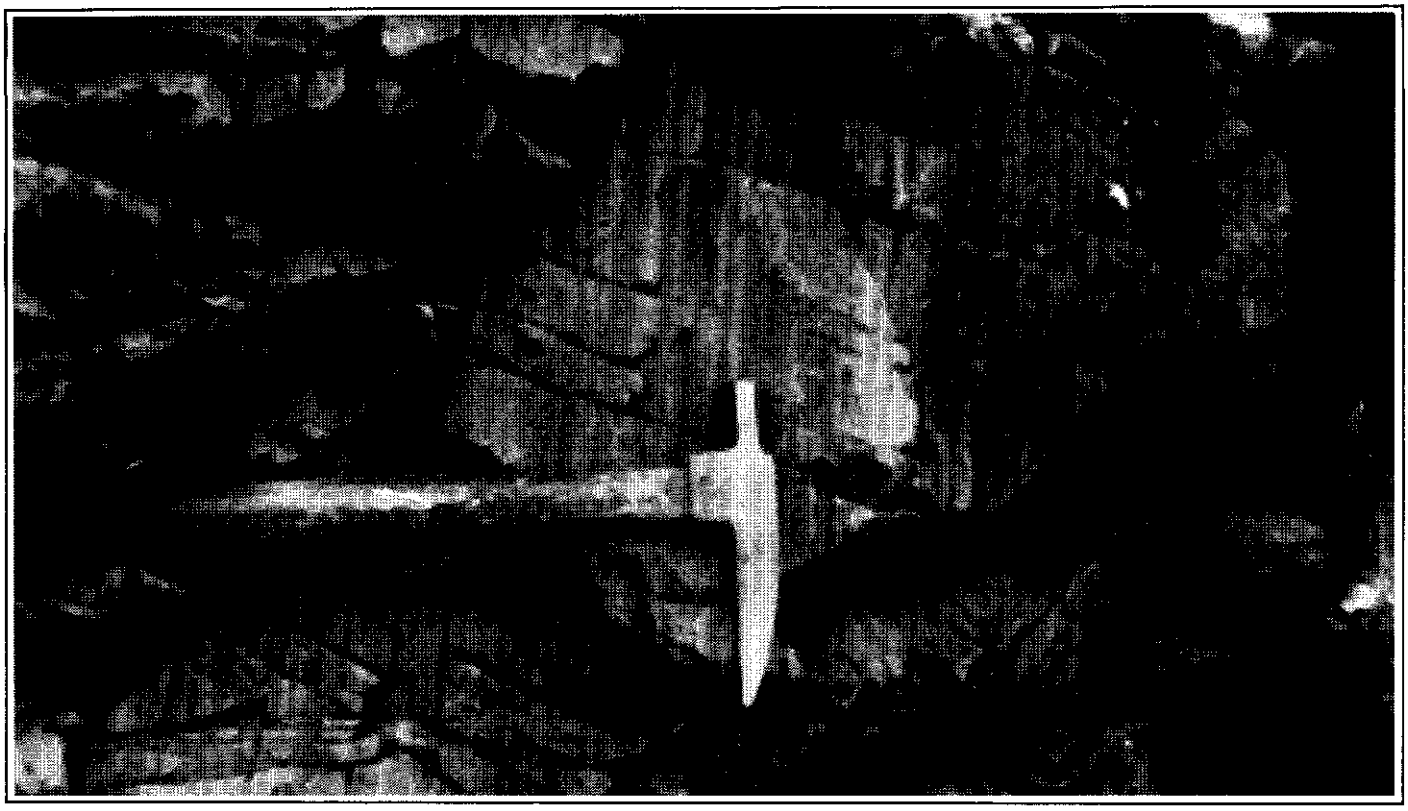

Figure 5a. Heterolithic facies 4.1, consisting of interbedded, ungraded sandstone and mudstone. Hammer for scale.

Figure 5b. Load-deformed ripple trains in ungraded sandstone-mudstone. Graded sandstone bands lie immediately above the lens cap.

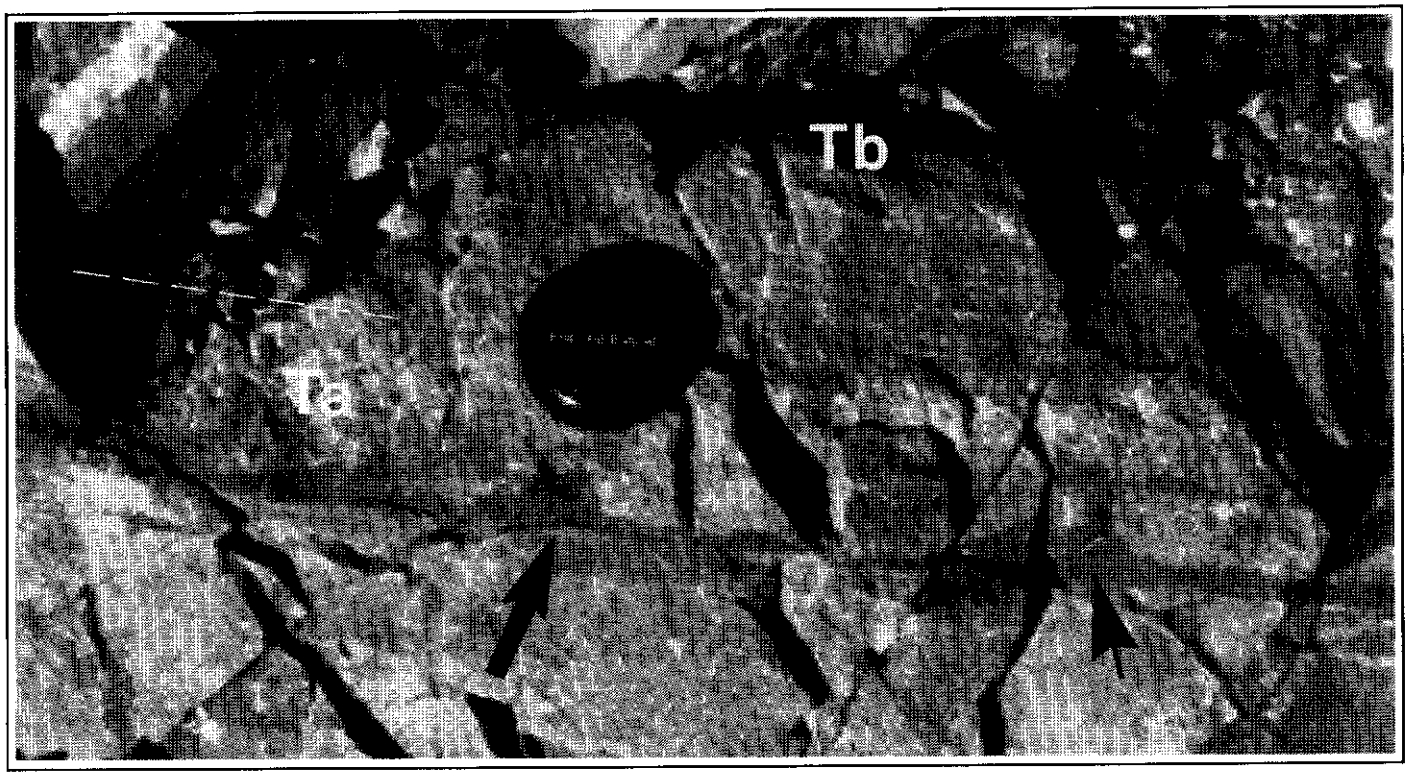

Figure 5c. Partial Bouma sequence in medium-grained sandstone. Ta and Tb divisions are marked. Rapid sediment loading caused load-injection of mudstone tongues (arrows) into the overlying sandstone during rapid fluid expulsion.

Figure 5d. Clast-supported cobble-boulder conglomerate (facies 10.2) with lens cap for scale. Note medium-grained to megacrystic biotite-hornblende granodiorite (pale clasts). A subangular clast of interbedded cross-stratified sandstone/black mudstone lies to the immediate upper left of the lens cap. This indicates certain cohesionless debris flows obviously possessed erosive turbulent energy, yet such clasts are exceedingly rare at this locality and tend to be restricted to the base of Unit (2).

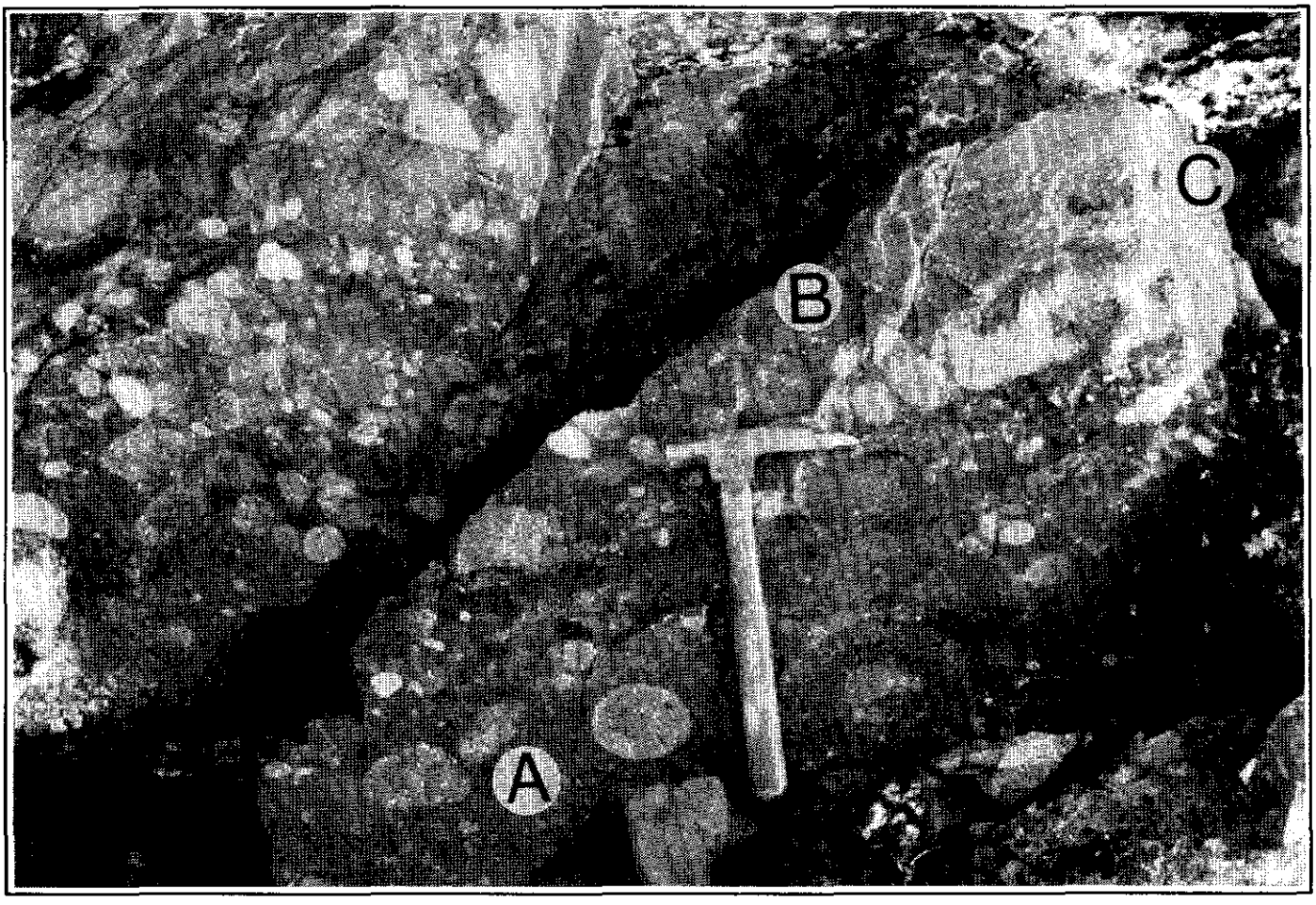

Figure 6. Graded-stratified conglomerate (facies 9.1). A: basal zone of massive, clast-supported conglomerate (cohesionless dispersion/ debris flow); B: medial zone of planar-stratified gravel; C: upper zone, containing upper plane-beds in medium-grained sandstone.

divisions are abundant, yet tend to be fine-grained and thin. Banded, cherty mudstone (to siltstone) is abundant higher in the section. While thinly bedded mudstones are locally massive, T^{2-6} mud turbidite divisions (Stow and Shanmugam, 1980) are abundant.

Banded mudstone was deposited by low-concentration turbidity currents and possible pelagic fallout. Authigenic pyrite is common, and tends to be associated with ammonite-bearing horizons. Planar pyritic and organic laminae formed along a highly reducing, oxygen poor and (seawater) sulphate-rich substrate.

Ammonites from Unit (3) (GSC Loc. No. 117414), including Protogrammoceras paltum, Protogrammoceras aff. pectinatum, Tiltonoceras aff. propinquum and Tiltonoceras facetum(?) belong to the Carlottense biochronozone of the uppermost Pliensbachian (H. Tipper, 1989, pers. comm.). Burrows are rare, but possible Zoophycos suggests a deep, poorly oxygenated environment. Locally, Nereites trace fossils occur. These are typical of bathyal settings which are frequently overrun by turbidity currents (Frey and Pemberton, 1984).

Deep marine trace fossils, pelagic fauna (ammonites), and extremely distal mass-flow processes (mud turbidites and associated facies) indicate a slope (to rise?) system.

Unit (4): Upper Conglomerate

Sequential stacking of clast-supported and matrix-supported conglomerate has created a conglomerate lithozone that is traceable along strike for over 5 km (Hart and Pelletier, 1989). A statistically significant facies stacking order is not present. Instead, vertical facies arrangements tend to be chaotic. MPS and Bth trends show fining and bed-thickening upward trends, indicative of ponding of mass flow gravels across the slope (Fig. 10). The lateral persistence of both individual beds and the entire conglomerate lithozone (Unit 4) combined with chaotic vertical ordering of mass-flow facies suggests a slope-apron interpretation.

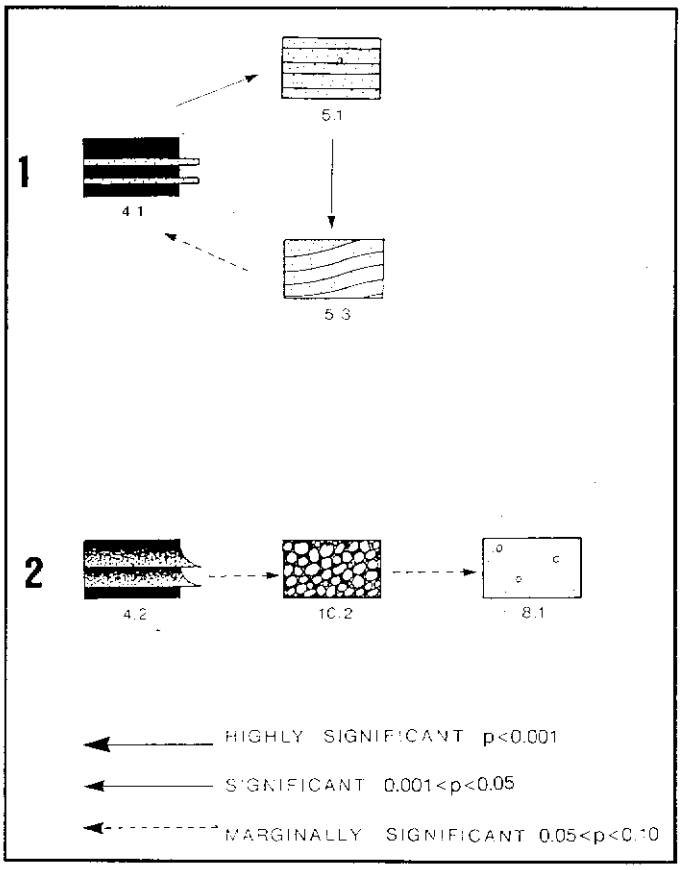

Figure 7. Statistically weighted facies transitions defining high-probability sequences. Sequence 1 shows a cyclic relationship between ambient prodelta shale sedimentation, later overrun by upper regime, plane-bedded sandstone and wavy-stratified (storm wavebase) sandstone. Sequence 2 defines a marginally significant succession between truncated turbidites, cohesionless debris flow-origin conglomerate, and pebbly sandstone (submarine hyperconcentrated flows).

DISCUSSION AND CONCLUSIONS

Sinemurian to Toarcian beds of the Conglomerate Formation overlie Hettangian to Pliensbachian (and Bajocian) Richthofen Formation shales throughout the Whitehorse Trough. Tempelman-Kluit (1985) described these units as formations of the Laberge Group, yet the units are strongly intercalated. They occur as laterally-equivalent lithozones, reflecting contemporaneous deposition of (coarse-grained) axial and (fine-grained) marginal portions of steep-gradient, mass-transport dominated submarine fans (Dickie, 1989). Lateral shifts in the locus of deposition, combined with variable sediment supply rates, created lithologic variability without a significant change in the environment of deposition. The intercalated and diachronous nature of the contact between these conglomerates and shales is well exposed at Brute Mountain. This stratigraphic relationship is inherent to the Laberge Group depositional systems as a whole. Thus, lithostratigraphic units may only have environmental significance in a very local sense.

Sedimentary facies, sequences and megasequences suggest that the Brute Mountain succession formed through an advancing prodelta lobe (Unit 1), entrenchment of a conglomeratic chute network (Unit 2), coarse-grained sediment "starvation" during chute/gully abandonment, continued deposition of deeper-water shales during a marine highstand (Unit 3), and ponding of mass flow gravel against the slope (Unit 4) (Fig. 11).

Based on the thickness of Unit (2) and the age range of Kunae and Carlottense ammonite zones (3.2 Ma) it is estimated that gravel accumulated at a rate of approximately 6.5 cm per thousand years. Considering that Unit (2) mass-flow conglomerates are typically 1-3 m thick, this low sedimentation rate suggests net bypass of the upper slope rather than accumulation in chutes. These conduits (chutes or shallow gullies) funnelled sediment deeper into the basin, preventing local buildup of gravel. Unit (3) shales document the cessation of coarse-grained sediment transport. These facies reflect even deeper marine conditions than those represented by Unit (2). Continued sea level rise coincided with a diminished gravel supply.

The Brute Mountain succession responded to continued marine transgression throughout the Middle to Late Pliensbachian. Stacking of Units 1-4 suggests variability in sediment supply rates, as opposed to transgressive and regressive control. No evidence exists for vertical shallowing; instead, facies indicate balanced sedimentation-subsidence rates. Gravel deprivation (Units 1 and 3) was compensated by continued deep-water, fine-grained processes.

Eustatic sea level charts for the Early to Middle Jurassic (Haq et al., 1987) show similarities to the trends expressed in the Brute Mountain section. However, long-term eustatic trends do not agree with these observed in the Whitehorse Trough, and coeval sections studied elsewhere in the basin exhibit a pronounced deviation from those of Brute Mountain (Dickie, 1989). While slope facies successions cannot be readily compared to shelf systems tracts, it must be possible to identify similar relationships (i.e. transgressive/ regressive) in slope basins where shelves are minimal or lacking. Bounding disconformities should be equivalent to conformable offlap successions in a slope setting (c.f. Haq et al., 1987).

A relative sea level rise due to tectonic subsidence is invoked to explain the depositional characteristics of the Brute Mountain succession. Sediment supply rates varied as a result of tectonic changes in the arc source area and possibly as a result of the activation of new feeder systems. The upper slope was an area of net sediment bypass until the Earliest Toarcian (Unit 4). At that time, gravel mass flows constructed a clastic apron parallel to the arc.

The presence of deep marine (i.e. slope) facies at Brute Mountain shows that a deep basin existed throughout the Pliensbachian and into the Toarcian. Thus, closure of the intervening seaway (Anvil Ocean - Whitehorse Trough)

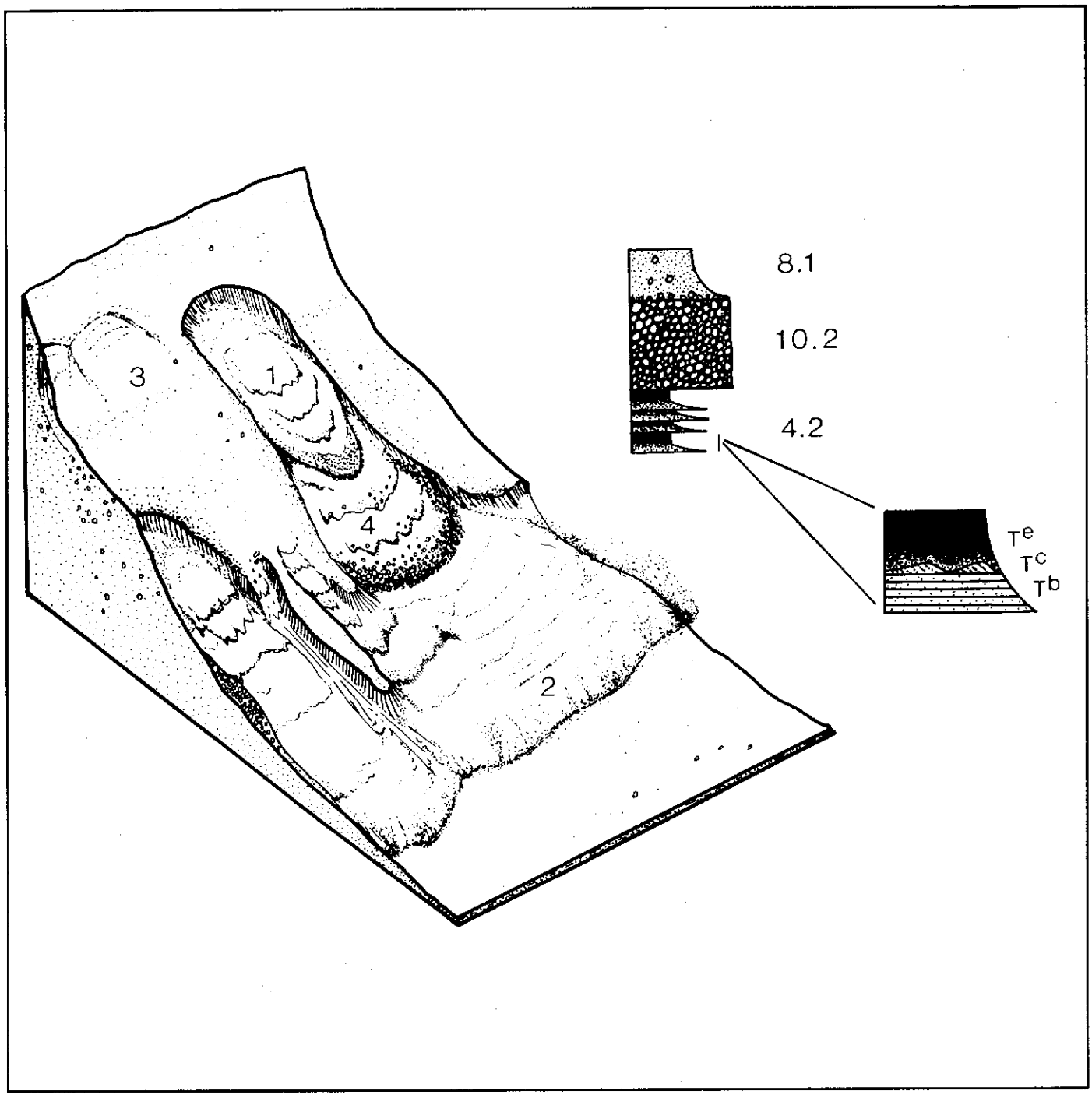

Figure 8. Schematic diagram showing the genetic interpretation of Sequence 2. 1: Facies 8.1 pebbly sandflow (hyperconcentrated) proceeds along a slide gully cut by the preceding mass flow. 2: The slide generates turbulence, homogenizing the flow and resulting in gravity-winnowing of fines (runout turbidite). 3: Incipient slide scar. 4: Cohesionless debris flow later overruns the turbidite apron.

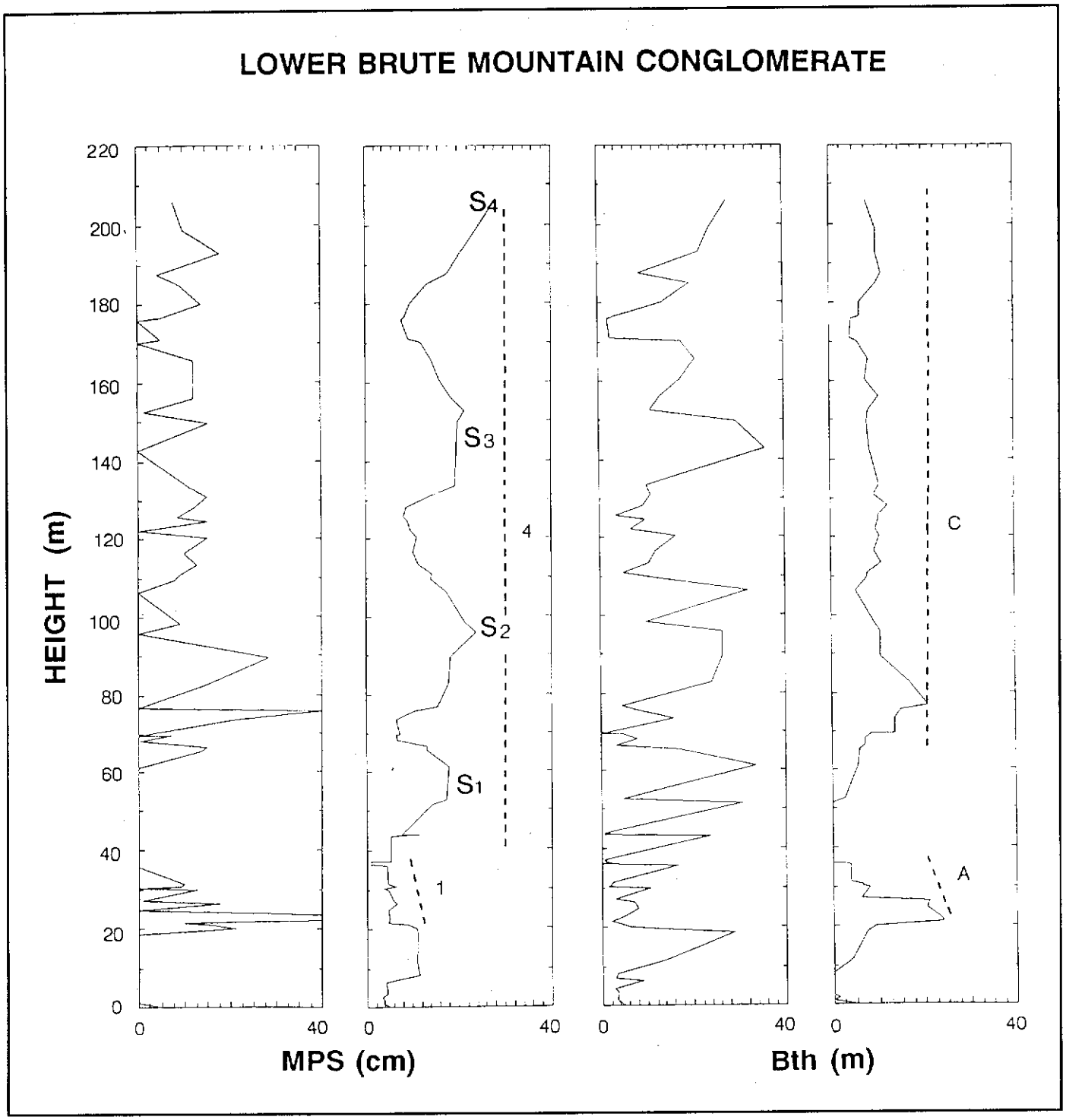

Figure 9. MPS and Bth trends for Lower Brute Mountain conglomerate (Unit 2). Mass-flow progradational sequences (S1-S4) are shown. The thick-bedded conglomerates of sequences 1-4 form an upward-fining and bed-thinning megasequence (1A) and an aggradational megasequence (4C). Plots, left to right, show raw and smoothed (3-point moving average) data for MPS (left two plots) and Bth (right two plots).

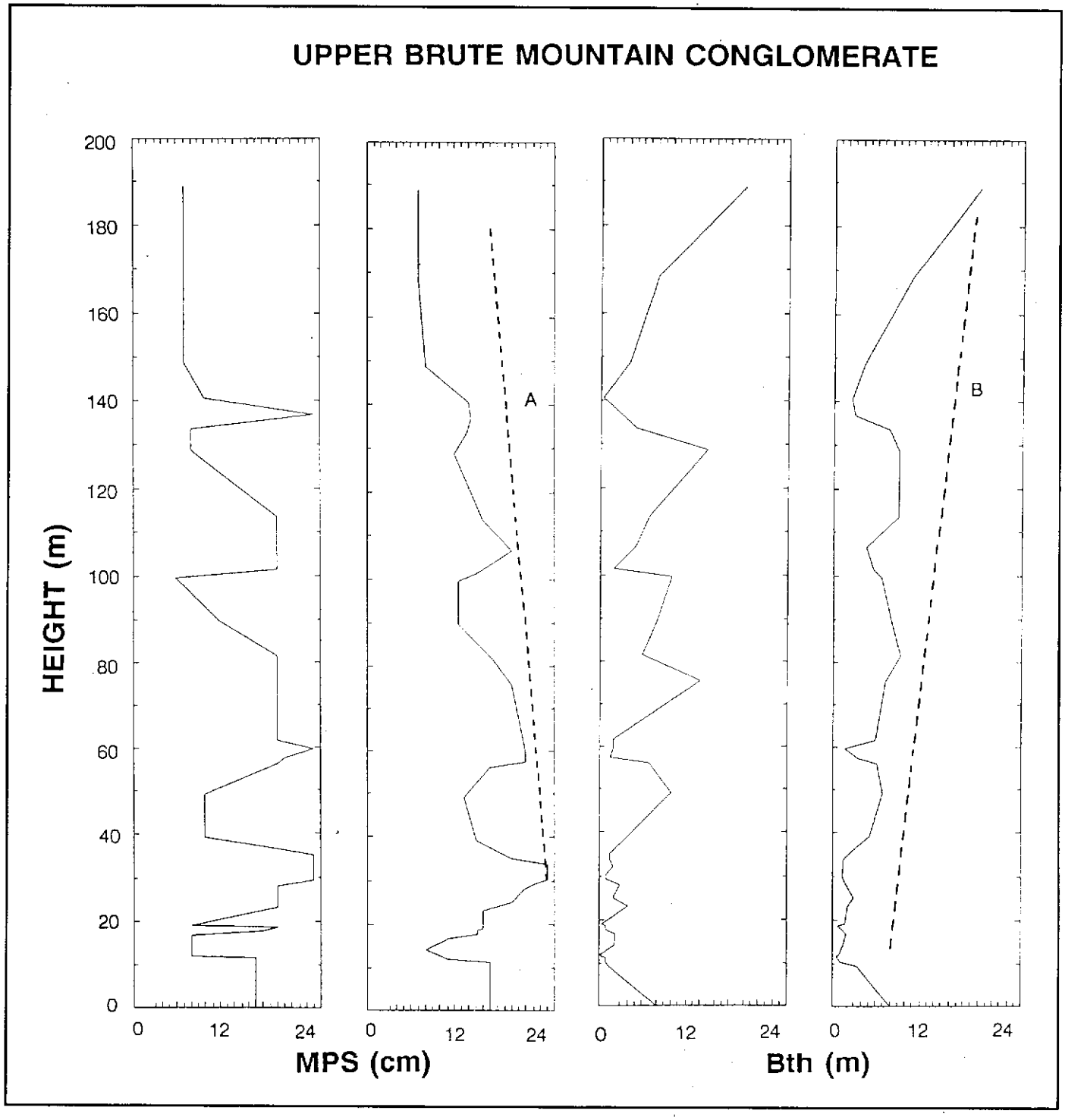

Figure 10. MPS and Bth trends for Upper Brute Mountain conglomerate (Unit 4). Coarsening-fining sequences correspond to thickening-thinning trends, suggestive of mass-flow ponding. Megasequence AB indicates long-term ponding and decreasing flow competence and possible source retreat. Raw (left) and smoothed (right; 3-point moving average) data are shown.

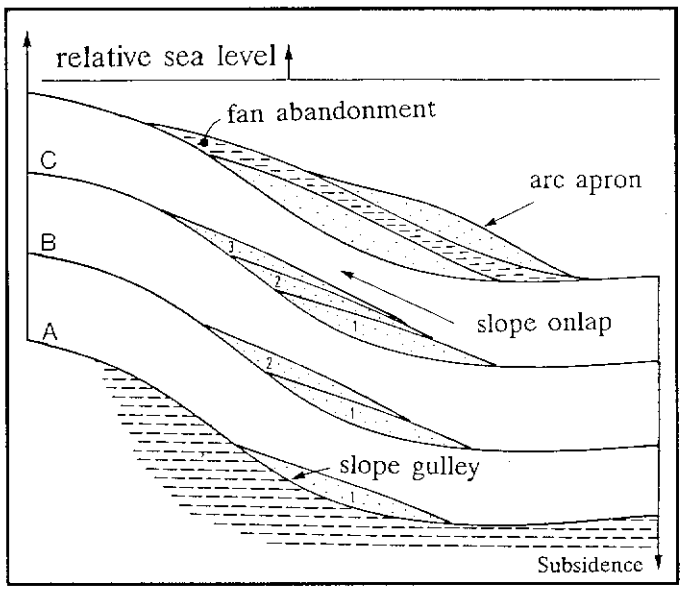

Figure 11. Schematic diagram depicting the general onlap relationship of the Brute Mountain succession. 1-3 represent successive sequences stacked against the upper slope, below the shelf break. Time series A-C (A is oldest) shows the general response to uplift and erosion in the sourceland coupled with tectonic subsidence across the slope and rise. Marine transgression continued during the cessation of coarse-grained input (Unit 3). (See text for additional discussion.)

between the Lewes River Island Arc and the North American continent did not produce the shallowing-upward successions expected of an infilling basin during this time. Significant closure of the Anvil Ocean basin and the start of arc obduction (c.f. Tempelman-Kluit, 1979) did not produce distinctive features in the stratigraphic record of the Whitehorse Trough until the Middle Jurassic.

ACKNOWLEDGEMENTS

The first author would like to thank Tom Pinkerton for able assistance in the field. Dr. Howard Tipper (Geological Survey of Canada) kindly identified ammonites collected by the first author. Craig Hart (Aurum Geological Consultants) released preprint copies of maps and was very informative during fascinating discussions on the geology of the Montana Mountain region. Funding and logistical support for the Brute Mountain study was through Exploration and Geological Services, Northern Affairs, Yukon, Canada, and a Northern Studies grant to J. Dickie.

REFERENCES

BECK Jr., M.E., 1983. On the mechanism of tectonic transport in zones of oblique subduction. Tectonophysics, Vol. 93, p. 1-11

BOUMA, A.H., 1962. Sedimentology of some Flysch Deposits: A Graphic Approach to Facies Interpretation. Elsevier: Amsterdam, 168 p.

COLEMAN, J.M., 1976. Deltas: Processes of deposition and models for exploration. Continuing Education Publication Company, Inc., Illinois, 102 p.

DICKIE, J.R., 1989. Sedimentary response to arc-continent transpressive tectonics: Laberge conglomerates (Jurassic), Whitehorse Trough, Yukon Territory. Unpublished M.Sc. thesis, Dalhousie University, Halifax, Nova Scotia, 365 p.

DICKIE, J.R. and HEIN, F.J., 1988. Facies and depositional setting of Laberge conglomerates (Jurassic), Whitehorse Trough, Yukon. In: Yukon Geology, Vol. 2; Exploration and Geological Services Division, Yukon, Indian and Northern Affairs Canada, p. 26-32.

FITCH, T.J., 1972. Plate convergence, transcurrent faults, and internal deformation adjacent to Southeast Asia and the western Pacific. Journal of Geophysical Research, Vol. 77, p. 4432-4461.

FREY, R.W. and PEMBERTON, S.G., 1984. Trace fossil facies models. In: Facies Models, R.G. Walker, (ed.); Geoscience Canada Reprint Series 1, p. 189-207.

HANSEN, V.L., 1987. Structural, metamorphic, and geochronologic evolution of the Teslin Suture Zone, Yukon: Evidence for Mesozoic oblique convergence outboard of the North American Cordillera. Unpublished Ph.D. thesis, University of Southern California, Los Angeles, California, 261 p.

HANSEN, V.L., 1988. A model for terrane accretion: Yukon-Tanana and Slide Mountain Terranes, northwest North America. Tectonics, Vol. 7, p. 1167-1177.

HAQ, B.Q., HARDENBOL, J., and Vail, P.R., 1987. Chronology of fluctuating sea levels since the Triassic. Science, Vol. 235, p. 1156-1166.

HARPER, C.W. (Jr.), 1984. Improved methods of facies sequence analysis. In: Facies Models, R.G. Walker, (ed.); Geoscience Canada Reprint Series 1, p. 11-13.

HART, C.J.R. and PELLETIER, K.S., 1989. Geology of Carcross (105D/2) and part of Robinson (105D/7) map areas. Exploration and Geological Services Division, Yukon, Indian and Northern Affairs, Canada, Open File 1989-1, 84 p.

MONGER, J.W.H., PRICE, R.A. and TEMPELMAN-KLUIT, D.J., 1982. Tectonic accretion and the origin of the two major metamorphic and plutonic welts in the Canadian Cordillera. Geology, Vol. 10, p. 70-75.

MORRISON, G.W., 1981. Setting and origin of skarn deposits in the Whitehorse Copper Belt, Yukon. Unpublished Ph.D. dissertation, University of Western Ontario, 306 p.

STOW, D.A.V. and SHANMUGAM, G., 1980. Sequence of structures in fine-grained turbidites; comparison of recent deep-sea and ancient flysch sediments. Sedimentary Geology, Vol. 25, p. 23-42.

TEMPELMAN-KLUIT, D.J., 1979. Transported cataclasite, ophiolite and granodiorite in Yukon: Evidence of arc-continent collision. Geological Survey of Canada, Paper 79-14, 27 p.

TEMPELMAN-KLUIT, D.J., 1985. Maps of Laberge (105E) and Carmacks (115I) map-areas. Geological Survey of Canada, Open File 1101.

TURK, G., 1979. Transition analysis of structural sequences. Discussion and reply. Geological Society of America Bulletin, Vol. 90, p. 989-991.

WHEELER, J.O., 1961. Whitehorse map-area, Yukon Territory 105D. Geological Survey of Canada, Memoir 312, 156 p.

Table 1. Summary facies table for Laberge conglomerates and associated lithofacies.

Class 1:	Micritic Limestone
Facies 1.1:	Micrite to Floatstone
Process:	Chemical precipitation of carbonate
Class 2:	Clastic limestone
Facies 2.1:	Calcarenite to rudite
Process:	Bedload transport; winnowing
Class 3:	Mudstone
Facies 3.1:	Red, desiccated silty mudstone
Process:	Suspension deposition of mud; minor tractional transport of silt to fine sand (cyclic); waning turbulent mass-flow; dehydration of mud; caliche development
Facies 3.2:	Red, bioturbated silty mudstone
Process:	Suspension deposition of mud (submarine); minor tractional transport of silt to fine sand under oscillatory flow; waning turbulent mass-flow; bioturbation by marine organisms
Class 4:	Heterolithic Facies
Facies 4.1:	Non-graded, interbedded sandstone-mudstone
Process:	Cyclic alteration of bedload sand transport with hemipelagic fallout. Minor current drift across ripple tops. Bioturbation indicates moderately anaerobic conditions
*Subfacies 4.1.1:	Non-graded sandstone; mudstone veneer
Process:	Cyclic alteration of bedload transport with carbonaceous mud fallout. Ripple drift indicates bedform aggradation
*Subfacies 4.1.2:	Convolute sandstone-mudstone
Process:	Fluidization of interbedded facies; slide folding of facies 4.1; ductile deformation followed by brittle failure
Facies 4.2:	Graded, interbedded sandstone-mudstone
Process:	Waning moderate to low-concentration turbidity currents
*Subfacies 4.2.1:	Graded siltstone-mudstone
Process:	Low-concentration turbidity currents; sorting of silt grains clay flocs in the subviscous flow layer (grading)
Facies 4.3:	Interbedded sandstone-carbonaceous mudstone
Process:	Alternating upper plane bed or turbulent mass-flow of sand or, rarely, bedform migration (trough cross-sets) and fallout of organic mud
Class 5:	Stratified sandstone
Facies 5.1:	Planar stratified sandstone
Process:	Upper regime plane bed flow; rarely lower plane bed deposition
*Subfacies 5.1.1:	Graded, planar-stratified sandstone
Process:	Frictional freezing of thin, sandy turbidity currents
Facies 5.2:	Low-angle stratified sandstone
Process:	Bidirectional upper regime flow across an inclined surface
Facies 5.3:	Wavy stratified sandstone
Process:	Rapid deposition through frictional freezing of thin, sandy turbidity currents under oscillatory flow influence (combined flow origin)
Class 6:	Massive sandstone
Facies 6.1:	Non-graded to normally graded sandstone
Process:	High concentration turbidity currents; grain flow

Class 7:	Cross-stratified sandstone
Facies 7.1:	Trough cross-stratified sandstone
Process:	Lower regime bedload transport
*Subfacies 7.1.1:	Vortex ripple-stratified sandstone
Process:	Reversing-flow bedload transport
Facies 7.2:	Planar-tabular cross-stratified sandstone
Process:	Bedload transport, migration of linear crested ripples
*Subfacies 7.2.1:	Cross-bedded sandstone-mudstone
Process:	Cyclic waning bedload, alternating bedform migration and abandonment
Facies 7.3:	Hummocky cross-stratified sandstone
Process:	Combined flow (storm suspension and bedload traction)
Class 8:	Pebbly sandstone
Facies 8.1:	Massive pebbly sandstone
Process:	Waning, semi-cohesive turbulent flow
Facies 8.2:	Trough cross-bedded pebbly sandstone
Process:	Cyclically waning bedload transport of sand and gravel; migration of large-amplitude sinuous crested bedforms
Facies 8.3:	Low-angle stratified pebbly sandstone
Process:	Scour filling by basal lag gravel; migration of sinuous crested bedforms under very shallow flow conditions
Class 9:	Graded-stratified conglomerate
Facies 9.1:	Graded-stratified conglomerate
Process:	Alternating suspension/traction deposition in high concentration turbidity flows experiencing velocity fluctuation
Facies 9.2:	Planar-tabular cross-bedded conglomerate
Process:	Upper regime bedload gravel transport; waning flow avalanche foreset grading
Class 10:	Clast-supported conglomerate
Facies 10.1:	Openwork conglomerate
Process:	Bedload transport of gravel; gradual waning flow-winnowing of matrix
Facies 10.2:	Massive to normally graded conglomerate
Process:	Cohesionless debris flow, low- or high-concentration turbidity flow (see text)
Facies 10.3:	Boulder conglomerate
Process:	Cohesionless, turbulent flow; rolling, saltation
Class 11:	Matrix-supported conglomerate
Facies 11.1:	Normally graded conglomerate
Process:	Hyperconcentrated flow
Facies 11.2:	Inversely graded conglomerate
Process:	Cohesive debris flow
Class 12:	Non-welded tuff
Facies 12.1:	Crystal tuff/tuffaceous sandstone
Process:	Subaqueous and subaerial pyroclastic flows; epiclastic equivalents
*Subfacies 12.1.1:	Calcareous tuff/tuffaceous sandstone
Process:	Turbulent ash flow across carbonate lagoon facies

GOLD-SULPHIDE QUARTZ VEINS IN METAMORPHIC ROCKS AS A POSSIBLE SOURCE FOR PLACER GOLD IN THE LIVINGSTONE CREEK AREA, YUKON TERRITORY, CANADA

L. Stroink

and

G. Friedrich

Institute of Mineralogy and Economic Geology
Aachen University of Technology
Wüllnerstr. 2, 5100 Aachen
Aachen, Germany

STROINK, L., and FRIEDRICH, G., 1992. Gold-sulphide quartz veins in metamorphic rocks as a possible source for placer gold in the Livingstone Creek area, Yukon Territory, Canada. In: Yukon Geology, Vol. 3; Exploration and Geological Services Division, Yukon, Indian and Northern Affairs, Canada, p.87-98

ABSTRACT

The Livingstone Creek area is located 100 km northeast of Whitehorse, Yukon Territory, Canada. Hydrothermal gold-sulphide mineralization (MINFILE 105E 001) occurs in quartz-carbonate veins and veinlets which cut Paleozoic metamorphic rocks of the Teslin Suture Zone. The metamorphic rocks are also cut by Cretaceous(?) feldspar-porphyry dykes with an average thickness of 2 m.

The mineralization appears to be structurally controlled by NNE-striking faults and a set of NNW-trending joints. The vein minerals consist of gold, pyrite, chalcopyrite, galena, hessite/stuetzite, tetradymite, Au-Ag tellurides, tennantite, hematite, pyrrhotite, quartz, and carbonate. Gold occurs as: (1) "free gold" in cracks and interstices of quartz gangue (2) inclusions in galena, usually rimmed by hessite (3) minute grains associated with chalcopyrite and galena in aggregates of coarse grained pyrite (4) individual grains or fracture fillings in iron hydroxides.

The coarse-grained gold in Livingstone Creek appears to be derived from gold-quartz veins in the metamorphic bedrock. This is indicated by: (1) similar silver and mercury contents in primary and placer gold (2) identical trace element composition of galena from gold-quartz veins and galena inclusions in placer gold (3) similar telluride mineral assemblages in both in gold-quartz veins and placer gold grains (4) similar homogenization temperatures and salinities in fluid inclusions from both gold-quartz veins and placer nuggets.

A limited amount of gold appears to have formed by supergene leaching and precipitation. This kind of gold occurs as irregular-shaped grains in the stream placers and in iron hydroxide along fractures in quartz veins. Relative to the primary gold it is enriched in silver and mercury.

RÉSUMÉ

La région du ruisseau Livingstone est située à 100 km au nord-est de Whitehorse (territoire du Yukon) au Canada. Il y a minéralisation hydrothermale en or et en sulfures dans des veines et veinules de quartz et carbonate dans les roches métamorphiques paléozoïques de la zone de suture de Teslin. Les roches métamorphiques sont également recoupées par des dykes de feldspath et porphyre du Crétacé (?) d'une épaisseur moyenne de deux mètres.

La minéralisation semble structuralement définie par une faille d'orientation NNE et un ensemble de diaclases d'orientation NNW. L'assemblage de minéraux des veines consiste en or, pyrite, chalcopyrite, galène, hessite/stuetzite, tétradymite, tellurures d'Au et d'Ag, tennantite, hématite, pyrrhotine, quartz et carbonate. L'or prend la forme : 1) d'«or libre» dans des fissures et interstices de la gangue de quartz, 2) d'inclusions dans la galène, habituellement entourées de hessite, 3) de minuscules grains associés à la chalcopyrite et à la galène dans des agrégats de pyrite de granulométrie grossière et 4) de grains individuels ou de remplissage de fractures dans des hydroxydes de fer.

L'or de granulométrie grossière dans le ruisseau Livingstone semble provenir de veines de quartz aurifère dans le socle rocheux métamorphique, ce qui est indiqué par 1) des teneurs en argent et en mercure similaires dans l'or primaire et dans l'or placérien, 2) des compositions identiques en éléments à l'état de traces dans la galène des veines de quartz et or et dans la galène des inclusions dans l'or placérien, 3) des assemblages de tellurures minéraux similaires dans les veines d'or et quartz et dans les grains d'or placérien et 4) des températures d'homogénéisation et des salinités similaires des inclusions fluides provenant des veines d'or et quartz et des pépites placériennes.

Une quantité limitée d'or semble s'être formée par lixiviation et précipitation secondaires. Ce type d'or prend la forme de grains de formes irrégulières dans les dépôts alluvionnaires des cours d'eau et dans les fractures avec hydroxyde de fer dans les veines de quartz. Il est enrichi en argent et en mercure par raport à l'or primaire.

INTRODUCTION

The Livingstone Creek placer gold camp is located approximately 100 km northeast of Whitehorse at latitude 61°19'N and longitude 134°17'W on N.T.S. map sheet 105 E 8 (Fig. 1). It comprises eight tributaries of the South Big Salmon River. The first discovery of placer gold was in 1898. In the first decade of the following century the Livingstone placer area became a booming camp with an estimated production of about $1,000,000.00 in gold (Bostock, 1938). From an economic standpoint, Livingstone Creek has been the most important creek in the camp, and placer gold deposits are still being mined.

The geology and placer gold deposits of the Livingstone Creek area were first described by McConnell (1901). Regional geological mapping was carried out by Bostock and Lees between 1929 and 1934 (Laberge sheet; Map 372A) and by Tempelman-Kluit (1978,1979). Hansen (1986a,b) described the tectonic setting in detail.

The origin of placer gold of the Livingstone Creek was unknown for a long time. Bostock (1938) supposed quartz veins in the metamorphic bedrock were possible contributors of the gold. A 1983 assay of dump material beside a small mineral occurrence on the north side of Livingstone Creek (MINFILE 105E 001) assayed up to 1.58 opt Au, 16.6 opt Ag and 9.9% Pb (Archer, Cathro & Associates (1981) Ltd internal report, 1986). Visible gold, however, has not previously been reported.

This paper describees the paragenesis of gold-quartz veins in relation to placer deposits in the Livingstone Creek area. It is based on data obtained by chemical and mineralogical investigations of gold-bearing quartz-carbonate veins and placer deposits. Field work was carried out during an eight week period in 1986 as part of the Canada/Germany Science and Technology Exchange program.

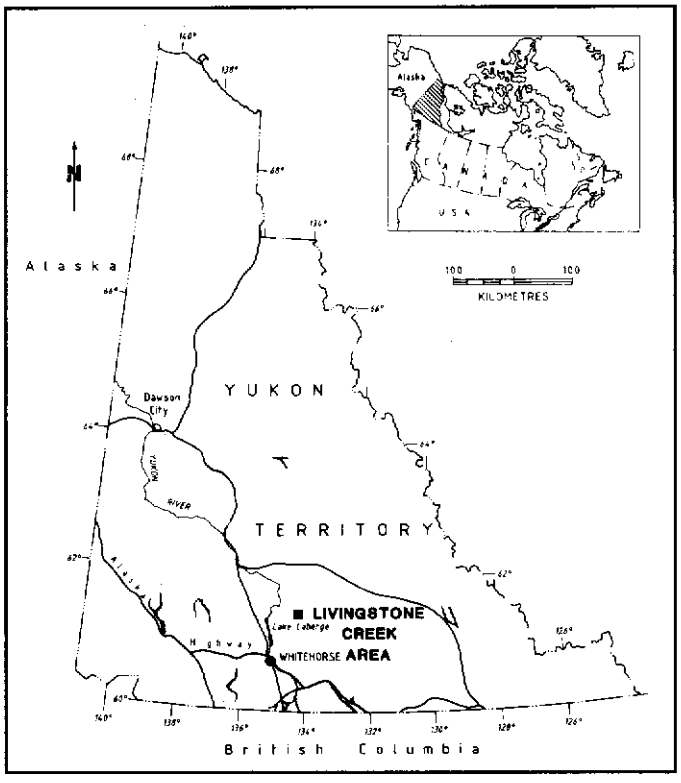

Figure 1. Location of the study area.

REGIONAL GEOLOGY

Cataclastic rocks of the Teslin Suture Zone (TSZ) underlie the area. The TSZ is interpreted as the fundamental boundary between eastern autochthonous rocks of the ancient North American Craton and allochthonous terranes to the west (Tempelman-Kluit, 1979). Cataclastic rocks of the TSZ are divided into three assemblages. The Nisutlin Allochthon, a schist-quartzite assemblage is derived from a protolith of synorogenic clastics with interlayered intermediate volcanics. The Anvil Allochthon is a sheared ophiolite complex consisting of basalt, gabbro and peridotite. The Simpson Allochthon consists of granitic cataclasites (Tempelman-Kluit, 1979). TSZ rocks were metamorphosed to greenschist or amphibolite facies in Late Triassic to Mid-Jurassic time (Tempelman-Kluit, 1979). The silicate mineral assemblage records maximum temperatures of 625°C, and pressures to 8 kbars (Hansen, 1986).

LOCAL GEOLOGY

Bedrock in the study area consists of southwest-dipping metamorphic rocks, intruded by two unmetamorphosed

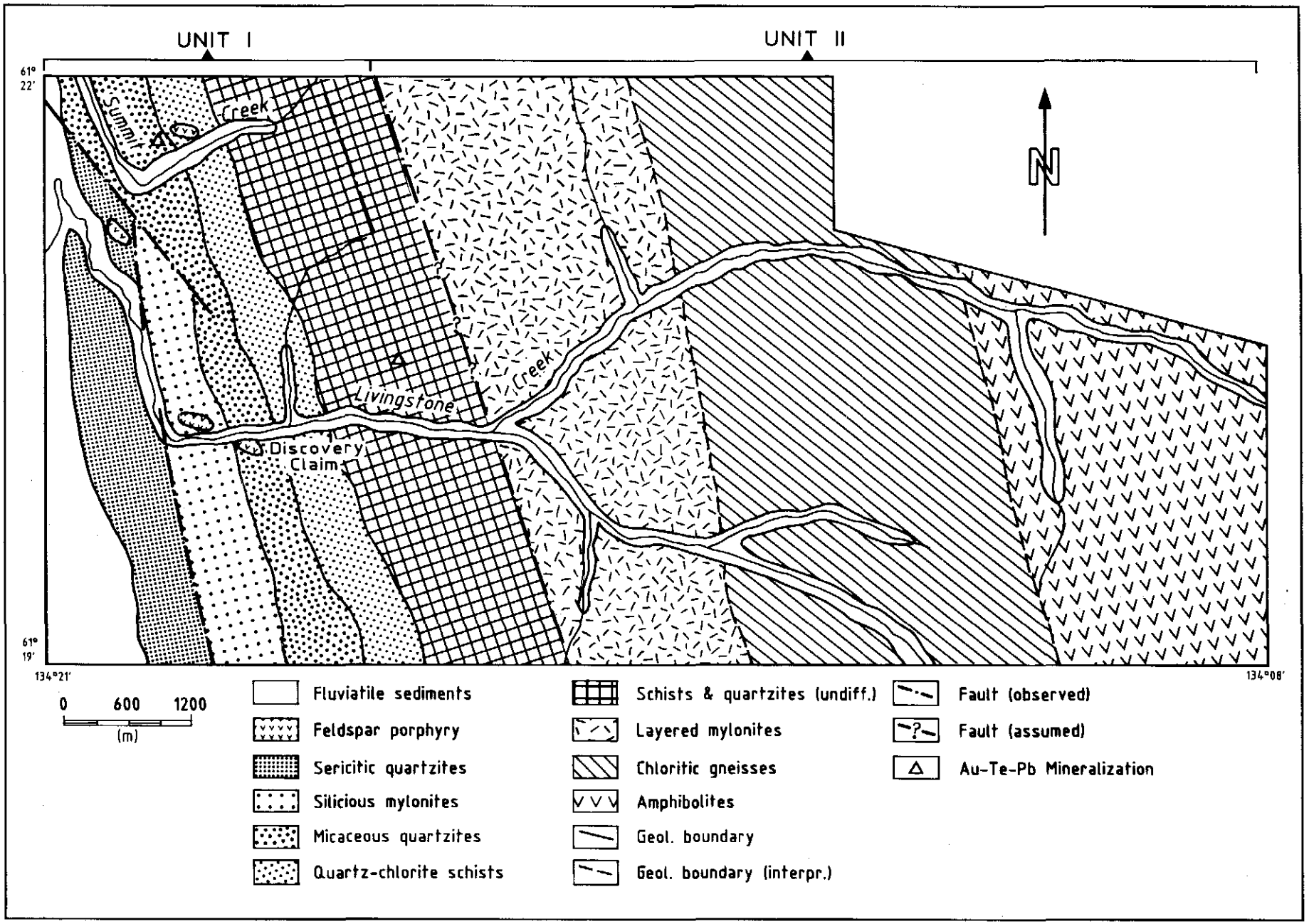

Figure 2. Geological map of the study area.

feldspar-porphyry dykes (Fig. 2). Exposure is poor, with good outcrops confined to the narrow canyon-like valleys of Livingstone Creek and Summit Creek, and to the ridges north,south and west of the two creeks.

Three distinct lithologic units are recognized. Unit 1 consists of siliceous tectonites derived from sedimentary and/or volcanic protoliths, and is assigned to the Nisutlin Allochthon. Unit 1 rocks are subdivided into five subunits. From west to east these are: (1) sericitic quartzite and metagreywacke; (2) siliceous mylonite intercalated with quartz-mica schist and lenses of silica-rich marble; (3) micaceous quartzite; (4) quartz-chlorite schist and (5) undifferentiated quartzite and mica-schist. The Unit 1 schists and quartzites are generally fine grained and consist mostly of quartz and sericite with minor sodic plagioclase, potassium feldspar, chlorite, biotite, epidote, clinozoisite, actinolite and carbonate, and accessory zircon, rutile, pyrite and magnetite.

Unit 2 is a metavolcanic unit of layered mylonite, chloritic gneiss and amphibolite. It is interpreted as part of the Anvil Allochthon, separated from Unit 1 by a NNW-trending fault zone. The layered mylonite consists of Mg-rich chlorite, epidote, clinozoisite, amphibole (barroisite and tschermakite), potassium feldspar, quartz, oligoclase, calcite, biotite and sericite. Amphibole (tschermakite) and plagioclase (oligoclase) are the main components of the dark green, medium-grained amphibolites. Minor components include epidote, iron-rich chlorite, garnet, sphene, clinozoisite and quartz. The Unit 2 amphibolites have a mafic igneous composition, and have been metamorphosed to upper greenschist or lower amphibolite grade. According to Spry's (1969) classification, cataclastic rocks in the study area range from protomylonites to mylonites and ultramylonites.

Unit 3 rocks are northwest-trending hornblende-feldspar porphyry dykes with an average thickness of two metres. The porphyritic texture is produced by phenocrysts of euhedral plagioclase (18 $\pm$ 0.4%) up to 2 cm in size, amphibole (hastingsite,(34 $\pm$ 1.3%) and biotite (3 $\pm$ 0.5%) in a fine-grained groundmass (45%). Their chemical composition suggests that they are banakites. They are most likely subvolcanic equivalents of the Late Cretaceous Carmacks Group volcanics (Glasmacher, 1989).

PRIMARY MINERALIZATION

Gold and sulphide minerals occur in quartz-carbonate veins and veinlets. The veinlets crosscut sheared micaceous quartzite of Unit 1 and are generally confined to NNW-striking joints. They are best exposed in Summit Creek valley. The main sulphide minerals in the veinlets are pyrite, pyrrhotite and chalcopyrite. Galena, gold, Bi-tellurides and hematitite occur to a lesser extent.

The major lode occurrence is a gold-quartz vein on the Horseshoe claim north of Livingstone Creek (MINFILE 105E 001). Average thickness of the vein is about 70 cm. The mineral assemblage consists of gold, pyrite, galena, chalcopyrite, tennantite, Au-Ag tellurides, hessite/stuetzite, quartz and minor carbonate gangue.

Gold forms visible grains in cracks and interstices of quartz gangue (Fig. 3) and inclusions of microscopic scale in galena (Fig. 4). It also occurs as relict particles in iron hydroxide (Fig. 5) and newly formed along microfractures (Fig. 6). Petrologic and electron microprobe studies reveal distinct differences in morphology and composition between gold grains from unoxidized and partly oxidized vein material.

Individual gold grains in quartz gangue and in unoxidized galena (Figs. 3, 4) reach 0.2 cm in diameter and commonly exhibit smooth grain boundaries. The silver and mercury contents in gold of this type of gold range from 13 to 16 weight per cent Ag (modal value 14%) and 0.2 to 0.9 weight per cent Hg (modal value 0.2%)(Figs. 11, 12). The average Au:Ag ratio is 5.9.

Relict gold particles found in iron hydroxides are characterized by corroded grain boundaries (Fig. 5) and similar chemical composition to those gold grains described above. In contrast, gold on fractures in iron hydroxides occurs as irregular shaped particles (Fig. 6). These irregular fracture-hosted particles show significantly higher silver values (16 to 23 weight per cent) and mercury (2 to 4 weight per cent)(Figs. 11, 12). The Au/Ag ratio decreases to an average value of 3.8.

Telluride minerals found in quartz veinlets of lower Summit Creek valley and in the Horseshoe quartz vein include hessite (Ag_2Te), stuetzite ($Ag_{5-x}Te_3$), Au-Ag tellurides of varying composition close to ideal petzite ($Au\text{-}Ag_3Te_2$), and tetradymite (Bi_2Te_2S).

Silver tellurides are restricted to the Horseshoe quartz vein. They usually occur as microscopic inclusions in unweathered galena, occasionally forming small rims around enclosed gold grains (Fig. 4). The silver tellurides contain between 57 and 62 weight per cent silver, and have been identified as hessite and/or stuetzite. Gold is below the detection limit (<0.2%).

Gold-silver tellurides have a restricted distribution and can only be identified by electron microprobe analysis. They occur either as small inclusions ($<3\mu$) in galena and pyrite, or intergrown with Bi-tellurides in quartz gangue. Figure 14 shows the compositions of the Au-Ag tellurides.

Bismuth tellurides have been found in quartz-carbonate veinlets cutting metamorphic rocks of the lower Summit Creek valley, where they are associated with pyrite, chalcopyrite, pyrrhotite and gold. They occur (1) as inclusions in pyrite, partly intergrown with galena and chalcopyrite (2) in quartz gangue intergrown with chalcopyrite or hematite (3) as individual phases in quartz gangue. The bismuth telluride crystals are generally anhedral with a maximum grain sizes of about 0.2 mm. The average composition of the bismuth tellurides (57.5 weight per cent Bi; 34.98 weight per cent Te; 4.48 weight per cent S) corresponds to tetradymite (Bi_2Te_2S).

Pyrite is ubiquitous in quartz-carbonate veins and veinlets.It forms euhedral crystals in the quartz carbonate veins or is disseminated and intergrown with rutile in highly silicified metamorphic wall rocks. Microprobe analyses indicate that both kinds of pyrite contain less than 0.11 weight per cent gold.

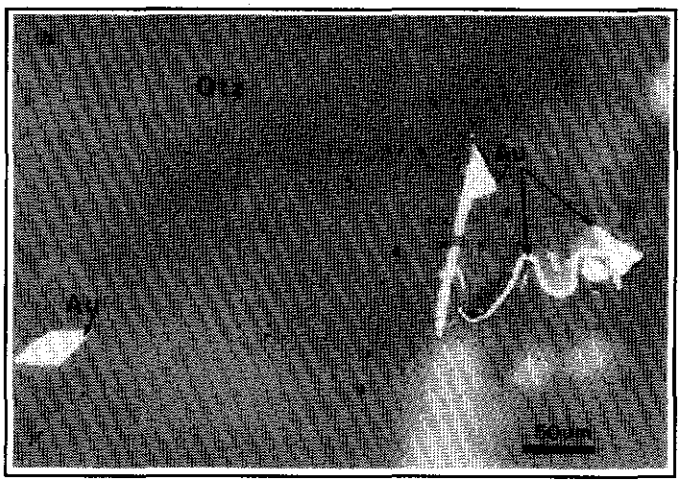

Figure 3. Interstital gold in quartz gangue (Horseshoe claim).

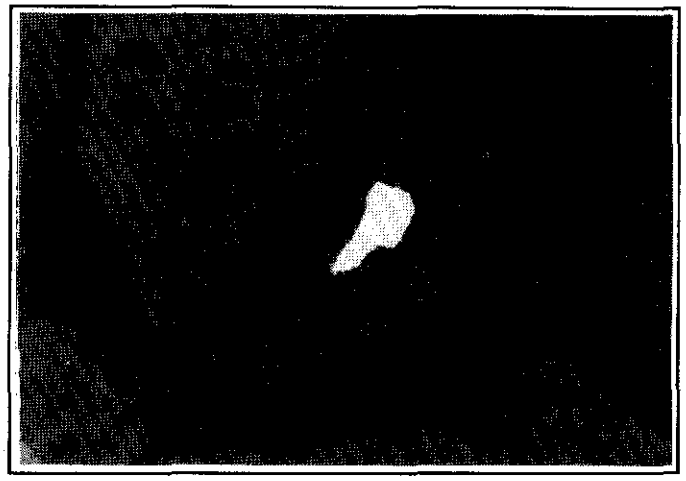

Figure 5. Gold rimmed by hessite, forming inclusions in galena.

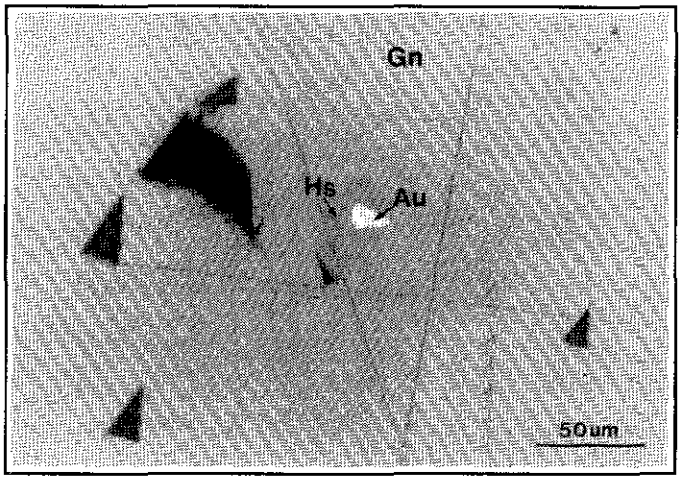

Figure 4. Gold rimmed by hessite, forming inclusions in galena.

Figure 6. Gold along fractures in iron hydroxide, Horseshoe claim.

Galena in gold-quartz veins generally forms coarse aggregates up to 2 cm in size. It often contains inclusions of gold which are usually rimmed by hessite (Fig. 4). Fracturesin galena are healed by tennantite and chalcopyrite. In the veinlets, galena occurs as small inclusions or along microfractures in pyrite. Microprobe analyses reveal traces of silver (average 0.41 weight per cent) and bismuth (average 0.74 weight per cent). Antimony has not been detected.

Chalcopyrite usually occurs as subhedral to anhedral crystals or as coarse grained aggregates intergrown with or cementing pyrite and galena. In minor amounts it is associated with hematite or occurs with galena along small fractures in pyrite.

Tennantite is exclusively intergrown with chalcopyrite in quartz gangue or along cracks in galena. It has an average arsenic content of 17.9 weight per cent. Traces of antimony (0.35 weight per cent), bismuth (1.0 weight per cent), silver (0.13 weight per cent) and mercury (0.08 weight per cent) have also been detected.

Hematite is common in veinlets of Summit Creek valley as needle-like crystals up to 1 mm in size. Hematite also occurs as symplectic intergrowths with chalcopyrite associated with pyrite. It also replaces fine disseminated magnetite in the metamorphic host rocks.

Coarse grained quartz is the main gangue mineral. Fluid inclusion data are presented in Fig. 15. Homogenization temperatures from primary fluid inclusions in quartz from the Horseshoe vein range from 110°C to 200°C with a maximum at 150°C (Blum, 1987). Salinities are about 4.5 weight per cent NaCl equivalent.

Wallrock alteration near mineralized veins includes pyritization, kaolinitization, dolomitization, sericitization, and chloritization. Quantitative studies of element enrichment and depletion in altered metasedimentary and volcanic rocks demonstrate elevated levels of gold and arsenic in altered wallrocks. Close to a NNE-trending fault zone, pyritized,

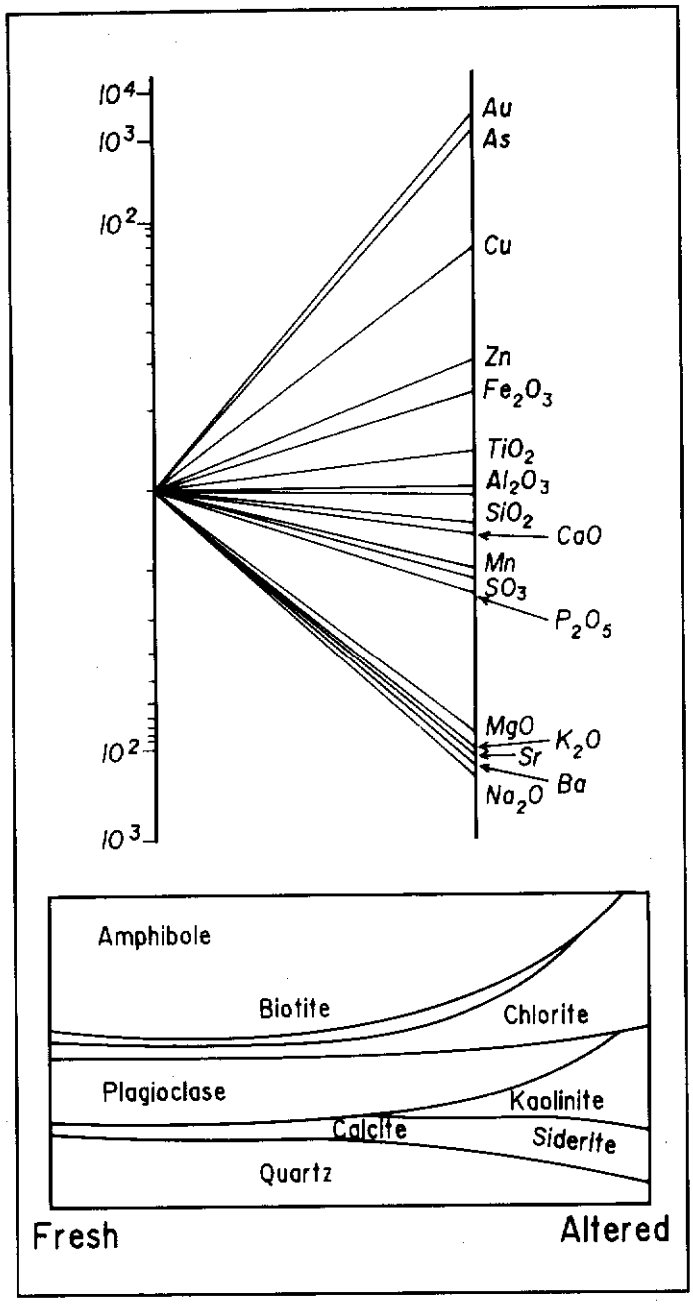

Figure 7. Element enrichment and depletion in altered feldspar porphyry.

kaolinized and sericitized porphyry dykes also show considerably increased levels of gold and arsenic (Fig. 7). The positive correlation between arsenic and gold allows arsenic to be used as a "pathfinder" element in this area. Mercury might also be used as a pathfinder element, as gold-silver alloys in the Horseshoe quartz vein contain up to 4 eight per cent mercury.

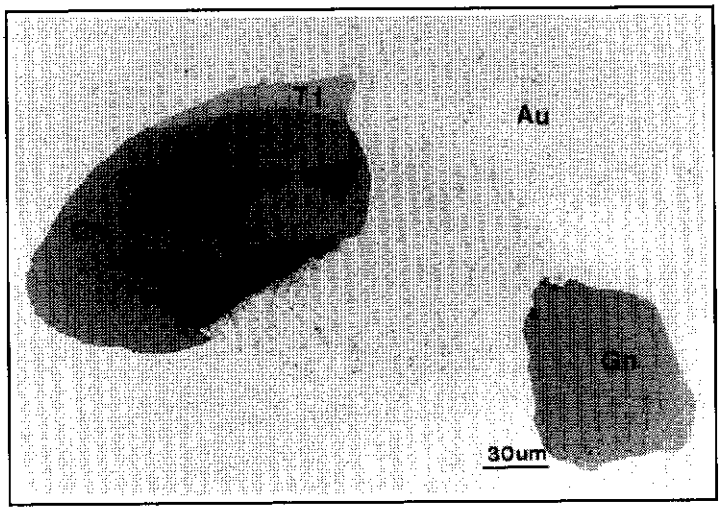

Figure 8. Intergrown galena and tetradymite, enclosed in placer gold grains from Livingstone Creek.

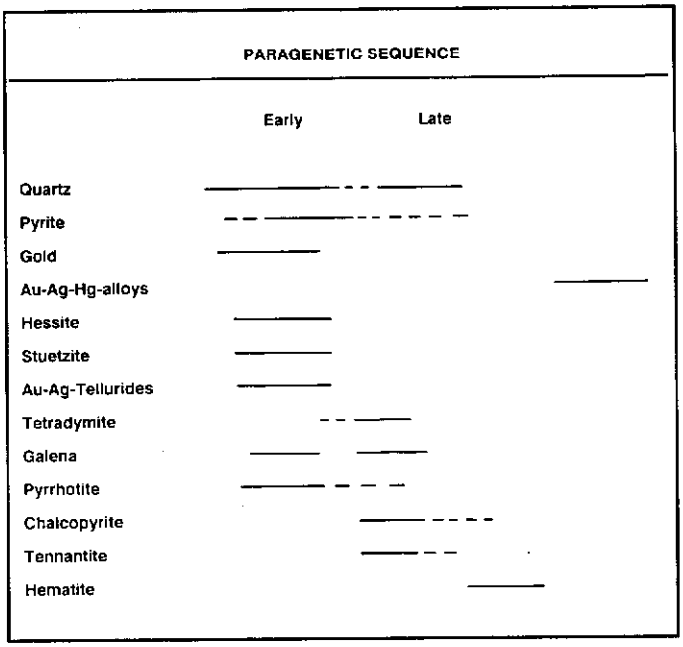

Figure 9. Paragenetic sequence for primary mineralization.

PLACER DEPOSITS

Alluvium in Livingstone Creek contains a heavy mineral assemblage which includes gold, galena, pyrite, arsenopyrite, cassiterite, cinnabar, epidote, garnet, hematite, ilmenite, pyrite, tourmaline, rutile, zircon and magnetite. Free gold particles consist of gold nuggets (grain size from 4.75 to >29 mm), "jewellery gold" (grain size from 1.7 to 3.4 mm) and fine gold (grain size <1.7 mm). Individual gold grains vary considerably in shape and internal structure. Four main types are recognized (Friedrich and Wiechowski, 1987): (1) Rounded gold grains, sometimes flat, with a smooth surface. Limonite is rare, usually confined to embayments in the

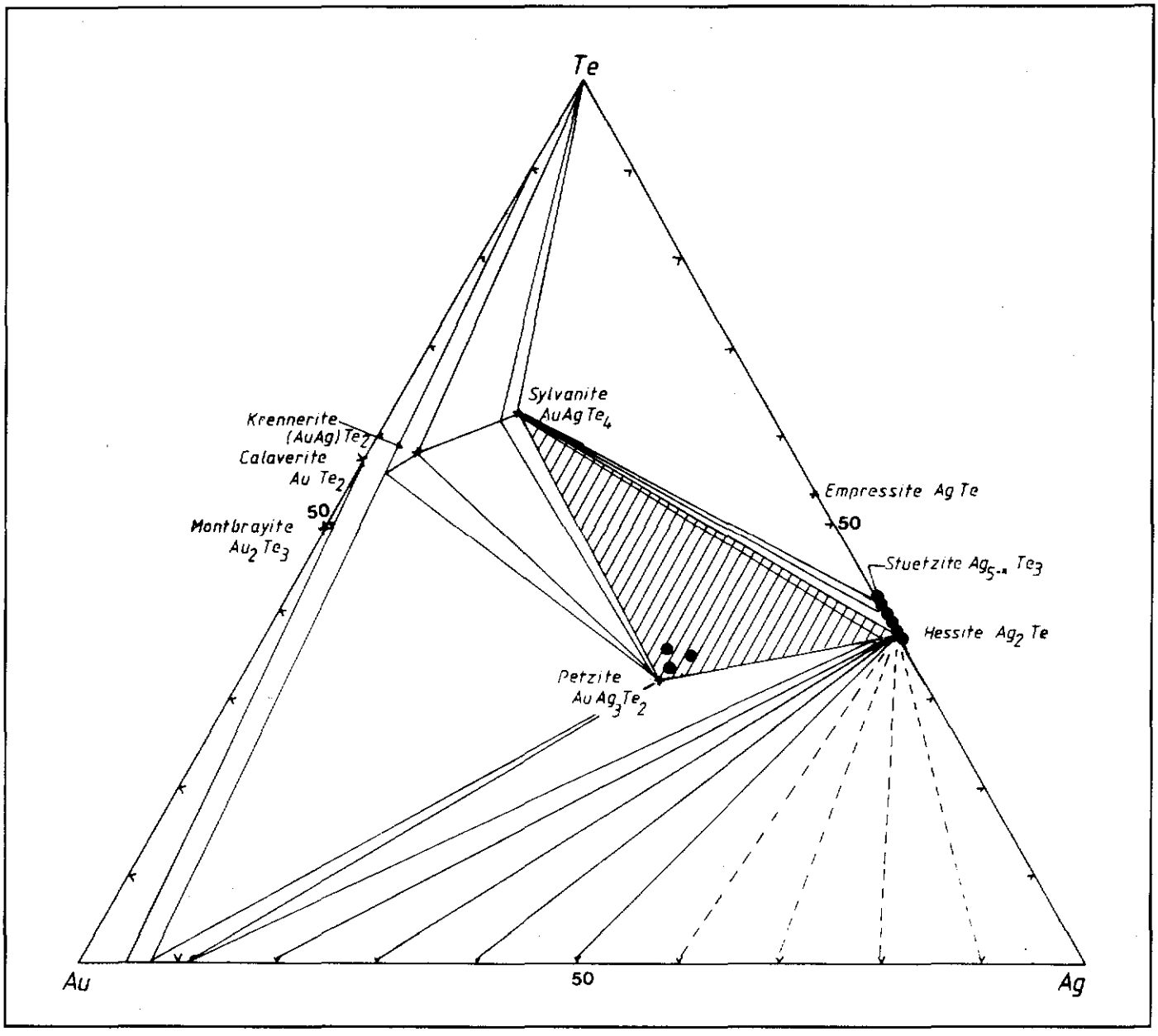

Figure 10. Minerals in the Au-Ag-Te system. Tie lines are indicated by natural mineral assemblages. (After Cabri, 1965). Dots indicate telluride minerals of the Livingstone Creek area.

surface. Larger nuggets often consist of an aggregate of gold leaves which are believed to have accreted during alluvial transport. (2) Flat, frequently elongated gold grains with smooth surfaces and rounded edges, characterized by dendritic growth structure. (3) Irregular gold grains with rugged or partly rounded surfaces, often intergrown with quartz. Irregular grains are rimmed with limonite, especially near embayments. (4) Thin flakes of gold with a smooth to verrucose surface and occasional curved rims.

Many gold nuggets contain inclusions of galena intergrown with tetradymite (Fig. 8), as well as hessite (Ag_2Te) and stuetzite ($Ag_{5-x}Te_3$).

Microprobe data reveal that the chemical composition of individual gold grains does not vary significantly, except for the mercury content. Fig. 11 shows the frequency distribution of silver values in placer gold grains. The outer rims generally return very low silver values due to leaching. The frequency distribution pattern of silver shows a range of values from 4-19 weight per cent, with a maximum at 12 weight per cent. There is no apparent correlation between silver content and grain size or shape of gold. The mercury content varies from <0.2 to 2.92 weight per cent (modal value 0.2 weight per cent) in primary gold grains and within individual gold nuggets (Fig. 12). Considerably higher mercury values (2-4 weight per cent) are found in irregular gold grains which are inferred to have a supergene origin.

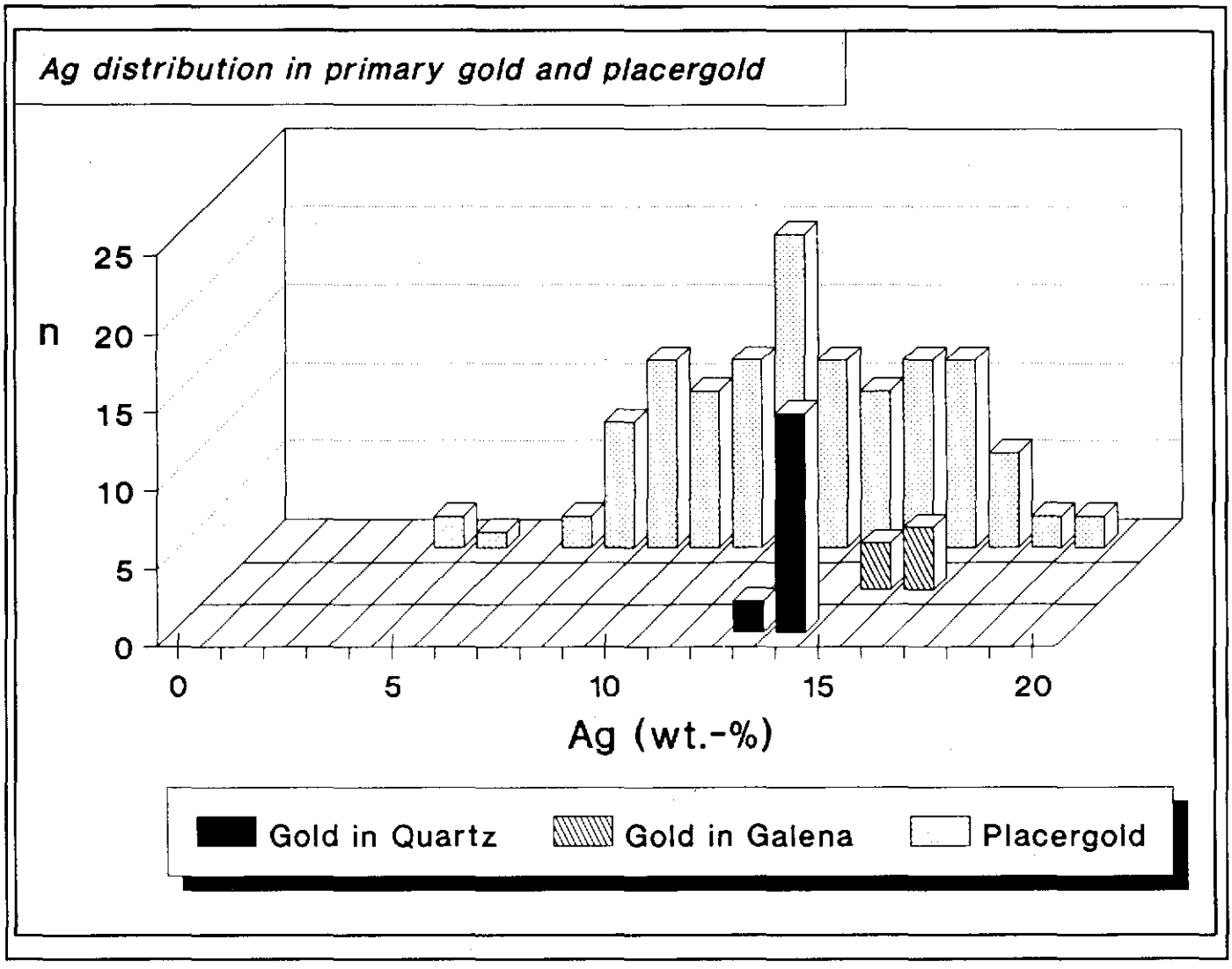

Figure 11 Frequency distribution of silver in placer gold and in vein gold from the Horseshoe claim.

Trace element compositions of galena inclusions in placer gold grains are shown in Fig. 13. Antimony is below detection limit. Average bismuth values range from 0.4 to 0.8 weight per cent and the silver content does not exceed 0.5 weight per cent.

Hessite and stuetzite inclusions in placer gold grains show slightly variable Ag/Te ratios (1.7 to 1.9). The gold content of the inclusions is very low and varies from 0.3 to 2 weight per cent. The composition of the Te-bearing minerals (including Au-Ag-Te inclusions in placer gold grains) is shown in Fig. 14.

Most of the placer gold deposits formed by physical transport and gravity concentration. Minor dissolution, migration, and reprecipitation of gold, however, is suggested by gold grains with silver-depleted rims.

DISCUSSION

The paragenetic sequence shown in Fig. 9 is defined by cross cutting relationships and replacement textures. The first stage of mineralization deposited milky quartz, coarse-grained pyrite, gold hessite, stuetzite, galena (I), and gold-silver tellurides. Later fracturing allowed earlier sulphides like galena and pyrite to be partially replaced or enclosed by chalcopyrite, galena (II), tetradymite, pyrrhotite and tennantite. Hematite formed last, as indicated by its lack of replacement textures, and massive hematite veinlets which crosscut earlier quartz-sulphide veinlets.

Assumptions about the temperature of mineralization are based on the occurrence and stability of Au-Ag-Te minerals. At temperatures above 170°C, compositions within the sylvanite-petzite-hessite field (Fig. 10) form the metastable gamma-phase (Cabri, 1965). The gamma phase breaks down at temperatures below 120°C forming stuetzite associated with hessite and petzite. The coexistence of stuetzite, hessite and other tellurium minerals with end-menber petzite in the Horseshoe vein indicates that the earliest telluride minerals were deposited at temperatures above 170°C.

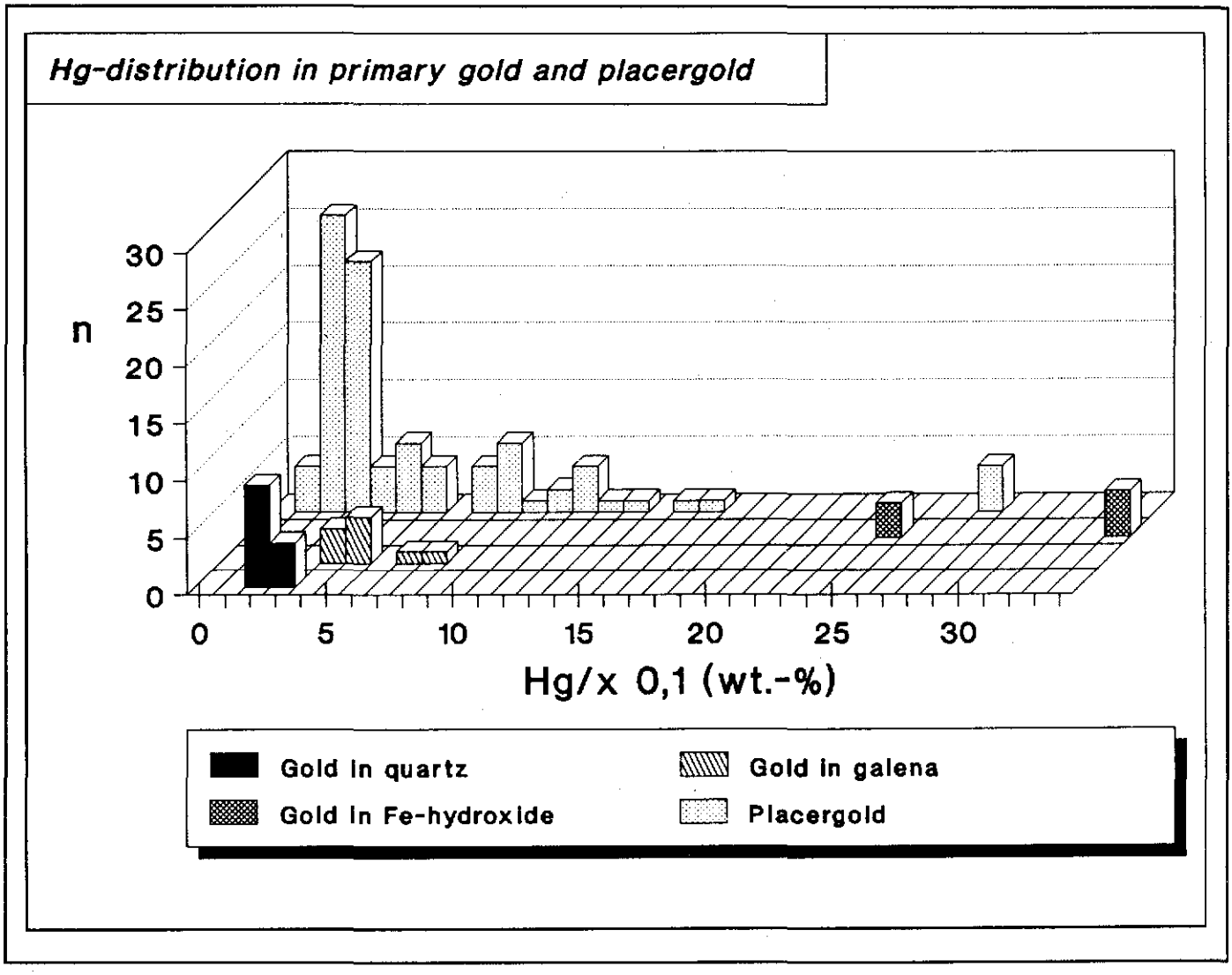

Figure 12 Frequency distribution of mercury in placer gold, and in vein gold from the Horseshoe claim.

Oxidized material from the gold-bearing quartz vein north of Livingstone Creek contains numerous tiny grains of visible gold. Relict gold particles in the iron hydroxide have a similar composition to the gold in unoxidized quartz and galena and show corroded grain boundaries due to partial dissolution. They are inferred to be residual.

Irregular-shaped gold particles in iron hydroxide-filled fractures are believed to have formed entirely as a result of supergene leaching and precipitation. Relative to gold grains in quartz gangue and galena, supergene gold is enriched in silver and mercury.

CONCLUSIONS

Comparison of gold and gold-silver tellurides from placer deposits and the Horseshoe vein suggests that most of the placer gold in Livingstone Creek is derived from gold-bearing quartz veins which crosscut the metamorphic bedrock. The following evidence supports this conclusion: (1) The vein and placer gold have very similar chemical composition (Fig. 11, 12); (2) galena inclusions in placer gold grains and primary galena in the gold quartz vein have identical trace element compositions (Fig. 13); (3) a similar suite of telluride minerals is associated with both the placer and vein occurrences; (4) Fluid inclusions in primary gold-quartz intergrowths in placer nuggets and in gold-quartz veins show similar patterns of homogenization temperatures (Fig. 15). Gold telluride compositions and fluid inclusion evidence shows that the veins were deposited from low-salinity epithermal fluids at a temperature of 170-200°C and a shallow or moderate depth. The age of the veins is unknown but they clearly post-date Late Cretaceous porphyry dykes in the area.

Gold is enriched in altered wallrocks along a NNE-trending fault, and there is a strong correlation between primary gold and arsenic.

Some gold grains in Livingstone Creek and in iron hydroxide-filled fractures in quartz show evidence of supergene leaching and redeposition. Gold grains of inferred

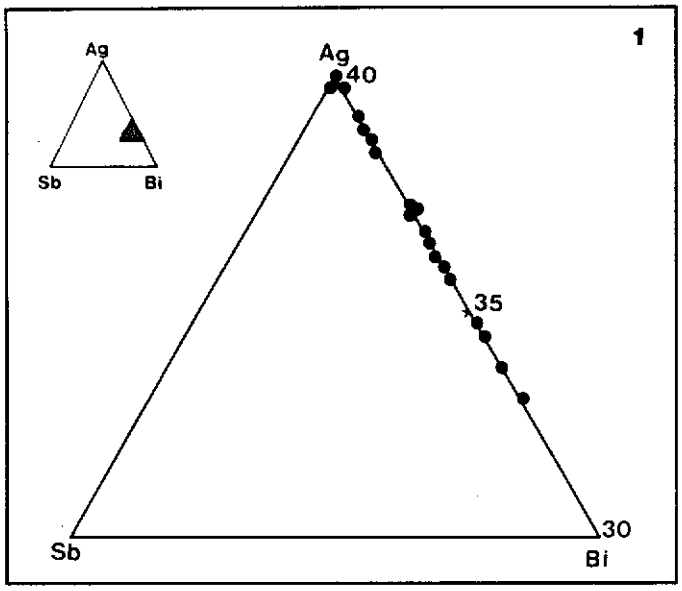

Fig. 13(1) Relative distribution of silver and bismuth in galena from gold-bearing quartz vein on the Horseshoe claim.

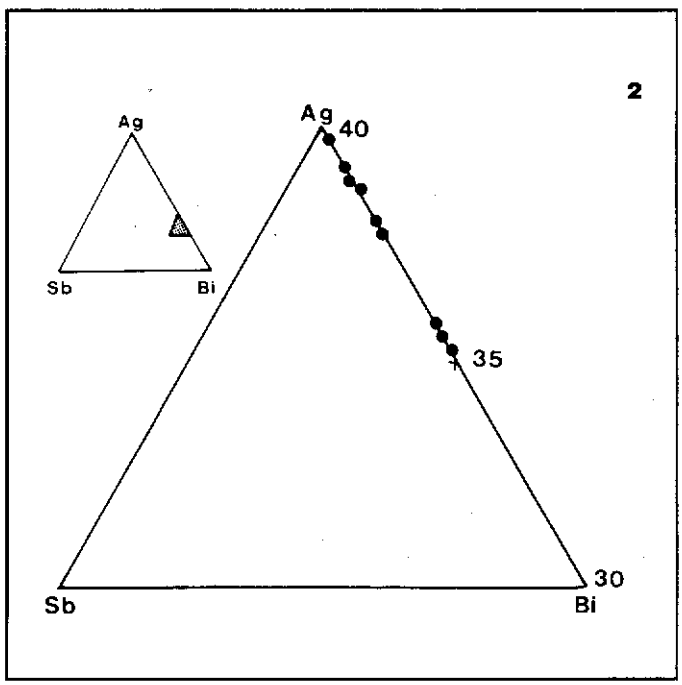

Fig. 13(2) Relative distribution of silver and bismuth in galena inclusions in placer gold.

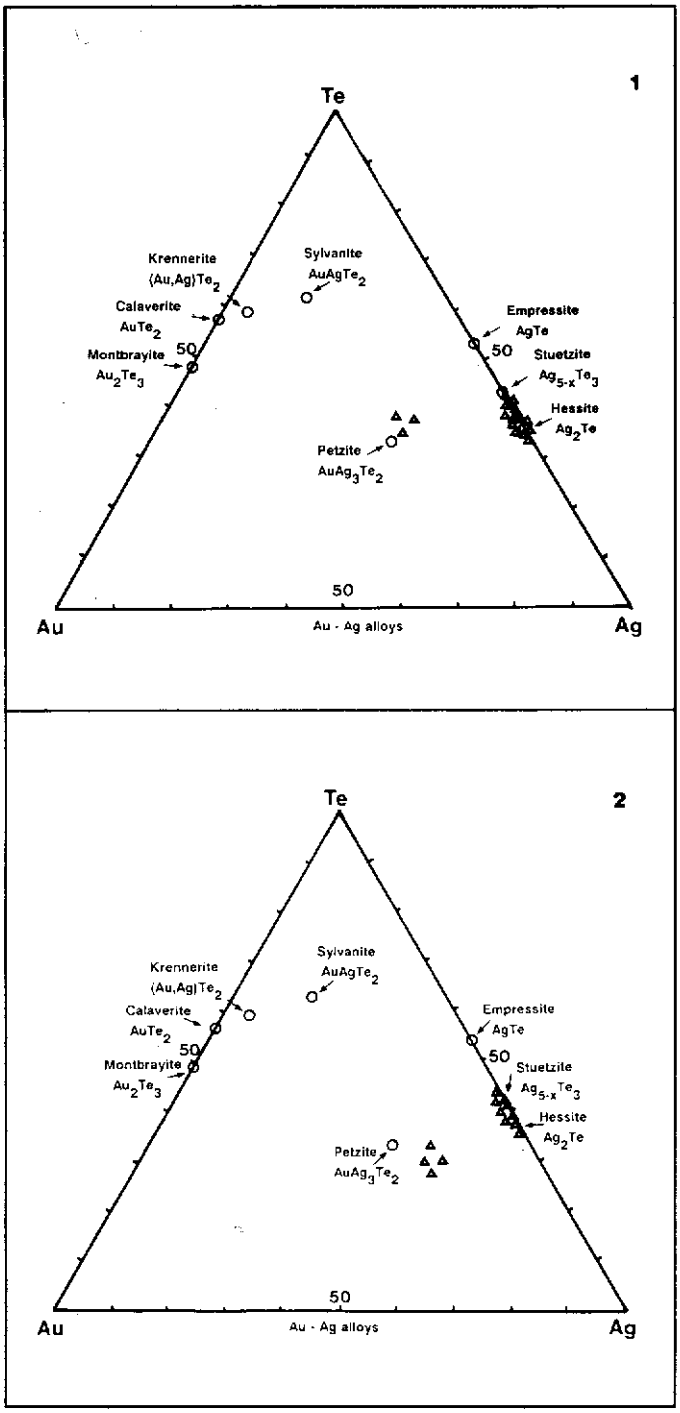

Figure 14. Composition of Ag- and Au-Ag- tellurides (triangles) from (1) gold bearing-quartz vein on the Horseshoe claim, and (2) telluride inclusions in placer gold.

supergene origin are distinguished by their irregular morphology and considerably higher silver and mercury content.

ACKNOWLEDGEMENTS

This project was part of the Canada/Germany Science and Technology Exchange Agreement organized by the Geological Survey of Canada and the Federal Institute for Geosciences and Mineral Resources (BGR). It received extensive support

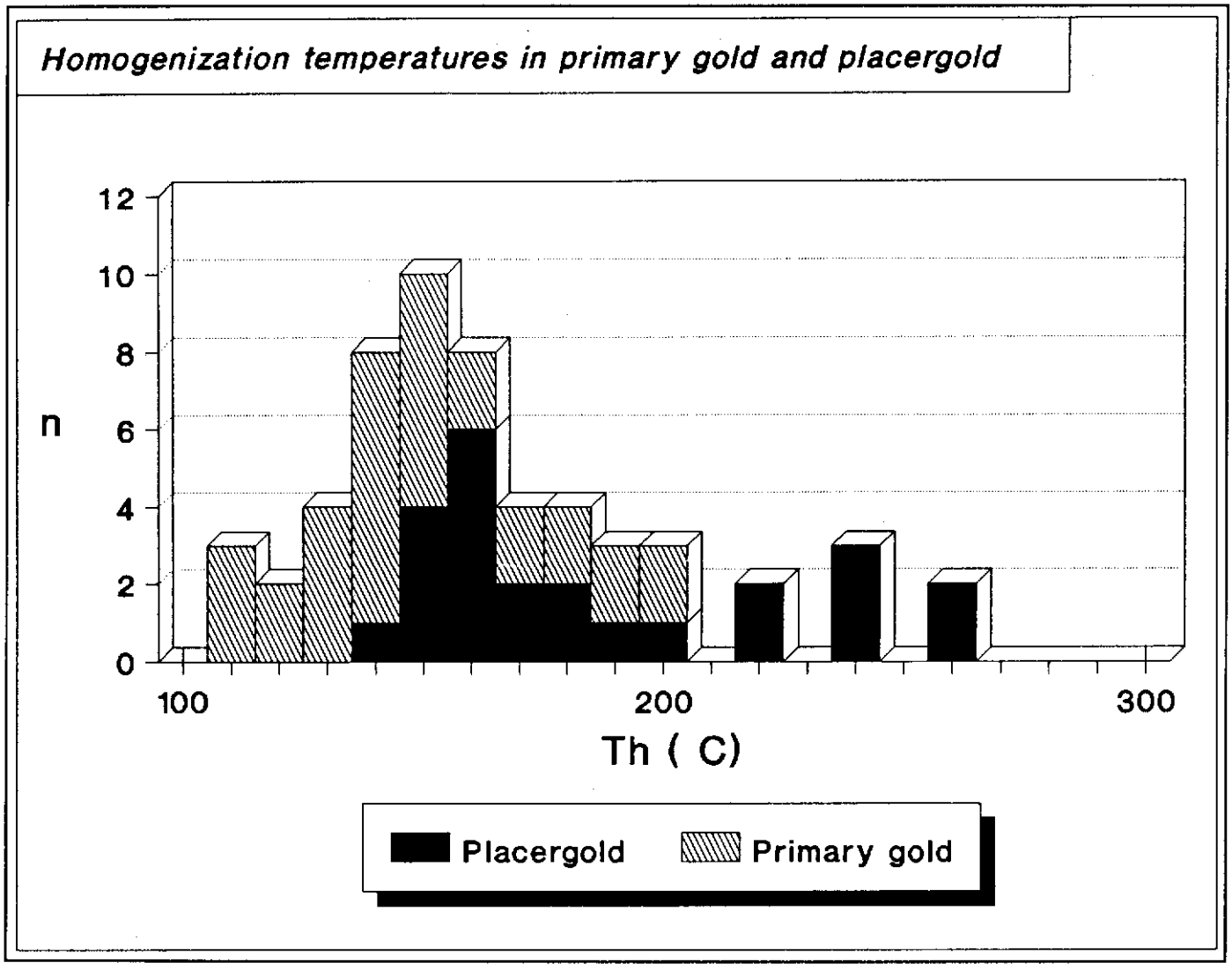

Figure 15. Homogenization temperatures of fluid inclusions in quartz-gold intergrowths from (1) gold-bearing quartz vein on the Horseshoe claim, (2) placer deposits.

from the German Ministry of Research and Technology and from the Exploration and Geological Services Division of Indian and Northern Affairs Canada, Whitehorse. We would like to thank J. Morin, G. Abbott, S. Morison and U. Glasmacher for their help and guidance. Many thanks go also to M. Fuerstner and R. Asachuck for the permission to work on their claims and for their hospitality and cooperation in the field. Trevor Bremner reviewed the manuscript.

REFERENCES

BLUM, M., 1987. Vergleichende mikrothermometrische Untersuchungen an Flussigkeitseinschlussen in Quarzen des Livingstone Gebietes, Yukon Territorium, Kanada. Unpubl. report, RWTH Aachen, 56 p.

BOSTOCK, H.S., 1931. The mining industry of Yukon-Selected field reports of the G.S.C. (1898-1933). Geological Survey of Canada, Memoir 284, p. 620-631.

BOSTOCK, H.S., and LEES, E.J., 1938. Laberge map-area, Yukon. Geological Survey of Canada Memoir 217.

BOYLE, R.W., 1979. The geochemistry of gold and its deposits. Geological Survey of Canada, Bulletin 280, p. 584.

CABRI, L.J., 1965. Phase relations in the Au-Ag-Te system and their mineralogical significance. Economic Geology, Vol. 60, p. 1570-1605.

FRIEDRICH, G., and WIECHOWSKI, A., 1987. Microprobe studies on alluvial gold, Livingstone Creek, Yukon Territory, Canada. Unpublished paper, RWTH Aachen, Germany, 18 p.

GLASMACHER, U., 1990. Petrogenetische und metallogenetische Entwicklung ausgewählter Gebiete im Yukon-Tanana Terrane und Stikine Terrane (Yukon Territorium, Kanada) während der Oberkreide und des Alttertiärs. Unpublished PhD thesis, Aachen University of Technology.

HANSEN, V.L., 1986a. Preliminary structural and kinematic analysis of mylonitic rocks of the Teslin Suture Zone, 105 E, Yukon. In: Yukon Geology, vol. 1; Exploration and Geological Services Division, Yukon, Indian and Northern Affairs, Canada, p. 119-124.

HANSEN, V.L., 1986b. Petrotectonic study of the Teslin Suture Zone, Yukon. A progress report. In: Yukon Geology, Vol. 1; Exploration and Geological Services Division, Yukon, Indian and Northern Affairs, Canada, p. 125-130.

MCCONNELL, R.G., 1901. Salmon River gold fields, including Livingstone and neighbouring placer creeks, Yukon Territory. In: H.S. Bostock, (ed.), Selected field reports of the Geological Survey of Canada, 1898-1933, Memoir 284, p. 37-48.

SPRY, A., 1969. Metamorphic textures. Pergamon Press, Oxford, p. 352.

STROINK, L., 1987. Geology, Petrology and Mineralization of Livingstone Creek, Yukon Territory, Canada. Unpublished Diploma-thesis, Aachen Technical University, p. 150.

TEMPELMAN-KLUIT, D., 1978. Reconnaissance geology, Laberge map area, Yukon. In: Current Research, Part A, Geological Survey of Canada, Paper 78-1A, p. 61-66.

TEMPELMAN-KLUIT, D., 1979. Transported cataclasite, ophiolite and granodiorite in Yukon. Evidence of Arc-Continent Collision. Geological Survey of Canada, Paper 79-14.

THE SEDIMENTOLOGY OF PLEISTOCENE DEPOSITS ASSOCIATED WITH PLACER GOLD BEARING GRAVELS IN THE LIVINGSTONE CREEK AREA, YUKON TERRITORY

Vic Levson
B.C. Geological Survey
553 Superior St
Victoria, B.C.
V8V 1X4

LEVSON, V., 1992. The sedimentology of Pleistocene deposits associated with placer gold bearing gravels in the Livingstone Creek area, Yukon Territory. In: Yukon Geology, Vol. 3; Exploration and Geological Services Division, Yukon, Indian and Northern Affairs Canada, p.99-132

ABSTRACT

Due to the depletion of traditional economic gold placer deposits in unglaciated areas of the Yukon, the study of the relationship of placer gravels to overlying glacial sediments in ice covered regions is important to future exploration activities. The Livingstone Creek area in south central Yukon has supported placer mining operations for over 90 years. Present activity is centred on gold-bearing gravels buried by thick Pleistocene glacial deposits. The placer gravels are associated with coarse interglacial stream and gulch deposits and they are overlain by fine grained, proximal, glaciolacustrine sediments.

During the last glaciation, damming of gold-bearing, high gradient interglacial tributary stream channels by main valley ice caused rapid environmental changes. Depositional processes dominated over erosion in the ice-marginal lakes, and thick sequences of fine grained suspension deposits, debris flow sediments, and deltaic sands and gravels accumulated. In addition, when glaciers expanded and overrode the area, these thick deposits protected the underlying placer gravels from subglacial erosion and dilution. Subglacial tills were probably deposited by lodgement, meltout and flow. During deglaciation, ice-marginal sedimentation again dominated. Post-glacial streams later cut through the glacial sediments and re-exposed the gold bearing gravels.

Stratigraphic, sedimentologic and geomorphic evidence from the Livingstone Creek area suggests that small tributary valleys, oriented transverse to the former direction of ice flow in the adjacent main valleys, would make good exploration targets in regions of new placer interest.

RÉSUMÉ

L'étude de la relation entre les graviers alluvionnaires et les sédiments glaciaires sus-jacents dans les régions recouvertes de glace est importante pour les activités futures d'exploration en raison de l'épuisement des classiques gisements rentables d'or placérien dans les régions non glaciées du Yukon. L'or placérien est exploité depuis plus de 90 ans dans la région du ruisseau Livingstone dans la partie méridionale centrale du Yukon. Actuellement, les activités sont centrées sur les graviers aurifères enfouis sous d'épais dépôts glaciaires du Pléistocène. Les graviers alluvionnaires sont associés à des dépôts de cours d'eau et de ravins interglaciaires à grains grossiers et ils sont recouverts de sédiments glaciolacustres proximaux à grains fins.

Pendant la dernière glaciation, l'endiguement d'affluents interglaciaires à forte pente par la glace de vallées principales a entraîné de rapides changements environnementaux. Les processus de dépôt, plutôt que l'érosion, ont été dominants dans les lacs de marges glaciaires et d'épaisses séquences de dépots à grains fins en suspension, de sédiments de coulées de débris et de sables et graviers deltaïques se sont accumulées. De plus, lorsque les glacier se sont agrandis et ont chevauché la région, ces épais dépôts ont protégé de l'érosion et de la dilution les graviers alluvionnaires sous-jacents. Les tills subglaciaires ont probablement été déposés sur le fond, par la fonte et l'écoulement. Pendant la déglaciation, la sédimentation aux marges glaciaires a de nouveau dominé. Les cours d'eau postglaciaires ont plus tard entaillé les sédiments glaciaires et de nouveau mis à nu les graviers aurifères.

Les indications stratigraphiques, sédimentologiques et géomorphologiques dans la région du ruisseau Livingstone suggèrent que les vallées de petits affluents orientées perpendiculairement à l'ancienne direction de l'écoulement de la glace dans les vallées principales adjacentes constitueraient de bonnes cibles d'exploration dans les régions d'intérêt pour les nouveaux gisements alluviaux.

INTRODUCTION

Yukon placer deposits have produced more than 11 million ounces (342 million grams) of gold since 1885 (Debicki, 1983). Record productions have occurred in recent years, with 1987-1990 ranked as the four best years in the last 72 (Latoski, 1991). In 1989, the highest production since 1917 was recorded: 165 571 crude ounces (5 151 510 million grams), valued at over Cdn $57.6 million (Latoski, 1991). Most placer mining activities in the Yukon have traditionally been in unglaciated regions such as the Klondike, Indian River and Sixtymile River areas but economic placer deposits also exist in glaciated areas, and generate about 25% of the total placer gold production (LeBarge, 1990). The focus of this study, an important placer occurrence in the Livingstone Creek area, is at least 125 km inside the limit of Pleistocene glacial advances (Hughes et. al., 1969). The reason for the preservation of the placer gravels in this area is unknown, although it has been suggested that they occur in valleys oriented perpendicular to the regional flow direction of Pleistocene glaciers (Bostock and Lees, 1938). Detailed stratigraphic and sedimentologic relationships of the placer gravels to the overlying glacial deposits were previously undocumented.

The objectives of this study were to investigate the sedimentary properties of the glacial sediments overlying the placer gold bearing deposits in the Livingstone area in order to document: (1) the stratigraphic and sedimentologic characteristics of the glacial sediments, (2) any relationship of these characteristics to the preservation of the gold bearing gravels, and (3) any unique features that might be used to identify potential exploration targets in other glaciated regions.

Placer gold was first discovered in the Livingstone Creek area (Figure 1) in 1898 and in the first forty years of activity the camp produced more than $1,000,000 in gold (Bostock and Lees, 1938). The area continued to produce gold over the next fifty years. Seven of the creeks had active operations between 1978 and 1990 which produced more than 3300 ounces of gold, a total value of about $1.3 million (Debicki, 1983; LeBarge, 1990; Latoski, 1991). Mining activities were observed on three creeks in the area during this study.

STUDY AREA

The Livingstone Creek area is located about 80 km northeast of Whitehorse (Figure 1, inset) and has two dirt airstrips and a winter road for access. Virtually all the gold production in the area has come from several small creeks that flow down the eastern slopes of the Big Salmon Range into the South Big Salmon River (Figure 1). Good exposures on Martin, Livingstone and Summit Creeks were the focus of this study. The creeks head in broad, shallow, glaciated basins that narrow into steep gradient canyons where the streams enter the main valley. A narrow, bedrock-walled valley along the eastern edge of the South Big Salmon River valley is responsible for the sharp northward diversions of Livingstone and Summit Creeks from their otherwise westerly drainage (Figure 1).

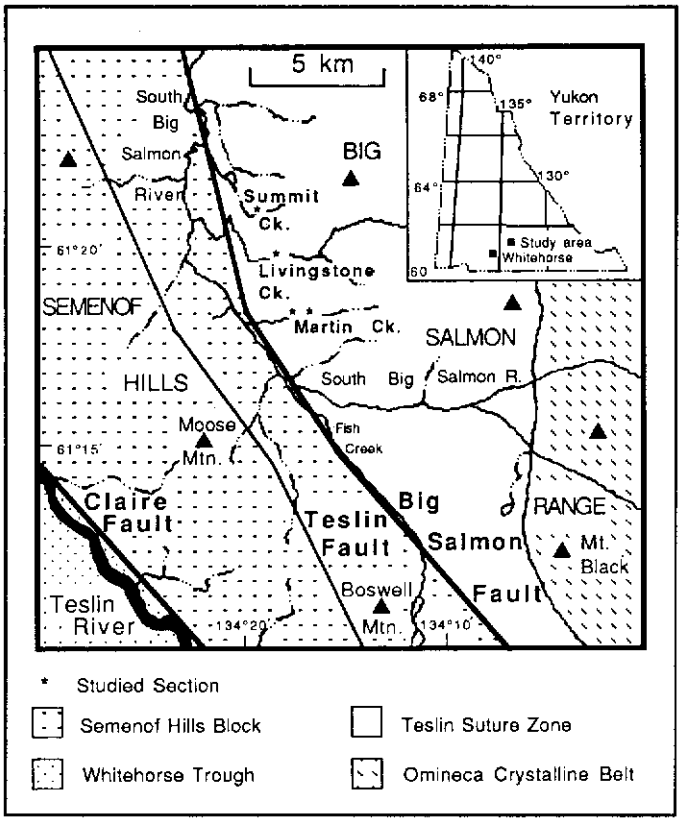

Figure 1. Locations of studied sections and bedrock geology of Livingstone Creek area.

Peaks on the Big Salmon Range rise to elevations of about 2000 m; Mt. Black (2158 m) at the SE end of the range is the highest mountain in the region (Figure 1). The Livingstone Creek area is separated from the Teslin River valley by the Semenof Hills. Several north-south trending valleys, such as between Moose and Boswell Mountains, cross the hills.

The gold-bearing gravels at the three creeks studied directly overlie bedrock. They are poorly exposed due to mining activity which has undercut the sections, resulting in the collapse of the overlying glacial deposits. This same collapse produced the fresh exposures in the upper part of the sections described in this paper (Figures 2 to 5).

PREVIOUS WORK

Few detailed studies of this nature have been carried out on placer deposits in glaciated parts of the Yukon. Morison (1983, 1984), however, provided a sedimentologic description of placer gold sediments and associated deposits in the glaciated Clear Creek basin. He concluded that placer deposits buried below till were preserved because the area is located near the limits of glaciation where subglacial erosion was decreased. The glacial sediments were probably deposited by mainly nonerosional processes such as meltout and resedimentation (Morison, 1984). Similar studies of placer deposits have recently been conducted in northwest British

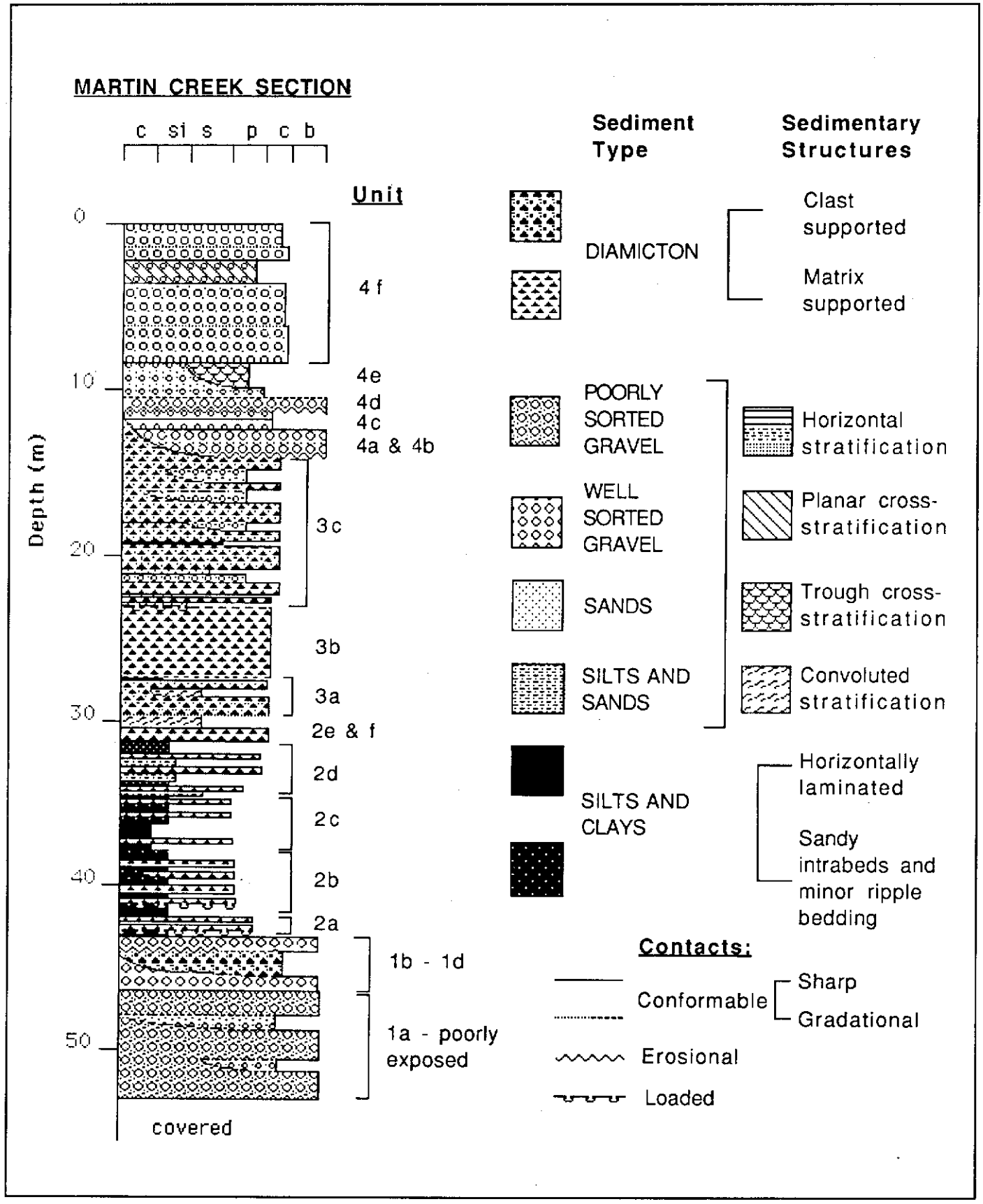

Figure 2. Composite stratigraphic column of the main Martin Creek section.

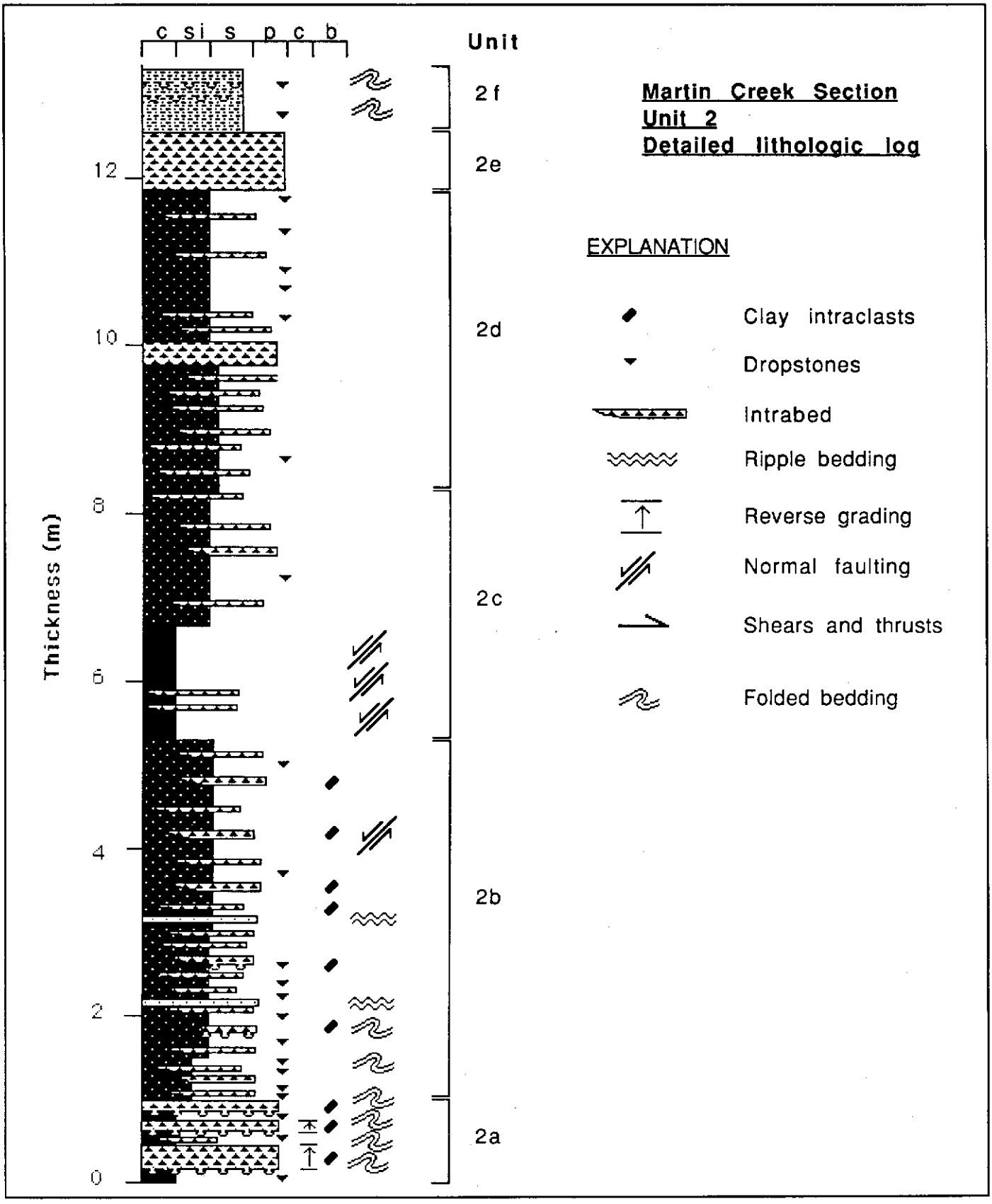

Figure 3. Detailed sedimentologic log of unit 2 at the Martin Creek section. Refer to Figure 2 for explanation of lithologic symbols.

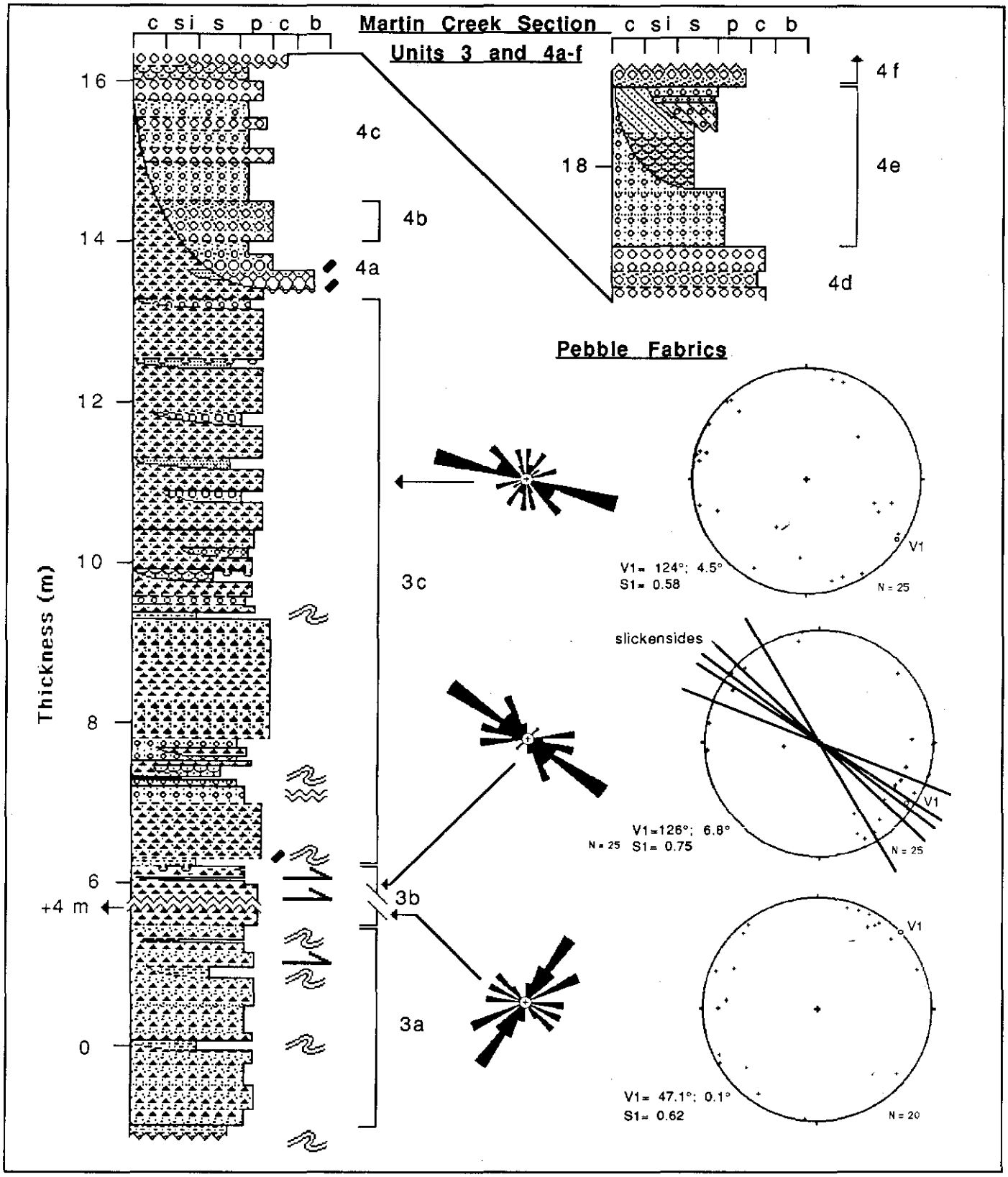

Figure 4. Detailed sedimentologic log of units 3a to 4f at the Martin Creek section. Rose diagrams and corresponding equal area density plots are shown for units 3b and 3c. V1 parallels the axis of maximum clustering of the a-axes of blade and prolate shaped clasts. S1 is the normalized eigenvalue corresponding to the V1 eigenvector. Refer to Figures 2 and 3 for explanation of symbols.

Summit Creek

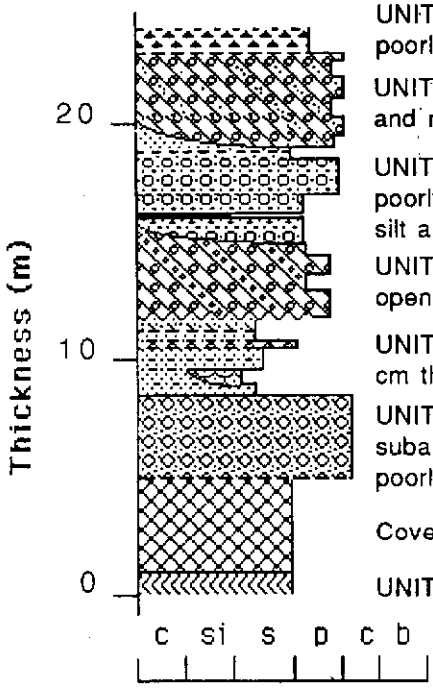

UNIT 7: diamicton; massive; clast to matrix supported; unsorted to poorly sorted; poorly exposed.

UNIT 6: pebble to cobble gravels; beds dip 23-31° NE (055°); open work and matrix filled beds; lower contact erosional and dips gently (5°) NE.

UNIT 5: sandy gravel; horizontal bedding to gently inclined planar crossbedding; poorly sorted; clasts mainly angular to subangular; minor horizontally laminated silt and fine sand beds; lower contact erosional and dips gently (5°) NE.

UNIT 4: pebble gravel; beds dip 15-20° NE (052°); clast supported; mainly openwork; moderately to well sorted; clasts mainly angular to subangular.

UNIT 3: sands; horizontally stratified; well to very well sorted; strata 0.1-10 cm thick; minor granule beds; some planar and trough cross-bedding; dropstones

UNIT 2: coarse gravel; clast supported; poorly sorted; 60-80% clasts, subangular to subrounded, up to boulder size; matrix sandy; disorganized fabric; poorly exposed; lower contact covered.

Covered interval.

UNIT 1: schist; vertical foliation; minor quartz veins and fracturing.

Livingstone Creek Section

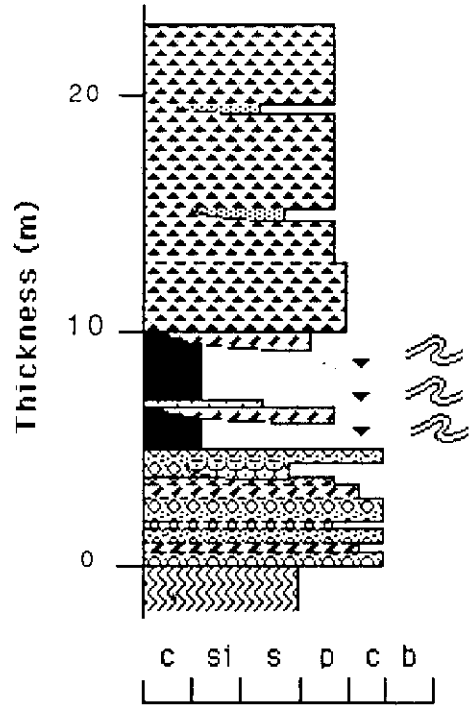

UNIT 5: diamicton; massive; matrix supported; silty mud matrix; 20-40% clasts, up to bouder sized, subangular to subrounded, striations common; light brown color; minor sorted sand lenses; poorly exposed.

UNIT 4: diamicton; as above except sandy silt matrix and dark grey

UNIT 3: silts and clays; parallel laminated; intense folding; pebble breccia intrabeds of very angular, local lithology; rounded erratics common as dropstones but rare in intrabeds; minor oxidized sands.

UNIT 2: gravels; horizontal bedding; clast supported; matrix filled; clasts up to boulder sized, well rounded to sub rounded; poorly to moderately sorted; some imbricated, cobble breccia beds of local schist; minor open work pebble gravel and trough cross-bedded sands.

UNIT 1: bedrock; blocky quartzite and schist; vertical foliation; silicified with abundant pyrite crystals oriented parallel to foliation; numerous near vertical quartz veins

Figure 5. Composite stratigraphic columns for the Summit Creek and Livingstone Creek sections. See Figures 2 and 3 for explanation of symbols.

Columbia, just south of the Yukon border (Levson, 1991; Levson and Kerr, 1991) and in central British Columbia (Levson and Giles, 1990; Levson, 1991).

Glacial features and surficial deposits in the area were mapped by Hughes (1968), and Klassen and Morison (1987). Surficial deposits in the area are mainly thin till and colluvium. An irregular glaciofluvial complex occurs in the South Big Salmon Valley near the mouth of Martin Creek (Klassen and Morison, 1987). The prominent valley that diverts the westerly flow of Livingstone and Summit Creeks is an ice-marginal channel (Hughes, 1968). Indicators of former ice flow direction, mapped by Hughes (1968) and Klassen and Morison (1987), suggest that glaciers flowed north along the low valleys that cross the Semenof Hills into the South Big Salmon River Valley in the Livingstone Creek area.

BEDROCK GEOLOGY

The Livingstone Creek area occurs within the Teslin Suture Zone (Figure 1), which is separated from the Semenof Hills Block, to the west, by the Big Salmon Fault (Tempelman-Kluit, 1980 and 1984). This fault closely parallels the South Big Salmon River in the area directly west of the studied sections (Figure 1). Local bedrock in the drainage basins of the investigated creeks is dominantly dark green, cataclastic, fine grained amphibolite and amphibolitic greenstone that grades into massive, melanocratic, dioritic to quartz dioritic hornblende augen gneiss. These rocks belong to the Anvil allochthonous assemblage and are associated with muscovite-quartz schist and muscovite quartzite of the Nisutlin assemblage (Tempelman-Kluit, 1984). Outcrops close to the Martin Creek section are dark, fine grained, strongly foliated and faulted greenstone and schist with some soft, strongly altered (kaolinitic?) and silicified zones (Figure 6a). Quartz veins are conspicuous throughout. Schist and quartzite are exposed at the base of the Summit Creek and Livingstone Creek sections. Quartz veins are present at both locations and are particularly numerous at Livingstone Creek, where the bedrock is also strongly silicified and pyritized. A belt of sheared granodiorite extends north from Livingstone Creek across the headwaters of Summit Creek (Bostock and Lees, 1938).

The Omineca Crystalline Belt occurs just east of the study area in the eastern Big Salmon mountains, the headwaters of the South Big Salmon River (Figure 1). Rocks outcropping in this area include Middle Cretaceous biotite granite, dolomite, siltstone, quartzite and shale of the Paleozoic Hogg and Nasina Formations, and granodiorite gneiss with intercalated mica-quartz schist of the Proterozoic and Lower Cambrian Ketza Group (Tempelman-Kluit, 1984).

Phyllite, greywacke, chert, chert conglomerate, and limestone of the Boswell Formation outcrop directly west of the study area in the Semenof Hills Block. Volcanic rocks of the Semenof and Open Creek Formations occur further to the east and south. Even further southeast, beyond the Teslin River, the Whitehorse Trough (Figure 1) is dominated by shale, greywacke and conglomerate of the Laberge Group with minor limestone (the Hancock Member)(Tempelman-Kluit, 1984). The Whitehorse Trough is the most probable source of rounded monzonite, granodiorite and syenite erratics found in the study area, and their presence indicates long distance ice transport. Two small bodies of porphyritic granodiorite and monzonite intrude Whitehorse Trough rocks directly south of the study area (Bostock and Lees, 1938).

SECTION DESCRIPTIONS AND INTERPRETATIONS

Martin Creek Section

Two sections were described at Martin Creek. A summary of the sequence of deposits exposed at the main Martin Creek Section (units 1 to 4) is provided in Figure 2. Unit 5 is exposed further down valley in a shallow exposure about 140 m in length which is referred to as the west Martin Creek section (Appendix 1). Detailed sedimentologic logs of units 2 and 3 at the main section are provided in Figures 3 and 4, respectively. A complete description of the Martin Creek Sections is provided in Appendix 1.

Unit 1

The lowest exposed sediments at Martin Creek (units 1a to 1d; Figure 2 and Appendix 1) are poorly sorted, coarse, mainly clast-supported gravels (Figure 6b). Lithologic analyses indicate that a high proportion of the clasts are derived from the local drainage basin (Figure 7) and some very angular clasts have come from the bedrock directly upstream of the section.

Several gradationally interbedded facies are recognized:

(1) Clast supported, with matrix-filled gravels dominant (Figure 6c). These gravels are poorly sorted, containing clay to boulder sized materials. They are structureless with a disorganized fabric and contain numerous angular clasts.

(2) A second gravel facies, better sorted, with more rounded clasts, and minor open work beds (Figure 6d). Some beds exhibit weak imbrication and crude, sub-horizontal stratification due to variations in clast size and sorting between beds. Sorting is generally poor, but a few pebble beds are moderately well sorted. Stratified clay, silt, sand and pebbly sands occur around some clasts (Figure 6d). Clasts are mainly rounded to subrounded.

(3) The coarsest beds in unit 1 contain clasts up to 1 m in diameter, which occur in disorganized clusters surrounded by sorted beds of finer material (Figure 6e). Pebble and pebbly sand beds generally occur downstream of the clusters whereas pebble to cobble beds occur upstream. A weak imbrication is locally developed.

(4) Gravel facies grade into massive, matrix to clast-supported diamicton beds (eg. unit 1c Appendix 1; Figure 6f). The shape and size ranges of clasts in the diamictons are similar to gravels of facies 1 above but the diamictons contain a much higher proportion of matrix.

The massive structure, high matrix component, and the presence of angular clasts in the poorly sorted gravels (facies

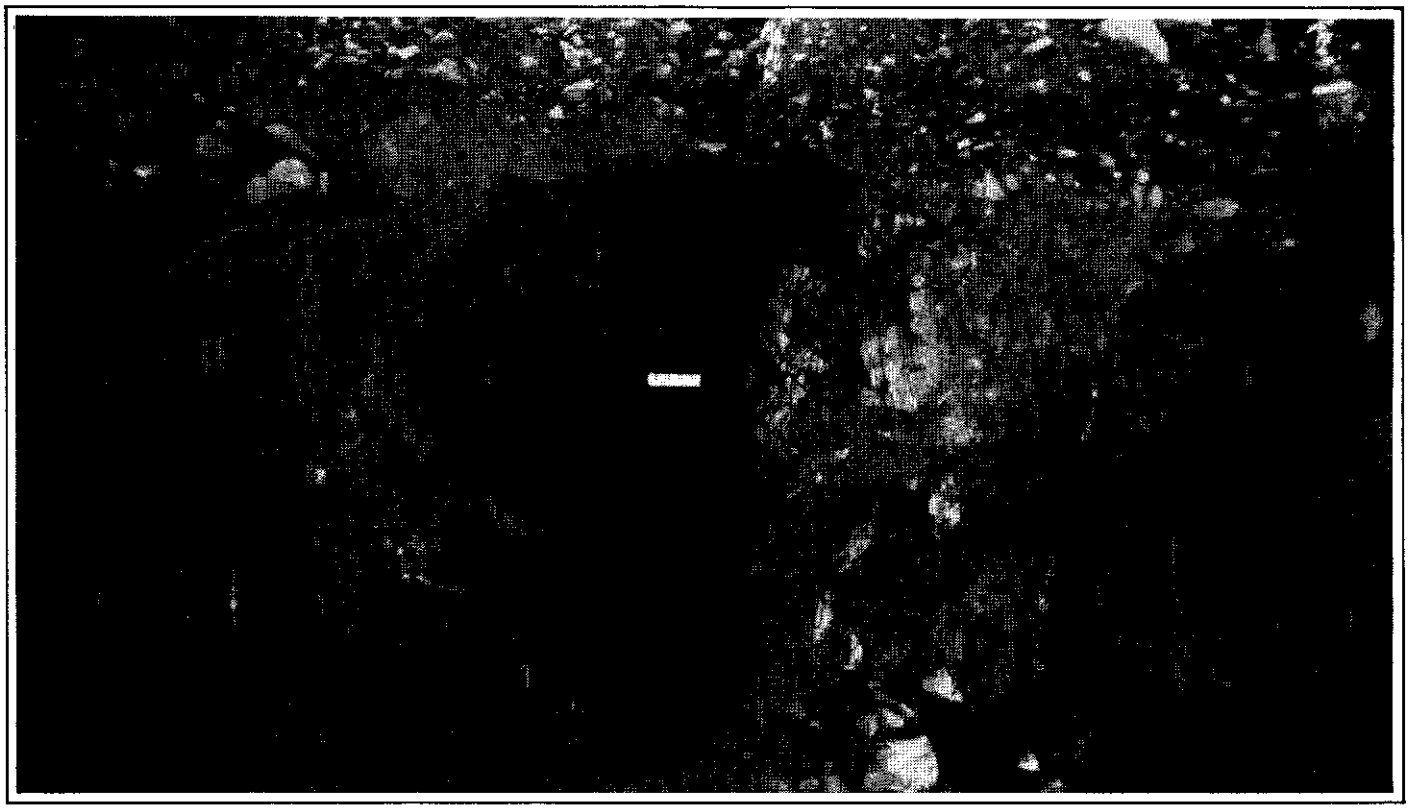

Figure 6. Bedrock and unit 1 gravels at Martin Creek. Paleo-flow is from left to right in all cases. (a) Local bedrock outcrop with a highly altered and silicified zone on the right in sharp contact with fine grained melanocratic rocks on the left. The outcrop has abundant quartz veins, is about 1 m high, and is overlain by gravel tailings.

Fig. 6(b). Poorly sorted coarse gravels typical of unit 1. Rod is 1.5 m long.

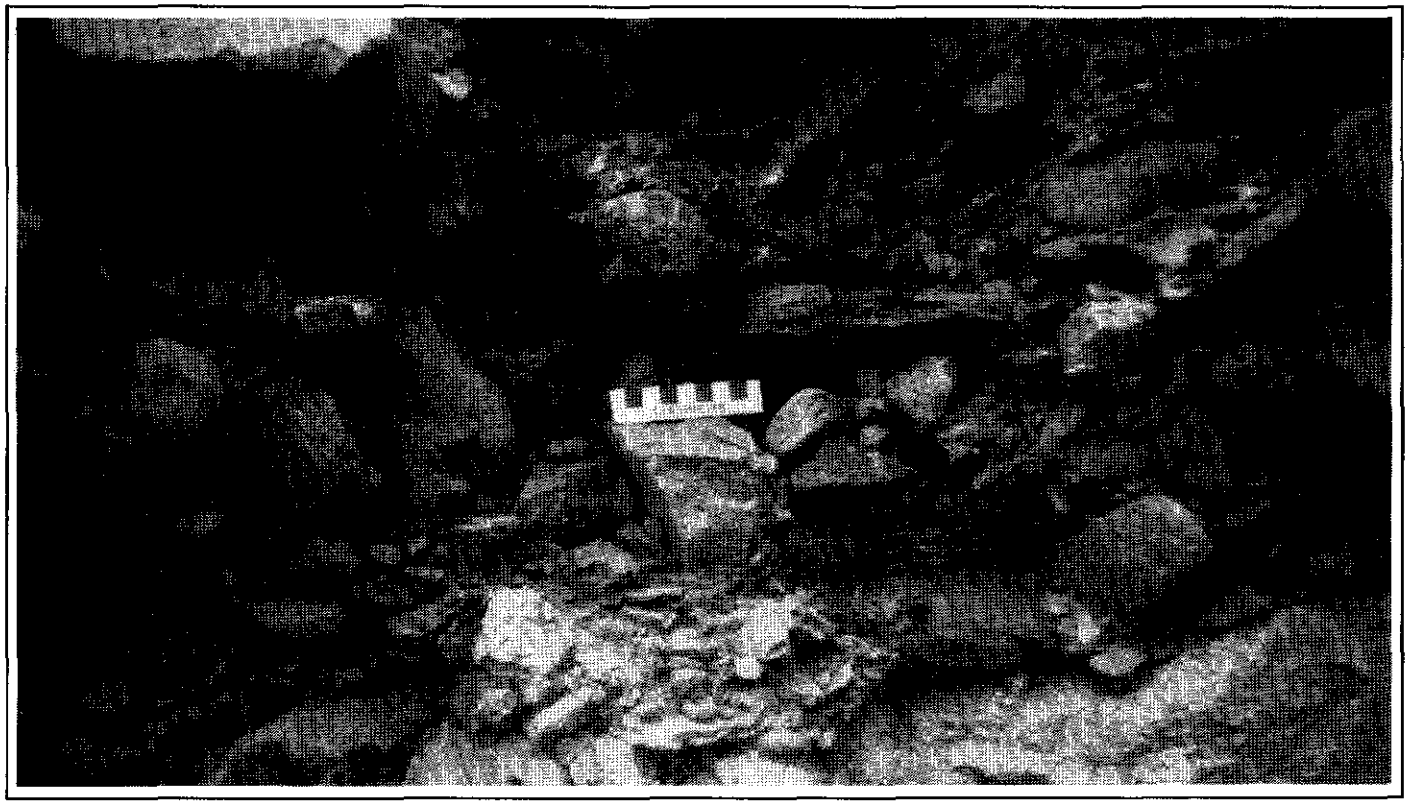

Fig. 6(c). Structureless, clast-supported, matrix filled gravels (facies 1).

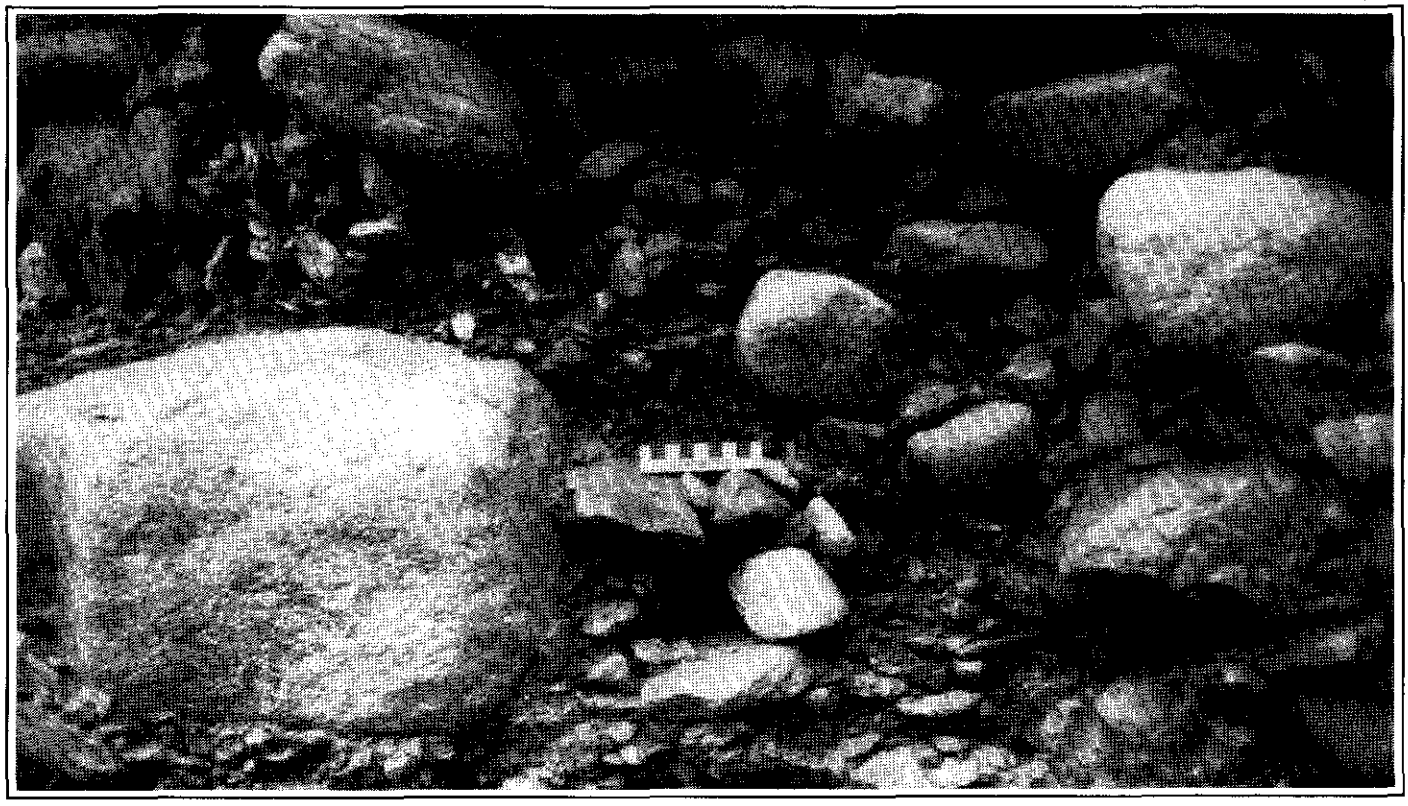

Fig. 6(d). Poorly to moderately sorted, clast-supported gravels with crude horizontal stratification and imbrication (facies 2). Note the open-work bed at the top and the finer gravel surrounding the cobble at the left. Scale in centimetres.

Fig. 6(e). Disorganized cobble and boulder cluster with an accumulation of coarse pebbles and small cobbles up flow (right) and mainly small to medium pebbles in the lee of the cluster. Pick is 65 cm long.

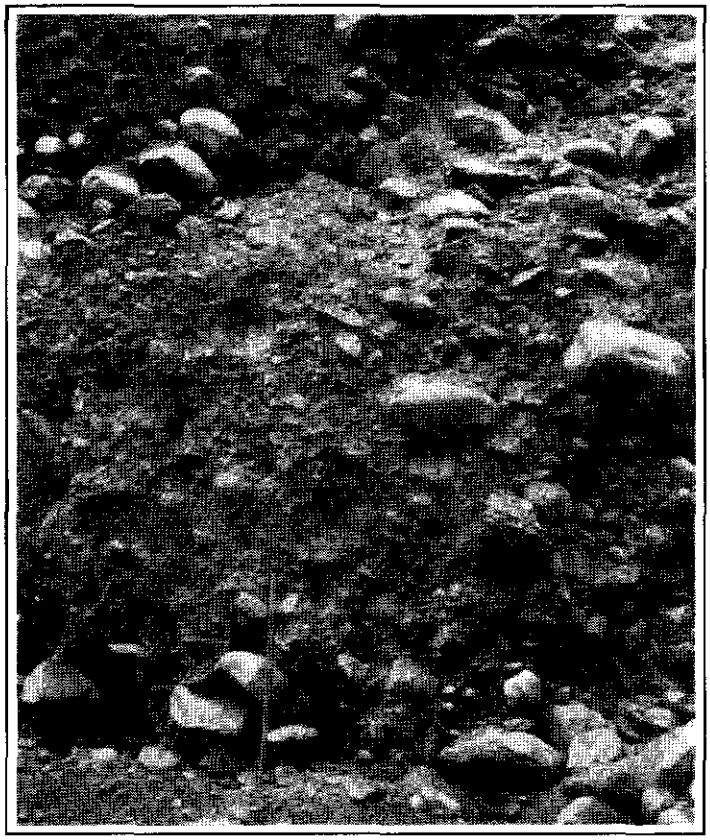

Fig. 6(f). Massive, matrix- to clast-supported debris flow deposits (facies 4) in unit 1c.

1) and diamicton beds (facies 4) suggest deposition by mass-flow processes. The large clast size and poor sorting indicate high energy flows with rapid deposition. Massive, poorly sorted sediments with a fine matrix, disorganized fabric and gradational bed contacts are typical of debris flow deposits (Fisher, 1971; Bull, 1972; Harvey, 1984; Kochel and Johnson, 1984; Wells, 1984).

Matrix support and higher mud contents in some facies 4 beds suggest that some flows were viscous and that clasts were supported by the cohesive strength of the matrix. Smeared and vertically slickensided clay coatings on clasts in some diamicton beds (unit 1c, Appendix 1) probably result from confined, vertical movement of the clasts through a highly viscous matrix. In contrast, the lower matrix content of some gravelly facies 1 beds suggests deposition from flows in which clasts remained mostly in contact with each other. Similar deposits with few fines and a massive, ungraded character were interpreted by Larsen and Steel (1978) and Burgisser (1984) as gravelly debris flows. Particles were probably suspended in these flows by buoyancy and grain to grain contact rather than by the cohesive strength of the matrix. These grain support mechanisms are typical of gravelly debris flows (Pierson, 1981; and Burgisser, 1984).

Better sorting and the presence of more rounded clasts and open-work beds suggests that some beds in unit 1 (facies 2) may have been deposited by more fluvial-dominated processes. Crude, sub-horizontal stratification has been well documented in shallow, gravelly, braided streams (Boothroyd and Ashley,

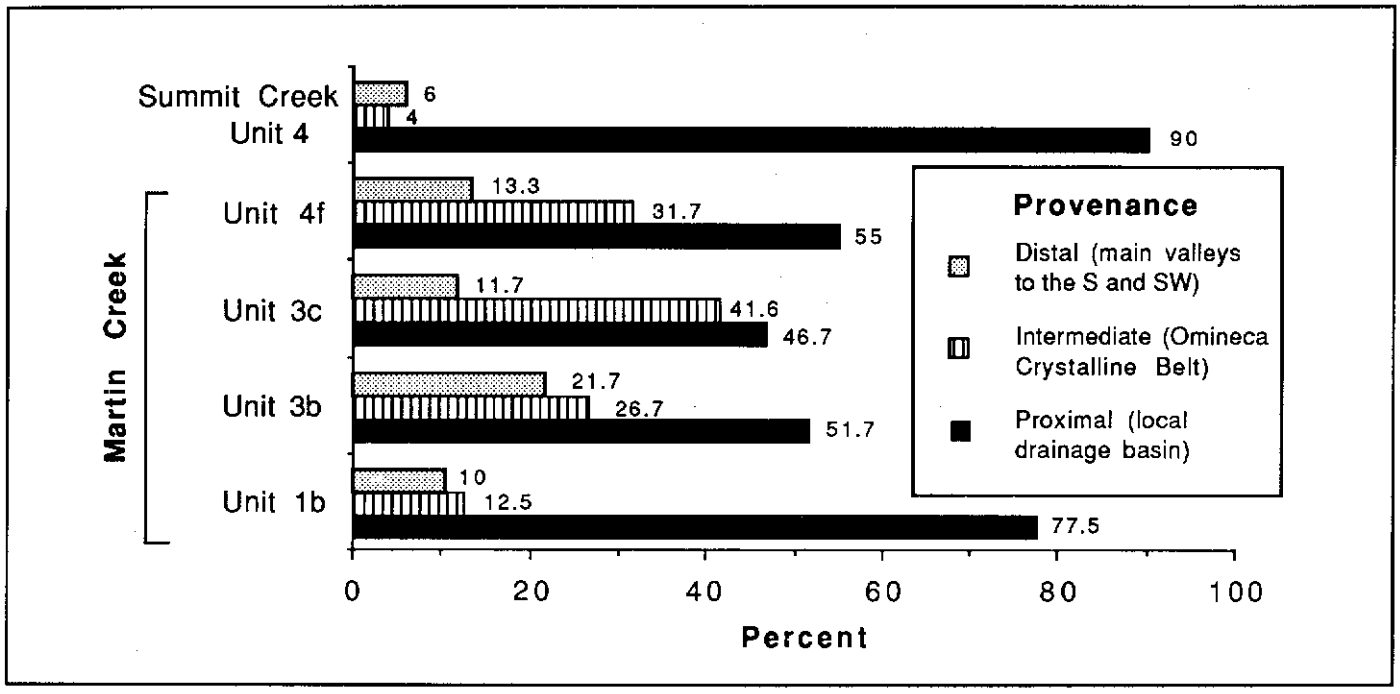

Figure 7. Provenance of pebbles from sampled beds at Martin and Summit Creeks.

1975; Church and Gilbert, 1975; Hein and Walker, 1977). Weak imbrication and rounded clasts indicate bedload transport. Sorting around clasts may be due to localized increases in turbulence in the more fluid flows or to the infiltration of finer materials as the flow waned. The distinction between deposits from watery debris flows and those from high velocity streams carrying high sediment concentrations is unclear and transitions from viscous to fluid flow may even occur during the same event (Johnson, 1970; Lowe,1979; Middleton and Hampton, 1976; Nardin et. al., 1979; Morison and Hein, 1987). Partly turbulent, hyperconcentrated flood flows, with sediment/water ratios intermediate between cohesive debris flows and normal stream flows, produce similar deposits (Smith, 1986,1987; Waresbach and Turberville, 1990).

Disorganized to weakly imbricated clast clusters, similar to those described above (facies 3), were observed by Brayshaw, (1984) in natural channels and flume experiments. The clusters developed subsequent to the deposition of large clasts (median size, D95, i.e. coarser than 95% of the bedload) which obstruct the flow. Fine grained (D8 to D46) wake accumulations are deposited in the obstacle shadow and comparatively coarse (D74 to D94) clasts accumulate in a cluster on the stoss-side (Brayshaw, 1984). The preservation of underlying fine grained sediments is due to the armouring effect of the cluster. Cluster bedforms develop during the falling stage of flood discharges.

Taken together, these facies are interpreted as high energy, stream channel or gulch sediments. Deposition occurred from both high velocity, channelized fluvial flows and debris flows. Large, lateral and vertical differences in grain size and sorting indicate substantial spatial and temporal variability in flow and/or sediment load. Unsorted beds, in part, matrix-supported, are probably debris flow deposits and form one end of a continuum. Weakly imbricated and stratified beds of poorly sorted gravel indicate more fluvial-dominated sedimentation. Discharges sufficient to move clasts up to 1 m or more in diameter probably occurred only after unusually large storm or spring runoff events. Gradational changes in grain size distribution suggest fluctuations in flow were gradual. The presence of clasts of erratic lithology (Figure 7) indicates that the gravels are interglacial (or interstadial) and not preglacial.

Unit 2

The gravels of unit 1 are overlain by almost 12 metres of interbedded fine grained sediments and diamicton (units 2a to 2f; Figures 2 and 3 and Appendix 1). Parallel laminated silts and clays dominate with minor ripple bedded sands (Figures 8a and 8b). Diamicton interbeds are matrix-supported and vary in thickness from a few centimetres or less (Figures 8a and 8c) to tens of centimetres (Figure 8d). Silt and clay beds commonly contain stones that are often striated, draped by overlying strata and deform underlying beds (Figures 8a to 8c). Folded bedding, faults, slump structures, load structures and mud intraclasts are abundant (Figures 8d to 8h). Beds dip about 10° to the northeast (50°), opposite to the regional slope. The abundance and thickness of diamicton beds and striated clasts increases up-section toward the southwest. Some diamicton beds are capped by gravel concentrations and exhibit inverse, coarse-tail grading (Figure 8d). Some clasts protrude from the tops of the beds (Figures 8d and 8f). In

diamicton beds in the lower part of the unit (eg. unit 2a), numerous pebble to cobble sized clasts occur in a silty clay matrix. Many of the stones are angular and derived from the local bedrock.

Deposits similar to those in unit 2 are typical of proximal glaciolacustrine environments (Ashley, 1988; McCabe and Eyles, 1988). Parallel-laminated clay and silt beds and ripple-bedded sands are interpreted as quiet water suspension and density underflow deposits. The abundance of striated clasts, inferred to be dropstones, indicate the proximity of ice. Interbeds of matrix-supported diamicton are interpreted as debris flow deposits. Modern debris flow sediments have characteristics similar to those described above (Bull, 1972; Kochel and Johnson, 1984). Massive, disorganized, matrix-supported diamictons with sharp, non-erosional lower contacts were interpreted as debris flow deposits by Harvey (1984) and Wells (1984). Clasts that project above bed tops are characteristic of viscous debris flows (Johnson, 1970; Nardin et. al., 1979) and imply a high matrix strength. The presence of inverse grading also suggests a debris flow origin for these deposits (Fisher, 1971 and Lowe, 1979). This interpretation is further supported by the occurrence of recumbent and overturned isoclinal folds inferred to be flow structures, abundant evidence of loading, and numerous inclusions of silt and clay which are interpreted as rip up clasts (Figures 8e and 8f).

The upslope dip of beds, indicates that the flows were derived from a high surface to the southwest, probably a glacier in the main valley. This is also suggested by an increase in abundance and thickness of diamicton beds toward the southwest. Instability in the ice-marginal lake sediments is indicated by abundant folds and faults. Normal faults (Figures 8c and 89), common in unit 2 (Figures 3 and 8), probably developed as a result of movement in the adjoining glacier.

The fine grained matrix of the debris flows likely originated by intraformational slumping of the unstable silts and clays (Figure 8h). The abundant local, angular stones in some diamicton beds in the lower part of the unit were probably eroded by the glacier shortly before incorporation in the debris flows. Similarly, large clasts transported by the glacier were undoubtedly incorporated in the flows. Textural inversions, characterized by angular and/or large clasts in a fine grained matrix, are typical of sediments produced by mixing of deposits from two different environments (Folk, 1980). Similar, texturally inverted, matrix-rich conglomerates and granule sandstones with associated loading, slumping and faulting, were interpreted by Larsen and Steel (1978) as subaqueously resedimented deposits of mixed debris flow and lacustrine origin. Diamicton beds formed by gravitational flows of coarse grained material over fine grained glaciolacustrine sediments should typify ice-marginal deltaic environments (Cohen, 1983). The pronounced and widespread upvalley dip of beds in unit 2 is consistent with the interpretation of an ice-marginal deltaic or pro-deltaic depositional environment.

Gravel concentrations capping some diamicton beds (eg. Figure 8d) probably result from winnowing by bottom currents or subaerial exposure. Periodic traction deposition is indicated by minor ripple and cross-bedded sand, pebbly sand and pebbly gravel beds. The increase in thickness of diamicton beds and traction deposits up section indicates a gradual infilling of the ice-marginal lake. The upward increase in the total number of erratic and striated clasts suggests the increased influence of glacier expansion in the main valley.

Unit 3

Unit 3 is dominated by matrix-supported diamicton (Figure 9a). The lower part of the unit (unit 3a; Figures 2 and 4 and Appendix 1) exhibits weak, horizontal stratification due to textural variations in the diamicton and the presence of numerous silt and fine sand beds and laminae. Load structures and folded laminae are common.

Almost five metres of dense, massive diamicton (Figure 9b) with numerous striated and glacially shaped clasts and polished subhorizontal partings occurs in the middle of unit 3 (unit 3b; Figure 2). Small lenses of silt, clay and sand near the top of unit 3b commonly exhibit compressive deformation structures such as thrust faults, reverse faults, folds and sub-horizontal shear zones (Figure 9c). Slickensides on shear zones (Figure 4) trend 110° to 150°, approximately parallel to the South Big Salmon River valley. The lower contact of unit 3b is gradational.

Unit 3c consists of about 7 m of sandy, loosely consolidated diamicton interbedded with silt, sand and gravel (Figure 9b). Diamicton beds are matrix to clast-supported (Figure 9d) with the total clast and sand content increasing towards the top of the unit. Massive or horizontally stratified sand and silt beds and trough cross-stratified sand and gravel lenses are common throughout the unit (Figure 9e).

Diamicton beds in unit 3a are interpreted as debris flow deposits. The presence of folded laminae believed to be flow folds support this interpretation. Load structures and deformed bedding indicate that the diamictons were deposited rapidly over unconsolidated sediments. The horizontal stratification, fine grain size and excellent sorting of the silt and sand beds suggests that they are mainly lacustrine sediments. The abundance of silty laminae and the association of these sediments with the underlying glaciolacustrine deposits suggests that the debris flows were dominantly subaqueous. Similar stratified diamictons with silt and sand laminae were interpreted as ice-marginal, subaqueous debris flows by Boulton (1968), Evenson et al. (1977), Eyles (1987) and Levson and Rutter (1988).

The diamicton in unit 3b is interpreted as a subglacial till probably deposited by lodgment processes. The sedimentary characteristics of the diamicton are typical of lodgment tills (Dreimanis, 1988). Partings, faults and shear zones probably formed at or near the sliding base of an overriding glacier. This is supported by the orientation of slickensides parallel to the inferred direction of former ice flow down the South Big Salmon River valley. Pebble fabric data from the upper part of unit 3b (Figure 4) also support this interpretation. The long axes of pebbles have a strong (S1 = 0.75) preferred

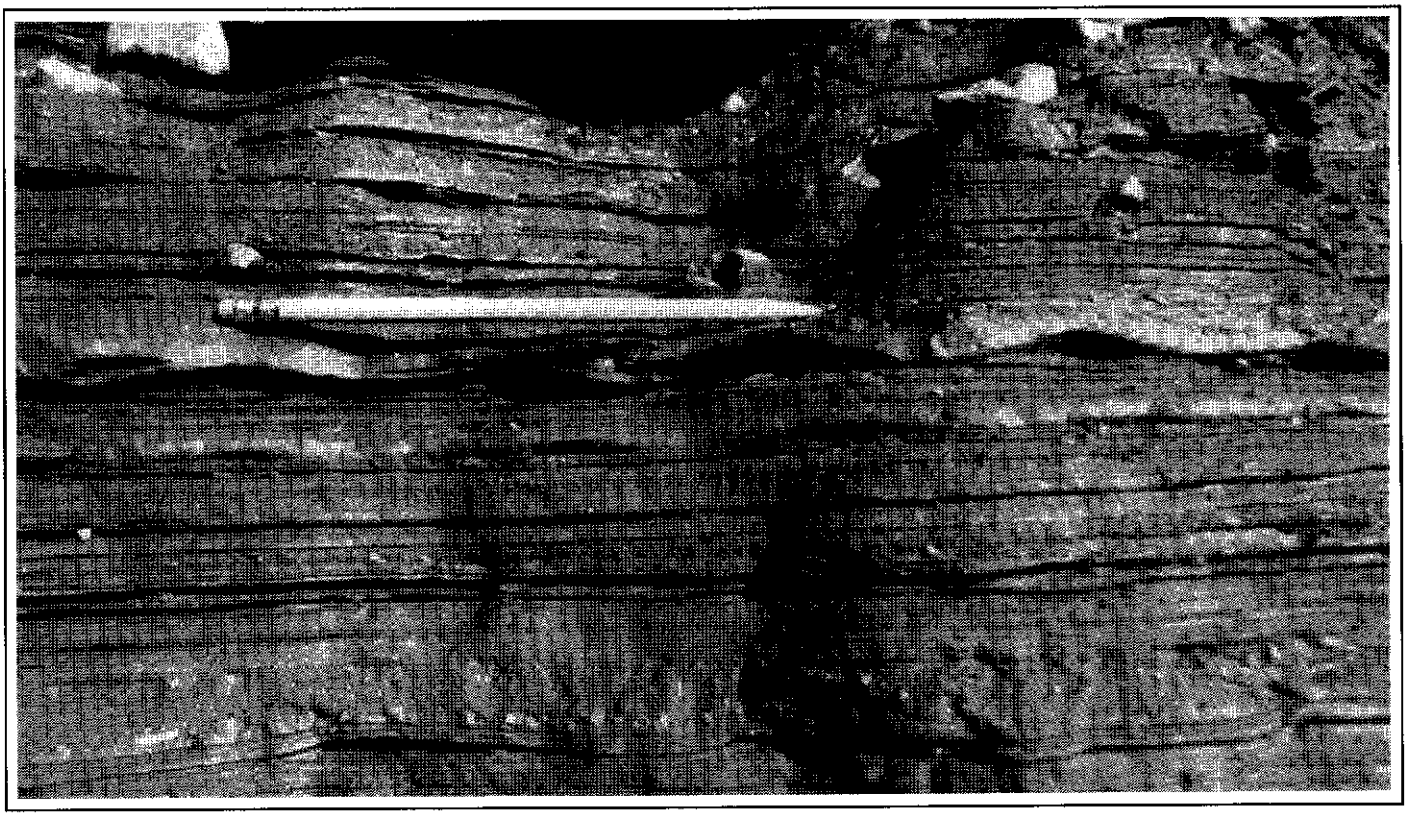

Figure 8. Proximal glaciolacustrine sediments of Unit 2 at Martin Creek. (a) Parallel-laminated silts and clays with thin intrabeds of diamicton and ripple-bedded fine sand and numerous dropstones.

Fig. 8(b). Deformed strata under dropstone in unit 2b. Note: 1 cm thick fine sand bed below scale and diamicton bed at top.

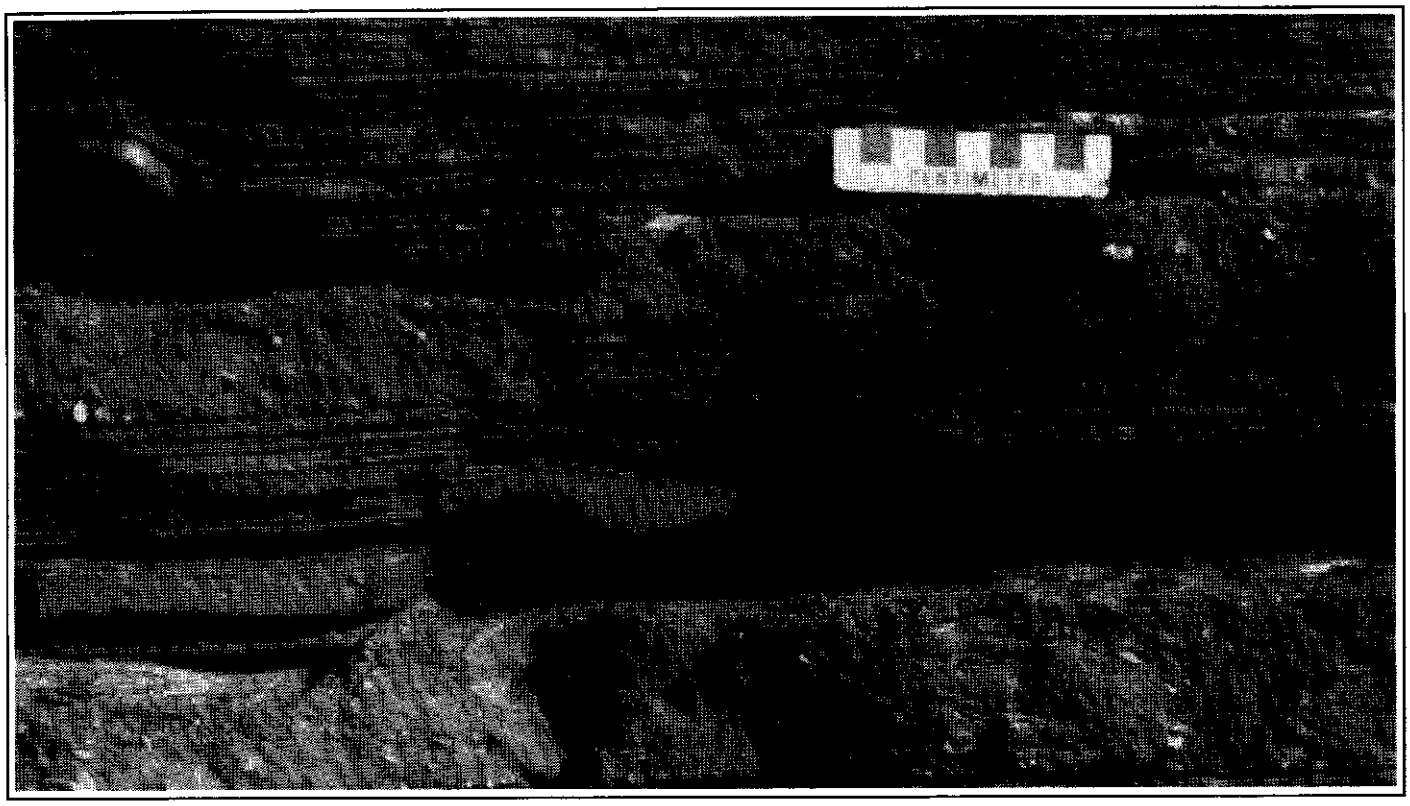

Fig. 8(c). Normal fault in interbedded diamicton and fines.

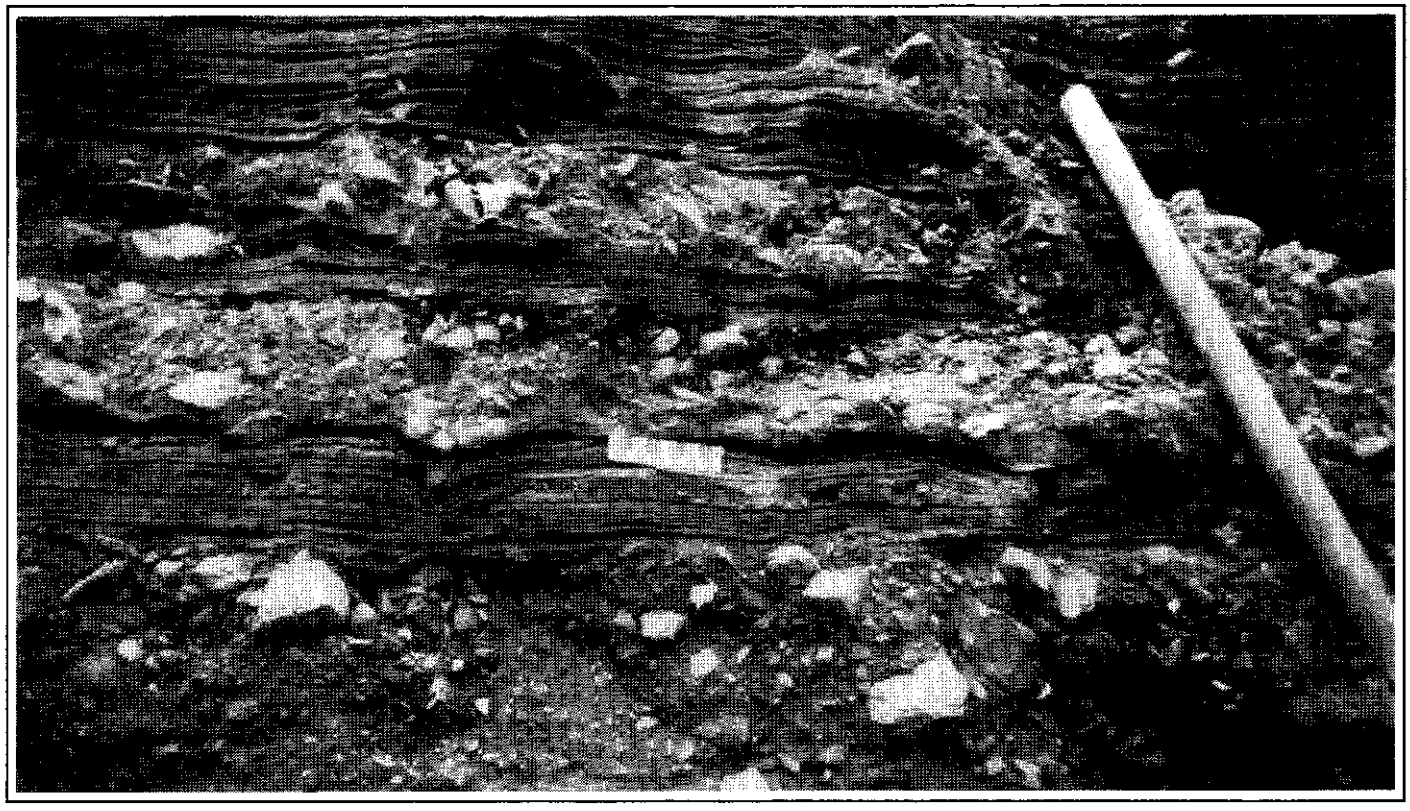

Fig. 8(d). Reversely graded debris flow deposits in laminated silts and clays. Note: gravel concentration at top of diamicton bed above small scale bar.

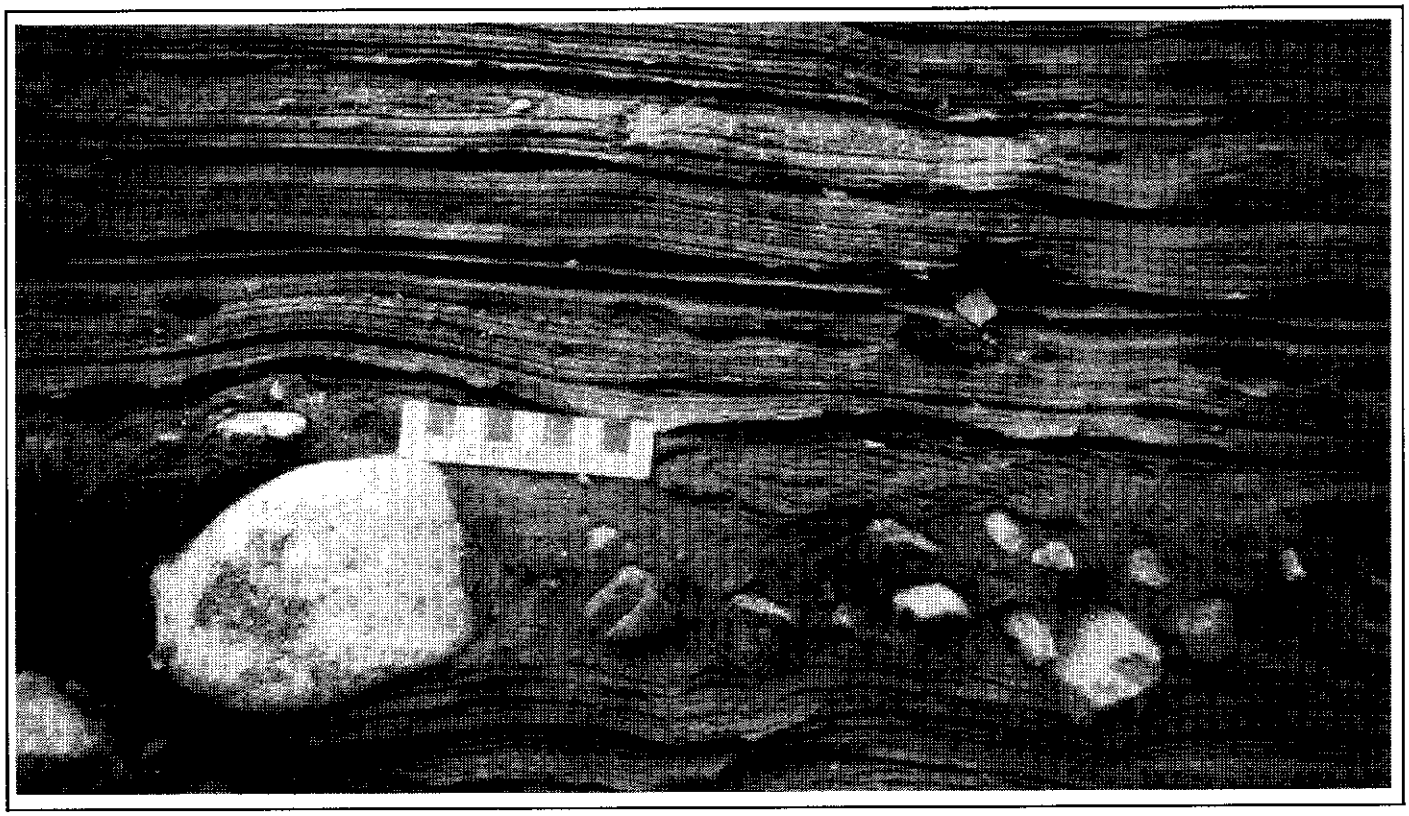

Fig. 8(e). Folded silt and clay intraclasts within diamicton bed.

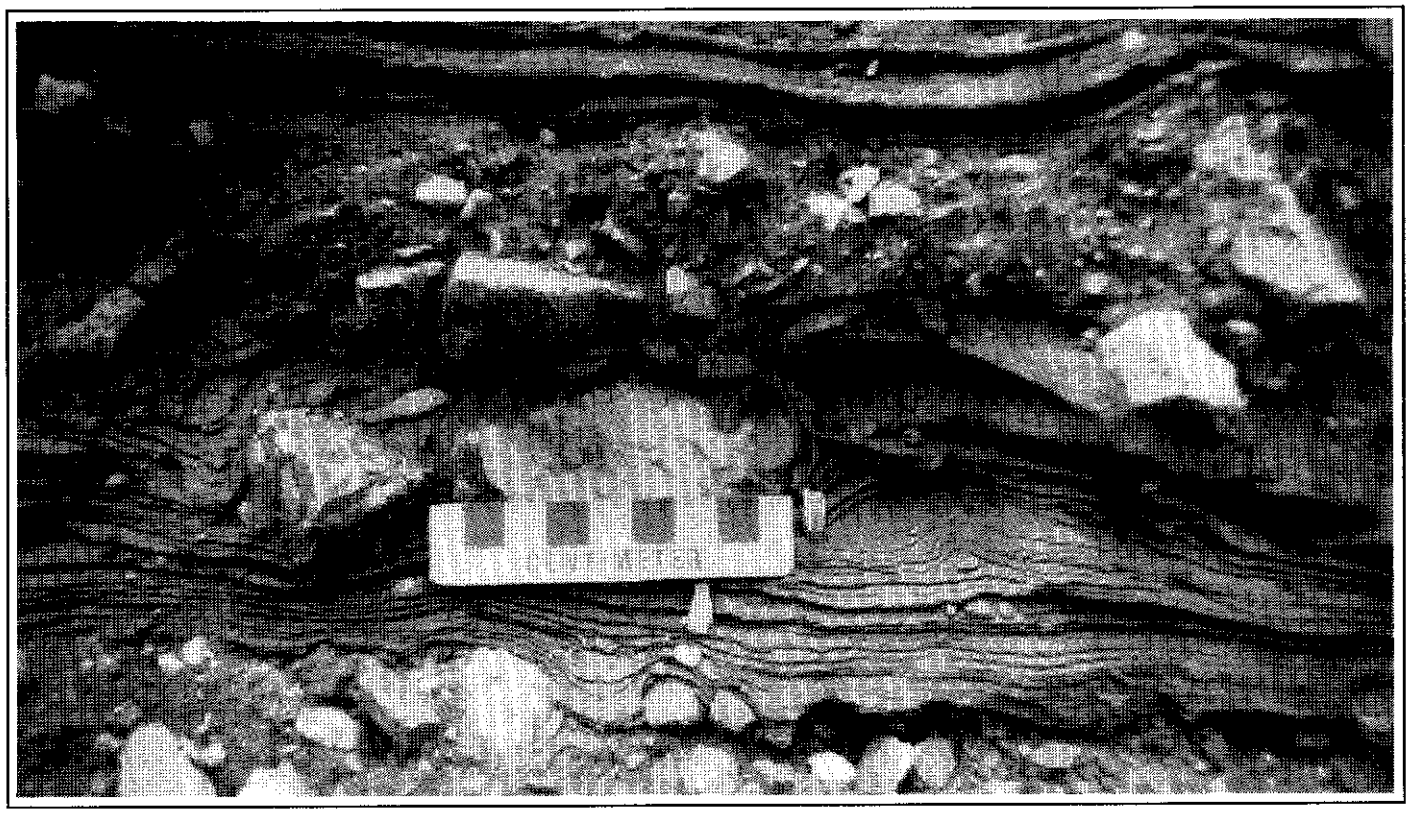

Fig. 8(f). Large mud intraclast in diamicton bed (above and right of scale) and mud drapes over clasts protruding from the top of the lower diamicton bed.

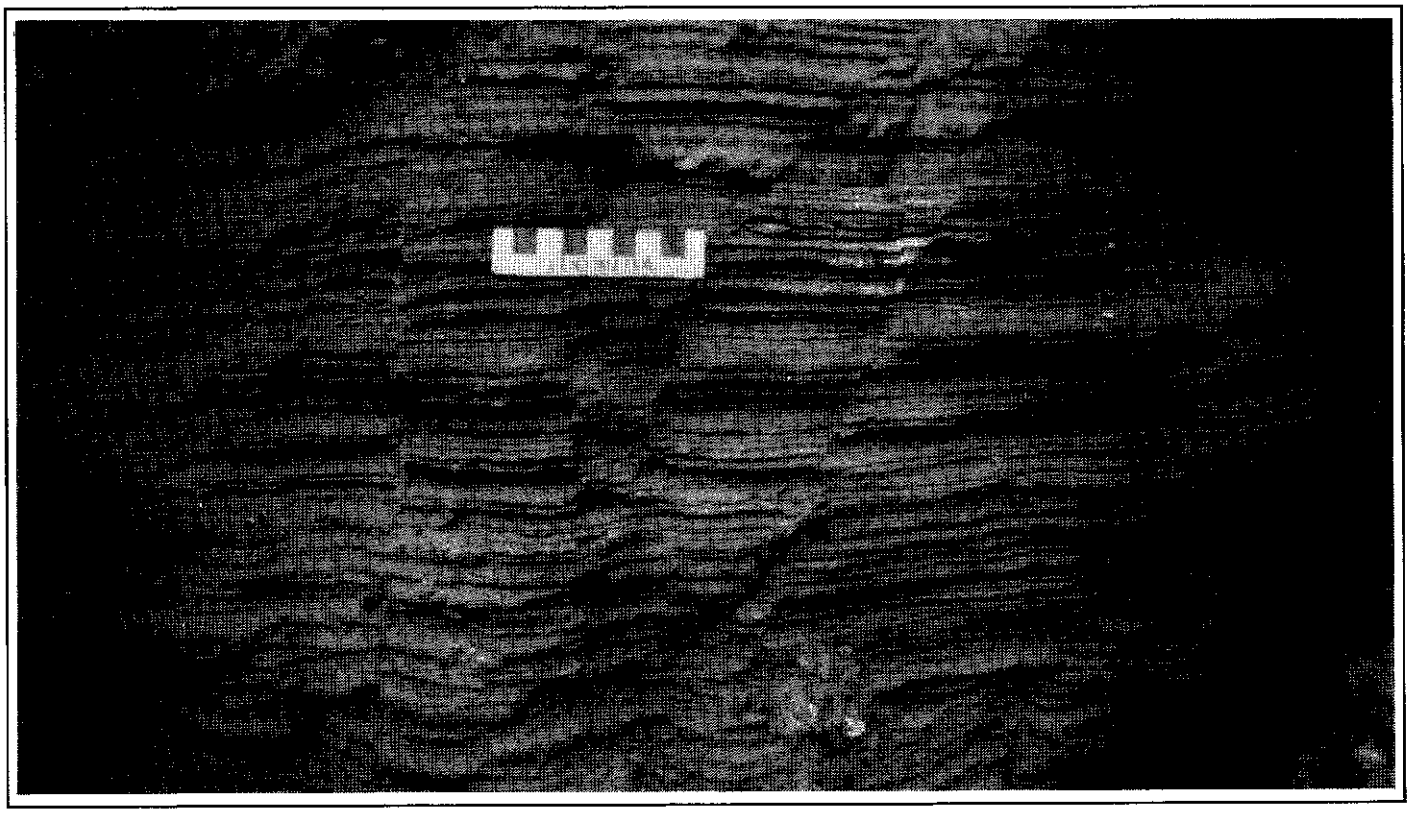

Fig. 8(g). Abundant normal faults in unit 2c.

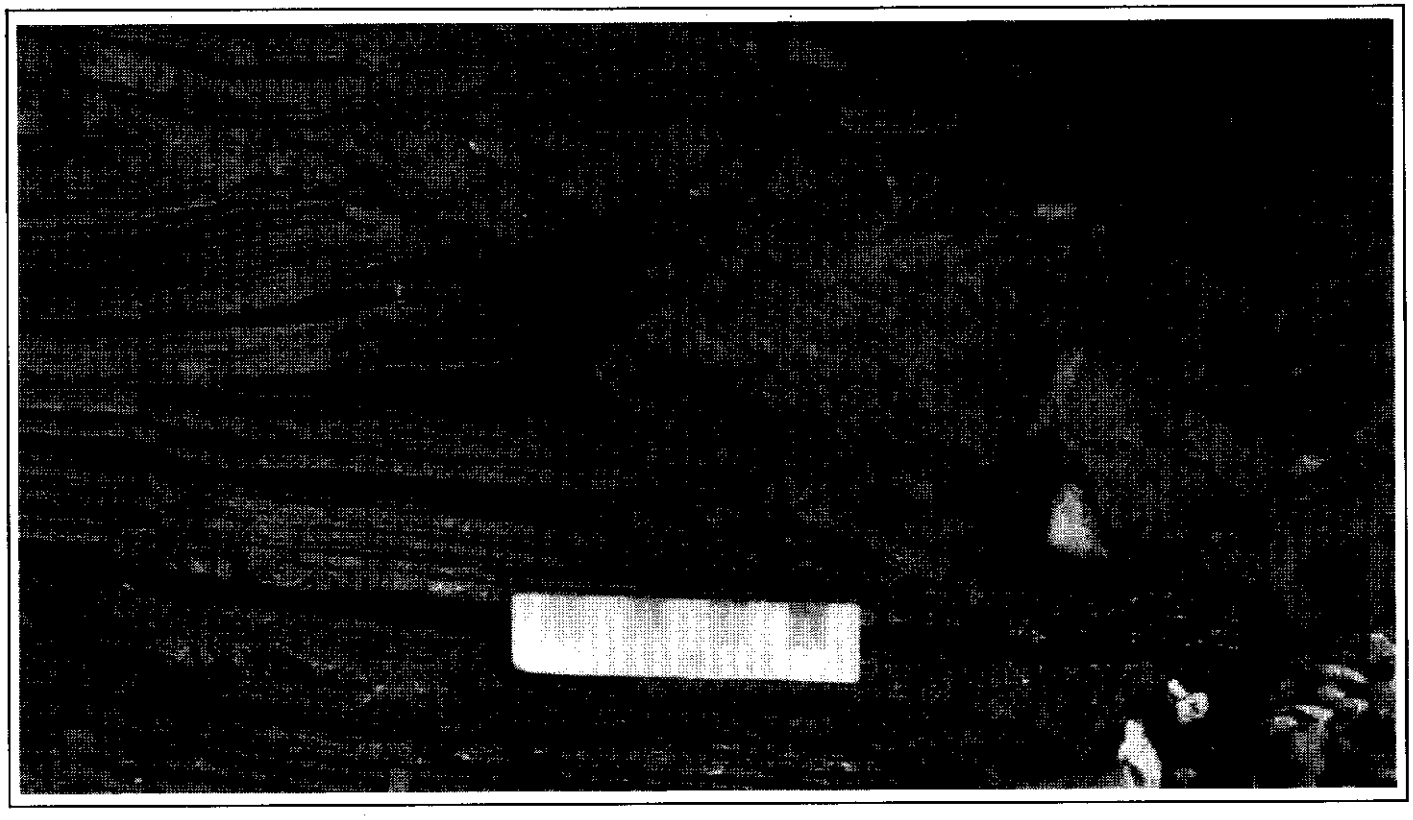

Fig. 8(h). Intraformational slump structure.

Figure 9. Sedimentary characteristics of units 3 and 4 at Martin Creek. (a) Matrix-supported diamicton with weak textural stratification in unit 3a.

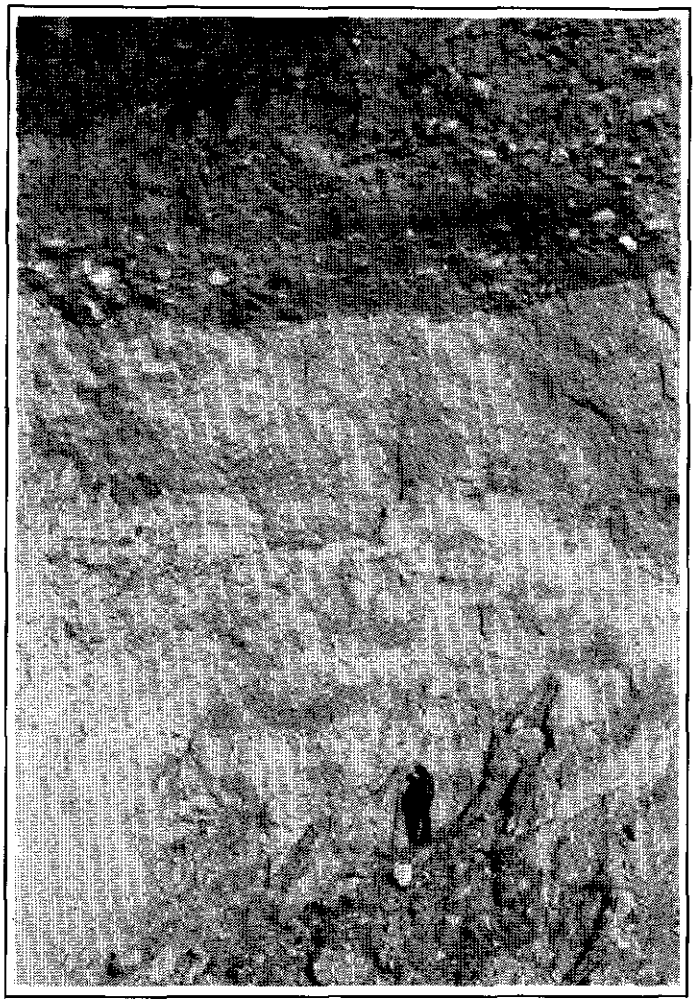

Fig. 9(b). Massive diamicton of unit 3b grading up into unit 3c and unconformably overlain by unit 4.

orientation (V1 = 126°) parallel to the trend of slickensides and the main valley (Figure 4). Pebbles at the base of unit 3b have a relatively weak (S1 = 0.62) preferred orientation at right angles (V1 = 047°) to the trend of the main valley but parallel to the Martin Creek valley (Figure 4). This suggests that the lower part of unit 3b may have a debris flow origin similar to the underlying diamicton of unit 3a.

The large number of clasts of erratic lithology in unit 3b also supports a glacial origin. The provenance of the clasts indicates a substantial input of debris from glaciers which originated in the main valleys to the south and, to a lesser degree, in tributary valleys to the southwest. The higher percentages of clasts derived from the Omineca Crystalline Belt in overlying units (Figure 7) may reflect the increased influence of an inset tributary glacier that likely originated in the Big Salmon Range and flowed down the upper South Big Salmon River valley.

The high clast content and sandy texture of the diamictons in unit 3c is typical of debris flow deposits that have been washed during one or more cycles of resedimentation (Lawson,1979; 1981a; and 1981b). The weak (S1 = 0.58) preferred orientation of pebbles in unit 3c (Figure 4) is also typical of debris flow deposits. Lenses and beds of sorted material are interpreted as fluvial sediments deposited between debris flow events. Lawson (1979) found that thin layers of sand and silt often separate diamictons deposited by individual flows. A decrease in the number of striated clasts and increased sorting toward the top of the unit probably reflects greater dominance of fluvial activity. All of unit 3c occurs in a wide (> 50 m), trough-shaped body which is interpreted as a broad channel that presumably developed along the ice margin during deglaciation.

Unit 4

Unit 4 consists of about 12 m of mainly horizontally stratified gravels (Figures 9b, 9f, and 9h). Beds of open-work, poorly sorted, cobble to boulder gravel are interbedded with poorly to moderately sorted, matrix-filled, pebbly gravel and sand beds (Figure 9f). Some lenses of well sorted, horizontally stratified and planar and trough cross-stratified sand lenses also occur (Figure 9g). Lower bed contacts are commonly erosional. The lower contact of unit 4 is

Fig. 9(c). Subhorizontal shear zones and compressively deformed strata (arrows are 1 cm long and point to a sample reverse fault) at the top of unit 3b.

unconformable and forms a large scour (Figure 9h) similar in size and shape to the channel shaped lower contact of unit 3c. Deposits of this type are typical of gravelly, proximal, braided rivers in glacial environments (Rust, 1972; Church and Gilbert, 1975; Boothroyd and Ashley, 1975).

Crude horizontal stratification is commonly formed in longitudinal bars which characterize gravel-bed braided streams (Smith, 1974). Scoured lower bed contacts and sharp variations in grain size distribution are typical of ice-marginal streams where large variations in discharge occur and sedimentation is highly episodic (Church and Gilbert, 1975). The similar size and shape of the lower contacts of units 3 and 4, suggests that unit 4 was deposited in the same ice-marginal channel as unit 3c. During deposition of unit 4, however, fluvial processes dominated over, or eroded any evidence of, debris flow sedimentation.

Unit 5

In an area of highly irregular or hummocky topography directly south of the main Martin Creek Section, shallow exposures reveal a complexly interbedded series of diamicton, gravel and sand beds described here as unit 5 (Appendix 1). Although the lower contact is not exposed, unit 5 apparently overlies unit 3 and is laterally equivalent to unit 4.

At the SW end of the exposure (Figure 10a) a large trough shaped unit of diamicton (unit 5a, Appendix 1) is conformably overlain by large scale trough cross-stratified sands (unit 5b). The NE limb of the trough grades into crudely stratified gravel, sand and diamicton beds (unit 5c) that dip upstream (NE) as much as 30°. These beds are conformably overlain by bouldery gravel (unit 5d). Strata in unit 5d are folded into a large (about 10 m wide) wedge-shaped feature (with beds dipping 60-80° in opposing directions). This is interpreted as a collapse structure (Figure 10b). The section here is capped by large troughs of well stratified sand and gravel (unit 5e). Folds and normal faults are common and increase in intensity towards the base of the unit (Figure 10c). At the NE end of the exposure, closest to the main Martin Creek Section, sand and gravel beds (unit 5f) dip about 20° downstream (Figure 10d). They are unconformably overlain by interbedded and convoluted diamicton, gravel and sand beds (unit 5g) that dip 20° upstream (Figure 10d).

Unit 5 is interpreted as an ice-marginal glaciofluvial complex. The unusually large and sharp changes in grain

Fig. 9(d). Sand bed and matrix to clast-supported diamicton at base of unit 3c.

size, sorting, bedding dip and dip direction support this interpretation. The presence of closely juxtaposed sorted deposits ranging from silts and sands to boulder gravels is typical of proximal glaciofluvial sediments (Boulton and Eyles, 1979; De Jong and Rappol, 1983). Large scale trough cross-stratification is interpreted as channel-fill bedding. The associated sands and gravels are inferred to be glaciofluvial sediments that infilled small ice-marginal channels. Diamicton and poorly sorted gravel beds were probably deposited by resedimentation processes. Such processes are common in ice-marginal environments (Lawson, 1979, 1981a, 1981b and 1982). The abundance of deformation structures is also typical of ice contact deposits (Schwan and Van Loon, 1979; and Hambrey, 1984). Normal faults and collapse structures probably formed as a result of melting of underlying or adjacent ice. The irregular and hummocky topography are also strongly suggestive of an ice contact origin. The stratigraphic position and surface expression of these sediments suggests that they were deposited along the ablating margin of the last glacier to occupy the area.

Livingstone Creek Section

A stratigraphic column and brief unit descriptions for the Livingstone Creek Section are provided in Figure 5. The general stratigraphy of the section is very similar to the Martin Creek Section and is not discussed in detail here.

The gravels immediately overlying the bedrock are coarse, poorly sorted and clast-supported. They exhibit weak horizontal bedding with minor open work pebble gravel and trough cross-bedded sand layers. Although most clasts are well rounded to subrounded some beds are dominated by very angular clasts of local origin. These gravels are similar to the gravel facies of unit 1 at Martin Creek. They are also interpreted as high energy stream channel and gulch sediments deposited by channelized fluvial flows and gravelly debris flows.

Parallel-laminated silts and clays with numerous erratic dropstones and pebble intrabeds in unit 3 are similar to those exposed in unit 2 at Martin Creek. They exhibit sedimentary structures typical of proximal glaciolacustrine sediments (Ashley, 1988). Intense folding of some silt and clay beds indicates remobilization of the lake sediments. Intrabeds of local, brecciated gravel with some rounded erratic clasts in a clay matrix were probably deposited by subaquatic debris flows that mixed pre-existing gravels with the finer lake sediments (Larsen and Steel, 1978). The lensoid shape of the beds and presence of soft-sediment intraclasts indicates that the flows were erosive.

The presence of lake sediments at similar stratigraphic positions in the Martin and Livingstone Creek valleys supports the interpretation that a glacier, flowing down the South Big Salmon River valley, blocked the tributaries and caused small ice-marginal lakes to form. Instability of the local bedrock slopes was probably caused by the presence of the lake water and the movement of the adjacent glacier, resulting in mass movements of local materials into the lake. This would explain the dominance of local, angular clasts in the pebble intrabeds.

The diamicton units capping the Livingstone Creek Section (Figure 5) are not well exposed. They are matrix-supported and contain numerous striated clasts suggesting a glacial origin. Units 4 and 5 have stratigraphic and sedimentary characteristics similar to units 3a and 3b at Martin Creek and may also have been deposited, respectively, as debris flows and subglacial tills. The upward decrease in sand content may be due to a vertical progression from resedimented deposits to mainly till deposited directly by ice (Levson and Rutter, 1988).

Summit Creek Section

Bedrock (unit 1) at the Summit Creek section (Figure 5) is overlain by clast-supported, disorganized, coarse gravels (Figure 11a) similar to unit 1 at Martin Creek. These gravels are also interpreted as stream channel and debris flow

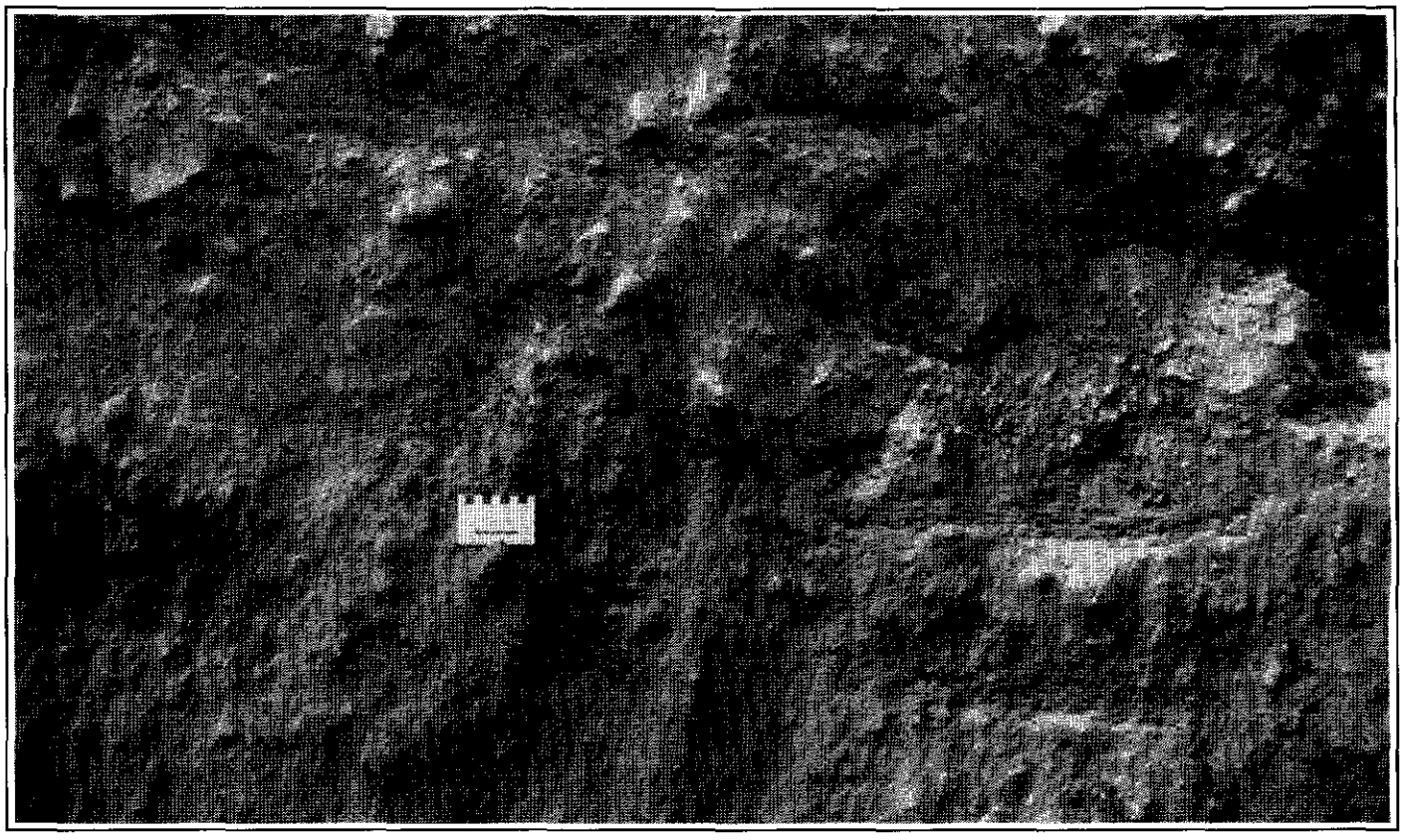

Fig. 9(e). Sandy diamicton with numerous stratified sand and gravel lenses near top of unit 3c.

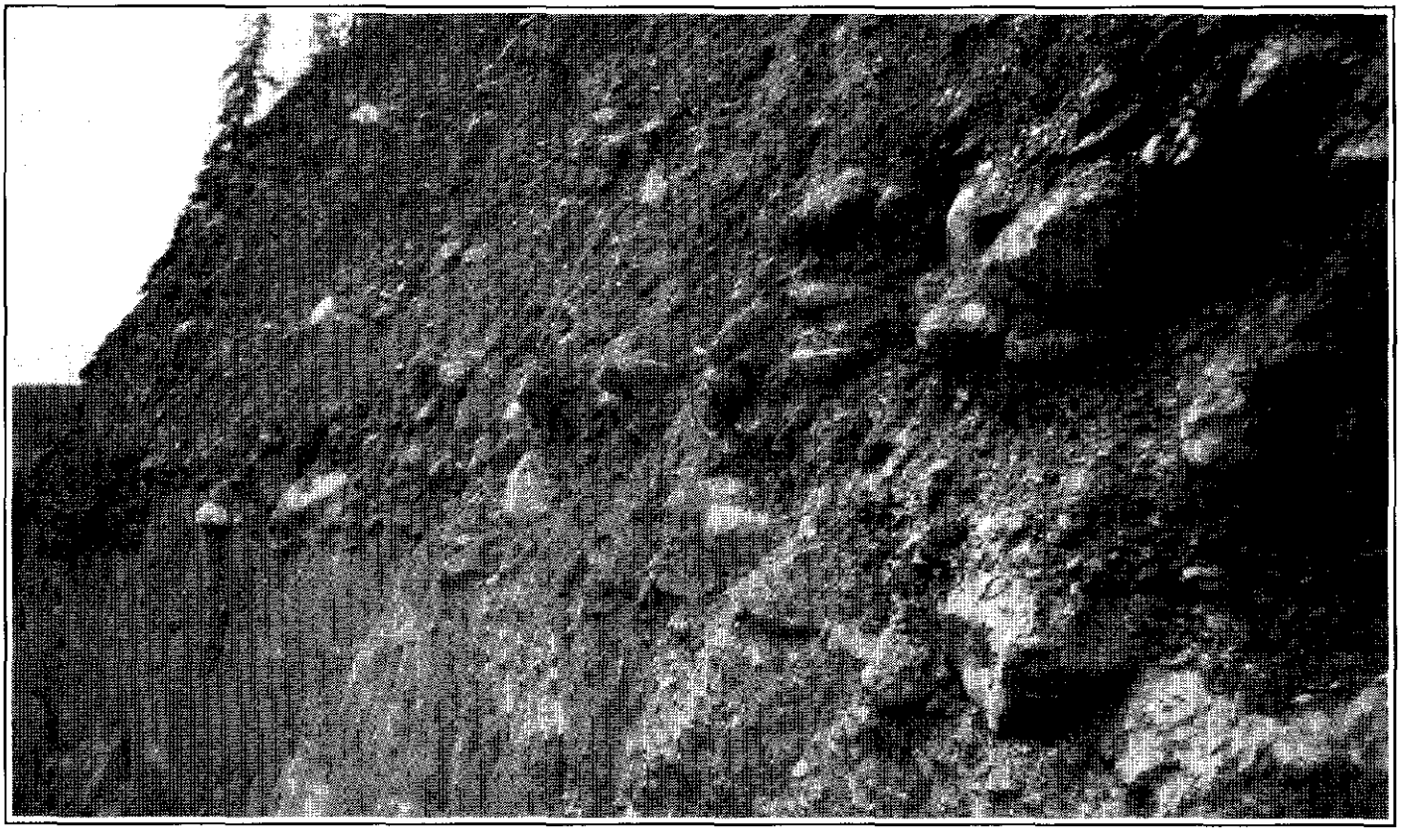

Fig. 9(f). Horizontally stratified, pebble to boulder gravels of unit 4 with erosional lower contact. Large boulders on right are nearly 1 m in diameter.

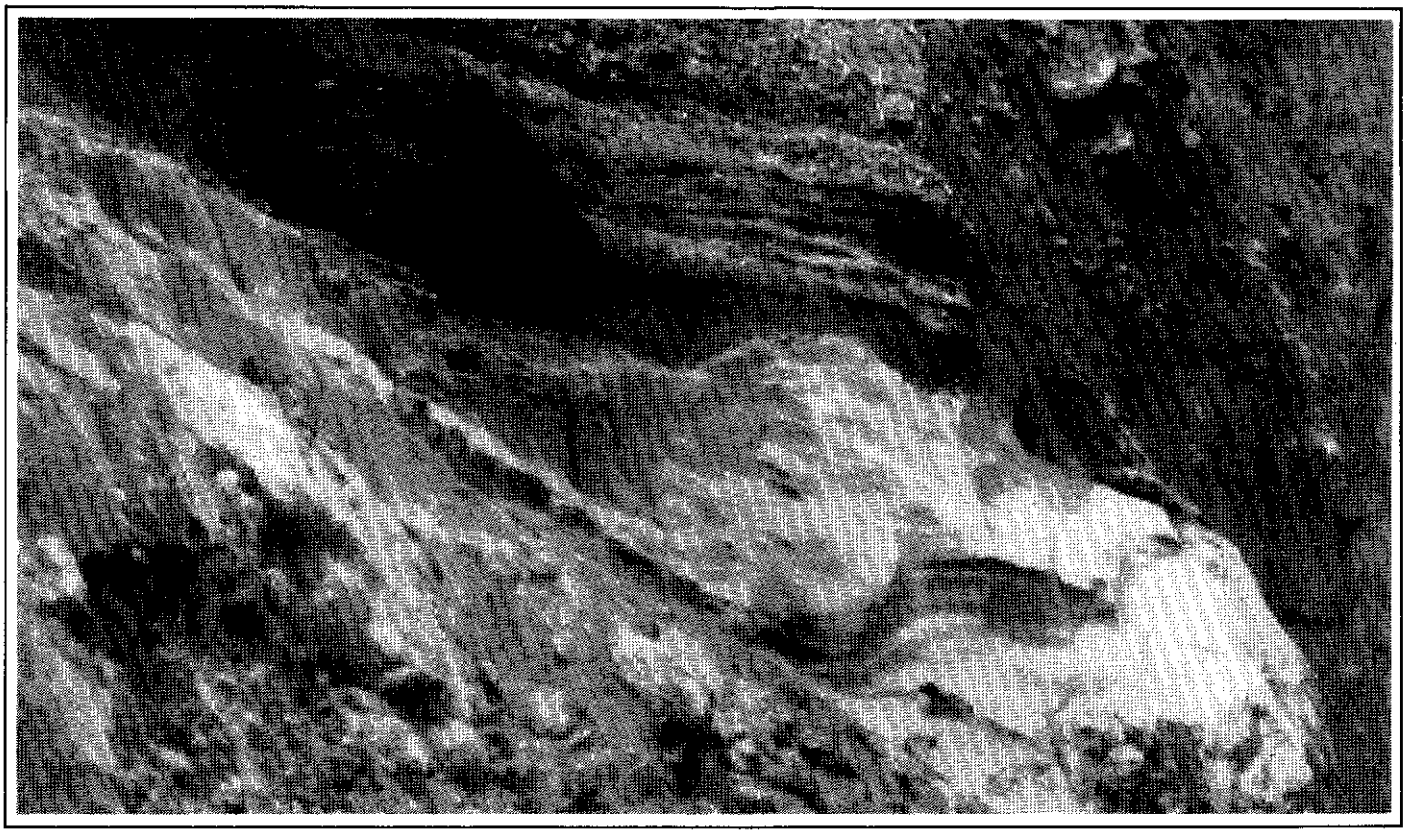

Fig. 9(g). Well sorted and cross-stratified sands interbedded with pebbly sands in a trough-shaped lens at the base of unit 4.

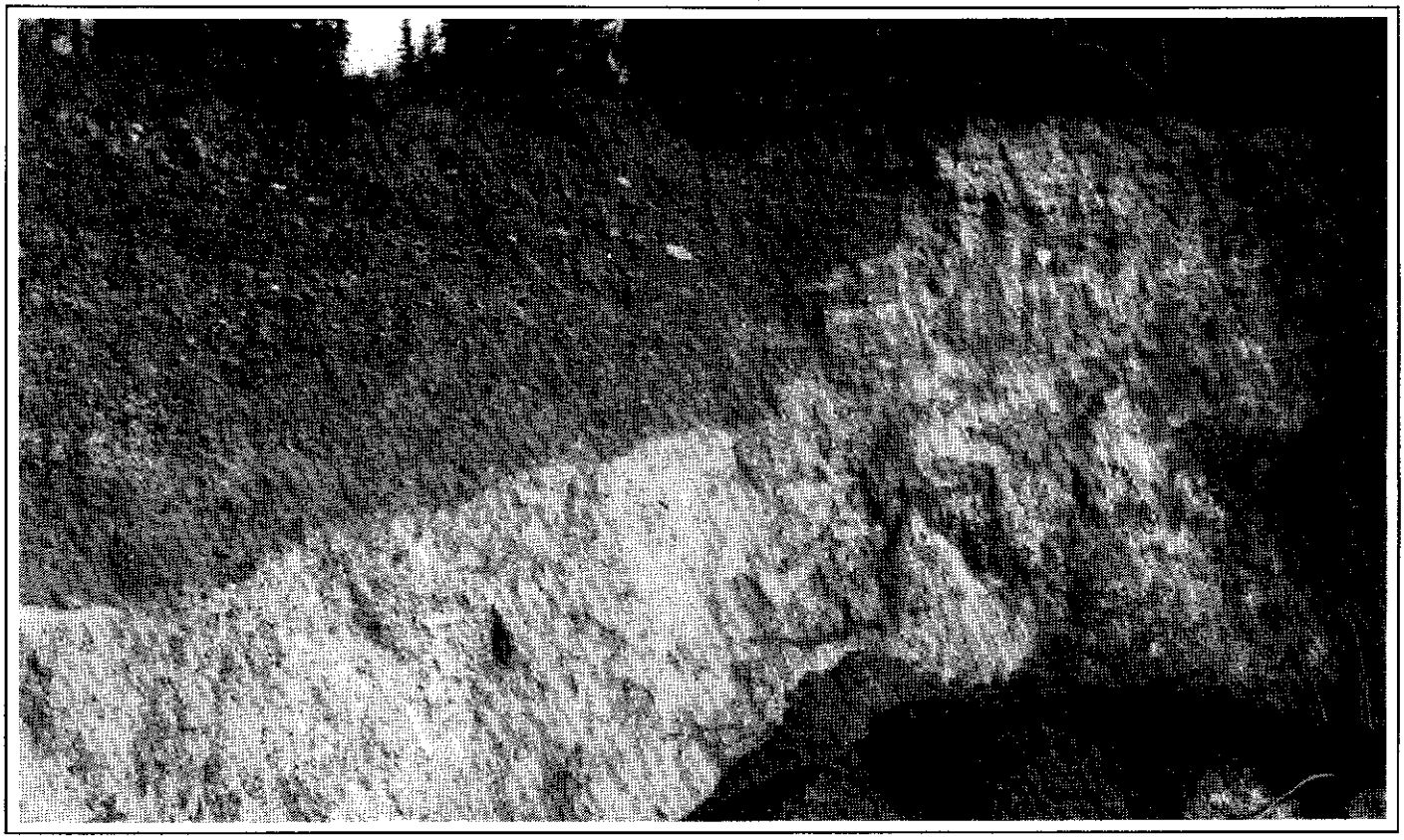

Fig. 9(h). Pronounced basal scour and channel shape of unit 4 gravels.

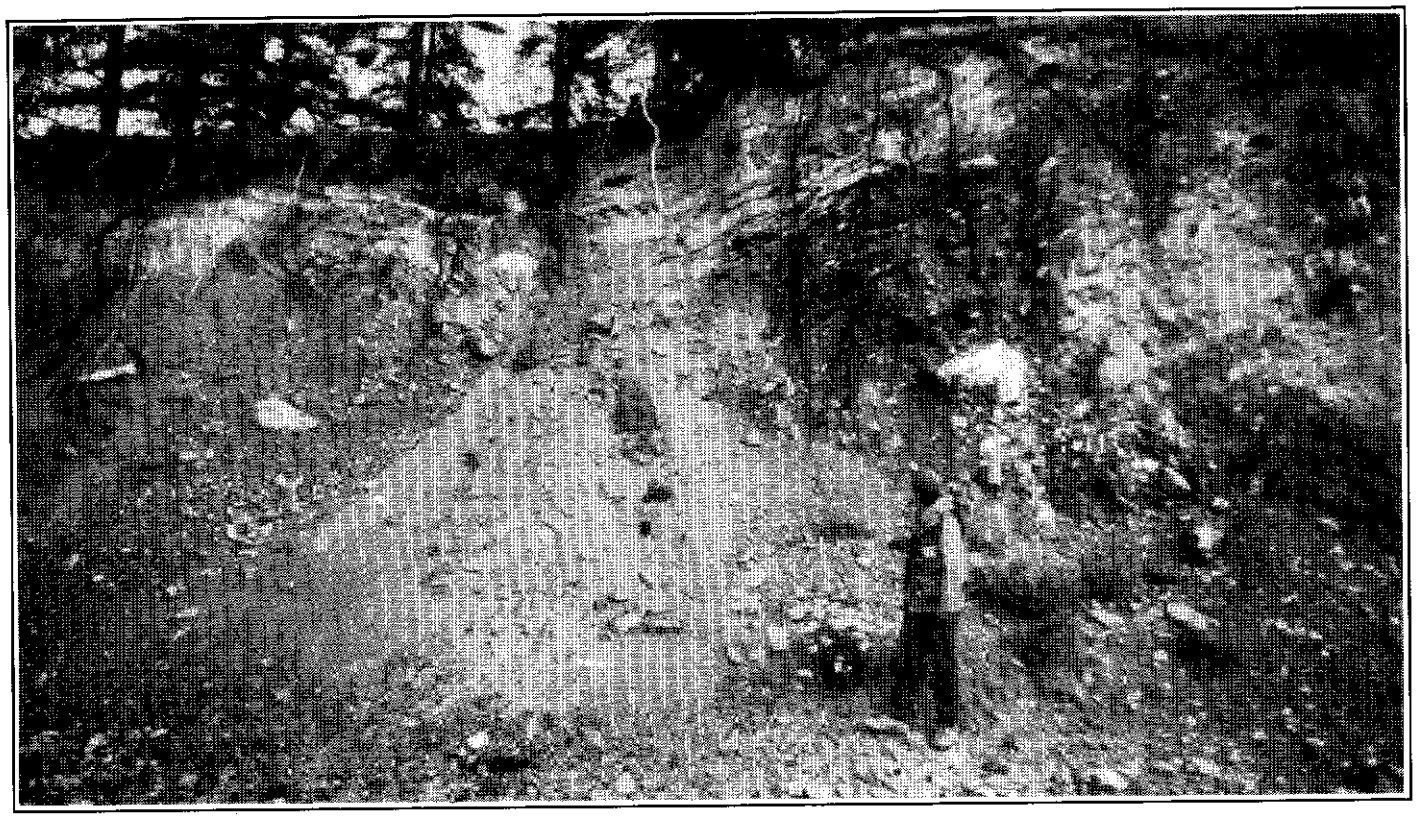

Figure 10. Ice-marginal, glaciofluvial deposits (unit 5) at the Martin Creek west exposure. (a) Diamicton of unit 5a overlain by channel sands and gravels (unit 5b).

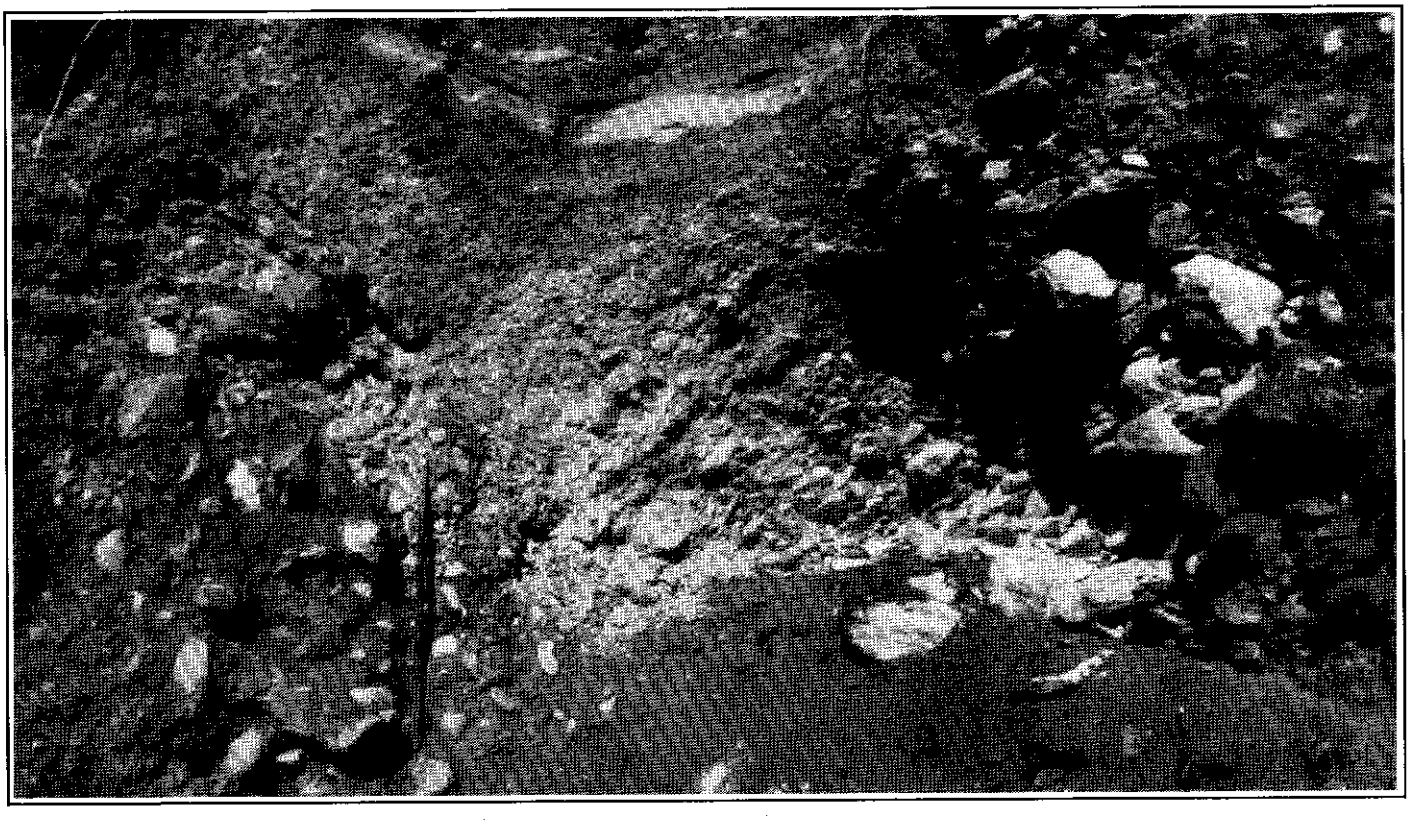

Fig. 10(b). Collapse structure in poorly sorted coarse gravel (beds dip towards photo center from both sides) (unit 5d) overlain by channel sands and gravels (unit 5e).

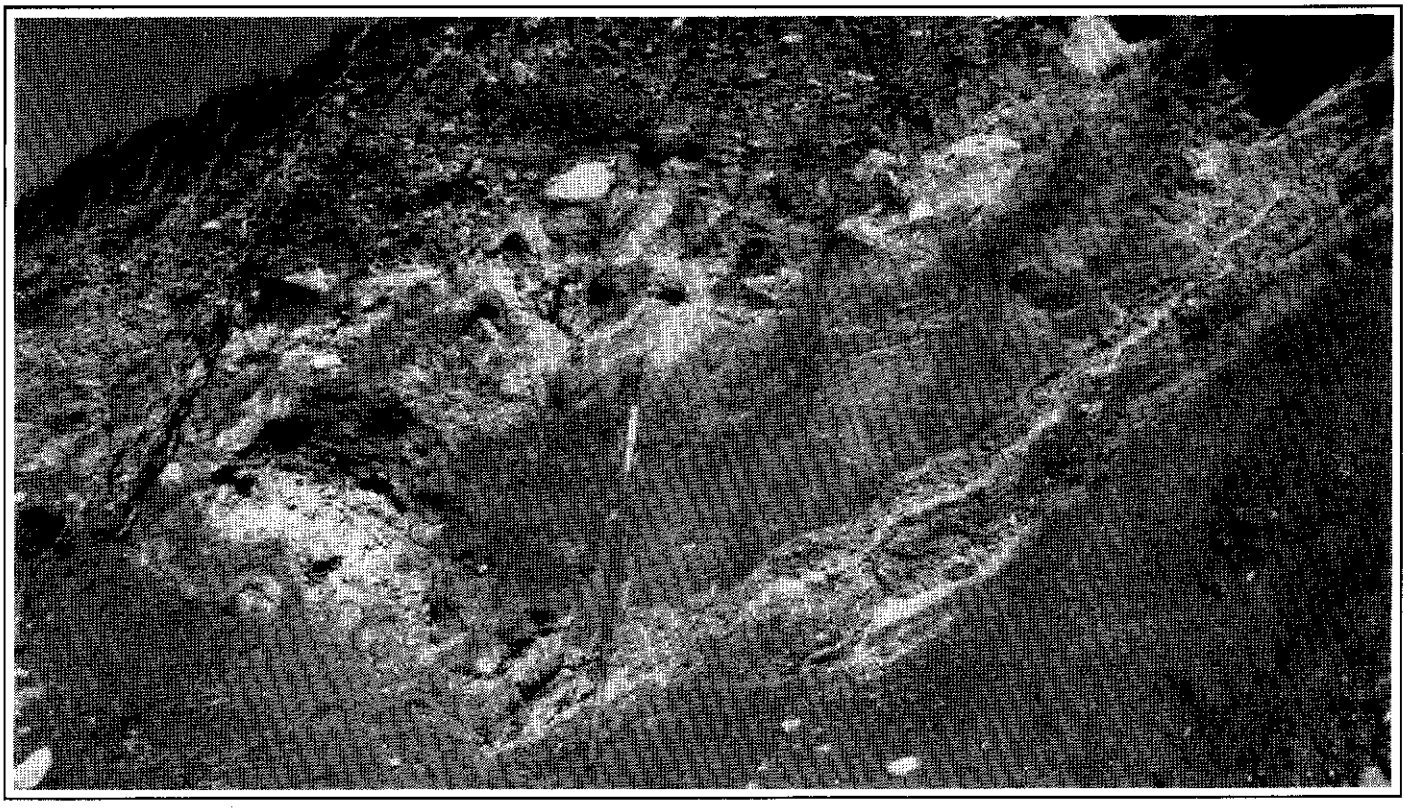

Fig. 10(c) Faults and folds at the base of unit 5e.

Fig. 10(d) Beds with opposing dip directions in ice-contact sand and gravel deposits of units 5f (right) and 5g (left).

deposits. They are overlain by horizontally stratified sands (Figure 11 b) which are interpreted as glaciolacustrine sediments. The lateral continuity of beds, uniform grain size, rarity of channelized features and presence of dropstones supports this interpretation.

Units 4 to 6 (Figures 5 and 11c) consist of clast-supported, well stratified, mainly open work, pebble to cobble gravels. A few boulder beds also occur. Planar cross-beds, dipping up to 31° to the northeast (opposite to the regional slope), dominate units 4 and 6 (Figures 11c and 11d). Individual cross strata are traceable for more than 5 m and are interpreted as deltaic foresets. In contrast to the good sorting and mainly open work structure of units 4 and 6, unit 5 gravels are poorly sorted and matrix-filled (Figure 11e). They exhibit horizontal to gently inclined planar bedding and are interbedded with parallel laminated silts and sands (Figures 11c and 11e). Pronounced erosional surfaces separate unit 5 from units 4 and 6 (Figure 11c).

The deposits of unit 5 are interpreted as delta front and pro-delta sediments, with the poorly sorted sandy gravels deposited by slumping and turbidity currents and the fine grained sediments representing quiet water sedimentation. Cohen (1983) interpreted similar interbedded fine grained and gravelly sediments in an ice-marginal deltaic sequence as the product of alternating foreset and bottom-set deposition induced by shifting sources of discharge and sediment supply.

The up-valley dip direction of bedding in units 4 to 6 indicates a debris source to the southwest in the South Big Salmon River valley. The only plausible explanation for this is that a glacier occupied the main valley and debris was washed from the ice surface or along the ice margin into the Summit Creek valley. This interpretation, combined with the presence of the delta and pro-delta sediments, indicates that an ice-dammed lake occupied the Summit Creek valley. Again, the presence of glaciolacustrine sediments in adjacent valleys at stratigraphically similar positions strongly supports this interpretation.

Clasts in units 4 to 6 are angular to subangular (Figure 11f) and up to 90% are locally derived (Figure 7), indicating that local bedrock was eroded by the ice or its meltwater and the clasts were transported only a short distance before being redeposited in the ice-marginal deltaic complex. The dominance of open-work beds of widely varying grain size is indicative of high and variable discharges typical of proximal glaciofluvial deposits. Changes from foreset (units 4 and 6) to pro-delta (unit 5) sedimentation indicate that the lake level must have fluctuated. Such variations are typical of ice-dammed lakes (Ashley, 1988). A rise in lake level must have occurred after deposition of unit 4 to allow for the deposition of the pro-delta sediments of unit 5. The prominent erosional surface separating units 4 and 5 probably formed as a result of slumping induced by the higher lake level. Progradation of unit 6 over unit 5 resulted in a sharp contact between the pro-delta (bottom set) sediments and the overlying delta front (foreset) beds.

The origin of the diamicton and poorly sorted gravel (unit 7) at the top of the section can not be determined due to poor exposure and inaccessibility. The poor sorting and high matrix component suggest that these sediments may be debris flow deposits or till, although a proximal glaciofluvial component is also likely.

SUMMARY

The coarse, dominantly local gravels exposed at the base of the Martin (unit 1), Livingstone (unit 2) and Summit (unit 2) Creek sections are interpreted as interglacial stream or gulch gravels. Concentrated fluvial and debris flow sedimentation likely occurred in response to unusually high storm or spring runoff events. The advance of a glacier down the South Big Salmon River valley resulted in damming of the channelized flows that deposited the underlying gravels. Ice-marginal lakes formed in each of the tributary valleys. Parallel-laminated clays, silts and sands were deposited in the ice dammed lakes along with debris flow deposits derived mainly from the ice margin (units 2 and 3a at Martin Creek and unit 3 at Summit Creek, and units 3 and 4 at Livingstone Creek). Ice-rafted debris and deformation structures characterize these sediments and are typical of proximal glaciolacustrine deposits. At Summit Creek a thick glaciofluvial delta complex (units 4 to 6) developed in the lake ponded in that valley.

As the glacier in the South Big Salmon River valley expanded, the lakes diminished in size and debris flow sedimentation increased until the area was overridden by ice. A thick till (unit 3b at Martin Creek, unit 5 at Livingstone Creek and unit 7 (?) at Summit Creek) was deposited at the base of the glacier. During deglaciation, a glaciofluvial complex developed along the ice margin in the Martin Creek area. Sedimentation occurred in an ice-marginal channel and was initially dominated by debris flow deposits (unit 3c). Glaciofluvial activity gradually increased in importance and eventually deposited a thick sequence of gravel (unit 4). Elsewhere the ice-marginal deposits developed an irregular glaciofluvial complex (unit 5). The series of meltwater channels that extend from south of Martin Creek to well north of Summit Creek, formed along the side of the South Big Salmon Valley in association with the ice-marginal deposits. Postglacial river erosion has incised through all of the overlying glacial deposits and has re-exposed the gold bearing gravels that have been mined throughout the twentieth century.

DISCUSSION

Damming of ice-marginal lakes in the all of the tributary valleys studied may have been critical for the preservation of the older gold bearing deposits. The lakes provided a quick transition from the subaerial stream gulch environment to a mainly depositional, quiet water environment. Sedimentation in the lakes was dominated by suspension settling, ice rafting, turbidity current, and debris flow processes. These processes are mostly depositional and none were sufficiently erosive to remove the underlying, coarse, interglacial gravels.

Figure 11. Summit Creek Section. (a) Poorly sorted, disorganized gravel (facies 1) in unit 2.

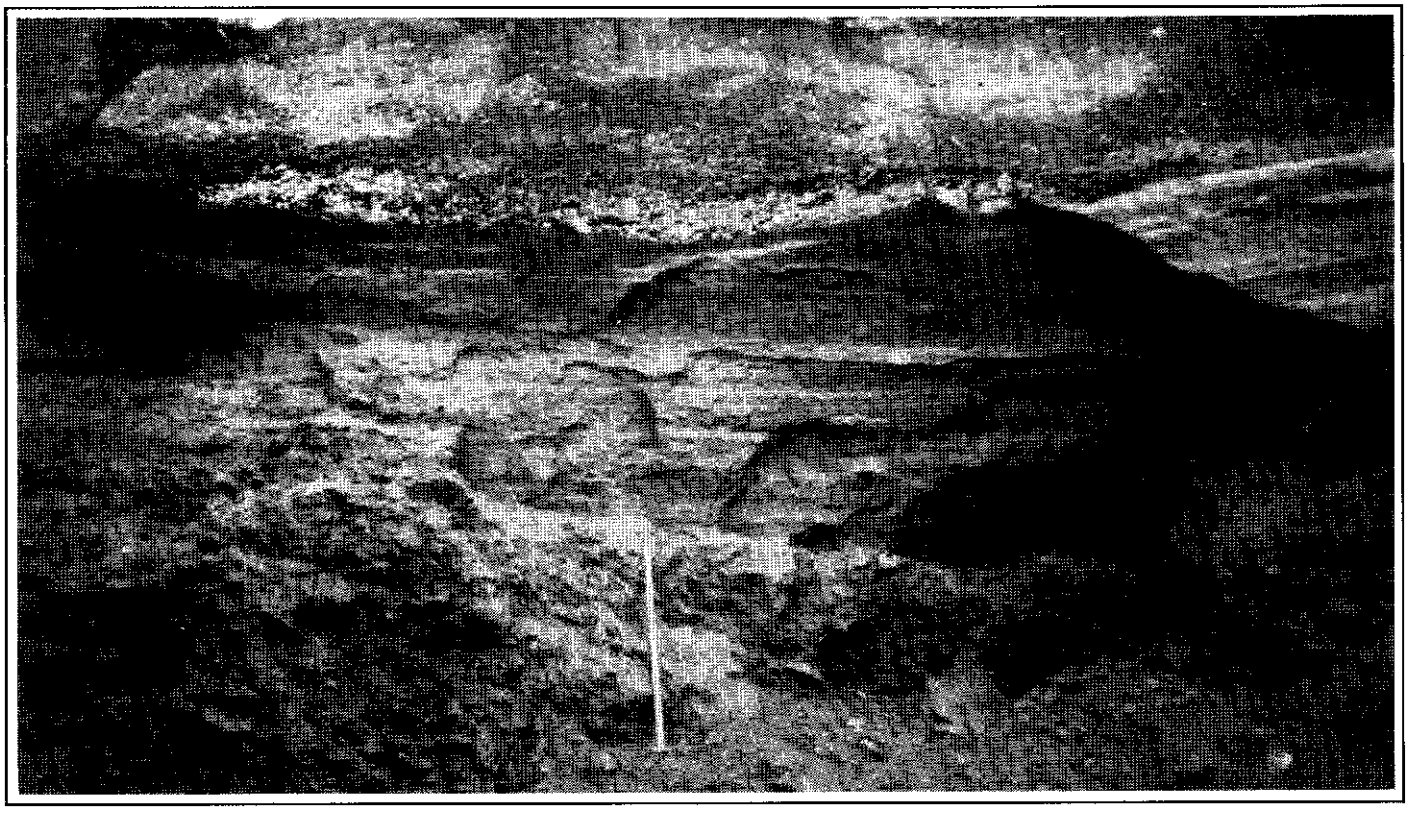

Fig. 11(b). Horizontally stratified bottom set sands (unit 3) overlying unit 2 gravels and unconformably overlain by unit 4 gravels. The top of the 1.5 m long rod is near the top of unit 2.

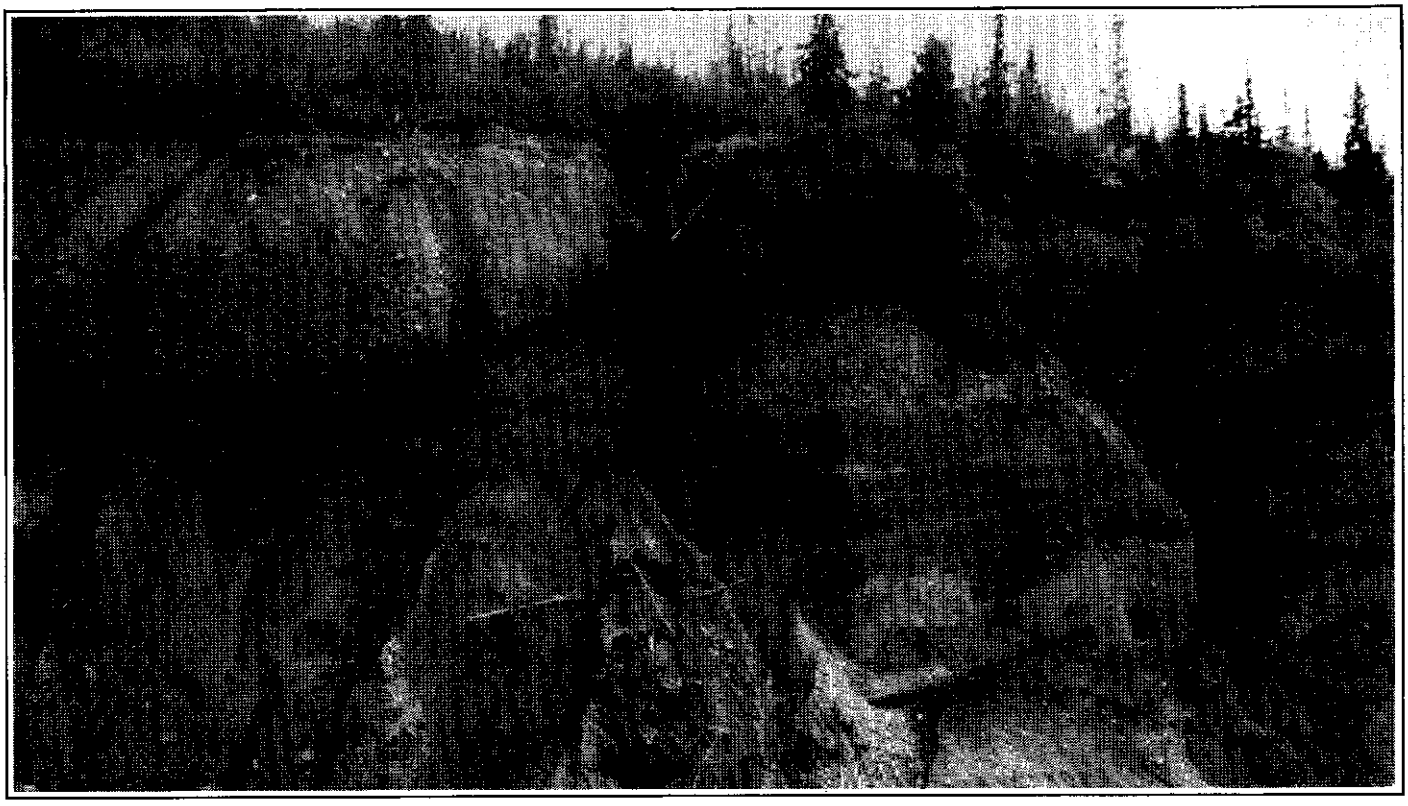

Fig. 11(c). Deltaic foreset gravels of unit 4 (lower right) and unit 6 (upper left) dipping steeply upvalley (left). Gently dipping, interbedded, sand and gravel strata of unit 5 (section center) are interpreted as delta front and pro-delta sediments. Pronounced unconformities separating unit 5 from units 4 and 6 probably resulted from major changes in water level or sediment source. Section is capped by a few metres of diamicton.

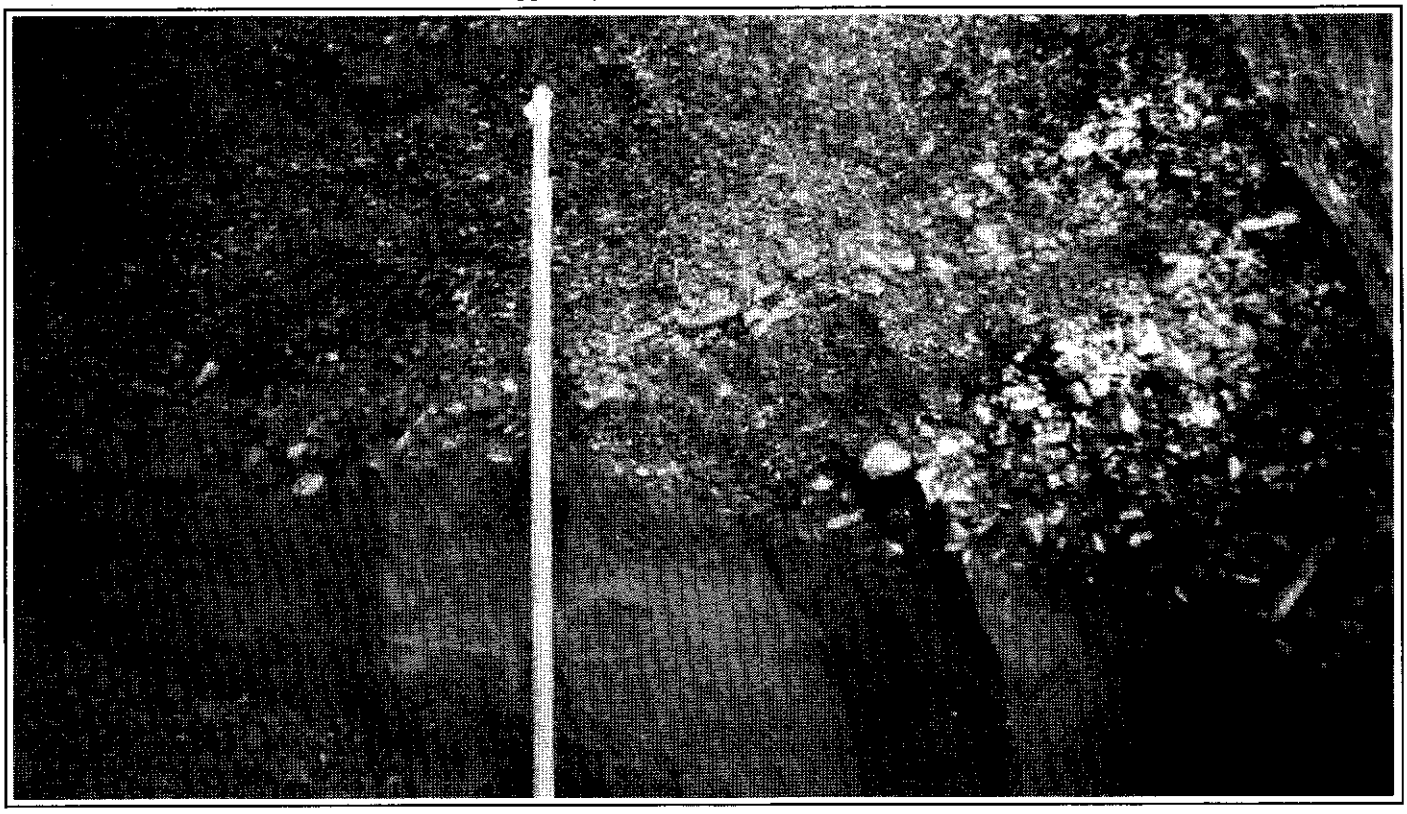

Fig. 11(d). Foreset gravels (unit 4) unconformably overlying bottom set beds (unit 3).

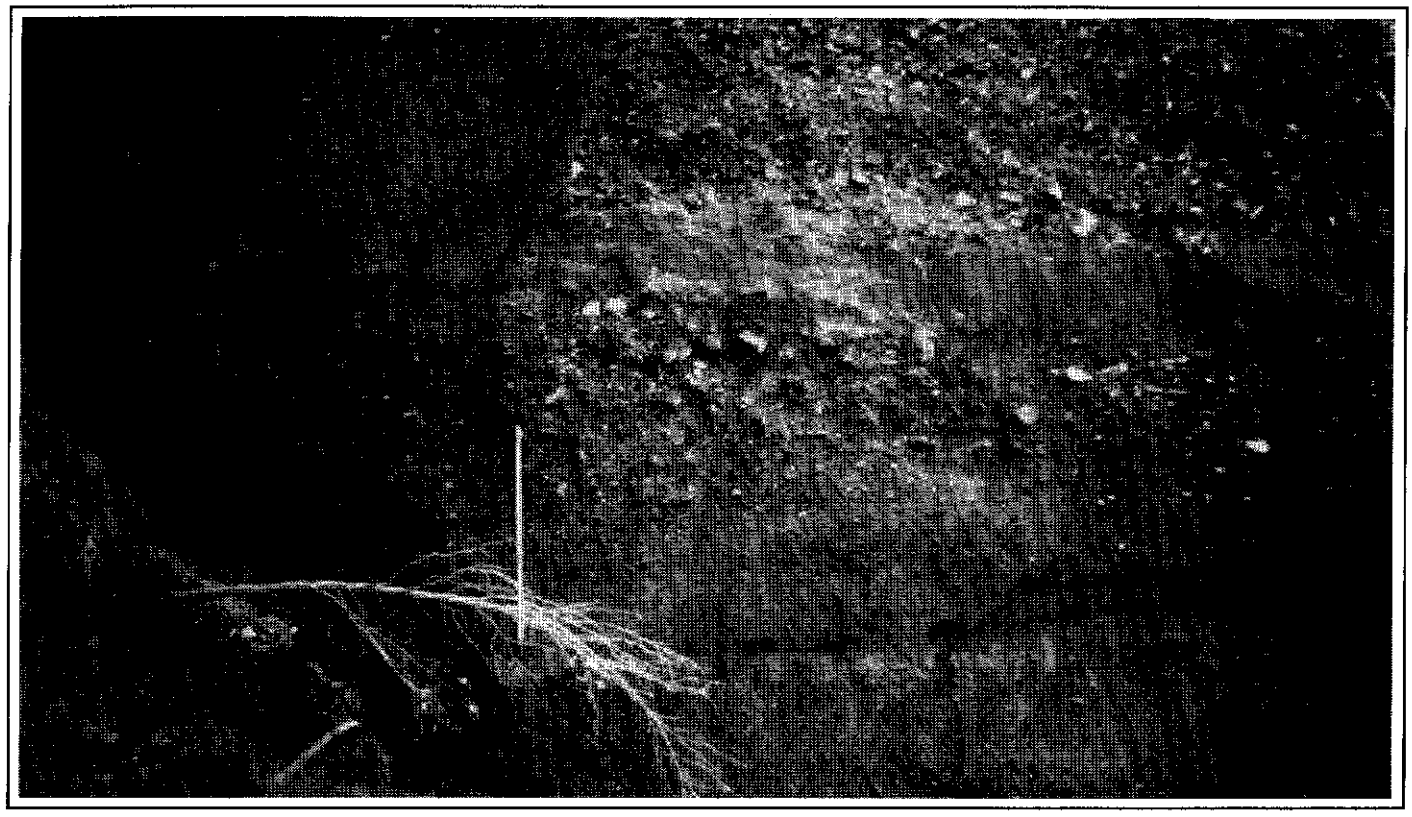

Fig. 11(e). Poorly sorted sediment-flow deposits of unit 5 (centre).

Fig. 11(f). Angular clasts in open-work bed typical of units 4 and 6.

Glaciolacustrine sediments overlie the interglacial gravels at all three of the studied sites and, at Livingstone and Martin Creeks, they are especially thick and have a high silt and clay content. The cohesive nature and low permeability of these fine grained sediments would also have acted to resist the erosive power of ice-marginal and subglacial meltwaters .

If ice-marginal lakes had not developed in the tributary valleys, the gold bearing sediments may have been eroded by meltwaters from the advancing glaciers. Such a situation might have occurred, for example, if glaciers developed in the Big Salmon Range to the east, and flowed into these valleys prior to the arrival of glaciers in the South Big Salmon Valley. Meltwater from the glaciers to the east would have had a free outlet and could have deeply eroded the gold bearing gravels. Discharges in these meltwater streams would potentially have been of much higher magnitude than normally encountered in the drainage basins in nonglacial times. In addition, as glaciers advanced down the tributary valleys, substantial erosion by the ice could have occurred.

During glacial advances, erosion of the gold-bearing gravels by the overriding glaciers was minimal, probably for two reasons. First, the gravels were buried by a thick sequence of glaciolacustrine, glaciofluvial and ice-marginal debris flow deposits. Second, these deposits accumulated in narrow and deep valleys that were oriented transverse to the regional direction of ice flow. The sediments within the tributary valleys were thus protected from ice erosion by the high bedrock walls flanking the valleys. The dominance of depositional over erosive processes in similar topographic situations has been observed in several other areas (egs. Garnes and Bergerson, 1977; Haldorsen, 1982, Levson and Rutter, 1986).

During deglaciation, glaciofluvial activity resulted in the deposition of a thick sequence of sand and gravel deposits and erosion of a meltwater channel system along the ice margin. The meltwater channels are incised partly into bedrock and probably removed or disrupted any underlying placer deposits. It is unlikely that any of the gravels deposited during deglaciation are gold bearing.

CONCLUSIONS

Three factors that contributed to the preservation of gold bearing gravels in tributary valleys in the Livingstone Creek region are: (1) Glaciers did not flow down the tributary valleys before ice occupied the main valley. This prevented the erosion of older deposits by water and ice moving down the valleys. (2) Ice-marginal lakes formed in the tributary valleys during the early stages of glaciation causing depositional processes to predominate. (3) The valleys are oriented transverse to the former regional direction of ice flow thus minimizing direct erosion by ice. As a result of these factors, the transverse valleys became depositional sinks, and erosion of the gold bearing deposits by glaciers and glacial meltwaters was minimal, both immediately prior to and, during glaciation. The recognition of areas with similar glacial histories may be important for the identification of potential exploration targets in other placer gold regions in glaciated terrains.

ACKNOWLEDGEMENTS

Funding and technical support for this research was provided by the Exploration and Geological Services Division of the Mineral Resources Directorate, Yukon Region. The study was directed by S. R. Morison of that division. Sections were examined with the kind permission of placer lease holders D. Gonder, M. Fuerstner and R. Asuchak. Mr D. Gonder generously offered the use of his placer camp for the duration of the study. Field assistance and lithologic studies were ably carried out by Bill LeBarge.

REFERENCES

ASHLEY, G.M. 1988. Classification of Glaciolacustrine sediments. In: Genetic classification of glacigenic deposits; R.P. Goldthwait and and C. L. Matsch (eds), Balkema, Rotterdam, p. 243-260.

BOOTHROYD, J.C. and ASHLEY, G.M. 1975. Processes, bar morphology, and sedimentary structures on braided outwash fans, northeastern gulf of Alaska. In: Glaciofluvial and glaciolacustrine sedimentation, A.V. Jopling and B.C. McDonald (eds); Society of Economic Paleontologists and Mineralogists, Special Publication 23, p. 193-222.

BOSTOCK H.S. and LEES E.J. 1938. Laberge map area, Yukon. Geological Survey of Canada, Mem. 217.

BOULTON, G.S. 1968. Flow tills and related deposits on some Vestspitzbergen glaciers. Journal of Glaciology, Vol. 7, p. 391-412.

BOULTON, G.S., and EYLES, N. 1979. Sedimentation by valley glaciers, a model and genetic classification. In: Moraines and varves, C.M. Schluchter, (ed); Balkema Press, Rotterdam, p. 11-25.

BRAYSHAW, A.C., 1984. Characteristics and origins of cluster bedforms in coarse-grained alluvial channels. In: Sedimentology of gravels and conglomerates, E.H. Koster and R.J. Steel (eds); Canadian Society of Petroleum Geologists, Memoir 10, p. 77-85.

BULL, W.B. 1972. Recognition of alluvial fan deposits in the stratigraphic record. In: Recognition of ancient sedimentary environments, J.K. Rigby and Wm. K. Hamblin,(eds); Society of Economic Paleontologists and Mineralogists, Special Publication 16. p. 63-83.

BURGISSER, H.M. 1984. A unique mass flow marker bed in a Miocene stream flow molasse sequence, Switzerland. In: Sedimentology of gravels and conglomerates, E.H. Koster and R.J. Steel (eds); Canadian Society of Petroleum Geologists, Memoir 10, p. 147-163.

CHURCH, M.A., and GILBERT, R. 1975. Proglacial fluvial and lacustrine environments. In: Glaciofluvial and glaciolacustrine sedimentation, A.V. Jopling and B.C. McDonald (eds); Society of Economic Paleontologists and Mineralogists, Special Publication 23, p. 22-100.

COHEN, J. M. 1983. Subaquatic mass flows in a high energy ice-marginal deltaic environment and problems with the identification of flow tills. In: Tills and related deposits, E.B. Evenson, C.H. Schluchter and J. Rabassa (eds); Proceedings of the INQUA Symposia on the genesis and lithology of Quaternary deposits, A.A. Balkema (ed); Rotterdam, p. 255-267.

DEBICKI R.L. 1983. Yukon Placer Mining Industry, 1978-1982. Exploration and Geological Services Division, Yukon, Indian and Northern Affairs Canada, 203 p.

DE JONG, M.G.G. and RAPPOL, M. 1983. Ice-marginal debris flow deposits in western Allgau, southern West Germany. Boreas, Vol. 12, p. 57-70.

DREIMANIS, A. 1988. Tills: their genetic terminology and classification. In: Genetic classification of glacigenic deposits, R.P. Goldthwait and C.L. Matsch (eds); Balkema, Rotterdam, p. 17-83.

EVENSON E.B., DREIMANIS A. and NEWSOME, J.W. 1977. Subaquatic flow tills: a new interpretation for the genesis of some laminated till deposits. Boreas, Vol. 6, p. 115-133.

EYLES, N., 1987. Late Pleistocene debris flow deposits in large glacial lakes in British Columbia and Alaska. Sedimentary Geology, Vol. 53, p. 33-71.

FISHER, R.V., 1971. Features of coarse grained, high concentration fluids and their deposits. Journal of Sedimentary Petrology, Vol. 41, p. 916-927.

FOLK, R.L., 1980. Petrology of sedimentary rocks. Hemphill Publishing Company, Austin, Texas. 184 p.

HAMBREY, M.J., 1984. Sedimentary processes and buried ice phenomena in the pro-glacial areas of Spitsbergen glaciers. Journal of Glaciology, Vol. 30, p. 116-119.

HARVEY, A.M. 1984. Debris flows and fluvial deposits in Spanish Quaternary alluvial fans: implications for fan morphology. In: Sedimentology of gravels and conglomerates, E.H. Koster and R. J. Steel (eds); Canadian Society of Petroleum Geologists, Memoir 10, p. 123-132.

HEIN, F.J. and WALKER R.G., 1977. Bar evolution and development of stratification in the gravelly braided Kicking Horse River, B.C. Canadian Journal of Earth Sciences, Vol. 14, p. 562-572.

HUGHES, O.L. 1968. Glacial map of Yukon Territory. Geological Survey of Canada Map 1968-6, scale 1:1,000,000.

HUGHES, O.L., CAMPBELL, R.B. MULLER, J.E. and WHEELER, J.O. 1969. Glacial limits and flow patterns, Yukon Territory, south of 65 degrees north latitude. Geological Survey of Canada, Paper 68-34.

JOHNSON, A.M., 1970. Physical Processes in Geology. Freeman, Cooper and Company, San Francisco, 577 p.

KLASSEN, R.W. 1987. The Tertiary-Pleistocene stratigraphy of the Liard Plain, southeastern Yukon Territory. Geological Survey of Canada, Paper 86-17.

KLASSEN, R.W. and MORISON, S.R. 1987. Surficial Geology, Laberge, Yukon Territory. Geological Survey of Canada, Map 8-1985, scale 1:250,000.

KOCHEL, R.C. and JOHNSON, R.A., 1984. Geomorphology and sedimentology of humid-temperate alluvial fans, central Virginia. In: Sedimentology of gravels and conglomerates, E.H. Koster and R. J. Steel, (eds), Canadian Society of Petroleum Geologists, Memoir 10, p. 109-122.

LARSEN, V. and STEEL, R.J., 1978. The sedimentary history of a debris flow dominated alluvial fan: a study of textural inversion. Sedimentology, Vol. 25, p. 37-59.

LATOSKI, D.A., 1991. An overview of the Yukon Placer Mining Industry 1989 and 1990. In: Yukon Placer Mining and Exploration, 1985 to 1988, W.P. Lebarge and S.R. Morison (eds); Exploration and Geological Services Division, Yukon, Indian and Northern Affairs Canada, p. V-IX.

LEBARGE, W.P. 1990. Yukon placer mining industry 1985-1988: an overview. In: Yukon Placer Mining Industry 1989-1990, A.R. Waroway and D.A. Latoski (eds); Exploration and Geological Services Division, Yukon, Indian and Northern Affairs Canada, p. III-VII.

LAWSON, D.E., 1979. A sedimentological analysis of the western terminus of the Matanuska Glacier, Alaska. United States Army Cold Regions Research and Engineering Laboratory, Hanover, NH, Report 79-9.

LAWSON, D.E., 1981a. Distinguishing characteristics of diamictons at the margin of the Matanuska Glacier, Alaska. Annals of Glaciology, Vol. 2, p. 78-84.

LAWSON, D.E., 1981b. Sedimentological characteristics and classification of depositional processes and deposits in the glacial environment. United States Army Cold Regions Research and Engineering Laboratory, Hanover, NH, Report 81-27.

LAWSON, D.E., 1982. Mobilization, movement and deposition of active subaerial sediment flows, Matanuska Glacier, Alaska. Journal of Geology, Vol. 90, p. 279-300.

LEVSON, V.M. 1991. Geologic controls on alluvial gold mining in the Cariboo District, British Columbia, Canada. In: Alluvial Mining; Elsevier Science Publishers for Institute of Mining and Metallurgy, London, England, p. 245-267.

LEVSON, V.M. 1992. Quaternary geology of the Atlin area (104N/11W, 104N/12E). In: Geological Fieldwork 1991, B.C. Ministry of Energy, Mines and Petroleum Resources, Paper 1992-1, p. 375-390.

LEVSON, V.M., and GILES, T.R., 1991. Stratigraphy and geologic settings of gold placers in the Cariboo Mining District (93A,B,G,H). In: Geological Fieldwork 1990; B.C. Ministry of Energy, Mines and Petroleum Resources, Paper 1991-1, p. 331-344.

LEVSON, V.M., and KERR, D.K., 1992. Surficial geology and placer gold settings of the Atlin - Surprise Lake area, NTS 104N/11,12. B.C. Ministry of Energy, Mines and Petroleum Resources, Open File 1992-7; 1:50 000 scale map.

LEVSON, V.M., and RUTTER, N.W., 1986. A facies approach to the stratigraphic analysis of Late Wisconsinan sediments in the Portal Creek area, Jasper National Park, Canada. Geographie physique et Quaternaire, Vol. 40, p. 129-144.

LEVSON, V.M., and RUTTER, N.W., 1988. A lithofacies analysis and interpretation of depositional environments of montane glacial diamictons, Jasper, Alberta, Canada. In: Genetic classification of glacigenic deposits, R.P. Goldthwait and C. L. Matsch (eds), Balkema, Rotterdam, p. 117-140.

LOWE, D.R., 1979. Sediment gravity flows: their classification and some problems of application to natural flows and deposits. In: Geology of continental slopes, O.H. Doyle and O. H. Pilkey (eds). Society of Economic Paleontologists and Mineralogists, Special Publication 27, p. 75-82.

MIDDLETON, G. V. and HAMPTON, M. A. 1976. Subaqueous sediment transport and deposition by sediment gravity flows. In: Marine sediment transport and environmental management, D.J. Stanley and D.J.P. Swift (eds); John Wiley and Sons, p. 197-218.

MORISON, S.R., 1983. A sedimentologic description of Clear Creek fluviatile sediments, 115 P, Central Yukon. In: Yukon Exploration and Geology 1982, Exploration and Geological Services Division, Yukon, Indian and Northern Affairs Canada, p. 50-54.

MORISON, S.R., 1984. Placer deposits of Clear Creek drainage basin 115 P, central Yukon. In: Yukon Exploration and Geology 1982; Exploration and Geological Services Division, Yukon, Indian and Northern Affairs Canada, p. 88-93.

MORISON, S.R. and HEIN, F.J., 1987. Sedimentology of the White Channel Gravels, Klondike area, Yukon Territory: fluvial deposits of a confined valley. Society of Economic Paleontologists and Mineralogists, Special Publication 39, p. 205-216.

NARDIN, T.R., HEIN, F.J., GORSLINE, D.S., and EDWARDS, B.D., 1979. A review of mass movement processes, sediment and acoustic characteristics, and contrasts in slope and base-of-slope systems versus canyon-fan-basin floor systems. In: Geology of continental slopes, 0.H. Doyle and O. H. Pilkey (eds); Society of Economic Paleontologists and Mineralogists, Special Publication 27, p. 61-73.

PIERSON, T.C., 1981. Dominant particle support mechanisms in debris flows at Mt. Thomas, New Zealand, and implications for flow mobility. Sedimentology, Vol. 28, p. 49-60.

RUST, B.R., 1972. Structure and processes in a braided river. Sedimentology, Vol. 18, p. 221-245.

SCHWAN, J., and VAN LOON, A.J., 1979. Structural and sedimentological characteristics of a Weichselian kame terrace at Sonderby Klint, Funen, Denmark. Geologie en Mijnbouw, Vol. 58, p. 305-319.

SMITH, G.A., 1986. The influence of explosive volcanism on fluvial sedimentation: the Deschutes Formation (Neogene) in central Oregon. Journal of Sedimentary Petrology, Vol. 57, p. 613-629.

SMITH, G.A., 1987. Coarse grained non-marine volcaniclastic sediments. Terminology and deposition processes. Geological Society of America Bulletin, Vol. 97, p. 1-10.

SMITH, N.D., 1974. Sedimentology and bar formation in the upper Kicking Horse River, a braided outwash stream. Journal of Geology, Vol. 82, p. 205-223.

TEMPELMAN-KLUIT, D., 1980. Highlights of fieldwork in Laberge and Carmacks map areas, Yukon Territory. Geological Survey of Canada, Paper 80-1A, p. 357-362.

TEMPELMAN-KLUIT, D., 1984. Geology, Laberge (105E) and Carmacks (1151), Yukon Territory. Geological Survey of Canada, Open File 1101.

WARESBACK, D.B., and TURBEVILLE, B.N., 1990. Evolution of a Plio-Pleistocene volcanogenic-alluvial fan: the Puye Formation, Jemez Mountains, New Mexico. Geological Society of America Bulletin, Vol. 102, p. 298-314.

WELLS, N.A., 1984. Sheet debris flow and sheet flood conglomerates in Cretaceous cool-maritme alluvial fans, South Orkney Islands, Antarctica. In: Sedimentology of gravels and conglomerates, E.H. Koster and R.J. Steel, (eds); Canadian Society of Petroleum Geologists, Memoir 10, p. 133-145 .

Appendix 1. Martin Creek Section Description

Main Section

Unit 1a: Bouldery gravel: 6.7 m thick; very poorly sorted; clast-supported; 50% boulders up to 1 m in diameter, 20% cobbles, 20% pebbles and 10% silt to coarse sand; clasts mainly subangular to subrounded; some poorly defined pebble to cobble gravel lenses, generally about 25 cm thick and 100 cm wide, poorly to moderately sorted; disorganized fabric; strong oxidation in basal 2 m; unit is poorly exposed; lower contact covered.

Unit 1b: Boulder-cobble gravel: 3.5 m thick; clast-supported, matrix-filled; some crude horizontal to low angle stratification; beds are poorly defined with gradational boundaries on all sides; 50% cobble and pebble beds increasing towards the top; beds generally 25 to 50 cm thick (P28 R17); boulders occur in disorganized clusters and beds up to 2 m thick with a clast size distribution similar to unit 1a; sorting generally poor except for a few pebble beds with an open work to sandy matrix; sorted layers of laminated clay, silt and sand and pebbly sands (Figure 6d) occur around some clasts with thicker sorted layers below the clast; clasts mainly rounded to subrounded (especially boulders and cobbles) but some angular, local clasts of quartzite and schist; weak imbrication locally developed; some oxidized patches and heavily altered clasts; lower contact covered.

Unit 1c: Diamicton: up to 3.5 m thick; lens shaped; massive; mainly clast-supported with a silty sand matrix; a few pockets of matrix-supported diamicton and poorly sorted cobble or pebble gravel; 60 to 80% clasts; disorganized fabric; oxidation patchy; shape and size range of clasts similar to unit 1b; some clasts have 1 - 2 mm thick, smeared and polished silt and clay coatings; slickensides weak and near vertical; lower contact gradational and irregular.

Unit 1d: Boulder-cobble gravel: similar to, and laterally continuous with, unit 1b; discontinuous lenses and beds up to about 1.5 m thick; lower contact gradational to erosional.

Unit 2: Interbedded clay, silt, sand and diamicton: 11.85 m thick; *Silt and clay beds:* 5 - 50 cm thick, parallel laminated, locally with numerous dropstones that deform underlying laminae, minor convoluted laminae and flaser bedding, lower contacts generally sharp and planar, upper contacts mainly gradational. *Diamicton beds:* generally 10 - 60 cm thick although thin (1cm) intrabeds are also common; generally matrix-supported; matrix silty to silty sand commonly with angular inclusions of laminated silts and clays (Figure 8f); clay, silt and sand laminae and intrabeds are common and often are folded (Figure 8e); clasts are mainly small to large pebbles; total clast content 50 - 70% near the base of the unit to 10-20% near the top, some clasts striated, mostly subrounded and subangular although angular clasts locally dominate; beds are mainly ungraded or normally graded; clasts at the base of the diamicton beds commonly deform underlying sediments and clasts at the top commonly protrude into, and are draped by, overlying strata (Figure 8f). *Sands:* Some fine to medium sand beds with parallel laminae; cross laminae and ripple bedding and minor pebbly sand beds occur. Minor irregular pebble gravel layers; some normal faults. Thickness and abundance of diamicton layers increases towards the SW. Contacts between beds are mainly conformable except for loading and deformation structures at the base of some diamicton beds. Lower contact of unit dips steeply (25° - 30°) to the west (220° - 295°) at the SW end of section and is marked by a 20 cm thick layer of sheared (fractured and slickensided) clay, silt and gravel (probably due to "recent" slumping). At the NE end of the section beds consistently dip about 10° to the NE (50°). The lower contact at the NE end of the section is covered. Near the section centre the contact is inaccessible but appears conformable, and unit 2 is locally interbedded with unit 1.

Unit 2a: Diamicton: 1.0 m thick; beds mainly 10 - 20 cm thick, clast to matrix-supported, matrix silty sand, total clast content 50 - 70%. 60% of clasts clasts are angular, siliceous, rocks of local origin, some beds inversely graded and capped by gravel concentrations (Figure 8d), lower contacts loaded. Silts and clays as above.

Unit 2b: Silt, clay, sand and diamicton: 4.25 m thick; silts and clays with some fine sand laminae (< 0.1 mm to 0.5 cm thick), abundant dropstones; numerous thin (< 1 - 10 cm) granular to pebbly diamicton beds, commonly with flow folds and silt/clay intraclasts; minor ripple bedded sands with silts infilling ripple troughs; thickness of diamicton beds and sand laminae increases towards the top of the unit; minor normal faulting (Figure 8c) near top of unit (dip 49°, dip direction 245°); bed contacts mainly conformable except for small scale load structures.

Unit 2c: Silts and clays: 2.0 m thick; thinly laminated silts and clays with few diamicton beds; number of diamicton beds and sand laminae increase towards the top of the unit; abundant normal faults in lower half (Figure 8g).

Unit 2d: Silts and fine sands: 3.6 m thick; thinly to thickly laminated silts and fine sands with little clay; diamicton beds 2-5 cm thick except for one 30 cm thick bed; matrix silty clay in thickest beds, otherwise silty sand; numerous silt and sand laminae (partings) in diamicton beds; numerous dropstones in upper part; contacts distinct and conformable.

Unit 2e: Diamicton: 0.7 m thick; matrix-supported; matrix silty sand; clasts pebble to small cobble sized, mostly subangular with abundant striations; numerous rounded mud clasts; total clast content 30 - 40%; lower contact gradational and indistinct.

Unit 2f: Pebbly sands and silts: 0.75 m thick; parallel laminae with intense small scale folding; abundant load structures, especially in the upper half of the unit where stratification is very indistinct.

Unit 3a: Diamicton interbedded with silt and fine sand: 2.5 m thick; diamicton matrix-supported with a silty sand matrix (figure 9a); clasts up to cobble size, subangular to rounded; diamicton beds are 20 to 50 cm thick and contain numerous discontinuous sand laminae; bedding is horizontal but is weakly defined; it is due to textural and color banding in the diamicton, and is enhanced by the sand and silt beds; horizontal laminae within sand and silt beds are generally discontinuous and highly deformed (loaded and folded); some polished and lineated (sheared?) surfaces occur in the upper part of the unit; lower contact is gradational.

Unit 3b: Diamicton: 4.5 m thick; matrix-supported, silty clay to silty sand matrix; dense; polished sub-horizontal partings are common in clay rich areas. Clasts mainly medium to large pebbles, cobbles and boulders rare, mainly subangular to subrounded, numerous striated and glacially shaped clasts, total clast content 20 - 40%; unit oxidizes readily resulting in mottling with grey, recently exposed diamicton occurring in patches on the dominantly brown, weathered surface. Small (< 20 cm thick), poorly defined, irregular, lenses of silt, clay and sand occur in the upper part of the diamicton; the lenses commonly exhibit compressive deformation structures such as thrust faults, reverse faults, folds and subhorizontal shear zones; slickensides on shear zones trend 110° to 150°. Lower contact gradational.

Unit 3c: Diamicton interbedded with silt, sand and gravel: *Diamicton:* (Figure 9d) matrix- to clast-supported, matrix silty sand to sand, little silt or clay; loosely consolidated; clasts pebble to cobble sized, subangular to subrounded, striated clasts common at base but decrease in abundance up section, 50 - 80% total clast content; sand and gravel content increases towards the top of the unit; beds 5 cm to 1.5 m thick. *Sands and silts:* beds 2 - 10 cm thick; massive to crudely horizontally stratified; minor ripple bedding and convoluted laminae; some irregular clay inclusions; trough cross-laminated sand (and gravel) lenses 2-10 cm thick and 10 - 100 cm wide occur throughout the unit (Figure 9e); moderately to very well sorted; beds laterally continuous for up to several metres before grading into diamicton. *Gravels:* occur in thin beds and lenses with horizontal to gently inclined planar bedding and some trough cross-bedding; poorly to moderately sorted, clasts mainly granule to medium pebble in size; lower contacts locally erosional. All of unit 3c occurs in a broad (50 m wide) trough-shaped body. Beds generally are near horizontal and contacts are diffuse, irregular and locally exhibit load structures. Lateral variations in sorting and stratification are common, especially in the lower part of this unit where horizontal and cross-stratified sands and pebbly sands locally dominate.

Unit 4a: Gravels: 0.6 m thick; open-work bouldery gravel fining up into matrix-filled pebbly gravel; poorly to very poorly sorted; clast-supported; crude horizontal stratification marked by pebbly beds about 10 cm thick; fabric disorganized to weakly imbricated [a(p), a(i)] indicating paleoflow to the NW (320°); some diamicton intraclasts; trough-shaped, erosional lower contact.

Unit 4b: Boulder gravel: 0.5 m thick; clast-supported, clasts large pebbles to boulders; open work; oxidized.

Unit 4c: Pebble gravel: 1.7 m thick; clast-supported; matrix filled; poorly to moderately sorted; horizontal stratification due to very large pebble to small cobble open work beds about 20 cm thick; unit fines up into trough cross stratified sands and pebbly sands.

Unit 4d: Boulder gravel: 0.8 m thick; same as unit 4b.

Unit 4e: Pebbly gravels and sands: 2.0 m thick; horizontally stratified; gravels clast-supported, matrix filled and moderately sorted; sands horizontally laminated with some trough cross laminae; unit grades laterally into well to very well sorted, trough and planar cross-stratified, fine to medium sands and horizontal and planar cross-stratified sands and pebbly sands (Figure 9g); lower contact erosional.

Unit 4f: Large pebble to boulder gravel: 8.4 m thick; crude horizontal stratification; clast-supported; matrix filled with some lenses of open-work, oxidized gravel; some well sorted pebbly layers with weak planar cross bedding; blade shaped clasts common; mostly rounded to subrounded; poorly to moderately sorted; sorting and stratification are poorer to the NE and SW; this unit is in almost vertical contact with diamicton of unit 3 to the NE.

West Section

Unit 5: Complexly interbedded sand, gravel and diamicton: (Note: This unit is exposed only at the west exposure of the Martin Creek Section.) The unit thickness varies laterally from about 1 to 10 m. At the SW end of the section the unit is dominated by a large trough of diamicton (unit 5a) overlain by sands (unit 5b). Unit 5a grades upstream into interbedded gravel, sand and gravelly diamicton (units 5c and 5d) over a distance of about 50 m. These sediments are overlain by two large troughs of sand and gravel (unit 5e), and they grade laterally (upstream) into interbedded diamicton, gravel and sand (unit 5g) unconformably underlain by sand and gravel.

Unit 5a: Sandy diamicton: up to 5 m thick; 70-80% clasts; unsorted to poorly sorted; interbedded with well stratified sand lenses; weak, large scale (20 m wide), trough shaped, cross bedding; lower contact covered.

Unit 5b: Fine to coarse sands and pebbly sands: 3 m thick; moderately to very well sorted; large scale trough cross-stratification as above (channel-fill bedding); lower contact conformable.

Unit 5c: Interbedded gravel, sand and diamicton: 9 m thick; gravels are pebble to cobble sized, clasts supported, poorly sorted, disorganized and have a silty sand matrix; sands and pebbly sands are poorly to well sorted and massive or planar cross-stratified; diamicton is matrix-supported and gravelly; gravel grades laterally and vertically into diamicton; the unit is crudely bedded with horizontal beds at the base; beds dip 25-30° up-valley (025°) in the middle of the unit; lower contact covered.

Unit 5d: Bouldery gravel: about 3 m thick; poorly sorted, clast-supported, some open work beds and vertically oriented clasts; beds dip (60-80°) in opposing directions to form a wedge about 10-15 m wide and 3-5 m high; these beds can be traced up-valley into nearly horizontal bedding; lower contact conformable.

Unit 5e: Interbedded sands and gravels: 3-6 m thick; sands fine to coarse, well sorted and parallel-laminated; minor silt beds occur with sands; gravels are pebble to boulder-sized, clast-supported, matrix-filled and poorly sorted; unit occurs in two large (20 -30 m wide) trough-shaped bodies at the top of the section; deformation (folding and normal faulting) increases towards the base; lower contact erosional.

Unit 5f: Sands, pebbly sands and pebble gravels: 2-5 m thick (unit thickens to the NE); well to poorly sorted; planar cross-stratified; beds dip about 20° downstream (250°); lower contact covered.

Unit 5g: Diamicton, gravel and sand: about 5 m thick; diamicton sandy, matrix to clast-supported; similar to unit 3c above; interbedded gravels are clast-supported, matrix-filled to open-work, and mainly pebble sized except for a large bouldery bed at the top of the unit; sands are planar cross-laminated, well to moderately well sorted; some pebbly sands; beds dip 20° upstream (070°) and unconformably overlie beds of opposing dips in unit 5f; beds in the centre of the unit are convoluted; the proportion of diamicton initially increases to the SW (downstream) and then decreases as the unit grades laterally into unit 5d; lower contact erosional.

GEOLOGY, MINERALOGY AND GEOCHEMISTRY OF TIN AND TUNGSTEN VEINS, BRECCIAS AND SKARNS, MCQUESTEN RIVER REGION (115 P (NORTH) AND 105 M 13), YUKON

Diane Emond
Exploration and Geological Services Division
Indian and Northern Affairs Canada
200 Range Road
Whitehorse, Yukon
Y1A 3V1

Teresa Lynch (née Potter)
2961 de Vincennes
Ste-Foy, P.Q.
G1W 2E5

EMOND, D.S. and LYNCH, T., 1990. Geology, mineralogy and geochemistry of tin and tungsten veins, breccias and skarns, McQuesten River region (115 P (north) and 105 M 13), Yukon. In: Yukon Geology, Vol. 3; Exploration and Geological Services Division, Yukon, Indian and Northern Affairs Canada, p.133-159

ABSTRACT

Tin and tungsten-bearing veins, breccias and skarns occur in a 60 km long belt trending west from Keno Hill to the Tintina Fault. They are hosted by mid-Cretaceous felsic intrusions, or adjacent metasedimentary rocks of Upper Precambrian to Mississippian age. Tin occurrences are mainly associated with two-mica granites in the southern part of the belt, while the tungsten lodes are more commonly associated with biotite-hornblende granitoids. Tin- and silver-bearing veins are associated with the central granite phase of a zoned intrusion in the northwest part of the belt (the Syenite Range). The zoned intrusion ranges in composition from tourmaline orbicular granite to granite to quartz monzonite to syenite.

Most skarns are tungsten-dominant, whereas most breccias and veins are tin-bearing. The skarns are calcic and reduced. Three stages of skarn mineral formation and associated minerals are recognized: (1) isochemical contact metamophism, including diopside, grossular, wollastonite, and tremolite; (2) metasomatic skarn formation including andradite, idocrase, hedenbergite, axinite, and some sulphide minerals; and (3) retrograde alteration including actinolite, chlorite, clinozoisite, epidote, calcite, biotite, scheelite, cassiterite and sulphide minerals. Sulphide minerals are mostly minor, with pyrrhotite and pyrite predominant.

Breccias, veins and sheeted veins of tin and tungsten occur in steeply dipping tabular bodies close to felsic intrusions. The veins consist of quartz, tourmaline or chlorite. Tin-bearing veins and breccias contain all three gangue minerals plus pyrrhotite, pyrite, sphalerite, chalcopyrite, arsenopyrite and galena. Tungsten is only found in quartz (-orthoclase) veins which contain minor pyrite and molybdenite.

Sheeted vein systems consist of three mineral assemblages: (1) quartz-orthoclase-scheelite, (2) quartz-orthoclase-cassiterite, and (3) tourmaline-cassiterite. The first assemblage is present both in the endo- and exocontact of felsic intrusions, whereas the second and third occur further away from the granite in metasedimentary rocks which generally lie outside the thermal aureole of the intrusion.

Breccia clasts consist of quartzite, schist, and/or vein fragments (quartz, tourmaline, or chlorite). The breccias are either clast-supported with a matrix of rock flour, or matrix-supported with a matrix (groundmass) of crystalline quartz, tourmaline or chlorite similar to vein material.

Geochemical studies of the McQuesten River occurrences indicate that: (1) Some properties are exclusively tin or tungsten properties, but others contain both metals. There is a positive correlation between tungsten and tin in some tin-bearing rocks. (2) Silver is common in veins and skarns which contain over 50 ppm Sn. (3) Gold occurs in significant quantities in most skarns and in several veins. (4) There is a positive correlation between gold and bismuth in the skarns. Bismuth can be used as a pathfinder for gold in these skarns.

RÉSUMÉ

On trouve des veines, des brèches et des skarns renfermant de l'étain et du tungstène dans une zone d'une longueur de 60 km s'allongeant vers l'ouest depuis la colline Keno jusqu'à la faille de Tintina. Ils se situent à l'intérieur d'intrusions felsiques du Crétacé moyen ou dans les roches sédiementaires métamorphisées adjacentes datant du Précambrien supérieur au Mississippien. Les indices minéralisés en étain sont principalement associés aux granites à deux micas de la partie méridionale de la zone alors que les filons de tungstène sont plus couramment associés aux granitoïdes à biotite et hornblende. Les veines renfermant de l'étain et de l'argent sont associées à la phase granitique centrale d'une intrusion zonée dans la partie occidentale de la zone (la chaîne Syenite). La composition de l'intrusion zonée passe du granite orbiculaire à tourmaline au granite à la monzonite quartzique à la syénite.

La plupart des skarns renferment principalement du tungstène alors que la plupart des brèches et des veines renferment de l'étain. Les skarns sont calciques et réduites. Trois stades de formation de minéraux et de minéraux associés dans les skarns ont été reconnus : 1) métamorphisme topochimique de contact (incluant diopside, grenat grossulaire, wollastonite et trémolite), 2) formation de skarn métasomatique (incluant andratite, idocrase, hédenbergite, axinite et certains minéraux sulfurés) et 3) altération rétrograde (incluant actinolite, chlorite, zoïsite monoclinite, épidotite, calcite, biotite, scheelite, cassitérite et minéraux sulfurés). Les minéraux sulfurés sont principalement présents en quantités mineures, la pyrrhotine et la pyrite étant les principaux.On trouve des brèches, des veines et des groupes de filons séparés de stériles renfermant de l'étain et du tungstène dans des masses tabulaires d'un fort pendage à proximité des intrusions felsiques. Les veines se composent de quartz, de tourmaline ou de chlorite. Les veines stannifères et tungstènifères renferment toutes trois minéraux de gangue en plus de pyrrhotine, de pyrite, de sphalérite, de chalcopyrite, d'arsénopyrite et de galène. Le tungstène n'est présent que dans les veines de quartz (-orthoclase) qui renferment des quantités mineures de pyrite et de molybdénite.

Les réseaux de filons séparés de stériles consistent en trois assemblages de minéraux : 1) quartz-orthoclase-scheelite, 2) quartz-orthoclase cassitérite et 3) tourmaline-cassitérite. Le premier de ces assemblages est présent dans les intrusions felsiques des côtés intérieur et extérieur du contact alors que les deuxième et troisième se retrouvent plus loin du granite dans les roches sédimentaires métamorphisées qui se trouvent généralement à l'extérieur de l'auréole thermique de l'intrusion.

Les fragments des brèches consistent en quartzite, en schiste et/ou en fragments de veines (quartz, tourmaline ou chlorite). Les brèches sont soit à base de fragments avec une matrice de poussière de roche, soit à base de matrice avec une matrice (pâte) de quartz cristallin, de tourmaline ou de chlorite similaires aux matériaux des veines.

Les études géochimiques des indices minéralisés de la rivière McQuesten indiquent 1) qu'il existe une corrélation positive entre la présence du tungstène et de l'étain dans certaines roches stannifères. Certaines propriétés sont exclusivement stannifères ou exclusivement tungstènifères, mais dans d'autres l'on trouve les deux métaux. 2) L'argent est commun dans les veines et dans les skarns renfermant plus de 50 ppm de Sn. 3) Il y a des quantités importantes d'or dans la plupart des skarns et dans plusieurs veines. 4) Il existe une corrélation positive entre la présence de l'or et du bismuth dans les skarns. Le bismuth peut être utilisé comme élément indiquant la présence d'or dans ces skarns.

INTRODUCTION

The McQuesten River - Mayo region is one of the most intensely mineralized in the northern Cordillera. Placer gold has been mined since the turn of the century mainly from Haggart, Highet, Johnson, Clear, Duncan and Swede Creeks. Silver-lead veins (MINFILE 105M 001 etc.) have been mined in the Keno and Galena Hill district since 1913, producing over 6.4 billion grams of silver (Watson 1986). Tin and tungsten lodes occur in a west-trending belt extending from the western edge of the Keno-Galena Hill district to the Tintina Fault (Figs. 1 and 2), and represent a different component of the same metallogenic event (i.e., deposits related to Cretaceous intrusions). The most notable deposit is the RAY GULCH tungsten skarn (MINFILE 106D 027) with probable and possible reserves of 5.4 million tonnes of 0.82% WO_3 (Lennan 1986).

Following a study of the Oliver Creek tin-silver breccias (MINFILE 115P 030)(Emond, 1985), the authors visited most of the tin and tungsten occurrences in 1985 (Emond 1986, INAC 1989). Lynch completed a B.Sc. research paper on the petrography of these occurrences (Potter 1987). This paper summarizes the detailed mineralogy, geochemistry and distribution of metals in the mineral occurrences. The McQuesten occurrences have been previously explored mainly for tin and tungsten, but this new geochemical data indicates local enrichment in gold.

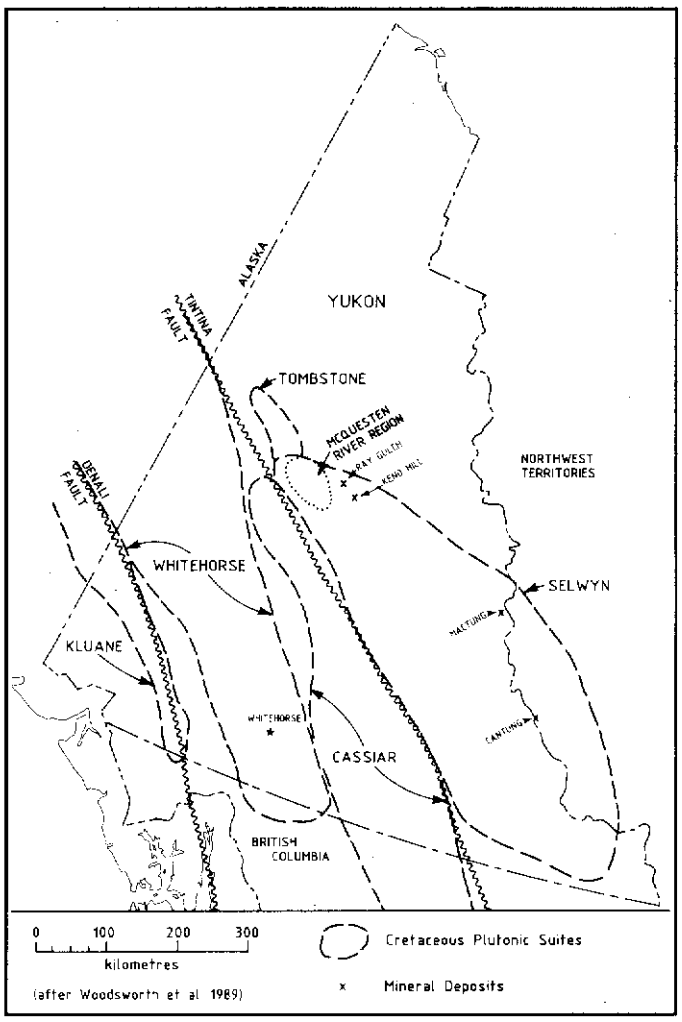

Figure 1. Location of the McQuesten River region in Yukon. Also outlines mid-Cretaceous felsic plutonic suites (after Woodsworth et al. 1989).

GEOLOGICAL SETTING

Tin- and tungsten-bearing veins, breccias and skarns occur in a 30 x 60 km belt that trends east from the Tintina Fault in the McQuesten River region (Fig. 1). They are closely associated with mid-Cretaceous plutons along the same trend, and occur in both the plutonic rocks and in Late Proterozoic to Mississippian metasedimentary rocks of the Late Precambrian to Early Cambrian Hyland Group ("Grit Unit"), the Ordovician-Silurian Road River Formation, and the Mississippian Keno Hill Quartzite (Bostock 1946 and 1964, etc). The only prominent large scale structure is the ENE-trending McQuesten Anticline. A strong foliation which strikes east-northeast cuts the metasedimentary rocks (Boyle 1965, Fig. 2).

The mid-Cretaceous plutons (83 to 108 Ma: biotite - K/Ar, Stevens et al. 1982) are small epizonal felsic intrusions with associated coeval lavas (85 Ma, whole rock, K/Ar, Hunt and Roddick 1987, Fig. 2). The felsic intrusive rocks (Emond 1992) belong to the post- to syn- collisional bimodal Selwyn Plutonic Suite, and are bounded by and may grade into the more alkaline Tombstone Plutonic Suite to the northwest (Fig. 1; Woodsworth et al. 1989). The lavas are most likely the northwesternmost exposure of the South Fork Volcanics (Gordey 1988).

The plutonic rocks are generally bimodal, "S" type, reduced granitoids, with biotite-muscovite (two-mica) granites mainly confined to the southern part of the belt, and biotite-hornblende granite, quartz monzonite, and granodiorite further north. At the north end of this belt, the rocks are more alkaline: a large stock zoned from hornblende-biotite syenite to quartz monzonite to granite towards the core has fractionally crystallized in situ (Abercrombie 1990, Emond 1992). Contact aureoles of biotite hornfels, andalusite porphyroblast hornfels, calc-silicate rocks and tourmalinite are common where pelitic metasedimentary rocks were intruded.

Each mineral occurrence is related to a particular type of granitoid (Fig. 2). Tin (-silver) occurrences are associated with evolved two-mica granites in the southern and northwestern part of the belt, while tungsten (-gold) occurrences are associated with less evolved biotite-hornblende granite, quartz monzonite and granodiorite throughout the belt (Emond 1992). In the southern part of the belt, where tungsten skarns are associated with biotite-hornblende granite, they are commonly polymetallic. The mineral associations in the McQuesten Plutonic Suite differ from those in the Selwyn Plutonic Suite. Tin-rich occurrences are more common in the McQuesten area, where they are associated with two-mica granites. Tungsten occurrences in the McQuesten area are associated with biotite-hornblende granitoids, but larger and more numerous tungsten deposits occur in the Selwyn Mountains where they are associated with two-mica granites (Anderson, 1988).

STYLES OF MINERALIZATION AND MINERALOGY

There are two main styles of tin and tungsten mineralization: (1) skarns, and (2) veins and/or breccias (Emond 1986). Detailed descriptions of individual properties mentioned here are published in Yukon Exploration 1988. Petrography of the mineral occurrences is discussed separately below.

1. Skarns

Both the Hyland Group and the Road River Formation contain thin layers of marble and dolomite which pinch and swell along strike. These units form calcic skarns on the margins of intrusions. At the OLIVER CREEK (MINFILE 115P 030) tin occurrence, calcareous diorite intercalated with Hyland Group rocks is also skarnified. Tin skarn occurs at OLIVER CREEK (MINFILE 115P 030) and BOULDER CREEK (115P 048). Tungsten skarn occurs at SCHEELITE DOME (MINFILE 115P 004), LUGDUSH (MINFILE 115P

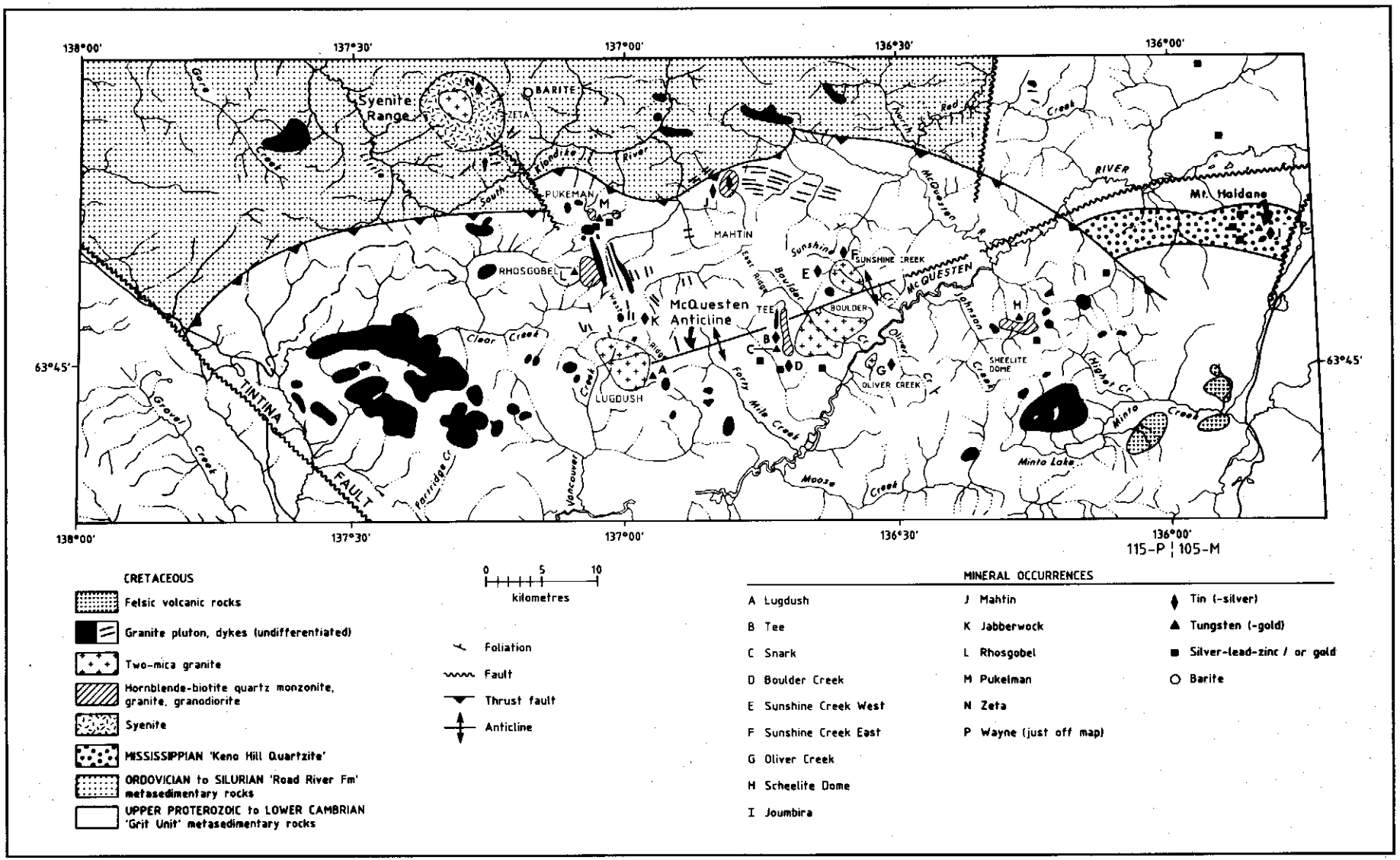

Figure 2. Geology and mineral occurrences, McQuesten River region. Plutonic phases are also distinguished where known.

009), RHOSGOBEL (MINFILE 115P 012) and RAY GULCH (MINFILE 106D 027)(Lennan 1986). Tin-tungsten skarn occurs at SNARK (MINFILE 115P 008b)(Fig. 2). These mineral occurences are documented in Table 1 in terms of host rock, associated intrusion, skarn mineral assemblage, size and geochemistry.

The best assays from the tungsten skarns came from SCHEELITE DOME (MINFILE 115P 004), where a 4 m chip sample of drill core contained 3620 ppm W and 2080 ppb Au. The best assays from tin skarns came from the OLIVER CREEK showing (MINFILE 115 P 030), where a 1.7 m drill intersection contained 0.9% Sn and 4 ppm Ag.

The skarns show a typical three-stage evolutionary pattern: (1) isochemical contact metamorphism accompanying crystallization of the magma; (2) metasomatic skarn formation accompanying crystallization of the magma and evolution of the ore fluid; and (3) retrograde alteration and continued ore deposition with the final cooling of the system (Einaudi et al. 1981). Table 2 places the skarn minerals in their respective evolutionary stages and summarizes the petrographic characteristics of the McQuesten River occurrences, such as mineral abundance, colour, grain size, form and alteration.

Stage 1. Isochemical Contact Metamorphism

In this prograde stage, metamorphic reactions involve changes in the amount of volatile components only, such as oxygen, carbon dioxide and water. Otherwise, on the scale of an outcrop, the system remains isochemical. Minerals from this stage in McQuesten area skarns consist mainly of diopside, grossular, wollastonite, and tremolite. Diopside is the most common mineral, occurring in both the tin and tungsten skarns. Grossularite occurs mostly in the tin skarns, while wollastonite is mainly restricted to the tungsten skarns. These iron-poor calcium-magnesium-aluminum silicates reflect the original limestone and dolomite host rocks. Though this stage was not a mineralizing event, the porosity increase resulting from the fracturing and volatile loss during intrusion probably controlled the later emplacement of the economic minerals (Einaudi et al. 1981).

Stage 2. Metasomatic Skarn Formation

The metasomatic minerals are formed by magmato-hydrothermal processes which, unlike the previous metamorphic ones, produce changes in the amounts of non-volatile components, such as calcium, iron, silica and boron (Einaudi et al. 1981). Minerals from this stage in McQuesten skarns include andradite, idocrase, hedenbergite and axinite. Complex skarns result from the overprinting of stage 2 on stage 1 assemblages. Minerals show iron enrichment trends (Emond 1985) due to infiltration of iron, silica and boron-rich magmatic fluids into the fractured host rock. Minor amounts of sulphides (pyrite, pyrrhotite, chalcopyrite, sphalerite and galena) were also deposited during this stage. Tin in the BOULDER CREEK (MINFILE 115P 012) tin skarn is inferred to be locked up in the andradite or axinite as no cassiterite was observed.

Stage 3. Retrograde Alteration

Retrograde minerals are formed by the final cooling of the system and the incursion of meteoric water, and typically reflect the composition of original skarn silicates, but modified by leaching of Ca, and the introduction of volatiles (Einaudi et al. 1981). Hydrous phases are typically formed. Minerals from this stage in McQuesten area skarns include actinolite, chlorite, clinozoisite, epidote, calcite and biotite. Scheelite precipitates at this stage, and calcium is released in solution (Figs. 3a and 3b). Cassiterite also precipitates at this stage as tin is released from calc-silicate minerals. Sulphide minerals continue to precipitate and reach a peak during retrograde alteration. The retrograde chlorite-actinolite-pyrrhotite-pyrite-cassiterite skarn (Fig. 3c) associated with chlorite-cassiterite breccias at OLIVER CREEK (MINFILE 115P 030) is an example of the importance of the retrograde stage in producing an economically viable tin prospect. At the PUKELMAN (MINFILE 115P 013) sheeted quartz-scheelite vein occurrence, scheelite occurs with retrograde biotite in hornfels, particularly in less calcic, more pelitic layers in the host rock.

Petrographic studies show clinozoisite and actinolite replacing diopside, and epidote and calcite replacing garnet. Actinolite also replaces idocrase and axinite. Fluorite is not abundant in the McQuesten area skarns, although some occurs locally in biotite hornfels.

Fluorite with abundant muscovite signals the onset of greisenization, an important retrograde alteration which improves the economic viability of tin deposits. In this area, only the OLIVER CREEK (MINFILE 115P 030) occurrence shows minor fluorite-sericite-chlorite alteration. Most of the skarns in the McQuesten region have not reached this stage.

Textures

Many of the tin and tungsten skarns are banded, with alternating 1-2 mm wide layers composed of quartz-orthoclase and diopside-clinozoisite ($\pm$ wollastonite or tremolite; Fig. 3d). This banding reflects the early regional metamorphic fabric. The foliation is believed to have exerted physical and chemical controls on the skarn mineralogy and textures (Fig. 3d). Only the coarse grained garnet-axinite-idocrase tin skarn at BOULDER CREEK (MINFILE 115P 048) is unfoliated.

Hornfels

Hornfels is defined as fine-grained, non-foliated rock composed of a mosaic of equidimensional grains with no preferred direction (Turner 1968). In the McQuesten River region, hornfelsed rocks occur within the contact aureole of the granitoid intrusions. They are composed of quartz, biotite, muscovite and actinolite, and are weakly foliated. Hornfels at the RHOSGOBEL property (MINFILE 115P 012) contains scheelite, and is intercalated with diopside-tremolite-biotite-scheelite skarn. The skarn-hornfels contact is sharp, and scheelite and sulphides are preferentially concentrated in the hornfels. Scheelite crystals occur in lens-shaped clusters associated with biotite. Scheelite concentrations run as high as 5% in hornfels, and 1-2% in skarn.

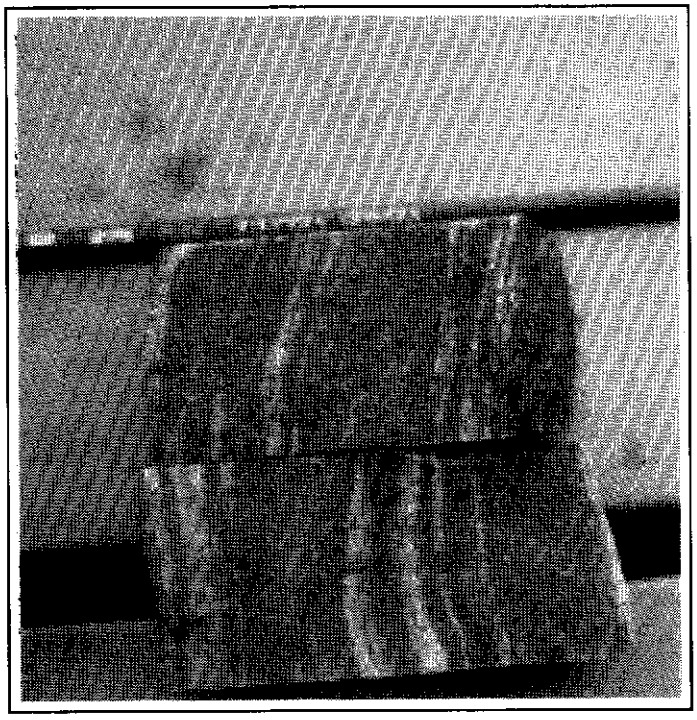

Figure 3a. Actinolite (dark)-quartz (light)-scheelite skarn from SCHEELITE DOME (MINFILE 115P 004).

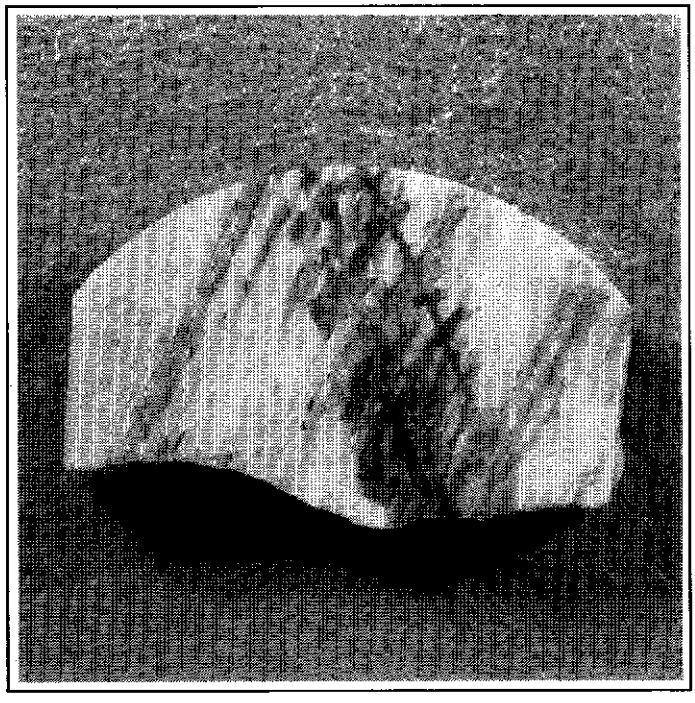

Figure 3b. Quartz-orthoclase-wollastonite (white) skarn cut by quartz-actinolite-scheelite (dark) vein and envelope, SCHEELITE DOME (MINFILE 115P 004).

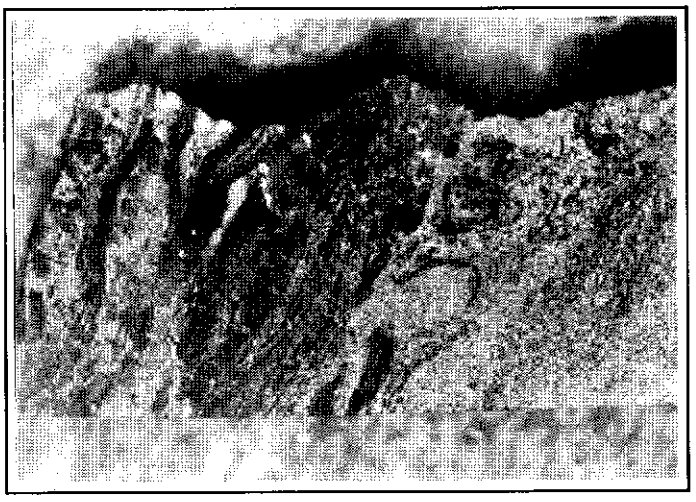

Figure 3c. Actinolite (dark), pyrrhotite (light-reflective), and cassiterite (microscopic) in skarn from OLIVER CREEK (MINFILE 115P 030).

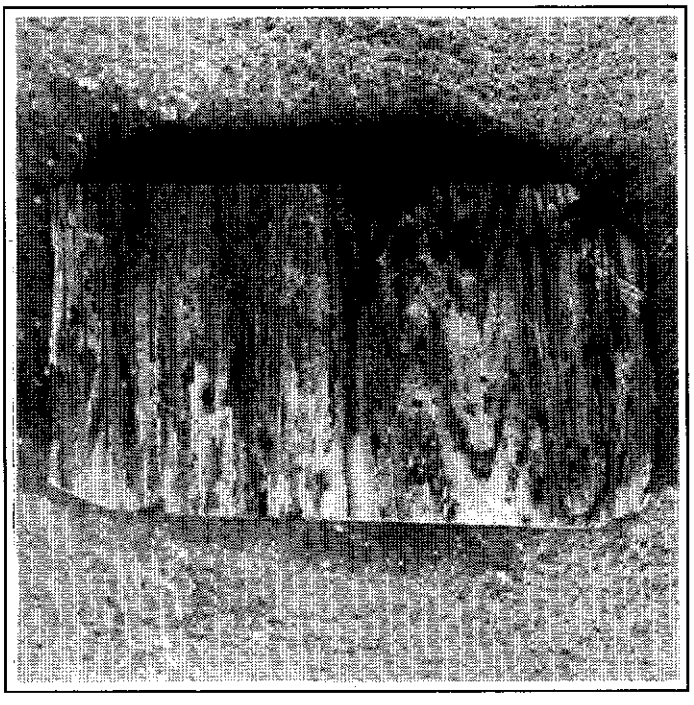

Figure 3d. Banded quartz-orthoclase (white) assemblage alternating with diopside (grey)-rich assemblage, SCHEELITE DOME (MINFILE 115P 004).

Tourmalinite

Tourmalinite also occurs in the contact aureoles of intrusions, and is most common near tin and tungsten showings. Pervasive tourmaline alteration occurs in mica-quartz schist, where the mica is altered to tourmaline, leaving alternating quartz and tourmaline layers on a millimetre to

centimetre scale. Sphene crystals approximately 0.1 mm long form 2-3% of the rock, and up to 2% topaz occurs locally.

Summary of Skarns

Petrographic analysis shows that skarns of the McQuesten River region incorporate features of both reduced and oxidized skarns as defined by Einaudi et al. (1981). Due to the predominance of pyrrhotite over pyrite and pyroxene over garnet, and the presence of some biotite and hornblende as retrograde minerals, they are appear to resemble Einaudi's reduced skarns. However, retrograde minerals common in oxidized skarns are also present, suggesting the onset of retrograde alteration was accompanied by an increase in oxidation state.

Temperatures typical of early skarn formation range from 500-600°C, and retrograde skarns form at 300-450°C (Einaudi et al. 1981). Newberry (1980) suggested that calcium released during breakdown of pyroxene and garnet during retrograde alteration contributes to tungsten precipitation. This is supported by the observation that biotite and sphene are closely associated in McQuesten River skarns. Calc-silicate gangue predominates over opaque minerals, in contrast to the sulphide or iron oxide replacement skarns which contain only minor amounts of low temperature calc-silicate minerals. Only the tin skarn at OLIVER CREEK and the tungsten skarn at SCHEELITE DOME contain massive sulphides, and these consist mainly of pyrrhotite, a low sulphur species (Fig. 3c).

The following three major evolutionary stages were involved in formation of the McQuesten River skarns: (1) Formation of a metamorphic aureole and local reaction skarns accompanying magma intrusion and expulsion of connate and ground water. (2) Melt crystallization and exchanges of components between the magmatic fluid and carbonate host rocks. Later stages of prograde skarn formation show an iron enrichment trend in the silicates which is reflected by the development of hedenbergite and axinite. (3) Cooling of the system and influx of meteoric water, leading to retrograde alteration of the skarn and hornfels. This is a very important stage in metal deposition.

(2) Breccias and Veins

Breccias, veins and sheeted veins containing tin and tungsten occur near the contacts of dykes and plutons with the metasedimentary rocks. They are especially common in the cupola region of the pluton. Sheeted veins in some cases extend from the pluton several hundred metres into the country rock. Breccias commonly grade into stockwork or veins, and have many of the characteristics of veins (Emond 1985). Most veins and breccias dip steeply and are fault or joint controlled (Fig. 4a).

The breccias form two main types: (1) rock flour breccias, consisting of quartzite or schist fragments in a matrix of finely ground quartzite (Fig. 5a); and (2) crystalline matrix breccias, consisting of a combination of quartzite (or schist) and/or vein material fragments in a matrix of vein minerals (Figs. 5b-d). The crystalline matrix breccias include three general types based on the dominant matrix mineral, which can be either quartz, tourmaline or chlorite.

Vein types are also defined by the same three dominant minerals. The three vein assemblages in order of paragenesis are: (a) quartz (± tourmaline, orthoclase, cassiterite, scheelite, topaz; (Fig. 5b)); (b) tourmaline (± sulphides, cassiterite; (Fig. 5c)); and (c) chlorite (± cassiterite, sulphides, biotite, muscovite; (Fig. 5d)). Calcite also forms crosscutting veins and breccias (Fig. 5a), but these are generally unmineralized.

Table 3 summarizes the tin and tungsten breccia/vein occurrences, including associated pluton, host rock, matrix or gangue, fragments, and geochemistry. The highest grade tin-silver breccia/vein occurrence is the OLIVER CREEK showing (MINFILE 115P 030), where a 1.7 m drill intersection assayed 0.9% Sn and 4 ppm Ag. The highest grade tungsten-gold sheeted vein occurrence is the PUKELMAN showing (MINFILE 115P 013) where a 4 m chip sample of drill core contained 3620 ppm W and 2080 ppb Au.

Rock Flour Breccias

Rock flour breccias consist of 70-95% angular to subrounded quartzite, schist, and/or tourmalinite fragments (<5 cm) in a finely comminuted matrix of quartz, tourmaline, muscovite, chlorite and occasional biotite (silt to sand size). Up to 5% cassiterite occurs in the matrix, and minor euhedral pyrite cubes occur locally. Other sulphide minerals are uncommon, except where chlorite or tourmaline veins are present. Topaz occurs with tourmaline, quartz and cassiterite in biotitized rock flour breccia, and limonite staining is common.

These breccias are common in fault zones and are not always mineralized. However, many are tin-bearing where crystalline-matrix breccias and/or veins are also present and on close examination, many of these accompanying breccias and veins also prove to contain rock flour (Table 3).

Rock flour breccia zones are closely associated with chlorite breccias at OLIVER CREEK (MINFILE 115P 030). These zones vary from a few centimetres to 15 m wide and were probably originally tectonic but were rebrecciated by pneumatolytic-hydrothermal processes accompanying the deposition of cassiterite (Emond 1985).

Crystalline Matrix Breccias and Veins

Crystalline matrix breccias are commonly vein-like in form, with similar mineralogy and texture to the veins. They consist of 30 to 70% angular to subrounded fragments (<5 cm) of quartzite, schist, tourmalinite and vein material (Figs. 5b-d). The breccias are matrix-supported with an average of 60% matrix, (mostly quartz, tourmaline and chlorite as separate phases). Veins associated with tin or tungsten showings usually occur in steeply-dipping to vertical sheeted sets, and are mainly confined to joints in the quartzite or the associated intrusion. Textures in matrix or vein material include comb-textured quartz and orthoclase. Tourmaline and

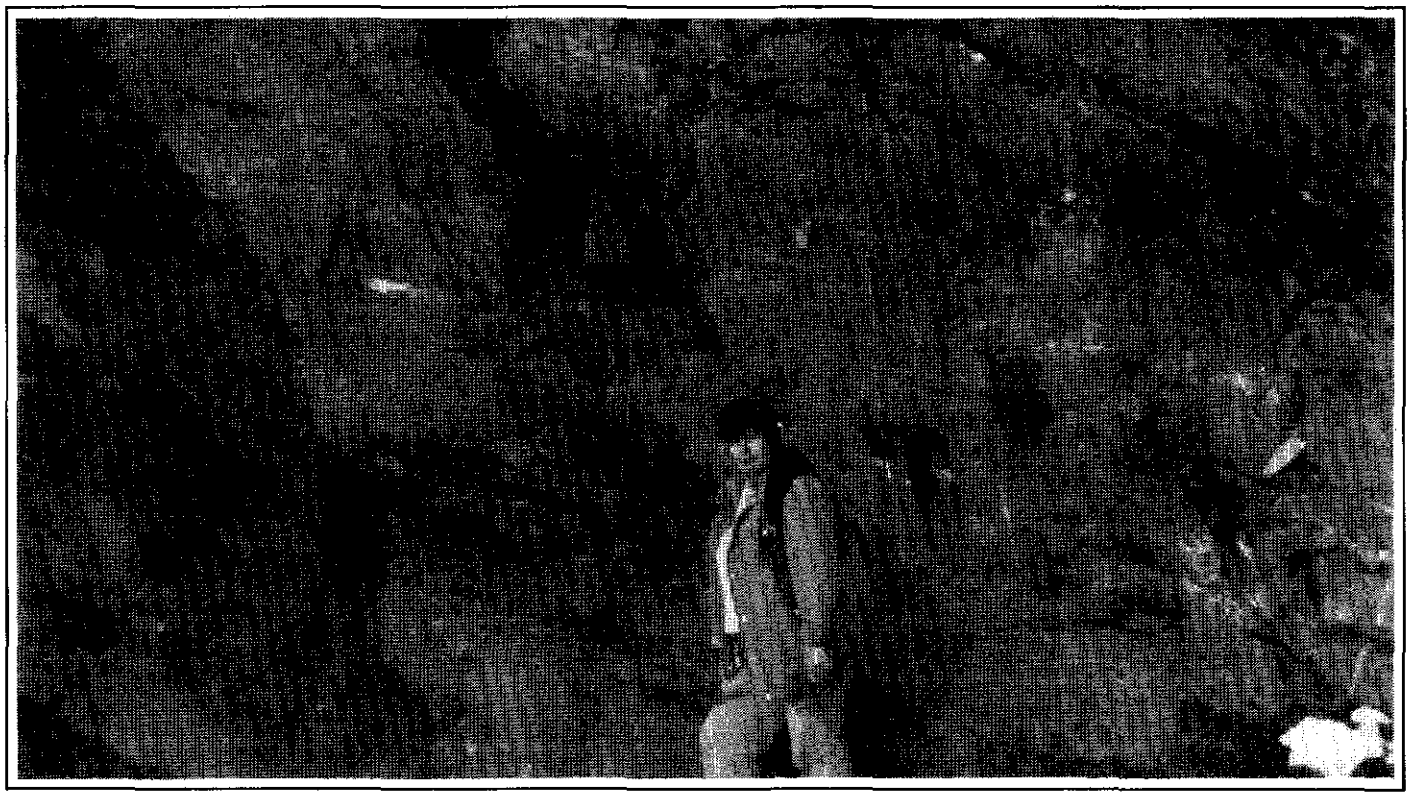

Figure 4a. Steeply dipping quartz-orthoclase-scheelite sheeted veins cutting hornfelsed, jointed metasedimentary rocks adjacent to the Pukelman quartz monzonite stock.

Figure 4b. Cassiterite crystals (small dark grey patches, at tip of pencil <2 mm) on joint surface of grey quartzite, JABBERWOCK (MINFILE 115P 051).

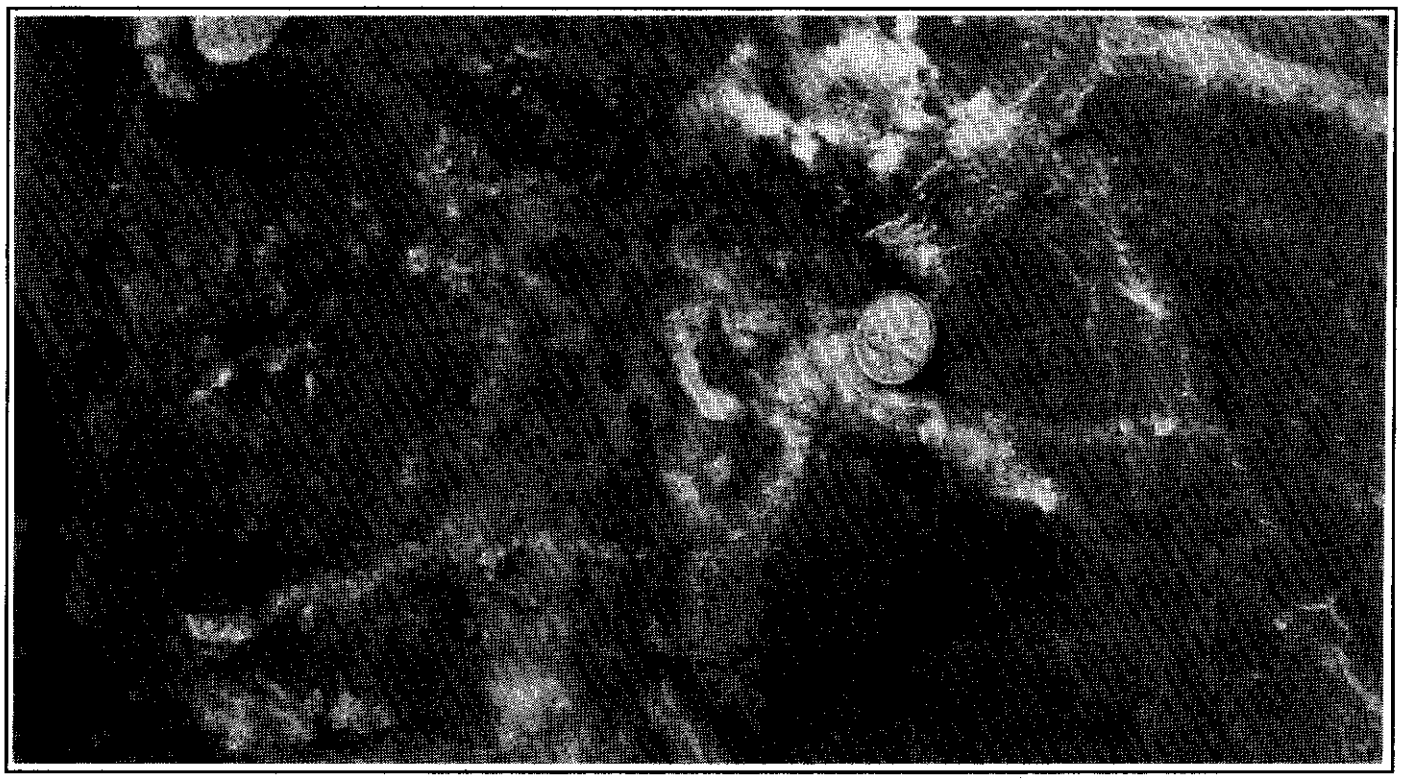

Figure 4c. Radiating tourmaline needle aggregates (black clots) with microscopic cassiterite on joint surfaces of Keno Hill quartzite with quartz veins, JOUMBIRA(MINFILE 105M 031).

chlorite occur locally in radiating aggregates in veins. Veins at OLIVER CREEK (MINFILE 115P 030) are zoned, with chlorite-cassiterite-sulphide cores and quartz margins. Oxidation of iron and manganese, and kaolinization of matrix and vein material occurs near surface.

The crystalline matrix breccias are locally heavily stained with limonite. Cassiterite crystals, crystal aggregates and fragmented crystals occur disseminated in the matrix or in vugs, forming up to 10% of the breccia. The crystals are anhedral to euhedral, display elbow twinning, and form aggregates up to 1 cm wide. Sulphides are rare, except at OLIVER CREEK (115P 030), MAHTIN (MINFILE 115P 007), and ZETA (MINFILE 115P 047).

Quartz crystalline-matrix breccias and quartz veins

Quartz crystalline matrix breccias are predominantly tin- and silver-bearing, and occur mainly at SUNSHINE CREEK WEST and EAST (MINFILE 115P 031a,b), and TEE (MINFILE 115P 008a)(Fig. 5b). They can be extensive; the SUNSHINE CREEK WEST breccia (MINFILE 115P 031a) is exposed over 200 m, and varies from 1 to 10 m wide. Up to 15% of the rock consists of open space. Tourmaline is common as an accessory phase, as an alteration of adjacent wallrocks (tourmalinite), and as fragments in breccias.

Sheeted quartz veins containing scheelite and gold occur mainly at PUKELMAN (MINFILE 115P 013)(Fig. 4a), within and on the margins of the Pukelman Stock. Most veins are 0.5 to 1.5 cm thick, but some reach 7 cm, and contain up to 10% scheelite. Molybdenite and pyrite are accessory minerals. Minor quartz stockwork containing molybdo-scheelite and scheelite cut metasedimentary rocks at SCHEELITE DOME (MINFILE 115P 004).

Relatively "dry" sheeted veins at JABBERWOCK (MINFILE 115P 051) contain cassiterite with only minor orthoclase (Fig. 4b). Orthoclase is a common accessory mineral in breccias (SUNSHINE CREEK (MINFILE 115P 031), TEE (MINFILE 115P 008a), MAHTIN (MINFILE 115P 007) and sheeted veins (both cassiterite-bearing at JABBERWOCK (MINFILE 115P 051), and scheelite-bearing at PUKELMAN (MINFILE 115P 013).

Tourmaline-dominant crystalline-matrix breccias and veins

Tourmaline-dominant breccias occur at OLIVER CREEK (MINFILE 115P 030)(Fig. 5c) and JABBERWOCK (MINFILE 115P 051), and veins occur at ZETA (MINFILE 115P 047). Pyrrhotite, pyrite, chalcopyrite and cassiterite are commonly associated with the tourmaline, along with stibnite, stannite, arsenopyrite, jamesonite and boulangerite at ZETA (Abercrombie 1990). Tourmaline also occurs as a common accessory in the granitoid rocks. At ZETA, the granite core of the zoned syenite stock contains fist-sized, tourmaline-rich orbicules. At OLIVER CREEK, intergranular granite- and aplite-hosted tourmaline is of similar composition to that from early tourmaline breccias, indicating their genesis from magmatic solutions derived from the associated granite plug (Emond 1985).

Figure 5a. Rock flour breccia with some calcite (white) stockwork (and breccia), OLIVER CREEK. Fragments are mostly quartzite.

Tourmaline also occurs in sheeted veins in the Keno Hill Quartzite and in crosscutting rhyodacite dykes at JOUMBIRA (MINFILE 1O5M 031) on Mt. Haldane. On the "FED showing" needle aggregates of tourmaline occur in relatively "dry" joints of the quartzite (Fig. 4c). Nearby, on the "PRO" showing, thin tourmaline veins cut a heavily sericitized and locally tourmalinized dyke. Cassiterite and fluorite occur within the tourmaline veinlets, mostly along and parallel to the margin of the 2 m wide dyke. At OLIVER CREEK, tourmaline forms steeply-dipping, millimetre size veinlets in quartzite. The veinlets are spaced several centimetres apart.

Chlorite breccias and veins

Chlorite breccias and veins are confined to the OLIVER CREEK occurrence (Fig. 5d). The chlorite matrix locally contains sphalerite, chalcopyrite, pyrite, pyrrhotite and rare galena. Cassiterite and silver are common. Due to the fine grain size, the silver mineralogy is unknown. The chlorite is a dark green, iron-rich variety and occurs in both radiating aggregates and in equant habits. Accesssory minerals are up to 5 mm in diameter. Several periods of brecciation and chlorite and cassiterite crystallization are generally evident.

Summary of Petrography

Tin and tungsten occurrences in the McQuesten River region are subdivided into (1) skarns and (2) breccias and/or veins. Most skarns are tungsten-dominated, whereas most breccias and veins are tin-bearing.

The skarns are calcic and reduced, and show evidence of a three stage evolution: (1) isochemical contact metamorphism of limestone to form diopside, wollastonite, tremolite and grossular garnet; (2) metasomatic formation of hedenbergite, andradite, axinite and sulphides; and (3) retrograde hydrolysis and formation of actinolite, clinozoisite, epidote, chlorite, sulphides and calcite. Scheelite, cassiterite and most sulphides are associated with the retrograde stage.

Early rock flour breccias were followed by crystalline-matrix breccias and veins with the following mineral paragenesis: (1) quartz (± orthoclase, cassiterite or scheelite); (2) tourmaline (± cassiterite and iron-sulphides); (3) chlorite (± cassiterite, sulphides, epidote, muscovite, biotite); (4) calcite, topaz, fluorite; (5) limonite, manganese oxide, kaolinite. Stages 2 and 3 are similar to the second and third stages of skarn mineral formation and indicate a similar genesis.

GEOCHEMISTRY

During property investigations, representative rock samples including grab and chip samples were collected from mineral showings. Samples include mineralized wallrock, wallrock adjacent to veins, barren skarn and mineralized skarn. Bondar-Clegg & Co. Ltd of Vancouver carried out 33 element ICP analysis of more than 110 samples. Elements analysed include Au, Sb, As, Ba, Cd, Cs, Cr, Co, Eu, Hf, Ir, Fe, La, Mo, Ni, Rb, Sc, Se, Ag, Ta, Th, W, U, Yb, Zn, Cu, Pb, F, Bi, Li, Sn and Nb. Appendix 1 lists analyses for Sn, W, Ag, Au, Pb, Zn, Cu, As, Sb, Bi, and F only.

The main problems addressed by this study are: (1) What are the relationships between tin and tungsten? (2) What are the relationships between tin/tungsten and precious metals? (3) Is bismuth a pathfinder element for gold?

The following discussion considers veins and breccias separately from skarns, and examines variations in the elements tin, tungsten, gold, silver and bismuth. Geochemical variations are displayed on two types of diagrams: (1) two metal plots (XY plots) where all samples are plotted to see if there is a correlation between the two metals; and (2) frequency diagrams (histograms) where all samples are plotted to study the variation in content of one metal.

Tin-Tungsten Relationship

Figure 6 is a plot of tungsten versus tin. It shows that some rocks are exclusively tin-rich, while other rocks are exclusively tungsten-rich. A third group of tin-rich samples (enclosed by dashed line) shows a general increase in tungsten with increasing tin content, although most samples with significant amounts of tungsten contain no tin.

Figure 7 is a frequency diagram which shows tungsten variation in samples from tin exploration targets. The figure shows that over 80% of these samples contain less than 50 ppm W. However, significant tungsten occurs in veins at JOUMBIRA (MINFILE 105M 031) and ZETA (MINFILE 115P 047)(up to 3600 ppm), and in skarn at SNARK (MINFILE 115P 008b)(up to 3270 ppm).

Figure 8 is a frequency diagram which shows tin variation in samples from tungsten exploration targets. It shows that over 80% of these samples have less than 25 ppm Sn. Significant tin occurs in skarn at SCHEELITE DOME (MINFILE 115P 004)(920 ppm) and LUGDUSH (MINFILE 115P 009).

Figure 5b. Quartz-matrix breccia, SUNSHINE CREEK WEST (MINFILE 115P 031). Rounded mica schist fragments with comb-textured quartz matrix.

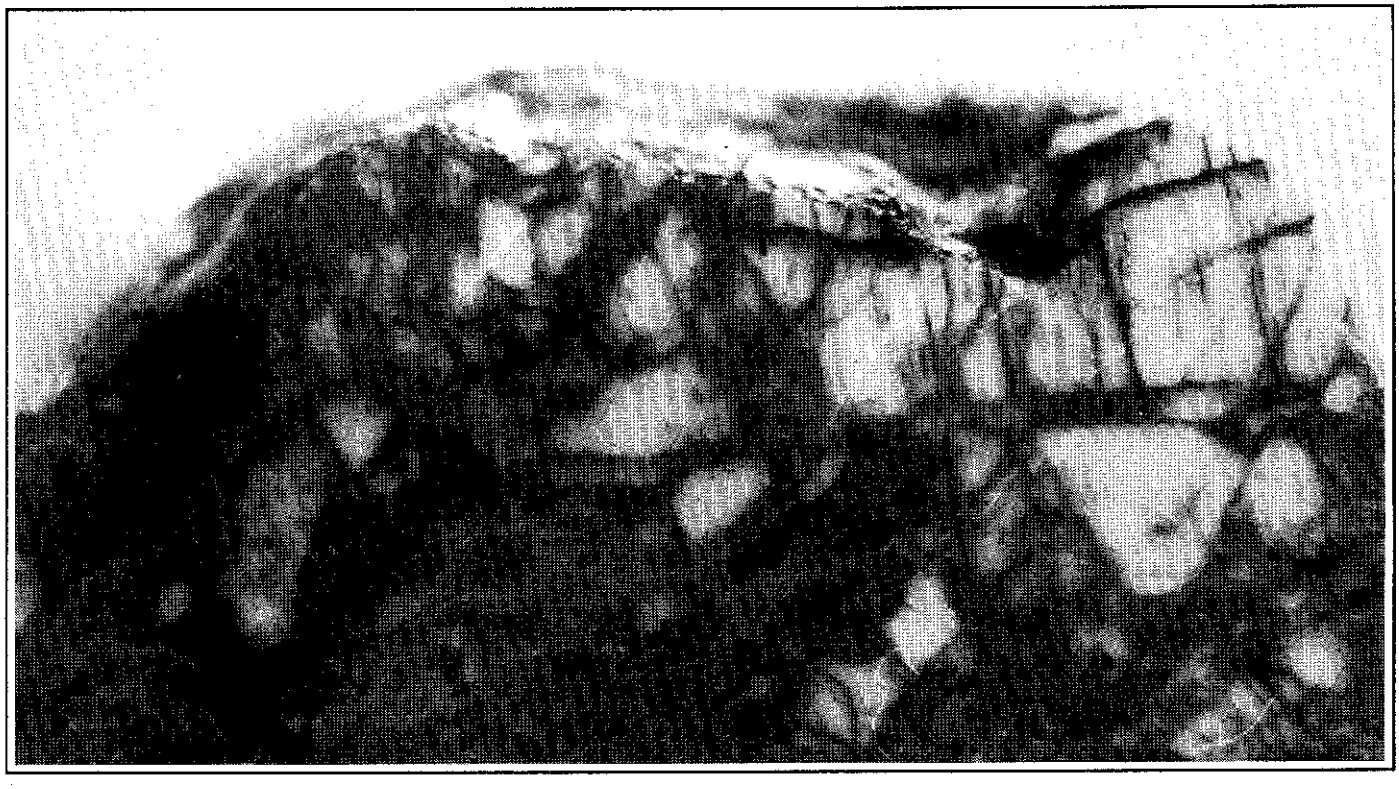

Figure 5c. Tourmaline-matrix breccia with quartz vein (white) and tourmaline vein (black) fragments, OLIVER CREEK (MINFILE 115P 030).

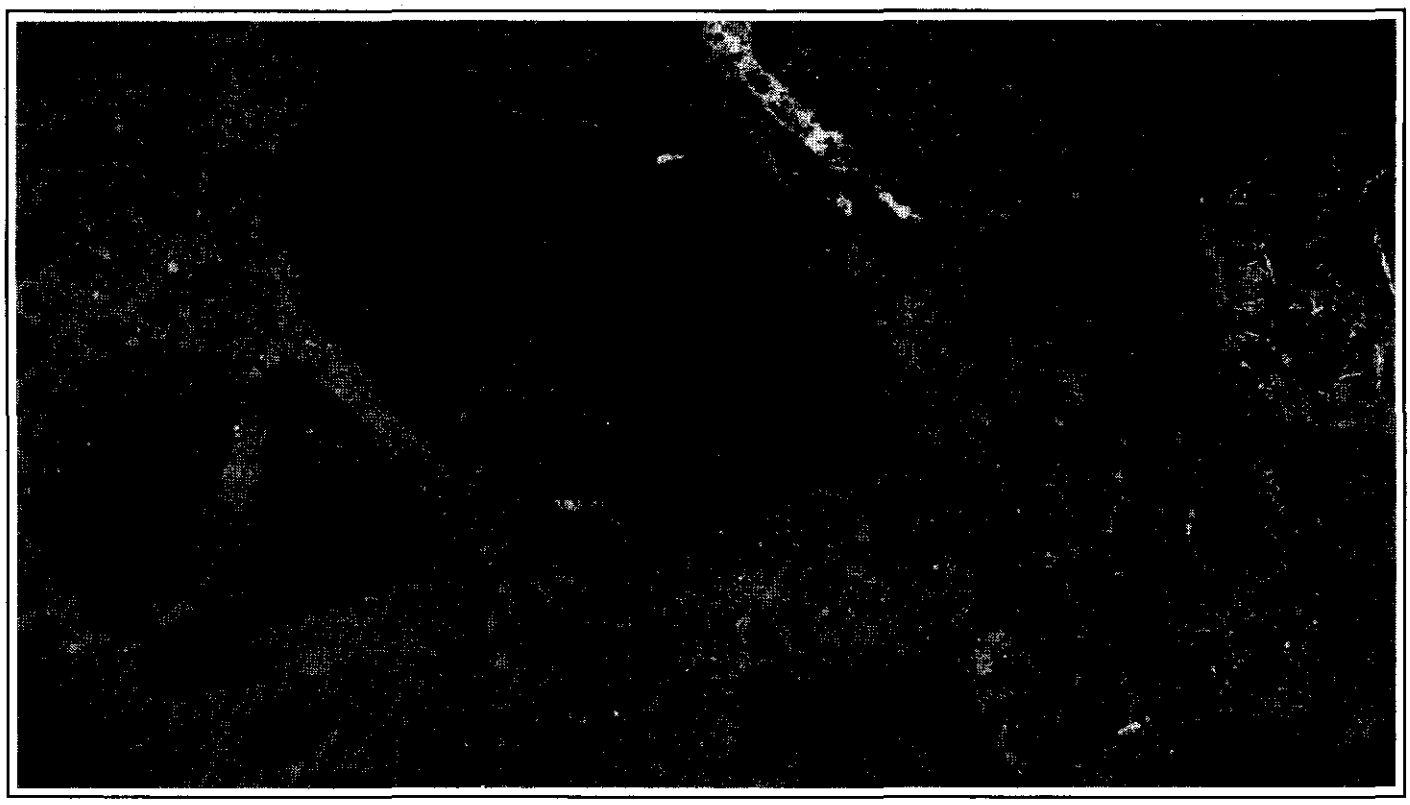

Figure 5d. Full view of thin section of chlorite-matrix breccia with quartzite (black) and chlorite vein (grey) fragments, OLIVER CREEK (MINFILE 115P 030).

Tin and Tungsten versus Precious Metals

a) Tin versus Silver

A plot of tin versus silver (Fig. 9) shows that most skarns contain no silver. A substantial group of number of mostly vein samples contain significant silver, but no correlation between tin and silver is evident. A gap in this random distribution exists: samples with less than 50 ppm tin contain little to no silver. Rocks containing over 50 ppm tin are more likely to contain some silver.

Figure 10 is a frequency diagram showing silver variation. Two groupings are evident in the data and represent: (i) tin exploration targets, and (ii) tungsten exploration targets. Almost 80% of the samples contain less than 5 ppm Ag. Also, almost all samples containing appreciable silver are from tin exploration targets. Samples from tungsten properties contain no silver. Properties containing significant silver include tin veins at ZETA (MINFILE 115P 047) up to 1060 ppm), TEE (MINFILE 115P 008a)(500 ppm), SUNSHINE CREEK (MINFILE 115P 031) and OLIVER CREEK (MINFILE 115P 030)(30 ppm); and some silver is contained in the tin skarn at SNARK (MINFILE 115P 008b).

b) Tin versus Gold

The plot of tin versus gold (Fig. 11) shows that most skarns contain gold. However, there is no direct relationship between the amount of tin and the amount of gold. Some tin-mineralized rock is gold-bearing and some is not.

c) Tungsten versus Gold

The plot of tungsten and gold (Fig. 12) also shows that most skarns contain gold. Many of the veins (mostly the tin-bearing type) contain no gold. The diagram shows a random distribution indicating that tungsten has no direct correlation with gold.

d) Gold Variation

The gold frequency diagram (Fig. 13) divides samples into: (1) tin exploration targets, and (2) tungsten exploration targets. More than 35% of the samples contain significant gold (>25 ppb). Gold is important in the WAYNE gold-tungsten occurrence (MINFILE 105M 029)(up to 22 700 ppb), the SCHEELITE DOME (MINFILE 115P 004) and TEE (115P 008a) tungsten skarns (2080 ppb), and in the PUKELMAN (MINFILE 115P 013) tungsten sheeted veins (7630 ppb). Gold is also important and was previously unrecognized in tin (-tungsten) skarn at SNARK (115P 008b)(3670 ppb), TEE, and MAHTIN (MINFILE 115P 007); and in tin-bearing veins at TEE (940 ppb). To stress the significance of these gold values: three 5m chip samples (15 m total width) across the SNARK tin-tungsten skarn assayed 2227 ppb Au (0.065 oz/t) along with 1210 ppm W and 951 pp Sn.

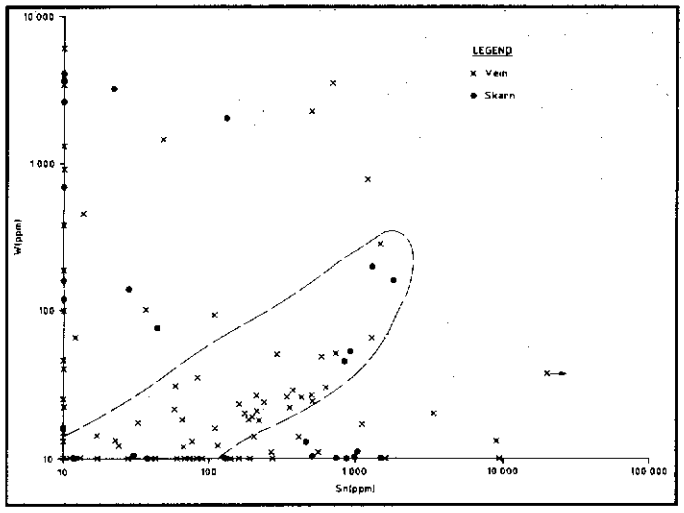

Figure 6. Graph of tungsten against tin.

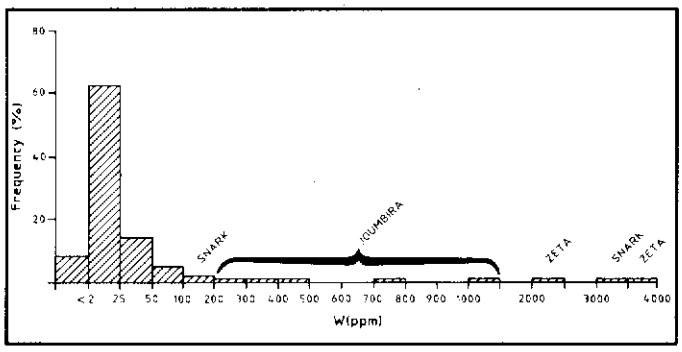

Figure 7. Frequency diagram of tungsten variation in samples from tin exploration targets.

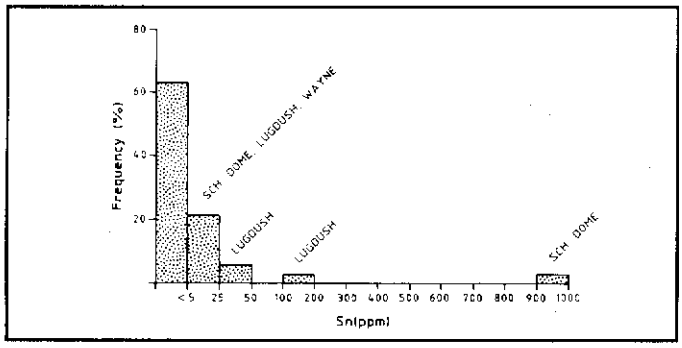

Figure 8. Frequency diagram of tin variation in samples from tungsten exploration targets.

e) Gold versus Bismuth

The plot of gold versus bismuth (Fig. 14) demonstrates that most gold-bearing skarns contain bismuth, and that there is a strong positive correlation between gold and bismuth. Many veins also contain bismuth, but no positive correlation between gold and bismuth is evident.

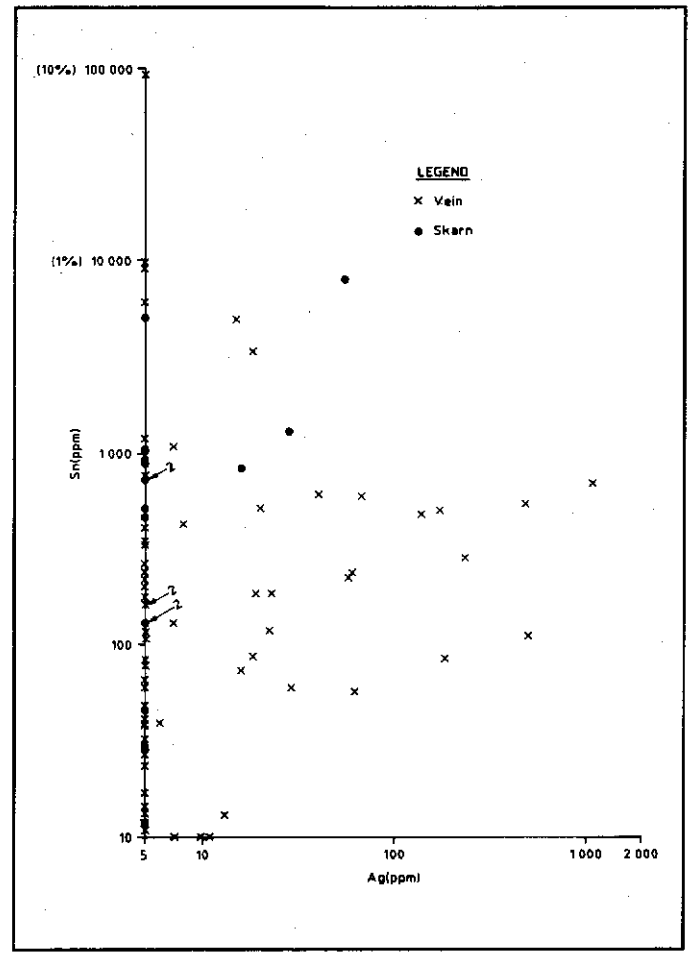

Figure 9. Graph of tin versus silver.

The frequency diagram for bismuth (Fig. 15) shows that over 70% of the samples contain less than 10 ppm Bi, and over 25% contain anomalous bismuth (up to 450 ppm at WAYNE (MINFILE 105M 029), and 264 ppm at SUNSHINE CREEK (MINFILE 115P 031)). The strong correlation indicated by the gold-bismuth plot (Fig. 14) suggests that skarns containing anomalous bismuth have a good gold potential. Most of the skarns contain high gold, except LUGDUSH (MINFILE 115P 009)(208 ppm Bi) which had only slightly anomalous values. The bismuth values at LUGDUSH suggest that the gold potential of this property should be re-evaluated.

Summary of Geochemical Results

(1) There is a positive correlation between tungsten and tin in some tin-bearing samples. Tungsten is evident in the ZETA (MINFILE 115P 047) and JOUMBIRA (MINFILE 1O5M 031) tin veins, and at the SNARK (MINFILE 115P 008b) tin (-tungsten) skarn properties. There is some tin at the SCHEELITE DOME (MINFILE 115P 004) and LUGDUSH (MINFILE 115P 009) tungsten skarn properties.

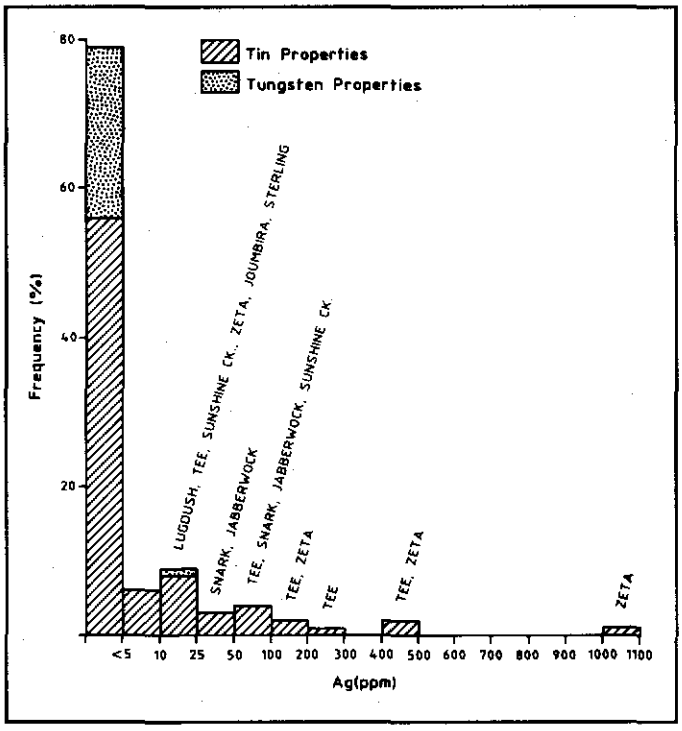

Figure 10. Frequency diagram of silver variation in samples from tin exploration targets and tungsten exploration targets.

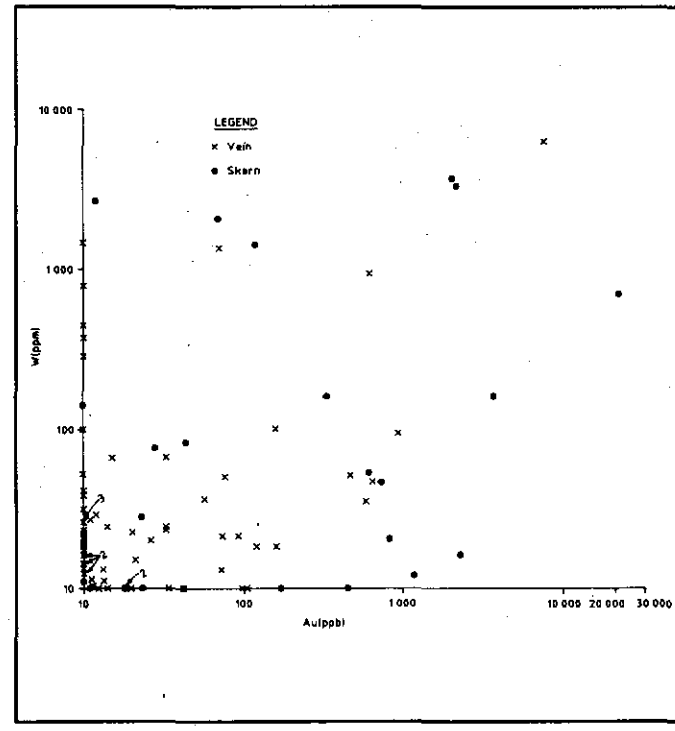

Figure 12. Graph of tungsten versus gold.

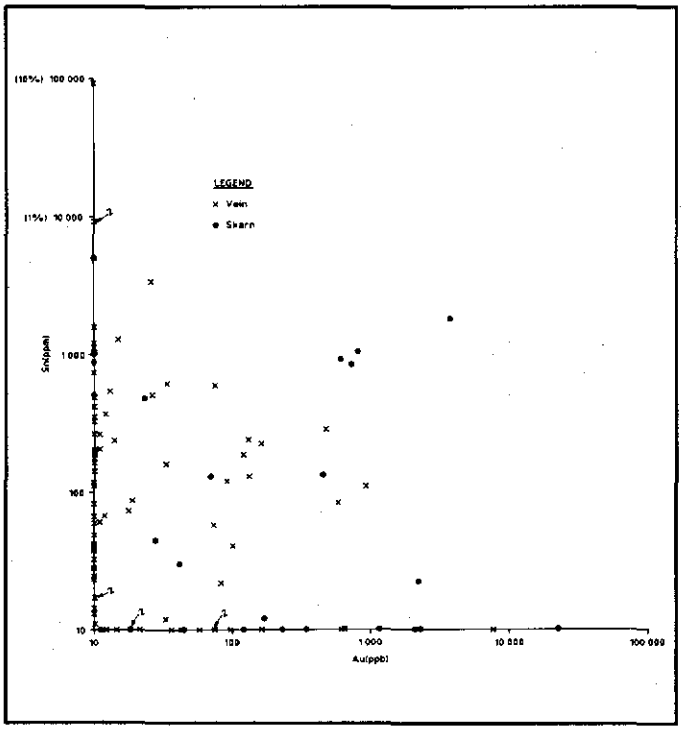

Figure 11. Graph of tin versus gold.

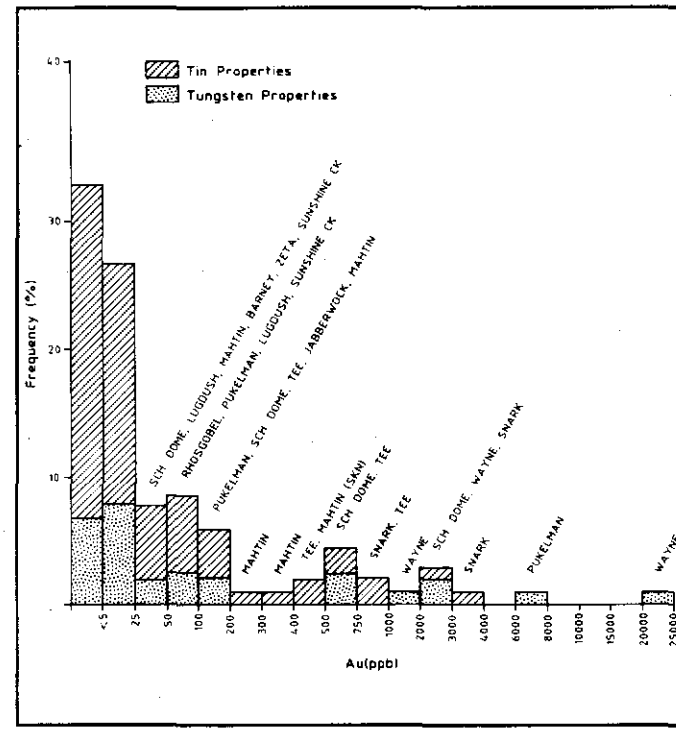

Figure 13. Frequency diagram of gold variation in samples from tin exploration targets and tungsten exploration targets.

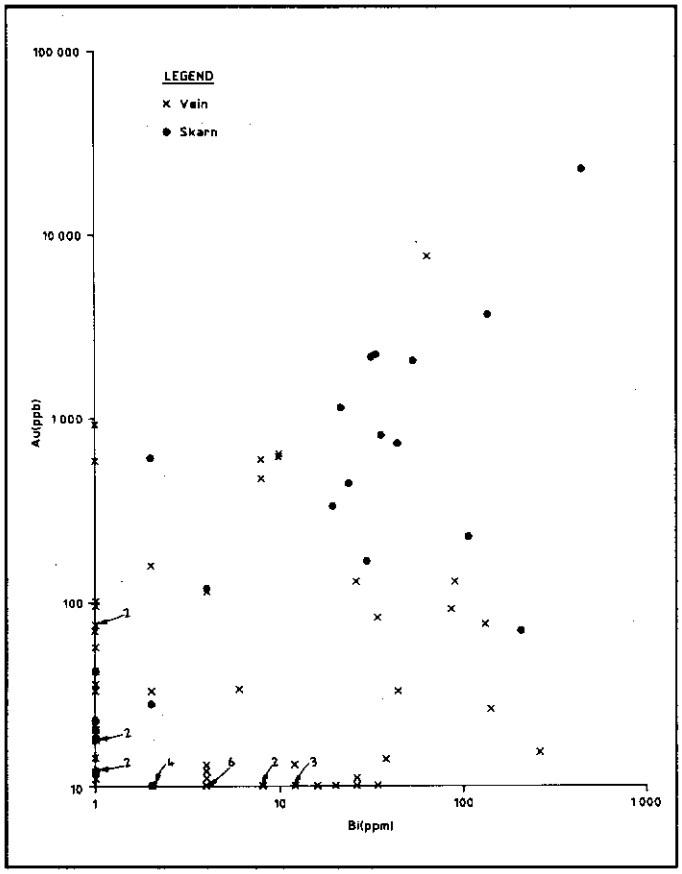

Figure 14. Graph of bismuth versus gold.

(2) Silver correlates with tin in veins containing more than 50 ppm Sn. Silver is important in the ZETA (MINFILE 115P 047), TEE (MINFILE 115P 008a), OLIVER CREEK (MINFILE 115P 030) and SUNSHINE CREEK (MINFILE 115P 031) tin veins and breccias, and in the SNARK (MINFILE 115P 008b) and OLIVER CREEK tin skarns. Other known tin showings probably also have silver potential, and in fact a silver-lead vein (the QUEST showing) was recently discovered by Silverquest Resources Ltd near the SNARK, BOULDER CREEK (MINFILE 115P 048) and TEE occurrences following the release of assessment reports on these properties.

(3) This study demonstrates that the McQuesten River area has gold as well as tin-tungsten potential. Most skarns and several veins contain appreciable gold, although no direct correlation exists between gold and either tin or tungsten. Significant gold values were previously known at the SCHEELITE DOME (MINFILE 115P 004) and WAYNE (MINFILE 105M 029) tungsten skarns. Gold also occurs in significant quantities in the SNARK (MINFILE 115P 008b), TEE (MINFILE 115P 008a) and MAHTIN (MINFILE 115P 007) skarns and in the TEE and PUKELMAN (MINFILE 115P 013) veins where it was previously unknown. Further discoveries may be expected. Recently a new gold-bearing vein, the RUM showing, was found by Goldrite Mining Corp.

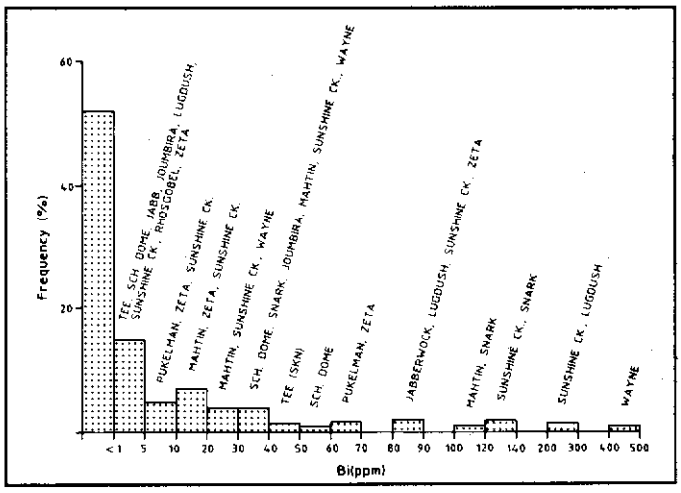

Figure 15. Frequency diagram of bismuth variation in all samples.

on the JOSEPHINE (MINFILE 115P 011) property, presently under option to Noranda Exploration Co. Ltd.

(4) Skarns show a strong positive correlation between gold and bismuth, demonstrating that bismuth can be used as a gold pathfinder. The LUGDUSH tungsten skarn (MINFILE 115P 009) contains significant bismuth and should be reexamined for gold.

CONCLUSIONS

Skarns, breccias, veins and sheeted vein systems of similar chemical composition form elongated belts in many tin-tungsten districts. Kwak (1987) explained: "Where carbonate is absent, other styles of similar mineralization such as vein systems may be interspersed between skarn deposits." The associated granitoids show a similar specialization pattern worldwide: W (-Mo-Cu) skarns containing little or no tin are commonly related to calcic magnetite-bearing granitic plutons (similar to RHOSGOBEL, (MINFILE 115P 012)), while Sn (W-F-Be-Li) skarns are typically related to low Ca, high Si & K, ilmenite-bearing plutons (LUGDUSH (MINFILE 115P 009), SCHEELITE DOME (115P 048), SNARK (MINFILE 115P 008B), BOULDER CREEK (MINFILE 115P 048), OLIVER CREEK (MINFILE 115P 030)(Kwak 1987).

Several conclusions from this study have implications for mineral exploration: (a) several tin and tungsten showings are open for staking; (b) several tin properties should be re-evaluated for tungsten potential and vice versa; (c) silver is expected in tin-bearing veins and skarn; (d) gold is important in most skarns and some veins, and was previously unrecognized at some of these properties; and (e) bismuth can be used as a pathfinder for gold in skarn and has defined several gold targets which were previously recognized only for tungsten, and (f) granitoid specialization defines the expected deposit type.

ACKNOWLEDGMENTS

Much appreciation goes to J.A. Morin who suggested the project, advised the author, provided advice on presentation of the geochemistry, and technically reviewed the paper. Thanks are extended to J.G. Abbott for his constructive comments, and to S.R. Morision for his encouragement. High quality drafting was provided by Drafting Services, Northern Affairs Program.

REFERENCES

ABERCROMBIE, S. M. 1990. Petrology, geochronometry and economic geology: The Zeta tin-silver prospect, Arsenic Ridge, west-central Yukon (115 P 14 and 116 A 3). Unpublished M.Sc. Thesis, University of British Columbia, Vancouver, B.C.

ANDERSON, R.G., 1988. An overview of some Mesozoic and Tertiary plutonic suites and their associated mineralization in the northern Canadian Cordillera. In: Recent Advances in the Geology of Granite Related Mineral Deposits, R.P. Taylor and D.F. Strong (eds); Canadian Institute of Mining and Metallurgy, Special Volume 39, p. 96-113.

BOSTOCK, H.S., 1946. Geology, Mayo area, Yukon Territory. Geological Survey of Canada, Map 890a.

BOSTOCK, H.S., 1964b. Geology, McQuesten River, Yukon Territory. Geological Survey of Canada, Map 1143A.

BOYLE, R.W., 1965. Geology, geochemistry and origin of the lead-zinc-silver deposits of the Keno Hill - Galena Hill area, Yukon Territory. Geological Survey of Canada, Bulletin 111, 302 p.

EINAUDI, M.T., MEINERT, L.D. and NEWBERRY, R.J., 1981. Skarn deposits. In: Seventy-Fifth Anniversary Volume, B.J. Skinner, (ed.); Economic Geology, p. 317-391.

EMOND, D.S., 1985. Geology, mineralogy and petrogenesis of tin-bearing breccia/veins at Oliver Creek, McQuesten River Area, Yukon. Unpublished M.Sc. thesis, Carleton University, Ottawa.

EMOND, D.S., 1986. Tin and tungsten veins and skarns in the McQuesten River area, central Yukon. In: Yukon Geology, Vol. 1.; Exploration and Geological Services Division, Yukon, Indian and Northern Affairs Canada, p. 113-118.

EMOND, D.S., 1992. Petrology and geochemistry of tin and tungsten mineralized plutons, McQuesten River region, Central Yukon. This volume.

GORDEY, S.P., 1988. The South Fork volcanics: mid-Cretaceous caldera fill tuffs in east-central Yukon. In: Current Research, Part E; Geological Survey of Canada, Paper 88-1E, p. 13-18.

HUNT, P.A. and RODDICK, J.C., 1987. A compilation of K-Ar ages, Report 17. In: Radiogenic Age and Isotopic Studies: Report 1; Geological Survey of Canada, Paper 87-2, p. 188.

KWAK, T.A.P., 1987. W-Sn Skarn Deposits and Related Metamorphic Skarns and Granitoids. Elsevier Scientific Publishers B.V., 451 p.

LENNAN, W.B., 1986. Ray Gulch tungsten skarn deposit. In: Mineral Deposits of Northern Cordillera, J.A. Morin (ed.); CIM Special Volume 37, p. 245-254.

NEWBERRY, R.J., 1980. The geochemistry of tungsten deposition in skarn deposits: a field and theoretical approach. Geological Society of America, Abstracts with Programs, Vol. 12, p. 492.

POTTER, T., 1987. Petrography of tin and tungsten occurrences and an electron microprobe mineralogical study of tourmaline from the McQuesten River area, Yukon Territory. Unpublished B.Sc. Research Paper, University of Alberta, Edmonton, Alberta.

STEVENS, R.P., LACHANCE, G.R. and DELABIO, R.N., 1982. Age determinations and geological studies. K-Ar isotopic ages, Report 16; Geological Survey of Canada, Paper 82-2, 56 p.

WATSON, K.W., 1986. Silver-lead-zinc deposits of the Keno Hill-Galena Hill area, central Yukon. In: Yukon Geology, Vol. 1; Exploration and Geological Services Division, Yukon, Indian and Northern Affairs Canada, p. 83-88.

WOODSWORTH, G.J., ANDERSON, R.G., BROOKFIELD, A. and TERCIER, P., 1989. Distribution of Proterozoic to Miocene plutonic suites in the Canadian Cordillera. Geological Survey of Canada, Open File 1982, 6 maps.

ABBREVIATIONS USED IN TABLES

GRAN	granite	GT	garnet
GRDI	granodiorite	HB	hornblende
QZIT	quartzite	ID	idocrase
QZMZ	quartz monzonite	JAM	jamesonite
PP	porphyry	LI	limonite
RHY	rhyolite	KA	kaolinite
RYOD	rhyodacite	KSP	K feldspar
SYEN	syenite	MN	manganese oxide
VN	vein	MO	molybdenite
VNQZ	vein quartz	MO-SCH	molybdoscheelite
AC	actinolite	MU	muscovite
ASP	arsenopyrite	OR	orthoclase
AX	axinite	PH	phlogopite
BI	biotite	PL	plagioclase
BOUL	boulangerite	PR	pyrrhotite
CB	carbonate	PY	pyrite
CC	calcite	QZ	quartz
CL	chlorite	RKFL	rock flour
CO,COR	corundum	SCH	scheelite
CP	chalcopyrite	SER	sericite
CT	cassiterite	SL	sphalerite
DI	diopside	STAN	stannite
EP	epidote	SX	sulphide minerals
FL	fluorite	TO	tourmaline
FS	feldspar	TOP	topaz
GL	galena	TR	tremolite
GOE	goethite	WO	wollastonite

Table 1. Skarn occurrences, including skarn from vein properties (location map in Fig. 1).

Property Name Minfile No. Location	Host Rock	Associated Pluton	Mineral Assemblages (stages)	Best Assay This Study (earlier)
Tungsten Skarns:				
LUGDUSH 115P 009 A	Hyland Gp (Grit Unit)	BI-MU GRAN Stock (mega-crystic PP)	DI-PL-OR-CO-QZ-CC-HB-PR-HB-SC	Best grab: 2050 ppm W, 8000 ppm Zn (800 X 150-200 m area, 0.1% WO_3; highest grab 2.18% WO_3)
SCHEELITE DOME 115P 004 H	Hyland Gp	HB-BI GRAN stock (PP)	WO-DI-CC-QZ-OR-PL(+/-GT) DI-AC-TR-QZ-CC-OR-BI-SC	4m Chip: 3620 ppm W, 2080 ppb Au (6.67 g/t Au over 3 m; 4800 ppm W over 1.5 m)
RHOSGOBEL 115P 012 L	Hyland Gp	BI-HB QZMZ Stock (PP)	QZ-DI-AC-PL-BI-SC QZ-DI-OR-WO-BI-SC	Best grab: 2630 ppm W
WAYNE 105M 029 (5 km E of Mt Haldane) P	Keno Hill Quartzite	MU-BI RHY? Dyke (PP)	DI-AC-CC-QZ-SC TR-CC-QZ-DI	Drill core: 22 700 ppb Au 696 ppm W 450 ppm Bi
Tin Skarns:				
TEE 115P 008a B	Hyland Gp	HB-BI GRDI Stock	AC-QZ-PR-CP-PY-AX	Grab: 845 ppm Sn 740 ppb Au 2.38% Zn 0.22% Cu 16 ppm Ag
SNARK 115P 008b C	Hyland Gp	MU-BI RYOD Dyke	AC-QZ-EP-AX-GL-PR-CP-SL-PY-SCH	Avg 3 grab over 15 m: 2227 ppb Au 28 ppm Ag 1210 ppm W 951 ppm Sn 5553 ppm Cu 3740 ppm Zn
BOULDER CREEK 115P 048 D	Hyland Gp	BI-MU GRAN Stock	AX-CC-AC-ID-GT-PL-EP-QZ	Avg 5 chip over 25 m exposure, 10-15 m thick: 1036 ppm Sn
OLIVER CREEK 115P 030 G	Hyland Gp	BI-MU GRAN	AC-CL-CC-DI-QZ-EP-PR-PY-SCH-CT	Drill core: 0.9% Sn, 4 ppm Ag over 1.7 m

Skarn from Vein Properties

MAHTIN **115P 007** **J**	Hyland Gp	BI-HB QZMZ	DI-CC-GT-QZ	Grab from
		Stock		10 X 4 m unit: 450 ppb Au 130 ppm Sn
			DI-TR-QZ-CC- -AS-PR-CP	Grab of float: 340 ppb Au 160 ppm W 870 ppm Cu 531 ppm As
SUNSHINE CREEK EAST **115P 031a** **F**	Hyland Gp	BI-MU GRAN	DI-TR-BI-QZ- OR-SCAP	low metal values

Table 2. Mineralogy of tin and tungsten skarns, McQuesten River region.

Mineral	Abundance	Size (mm)	Color	Habit	Diagnostic	Association	Other
ISOCHEMICAL STAGE							
Diopside	25-40%	0.1-2	Pale brown to green	Anhedral aggregates	Cleavages at 90°, moderate birefringence	Replaced by clinozoisite and actinolite	Most common isochemical mineral in both Sn & W skarns
Grossularite	10-60%	0.5-2	Light brown	Dodecahedral, often subhedral	Isotropic or anomalous isotropic extinction	Occurs with axinite, idocrase & diopside in Sn skarns. Replaced by calcite & epidote.	Often zoned
Wollastonite	30-60%	0.1-0.25	Colorless	Fibrous, radiating radiating	Fibrous habit, low birefringence	Occurs with quartz, fsp & diopside	More common in W skarns
Tremolite	20-30%	0.1-1.0	Colorless	Prismatic to anhedral	120° cleavages	Occurs with diopside	Found in W & Au-bearing skarns
Quartz	10-40%	0.1-1.5	Colorless	Anhedral, often strained	Low birefringence & relief	Forms interlocking mosaic with orthoclase	Found in almost all skarn assemblages; more where no metasomatic minerals have been introduced
Orthoclase	5-15%	0.1-0.5	Colorless	Anhedral	Lack of twinning, biaxial	Found with quartz	Common in Sn & W skarn assemblages
Calcite	5-20%	3.0 (approx.)	Colorless	Elongate prisms	Growth twinning, high interference colours	Occurs with axinite, garnet, idocrase	Occurs in Sn skarns in this stage.
Corundum	20-30%	0.1-0.3	Colorless	Granular	Low birefringence, uniaxial negative, sometimes biax., high relief	Associated with diopside, quartz & calcite in a W-bearing skarn	Rare. Only found in one thin section from Lugdush.
METASOMATIC STAGE							
Scapolite	5-15%	0.1-0.3	Colorless, with a mottled appearance	Anhedral aggregates	Low birefringence, uniaxial negative	Occurs with biotite and diopside	Rare. Found in only one section from Sunshine Creek
Axinite	30-40%	1-4	Colorless to light brown	Euhedral, wedge-shaped	"Axe-head" shape, low birefringence	Occurs with garnet & idocrase. Replaced by actinolite & epidote	Sn-skarns only
Idocrase	5-30%	1-2	Light brown	Equidimensional, sub-anhedral	Blue anomalous interference colours, high relief	Occurs with axinite & garnet in Sn skarns	Sometimes difficult to distinguish from garnet
Andradite	10-60%	0.5-2	Light brown	Dodecahedral, sub to anhedral	Isotropic or anomalous isotropic extinction	Occurs with axinite, idocrase, diopside in tin skarns	Commonly zoned; unable to distinguish from andradite, but assumed both the Al & Fe-rich varieties may exist
Pyrite	1-2%	0.5-4	Light yellow	Anhedral, disseminated flakes	Isotropic	Assoc. with clinozoisite, diopside, wollastonite, & other	Uncommon, minor in Sn & W skarns
Pyrrhotite	< 5%	0.5-1.5	Creamy brown	Anhedral disseminated	Strongly anisotropic	Assoc. with other sulphides	Most common sulphide mineral in skarns
Chalcopyrite	1-2%	0.5-1	Brassy yellow	Anhedral disseminated	Tarnish, weakly anisotropic	Assoc. with other sulphides	Not common
Sphalerite	< 3%	0.1-1	Gray	Anhedral aggregates	Isotropic	Assoc. with other sulphides	Not common
Galena	< 3%	1-3	White to light grey	Anhedral, diss. & veinlets	Isotropic	Assoc. with other sulphides	Not common

Mineral	Abundance	Size (mm)	Color	Habit	Diagnostic	Association	Other
RETROGRADE STAGE							
Actinolite	up to 65%	0.1-1	Light green	Acicular, fibrous aggregates	Green colour, habit, pleochroic	Replaces diopside, axinite	Very common in Sn & W skarns
Clinozoisite	5-20%	0.1-1	Colorless to light brown to light green	Anhedral masses	Anomalous blue interference colours	Replaces diopside, forms haloes around sulphides	Quite common, especially at at the Wayne occurrence
Epidote	5-40%	0.1-0.5	Pale green, moderately pleochroic	Anhedral aggregates, stubby prismatic	Green color, high relief, moderate birefringence	Replaces garnet & axinite, & associated with sulphides	Quite common
Calcite	5-10%	0.5-2	Colorless	Anhedral	High birefringence	Replaces garnet, wollastonite axinite, idocrase, diopside	Very common
Phlogopite	up to 30%	0.2-0.6	Colorless	Radiating bundles deformed	Very high birefringence	Occurs with calcite	Rare-seen in Sn skarn assemblage
Hornblende	2-5%	0.1-0.5	Pleochroic in shades of green	Anhedral-subhedral, prismatic	120° cleavage, green colour	Replaces diopside where actinolite is absent	Not common in Sn & W skarns
Biotite	5-35%	0.1-1	Pleochroic in shades of brown	Platy	Brown-green colour, perfect cleavages	Associated with sulphides & scheelite	Occurs in skarns in contact with biotite hornfels.
Scheelite	1-3%	0.2-2	Sugary-brown	Anhedral disseminated grains	Grainy appearance, high relief	Occurs with diopside/actinolite, sulphides & biotite	Found in W skarns

Table 3. Breccia and/or Vein Occurrences (for location map, see Fig. 2).

Property Name Minfile No. Location	Host Rock	Associated Pluton	Matrix-Gangue Minerals (% Matrix)	Fragments	Best Assay This Study (earlier)
Tin-Silver Breccias:					
TEE 115P 008a B	Hyland Gp	HB-BI GRDI Stock	QZ-OR (50-70%) 10% open sp. <3% CT	angular to subrounded, 1-5 mm QZIT, mod-poor sorting	0.1 to 1.5 m wide zone, over 150 m long, avg six grabs from six trenches 300 ppb Au, 139 ppm Ag, 1724 ppm Pb, 1485 ppm Zn, 105 ppm Sn, 167 ppm Cu
SUNSHINE CREEK WEST 115P 031a E	Hyland Gp	BI-MU GRAN Stock	QZ-OR-TO (50-70%) CT <15% open spaces	subangular to subrounded < 5 cm QZIT mod-poor sorting	1-10 m wide, 200 m long, avg 10 grabs at 20 m intervals along length: 308.5 ppm Sn, 877 ppm Pb, 263 ppm Cu, 1740 ppm As Other grab: 67 ppm Ag; Other grab:120 ppb Au, 600 ppm Sn, 900 ppm Pb; (Cominco drill int: 7.6 m 0.28% Sn)
SUNSHINE CREEK EAST 115P 031b F	Hyland Gp	Bi-MU GRAN Stock, RHYOD Dyke	QZ-TO-OR <1% CT (20-50%) No open space	angular to subangular <2 cm QZIT, TO, VNQZ mod-poor sorting	1 to 5 m wide, 10 m long, avg 2 grab sam: 2350 ppm Sn, 23 ppm Ag
OLIVER CREEK 115P 030 G	Hyland Gp	BI-MU GRAN	Rock Flour (10-30%); Crystalline: CL; TO; QZ; CC; MU; BI; KA (20-50%) <5% CT SL,CP,PY,PR,GL	angular to subrounded 1-4 cm QZIT, SCH, VN mat, mod-poor sorting	(Drill core: Over 3.7 m 0.94% Sn & 11.83 g/t Ag; Over 0.95 m 2.45% Sn & 2.1 g/t Ag - Billiton Canada)
MAHTIN 115P 007 J	QZMZ, Hyland Gp	HB-BI QZMZ	TO-ASP-PY; QZ-OR-SER-Rock Flour; QZ-CC-TO-SER- ASP-PY-STIB- CP veinlets	angular to subrounded, < 3 cm QZMZ, mod sorting	1 X 15 m zone: Best grab 7 ppm Ag, 1650 ppm Cu, 130 ppm Sn, 130 ppb Au, 299 ppm Sb; < 100 ppm Ag - (Best grab - < 100 ppm Ag: Billiton Metals Canada)

Table 3 (continued)

Property Name Minfile No. Location	Host Rock	Associated Pluton	Matrix-Gangue Minerals (% Matrix)	Fragments	Best Assay This Study (earlier)
Tin-Silver Veins, Sheeted Veins					
JOUMBIRA **115M 031** **I**	Keno Hill Quartzite	BI-QZ RYOD (PP), BI-MU GRAN	TO-CT-FL, QZ-MU, QZ-TO-MU-SL-PY-ASP QZ-SL-PY-GL	Sheeted veins in joints Vein	PRO showing: Grab 1200 ppm Sn & 798 ppm W; FED showing: Grab 740 ppm Sn & 1460 ppm W; Fortune Ck showing: Grab 10 000 ppm Zn, 1500 ppm Sn 283 ppm W, 15 ppm Ag
JABBERWOCK **115P 051** **K**	Hyland Gp	BI-HB RYOD (PP)	OR-QZ-CT	Sheeted veins in joints	Avg 2 grab samples 9450 ppm Sn
ZETA **115P 047** **N**	Syenite	HB-BI SYEN, QZMZ, GRAN	TO-MU-ASP-PY-JAM-BOUL-CT-STAN	Greisen vein	(<1 km long zone, 150 m str. length, 50 m depth, 2 m avg width; Shallow - 103-137 g/t Ag; Deeper - 686-1234 g/t Ag; Avg Sn throughout - 0.1% with up to 0.6% Sn locally (Noranda) Recent drill indicated silver reserves: 98 248 tonnes of 557.8 g/t Ag - Danra Resources)
Tungsten-gold Sheeted Veins					
PUKELMAN **115P 013** **M**	Hyland Gp, QZMZ	BI-HB QZMZ	QZ-OR-SCH QZ-ASP-GL	Sheeted veins in joints	Grab 7630 ppb Au, 6100 ppm W (200 x 200 m zone outlined) - 9 samples avg 0.05% WO_3 (Cathro); Grab of QZ-SX vein in HNFLS 19.3 g/t Au, 227.6 g/t Ag, 4.48% Pb)(Bema)

Abbreviations: see Appendix 2

Appendix 1. Hand sample description and geochemical analyses of mineralized rock.

Sample No.	Sn	W	Ag	Au	Pb	Zn	Cu	As	Sb	Bi	F	Description
BOULDER CREEK (MINFILE 115P 048)												
E-85-01	1050	11	<5	8	69	510	7	5	1.6	<1	510	Ophicalcite: CC-PH-CL-OR (-AX-QZ) skarn
-02	746	<2	<5	<5	35	<200	3	5	1.7	<1	470	GT-CC-AC-AX-SCH skarn
-03	1500	5	<5	<5	18	320	2	6	3.3	<1	580	AX-GT-EP-CC (-QZ-AC-PL-SCH) skarn
-04	1000	3	<5	<5	20	290	2	5	5.5	<1	490	ID-GT-CC-EP-AC-QZ-AX skarn
-05	885	<2	<5	<5	26	440	2	6	1.3	<1	420	AX-CC-AC-ID-GT-PL skarn
-06	68	4	<5	12	39	<200	42	132	7.0	<1	970	QZ stockwork and breccia
-200	510	4	<5	<6	32	250	4	84	44.4	<1	400	Garnetite: 60% GT, 25% DI, 10% AX, CC, AC
TEE (MINFILE 115P 008a)												
E-85-07	845	46	16	740	32	23,800	2200	15	0.9	44	550	QZ-OR-AC-ID-CC-DI (-TOP-GL-PR-PY-SL-CP-AX)
-08	40	5	<5	100	1770	6700	89	962	29.7	<1	530	QZ breccia and stockwork
-09	285	50	230	470	2.50%	4600	390	2910	133.0	8	650	QZ breccia and stockwork cutting skarn
-10	10	3	11	8	680	3400	196	117	6.3	4	430	QZ breccia with SER
-11	485	13	<5	23	150	4300	300	97	2.3	<1	760	QZ-OR-EP-AC (-SL-PY) skarn
-12	220	18	57	160	3500	3000	490	6370	56.9	8	580	QZ-OR (-CT) breccia
-13	73	3	16	18	280	3100	145	325	10.0	<1	240	QZ-OR (-CT) breccia
-14	84	35	180	593	4600	1300	87	1740	89.5	<1	340	QZ-OR (-CT) breccia
-15	110	94	500	942	420	210	164	1760	55.3	<1	430	QZ-OR (-CT) breccia
-16	57	21	63	73	82	<200	22	296	11.0	<1	870	QZ-OR (-CT) breccia
-17	<5	<2	<5	9	78	<200	6	16	1.2	<1	130	QZ-OR-WOL-EP-SER(-SX) skarn
-18	86	6	18	19	1460	1100	92	145	20.2	<1	470	QZ-OR (-CT) breccia
SNARK (MINFILE 115P 008b)												
E-85-19	1800	160	55	3670	20	4000	6900	1130	8.9	136	350	AC-ID-QZ-EP (-SCH-PY-AX-GT-CC) skarn
-20	1030	200	28	821	14	7000	9200	6840	4.9	36	330	EP-AC-CC-QZ-ID (-SCH-PY-PR-CP-SL-AX) skarn
-21	22	3270	<5	2190	18	220	560	23	5.3	116	220	EP-CC-AC-GT (-SCH-AX) skarn
SCHEELITE DOME (MINFILE 115P 004)												
E-85-22	920	53	<5	613	10	5900	1680	836	2.4	32	340	DI-CC-QZ-OR-AC (-PR-SCH) skarn
-23	12	67	<5	33	30	<200	38	40	1.1	2	550	QZ-KSP-PR-TO-MU greisen vein
-24	9	3620	<5	2080	16	330	176	9	5.2	54	210	DI-CC-QZ-CL-AC-SCH-PR-CP-GL (-PY) skarn
-25	<5	81	<5	44	46	<200	16	50	5.0	<1	350	DI-WOL-QZ-CC (-PY) skarn
-26	<5	28	<5	22	72	220	49	52	1.2	<1	240	WOL-DI-QZ-OR-CC-PL (-PR-PY-SCH) skarn
-27	<5	22	<5	20	152	<200	22	74	11.0	<1	24	QZ-CC (-SCH) stockwork
E-85-28	<5	8	<5	11	114	<200	8	17	7.6	<1	370	WOL-DI-QZ-CC-CL-OR (-SCH) skarn
-29	8	1410	<5	120	240	400	126	11	5.7	4	240	DI-AC-QZ-CC-CL (-SCH-PR-SL-CP) skarn
JABBERWOCK (MINFILE 115P 051)												
E-85-30	160	10	<5	7	240	<200	12	2800	3.0	<1	340	QZ-MU-TO-PY rock flour breccia
31	140	31	6	<6	24	<200	11	328	4.0	<1	550	Tourmalinite: 65% TO, QZ, MU (PY)
32	<5	5	<5	<5	44	<200	15	69	1.6	<1	210	QZ vein & tourmalinite (dissem. PY)
33	60	<3	29	11	7300	11.81%	1510	254	10.0	<1	80	QZ (-SL-CP-GL-PY) vein
34	77	13	<5	<11	100	2800	34	11400	6.8	4	75	ASP pods & SCOR in QZ (-PY) vein
35	9500	2	<5	<5	45	600	42	96	1.4	4	180	CT on joints of musc. quartzite
36	9400	13	<5	13	32	<200	24	357	1.7	4	130	Tourmalinized (QZ-TO-CT) rock flour breccia
37	240	<12	60	130	9400	430	24	16900	26.0	90	510	QZ vein with GL, ASP in FS-BI porphyry
38	9.32%	38	<5	<7	84	<200	14	801	1.9	8	330	CT-OR in fractures of quartzite

Appendix 1 (continued)

Sample No.	Sn	W	Ag	Au	Pb	Zn	Cu	As	Sb	Bi	F	Description
STERLING (MINFILE 115P 010)												
E-85-39	1600	<2	<5	<5	260	240	8	36	2.4	<1	60	QZ (-TO) vein
40	185	9	23	<8	2600	1300	48	2510	34.2	<1	150	Limonitic rock flour (-TO) breccia
41	115	12	<5	<5	45	<200	4	113	1.3	<1	230	TO veinlets within QZ vein
42	40	4	6	<5	660	5700	54	169	3.8	<1	250	Rock flour breccia
43	83	<2	<5	<5	260	270	7	16	2.1	<1	140	QZ vein with CL pods & veinlets
JOUMBIRA (MINFILE 105M 031)(Fed Showing)												
E-85-45	175	20	<5	<5	32	<200	6	37	0.9	<1	100	QZ vein with TO in joints in quartzite
46	195	19	<5	<5	32	270	9	684	1.0	<1	110	QZ vein in quartzite
47	740	51	<5	<5	48	210	9	1140	1.5	<1	110	QZ vein in quartzite
48	48	1460	<5	<5	14	<200	5	303	0.9	<1	160	LI stained QZ-TO vein in quartzite
49	37	100	<5	<5	19	<200	6	348	1.0	<1	55	QZ vein in quartzite
50	355	22	<5	<7	9	<200	5	245	0.8	2	130	QZ vein with TO filled fractures
51	28	9	<5	<5	78	1200	7	13	1.7	<1	130	QZ-SL vein
52	410	14	<5	5	16	<200	4	118	0.8	<1	140	QZ vein with TO-SER along fractures
53	23	13	<5	<5	45	520	11	254	1.5	<1	85	Fractured, limonitized quartzite
55	14	453	<5	<7	13	220	5	748	1.1	<1	130	QZ-TO veins in quartzite
JOUMBIRA (MINFILE 105M 031)(Creek Showing)												
56	24	12	<5	<5	39	<200	14	349	1.4	<1	870	SER-FS veins in quartzite
E-85-57	<5	3	<5	<5	10	<200	4	53	0.5	<1	180	QZ (-BI-FS) vein
58	32	17	<5	<6	56	<200	14	2960	3.9	<1	1600	QZ-FS (-SER) veins in quarzite
59	<5	377	<5	<5	10	<200	29	52	1.0	<1	160	QZ-FS veins with greisen envelopes in quartzite
61	11	7	<5	<5	18	310	10	1210	1.4	<1	530	QZ vein with MU selvage
62	1500	283	15	<10	58	15000	37	8120	18.0	34	650	QZ-TO-MU-CT (-PY-ASP-SL) vnlts in porph dyke
63	<5	5	7	<5	68	<200	3	108	1.7	2	140	QZ-MU stockwork with FS veins
JOUMBIRA (South)												
64	<5	<2	5	18	10	340	134	60	0.7	<1	210	Amphibolite
65	<5	<2	<5	<5	10	<200	160	226	0.7	<1	110	QZ-CB veins
JOUMBIRA (Pro Showing)												
60	59	31	<5	<5	21	<200	6	193	1.2	<1	130	TO veinlets in quartzite
99	6	10	<5	<5	33	1200	12	411	0.6	4	370	QZ porphyry dyke
100	1100	17	7	<5	51	<200	5	1290	2.2	4	470	TO-CT veinlets in QZ porphyry dyke, QZ-MU filled vugs
101	1200	798	<5	<5	15	<200	5	1060	1.0	4	300	QZ-MU vein with TO in fractures
102	<5	3	<5	<5	12	<200	2	35	0.7	2	120	TO-MU greisen vein
MAHTIN (MINFILE 115P 007)												
E-85-66	130	<120	7	130	32	<200	1650	>30000	299.0	26	630	QZ-FS vein cut by TO (-ASP-PY-CT) veinlets and TO breccia
67	12	6	<5	170	59	<200	700	1550	5.8	30	420	DI-TR-QZ-CC (-PR-CP-ASP-PY) skarn
68	<5	<25	<5	230	42	260	220	>30000	42.9	108	800	AC-QZ (-ASP-PY) skarn
69	30	3	<5	42	26	270	44	119	2.9	<1	310	DI-CC-ID-AC (-QZ) skarn with PR veinlets
70	9	160	<5	340	20	<200	870	531	3.6	20	470	DI-TR-QZ-CC (-PR-CP) skarn
71	215	<13	<5	82	37	290	115	17700	114.0	34	1250	QZ-CC-FS (-PY-ASP-CP) vein
72	130	4	<5	450	38	280	122	86	17.0	24	680	DI-QZ-PL-HB-CC (-SPH) skarn

Sample No.	Sn	W	Ag	Au	Pb	Zn	Cu	As	Sb	Bi	F	Description
BARNEY (MINFILE 115P 055)												
E-85-73	<5	21	<5	<5	70	<200	30	169	10.0	<1	580	Greisenized quartzite
74	<5	13	<5	73	14	<200	14	529	25.9	<1	200	Brecciated quartzite
75	<5	3	<5	42	133	<200	13	296	42.8	<1	170	Brecciated quartzite
76	<5	4	<5	35	26	<200	18	258	32.8	<1	270	QZ breccia
77	<5	6	<5	98	20	<200	13	1050	187.0	<1	170	Brecciated quartzite
RHOSGOBEL (MINFILE 115P 012)												
E-85-78	<5	<2	<5	<5	26	<200	26	16	1.1	<1	1100	BI quartzite
79	<5	2	<5	7	14	<200	26	11	1.6	<1	780	BI schist with PY-QZ pod, minor SCH
80	<5	<2	<5	7	10	<200	4	14	1.9	<1	190	QZ-AC-DI-PL (-SL) skarn
81	<5	2630	<5	12	54	<200	6	7	1.9	<1	300	DI-QZ-AC-PL (-SCH) skarn
82	<5	40	<5	<5	30	<200	14	30	1.8	<1	680	BI quartzite with TO-QZ veins
83	<5	9	<5	<5	26	<200	5	8	2.0	2	290	QZ-DI-AC-PL-BI (-OR-SL) skarn
84	<5	1340	<5	71	21	<200	16	9	0.7	2	320	QZ-PL-PH-DI-CC-AC (-SCH) skarn cut by QZ-SCH vein
PUKELMAN (MINFILE 115P 013)												
E-85-85	17	14	<5	<5	10	<200	11	151	3.5	<1	900	TO-BI (-CT-TOP) rock flour breccia
86	<5	6	<5	<5	24	<200	14	986	1.4	<1	440	BI quartzite with QZ veinlets
87	<5	5	<5	14	5	<200	6	1790	1.3	<1	550	QZ breccia cutting BI hornfels
88	<5	100	<5	160	11	<200	8	341	4.1	2	950	QZ-FS veinlets in FS granite porphyry
89	<5	46	<5	647	19	<200	12	7580	8.2	10	970	QZ-MO-PY vein in quartz monzonite
90	<5	15	<5	21	15	<200	16	82	4.2	<1	710	QZ vein in BI quartzite
91	<5	924	<5	616	6	<200	16	232	2.4	10	1800	BI-QZ schist cut by QZ-FS(-SCH) veins
92	<5	6100	<5	7630	11	<200	28	89	3.0	64	1300	Sheeted QZ-FS-SCH veins in BI quartzite
93	<5	3560	<5	57	5	<200	14	26	0.8	<1	3600	BI hornfels and QZ-BI-AC-OR (-SCH) skarn
LUGDUSH (MINFILE 115P 009)												
E-85-94	130	2050	<5	70	10	330	6	17	1.3	208	8000	DI-PL-QZ-CC-HB (-SCH) skarn (float)
95	<5	60	<5	<5	64	460	43	11	0.4	84	3600	Tourmalinite: 80% TO, OR, QZ
96	45	76	<5	28	48	440	10	12	1.8	2	1050	DI-OR-QZ-CC-HB (-SCH) skarn
97	28	140	<5	<5	18	390	6	5	0.6	2	460	DI-COR(20%)-QZ-OR-CC-PL (-PR-SCH) skarn
98	13	7	13	<5	148	<200	6	6	1.0	20	100	QZ vein with minor MO-SCH
ZETA (MINFILE 115P 047)												
E-85-103	140	8	<5	<5	34	<200	52	996	20.7	<1	1250	Syenite with TO (-PY-CT) veins
104	610	<30	40	34	690	1100	340	16600	507.0	6	1800	QZ(-LI-TO-PY-ASP) vein
105	480	<2	2.99°/t	nd*	4700	85	210	3.2%	0.70%	18	830	Radiating tourmaline in pods in granite
106	500	2300	3.12°/t	nd	5200	57	1320	6.1%	0.92%	5	1100	LI-stained TO (-SX) vein
107	600	<2	8.10°/t	nd	>10000	121	320	3.34%	3.64%	12	950	TO-QZ (-SX) breccia
108	450	<2	7.19°/t	nd	>10000	86	260	2.01%	2.56%	18	900	Tourminilized qranite: 10-20% TO, CT, PR
109	550	<2	9.10°/t	nd	>10000	225	104	1.16%	1.09%	4	520	QZ-TO (-SX) vein
110	<5	<20	10	<22	500	<200	53	1160	693.0	<1	150	FS porphyritic syenite with TO
111	<5	25	<5	<13	260	<200	10	339	329.0	<1	1150	HB-QZ syenite with TO veinlets
112	510	24	20	33	310	3000	133	864	312.0	<1	2200	LI-SCOR stained QZ (-ASP-PY-TO) vein in quartz monzonite
113	<5	3	<5	<9	67	<200	20	97	110.0	<1	340	TO (-PY) veins in quartzite
120	17	7	<5	<7	164	<200	4	69	51.0	<1	770	TO-QZ-(-CT) veins in greywacke
121	<5	4	<5	<9	220	<200	57	178	87.5	<1	650	SER veinlets in joints of quartzite
152	2900	<2	30.74°/t	nd	1.42%	151	720	3.26%	2.45%	88	1600	TO (-QZ-MU-CT-SX) breccia
153	700	3600	26.77°/t	nd	2100	92	260	4.83%	0.51%	64	1150	TO (-QZ-SX) vein

Appendix 1 (continued)

Sample No.	Sn	W	Ag	Au	Pb	Zn	Cu	As	Sb	Bi	F	Description
ZETA (MINFILE 115P 047)(East Showing)												
114	5	2	<5	<7	84	320	27	134	111.0	<1	800	CT-SER-LI in joints of SER quartzite
115	<5	3	<5	<6	60	410	35	124	78.5	<1	680	CT-SER-LI in joints of SER quartzite
116	<5	6	<5	<9	57	250	52	137	177.0	<1	740	CT-SER-LI in joints of SER quartzite
117	<5	5	<5	<7	123	<200	32	69	51.8	<1	680	CT-SER-LI in joints of SER quartzite
118	10	3	<5	<9	80	<200	22	66	88.2	<1	740	CT-SER-LI in joints of SER quartzite
SUNSHINE CREEK WEST (MINFILE 115P 031a)												
E-85-122	120	21	22	93	1900	<200	101	2340	80.1	86	300	QZ-TO (-SL) breccia and stockwork (0-20 m from SSW end of trench)
123	600	49	67	76	900	<200	220	3460	55.5	130	720	QZ-TO (-SL) breccia (20-40 m)
124	265	11	<5	11	340	<200	145	1180	40.3	4	770	Tourmalinite: 55% TO, 40% QZ, iron oxides (40-60 m)
125	500	26	<5	8	600	<200	149	1140	33.3	8	610	QZ breccia with TO veinlets and tourmalinite (60-80 m)
126	425	26	8	6	910	<200	120	1760	27.4	26	290	QZ-TO breccia (at 75 m, grab)
127	265	10	<5	9	900	<200	380	2220	62.9	16	470	TO-CL-QZ (-EP) breccia (80-100 m)
128	205	27	5	11	760	<200	360	1810	63.9	26	670	QZ breccia & stockwork, TO alteration & veins (100-120 m)
129	235	24	<5	14	950	<200	290	1280	34.6	38	370	TO-QZ breccia (120-140 m)
130	185	18	19	120	280	<200	185	1600	32.7	4	670	LI-stained QZ breccia with tourmalinite (140-160 m)
131	160	23	<5	33	1810	<200	310	1940	103.0	44	560	QZ breccia (160-180 m)
132	550	11	<5	13	330	220	490	426	29.0	12	720	QZ breccia (180-200 m)
141	7	3	<5	12	14	720	250	14	2.5	<1	1200	LI-MN-stained quartzite & BI schist
142	375	29	<5	12	59	200	88	298	14.0	4	1500	CL-QZ schist with TO band
SUNSHINE CREEK EAST (MINFILE 115P 031b)												
E-85-133	340	26	<5	<6	86	<200	167	537	8.0	12	440	GOE veins in quartzite
134	3400	20	18	26	116	<200	110	741	21.4	140	740	QZ breccia with TO veins
135	1300	66	28	15	800	<200	330	2400	15.0	264	1000	QZ-TO (-CT-LI) breccia
136	200	14	<5	<5	30	<200	168	51	5.0	12	200	TO veinlets in quartzite
137	38	5	<5	<5	53	<200	22	60	13.0	2	330	AC (-CL-CT) veinlets in BI quartzite
138	110	16	<5	9	41	<200	290	55	15.0	12	1950	BI schist with TO veins
139	66	18	<5	<5	15	<200	450	18	4.9	10	1700	Tourmalinite: 85% TO, 10% QZ, 3% TOP, CC, PY, CP, SL
WAYNE (MINFILE 105M 029)												
E-85-143	<5	696	<5	22700	66	<200	410	50	22.8	450	220	QZ-DI-CZ-AC-CC (-SL-PY-SCH) skarn
144	10	120	<5	1150	92	<200	76	89	28.8	22	870	AC-TR-DI-QZ (-PY) skarn
145	9	16	<5	2250	101	<200	137	204	80.2	34	1650	QZ-DI-TR-BI (-PY-SCH) skarn
147	<5	5	<5	18	109	490	4	18	3.1	<1	190	skarn with QZ-SL-PY

nd: not detected (for Au - detection limit is 0.002 oz/ton)
o/t: ounces per ton

DIFFERENTIAL UPLIFT ACROSS THE COAST PLUTONIC COMPLEX-NORTHERN STIKINE TERRANE CONTACT, YUKON: PRELIMINARY EVIDENCE FROM APATITE FISSION-TRACK THERMOCHRONOMETRY

by

John R. Dickie
Centre for Marine Geology
Dalhousie University
Halifax, Nova Scotia
Canada B3H 3J5

Alexander M. Grist
Fission Track Research Laboratory
Department of Earth Sciences
Dalhousie University
Halifax, Nova Scotia
Canada B3H 3J5

and

Raymond A. Donelick
Fission Track Research Laboratory
Department of Earth Sciences
Dalhousie University
Halifax, Nova Scotia
Canada B3H 3J5

DICKIE, J.R., GRIST, A.M., and DONELICK, R.A., 1992. Differential uplift across the Coast Plutonic Complex-Northern Stikine Terrane contact, Yukon: preliminary evidence from apatite fission-track thermochronometry. In: Yukon Geology, Vol. 3; Exploration and Geological Services Division, Yukon, Indian and Northern Affairs Canada, p.160-166

ABSTRACT

Six fission-track analyses were conducted on samples taken across a fault in the Takhini Hotsprings area, Yukon. The results indicate that samples taken on the east side of the fault cooled through 100°C at 104.4 ± 11.9 Ma, while the samples taken on the west side of the fault cooled through 100°C at 63.9 ± 8.5 Ma. Differential uplift and faster erosion on the west side of the fault between the mid-Cretaceous and the Early Paleocene could account for this difference in cooling history. This fault forms the approximate western edge of the Whitehorse Trough, and is marked by a dramatic change in the isopach of Jurassic and Triassic sedimentary and volcanic rocks which form a thin veneer over rocks of the Coast Plutonic Complex on the west side, and a very thick sedimentary sequence on the east side where basement rocks are not seen. Based on these observations, the fault is inferred to be a major zone of crustal weakness which could form the boundary between the Northern Stikine Terrane and the Coast Plutonic Complex in southern Yukon.

Similar results were obtained in a previous study of samples collected across the Llewellyn Fault Zone, which forms the boundary between the Northern Stikine Terrane and rocks of the Nisling Terrane and Coast Plutonic Complex in northwest B.C.

RÉSUMÉ

On a soumis à l'analyse des traces de fission dans l'apatite six échantillons recueillis le long d'un transect recoupant un prolongement septentrional de la zone faillée de Llewellyn au Yukon. Les échantillons recueillis dans la zone intramontagneuse présentaient une histoire de refroidissement différente de celle des échantillons recueillis dans l'acjacent complexe plutonique côtier. Les premiers se sont refroidis jusqu'à une température de 100 °C il y a 104,4 ±11,9 Ma et les derniers ont atteint cette même température il y a 63,9 ±8,5 Ma. Des résultats similaires obtenus pour des échantillons recueillis sur la zone faillée de Llewellyn dans le nord-ouest de la Colombie-Britannique indiquent une disparité régionale dans l'évolution thermique aux faibles températures de la zone intramontagneuse et du complexe plutonique côtier. Un soulèvement différentiel menant à une érosion plus rapide du côté occidental de la zone faillée pendant l'intervalle d'environ 104 à 64 Ma pourrait expliquer cette disparité dans les histoires thermiques. Sous forme d'une zone crustale affaiblie, la zone faillée de Llewellyn semble avoir facilité un soulèvement différentiel des roches du complexe plutonique côtier et des roches de l'adjacente zone intramontagneuse du Crétacé moyen au Crétacé tardif et au Paléocène précoce.

INTRODUCTION

Apatite fission-track techniques have revealed significantly different low-temperature cooling histories for rocks on either side of the Llewellyn Fault system in northwest British Columbia (e.g., Donelick and Dickie 1990). The Llewellyn Fault is a major crustal break which separates rocks of the Northern Stikine Terrane from the Nisling Terrane and the Coast Plutonic Complex (Fig. 1). The low-temperature thermal histories of samples taken across this structural boundary near the south end of Tagish Lake, British Columbia, are summarized by Donelick (1986, 1988), Donelick and Miller (1986), and Donelick and Dickie (1990). New results presented here show a similar change in low-temperature cooling history across a fault in southern Yukon. These results have important tectonic implications: we suggest that the observed difference in thermal history between rocks of the Northern Stikine Terrane and the Coast Plutonic Complex is due to differential uplift which occurred between the mid-Cretaceous and the Early Paleocene.

The study area lies approximately 20 km north of Whitehorse (Fig. 1). The samples were taken along a northeast-southwest transect across a north-trending fault zone which separates rocks of the Upper Triassic Lewes River Group from a thick sequence of Lower Jurassic Laberge Group clastics, east of Takhini Hotsprings (Fig. 2).

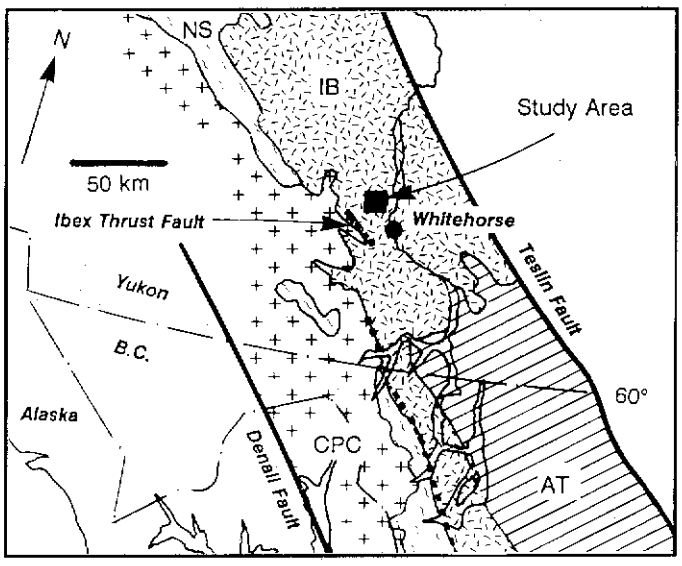

Figure 1. Study location map. The Northern Stikine Terrane (IB), Coast Plutonic Complex (CPC), Atlin Terrane (AT) and Nisling Terrane (NS) are depicted. The location of the Llewellyn Fault-Tally-Ho Shear system (dashed line) is based on data from Doherty and Hart (1988), Hart and Radloff (1990) and Mihalynuk and Mountjoy (1990).

GENERAL GEOLOGY

Two tectonic belts of the northern Cordillera are considered in this study. The Coast Plutonic Complex is a northwest-trending linear batholith comprised of Late Cretaceous to Eocene epizonal calc-alkaline plutons. It lies west of the Northern Stikine Terrane which, in southern Yukon, is predominantly represented by volcanic and sedimentary rocks of the Whitehorse Trough.

Mesozoic rocks of the Whitehorse Trough include (a) Carnian to Late Norian (to Hettangian?) calc-alkaline plagioclase- and augite-phyric volcanic flows, breccias and pyroclastics, volcanogenic sandstone, black argillite, and limestone of the Lewes River Group (e.g., Tozer 1958, Wheeler 1961, Hart and Radloff 1990), (b) Hettangian to Bajocian polymictic conglomerate, sandstone and argillite of the Laberge Group (e.g., Wheeler 1961, Dickie 1989, Hart and Radloff 1990, Dickie and Hein in press), (c) Oxfordian-Kimmeridgian (Hart and Radloff 1990) to Albian chert-pebble conglomerate, sandstone and coal of the Tantalus Formation (Lowey and Hills, 1988), and (d) Cretaceous andesitic to rhyolitic volcanic rocks.

The Whitehorse Trough sedimentary and volcanic rocks were deposited on the leading edge of the allochthonous Stikine Terrane during a Jurassic arc-continent collision (e.g., Tempelman-Kluit 1979, Dickie and Hein 1988, Dickie and Hein in press). They are now juxtaposed against quartzofeldspathic biotite-muscovite schist, quartzite, and marble of the Nisling Terrane (e.g., Wheeler and McFeely 1987, Hansen 1990, Hart and Radloff 1990) which form the basement to the Jurassic arc, but probably not to the forearc basin. Nisling rocks were originally classified by Cairnes (1916) as the Yukon Group and were later described as part of the Yukon Crystalline Terrane by Tempelman-Kluit (1976, 1979), and are intruded by igneous rocks of the Coast Plutonic Complex.

Whitehorse Trough developed as a fore-arc basin from Late Triassic to the Middle Jurassic (Tempelman-Kluit 1979, Dickie 1989, Dickie and Hein in press), and a plutonic belt formed along the western basin margin. These arc plutons range in composition from quartz diorite to granite and have yielded Late Triassic to Early Jurassic radiometric ages (e.g., Tempelman-Kluit and Wanless 1975, Morrison et al. 1979, Doherty and Hart 1988, Johnson 1988, Hart and Radloff 1990, Hart and Armstrong, unpublished data). Triassic-Jurassic radiometric dates (U/Pb method) from clasts of the Laberge Group conglomerate, and northeast to southeast-directed paleocurrents in the Jurassic basin-fill substantiate a link between this plutonic belt and the adjacent basin in the early Mesozoic (Hart, Dickie and Armstrong, unpublished data and in prep.). Plutons of the younger Coast Plutonic Complex follow the same trend as the Triassic-Jurassic plutons, but are much more numerous immediately west of the Triassic-Jurassic plutonic belt.

In northwest B.C. the Llewellyn Fault system separates Nisling Terrane metamorphic rocks to the west from the Whitehorse Trough to the east (e.g., Hart and Radloff 1990). Dickie and Hein (in press) suggest that in the southernmost Yukon, the Tally-Ho Shear Zone forms a similar boundary between Nisling Terrane metamorphic basement rock and younger rift-related transitional to oceanic crust flooring the Whitehorse Trough. This transition between continental and oceanic crust in many island arcs is a zone of mechanical weakness, subject to failure in the form of fore-arc transform fault zones (Turcotte et al. 1977).

The Llewellyn Fault and Tally-Ho Shear Zone are described in detail by Hart and Radloff (1990) and Mihalynuk and Mountjoy (1990). Hart and Radloff (1990) and Radloff et al. (1990) described evidence for two phases of deformation along the Tally-Ho Shear Zone: (a) penetrative, semi-ductile structures, indicative of Triassic sinistral transcurrent motion at a mid-crustal level, and (b) non-penetrative, brittle structures, indicative of Late Cretaceous dextral transcurrent motion at a shallow crustal level. The Tally-Ho Shear Zone is inferred to represent a more deeply exposed part of the same fault system which provides a record of the more ductile Triassic deformation, whereas the Llewellyn Fault to the south exhibits late Cretaceous brittle deformation textures which overprinted the older, ductile fabrics. The Tally-Ho Shear Zone is offset from the Llewellyn Fault at the Yukon-B.C. border along a northeast-trending strike-slip fault (Hart and Radloff 1990). The Tally-Ho Shear Zone has been traced north as far as Fish Lake, where it is overridden by the Ibex Thrust.

Like the Llewellyn Fault and Tally-Ho Shear Zone, the fault near Takhini Hot Springs which forms the subject of this study appears to form the boundary between the Northern Stikine Terrane and the Nisling Terrane/Coast Plutonic Complex. The three faults show a number of similarities, including: (a) a north to northwest trend, (b) semi-ductile deformational features overprinted by brittle fractures within Triassic Lewes River Group sandstone and argillite (c) sheared black argillite containing veinlets of chalcopyrite with malachite, galena, tetrahedrite and argentite (Dickie, unpublished data), and (d) location along the western margin of the Whitehorse Trough, indicated by coastal deposits of the Lewes River and Laberge Groups (Dickie 1989) and a dramatic decrease in the thickness and extent of Laberge Group strata west of the fault.

Late Cretaceous volcanic rocks cap the Takhini Hotsprings fault at its north end (Wheeler 1961, Tempelman-Kluit 1984), and constrain the timing of its last significant lateral movement.

The Tally-Ho Shear Zone has been traced north as far as Fish Lake. A northeast-trending fault similar to the one which connects the Llewellyn Fault with the Tally-Ho Shear Zone would have to be invoked in order to link the Takhini Hotsprings-area fault with the north end of the Tally-Ho system.

METHODS

Six samples were collected for fission-track geochronology from an area near Takhini Hotspring (Fig. 2). All samples were collected at a constant elevation of 900 m above sea level. Sample locations are shown in Figure 2 and are summarized in Table 1. The sample suite represents: (a) two samples from sedimentary and pyroclastic Lewes River Group strata close to a late Cretaceous granitic pluton of the Coast Plutonic Complex (Wheeler 1961), (b) two samples from sedimentary Lewes River Group strata nearer to the west side of the fault, and (c) two samples from sedimentary Laberge Group strata on the east side of the structure depicted in Figures 2 and 3. Full details regarding the mineral separation techniques, sample preparation procedures, and analytical methods employed for the fission-track analyses are presented in Donelick (1986, 1988). In this paper, each fission-track age is interpreted as the time when its sample cooled through the 100°C crustal isotherm. This interpretation results from the limited degree of fission-track annealing present in the apatites, revealed by relatively long mean etchable track lengths (e.g., Naeser and Forbes 1976, Green et al. 1986). Apatite fission-track ages were measured for all samples, which are labelled YT-1 to YT-6 (Fig. 2). It is convenient to consider the fission track data obtained for rocks exposed west and east of the fault in the study area separately (Fig. 2).

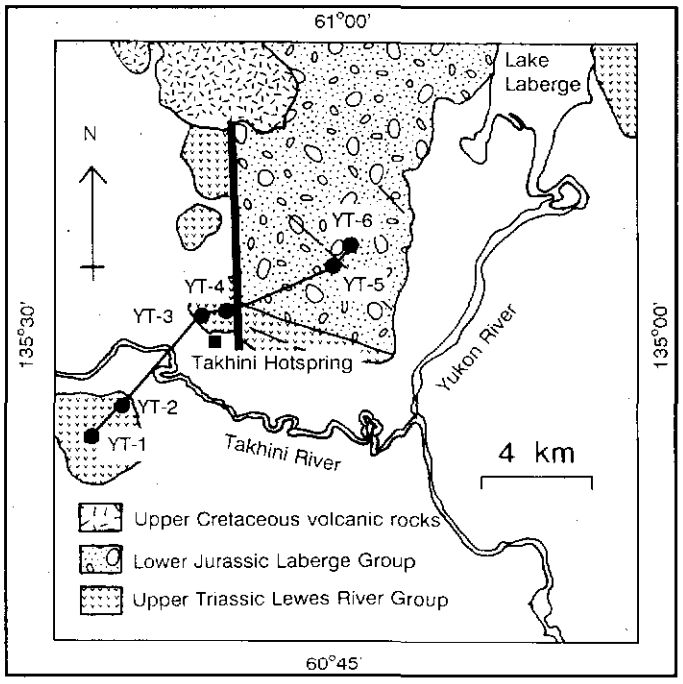

Figure 2. Detailed study location map showing the generalized outcrop patterns in the vicinity of Takhini Hotspring. The large solid line is the fault under study, which is believed to form the east boundary of the Coast Plutonic Complex, similar to the Llewellyn Fault in Northern B.C. Sample localities at 900 m elevation above sea level are depicted as YT-1 to YT-6.

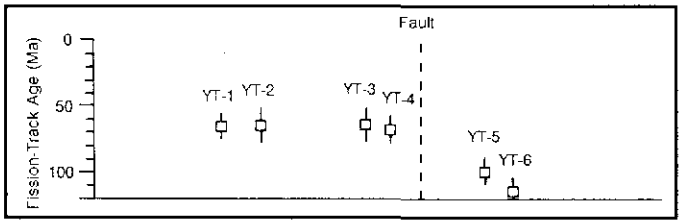

Figure 3. Summary cross-section of the sampling transect. Fission-track ages for samples YT-1 to YT-6, with error bars of one standard deviation, are plotted against relative distance from the fault (refer to Fig. 2 for localities). Notice that rocks on either side of the fault return significantly different cooling ages.

RESULTS

Although no previous work has been published on the low-temperature thermal history of the Coast Plutonic Complex in southern Yukon, relevant studies on the southern part of the Coast Plutonic Complex exist (e.g., Harrison et al. 1979; Parrish 1982, 1983; Donelick and Dickie 1991). These studies primarily document the large-scale cooling of much of the Cordillera following latest Cretaceous to Eocene compressive orogeny. Donelick and Dickie (1991) published the first detailed low-temperature history of this plutonic belt in the northern Cordillera. These results from northwestern British Columbia show cooling ages through the 100°C crustal isotherm of 63.7 ± 4.9 Ma to 48.3 ± 4.6 Ma with a mean age of 53.9 ± 4.6 Ma. No plutons of the Coast Plutonic Complex were sampled for fission-track thermochronometry in southern Yukon. It is expected, however, that rocks of the Lewes River Group directly overlying rocks of the Coast Plutonic Complex would have experienced a very similar low-temperature cooling history, whereas rocks separated from the Coast Plutonic Complex by a major fault might have a different low-temperature cooling history.

Samples YT-1 to YT-4 were collected from the Lewes River Group on the west side of the fault zone. These revealed latest Cretaceous to early Paleocene cooling ages, ranging from 67.7 ± 6.9 Ma to 61.8 ± 12.1 Ma (Table 2), providing a mean fission-track age of 63.9 ± 8.5 Ma. These results are slightly older than, but similar to, the results of Donelick (1986, 1988) and Donelick and Dickie (1990) for northwestern British Columbia.

Samples YT-5 and YT-6 are clasts collected from Laberge Group conglomerate east of the fault. These samples yielded 100°C cooling ages of 113.0 ± 10.0 Ma and 95.8 ± 10.5 Ma respectively (Table 2), providing a mean fission-track age of 104.4 ± 11.9 Ma. As a comparison, two conglomerate samples collected from the Laberge Group beside Tagish Lake and analysed by Donelick (1986, 1988) yielded apatite fission-track ages of 98.1 ± 10.1 Ma and 100.0 ± 11.0 Ma.

DISCUSSION AND CONCLUSIONS

The fission-track results are consistent with west-side up displacement across the fault in the study area between about 100 Ma and 60 Ma. This coincides with the intrusion of the Coast Plutonic Complex in this part of the Cordillera (e.g., Tempelman-Kluit and Wanless 1975, Hart and Radloff 1990) and may reflect a mechanical response to inhomogeneous thermal expansion across an existing crustal weakness. Uppermost Cretaceous volcanic rocks capping the northern part of the fault are consistent with this model. We believe that uplift across this boundary ceased immediately prior to the emplacement of those volcanic flows.

These fission-track results suggest that both in Yukon and in Northern British Columbia, the Whitehorse Trough and the adjacent Coast Plutonic Complex experienced significantly different low-temperature cooling histories. If the interpreted vertical movement on the major terrane-bounding faults between about 100 Ma and 60 Ma is related to the intrusion of the Coast Plutonic Complex, then these faults and associated splays are of interest for their economic potential, as the faults would have acted as conduits for hot fluids associated with the intrusions. Many hydrothermal fluids would contain sufficient heat to anneal fission tracks in wall-rock apatite. Because rocks east of the fault consistently return 100 Ma fission-track ages, post-100 Ma mineralizing events could be modelled on

the basis of "reset" fission-track ages.

ACKNOWLEDGEMENTS

Support for this project was supplied through a research agreement between JRD and Exploration and Geological Services Division, Yukon, Indian and Northern Affairs Canada. The authors gratefully acknowledge the use of facilities at the Dalhousie Fission Track Research Laboratory and to the Centre for Marine Geology. We would also like to express our sincere gratitude to Chief Geologist Steve Morison at Northern Affairs, and to Erwin Kreft at Takhini Hotsprings.

REFERENCES

CAIRNES, D.D. 1916. Wheaton District, Southern Yukon. Supplement to Geological Survey of Canada. Memoir 31, Summary Report for 1915.

DOHERTY, R.A. and HART, C.J.R. 1988. Preliminary geology of Fenwick Creek (105D/3) and Alligator Lake (105D/6) map areas. Exploration and Geological Services Division, Indian and Northern Affairs Canada, Open File 1988-2.

DONELICK, R.A. 1986. Mesozoic-Cenozoic thermal evolution of the Atlin Terrane, Whitehorse Trough, and Coast Plutonic Complex from Atlin, British Columbia to Haines, Alaska as revealed by fission track geothermometry techniques. Unpublished M.Sc. thesis, Renssalaer Polytechnic Institute, Troy, New York. 167 p.

DONELICK, R.A., 1988. Etchable fission track length reduction in apatite: Experimental observations, theory and geological applications. Unpublished Ph.D. thesis, Renssalaer Polytechnic Institute, Troy, New York. 414 p.
DONELICK, R.A., and MILLER, D.S. 1986. Low-temperature geothrmometry of the Coast Plutonic Complex, Whitehorse Trough and Atlin Terrane from Atlin, B.C. to Haines, AK. Geological Society of America, Abstracts with Programs, Vol. 18, p. 102.

DONELICK, R.A., and DICKIE, J.R. 1991. Low-temperature thermal history of the Coast Plutonic Complex and Intermontane Belt, northwest British Columbia (104M,N). In: Geological Fieldwork 1990; British Columbia Ministry of Energy, Mines and Petroleum Resources, Paper 1991-1, p. 139-144.

DICKIE, J.R. 1989. Sedimentary response to arc-continent transpressive tectonics: The Laberge Conglomerates (Jurassic), Whitehorse Trough, Yukon Territory. Unpublished M.Sc. thesis, Dalhousie University, Halifax, Nova Scotia. 361 p.

DICKIE, J.R., and HEIN, F.J., in press. Conglomeratic submarine fans of the Jurassic Laberge Group, Whitehorse Trough, Yukon: New constraints on an arc-continent collision model. Canadian Journal of Earth Sciences.

DICKIE, J.D., and HEIN, F.J. 1988. Laberge conglomerates, Yukon: Evidence of a Late Triassic-Jurassic arc-continent collision. Geological Association of Canada, Abstracts with Programs. p. A32.

GREEN, P.F., DUDDY, I.R., GLEADOW, A.J.W., LASLETT, G.M. and TINGATE, P.R. 1986. Thermal annealing of fission tracks in apatite - a qualitative description. Chemical Geology (Isotope Geoscience Section), Vol. 59, p. 237-253.

HANSEN, V.L. 1990. Yukon-Tanana terrane: A partial acquittal. Geology, Vol. 18, p. 365-369

HARRISON, T.M., ARMSTRONG, R.L., NAESER, C.W. and HARAKAL, J.E., 1979. Geochronology and thermal history of the Coast Plutonic Complex, near Prince Rupert, British Columbia. Canadian Journal of Earth Sciences, Vol. 16, p. 400-410.

HART, C.J.R., and RADLOFF, J.K. 1990. Geology of Whitehorse, Alligator Lake, Fenwick Creek, Carcross and parts of Robinson map areas (105D/11,6,3,2,7). Exploration and Geological Services Division, Yukon, Indian and Northern Affairs Canada, Open File 1990-4.

JOHNSON, S. 1988. The tectonic setting of the Aishihik batholith, southwesten Yukon. In: Yukon Geology Volume 2, Exploration and Geological Services Division, Yukon, Indian and Northern Affairs Canada, p. 37-41.

LOWEY, G.W., and HILLS, L.V., 1988. Lithofacies, petrology and environments of deposition, Tantalus Formation (Lower Cretaceous) Indian River area, west-central Yukon. Canadian Society of Petroleum Geologists Bulletin, Vol. 36, p. 296-310.

MIHALYNUK, M.B. and MOUNTJOY, K.J. 1990. Geology of the Tagish Lake area (104M/8, 9E). British Columbia Ministry of Energy, Mines and Petroleum Resources, Geological Fieldwork 1989, Paper 1990-1, p. 181-196.

MORRISON, G.W., GODWIN, C.I. and ARMSTRONG, R.L. 1979. Interpretation of isotopic ages and $^{87}Sr/^{86}Sr$ initial ratios for plutonic rocks in the Whitehorse map-area, Yukon. Canadian Journal of Earth Sciences, Vol. 16. p. 1988-1997.

PARRISH, R.R. 1982. Cenozoic thermal and tectonic history of the Coast Mountainsof British Columbia as revealed by fission-track and geological data and quantitative thermal models. Unpublished Ph.D. thesis, University of British Columbia, 166 p.

PARRISH, R.R., 1983. Cenozoic thermal evolution and tectonics of the Coast Mountains of British Columbia - Fission track dating, apparent uplift rates, and patterns of uplift. Tectonics, Vol. 2, p. 601-631.

RADLOFF, J.K., HART, C.J.R. and HANSEN, V.L. 1990. Late Triassic sinistral translation on the Tally-Ho Shear Zone, Yukon. Geological Society of America, Abstracts with programs, Vol. 22, p. 76-77.

TEMPELMAN-KLUIT, D.J. 1976. The Yukon Crystalline Terrane; enigma of the Canadian Cordillera. Geological Society of America Bulletin, Vol. 87, p. 1343-1357.

TEMPELMAN-KLUIT, D.J. 1979. Transported cataclasite, ophiolite and granodiorite in Yukon: evidence of arc-continent collision. Geological Survey of Canada, Paper 79-14.

TEMPELMAN-KLUIT, D.J. 1984. Maps of Laberge (105E) and Carmacks (115I) map areas, with legends. Geological Survey of Canada, Open File 1101.

TEMPELMAN-KLUIT, D.J., and WANLESS, R.K. 1975. Potassium-Argon age determinations of metamorphic and plutonic rocks in the Yukon Crystalline Terrane. Canadian Journal of Earth Sciences, Vol. 12, p. 1895-1909.

TOZER, E.T. 1958. Stratigraphy of the Lewes River Group (Triassic), Central Laberge area, Yukon Territory. Geological Survey of Canada, Bulletin 43.

TURCOTTE, D.L., AHERN, J.C. and BIRD, J.M. The state of stress at continental margins. Tectonophysics, Vol. 42, p. 1-28.

WHEELER, J.O. 1961. Whitehorse map-area, Yukon Territory (105D). Geological Survey of Canada, Memoir 312.

WHEELER, J.O., and McFeely, P. 1987. Tectonic assemblage map of the Canadian Cordillera and adjacent parts of the United States of America. Geological Survey of Canada, Open File 1565.

Table 1. Summary of Sample Lithologies and Locations

Sample	Lithology	Longitude	Latitude
YT-1	unwelded andesite tuff	135°28'	60°49'
YT-2	aphyric andesite[1]	135°27'	60°50'
YT-3	granite[1]	135°24'	60°51'
YT-4	volcanogenic sandstone	135°22'	60°51'
YT-5	hornblende granodiorite[2]	135°15'	60°52'
YT-6	augite-phyric andesite[2]	135°13'	60°53'

[1]Clasts in the uppermost Lewes River Group conglomerate
[2]Clasts in the Laberge Group conglomerate

Table 2. Summary of Apatite Fission-track Results

Sample	p_s[a]	N	p_i[a]	N	p_d[a]	N	GrainsChi²Test[b]	Fission-track Age (Ma)
YT-1	3.06E+05	129	1.12E+06	474	4.25E+06	5300	169.0289PASS	63.3 ± 6.6
YT-2	2.13E+05	73	7.92E+05	271	4.25E+06	5300	153.0931PASS	62.7 ± 8.5
YT-3	1.17E+05	34	4.40E+05	128	4.25E+06	5300	121.1447PASS	61.8 ± 12.1
YT-4	2.13E+05	137	7.33E+05	471	4.25E+06	5300	226.0711PASS	67.7 ± 6.9
YT-5	4.49E+05	75	1.19E+06	199	4.21E+06	3450	123.9354PASS	95.8 ± 13.9
YT-6	5.23E+05	282	1.17E+06	632	4.21E+06	3450	2010.5127PASS	113 ± 10.0

[a]in units of 10^6 tracks/cm²
[b]pass or fail at the 95% confidence level for Chi²
[c]zeta calibration factor 110 ± 3.0 (samples YT-1 to YT-4) and 121.8 ± 6.0 (samples YT-5 and YT-6) relative to neutron dosimeter glass standard CN1.
Error given is 1 standard deviation.

PETROLOGY AND GEOCHEMISTRY OF TIN AND TUNGSTEN MINERALIZED PLUTONS, MCQUESTEN RIVER REGION, CENTRAL YUKON

Diane S. Emond
Exploration and Geological Services Division
Indian and Northern Affairs Canada
200 Range Rd
Whitehorse, Yukon
Y1A 3V1

EMOND, D.S., 1992. Petrology and geochemistry of tin and tungsten mineralized plutons, McQuesten River region, Central Yukon. In: Yukon Geology Vol. 3; Exploration and Geological Services Division, Yukon, Indian and Northern Affairs Canada, p.167-195

ABSTRACT

Mid-Cretaceous plutons in the McQuesten River region intrude Upper Proterozoic to Mississippian miogeoclinal metasedimentary rocks of Selwyn Basin. They form a belt trending east from the Tintina Trench which can be roughly subdivided into two parallel belts. Plutonic rocks fall into three main groups: (1) biotite-muscovite (two-mica) granite in the southernmost belt which follows the trend of the McQuesten Anticline; (2) biotite-hornblende quartz monzonite, granite and granodiorite in the northern belt which follows the thrust faulted contact of the Hyland Group (Grit Unit) with the Road River Formation; and (3) hornblende-biotite syenite and associated quartz syenite, quartz monzonite, granite and tourmaline-orbicular granite along the north edge of the northern belt.

Tin-silver breccias veins and skarns are spatially associated with the two-mica granites, while tungsten-gold skarns and sheeted veins are associated with biotite-hornblende granite, quartz monzonite and granodiorite. The concentrically zoned syenite intrusion in the northern belt (ZETA) includes all the plutonic phases (two-mica granite, biotite-hornblende granitoids, and hornblende-biotite syenitoids), and links them cogenetically through the fractional crystallization process. The ZETA tin-silver veins (MINFILE 115P 047) are associated with the tourmaline orbicular granite, which is the most evolved phase of the concentrically zoned ZETA syenite intrusion.

Petrologic and geochemical variation between the three main rock groups is consistent with plutonic rocks of the belt being cogenetic, the two-mica granite being the most evolved phase. Trace and rare earth element variations further suggest that the entire McQuesten plutonic suite formed from melted sedimentary rocks, and that fractionation accounts for the evolution of the individual rock types and their associated mineral deposits.

Plutons in the McQuesten region resemble those of the Selwyn and Tombstone Plutonic Suites. They are post- to syntectonic, roughly circular in shape, and intrude miogeoclinal metasedimentary rocks of ancient North America. They show a concentric zonation and are surrounded by contact aureoles. The intrusive suite is bimodal, with a southern belt consisting of evolved two-mica granites and a northern belt consisting of less evolved biotite-hornblende granites. Lavas associated with the plutons are believed to be coeval.

The two main igneous types in each belt have been compared in detail. Both types are petrographically similar in that they contain quartz, plagioclase, K feldspar, microperthitic orthoclase and a range of accessory minerals including apatite, zircon, allanite, titanite and tourmaline.

Distinguishing features typical of the two-mica granites include their more quartz-rich nature, a more restricted potassium feldspar to plagioclase ratio, and a more common myrmekitic texture. Minerals in the two-mica granite generally have a more subhedral form and the biotite shows reddish brown pleochroism. The biotite-hornblende granitoids are distinguished by accessory dark green to brown pleochroic hornblende and dark brown pleochroic clinopyroxene. The biotite has chocolate brown pleochroism and an unusually large number of inclusions. The accessory minerals titanite, allanite and magnetite appear to be more abundant in the biotite-hornblende rocks. Red-brown biotite, pale green hornblende and beige clinopyroxene occur in the less abundant syenites, along with minor nepheline and enhanced amounts of magnetite and titanite.

Chemically, the rocks are subalkaline (two-mica and biotite-hornblende rocks) to alkaline (syenite).

The two-mica granites are characterized by normative corundum, higher alkalies and lower amounts of iron, calcium and magnesium than the biotite-hornblende rocks. The biotite-hornblende granites are distinguished by higher amounts of normative clinopyroxene, and the syenites by normative nepheline. Na_2O/K_2O, $Na_2O/K_2O/CaO$ and Rb/Ba/Sr ratios are similar to other S-type granites.

McQuesten region biotite-hornblende granodiorites are chemically distinguished from those of the Selwyn and Tombstone Suites by their peraluminous composition, lower modal quartz content, and higher iron to alkalies and magnesium ratios. Equivalent rocks of the Tombstone Plutonic Suite contain aegirine-augite indicating an A-type origin. In the McQuesten region, tungsten is associated with the biotite-hornblende rocks, whereas in the Selwyn area it is associated with two-mica granites.

RÉSUMÉ

Des plutons du Crétacé moyen pénètrent, dans la région de la rivière McQuesten, les roches sédimentaires métamorphisées miogéoclinales du bassin de Selwyn datant du Protérozoïque supérieur au Mississippien. Ils forment une zone s'allongeant vers l'est depuis le sillon de Tintina et qui peut grossièrement être subdivisée en deux zones parallèles. Il existe trois grands groupes de roches : 1) granite à biotite et muscovite (deux micas) dans la zone la plus méridionale qui suit l'orientation de l'anticlinal de McQuesten, 2) monzonite quartzique à biotite et hornblende, granite et granodiorite dans la zone septentrionale qui longe le contact par faille chevauchante entre le groupe de Hyland (unité de grit) et la formation de Road River et 3) syénite à hornblende et biotite et syénite quartzique associée, monzonite quartzique, granite et granite orbiculaire à tourmaline le long de la bordure de la zone septentrionale.

Les veines de brèche et les skarns stannifères et argentifères sont spatialement associés aux granites à deux micas alors que les skarns et les groupes de filons séparés de stériles renfermant du tungstène et de l'or sont associés au granite à biotite et hornblende, à la monzonite quartzique et à la granodiorite. L'intrusion de syénite à zonation concentrique de la zone septentrionale (ZETA) englobe toutes les phases plutoniques (granite à deux micas, granitoïdes à biotite et hornblende et syénitoïdes à hornblende et biotite) et les associe cogénétiquement les unes aux autres par le processus de la cristallisation fractionée. Les veines stannifères et argentifères ZETA sont associées au granite oprbiculaire à tourmaline qui constitue la phase la plus évoluée de l'intrusion de syénite à zonation concentrique ZETA.

Les variations pétrologiques et géochimiques entre les trois groupes confirment le caractère cogénétique des roches plutoniques de la zone, le granite à deux micas constituant la phase la plus évoluée. Les variations de la composition en éléments à l'état de traces et en terres rares suggèrent de plus que tout l'ensemble de la zone plutonique de McQuesten s'est formé à partir de roches sédimentaires fondues et que le fractionnement explique l'évolution des types individuels de roches ainsi que les dépôts de minéraux qui leurs sont associés.

Les plutons de la région de McQuesten sont quelque peu similaires aux suites plutoniques de Selwyn et de Tombstone. Ils sont contemporains du tectonisme, ou postérieurs à ce dernier, de forme approximativement circulaire et pénètrent les roches sédimentaires métamorphisées miogéoclinales de l'ancienne Amérique du Nord. Il présentent une zonation concentrique et sont entourés d'auréoles de contact. La suite intrusive est bimodale, comportant une zone méridionale qui consiste en granites à deux micas évolués et une zone septentrionale qui consiste en granites à biotite et hornblende moins évolués. Les laves associées aux plutons seraient contemporaines.

Les deux principaux types de roches ignées de chaque zone ont été comparés de manière détaillée. Les deux types sont pétrographiquement similaires du fait qu'ils renferment du quartz, du plagioclase, du feldspath potassique, de l'orthoclase microperthitique et une gamme de minéraux accessoires incluant l'apatite, le zircon, l'allanite, la titanite et la tourmaline.

Parmi les caractéristiques distinctives typiques des granites à deux micas mentionnons leur teneur plus élevée en quartz, un rapport feldspath potassique sur plagioclase moindre et une structure plus couramment myrmékitique. Les minéraux dans le granite à deux micas présentent généralement une forme davantage hypidiomorphe et la biotite présente un pléochroïsme brun rougeâtre. Les granitoïdes à biotite et hornblende se distinguent par la présence de hornblende pléochroïque vert foncé à brune et de clinopyroxène pléochroïque brun. La biotite présente un pléochroïsme brun chocolat et un nombre inhabituellement élevé d'inclusions. Les minéraux accessoires que sont la titanite, l'allanite et la magnétite semblent plus abondants dans les roches à biotite et hornblende. Les syénites, qui constituent les membres les moins abondants de ces suites, renferment de la biotite rouge-brun, de la hornblende vert pâle et du clinopyroxène beige. Parmi les minéraux accessoires mentionnons la néphéline, et des quantités accrues

de magnétite et de titanite.

Chimiquement, les roches sont de subalcalines (roches à deux micas et à biotite et hornblende) à alcalines (syénite). Les granites à deux micas sont caractérisés par la présence de corindon normatif, par des alcalinités plus élevées et par des quantités moindres de fer, de calcium et de magnésium que celles présentes dans les roches à biotite et hornblende. Les granites à biotite et hornblende se distinguent par des quantités plus grandes de clinopyroxène normatif et les syénites par la présence de néphéline normative. Les rapports Na_2O/K_2O, $Na_2O/K_2O/CaO$ et Rb/Ba/Sr sont similaires à ceux des autres granites de type S.

Les granodiorites à biotite et hornblende de la région de McQuesten se distinguent chimiquement de celles des suites de Selwyn et de Tombstone par leur composition hyperalumineuse, leur teneur moindre en quartz modal et leurs rapports fer sur métaux alcalins et magnésium plus élevés. Les roches équivalentes de la suite plutonique de Tombstone renferment de l'augite aegyrinique, ce qui indique une origine de type A. Dans la région de McQuesten, le tungstène est associé aux roches à hornblende et biotite alors que dans la région de Selwyn il est associé aux granites à deux micas.

INTRODUCTION

Felsic plutons form a 30 x 150 km belt that trends east from Tintina Trench to Mayo Lake (30 km east of Keno Hill) in central Yukon (Fig. 1). They are mid-Cretaceous and intrude Upper Proterozoic to Mississippian metasedimentary rocks of the North American miogeocline. These plutons include over 20 stocks and plugs, and abundant dykes, many with associated metallic mineral occurrences and deposits. Keno and Galena Hill silver-lead-zinc veins have produced over 6 400 tonnes (206 million ounces) of silver since 1913 (Watson 1986), and are genetically related to the Mayo Lake Batholith (distal; Lynch 1988). Pluton-proximal mineralization includes the Ray Gulch skarn (MINFILE 106D 027) which has probable and possible reserves of 5.4 million tonnes grading 0.82% WO_3 (Lennan 1986). In the McQuesten River region, eleven plutons are directly associated with tin-tungsten-silver-gold veins, breccias and/or skarns (Fig. 2; Emond and Lynch 1992; Emond 1986, 1985, 1983).

Mid-Cretaceous, felsic plutons in the northern Canadian Cordillera post-tectonically intrude folded miogeoclinal sedimentary rocks of the Foreland Fold and Thrust Belt (the Omineca Crystalline Belt) and adjoining ductilely deformed metasedimentary rocks of Yukon Tanana Terrane which overlie the continental crust of ancestral North America. Local studies by Anderson and others have resulted in the naming of several plutonic suites based partly on geographic location, and partly on intrusion characteristics (Fig. 1; Woodsworth et al. 1989).

The McQuesten plutonic belt is part of the Selwyn Plutonic Suite of eastern Yukon. In the southeast part of the Selwyn Plutonic Suite (in the Selwyn Mountains), tungsten-copper (zinc) skarn deposits are associated with peraluminous, two-mica plutons (Anderson 1988). These deposits include MacTung (MINFILE 105O 002), with defined geologic reserves of 32 million tonnes grading 0.92% WO_3 (Atkinson and Baker 1986); and the Cantung (NWT) deposit, which produced nearly 39 000 tonnes WO_3 to the end of 1982 (Sinclair 1986).

The Tombstone Plutonic Suite intrudes folded and thrusted passive continental margin carbonate and clastic rocks (Anderson 1988) in the Tombstone Mountains (Fig. 1). It shows similarities to the Selwyn Plutonic Suite. However, several Late Proterozoic periods of extension in this area probably thinned the crust substantially (Thompson and Eisbacher 1984), resulting in more alkalic compositions and minor mafic phases. Vein, breccia, skarn, and disseminated U-Th-Sb-W-Mo-Sn-Ag-Au and base metal occurrences are associated with these plutons. Plutons in the northwestern part of the McQuesten River region were previously included in the Tombstone Plutonic Suite.

Little information is available on the granites in the Mayo-McQuesten area (Abercrombie 1990, Sinclair 1986, Kuran 1982). This report provides descriptions of the petrology and geochemistry of the McQuesten plutons, and comparisons with the well-documented Selwyn and Tombstone Suites. Additional information about mid-Cretaceous plutonism in the northern Cordillera will assist in interpretation of related mineral deposits.

GEOLOGIC SETTING

The McQuesten River region lies in Selwyn Basin, within the Omineca Crystalline Belt of the Canadian Cordillera. North American miogeoclinal rocks of the Late Proterozoic-Early Cambrian Hyland Group (formerly known as the Grit Unit) were thrust northward onto Ordovician to Silurian Road River Formation and Mississippian Keno Hill Quartzite (Wheeler and McFeely 1987, Eisbacher 1981, Bostock 1946 and 1964) during Late Triassic to Early Jurassic arc-continent collision. Thrusting formed a prominent east-northeast-striking cataclastic foliation, as well as the McQuesten Anticline, the limbs of which dip north and south at a shallow angle (Boyle 1965; Fig. 2).

Felsic intrusions were emplaced in the metasedimentary rocks of the ancient continental margin in the mid-Cretaceous (83 to 108 Ma; biotite, K/Ar, Stevens et al. 1982) and coeval lavas were extruded (85 Ma; whole rock, K/Ar, Hunt and Roddick 1987; Fig. 2). Igneous rocks from the McQuesten River region have high initial Sr isotope ratios (generally over 0.71; Abercrombie 1990; Sinclair 1986) indicating addition of radiogenic Sr from sialic Precambrian crust.

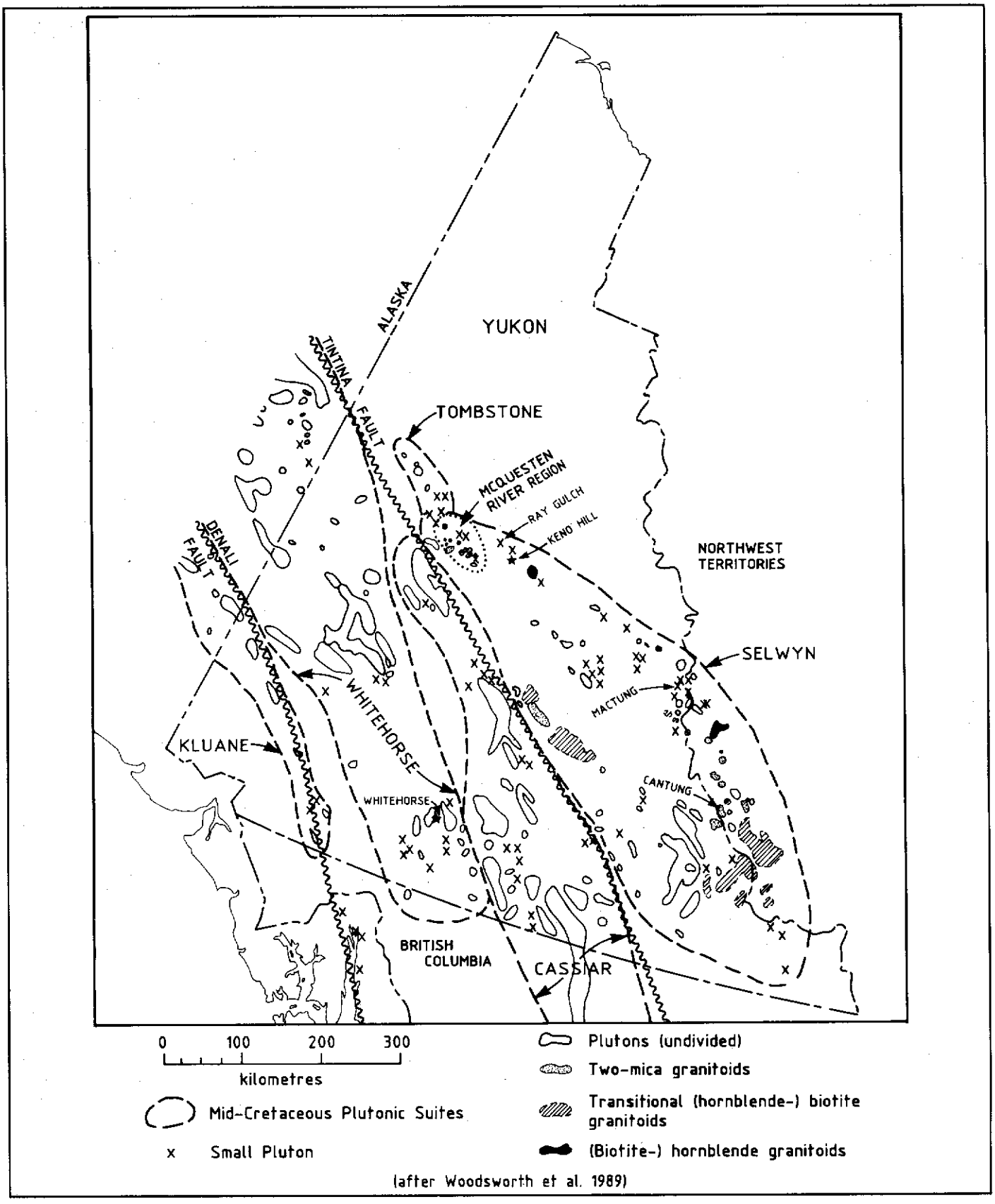

Figure 1. Location of the McQuesten River region and of mid-Cretaceous plutonic suites in Yukon (after Woodsworth et al. 1989).

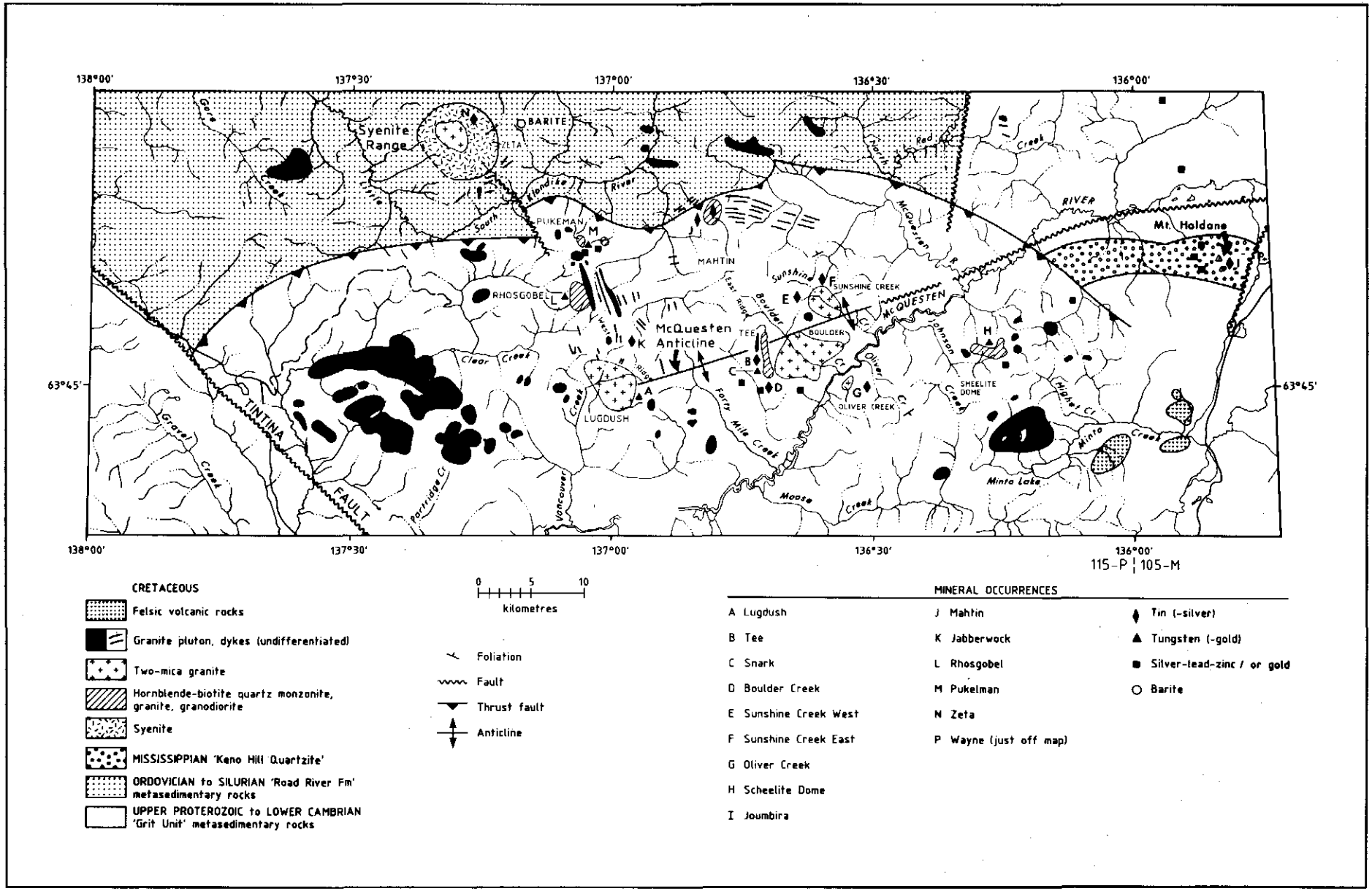

Figure 2. Geology and mineral occurrence map, McQuesten River region. Also shows distribution of two-mica granites, biotite-hornblende granitoids, hornblende-biotite syenites).

Field relations and regional geology show that the plutons were emplaced at a high level in Precambrian to Paleozoic sialic crust after a period of major deformation related to arc-continent collision. However, the coincidence of the suite along the McQuesten Anticline may indicate that some crustal warping was due to plutonism, and large batholiths may underlie the area.

CHARACTERISTICS OF INTRUSIONS

Stocks and plugs in the McQuesten River region outline two east-trending belts, a southern belt which follows the trend of the McQuesten Anticline, and a northern belt which follows the thrust faulted contact of the Hyland Group with the Road River Formation (Fig. 2).

Many of the intrusions are circular to subcircular in plan, and contacts with the surrounding metasedimentary rocks are discordant. Mineral foliation in the intrusions is restricted to and concordant with pluton margins. Xenoliths are uncommon except for large roof pendants in an intrusion near Minto Lake (Fig. 2) and fine grained diorite inclusions in some dykes. Contacts are sharp and in most cases plutons remain coarse grained to their margins, except the LUGDUSH (MINFILE 115P 009)[1] stock which has a fine-grained rim. Around the intrusions are contact aureoles of andalusite and/or biotite hornfels, calc-silicate hornfels, quartzite and minor tourmalinite.

Dykes are scattered through the metasedimentary rocks, and sheeted dyke systems also follow regional fault trends. One system in the MAHTIN (MINFILE 115P 007) area trends east-southeast, and another between JABBERWOCK (MINFILE 115P 051) and PUKELMAN (MINFILE 115P 013) trends north to north-northwest. Dykes also occur in the contact zones, both inside and outside the plutons. These dykes include tourmaline and muscovite-bearing aplites found in the endocontact zone at OLIVER CREEK (MINFILE 115P 030).

Intrusions are heterogeneous and commonly zoned from a more mafic rim to a more felsic core. This zoning is observed at ZETA (MINFILE 115P 047)(granite rimmed by syenite), SUNSHINE CREEK (MINFILE 115P 031)(granite rimmed by granodiorite), LUGDUSH (MINFILE 115P 009)(granite rimmed by dacite), BOULDER CREEK (MINFILE 115P 048) and TEE (MINFILE 115P 008a)(the BOULDER CREEK granite may be rimmed by the TEE granodiorite). Contacts between the zones vary from sharp to gradational. Rocks are medium to coarse-grained, and textures range from porphyritic to glomeroporphyritic, megacrystic and seriate.

There are three main groups of rocks. Biotite-muscovite ("two-mica") granite occurs in the southern belt (SUNSHINE CREEK (MINFILE 115P 031), BOULDER CREEK (MINFILE 115P 048), LUGDUSH (MINFILE 115P 009), OLIVER CREEK (MINFILE 115P 030) and JOUMBIRA (MINFILE 105M 031)). Biotite-hornblende quartz-monzonite, granite, and granodiorite are found mainly in the northern belt (at PUKELMAN (MINFILE 115P 013), RHOSGOBEL (MINFILE 115P 012), MAHTIN (MINFILE 115P 007), TEE (MINFILE 115P 008a) and SCHEELITE DOME (MINFILE 115P 004)). Hornblende-biotite syenite, quartz syenite, quartz monzonite, granite and tourmaline orbicular granite (ZETA (MINFILE 115P 047) zoned stock), and syenite dykes (MAHTIN (MINFILE 115P 007)), are confined to the northern belt. Intermediate and mafic rocks are rare.

PETROGRAPHY

Mineralogy and chemical composition separate the McQuesten plutonic belt into the three groupings described above. The following summary is based on petrographic descriptions of 50 samples of igneous rocks. Table 1 lists petrographic characteristics. Table 2 lists estimates of the mineral modes. Rocks were named according to Streckeisen (1973, Fig. 3).

(1) Two-mica Granite

Biotite-muscovite granite varies from allotriomorphic to hypidiomorphic granular and from equigranular to seriate or porphyritic. It contains mainly quartz and plagioclase, and locally K feldspar phenocrysts. Quartz and plagioclase are commonly glomerophyric, and K feldspar and quartz are megacrystic at LUGDUSH (MINFILE 115P 009). Myrmekite is common, especially in dyke rocks. Alteration includes sericitization of plagioclase, chloritization of biotite, and some microclinization and minor epidotization of the groundmass. Plagioclase varies from oligoclase to andesine and commonly shows concentric zoning. Inclusions of apatite, biotite and plagioclase occur in some plagioclase cores. Alkali feldspar phenocrysts consist of microperthitic orthoclase. Microcline is abundant in the groundmass of the JOUMBIRA (MINFILE 105M 031) plug, and is probably secondary. Quartz is strained, embayed, and has formed around phenocrysts. Interstitial biotite and muscovite consist of ragged, bent flakes. They occur both as separate grains and intergrown with each other. Pleochroic red-brown to light yellow biotite predominates. The biotite contains zircon inclusions with radiation haloes and minor apatite. Some muscovite is a fine grained alteration product, but other separate, medium sized grains appear primary (interstitial). It is pleochroic in shades of pink, clear and pale blue. Accessory minerals generally comprise less than 1 % of the rock and include apatite, zircon, tourmaline, fluorite, monazite, opaques and titanite. Euhedral to subhedral apatite is particulary abundant in the SUNSHINE CREEK (MINFILE 115P 031) stock where it reaches up to several per cent. Primary, concentrically-zoned tourmaline is abundant in the OLIVER CREEK (MINFILE 115P 030) plug, with orange-brown cores and blue rims (Emond 1985). Titanite occurs only in the SNARK (MINFILE 115P 008b) dyke. Associated fine to medium-grained porphryitic to equigranular dykes include aplite, rhyodacite and quartz latite. Quartz, plagioclase and K feldspar occur as phenocrysts, and minor biotite and muscovite occur in the groundmass. Quartz amgydules are found at SUNSHINE CREEK EAST

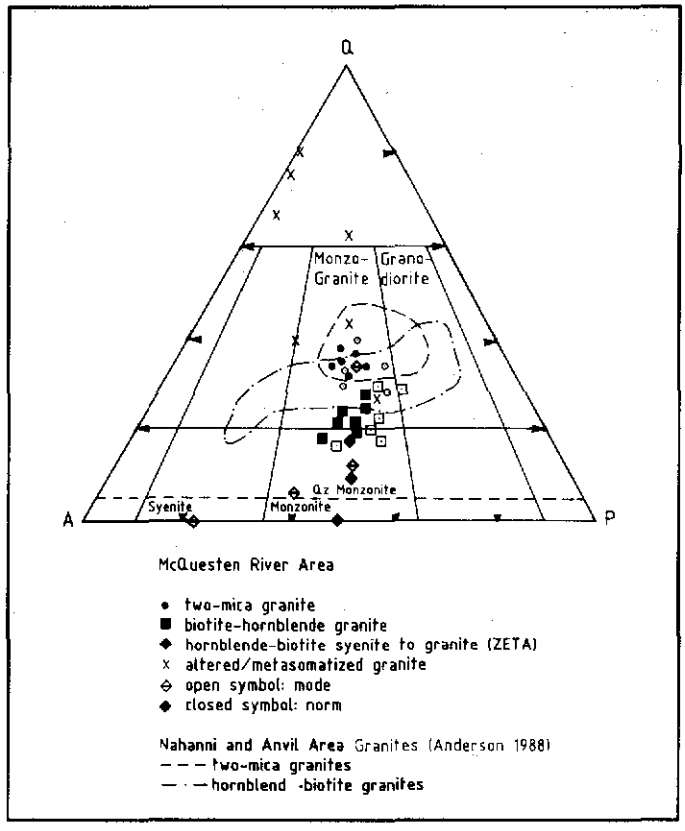

Figure 3. Quartz-orthoclase-plagioclase triangular diagram for felsic plutonic rocks of the McQuesten River region. Modes and normative composition are shown with the outline of the Streckeisen (1973) classification. Also shown is the outline of granitoids from the Selwyn Plutonic Suite (after Anderson 1988).

(MINFILE 115P 031b). Dykes are albitized, sericitized and tourmalinized at JOUMBIRA (MINFILE 105M 031) and OLIVER CREEK (MINFILE 115P 030), and sericitized and silicified at SUNSHINE CREEK (MINFILE 115P 031).

(2) Hornblende-Biotite Granite, Quartz Monzonite and Granodiorite

These rocks generally contain up to 20 % less modal quartz than the two-mica granites (Fig. 3). The hornblende-biotite granitoids are mainly hypidiomorphic and idiomorphic granular (locally allotriomorphic granular) and porphyritic. As well as normal phenocrysts of quartz, plagioclase and alkali feldspar, they contain perthitic K feldspar megacrysts, and quartz "clots" and glomerophyrs. Quartz phenocrysts commonly have square cross sections. Groundmass consists of perthite, plagioclase, hornblende, biotite and quartz in varying proportions. Myrmekite was not observed in these rocks. Alteration includes sericitization and microclinization of plagioclase, chloritization of biotite and hornblende, biotitization and epidotization of hornblende, uralitization of clinopyroxene, and minor secondary carbonate.

Plagioclase consists of slightly more calcic andesine, with more oscillatory zoning than in the two-mica granite. Alkali feldspar is mostly perthitic orthoclase, with minor replacement microcline. Quartz is strained.

Biotite and hornblende are interstitial and commonly intergrown. Biotite is more abundant than hornblende, and has higher absorption and cleaner edges than biotite in the two-mica granite. Pleochroism varies from chocolate brown to light yellowish brown at PUKELMAN (MINFILE 115P 013) and RHOSGOBEL (MINFILE 115P 012), to reddish brown at TEE (MINFILE 115P 008a) and SCHEELITE DOME (MINFILE 115P 004). Hornblende is mostly light brownish green to pale yellow, and also pinkish green and light bluish green, except at PUKELMAN and RHOSGOBEL, where it is grass green to pale yellow. Some hornblende is poikilitic, and some zoned. Up to 2% beige to clear pleochroic augite occurs with the hornblende and biotite.

Euhedral to subhedral accessory minerals include allanite, titanite, apatite, zircon, magnetite and other opaques. Locally, several percent titanite is associated with mafic minerals. Allanite is commonly twinned and has chlorite overgrowths.

Dykes are fine to coarse grained and porphyritic, with phenocrysts of plagioclase, perthite, quartz, hornblende and biotite. Composition varies mostly from quartz latite to latite. Alteration includes mainly chloritization of hornblende and some sericitization of plagioclase, but albite, carbonate, muscovite, epidote and tourmaline also occur as alteration minerals in places. Rare biotite-phyric lamprophyre occurs near SCHEELITE DOME (MINFILE 115P 004).

(3) Hornblende (-Biotite) Syenite, Quartz Syenite, Quartz Monzonite and Granite

These rocks form a zoned intrusion (ZETA; MINFILE 115P 047), in the Syenite Range. According to Abercrombie (1990), the modal composition of these rocks varies from syenite at the rim through quartz syenite and granite to tourmaline orbicular granite in the core. The present study showed variation from syenite to low-quartz quartz monzonite to quartz monzonite to tourmaline orbicular granite. Textures range from equigranular to porphyritic, with euhedral alkali feldspar phenocrysts.

In the syenite, plagioclase and hornblende are intersitial or occur along fractures. Nepheline occurs in the syenite as a late magmatic mineral along grain boundaries, and is commonly scarred by inclusion tracks. Late magmatic overgrowths of hornblende occur on clinopyroxene. A myrmekitic texture occurs along the margins of perthite phenocrysts. Alteration consists of K feldspathization of plagioclase, biotitization of hornblende, and late calcite.

The central part of the intrusion is perthite and plagioclase-phyric quartz monzonite to equigranular granite with a core of tourmaline orbicular granite. "Epitactic" texture, an intergrowth of K feldspar, tourmaline, interstitial quartz and sericitic plagioclase, is common in the orbicules

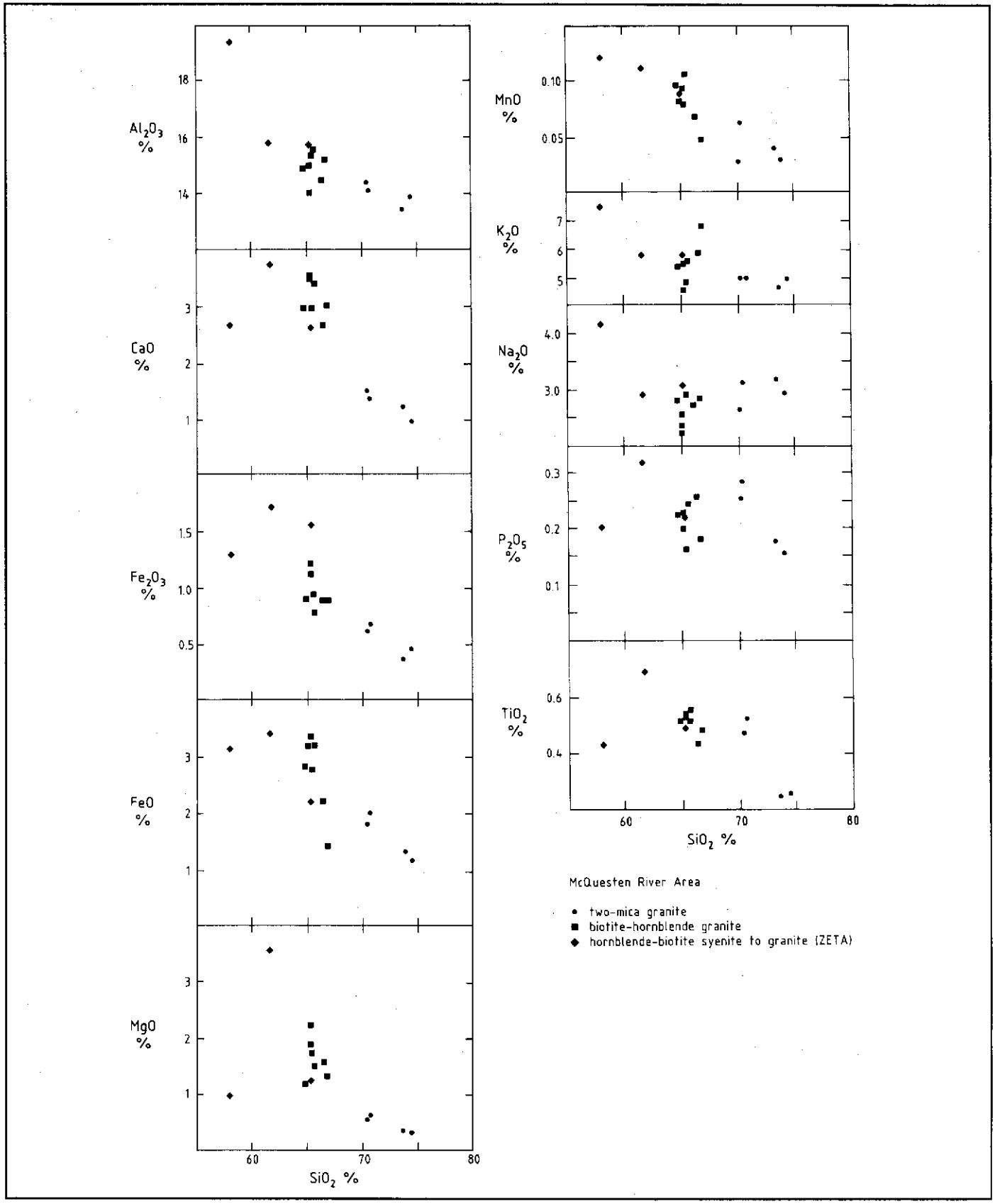

Figure 4a. Harker diagrams for felsic plutonic rocks of the McQuesten River region. (a) Major elements vs SiO_2.

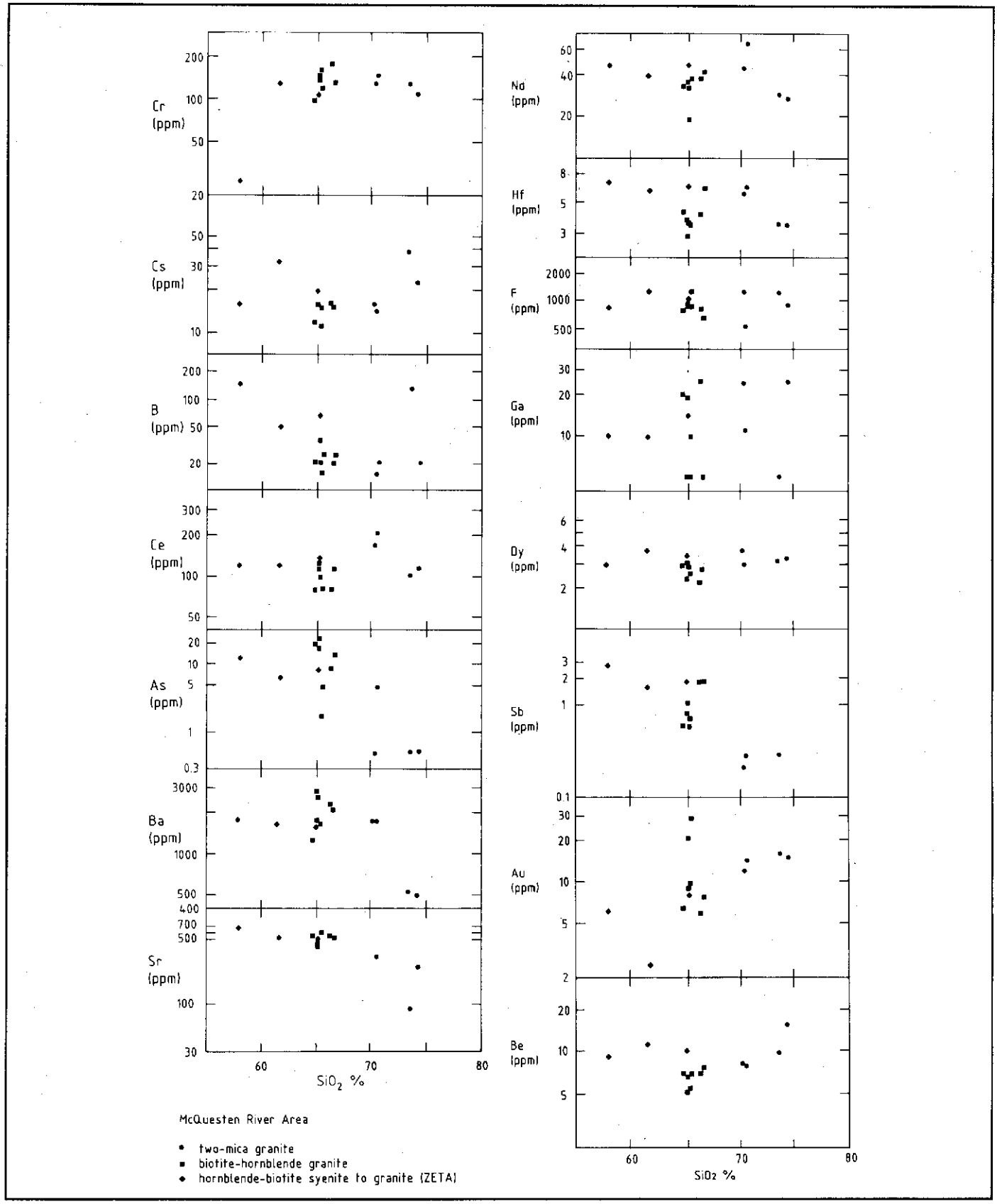

Figure 4b. Harker diagrams for felsic plutonic rocks of the McQuesten River region. (b). Minor and trace elements vs SiO_2.

which range up to 10 cm or more in diameter. Up to 1% tourmaline also occurs disseminated in the granite. The tourmaline includes both brown to black and blue to clear pleochroic varieties. Up to 2% muscovite occurs as free grains and as sericitic alteration of feldspar. Cassiterite is intergrown with the tourmaline.

Both the quartz monzonite and the quartz syenite (Abercrombie 1990) contain approximately 5% modal quartz and lie compositionally and spatially between the syenite and the quartz monzonite to granite core.

Petrographically, the hornblende-biotite syenite and quartz monzonite resemble the biotite-hornblende granitoids, and the granite resembles the two-mica granites (see sections 1 and 2). Points of similarity include mineral morphology and pleochroism. Alkali feldspar is perthite, and plagioclase is oligoclase or andesine. Hornblende predominates over biotite, and has strong absorption with dark green-brown to red-brown to yellow-green pleochroism, with a bright green variety in the granite. Biotite also shows strong absorption, with dark red-brown to light yellow-brown pleochroism in the syenite, and chocolate brown to light yellow-brown pleochroism in the granite. Up to 5% of the rock consists of medium to light brown pleochroic clinopyroxene, probably augite. Inclusion-rich augite cores are commonly overgrown by hornblende with a similar orientation. Euhedral to subhedral accessory minerals include tourmaline, muscovite, allanite, titanite, cassiterite, apatite, zircon and rutile. After tourmaline in the tourmaline-rich granite, allanite (up to 1%) is the most abundant accessory mineral. Tourmaline, muscovite and cassiterite occur mainly in the orbicular granite. According to Abercrombie (1990), the syenite and quartz syenite contain magmatic epidote, indicating lithostatic pressure of crystallization greater than 8 kbar (Zen and Hammerstrom, 1984).

Quartz-plagioclase porphyry dykes occur just inside the contact of the syenite intrusion at ZETA (MINFILE 115P 047). The dykes contain round quartz phenocrysts, and both biotite and muscovite are present. Greisenization, including abundant sericitization and tourmalinization, is common, especially near the tourmaline-rich tin-silver veins. Radiating aggregates of tourmaline needles, which locally make up more than 10% of the rock, are associated with cassiterite.

Sheeted porphyry dykes, including hornblende syenite, latite and quartz latite, occur near a hornblende-biotite intrusion at MAHTIN (115P 007). Phenocrysts consist mostly of alkali feldspar, plagioclase and hornblende, with minor quartz and biotite. Accessory minerals include augite and titanite, and minor zircon, apatite, epidote and calcite.

GEOCHEMISTRY

Twenty-five samples of plutons and dykes associated with tin and tungsten mineralization, some from each of the three groups of rocks outlined above, were analysed for major, minor, trace and some rare earth elements (Table 2).

Generally CIPW normative mineralogy is similar to modal estimates (Fig. 3). The two-mica granite, biotite-hornblende granite, and hornblende-biotite syenite are geochemically distinct. The more evolved phases from the core of the ZETA (MINFILE 115P 047) syenitic intrusion are similar to the hornblende-biotite granitoids and two-mica granites from the rest of the region. The phases grade from hornblende-biotite syenite to quartz monzonite to biotite-hornblende granite to two-mica granite. Harker diagram variation trends are irregular, although some useful patterns were recognized (Fig. 4). Some exceptions to trends noted below may be significant to individual plutons, but are not discussed here. All rocks are peraluminous (Shand index A/CNK = molar $Al_2O_3/(CaO + Na_2O + K_2O)$ greater than 1.0), but the two-mica granites have a slightly higher ratios (greater than 1.1; Fig. 5) than the hornblende-biotite granitoids.

In the following paragraphs, the term 'average' as applied to granite, granodiorite, syenite, etc. is based on analytical data published by Cox et al. (1979).

(1) Two-mica Granites

The two-mica granites are peraluminous, with higher SiO_2, K_2O and P_2O_5, and lower Fe_2O_3, MnO, MgO, CaO and Na_2O than 'average' granite. Analyses indicate 1.86 to 2.59% normative corundum and 2.34 to 4.09% hypersthene (Fig. 6). The sum of normative albite, orthoclase and quartz ("Differentiation Index" (D.I.) of Thornton and Tuttle, 1960) makes up 82 to 89% of the calculated norm, and normative anorthite ranges from 4.32 to 10.07%. Normative quartz, plagioclase and orthoclase are subequal, with slightly higher quartz. Average compositions are shown in Table 3. Harker diagram patterns are regular: SiO_2 and Na_2O (and trace elements Rb, Be, Sb, B, Cs, Au and Y) increase; and Al_2O_3, CaO, Fe_2O_3, FeO, MgO and TiO_2 (as well as Ba, Hf and Sr) decrease (Fig. 4a and 4b). This indicates that fractional crystallization probably controlled the formation of these granites. Analyses resemble those of low calcium, low magnesium, high potassium calc-alkaline granitoids (White and Chappell 1983). They also are similar in SiO_2, Al_2O_3, TiO_2, MnO and P_2O_5 content to the "tin granites" of the Seward Penninsula (Hudson and Arth 1983), but higher in K_2O, lower in Fe_2O_3 and Na_2O, and slightly lower in MgO and FeO.

(2) Hornblende-biotite Granitoids

Hornblende-biotite granite, quartz monzonite and granodiorite have levels of SiO_2, TiO_2, CaO, MgO, MnO and P_2O_5 similar to 'average' granodiorite, but much higher amounts of K_2O (Sb and Sr), and lower Na_2O, Al_2O_3, Fe_2O_3, Be, Au and Y (Fig. 4a and 4b). They are less evolved than the two-mica granites, with lower SiO_2, Na_2O+K_2O versus Fe-oxides, MgO, CaO, Rb, Y and Nb (Figs. 5, 7, 8 and Table 3), and higher levels of Ca, Fe and Mg oxides, TiO_2, MnO, Al_2O_3, Sr, Ba, Sb, As and Ba/Rb (Fig. 9, Table 3). Other distinguishing features include a lower D.I. (70 to 81%), higher normative pyroxene (3.42 to 9.43% hypersthene, up to 4.03% diopside), and zero normative corundum except at TEE (MINFILE 115P 008a) and SCHEELITE DOME

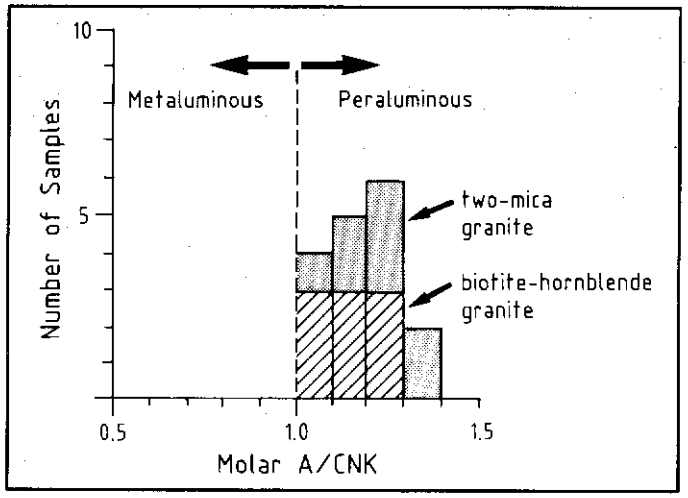

Figure 5. Shand Index diagram (histogram of molar $Al_2O_3/(CaO+Na_2O+K_2O)$.

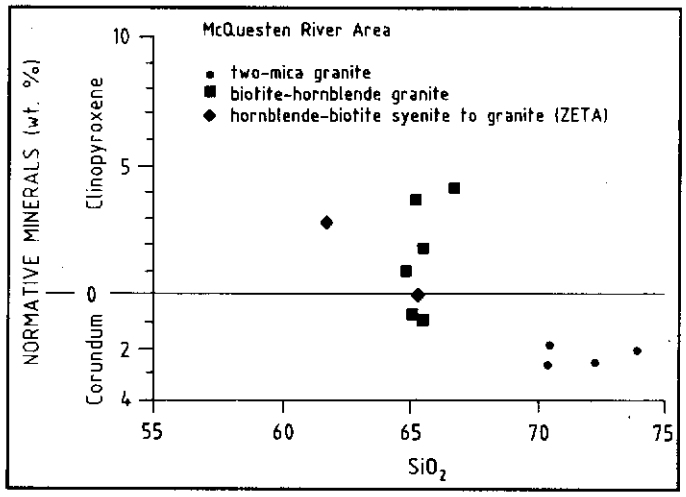

Figure 6. Normative clinopyroxene and corundum vs SiO_2.

(MINFILE 115P 004)(up to 0.89%). Internal variations are shown by Harker diagrams (Figs. 4a and 4b). SiO_2, K_2O and Na_2O increase, and CaO, FeO, MnO and TiO_2 decrease. Trace elements are less variable than in the two-mica granites.

(3) ZETA Zoned Intrusion (Syenite-Quartz Monzonite-Granite)

The D.I. for these rocks varies from 67 to 77%. A/CNK values are all surprisingly high, ranging from 1.09 to 1.15. Hornblende (-biotite) syenite is characterized by normative and modal nepheline, olivine, very minor corundum, and no pyroxene (Table 3). Modal SiO_2 and Na_2O resemble 'average' syenite, but Al_2O_3, CaO, K_2O and P_2O_5 are more similar to 'average' phonolite, except for FeO which is at least 1% higher, and TiO_2 which is slightly lower.

The quartz monzonite is characterized by 12.85% normative hypersthene and 2.9% diopside, and also has the highest normative magnetite and ilmenite of all rocks analysed. Its composition is mostly intermediate between the syenite and granite, although it has the lowest D.I. of the three. Chemically it is also similar to the hornblende-biotite granitoids.

The tourmaline orbicular granite in the core of the ZETA intrusion is not strictly comparable with the other granitoids, due to the high silica (78.5%) and boron (2850 ppm) content associated with the large orbicules (analysis not shown in Table 2). However, the interstitial granitic material resembles the two-mica granite in modal and trace element composition (Fig. 3). It appears to be slightly more evolved than the two-mica granite. The tourmaline orbicular granite shows several notable features when compared to other granitoids: (1) severe depletion of Ba, (2) depletion of Ce, Dy, F, Ga, Au, Hf, Nd, Sr and Y, and (3) enrichment in Sb.

Variation from syenite to quartz monzonite to granite corresponds to Harker trends, with increasing SiO_2 and decreasing MnO, but little variation in trace elements. Variation from syenite to quartz monzonite is marked by an increase in SiO_2, CaO, Fe_2O_3, FeO, MgO, P_2O_5 and TiO_2 and the trace elements Cs, Cr and F, and a sharp decrease in Na_2O, K_2O, Sb, As, B and Au. Variation from quartz monzonite to granite is marked by a decrease in SiO_2, CaO, Fe_2O_3, FeO, MgO, P_2O_5 and TiO_2, and an increase in Na_2O, B, Ga and Au. The variation in Ca, Fe, Mg, P and Ti is probably due to pyroxene, apatite and sphene fractionation.

Compared to both the two-mica and hornblende-biotite granitoids, the zoned syenite to quartz monzonite to granite intrusion contains similar amounts of As, Ba, F, Ga, Sr and Y, slightly higher amounts of Be, Sb, B, Ce, Cs, Dy, Hf and Nd; and slightly lower values of Cr and Au (Fig. 4b and Table 3). The quantities of Be, B, Ce, Cs and Dy in the ZETA intrusion rocks are similar to those in the highly evolved phases of the two-mica granites.

Rb-Ba-Sr Relationships

The two-mica granite is significantly enriched in Rb with respect to Ba and Sr compared to the hornblende-biotite granite, with the core of the SUNSHINE CREEK (MINFILE 115P 031) intrusion being the most enriched (Fig. 9). The Ba/Sr and Ba/Rb ratio increases in the hornblende-biotite granites and syenites from the less evolved PUKELMAN, RHOSGOBEL (MINFILE 115P 012) and ZETA (MINFILE 115P 047) intrusions, through the MAHTIN (MINFILE 115P 007) intrusions, to the more evolved TEE (MINFILE 115P 008a) and SCHEELITE DOME (MINFILE 115P 004) intrusions. The latter intrusions have similar Ba/Sr and Ba/Rb ratios to the least evolved of the two-mica granites.

RARE EARTH ELEMENTS

The following rare earth elements (REE's) were analysed: La, Ce, Nd, Sm, Eu, Gd, Tb, Dy, Yb and Lu (Table 2).

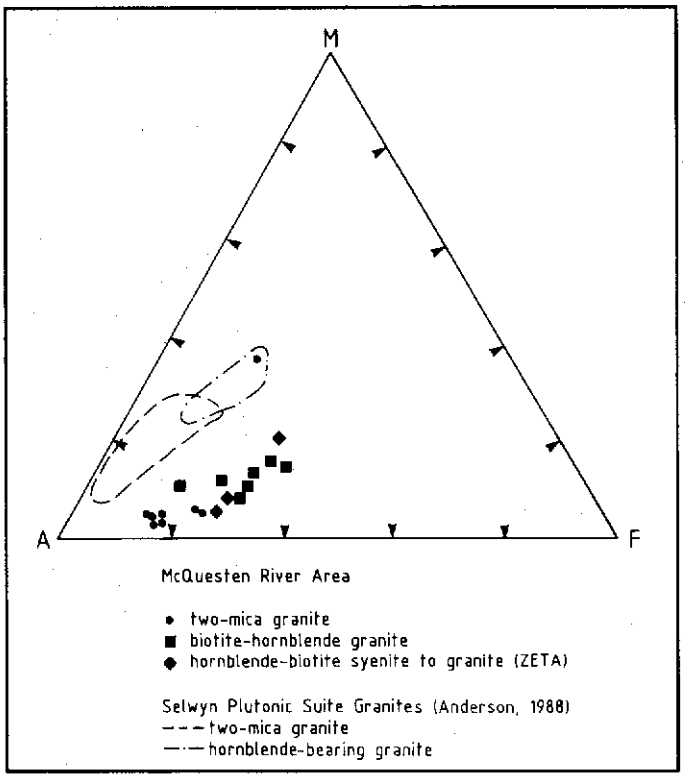

Figure 7. AFM diagram (triangular, Na_2O+K_2O vs Fe_2O_3+FeO vs MgO).

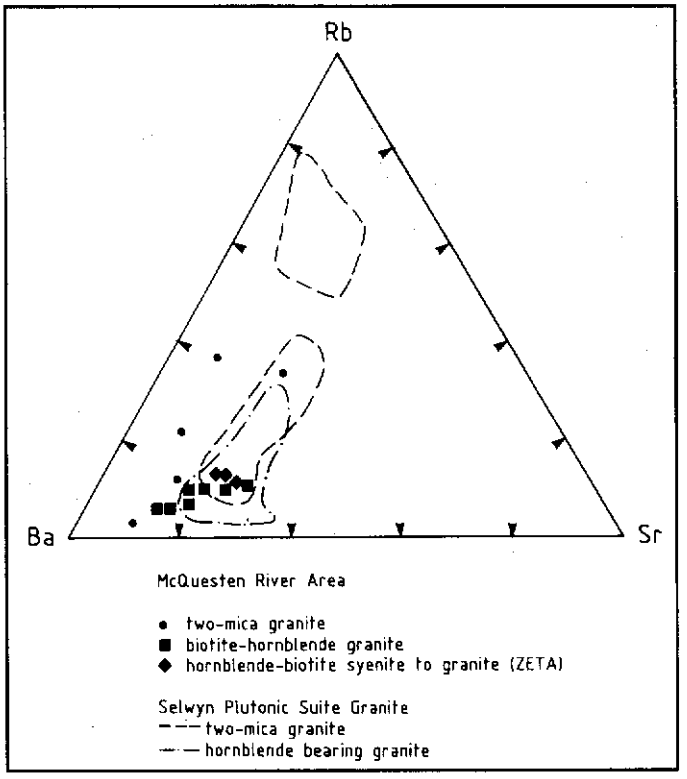

Figure 9. Rb-Ba-Sr triangular diagram (ratios of ppm quantities).

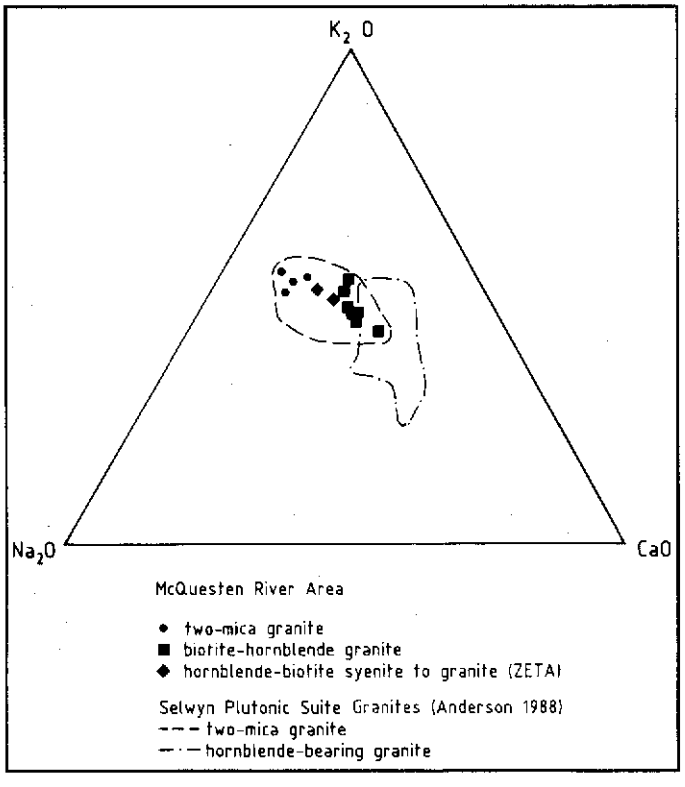

Figure 8. Na_2O-K_2O-CaO triangular diagram.

Chondrite normalized graphs were used as an aid to interpretation (Fig. 10). However, due to the detection limits of Eu and Gd (2 ppm and 200 ppm, respectively), the graphs are abnormal, with a positive Gd anomaly but no negative Eu anomaly.

All patterns have negative slopes showing light rare earth (LREE) enrichment, and lower abundances of heavy rare earths (HREE). The following rock types are listed in decreasing order of LREE enrichment: (1) two-mica granite from LUGDUSH (MINFILE 115P 009); (2) two-mica granite from the rim of SUNSHINE CREEK (MINFILE 115P 031), syenite and quartz monzonite from ZETA (MINFILE 115P 047), hornblende-biotite granodiorite from TEE (MINFILE 115P 008a), hornblende-biotite granite from RHOSGOBEL (MINFILE 115P 012) and PUKELMAN (MINFILE 115P 013), and two-mica granite from the core of SUNSHINE CREEK (MINFILE 115P 031); (3) two-mica rhyodacite dyke from JOUMBIRA (105M 031), sericitized dacite rim of LUGDUSH (MINFILE 115P 009)(hornblende-biotite), and rhyodacite dykes from SNARK (MINFILE 115P 008b), ZETA (MINFILE 115P 047), SUNSHINE CREEK WEST (MINFILE 115P 031) and WAYNE (MINFILE 105M 029). The third group shows less LREE enrichment and slightly more HREE depletion. The rim of the SUNSHINE CREEK pluton is enriched in LREE relative to the core. This is explained by fractionation of apatite, which forms more than

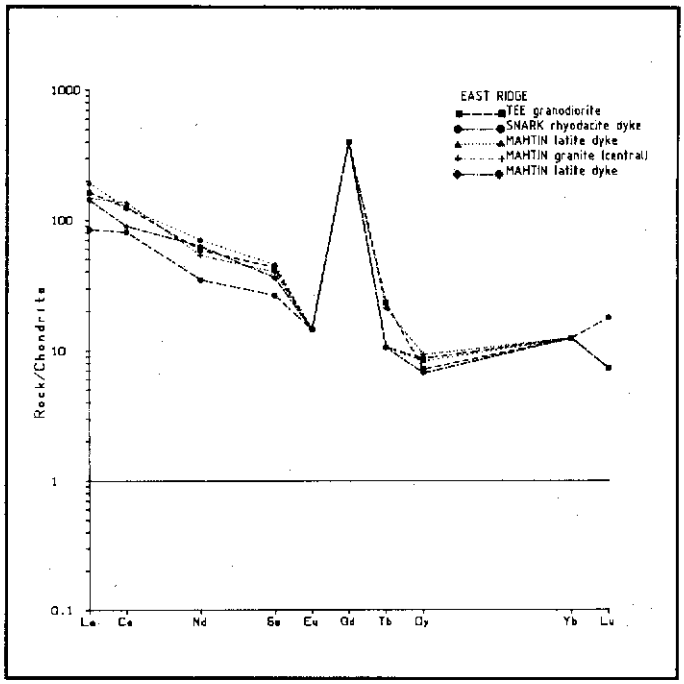

Fig. 10a Chondrite-normalized rare earth element diagram: East Ridge.

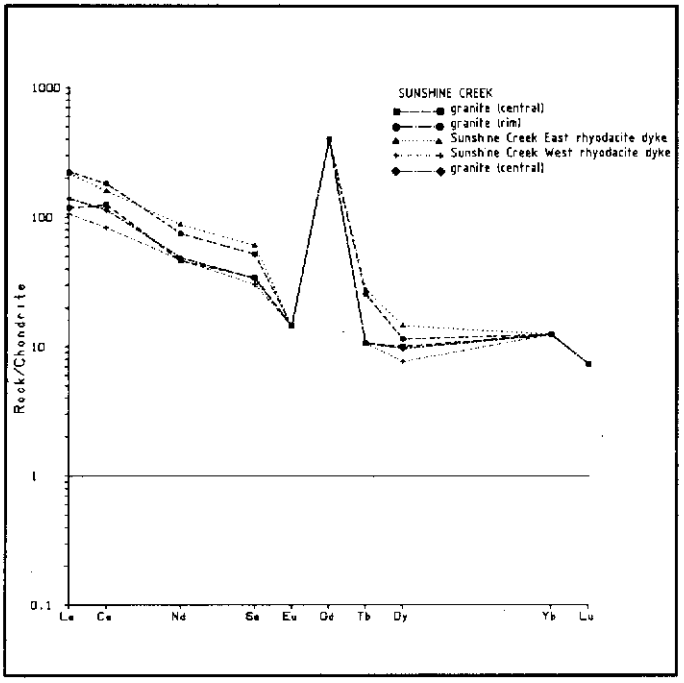

Fig. 10b Chondrite-normalized rare earth element diagram: Sunshine Creek.

2% of the rim. Most phases of the zoned syenite to granite intrusion at ZETA are similar, but the orbicular granite is relatively depleted in HREE, an indication of its highly evolved nature.

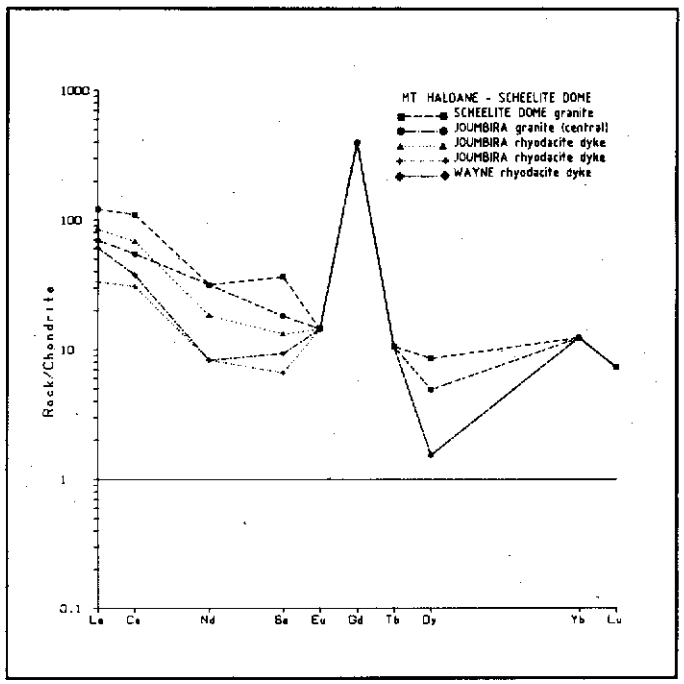

Fig. 10c Chondrite-normalized rare earth element diagram: Mt. Haldane & Scheelite Dome.

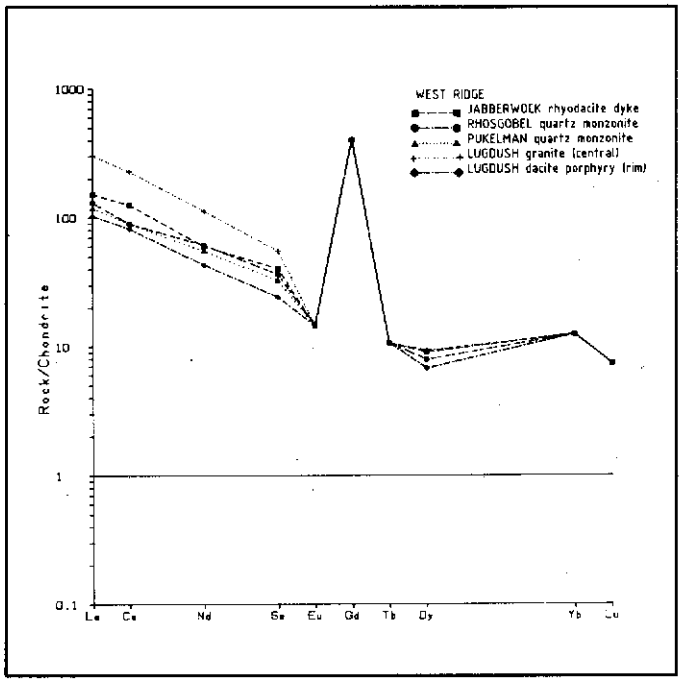

Fig. 10d Chondrite-normalized rare earth element diagram: West Ridge.

INCOMPATIBLE AND RARE EARTH VARIATION AS AN AID TO TECTONIC INTERPRETATION

Pearce et al. (1984) used trace element variations to distinguish between granites from different tectonic settings. They defined a granite as any plutonic rock containing more

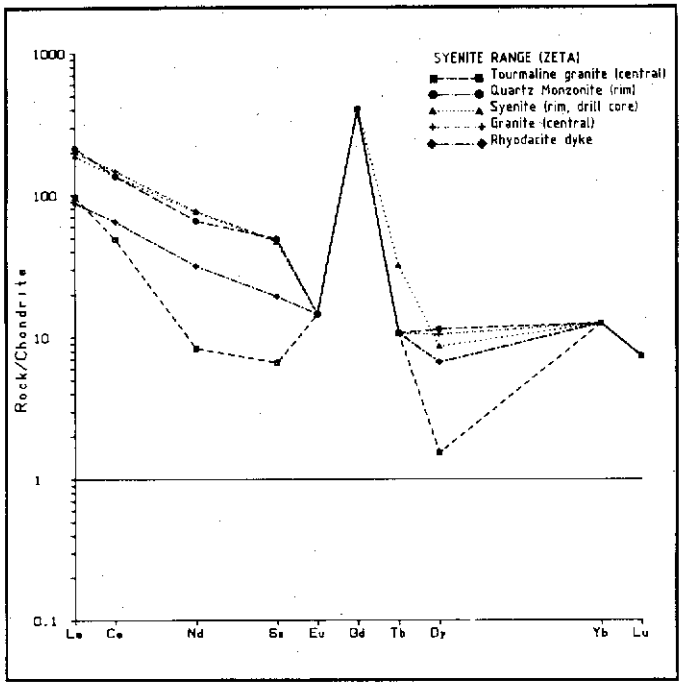

Fig. 10e. Chondrite-normalized rare earth element diagrams from Syenite Range (Zeta).

than 5% modal quartz. The following four groups of granites were established: (1) ocean ridge (ORG), (2) volcanic arc (VAG), (3) within plate (WPG), and (4) collision (COLG) granites. These groups were further subdivided according to their precise setting: for instance the latter group was divided into syn- and post-COLG's. "Using ORG-normalized geochemical patterns and element-SiO_2 plots ... most granite groups exhibit distinctive trace element characteristics ... Post-collision granites present the main problem of tectonic classification, since their characteristics depend on the thickness and composition of the lithosphere involved in the collision event and on the precise timing and location of magmatism. Provided they are coupled with a consideration of geological constraints, however, studies of trace element compositions can clearly help in the elucidation of post-Archean tectonic settings." (Pearce et al. 1984, p. 956).

Elements included in the diagrams are restricted to those thought to behave incompatibly during fractionation of MORB to felsic composition. The rare earth elements are represented by Ce, Sm and Yb. In the diagrams, the elements are plotted in order of increasing incompatibility during MORB genesis (from Yb to Rb). Flat patterns (near unity) reflect granite with a simple genetic history: derived from convecting upper mantle, derived from a basalt parent by fractional crystallization, or unaffected by crustal melting, assimilation or volatile-dominated processes. Deviations from these flat patterns indicate a more complex genetic history for the granite.

ORG-normalized diagrams for the McQuesten plutonic rocks are shown in Figures 11a-e. Some examples of collision and volcanic arc granites from Pearce et al. (1984) are shown in Figures 11f-h. The McQuesten rocks show patterns similar to "collision" and Chilean "volcanic arc" granites. All of the samples have very high values which are 30 to 90 times the norm, (a feature typical of evolved granites), high Rb and Th compared to Ta and Nb, with Th to Ta ratios ranging from 5:1 to 50:1 (typical of "crust-dominated" plutons), and a general increase in the trace elements from Yb to Rb. Several patterns also show negative Ba anomalies, and/or positive Ce and Sm anomalies with respect to adjacent elements, another "crust-dominated" feature.

Negative Ba anomalies are characteristic of two-mica granites at SUNSHINE CREEK (MINFILE 115P 031) and LUGDUSH (MINFILE 115P 009). The rim of the SUNSHINE CREEK (MINFILE 115P 031) pluton is similarly depleted in barium with respect to the core. This is consistent with Ba depletion in the magma at a late stage in the differentiation process. The syenite from ZETA (MINFILE 115P 047) shows a pattern similar to the other granites, but without the Ba anomaly. The hornblende-biotite granites show a consistent decrease from Rb to Ba to Th, or a slight positive Ba anomaly.

Positive Ce and Sm anomalies occur in the two-mica granite at LUGDUSH (MINFILE 115P 009), but are absent in the centre of the SUNSHINE CREEK (MINFILE 115P 031) stock. The latter is probably due to apatite crystallization in the rim causing depletion of LREE in the residual magma. Positive Ce and Sm are also associated with in hornblende-biotite granite at SCHEELITE DOME (MINFILE 115P 004), TEE (MINFILE 115P 008a) and MAHTIN (MINFILE 115P 007).

Some positive Zr anomalies are present in hornblende-biotite granites at RHOSGOBEL (MINFILE 115P 012), PUKELMAN (MINFILE 115P 013) and SCHEELITE DOME (MINFILE 115P 004), and in tourmaline orbicular granite and dyke rock from ZETA (MINFILE 115P 047). This can be explained by accumulation of zircon crystals at more mafic compositions (Pearce et al. 1984).

Hornblende-biotite syenite and granite from ZETA (MINFILE 115P 047), MAHTIN (MINFILE 115P 007), PUKELMAN (MINFILE 115P 013) and RHOSGOBEL (MINFILE 115P 012)(the northern belt), have a lesser Th:Ta ratio, and are richer in Nb than other granites (both hornblende-biotite and two-mica granites), indicating a less crust-dominated origin.

A rhyodacite dyke and the central two-mica granite plug at JOUMBIRA (MINFILE 105M 031), and the dacite rim of LUGDUSH (MINFILE 115P 009) each show a positive Ba anomaly, very low Y and a slight Zr anomaly. The positive Ba and low Y could be due to alteration, since the feldspar is commonly sericitized.

The general similarities in these trace element patterns and abundances suggest that melted sedimentary rocks formed the entire McQuesten plutonic belt. Even rocks which show evidence of alteration or metasomatism in thin section show strikingly similar trace element patterns.

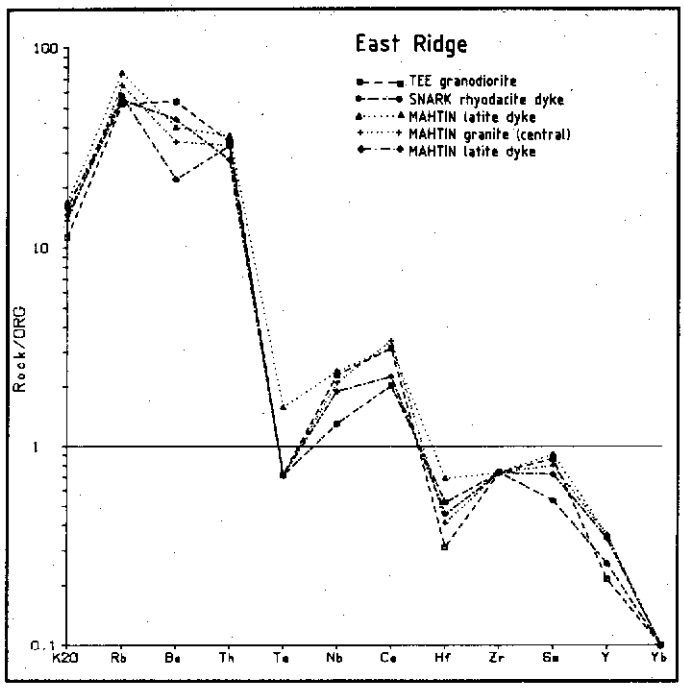

Fig. 11a.

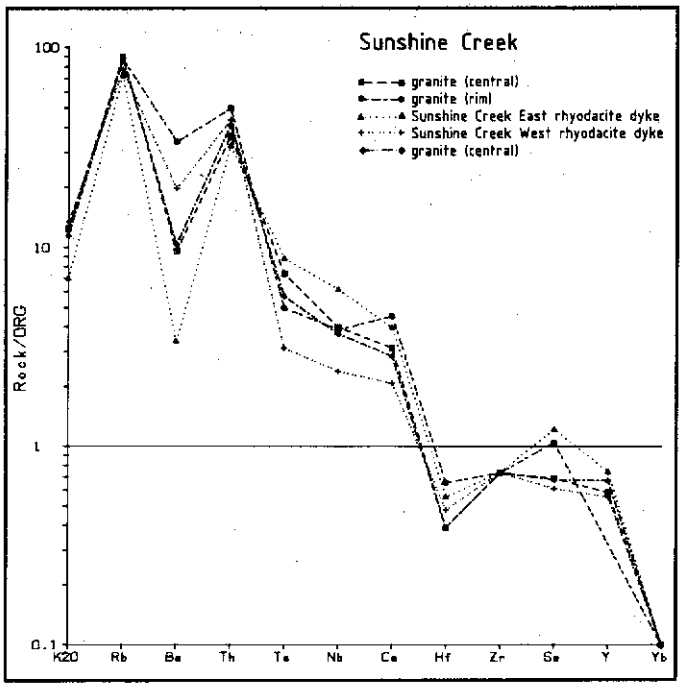

Fig. 11b.

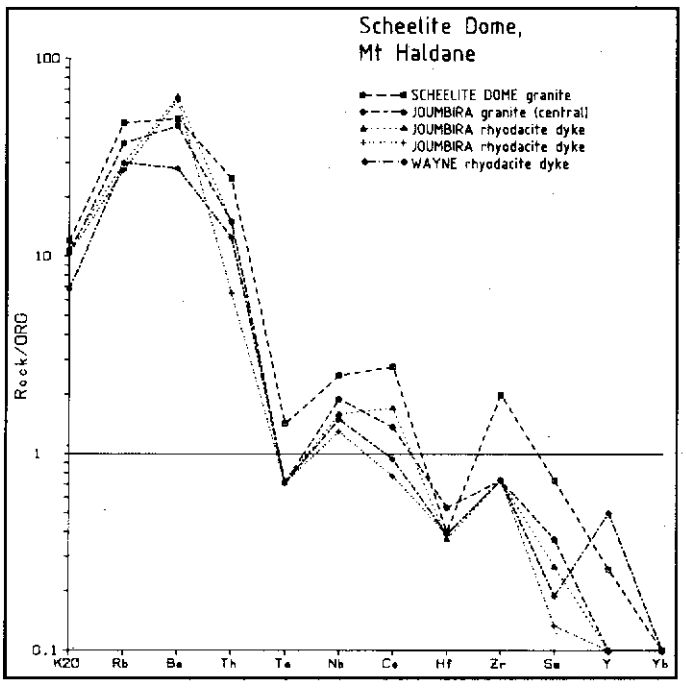

Fig. 11c.

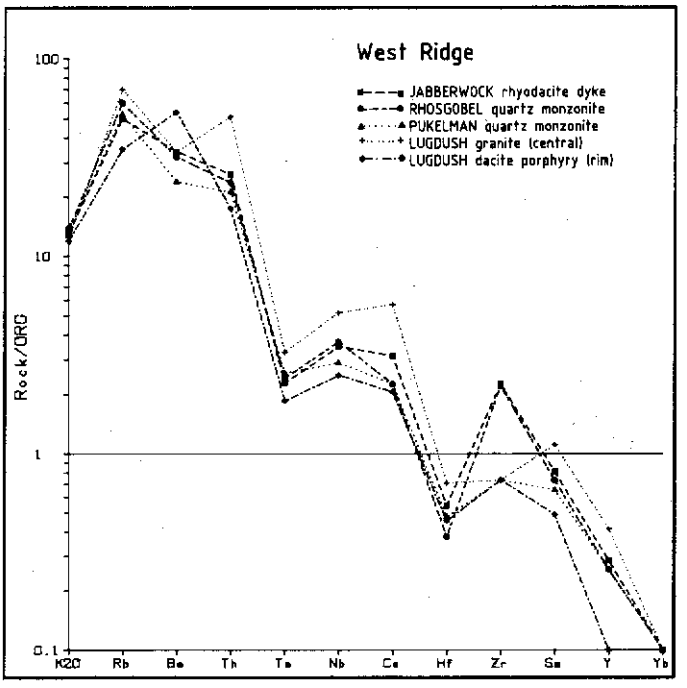

Fig. 11c.

Figure 11. Ocean Ridge-normalized diagrams for trace elements (normalized according to values given by Pearce et al. (1984)) for felsic plutonic rocks from the McQuesten River region. (a) East Ridge, (b) Sunshine Creek, (c) Mt Haldane and Scheelite Dome; (d) West Ridge.

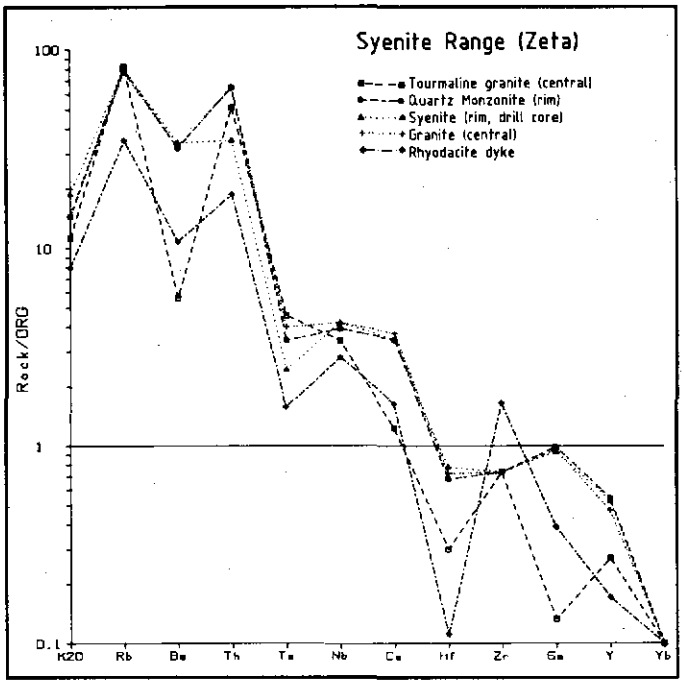

Fig. 11e.

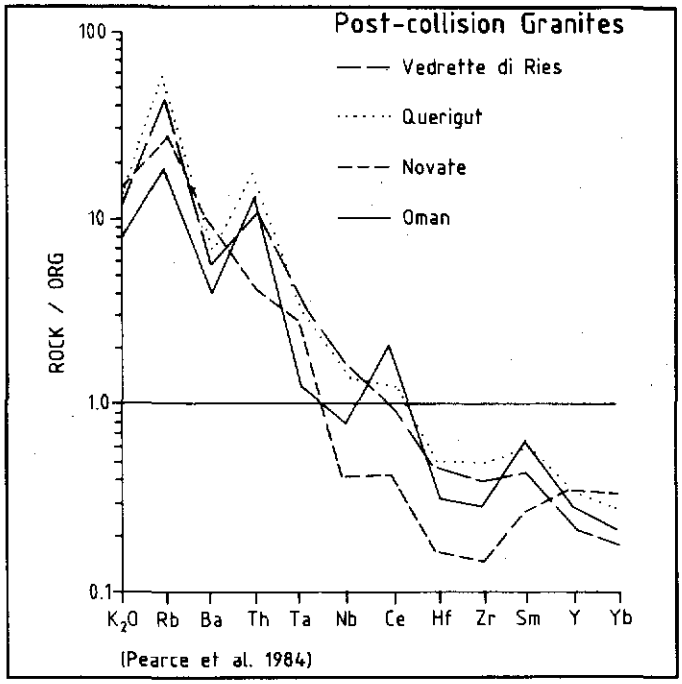

Fig. 11f.

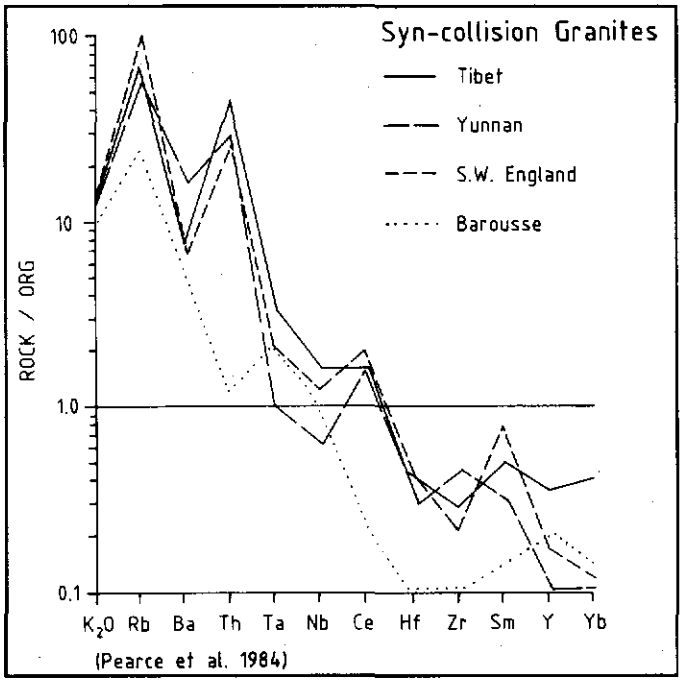

Fig. 11g.

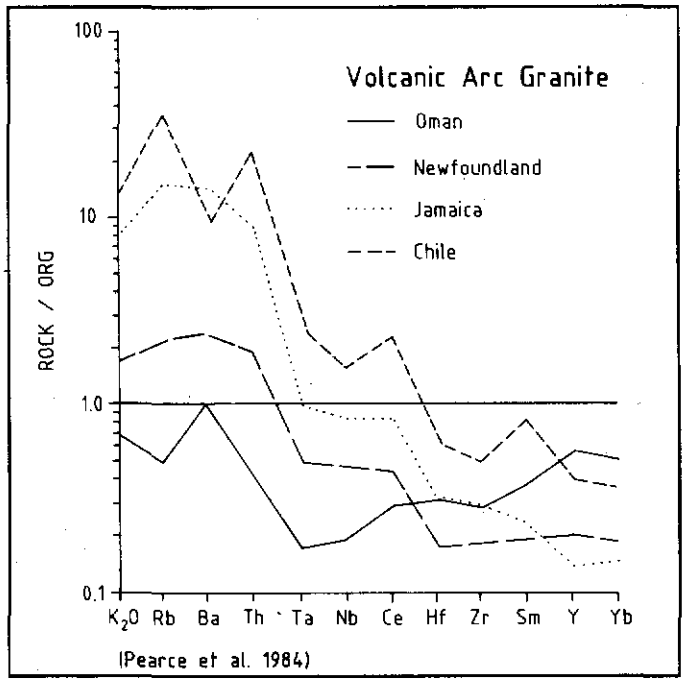

Fig. 11h.

Figure 11. Ocean Ridge-normalized diagrams for trace elements (normalized according to values given by Pearce et al. (1984)) for felsic plutonic rocks from the McQuesten River region. (e) Syenite Range (Zeta); and examples from Pearce et al. (1984): (f) Post-collision granites, (g) Syn-collision granites, and (h) Volcanic arc granites.

Trace Element Variation Diagrams used in Tectonic Interpretation

Pearce et al. (1984) were able to discriminate further between ocean ridge (ORG), volcanic arc (VAG), within plate (WPG) and collision (COLG) granites by graphing Y, Yb, Rb, Ta and Nb versus SiO_2, and also Nb vs Y, Ta vs Yb, Rb vs Y+Nb, and Rb vs Yb+Ta. McQuesten area samples plot mostly in the field of collision granites, but some show compositional similarity to within-plate granites. Calculated ratios of Y, Yb, Rb and Ta versus SiO_2, as well as the ratios Ta vs Yb and Rb vs Yb+Ta plot mostly within the COLG and VAG fields as expected (Fig. 12)[2]. However, Y vs SiO_2, and Nb vs Y diagrams show that samples from SUNSHINE CREEK (MINFILE 115P 031), ZETA (MINFILE 115P 047) and LUGDUSH (MINFILE 115P 009) have WPG affinities. Niobium is somewhat high compared to COLG, and samples plotted on an Nb vs SiO_2 graph almost all lie in the WPG and ORG fields (Fig. 12b). Most samples on the Rb vs Y+Nb diagram plot in the syn-COLG and VAG fields, but several fall near or within the WPG field (Fig. 12c).

Whalen et al. (1987) used Ga/Al ratios, various major element ratios and Y, Ce, Nb and Zr as discriminants in distinguishing A-type granites from M-, I- and S-type granites. Similar plots were made using analyses of McQuesten area plutonic rocks (Fig. 13). Two-mica granites mostly show Ga/Al ratios typical of I- and S-type granites, but a few plutons such as SUNSHINE CREEK (MINFILE 115P 031) have higher ratios more typical of fractionated felsic granites (Whalen et al., 1987). The biotite-hornblende granites gave lower (K_2O + Na_2O)/CaO and FeO/MgO ratios (Fig. 13a, b). Also K_2O + Na_2O, Zr, Ce and Zn values in some samples are higher than for most regular I- and S-type granites, again explainable by fractionation. Nb values are all higher than I- and S-types (Fig. 13c). Diagrams using the sum of Zr, Nb, Ce and Y on the abscissa were used similarly to Ga/Al plots. Due to high Nb and Y content, the samples plotted out of the field of OGT (unfractionated M-, I- and S-type granites), slightly toward the A type average (Fig. 13d). Most major element ratios, including FeO/MgO, (K_2O + Na_2O)/CaO, and Rb/Ba, plotted outside the OGT field. These granites are not believed to have an A-type origin, but it appears that fractionation has played an important role in their formation.

COMPARISON WITH SELWYN AND TOMBSTONE PLUTONIC SUITES

Intrusive phases similar to those in the McQuesten region occur in the Selwyn and Tombstone Plutonic Suites (Anderson 1987, 1988; Pigage and Anderson 1985). Composite and zoned syenites in the Selwyn Mountains are documented by Smit et al. (1985) and similar rocks in the Tombstone Mountains are documented by Anderson (1987).

Overall similarities

Points of overall geological similarity are listed in Table 4, and are summarized below: (1) The intrusions are post- to syn-tectonic. (2) They intrude upper Proterozoic to Jurassic, miogeoclinal metasedimentary host rocks. (3) They have a subcircular form indicative of forceful emplacement. (4) They have formed contact aureoles with andalusite and biotite (typical of shallow emplacement). (5) Some intrusions, especially syenitic plutons at Emerald Lake and in the Tombstone Range, show concentric zoning indicative of fractional crystallization in situ. (6) Each suite has bimodal characteristics, with the southernmost intrusions consisting oftwo-mica granite, and the northernmost intrusions consisting of less evolved biotite-hornblende granite. Bimodal characteristics of the Selwyn Plutonic Suite were documented by Anderson (1983). (7) Coeval volcanic rocks and dykes accompany the intrusions, for example the South Fork Volcanics in the Tay River area.

Petrographic similarities

Petrographic analysis shows the following similarities between the three different plutonic suites. (1) Modal compositions show that the two-mica granites are more quartz-rich, and more restricted in K feldspar:plagioclase ratio than the hornblende-biotite granites. McQuesten area granites are similar to the Nahanni and Anvil area granites as shown in Fig. 3, although batholiths in the Nahanni-Flat River area show less variation between phases, and include a "transitional phase" of two-mica granite with minor hornblende (Anderson 1988). (2) Igneous texture varies from hypidiomorphic to allotriomorphic granular in the two-mica granite, to hypidiomorphic and idiomorphic granular in biotite-hornblende granite. (3) Feldspar and quartz phenocrysts show similar morphology. Microperthitic orthoclase megacrysts are characteristic. (4) Biotite is ubiquitous as an accessory mineral. Other distinctive accessory minerals include muscovite in the two-mica granites, hornblende and minor clinopyroxene in the biotite-hornblende granites, and nepheline in the syenites. (5) Biotite has chocolate brown pleochroism in biotite-hornblende granites compared to reddish brown in the two-mica granites. Hornblende is a darker green to brown compared to pale green in the two-mica granites, and clinopyroxene is dark brown, compared to beige in the two-mica granites. (6) Other accessory minerals include apatite, zircon, allanite, titanite, and tourmaline. Monazite occurs mainly in the two-mica granites. Titanite, allanite and magnetite are mostly associated with the hornblende-biotite granites. Magnetite and titanite are confined to the syenite. (7) Inclusions of zircon and allanite in biotite are more abundant in the hornblende-biotite granite. (8) Myrmekitic (or granophyric) texture is particularly common in the two-mica granites.

Anderson (1988) described two-mica granites with minor hornblende, confined mainly to large batholiths in the southeastern part of the Selwyn Plutonic Suite, as "transitional". Their chemistry is intermediate between the hornblende-biotite and two-mica granites. Uncommon but

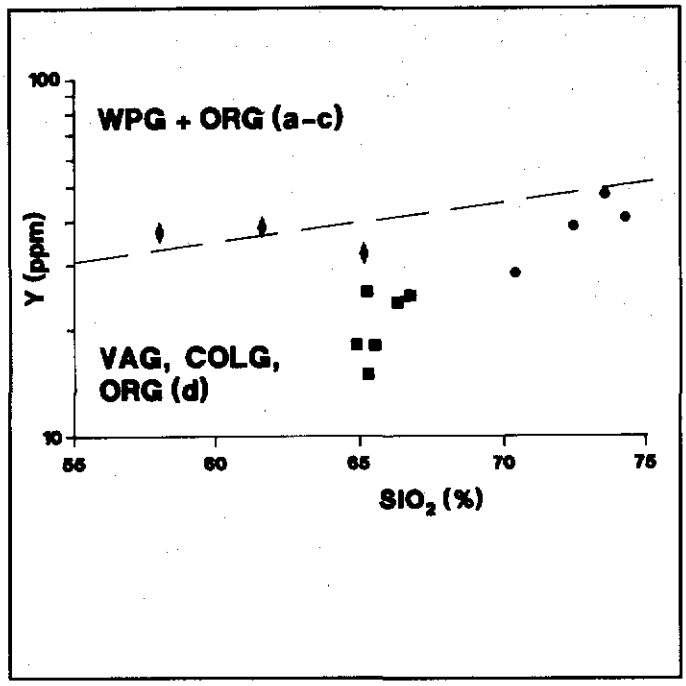

Fig. 12a.

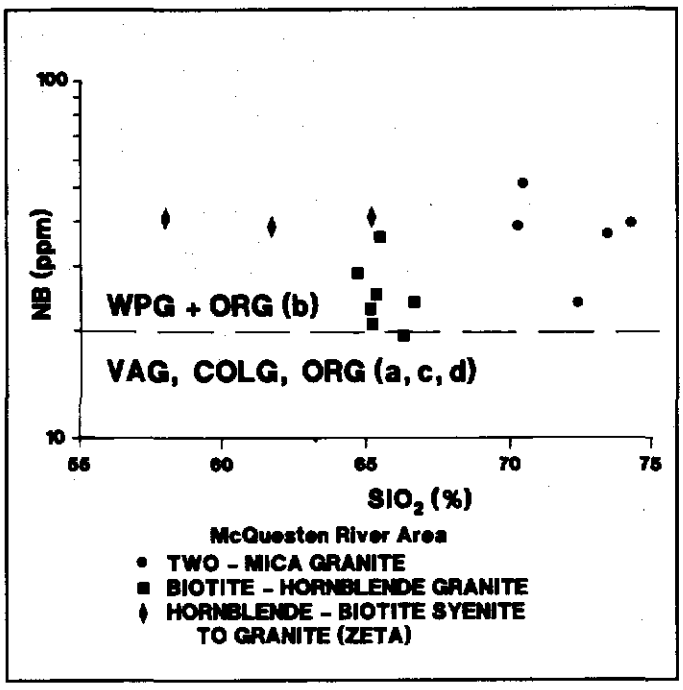

Fig. 12b.

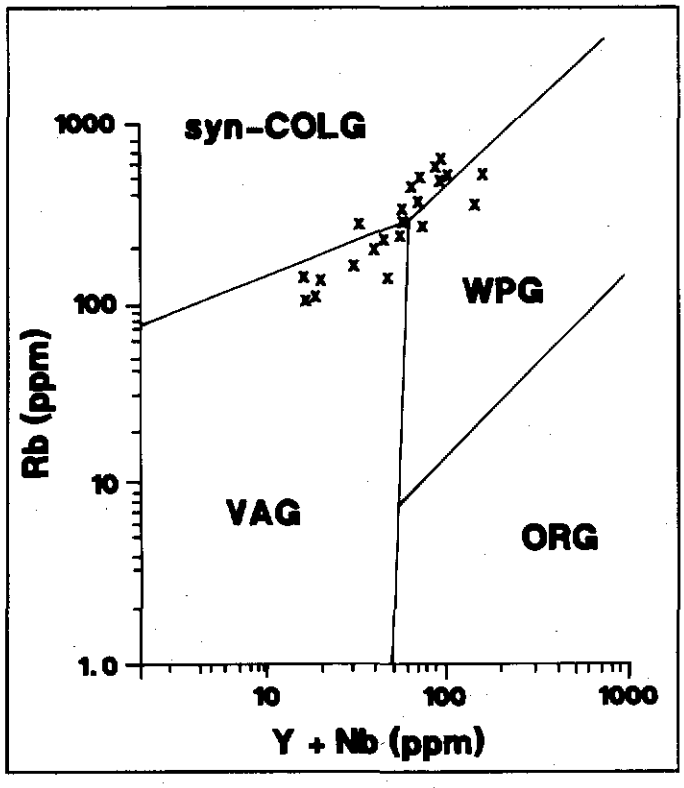

Fig. 12c.

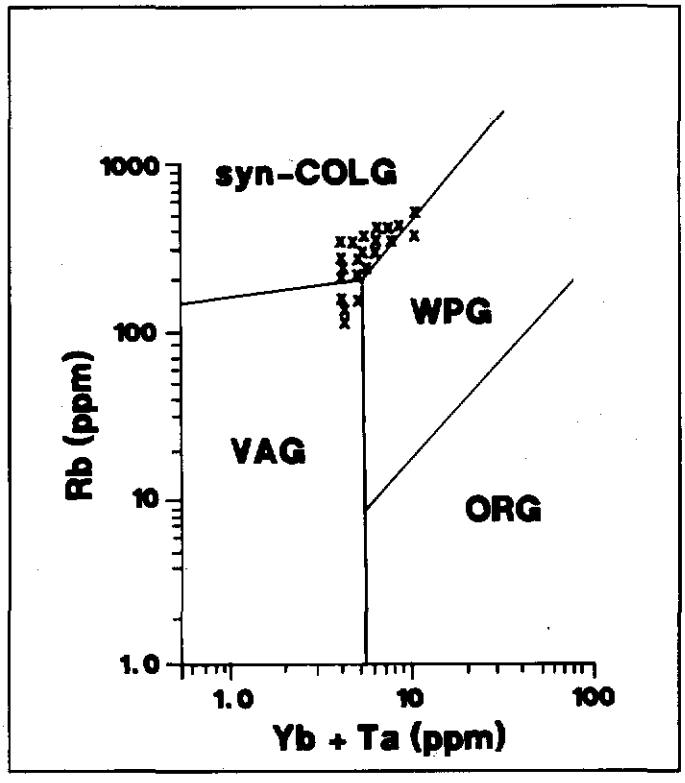

Fig. 12d.

Figure 12. Trace element diagrams for indicating tectonic origin of granites (fields as defined by Pearce et al. (1984)): (a) Y vs SiO_2, (b) Nb vs SiO_2, (c) Rb vs Y+Nb, (d) Rb vs Yb + Ta; Terms: WPG= within plate granites; ORG = ocean ridge granites; VAG = volcanic arc granites; COLG = collision granites.

Trace Element Variation Diagrams used in Tectonic Interpretation

Pearce et al. (1984) were able to discriminate further between ocean ridge (ORG), volcanic arc (VAG), within plate (WPG) and collision (COLG) granites by graphing Y, Yb, Rb, Ta and Nb versus SiO_2, and also Nb vs Y, Ta vs Yb, Rb vs Y+Nb, and Rb vs Yb+Ta. McQuesten area samples plot mostly in the field of collision granites, but some show compositional similarity to within-plate granites. Calculated ratios of Y, Yb, Rb and Ta versus SiO_2, as well as the ratios Ta vs Yb and Rb vs Yb+Ta plot mostly within the COLG and VAG fields as expected (Fig. 12)[2]. However, Y vs SiO_2, and Nb vs Y diagrams show that samples from SUNSHINE CREEK (MINFILE 115P 031), ZETA (MINFILE 115P 047) and LUGDUSH (MINFILE 115P 009) have WPG affinities. Niobium is somewhat high compared to COLG, and samples plotted on an Nb vs SiO_2 graph almost all lie in the WPG and ORG fields (Fig. 12b). Most samples on the Rb vs Y+Nb diagram plot in the syn-COLG and VAG fields, but several fall near or within the WPG field (Fig. 12c).

Whalen et al. (1987) used Ga/Al ratios, various major element ratios and Y, Ce, Nb and Zr as discriminants in distinguishing A-type granites from M-, I- and S-type granites. Similar plots were made using analyses of McQuesten area plutonic rocks (Fig. 13). Two-mica granites mostly show Ga/Al ratios typical of I- and S-type granites, but a few plutons such as SUNSHINE CREEK (MINFILE 115P 031) have higher ratios more typical of fractionated felsic granites (Whalen et al., 1987). The biotite-hornblende granites gave lower $(K_2O + Na_2O)/CaO$ and FeO/MgO ratios (Fig. 13a, b). Also $K_2O + Na_2O$, Zr, Ce and Zn values in some samples are higher than for most regular I- and S-type granites, again explainable by fractionation. Nb values are all higher than I- and S-types (Fig. 13c). Diagrams using the sum of Zr, Nb, Ce and Y on the abscissa were used similarly to Ga/Al plots. Due to high Nb and Y content, the samples plotted out of the field of OGT (unfractionated M-, I- and S-type granites), slightly toward the A type average (Fig. 13d). Most major element ratios, including FeO/MgO, $(K_2O + Na_2O)/CaO$, and Rb/Ba, plotted outside the OGT field. These granites are not believed to have an A-type origin, but it appears that fractionation has played an important role in their formation.

COMPARISON WITH SELWYN AND TOMBSTONE PLUTONIC SUITES

Intrusive phases similar to those in the McQuesten region occur in the Selwyn and Tombstone Plutonic Suites (Anderson 1987, 1988; Pigage and Anderson 1985). Composite and zoned syenites in the Selwyn Mountains are documented by Smit et al. (1985) and similar rocks in the Tombstone Mountains are documented by Anderson (1987).

Overall similarities

Points of overall geological similarity are listed in Table 4, and are summarized below: (1) The intrusions are post- to syn-tectonic. (2) They intrude upper Proterozoic to Jurassic, miogeoclinal metasedimentary host rocks. (3) They have a subcircular form indicative of forceful emplacement. (4) They have formed contact aureoles with andalusite and biotite (typical of shallow emplacement). (5) Some intrusions, especially syenitic plutons at Emerald Lake and in the Tombstone Range, show concentric zoning indicative of fractional crystallization in situ. (6) Each suite has bimodal characteristics, with the southernmost intrusions consisting oftwo-mica granite, and the northernmost intrusions consisting of less evolved biotite-hornblende granite. Bimodal characteristics of the Selwyn Plutonic Suite were documented by Anderson (1983). (7) Coeval volcanic rocks and dykes accompany the intrusions, for example the South Fork Volcanics in the Tay River area.

Petrographic similarities

Petrographic analysis shows the following similarities between the three different plutonic suites. (1) Modal compositions show that the two-mica granites are more quartz-rich, and more restricted in K feldspar:plagioclase ratio than the hornblende-biotite granites. McQuesten area granites are similar to the Nahanni and Anvil area granites as shown in Fig. 3, although batholiths in the Nahanni-Flat River area show less variation between phases, and include a "transitional phase" of two-mica granite with minor hornblende (Anderson 1988). (2) Igneous texture varies from hypidiomorphic to allotriomorphic granular in the two-mica granite, to hypidiomorphic and idiomorphic granular in biotite-hornblende granite. (3) Feldspar and quartz phenocrysts show similar morphology. Microperthitic orthoclase megacrysts are characteristic. (4) Biotite is ubiquitous as an accessory mineral. Other distinctive accessory minerals include muscovite in the two-mica granites, hornblende and minor clinopyroxene in the biotite-hornblende granites, and nepheline in the syenites. (5) Biotite has chocolate brown pleochroism in biotite-hornblende granites compared to reddish brown in the two-mica granites. Hornblende is a darker green to brown compared to pale green in the two-mica granites, and clinopyroxene is dark brown, compared to beige in the two-mica granites. (6) Other accessory minerals include apatite, zircon, allanite, titanite, and tourmaline. Monazite occurs mainly in the two-mica granites. Titanite, allanite and magnetite are mostly associated with the hornblende-biotite granites. Magnetite and titanite are confined to the syenite. (7) Inclusions of zircon and allanite in biotite are more abundant in the hornblende-biotite granite. (8) Myrmekitic (or granophyric) texture is particularly common in the two-mica granites.

Anderson (1988) described two-mica granites with minor hornblende, confined mainly to large batholiths in the southeastern part of the Selwyn Plutonic Suite, as "transitional". Their chemistry is intermediate between the hornblende-biotite and two-mica granites. Uncommon but

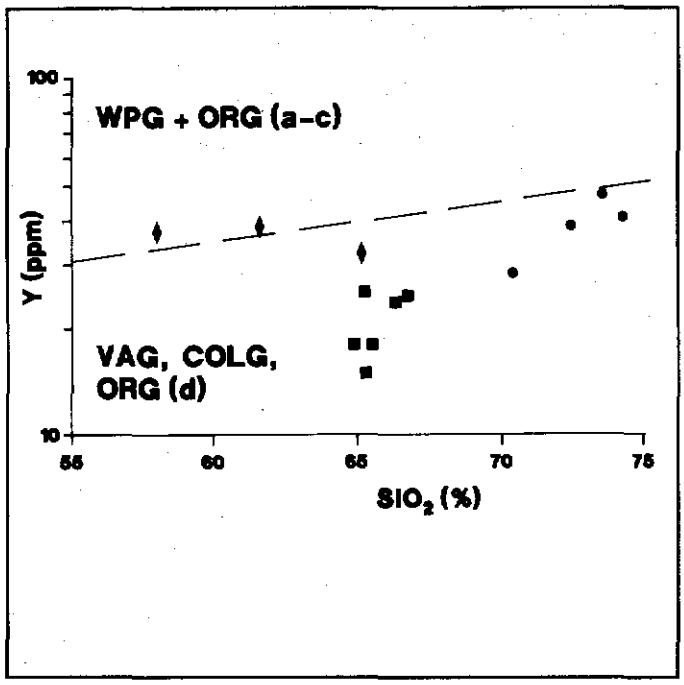

Fig. 12a.

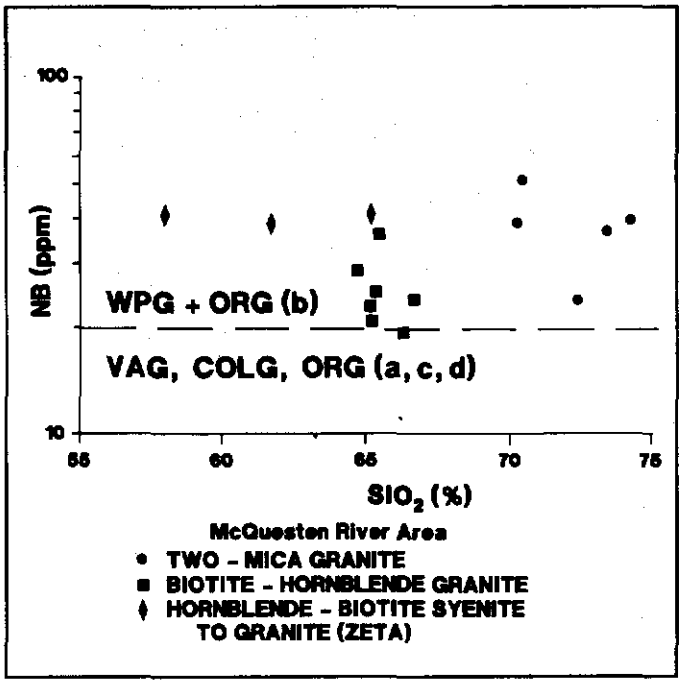

Fig. 12b.

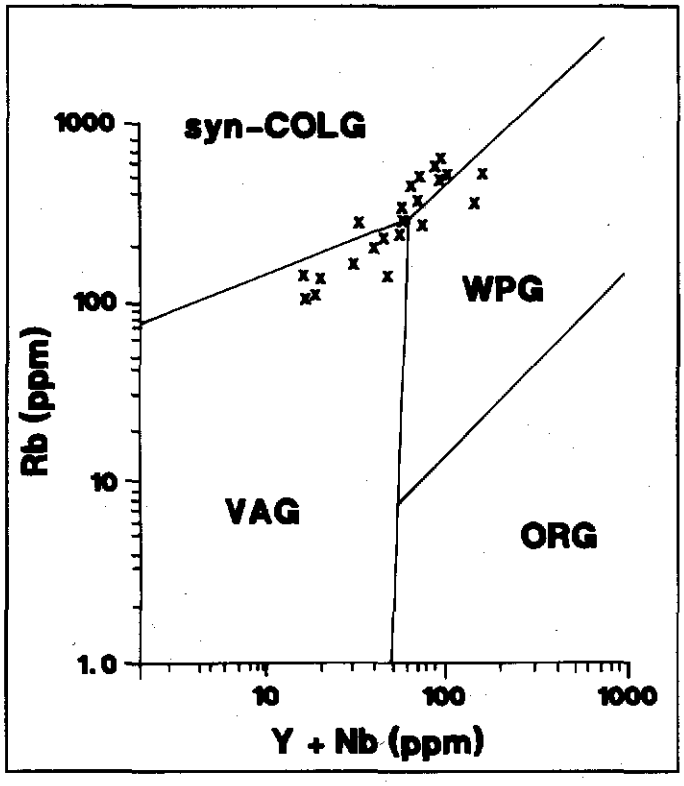

Fig. 12c.

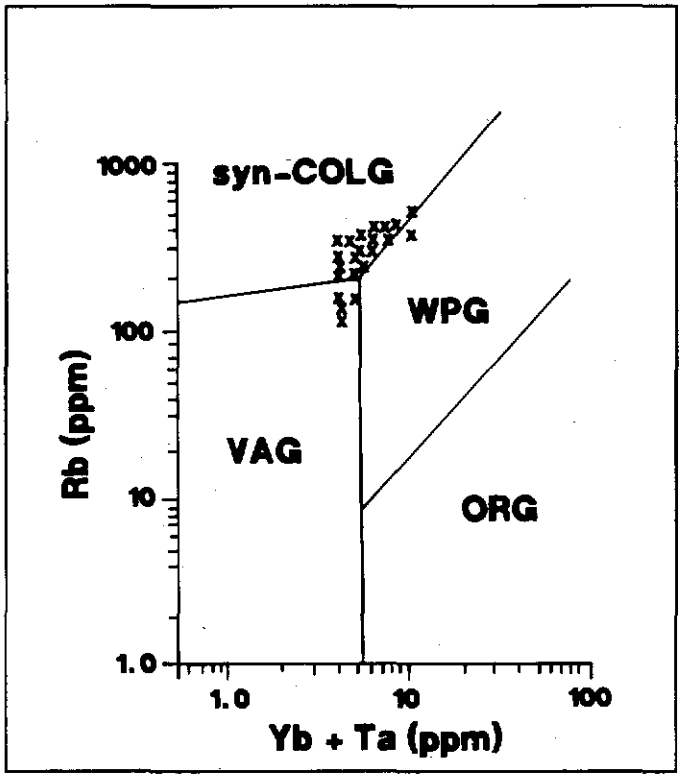

Fig. 12d.

Figure 12. Trace element diagrams for indicating tectonic origin of granites (fields as defined by Pearce et al. (1984)): (a) Y vs SiO_2, (b) Nb vs SiO_2, (c) Rb vs Y+Nb, (d) Rb vs Yb + Ta; Terms: WPG= within plate granites; ORG = ocean ridge granites; VAG = volcanic arc granites; COLG = collision granites.

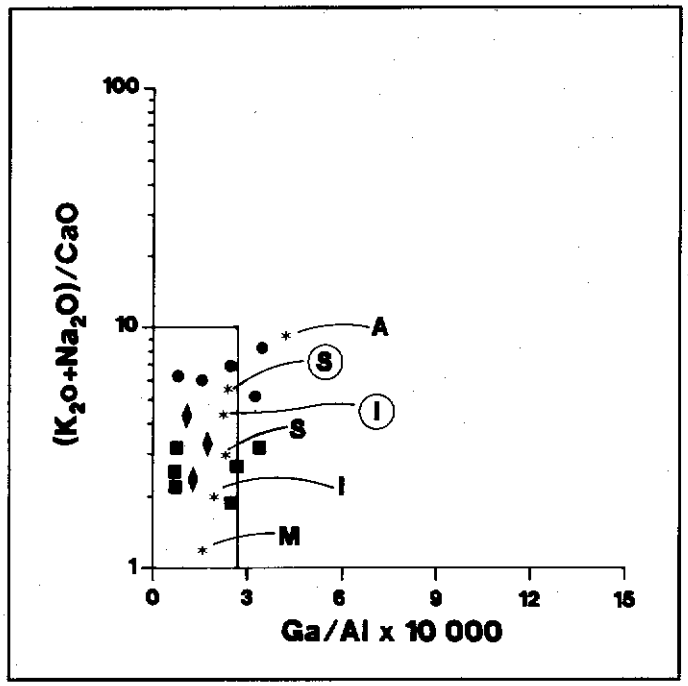

Fig. 13a. $(K_2O+Na_2O)/CaO$ vs Ga/Al*10000

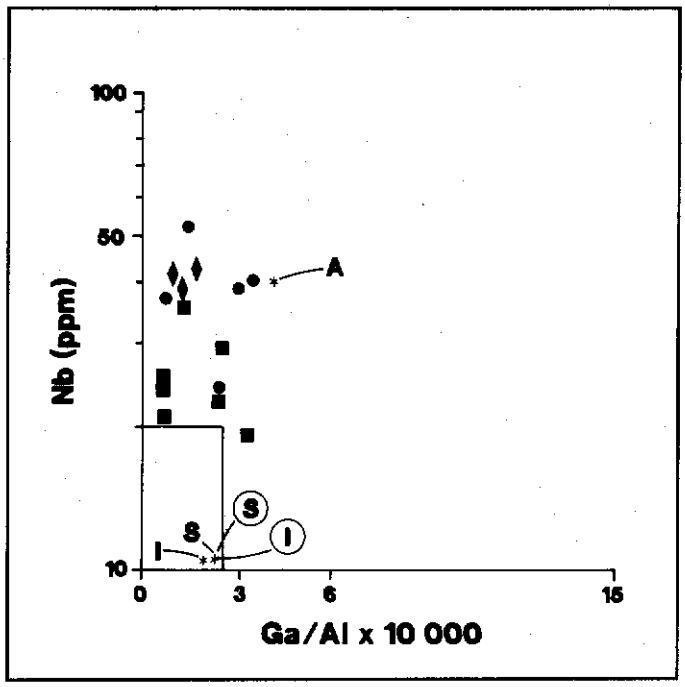

Fig. 13c. Nb vs Ga/Al*10000;

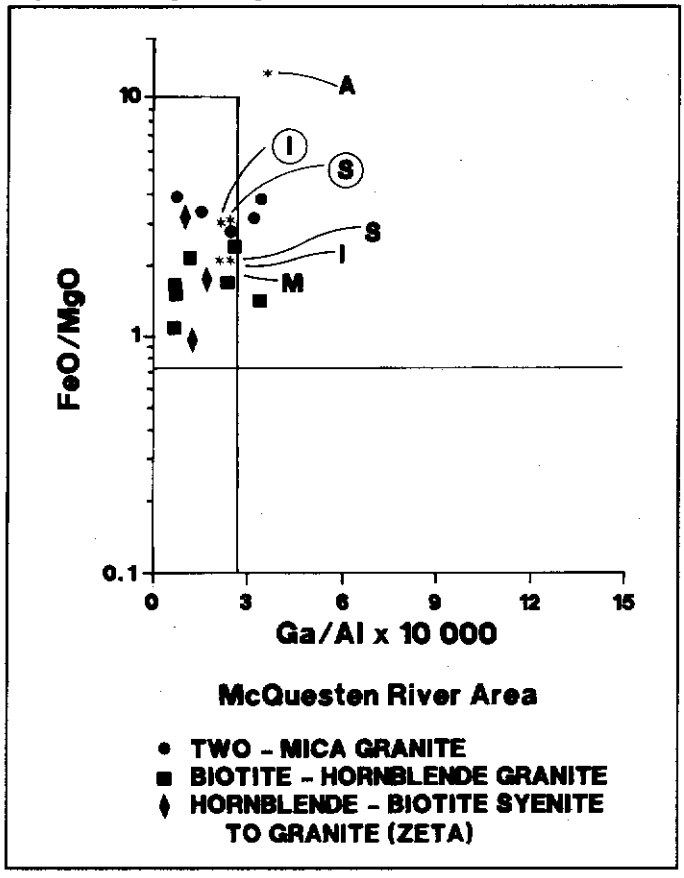

Fig. 13b. FeO/MgO vs Ga/Al*10000

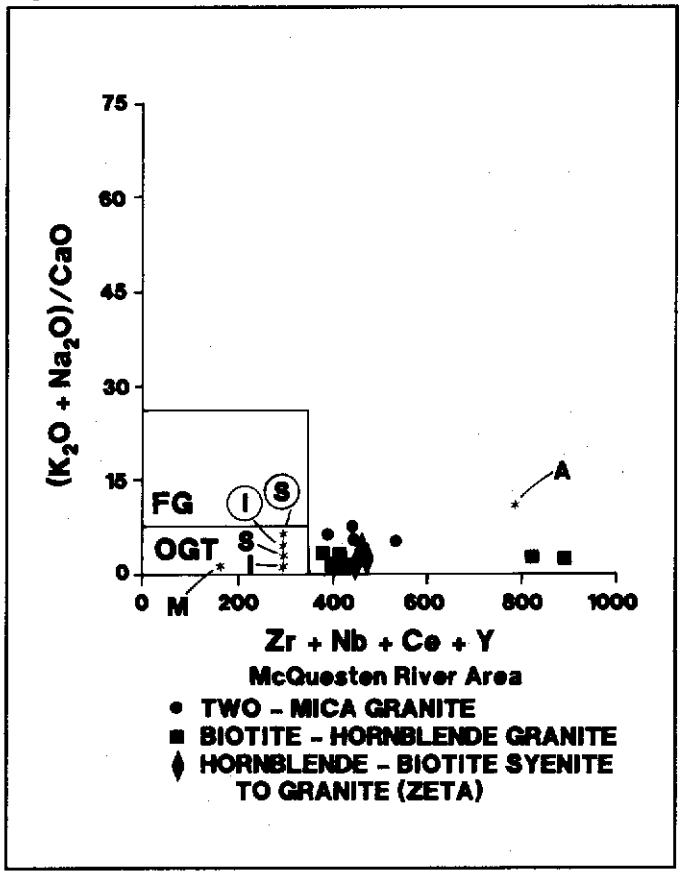

Fig. 13d. $(K_2O+Na_2O)/CaO$ vs Zr+Nb+Ce+Y.

Figure 13. Trace element diagrams for indication of petrogenesis (fields of OGT=unfractionated M, I and S granites; and FG=fractionated granites as defined by Whalen et al. (1987)). Average M, I, S and A types are shown by their respective letters; while fractionated I and S types are circled.

Apparently similar rocks occur in the McQuesten region, for instance on the margin of the LUGDUSH (MINFILE 115P 009) stock. This is a medium grained biotite-quartz-feldspar porphyry which contains sericite and chlorite pseudomorphs after hornblende, and has a composition intermediate between the two major granite types.

Petrographic characteristics of the McQuesten area rocks which are not recognized in the Selwyn Plutonic Suite include glomerophyric quartz and plagioclase, most notably in the two-mica granite, tourmaline orbicules (such as at ZETA (MINFILE 115P 047)), and microclinization and albitization of feldspar. These characteristics may indicate that the McQuesten granites are slightly more evolved.

Geochemical similarities

McQuesten area rocks show geochemical similarities to the Selwyn and Anvil suites (Gordey and Anderson, in press; Anderson 1988). (1) The two-mica granites contain normative corundum, while the hornblende-biotite granites contain normative clinopyroxene and little or no normative corundum. The syenites contain normative nepheline. (2) The two-mica and hornblende-biotite granites form two subalkaline groups, the former containing more than 70% silica and the latter, less than 67% silica (Fig. 14). The syenite and quartz monzonite are alkaline, similar to the Tombstone syenite. (3) The rocks are mainly subalkaline to calc-alkaline, and from hornblende-biotite to two-mica granite the composition shifts toward higher alkalis and lower Fe and Mg (Fig. 7). (4) The rocks have similar Na_2O to K_2O ratios which plot in the field of S-type granites. (5) They have similar Na_2O to K_2O to CaO ratios. Alkalis increase and calcium decreases from the hornblende-biotite to the two-mica granites (Fig. 8). (6) They have similar Rb-Ba-Sr relationships, except that some of the Selwyn two-mica granites have higher Rb values.

Differences:

There are some notable differences between the McQuesten granites and rocks of the Selwyn and Tombstone Suites. (1) Biotite-hornblende granites of the McQuesten region have a lower ratio of modal quartz to alkali feldspar and plagioclase than those in the Selwyn and Anvil regions (Fig. 3). (2) The McQuesten rocks are all peraluminous, whereas in the Selwyn and Anvil plutonic suites only the hornblende-biotite granite is metaluminous, and only the two-mica granite is peraluminous. (3) The McQuesten granites contain more iron compared to alkalis and magnesium (Fig. 7). (4) Unlike rocks of the Tombstone Suite which contain aegirine-augite, the McQuesten syenite and quartz monzonite intrusions entirely lack A-type characteristics.

DISCUSSION

Plutonic rocks in the McQuesten River region are generally bimodal, with two-mica granites in the south and hornblende-biotite granitoids and syenitoids in the north. There is a broad transition from hornblende-bearing nepheline syenite, to poorly evolved hornblende-bearing, clinopyroxene-normative biotite quartz monzonite, to granite, to more evolved, peraluminous, corundum-normative muscovite-bearing biotite granite (Fig. 3). The coexistance of all three of the above phases in the ZETA (MINFILE 115P 047) zoned intrusion suggests they form a comagmatic suite. This is supported by Rb-Ba-Sr trends. A primary trend of Ba enrichment is observed in the less evolved biotite-hornblende granites, and a secondary trend of Rb enrichment is seen in the more evolved two-mica granites. This is consistent with differentiation trends for felsic magmatic suites (Bouseily and Sokkary 1975). All phases of the McQuesten Plutonic Suite show similar patterns of trace elements (normalized to ocean ridge granite), providing further evidence of a comagmatic origin. These trace element patterns are doubly useful in that they have not been affected by alteration processes. The patterns recognized include high Ba and Th with respect to Ta and Nb, high Ce and Sm values with respect to adjacent elements, and an increase in abundance of trace elements from Yb to Rb. These trace element patterns are typical of collision and volcanic arc granites with a "crust-dominated" source. Other trace elements are consistent with this interpretation, except for slightly elevated Nb and Y values which are more typical of granite originating within a plate. The original magmas were probably melts of, or melts contaminated by, sialic lower crustal material. Rb/Sr ratios greater than 0.71 reported by Abercrombie (1990), and Kuran (1982) support this conclusion.

Crustal trace element patterns such as a lower Th:Ta ratio and higher Nb values are more characteristic of the two-mica granites and the hornblende-biotite granitoids of the southern belt than of hornblende-biotite granitoids of the northern McQuesten belt. The hornblende-biotite granitoids in the south even have positive Ce and Sm anomalies, whereas those in the north do not.

High Rb and negative Ba anomalies indicate the highly evolved nature of the two-mica granites in the southern belt. Lower Rb and less negative Ba anomalies are apparent in the less evolved biotite-hornblende phase, especially in the north.

Two-mica granites from the McQuesten region have typical S-type characteristics. For instance, they are peraluminous, have K_2O greater than Na_2O (Fig. 15), relatively low TiO_2, and FeO greater than Fe_2O_3 (Fig. 16). However, the biotite-hornblende granitoids contain less SiO_2 and show petrographic features (e.g., darker, chocolate brown biotite) more similar to 'I-type' granites of the Selwyn Plutonic Suite (Gordey and Anderson, in press). Any A-type characteristics, i.e. a few high Ga/Al ratios and high Zr+Nb+Ce+Y values (due to high Nb and Y), are likely due to fractionation of S-, or I-type magmas.

Major metals are also partitioned between the two main igneous phases in the McQuesten River region. Tin-(silver) mineralization is associated with the two-mica granite at OLIVER CREEK (MINFILE 115P 030), SUNSHINE CREEK (MINFILE 115P 031), BOULDER CREEK (MINFILE 115P 048) and JOUMBIRA (MINFILE 105M 031) in the southern belt, and ZETA (MINFILE 115P 047) in the northern belt, while tungsten (-gold) mineralization is associated with

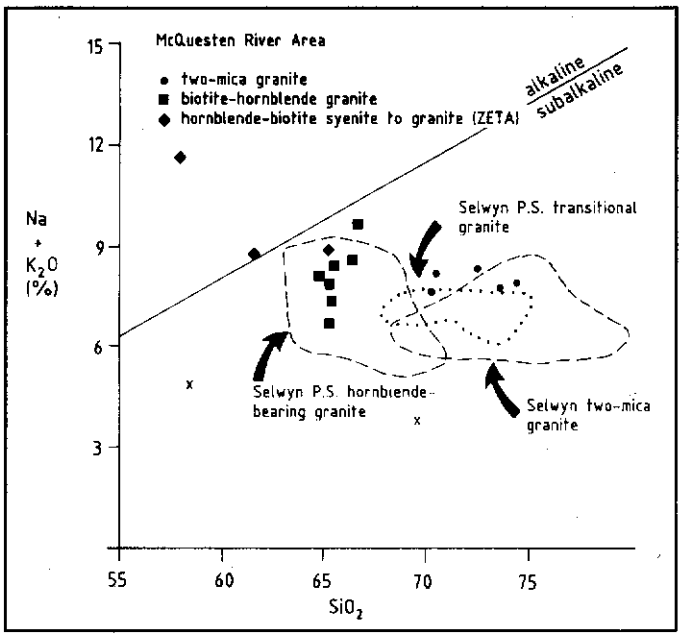

Figure 14. Na_2O+K_2O vs SiO_2 of McQuesten River plutonic rocks. Outline of composition of granites from the Selwyn Plutonic Suite (after Anderson 1988) is also shown.

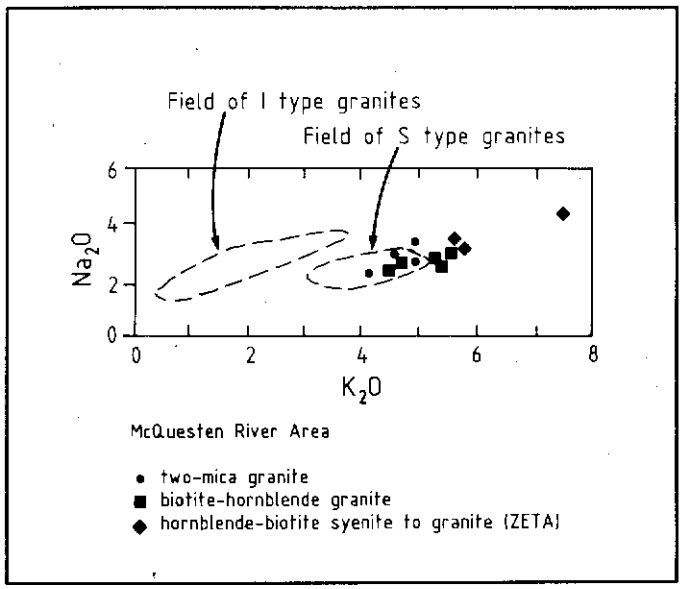

Figure 15. Plot of Na_2O vs K_2O for I and S type granites.

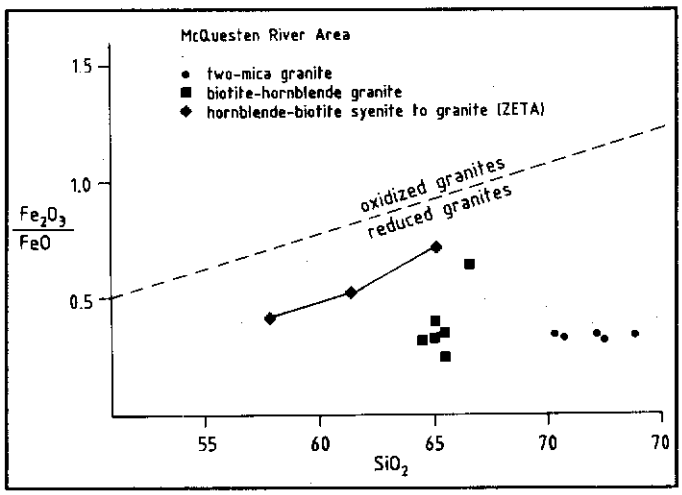

Figure 16. Fe_2O_3/FeO vs SiO_2 of McQuesten River plutonic rocks showing oxidized and reduced granitoid classification.

biotite-hornblende granite at PUKELMAN (MINFILE 115P 013) and RHOSGOBEL (MINFILE 115P 012) in the northern belt and at SCHEELITE DOME (MINFILE 115P 004) and LUGDUSH (MINFILE 115P 009) in the southern belt (Emond, 1992). The LUGDUSH (MINFILE 115P 009) pluton is mainly a two-mica granite, but it is rimmed with sericitized hornblende-biotite dacite which formed the associated W skarn. At SCHEELITE DOME (MINFILE 115P 004), TEE (MINFILE 115P 008a) and SNARK (MINFILE 115P 008b) the tungsten skarns associated with biotite-hornblende granite also contain sulphide minerals and tin.

Metallic minerals help to characterize the McQuesten plutonic suite as a unique entity, distinct from the Selwyn and Tombstone plutonic suites. Numerous tin showings occur in the McQuesten belt, and its tungsten deposits are associated with biotite-hornblende rocks, whereas the southeast part of the Selwyn Plutonic Suite contains larger and more numerous tungsten deposits which are associated with two-mica granites (Anderson, 1988).

The Selwyn Plutonic Suite postdated the arc-continent collision (Tempelman-Kluit 1981, 1979). The magmas which formed these rocks are commonly believed to have formed by relaxation of isotherms associated with post-collision crustal thickening causing melting of the lower crust. However, it is also possible that these magmas were formed by low angle east-dipping subduction originating west of the 'Stikine arc' (Tempelman-Kluit 1979) causing melting of the lower crust or the 'downgoing slab'. Formation by subduction could possibly explain the bimodal distribution of the Selwyn intrusions and also some of their 'I' type characteristics.

The presence of syenite along the north edge of the McQuesten region links rocks of the McQuesten region to the syenites and 'A' type granites in the Tombstone Mountains to the northwest. There, a different intrusive suite was emplaced as a result of extensive Proterozoic crustal thinning and a difference in the composition of the lower crust (Anderson 1987). Since the granitoid rocks in the northern McQuesten region lack 'A' type characteristics, they have been included in the Selwyn Plutonic Suite, and may mark the southern margin of thinned crust. Syenites in the McQuesten region show a close relationship to the granites, particularly at the ZETA property (MINFILE 115P 047) where the syenites and granites appear to be differentiation products of a single magma.

SUMMARY

Plutonic rocks of the McQuesten River region are comagmatic and consist mainly of hornblende syenite, biotite-hornblende granite and two-mica granite. Small plutons were forcefully emplaced at a high level in the crust and fractionally crystallized in place. The plutonic rocks form two east-trending belts: a northern belt with more mafic biotite-hornblende granitic and syenitic rocks, and a southern belt with more felsic biotite-muscovite (two-mica) granites. The two-mica granite, which crystallized from the most evolved and therefore volatile-rich (i.e., boron-rich) melt, is associated with tin-silver veins and skarns. The less evolved biotite-hornblende granite is associated with tungsten-gold skarns and veins.

The McQuesten Plutonic Belt is broadly similar to the Selwyn Plutonic Suite in its geometry and bimodal character. Differences in chemistry and metallization, however, indicate that the McQuesten intrusions are more highly evolved.

ACKNOWLEDGMENTS

The author appreciates the time, energy and expertise spent by J.A. Morin, W.D. Sinclair, and J.G. Abbott in critical review of the paper. Special thanks are due to S.R. Morison and J.A. Morin for their encouragement and provision of office facilities. Thanks are also to due to S. Abercrombie for interesting discussion of her thesis material, and to L. Pigage for providing further geochemical data on granites of the Anvil area. The drafting services of Northern Affairs, Whitehorse are also greatly appreciated.

REFERENCES

ABERCROMBIE, S.M. 1990. Petrology, geochronometry and economic geology: The Zeta tin-silver prospect, Arsenic Ridge, west-central Yukon (115 P 14 and 116 A 3). Unpublished M.Sc. Thesis, University of British Columbia, Vancouver, B.C.

ANDERSON, R.G., 1987. Plutonic rocks in the Dawson map area, Yukon Territory. In Current Research, Part A, Geological Survey of Canada, Paper 87-1A, p. 689-697.

ANDERSON, R.G., 1988. An overview of some Mesozoic and Tertiary plutonic suites and their associated mineralization in the northern Canadian Cordillera. In: Recent Advances in the Geology of Granite Related Mineral Deposits, R.P. Taylor and D.F. Strong (eds.); Canadian Institute of Mining and Metallurgy, Special Volume 39, p. 96-113.

ATKINSON, D. and BAKER, D.J., 1986. Recent developments in the geologic understanding of MacTung. In: Mineral Deposits of Northern Cordillera, J.A. Morin, (ed.); CIM Special Volume 37, p. 234-244.

BOSTOCK, H.S., 1946. Geology, Mayo area, Yukon Territory. Geological Survey of Canada, Map 890A.

BOSTOCK, H.S., 1964. Geology, McQuesten River, Yukon Territory. Geological Survey of Canada, Map 1143A.

BOUSEILY (EL), A.M. and SOKKARY (EL), A.A., 1975. The relation between Rb, Ba and Sr in granitic rocks. Chemical Geology, Vol. 16, p. 207-219.

BOYLE, R.W., 1965. Geology, geochemistry and origin of the lead-zinc-silver deposits of the Keno Hill - Galena Hill area, Yukon Territory. Geological Survey of Canada, Bulletin 111, 302 p.

COX, K.G., BELL, J.D. and PANKHURST, R.J., 1979. The Interpretation of Igneous Rocks. George Allen & Unwin Ltd, London, 450 p.

EISBACHER, G.H., 1981. Sedimentary tectonics and glacial record in the Windermere Supergroup, Mackenzie Mountains, northwestern Canada. Geological Survey of Canada, Paper, p. 80-27.

EMOND, D.S., 1983. Geology of the EPD stanniferous breccia deposit, McQuesten area, 115 P, Yukon. In: Yukon Exploration and Geology 1982; Exploration and Geological Services Division, Yukon, Indian and Northern Affairs Canada, p. 26-33.

EMOND, D.S., 1985. Geology, mineralogy and petrogenesis of tin-bearing breccia/veins at Oliver Creek, McQuesten River Area, Yukon. Unpublished M.Sc. thesis, Carleton University, Ottawa, Ontario.

EMOND, D.S., 1986. Tin and tungsten veins and skarns in the McQuesten River area, central Yukon. In Yukon Geology, Vol. 1; Exploration and Geological Services Division, Yukon, Indian and Northern Affairs Canada, p. 113-118.

EMOND, D.S. and LYNCH, T., 1992. Geology, mineralogy and geochemistry of tin and tungsten veins, breccias and skarns, McQuesten River area (115 P (north) and 105 M 13), Yukon. In: Yukon Geology Volume 3; Exploration and Geological Services Division, Yukon, Indian and Northern Affairs Canada (this volume).

GORDEY, S.P. and ANDERSON, R.G., in press. Evolution of the northern Cordilleran miogeocline, Nahanni map area (105 I), Yukon Territory and District of McKenzie. Geological Survey of Canada, Memoir.

HUDSON, T. and ARTH, J.G., 1983. Tin granites of Seward Peninsula, Alaska. · Geological Society of America Bulletin, Vol. 94, p. 768-790.

HUNT, P.A. and RODDICK, J.C., 1987. A compilation of K-Ar ages, Report 17. In: Radiogenic Age and Isotopic Studies: Report 1; Geological Survey of Canada, Paper 87-2, p. 188.

KURAN, V.M., GODWIN, C.I. and ARMSTRONG, R.L., 1982. Geology and geochronometry of the Scheelite Dome tungsten-bearing skarn property, Yukon Territory. Canadian Institute of Mining and Metallurgy Bulletin, Vol. 75, p. 137-142.

LENNAN, W.B., 1986. Ray Gulch tungsten skarn deposit. In: Mineral Deposits of Northern Cordillera, J.A. Morin, (ed.); Canadian Institute of Mining and Metallurgy, Special Volume 37, p. 245-254.

LYNCH, J.V.G., 1989. Hydrothermal zoning in the Keno Hill Ag-Pb-Zn vein system, Yukon: A study in structural geology, mineralogy, fluid inclusions, and stable isotope geochemistry. Unpublished Ph.D. Thesis, University of Alberta, Edmonton, Alberta, 218 p.

PEARCE, J.A., HARRIS, N.B.W. and TINDLE, A.G., 1984. Trace element discrimination diagrams for the tectonic interpretation of granitic rocks. Journal of Petrology, Vol. 25, p. 956-983.

PIGAGE, L.C. and ANDERSON, R.G., 1985. The Anvil plutonic suite, Faro, Yukon Territory. Canadian Journal of Earth Sciences, Vol. 22, p. 1204-1216.

SINCLAIR, W.D., 1986. Molybdenum, tungsten and tin deposits and associated granitoid intrusions in the northern Canadian Cordillera and adjacent parts of Alaska. In: Mineral Deposits of Northern Cordillera, J.A. Morin, (ed.); Canadian Institute of Mining and Metallurgy, Special Volume 37, p. 216-233.

SMIT, H., ARMSTRONG, R.L., and VAN DER HEYDEN, P., 1985. Petrology, chemistry and radiogenic isotope (K-Ar, Rb-Sr, and U-Pb) study of the Emerald Lake pluton, eastern Yukon Territory. In: Current Research, Part B, Geological Survey of Canada, Paper 85-1B, p. 347-359.

STEVENS, R.P., LACHANCE, G.R. and DELABIO, R.N., 1982. Age determinations and geological studies, K-Ar isotopic ages, Report 16. Geological Survey of Canada, Paper 82-2, 56 p.

STRECKEISEN, A.L., 1973. Classification of plutonic rocks. Geotimes, Vol. 18, p. 26-30.

TEMPELMAN-KLUIT, D.J., 1979. Transported cataclasite, ophiolite and granodiorite in Yukon. Evidence of arc-continent collision. Geological Survey of Canada, Paper 79-14, 27 p.

TEMPELMAN-KLUIT, D.J., 1981. Geology of the southern Yukon. In: Yukon Geology and Exploration 1979-80; Exploration and Geological Services Division, Yukon, Indian and Northern Affairs Canada, p. 8-31.

THOMPSON, R.I. and EISBACHER, G.H., 1984. Late Proterozoic rift assemblages, northern Canadian Cordillera. Geological Society of America, Abstracts with Programs, Vol. 16, p. 336.

THORNTON, C.P. and TUTTLE, O.F., 1960. Chemistry of igneous rocks - I, Differentiation Index. American Journal of Science, Vol. 258, p. 664-684.

WATSON, K.W., 1986. Silver-lead-zinc deposits of the Keno Hill-Galena Hill area, central Yukon. In: Yukon Geology Volume 1; Indian and Northern Affairs Canada, Northern Affairs Program, Exploration and Geological Services Division, Yukon, p. 83-88.

WHALEN, J.B., CURRIE, K.L., and CHAPPELL, B.W., 1987. A-type granites: geochemical characteristics, dicrimination and petrogenesis. Contributions to Mineralogy and Petrology, Vol. 95, p. 407-419.

WHEELER, J.O. and MCFEELY, P., 1987. Tectonic assemblage map of the Northern Cordillera. Geological Survey of Canada, Open File 1565.

WHITE, A.J.R. and CHAPPELL, B.W., 1983. Granitoid types and their distribution in the Lachlan Fold Belt, southeastern Australia. In: Circum-Pacific Plutonic Terranes (J.A. Roddick, ed.); Geological Society of America, Memoir 159, p. 21-34.

WOODSWORTH, G.J., ANDERSON, R.G., BROOKFIELD, A. and TERCIER, P., 1989. Distribution of Proterozoic to Miocene plutonic suites in the Canadian Cordillera. Geological Survey of Canada, Open File 1982, 6 maps.

ZEN, E. and HAMMARSTROM, J.M., 1984. Magmatic epidote and its petrologic significance. Geology, Vol. 12, p. 515-518.

Appendix 1. Abbreviations (used in tables).

ALL,AL	allanite	NOS	nosean
AP	apatite	OP	opaque minerals
AN	anatase	OR	orthoclase
BI	biotite	PL	plagioclase
COR	corundum	PX	pyroxene
CAN	cancrinite	QZ	quartz
CPX	clinopyroxene	RU	rutile
DI	diopside	SPH	sphene
FL	fluorite	TO	tourmaline
GT	garnet	ZR	zircon
HB	hornblende	DAC	dacite
KSP	K feldspar	GRAN	granite
MEL	melanite	GRANODI	granodiorite
MON	monazite	QZMZ	quartz monzonite
MT	magnetite	RHYODAC	rhyodacite
MU	muscovite	SY	syenite
NE	nepheline		

1. In this report, the mineral property name is also used when referring to the associated pluton.

2. Due to space constraints, some of these diagrams have been omitted.

Table 1. Petrology of Plutonic Rocks of the McQuesten River Area[1]

	TWO-MICA GRANITE	HORNBLENDE-BIOTITE GRANITE	HORNBLENDE-(BIOTITE) SYENITE
MAIN MINERALS	QZ, PL(Ol-An), KSP	QZ, PL(An), KSP	KSP, PL(Ol-An), HB
ESSENTIAL MINERALS	BI > MU	BI > HB	HB > > BI
BIOTITE	reddish- to orange-brown to lt yellow brown	chocolate brown to lt yellow-brown -minor rusty brown	chocolate brown to dk red brown to lt yellow
HORNBLENDE	none	lt brownish green to yellow-clear to grass green - also pinkish clear, lt bluish green)	dk green-brown to red-brown to yellow-green
ACCESSORY MINERALS	AP, ZR, MON, TO (OP, SPH)	ALL, AP, ZR, SPH (OP-MT)	ALL, RU, AP, ZR, SPH, NE
TEXTURES	allotrio- to hypidiomorphic granular, myrmekite, ragged edges (mica), strained embayed quartz, quartz glomophyrs, megacrystic KSP, equigranular to seriate to porphyritic	hypidio- to idiomorphic granular, smooth edges (mica), strained quartz, quartz glomophyrs, KSP megacrysts and clots poikilolitic & zoned HB, porphyritic	idio- to hypidiomorphic granular myrmekite, porphyritic to equigranular
ALTERATION	ser. of PL chl. of BI perth. of KSP microcl. of KSP epidote	ser. of PL chl. of BI & HB microcl. of PL biot. of HB epidot. of HB carbonate albitization ural. of PX	biot. of HB ural. of PX perth. of HB carbonate

[1]Abbreviations: see Appendix 1.

Table 2. Major-element, normative mineral and modal composition of samples from the McQuesten Granite Belt

Associated Mineral	LUGDUSH	LUGDUSH	TEE	SUNSHINE CREEK	SUNSHINE CREEK	SUNSHINE CREEK	SCHEELITE DOME	JOUMBIRA	JOUMBIRA	MAHTIN	MAHTIN	RHOSGL	PUKELMAN	ZETA	ZETA	ZETA
Occurrence	Core	Rim	Stock	Central	Stock	Dyke		Plug	Dyke	Plug	Dyke			Margin	Margin	Core
Sample No.	242	237	203	281,2	279	275	208	219	244	227	221	235	236	264	256	258
(New)	(12)	(11)	(1)	(23,24)	(22)	(20)	(3)	(5)	(13)	(7)	(6)	(9)	(10)	(19)	(16)	(17)
Rock Type	GRAN	DAC	GRDI	GRAN	GRDI	RYOD	GRAN	GRAN	RYOD	GRAN	GRAN	QZMZ	QZMZ	SY	QZMZ	GRAN
Accessory Minerals	BI	BI-MU (HB?)	BI-HB	BI-MU	BI-MU	BI(HB?)	BI-HB	BI-MU	BI-HB	HB-BI	HB-BI	HB-BI	HB-BI	HB (BI)	HB-BI	HB-BI
Major Oxides(wt %)																
SiO_2	70.61	68.46	65.25	73.99	70.39	72.54	65.40	72.23	70.61	65.26	66.72	65.56	64.82	58.04	61.67	65.27
Al_2O_3	14.20	15.46	14.98	13.70	14.42	14.26	15.38	13.60	15.35	14.05	15.24	15.54	14.89	19.37	15.82	15.72
Fe_2O_3	0.67	0.98	1.20	0.42	0.63	0.35	0.94	0.53	0.65	1.12	0.89	0.78	0.90	1.30	1.72	1.57
FeO	2.00	2.25	3.20	1.22	1.80	1.10	2.75	1.55	0.75	3.35	1.40	3.20	2.80	3.15	3.40	2.20
MgO	0.60	0.99	1.87	0.32	0.57	0.40	1.71	0.71	0.37	2.21	1.31	1.47	1.16	0.98	3.55	1.25
CaO	1.36	2.54	3.49	0.94	1.49	1.21	2.97	1.76	2.15	3.53	3.02	3.40	2.97	2.67	3.74	2.63
Na_2O	3.12	3.08	2.22	3.04	2.65	2.86	2.60	2.20	2.84	2.36	2.83	2.89	2.80	4.14	2.92	3.08
K_2O	4.99	4.79	4.51	4.76	4.98	5.37	4.80	4.18	4.41	5.46	6.78	5.55	5.35	7.52	5.81	5.77
TiO_2	0.52	0.45	0.53	0.24	0.47	0.32	0.51	0.32	0.19	0.54	0.48	0.55	0.51	0.43	0.69	0.50
P_2O_5	0.28	0.16	0.23	0.16	0.25	0.21	0.16	0.14	0.09	0.20	0.18	0.24	0.23	0.20	0.32	0.23
MnO	0.06	0.06	0.08	0.04	0.03	0.03	0.08	0.03	0.01	0.09	0.05	0.10	0.09	0.12	0.11	0.09
LOI	0.80	1.40	0.80	0.70	1.10	1.00	0.70	0.90	1.10	0.80	1.10	0.90	1.20	0.90	0.80	0.90
Total	99.21	100.61	98.36	99.68	98.77	99.66	98.01	98.16	98.53	98.96	99.99	100.19	97.71	98.82	100.55	99.21
molar A/CNK	1.20	1.23	1.28	1.23	1.31		1.27	1.40	1.35	1.08	1.03	1.12	1.13	1.11	1.09	1.15
DIFF INDEX																
CIPW NORMS																
Q	29.16	24.20	23.28	34.97	31.52	32.14	21.65	38.03	31.66	19.11	16.49	17.24	19.01		8.34	16.60
C	1.86	0.97	0.65	1.96	2.56	2.04	0.89	2.59	2.21					0.04		0.17
OR	29.48	28.30	26.65	28.10	29.42	31.73	28.36	24.70	26.05	32.26	40.06	32.79	31.61	44.43	34.33	34.09
AB	26.40	26.06	18.78	25.72	22.42	24.20	22.00	18.61	24.03	19.96	23.94	24.45	23.69	30.97	24.70	26.06
AN	4.91	11.55	15.81	4.32	5.75	4.63	13.68	7.81	10.07	11.61	8.85	13.03	12.25	11.93	12.90	11.54
NE														2.19		
DI										3.77	4.03	1.87	0.81		2.90	
HY	4.09	5.85	9.43	2.52	3.74	2.34	8.18	3.90	2.94	8.51	3.42	7.01	6.44		12.85	7.09
MT	0.83	1.00	1.37	0.51	0.76	0.45	1.15	0.65	0.42	1.40	0.70	1.25	1.16	1.39	1.59	1.16
IL	0.98	0.85	1.00	0.46	0.89	0.60	0.96	0.60	0.36	1.02	0.91	1.04	0.96	0.81	1.31	0.94
FA	0.22	0.12	0.18	0.12	0.19	0.16	0.12	0.11	0.07	0.15	0.14	0.18	0.18	0.15	0.25	0.18
EN	1.49	2.46	4.65	0.80	1.41	0.99	4.25	1.76	0.92	4.51	2.06	3.23	2.71		7.96	3.11
FS	2.59	3.39	4.77	1.72	2.32	1.34	3.92	2.13	1.42	4.00	1.35	3.78	3.73		4.88	3.98
WOLL										1.91	2.06	0.94	0.40		1.48	
EN(DP)										0.98	1.19	0.43	0.17		0.87	
FS(DP)										0.87	0.77	0.50	0.23		0.53	
OL														5.62		
OL (FOR)														1.70		
OL (FAY)														3.91		

Table 2. (continued)

Associated Mineral	LUGDUSH	LUGDUSH	TEE	SUNSHINE CREEK	SUNSHINE CREEK	SUNSHINE CREEK	SCHEELITE DOME	JOUMBIRA	JOUMBIRA	MAHTIN	MAHTIN	RHOSGL	PUKEL	ZETA	ZETA	ZETA
Occurrence	Core	Rim	Stock	Central	Stock	Dyke		Plug	Dyke	Plug	Dyke			Margin	Margin	Core
Sample No.	242	237	203	281,2	279	275	208	219	244	227	221	235	236	264	256	258
(New)	(12)	(11)	(1)	(23,24)	(22)	(20)	(3)	(5)	(13)	(7)	(6)	(9)	(10)	(19)	(16)	(17)
Rock Type	GRAN	DAC	GRDI	GRAN	GRDI	RYOD	GRAN	GRAN	RYOD	GRAN	GRAN	QZMZ	QZMZ	SY	QZMZ	GRAN
Accessory Minerals	BI	BI-MU (HB?)	BI-HB	BI-MU	BI-MU	BI(HB?)	BI-HB	BI-MU	BI-HB	HB-BI	HB-BI	HB-BI	HB-BI	HB (BI)	HB-BI	HB-BI
Minor Elements (ppm)																
Large Cations																
Ba	1700	2700	2700	500	1700	990	2500	2300	3200	1700	2000	1600	1200	1700	1600	1600
Cs	14	11	16	30	16	10	11	14	4	16	15	15	12	16	32	20
Rb	280	140	210	360	350	310	190	150	120	260	300	240	210	320	320	310
Sr	315	510	455	162.5		145	475	305	380	420	515	555	520	655	525	495
Rb/Sr	0.90	0.27	0.46	2.21		2.14	0.4	0.49	0.32	0.62	0.58	0.43	0.40	0.49	0.61	0.63
Rare Earth Elements																
La	100	34	54	42	74	35	40	23	28	49	64	43	39	62	71	66
Ce	200	72	110	105	160	73	97.0	48.0	60	120	110	79	79	120	120	130
Nd	67	26	35	28	45	28	19	19.0	11	32	42	37	33	45	39	46
Sm	10.0	4.4	7.8	6.2	9.4	5.5	6.6	3.3	2.4	7.2	8.2	6.6	5.9	8.4	8.9	8.6
Tb	<1	<1	1	<1	1	<1	<1	<1	<1	1	<1	<1	<1	2	<1	<1
Dy	3	2	2	3	4	3	3	2	<1	3	3	3	3	3	4	3
High Valence Cations																
Th	41.0	14.0	27.0	31.0	40.0	35.0	20.0	12.0	12.0	26.0	29.0	19.0	17.0	28.0	51.8	51.3
U	4.8	4.7	9.2	14.8	12.0	8.8	9.1	5.4	4.1	7.2	5.0	7.3	8.2	5.6	13.0	10.0
Hf	6	4	3	4	6	4	4	5	3	4	6	3	4	7	6	7
Ta	2	1	<1	4	4	2	1	<1	<1	<1	1	2	2	2	2	3
Nb	52	25	23	38	39	24	25	19	16	21	24	37	29	42	39	42
Y	29	7	15	44		39	18	<5	<5	25	25	18	18	37	38	33
Ga	11	20	19	15*	24	18	<1	20	59	<10	<10	10	20	10	10	14
B	20	20	35	75	15	45	15	25	15	20	25	25	20	145	50	65
Zr	<500	<500	<500	<500	<500	<500	680	<500	<500	<500	<500	750	<500	<500	<500	<500
W	<2	<2	<2	6	<2	<2	11	<2	<2	<2	<2	<2	23	<2	13	<2
Mo	<2	<2	<2	2*	<2	<2	<2	<2	<2	<2	<2	<2	<2	<2	<2	<2
Th/U	8.5	3.0	2.93	2.1	3.3	4.0	2.20	2.22	2.92	3.61	5.8	2.60	2.07	5	3.98	5.13
Other Metals																
Au (ppb)	14	10	20	16	12	18	9	<5	7	9	8	28	6	6	<5	8
Ag	<5	<5	<5	<5	<5	7	7	<5	<5	7	<5	<5	<5	<5	<5	<5
Sb	0.3	0.6	0.8	0.2*	0.2	2.1	0.6	0.9	0.5	1.0	1.8	0.7	0.6	2.7	1.6	1.8
As	5	11	16	<1	<1	131	<3	0.9	0.5	22	13	4	19	12	6	8
Cr	150	120	140	120	130	86	160	101	15	150	130	120	98	<50	130	110
Zn	<200	<200	<200	<200	<200	210	<200	810	230	<200	<200	<200	<200	<200	<200	<200
Sc	5.2	5.5	11.0	4.9	7.0	3.4	11.0	3.9	1.4	13.0	8.3	9.5	7.1	3.8	11.0	6.9
Be	7.6	4.8	5.0	12.2	7.7	6.7	5.1	3.9	2.9	6.5	7.4	6.7	6.7	9.2	11.0	9.9
F	550	450	900	1120	1300	420	900	620	280	1000	660	1300	850	840	1250	1050

Analyses were performed by Bondar-Clegg & Company Ltd., North Vancouver using mainly the following methods: 1) major and minor elements - D.C. Plasma (also Titrimetric for FeO; and Gravimetric for Loss on Ignition); 2) trace elements - Neutron Activation (and also X-ray fluorescence for Sr, Y, Ga and In; D.C. Plasma for Ge; Turbidimetric for Cl; and Atomic Absorption for Be).

Abbreviations: see Appendix 1

Table 3. Average composition of Granitoid Rocks in the McQuesten River Area

	Two-Mica Granite n=4[1]		Hornblende-Biotite Quartz Monzonite, Granite n=6		Hornblende-Biotite Syenite n=1
MAJOR OXIDE ANALYSES (WT %)					
SiO_2	71.80 (70.39-73.99)		65.50 (64.82-66.72)		58.04
Al_2O_3	13.98 (13.60-14.42)		15.01 (14.05-15.54)		19.37
Fe_2O_3	0.56 (0.42-0.67)		0.97 (0.78-1.20)		1.30
FeO	1.64 (1.22-2.00)		2.78 (1.40-3.20)		3.15
MgO	0.55 (0.32-0.71)		1.62 (1.16-2.21)		0.98
CaO	1.38 (0.94-1.49)		3.23 (2.97-3.53)		2.67
Na_2O	2.75 (2.20-3.12)		2.61 (2.22-2.89)		4.14
K_2O	4.73 (4.18-4.99)		5.41 (4.51-6.78)		7.52
TiO_2	0.38 (0.24-0.52)		0.52 (0.48-0.55)		0.43
P_2O_5	0.25 (0.14-0.28)		0.21 (0.18-0.24)		0.20
MnO	0.04 (0.03-0.06)		0.08 (0.05-0.10)		0.12
molar A/CNK	1.28 (1.20-1.40)		1.15 (1.03-1.28)		1.11
DIFF INDEX					
CIPW NORMS					
Q	33.42 (29.16-38.03)		19.46 (16.49-23.28)		
C	2.24 (1.86-2.59)		0.26 (0-0.89)		0.04
OR	27.92 (24.70-29.48)		31.96 (26.65-40.06)		44.43
AB	23.29 (18.61-26.40)		22.14 (18.78-24.45)		30.97
AN	5.70 (4.32-7.81)		12.54 (8.85-15.81)		11.93
NE					2.19
DI			1.75 (0-4.03)		
HY	3.56 (2.52-4.09)		6.66 (3.42-9.3)		
MT	0.69 (0.51-0.83)		1.17 (0.70-1.40)		1.39
IL	0.73 (0.46-0.98)		0.98 (0.91-1.04)		0.81
FA	0.16 (0.11-0.22)		0.16 (0.12-0.18)		0.15
EN	1.37 (0.80-1.76)		3.57 (2.06-4.65)		
FS	2.19 (1.72-2.59)		3.59 (1.35-4.77)		
WOLL			0.88 (0-2.06)		
EN(DP)			0.46 (0-1.19)		
FS(DP)			0.40 (0-0.87)		
OL					5.62
OL(FOR)					1.70
OL(FAY)					3.91
MINOR ELEMENTS (PPM):					
Large Cations					
Ba	1550	(500-2300)	1950	(1200-2700)	1700
Cs	18	(14-30)	14	(11-16)	16
Rb	280	(150-360)	235	(190-300)	320
Sr	261	(162.5-315)	490	(420-555)	655
Rb/Sr	1.2	(0.49-2.21)	.48	(0.40-0.62)	0.49
Rare Earth Elements					
La	49	(23-100)	48	(39-64)	62
Ce	128	(48-200)	99	(79-120)	120
Nd	39	(19-67)	33	(19-42)	45
Sm	7.2	(3.3-10.0)	7.0	(5.9-8.2)	8.4
Tb	<1	(<1-1)	<1	(<1-1)	2
Dy	3	(2-4)	3	(2-3)	3
High Valence Cations					
Th	31.0	(12-41)	23.0	(17-29)	28.0
U	9.2	(4.8-14.8)	7.7	(5.0-9.2)	5.6
Hf	5	(4-6)	4	(3-6)	7
Ta	3	(<1-4)	1	(<1-2)	2
Nb	37	(19-52)	26	(21-37)	42
Y	25	(<5-44)	20	(15-25)	37
Ga	17	(11-24)	<10	(<10-20)	10
B	34	(15-75)	23	(15-35)	145
Zr	<500		<500	(<500-750)	<500
W	2	(<2-6)	6	(<2-23)	<2
Mo	<2	(<2-2)	<2		<2
Th/U	4.03	(2.1-8.5)	3.20	(2.07-5.80)	5
Other Metals					
Au (ppb)	11	(<5-16)	13	(6-28)	6
Ag	<5		<5	(<5-7)	<5
Sb	0.4	(0.2-0.9)	0.9	(0.6-1.8)	2.7
As	27	(<1-101)	12	(<3-22)	12
Cr	140	(120-170)	133	(98-160)	<50
Zn	280	(<2-810)	<200		<200
Sc	5.2	(3.9-7.0)	10.0	(7.1-13.0)	3.8
Be	7.8	(3.9-12.2)	6.2	(5.0-7.4)	9.2
F	900	(550-1300)	940	(660-1300)	840

[1]When n>1, the first value is the mean; this is followed by the range, in parentheses.

Table 4. Comparison of plutonic rocks of the McQuesten area with the Selwyn and Tombstone Plutonic Suites

	MCQUESTEN	SELWYN	TOMBSTONE
GEOLOGICAL SETTING	Late Proterozoic to Miss. metased. rx	Late Proterozoic to Miss. metased. & metavol. rocks	M. Proterozoic to Jurassic metased. rx. Zone of suspect Late Proterozoic extension.
INTRUSION CHARACTER-ISTICS	Zoned, nearby coeval volcs, contact aureoles, roof pendants, subcircular, heterogeneous, stocks, plugs, dykes	Zoned, composite, overlain by coeval volcs, subcircular, heterogeneous, batholiths, plugs, stocks, dykes	subcircular to circular, post-tectonic, cogenetic dykes & volcanics
PHASES	1) QZ-rich felsic (bi-mu granite)	1) QZ-rich felsic (hb-free bi-mu granite to granodi.	1) no two-mica granite
		1a) Transitional variety between 1) and 2: a two-mica granite with minor hb.	
	2) felsic (hb-bi quartz monz, granodi, granite)	2) felsic (hb-bi granite, granodi, quartz syenite)	2) siliceous felsic (hb-bi monzogranite)
	3) QZ-poor felsic (hb-bi (hb-bi syenite, quartz monzonite to granite)	3) QZ-poor felsic (hb-bi (hb-bi alkali feldspar syenite to syenite to qtz syenite to qtz monzonite to granite)	3) QZ-poor felsic (hb $\pm$ bi alkali to feldspar syenite)
			4) Mafic to Intermed. (Subordinate)(hb-clino-pyroxenite, hb-diorite, tinguaite, bi-monzonite)
ACCESSORY MINERALOGY	1) MU, BI, AP, ZR, TO, MON	1) MU, BI, GT, TO, AP, AL, ZR, AN, MON, HB, CPX	
	2) BI, HB, AL, SPH, AP, ZR, CPX, MT	2) BI, HB, MT, SPH, AP, AL,TO,ZR,CPX	2) HB, BI
	3) HB, BI, AL, SPH AP, ZR, RU, NE, CT, TO	3) HB, BI, SPH, MT, AP, ZR, AL	3) HB, BI, SPH, FL, AEGIRINE-AUGITE, MT, MEL, AP, CAN, NOS, NE
TEXTURES	allotriom. to hypid. gran. seriate, porph., megacrystic, glomerophyric, myrmekite, microperthite	hypid. gran., equigran, seriate, megacrystic, myrmekite microperthite	equigranular, megacrystic, porph., granophyric, graphic granite, myrmekite, microperthite
ALTERATION MINERALS	chlor., ser., microcliniz.,ep., calc., albit., uralit.	chlor., ser., ep., calc., sphene, saussur.	
ASSOCIATED MINERAL DEPOSITS	Sn-Ag veins, skarns assoc. with two-mica granite W-Au skarn & veins assoc. with hb-bi granite; Ag-Pb-Zn veins distal to plutons	large W-Cu skarns assoc. with two-mica granite Cu-Mo-Fe-As-Zn (Au-W) skarn & vein showings assoc. with hb-bi granite	F, U, Th, Sb, W, Sn, Mo, Ag, Au, base metal; sulphides dissem. & veins,
GEOCHEMISTRY	1) Corundum norm > 70% SiO_2 (70-75) $K_2O > Na_2O$	1) Corundum norm silicic, high K, low Ca & Mg,	
	2) CPX norm. < 70% SiO_2 (64-66)	2) CPX norm, lower norm. corundum & silica, higher cafemic, TiO_2,MnO,Sr,Ba,La,Y,K/Rb, Ba/Rb,lower salic oxides, D.I.,Rb,Rb/Sr,K/Ba	
	3) NE to COR norm. (from syenite to granite)< 60 % SiO_2 (58)		3) QZ or NE norm.
	Peraluminous (hb-bearing - lower Shand Ind.	Per- to metalum. (hb-bearing - lower Shand Index)	
	Subalkaline (minor alkaline)	Subalkaline (minor alkaline)	Alkaline to subalkaline
	Calc-alkaline (2-mica granite-higher alkalis, lower Fe, Mg)	Calc-alkaline (2-mica granite-higher alkalis, lower Fe, Mg)	

Abbreviations: see Appendix 1

DRIFT PROSPECTING FOR GOLD IN THE TINTINA TRENCH

by

Alain Plouffe
Geological Survey of Canada
601 Booth St
Ottawa, Ontario
K1A 0E8

and

Lionel E. Jackson, Jr.
Geological Survey of Canada
100 West Pender St
Vancouver, B.C.
V6B 1R8

Geological Survey of Canada Contribution #38389

PLOUFFE, A., and JACKSON, L.E., 1992. Drift prospecting for gold in the Tintina Trench. In: Yukon Geology, Vol. 3; Exploration and Geological Services Division, Yukon, Indian and Northern Affairs Canada, p.196-213

ABSTRACT

Two tills and related deposits are the products of at least two ice advances over the Tintina Trench near Ross River, Yukon Territory. These ice advances are termed the McConnell and pre-McConnell glaciations. Erosional remnants provide evidence of the pre-McConnell glaciation and indicate that the ice was flowing to the west or northwest. The onset of McConnell glaciation was marked by an early ice advance out of the Lapie River valley, which was followed by a general ice flow toward the west or northwest along the Tintina Trench. During the retreat of the McConnell glacier, an ice tongue advanced up the Lapie River valley, blocking the drainage and forming a glacial lake.

To develop and apply drift prospecting techniques in the Tintina Trench, 204 till samples were collected over the study area. The silt plus clay size fraction was analysed for Au and the clay fraction was analysed for 30 elements. Only the Au, Ag, Hg and Sb results are discussed in this paper. The geochemical data for till down-ice from the Grew Creek Au-Ag mineralization (MINFILE 105K 009) show a dispersal train for gold, but not for pathfinder elements such as Ag, As, Hg and Sb. A possible relationship between Au and Tertiary volcanic rocks is illustrated. However, closer-spaced samples would have to be taken to verify this hypothesis, since the length of the Au dispersal train is about 500 m, much smaller than the sampling interval.

RÉSUMÉ

Deux tills et les sédiments qui s'y rattachent ont été produits par un moins deux avancés glaciaires dans la dépression de Tintina dans la région de Ross River au Territoire du Yukon. Ces deux avancés sont appelées glaciations de McConnell et pré-McConnell. Les seuls évidences de la Glaciation pré-McConnell sont des restants d'érosion selon lesquels la glace se serait écoulée hors de la vallée de la Rivière Lapie et au point culminant de cette glaciation l'écoulement était généralement vers le nord-ouest et l'ouest dans la dépression de Tintina. Pendant la retrait de ce lobe glaciaire, une langue de glace s'est avancée en remontant la pente dans la vallée de la Rivière Lapie ce qui créa un lac glaciaire dans cette même vallée.

Deux cent quatre échantillons de till ont été ramassés de façon à développer et appliquer les techniques de prospection à l'aide de sédiments glaciaires dans la dépression de Tintina. La fraction silt et argile a été analysée pour une série de 30 éléments. Seuls les résultats pour l'Ag, As, Hg et Sb sont discutés dans cet article. Les données géochimiques permettent de définir un train de dispersion d'or, mais pas d'argent, d'arsenic, de mercure ou d'antimoine, en aval glaciare d'une minéralisation d'argent et d'or au Ruisseau

Grew (MINFILE 105K 009). Une relation possible entre l'or et les roches volcaniques Tertiaire est illustrée. Cependant, un échantillonage plus serré serait nécessaire pour vérifier cette hypothèse puisque le train de dispersion d'or possède une longeur d'environ 500 m, c'est-à-dire une longeur beaucoup plus courte que la distance entre chacun des échantillons.

INTRODUCTION

The discovery of a Tertiary epithermal gold-silver prospect (MINFILE 105K 009) in the Tintina Trench, Yukon Territory, has raised interest in the potential for analogous deposits buried by drift elsewhere along this structurally controlled depression (e.g. Duke, 1986; Duke and Godwin, 1986; Jackson et al., 1986). Jackson et al. (1986) cited circumstantial evidence linking the occurrence of placer gold, ice flow directions and Tertiary volcanics along the Tintina Trench. This relationship could not be tested by conventional exploration techniques (e.g. bedrock mapping, bedrock geochemistry, geophysics) because of the locally thick and fairly continuous glacial drift cover. For that reason, a drift prospecting study was carried out. The study conducted during the summer of 1987 consisted of three components: (1) a detailed study of the Quaternary geology of the area, including stratigraphy; (2) identification of ice flow configurations through the investigation of glacial dispersal of rock fragments; and (3) the interpretation of reconnaissance geochemical mapping of gold. This paper reports the results of the drift prospecting study.

SETTING

The study area (Fig. 1) is a narrow band centred on the Tintina Trench extending from Wolverine and Finlayson Lakes to just southeast of the town of Faro. It includes parts of Quiet Lake, Finlayson Lake and Tay River NTS map sheets (105F, 105G and 105K respectively). Two major roads cross the area: the Robert Campbell Highway, along which most of the till sampling has been done, and the Canol Road. Tintina Trench is bounded by the Pelly Mountains to the southwest and the Pelly and Macmillan Plateaus to the northeast. Differences in elevation between Tintina Trench and the surrounding terrain are significant. Elevations in the Trench range from 760 to 910 m, with a few high areas reaching 1070 m. The Pelly Mountains range in elevation from 1220 to 1830 m, with the highest peak reaching 2353 m in the Wolverine Lake area. Plateau surfaces vary in elevation from 910 to 1370 m.

Economic Geology

Several bedrock mineral occurrences and placer gold deposits have been found in the study area from exploration work conducted by private companies and prospectors. Most of the detailed exploration has occurred around the Grew Creek gold-silver prospect (MINFILE 105K 009) located halfway between the towns of Faro and Ross River. Rocks preserved in a graben at Grew Creek consist of felsic volcanic and volcaniclastic units overlain by interbedded coarse clastic sediments, basaltic flows and basaltic volcaniclastic beds (Duke, 1986; Duke and Godwin, 1986). Two zones of mineralization have been defined on the property: the Main and Tarn Zones. Intensive silicic and argillic hydrothermal alteration characterize Grew Creek mineralized rocks. High grade gold and silver mineralization occurs in chalcedonic quartz and K-feldspar veins which were intruded during volcanism (Duke and Godwin, 1986). Although both gold and silver are enriched in samples from boreholes, mineralized outcrops are characterized by high gold levels only (T. Christie, oral presentation, Geoscience Forum, Whitehorse, Yukon, 1988).

PREVIOUS WORK

Multiple glaciations in Yukon were first proposed by Bostock (1934) in the Carmacks area. Later, Bostock (1966) described two series of end moraines and other glacial deposits related to four different glacial stages: (1) the youngest McConnell glaciation (Wisconsinan age), (2) the more extensive Reid glaciation (Illinoian(?), Hughes, 1987), and (3) the oldest two pre-Reid glaciations. On the basis of air photo interpretation and limited ground observations, Hughes et al. (1969) reported that the Cordilleran Ice Sheet flowed west to northwest over the study area during the McConnell glaciation. Campbell (1967) gave the name "Selwyn Lobe" to this sector of the Cordilleran Ice Sheet. Hughes et al. (1969) suggested that: "a stage of alpine glaciation preceded the McConnell advance in mountainous areas lying within the limits of the ice sheet." Duke-Rodkin et al. (1986) reconstructed the profile of the Selwyn Lobe using the inferred McConnell age moraines and ice marginal channels associated with nunataks in the Glenlyon and Tay River map areas (105L and 105K). Jackson (1989) described the paleoglaciology of the Selwyn Lobe and the Quaternary stratigraphy of parts of the study area. He also mapped the regional Quaternary geology of the Pelly Mountains and Tintina Trench area (Jackson, 1986a; 1986b; 1987). Ward (1989) reported on the Quaternary stratigraphy and history of an area that extends along the Pelly River in Glenlyon and Carmacks map-areas.

QUATERNARY STRATIGRAPHY

The two most complete stratigraphic sections (Section 076 and 044) are exposed in the deeper valleys of the study area, i.e. the Pelly and Lapie River valleys. Other sections reveal key information for the Quaternary history. These sections are described below.

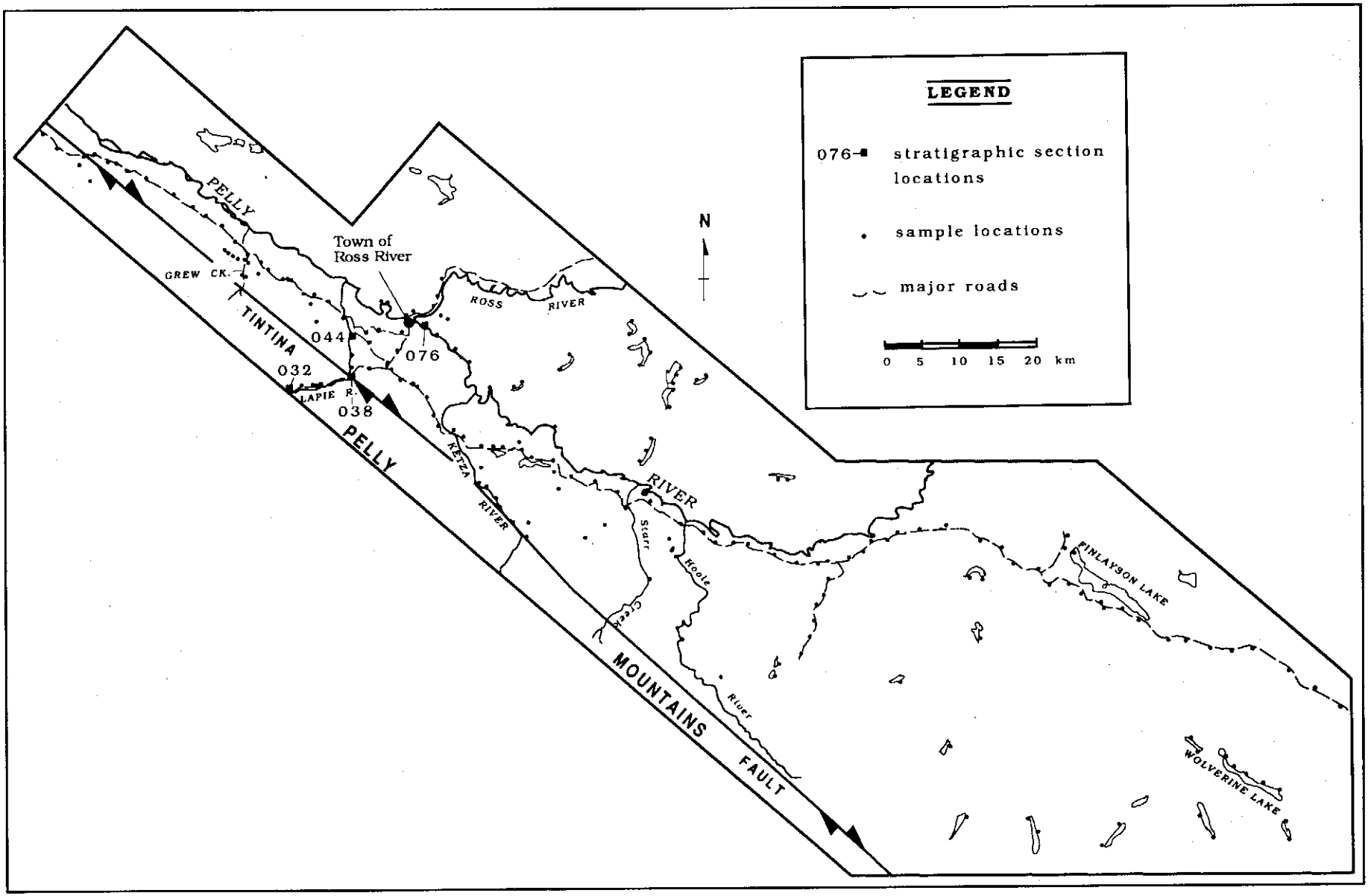

Figure 1. Location map of study area showing major stratigraphic sections and sample locations.

Section 076

This section is exposed along the Pelly River, 3 km due east of the town of Ross River (Fig. 1). Access is possible by helicopter or by motorized canoe. It has been reported by Jackson (1989) and is equivalent to his section 14686S-1.

The lowest unit exposed at this section is till deposited prior to McConnell glaciation (Fig. 2). It is overlain by glaciolacustrine sediments and horizontally stratified gravels. The gravel sequence coarsens upward, suggesting that it was deposited in front of the advancing glacial ice during McConnell glaciation. The overlying unit is the McConnell age till which is overlain essentially by the same sequence of sediments as below it: glaciolacustrine sediments and stratified gravels. These glaciolacustrine sediments are confined to the Pelly River valley and are omnipresent in sections along the river downstream from the town of Ross River. The stratified gravel above these glaciolacustrine sediments is tentatively identified as outwash gravel deposited in front of the retreating McConnell glacier on the basis of stratigraphic correlation with other exposures of outwash gravel along the Pelly River. At the top of the section, the White River Tephra (Lerbekmo et al., 1975) is exposed in a well sorted fine sand and silt unit thought to be eolian in origin.

Erratics in pre-McConnell and McConnell tills at this section include a large amount of metasediments and clastic sediments with rare ultramafic, quartz and calcareous clasts. These lithologies are interpreted as being derived from allochthons to the southeast (Tempelman-Kluit, 1977, Maps 105F and G). Since clast lithologies in the two tills are similar, ice flow directions were probably toward the west to northwest in the Pelly River valley during pre-McConnell and McConnell glaciations.

Fabrics have been measured in both tills at this section (Fig. 2 and Table 1). The a-axes of clasts are dominantly oriented northwest-southeast in the pre-McConnell till. Pebbles in the McConnell till at this site do not have an obvious preferred orientation (Table 1). This divergent orientation probably results from reworking of the drift by gravity flow after its deposition.

Section 044

Section 044 is exposed along the Lapie River, about 8 km southwest of the town of Ross River (Fig. 1). A bush road connects the top of the section with the Campbell Highway. The section was first reported by Jackson (1989), and is equivalent to his section 7686S-2.

As illustrated in Figures 2 and 3, the stratigraphy at this section is very similar to that exposed in Section 076 along the Pelly River. The oldest unit exposed is a poorly sorted, clast-supported, bouldery gravel, which is thought to be alluvial in origin. The interpretation of this unit is complicated by its relatively small exposure. A sharp erosional contact separates this gravel from the overlying pre-McConnell till. The contact between the till and the overlying outwash gravel sequence is abrupt. The outwash deposit is characterized by numerous beds of gravel, sand and diamicton. These beds of diamicton are thought to be gravity flow deposits because they are draped over the underlying units. Two cycles were defined in the outwash gravel without any major break between the two: a fining upward sequence going from the base of the unit to the middle of it, and a coarsening upward sequence in the upper part. This suggests that these gravels were deposited during retreat of the pre-McConnell glacier and advance of the McConnell ice or simply during fluctuations of the retreating pre-McConnell ice front. They are overlain by one to two metres of McConnell till. Finally, the section is capped by another two metres of outwash gravel and sand. White River Tephra is exposed at the top of the section in colluvium.

Clastic sedimentary and metasedimentary rocks are in the same ratio and by far the most abundant lithologies in both tills at this section. These lithologies indicate a provenance to the east or southeast (Tempelman-Kluit, 1977, Maps 105F and G) during McConnell and pre-McConnell glaciations.

Four till fabrics were measured at this section (Fig. 3 and Table 1). Pebble orientations seem to be parallel and transverse to the ice flow direction inferred from till lithologies. Clasts may have been transported with the a-axes parallel to the ice-movement direction re-oriented after deposition due to deformation by the active glacier (Boulton, 1970; Amark, 1986).

Section 038

This section is exposed along the South Canol Road at the front of the Pelly Mountains (Fig. 1). At this section, the McConnell till reaches a thickness of 18 metres and is overlain by 25 metres of ice-contact gravels (Fig. 4). Abrupt contacts and rapid grain size variation between individual beds, and abundant faulting characterize the ice-contact gravels at this section.

Till pebble lithologies were identified at three levels (Fig. 4). Lithologies are mostly clastics with variable proportions of calcareous and metasedimentary clasts. The lowest part of the till is enriched in calcareous sedimentary clasts and depleted in metasedimentary clasts compared to the upper part. This stratigraphic change in lithologies within the same till unit could be explained by two hypotheses:

(1) Ice might always have flowed parallel to the Tintina Trench, and the dominance of calcareous clasts in the lower portion simply reflects local bedrock. In other words, changes in clast lithologies could simply reflect flow lines in the glacier.

(2) On the other hand, the lower portion of the till, which is mostly enriched in calcareous sediment, might have been deposited by a valley glacier which flowed out of Lapie River valley where the major sources of calcareous bedrock are located (Tempelman-Kluit, 1977, Map 105F).

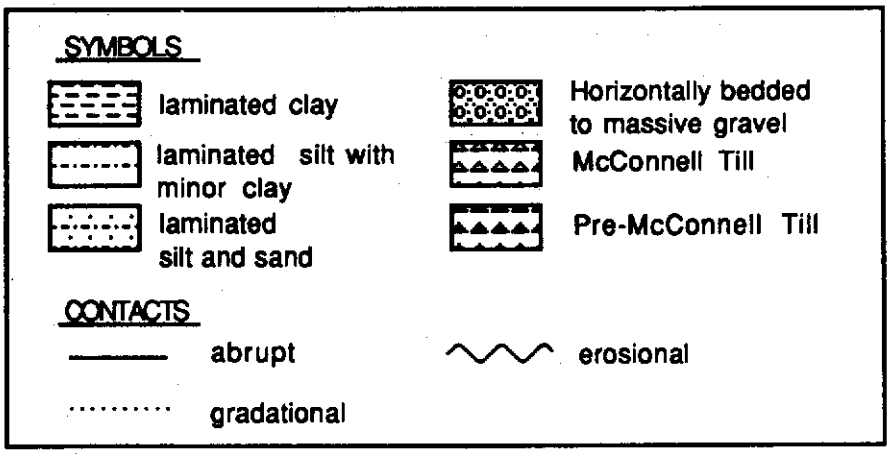

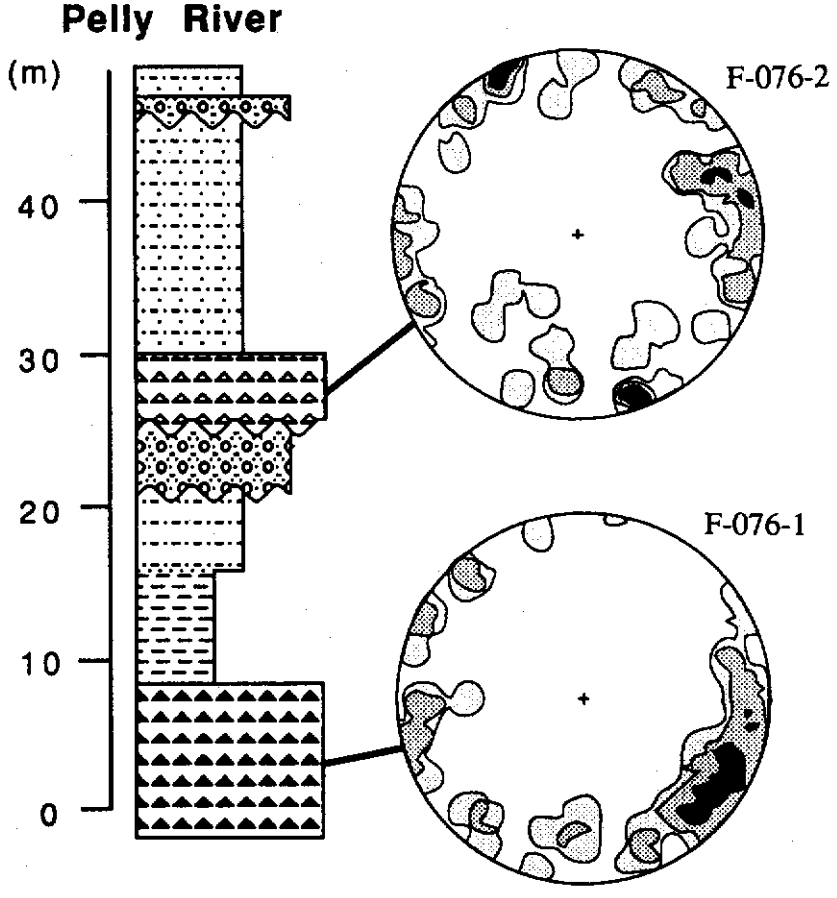

Figure 2. Stratigraphic column of section 076 with equal-area stereographic plots of long axes of stones (50 measurements in each case). See text for description.

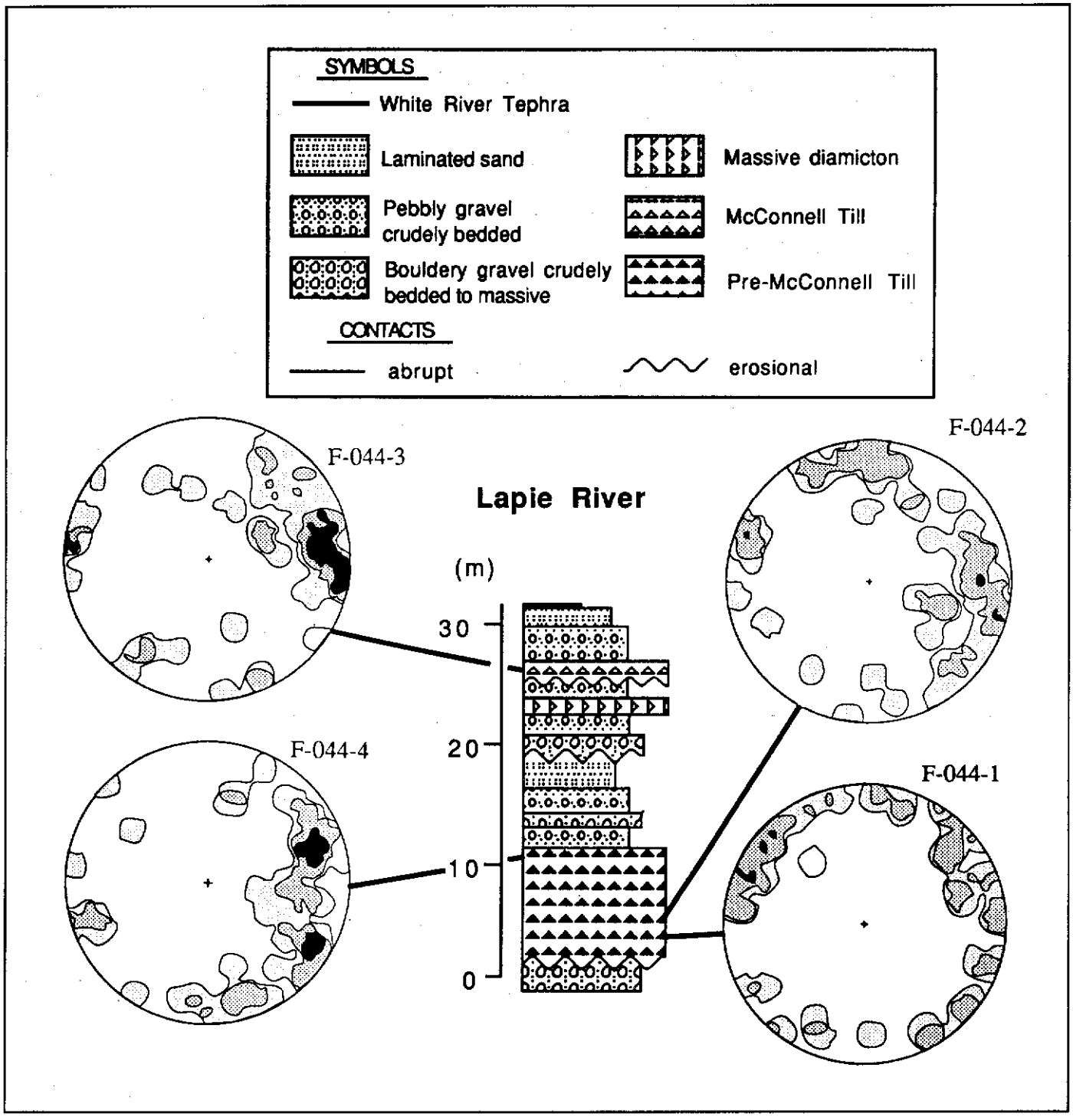

Figure 3. Stratigraphic column of section 044 with equal-area stereographic plots of long axes of stones (50 measurements in each case).

The greater abundance of metasediments in the upper part of the till could indicate a provenance from the Tintina Trench (Tempelman-Kluit, 1977, Maps 105F and G).

Till fabrics were measured at each of the three pebble sampling sites (Fig. 5 and Table 1). If clast a-axes are parallel to ice flow direction (which was the case for most fabrics measured in the McConnell till in the Tintina Trench), the till fabrics indicate an initial ice flow out of Lapie River valley, followed by flow parallel to the Tintina Trench. This supports hypothesis (2). However, the possibility remains that the a-axes in the lower fabrics are perpendicular to the ice flow direction, whereas the a-axes in the upper fabric are

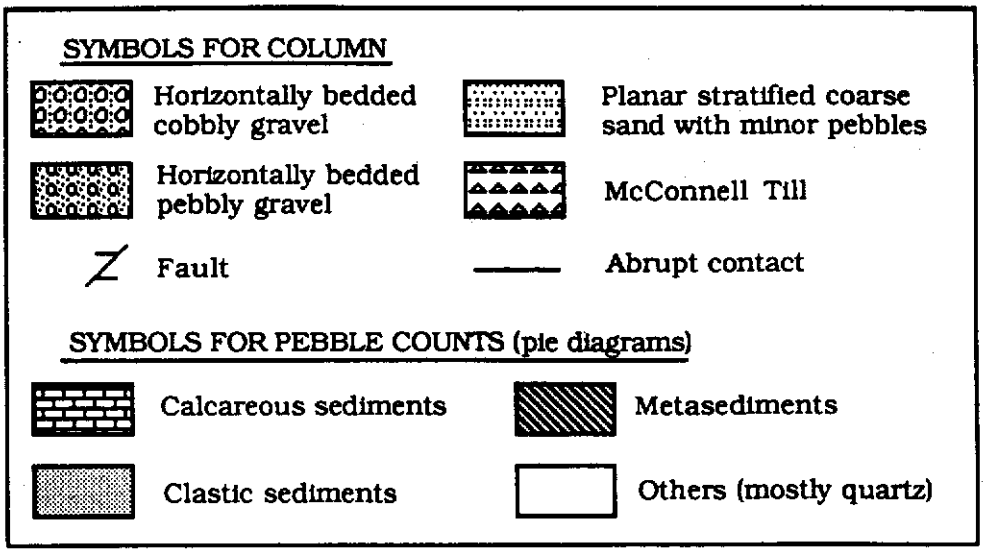

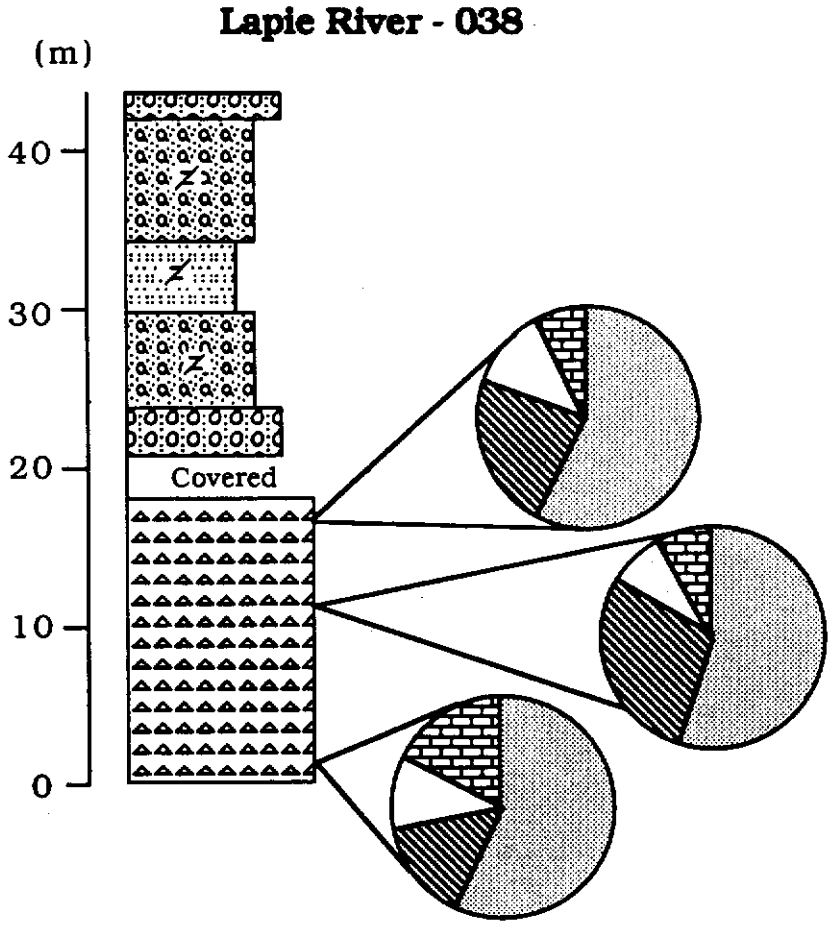

Figure 4. Composite stratigraphic column of section 038 with pie diagrams representing percentages of each lithology at three levels in till.

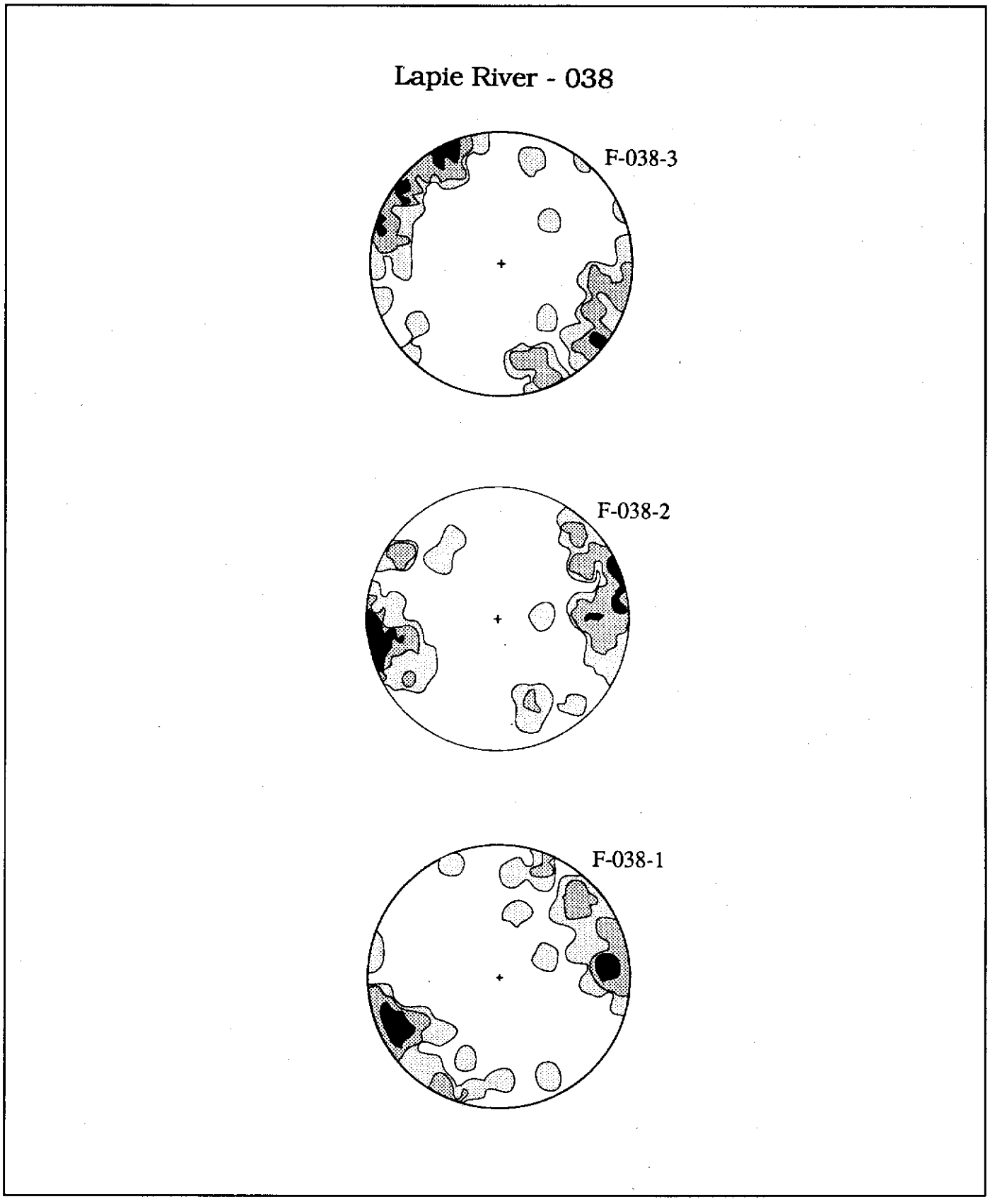

Figure 5. Equal-area stereographic plots of long axes of stones at section 038 (50 measurements in each case). Fabric locations are the same as pebble counts (see Figure 4).

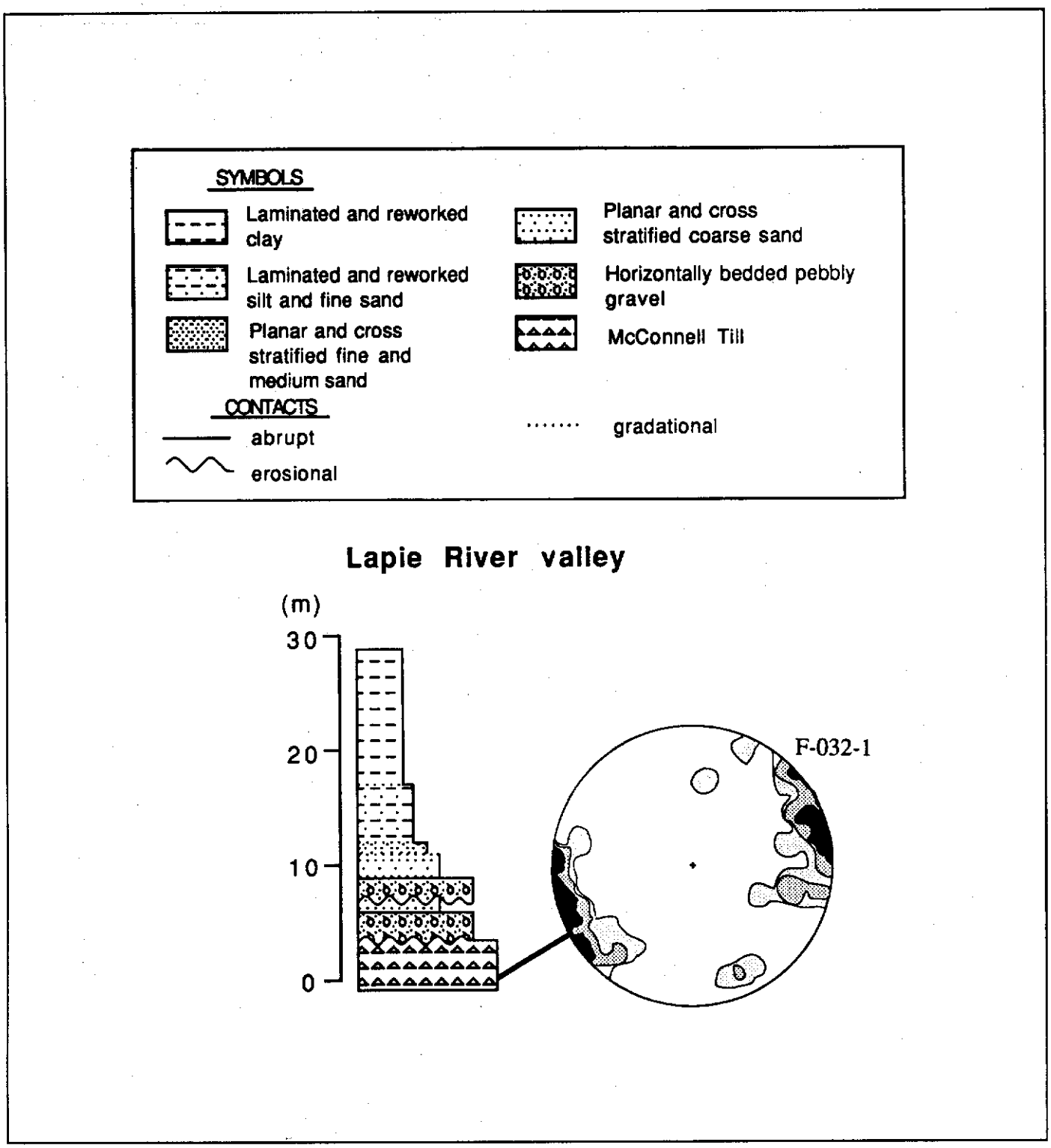

Figure 6. Stratigraphic column of section 032 with equal-area stereographic plot of long axes of stones (30 measurements).

parallel to it. Clast a-axes transverse to ice flow direction have been reported by Amark (1986) and Boulton (1970), among others.

Section 032

Section 032 is located along the South Canol Road in the Pelly Mountains (Fig. 1). The stratigraphy exposed at this section is depicted in Figure 6. About 4 m of McConnell age till is exposed at the bottom of this section. A single till fabric analysis reveals that elongated clasts have a preferred orientation parallel to the Lapie River valley (Fig. 6 and Table 1). A few cobbles of South-Fork Volcanics were recovered from the till. These could have been derived from outcrops of South-Fork Volcanics in the Macmillan Plateau (Gordey, 1988) or from unconsolidated sediments in the Tintina Trench (Plouffe, 1989). The till is overlain by stratified sand and gravels. A paleocurrent toward the west-southwest was measured on planar-cross stratified laminations in a well sorted sand bed. Pebbles of Tertiary rhyolite with a provenance to the northeast in the Tintina Trench (Tempelman-Kluit, 1977, Map 105F) were found in these gravels. Glaciolacustrine silt and clay overlie the gravels. These have been reworked by gravity flow; primary laminations are rare and discontinuous.

The stratified gravels are interpreted as subaqueous outwash fan deposits in a glacial lake which was dammed by ice advancing up Lapie River valley, based upon their stratigraphic position beneath glaciolacustrine sediments and their topographic location below the lowest possible outlet for the glacial lake. The water level elevation of this glacial lake was controlled by the ice dam, and the water drainage divide between the Lapie and Rose Rivers which is located higher in the Pelly Mountains at about 1080 m; gravels at this section are at about 945 m.

QUATERNARY HISTORY

The only clue about conditions prior to the pre-McConnell glacier event comes from the lowest gravels exposed at Section 044, which indicate a period of fluvial aggradation. Information gathered from the only two exposures of pre-McConnell till in the area unequivocally indicate that ice flowed toward the west to northwest during the pre-McConnell glaciation. Occurrences of pre-McConnell till are probably erosional remnants, and most of the drift was stripped off during the following glacial event. During deglaciation a glacial lake formed in the Pelly River valley and lasted for a long enough period of time to accumulate the thick sequences of laminated silt and clay now exposed at Section 076 (Fig. 2). During that time, areas adjacent to the Pelly River valley were characterized by glaciofluvial aggradation (Jackson, 1989). As part of the paraglacial processes (Jackson et al., 1982), major streams such as the Pelly River evolved from braided to meandering as the sediment load decreased (Jackson, 1989).

Assuming a-axes in Section 038 till fabrics are parallel to ice flow directions, a valley glacier flowed northward out of the Lapie River valley at the onset of McConnell glaciation. However, more field information is needed to verify this hypothesis. At the peak of the McConnell glaciation, ice flow in the Selwyn Lobe was west to northwest over the area, as indicated by till lithologies and till fabrics. At the end of the McConnell glaciation, an ice tongue advanced up the Lapie River valley from part of the Selwyn Lobe which still occupied Tintina Trench, blocking the Lapie River drainage and damming a glacial lake at about 1040 m, as estimated from the highest occurrence of glaciolacustrine sediments (Jackson, 1989). This is documented by clasts of South Fork Volcanics found in the McConnell till and Tertiary rhyolites in McConnell gravel, which were transported at least 9 km up valley from the mountain front.

Late glacial events were essentially the same for pre-McConnell and McConnell glaciations. During the retreat of the McConnell glacier, a glacial lake formed in the Pelly River valley under conditions similar to the pre-McConnell glacial retreat (Jackson, 1989).

TILL GEOCHEMISTRY SAMPLING AND ANALYSIS

In order to achieve the primary objective (drift prospecting study), 204 till samples were collected during the 1987 field season (Fig. 1). Samples were collected with the aid of a pick and shovel from river bank sections, road cuts, old trenches and hand dug pits. Care was taken to collect samples below the postglacial solum. In areas of easy access, like along the Campbell Highway, the distance between till samples averages 2 km.

Laboratory Procedures

Dry sieving was performed on till samples to separate the silt plus clay size fraction (<63 μm). The clay fraction (<2 μm) of till samples was separated by centrifuge, using standard procedures of the sedimentary laboratory of the Geological Survey of Canada. Determination of the silt/clay ratio was done by pipette analysis as described by Folk (1968). Till samples were wet sieved in order to separate the 125 to 250 μm size fraction. Heavy minerals were separated from this size range fraction with a shaking table and methylene iodide (s.g. 3.3) in the laboratory of Overburden Drilling Management Ltd., Nepean, Ontario. Geochemical analyses on clay and silt plus clay size fractions were done by Acme Analytical Laboratories Ltd., Vancouver, B.C. The clay fraction was analysed for Ag, As and Sb by ICP/MS (inductively coupled plasma mass spectrometry) after a hot (HCl-HNO_3-H_2O) acid leach using 0.5 g samples and Hg was analysed by flameless atomic absorption. The highest concentrations of most metals are found in the clay size fraction of oxidized till because (1) phyllosilicates have a primary metal enrichment within their structure, and (2) metals released by weathering of labile minerals are scavenged by colloidal particles such as clay minerals, oxides and hydroxides (Shilts, 1984). The <63 μm fraction was analysed for gold by atomic absorption using 10 g samples with a detection limit of 1 ppb. The silt plus clay size fraction was

analysed for gold, since Dilabio (1985) demonstrated that gold is preferentially enriched in the fine fractions of oxidized till. In the case of unoxidized till, such as samples collected from the measured sections, "gold is most abundant in grain size fractions that reflect the grain size of the glacially liberated and comminuted native gold and oxide or sulfide host minerals" (Dilabio, 1985). At Grew Creek (MINFILE 105K 009), the only well known Au mineralization in the area, gold occurs in bedrock as native particles with an average diameter of 7.5 μm (J.L. Duke, pers. comm., 1988). Consequently, assuming similar mineralization elsewhere into the Tintina Trench, it is likely that in unoxidized till gold is concentrated in the silt and finer size fractions. Using coarser fractions for analysis would dilute the gold content and reduce any anomaly contrast. Heavy minerals were analysed for Au by neutron activation at Bondar-Clegg & Co. Ltd, Ottawa, Ontario. The clay size fraction was also analysed for base metals and heavy minerals for a series of gold pathfinder elements; these results are discussed in Plouffe (1989).

RESULTS AND DISCUSSION

Several methods are presented in the literature to calculate a threshold for geochemical exploration (see Rose et al., 1979; Sinclair, 1974). However in this case, because of the scale of the geochemical survey, the 90th percentile was considered anomalous. In the case of Au in the silt plus clay size fraction of till, the 90th percentile is equivalent to 7 ppb.

Au in the silt plus clay size fraction of till

Textural analyses were performed on a series of samples to verify any possible relationships between the Au and silt contents, i.e. to determine if gold was preferentially concentrated in the silt size fraction compared to the clay size fraction. As illustrated in Figure 7, the correlation between the variables is very low. It is concluded that (1) size distribution of the <63 μm fraction does not affect gold values in this case, and (2) Au must be present in the clay fraction, probably bound as complexes to oxides, hydroxides and/or clay minerals (see Boyle, 1979; Boyle et al., 1975). At this point, there is a lack of data to indicate if gold in the silt plus clay size fraction is detrital and/or chemically remobilized. Detailed work on gold particles recovered from this fraction (e.g. fineness) could clarify whether their mode of transportation was detrital or chemical.

Forty-seven till samples were analysed twice in order to estimate the precision of the analytical method. These samples were chosen at random throughout the entire set of 204 samples. Results obtained after the first and second analyses are depicted in Figure 8 (using a graphic technique modified from Shilts, 1975). Vertical shading indicates values above background (>7 ppb or 90th percentile) after the first analysis; horizontal shading indicates values above background after the second analysis. Samples which returned anomalous values from both analyses are in the cross-hatched field. Finally, background samples are represented by dots in the clear field. Also shown in Figure 8 is a slope of 1, which is used here as a fast way to verify the precision of the analytical method. Since several samples plot well off the line, one can say that the precision is low. Samples falling in the cross-hatched field are most likely related to true anomalies. However, samples in the vertical and horizontal fields are not necessarily false anomalies because the analytical method has a poor precision. The poor precision of the analytical method for the silt plus clay size fraction is attributable to (1) heterogeneity of the samples, and (2) most measurements, even anomalous ones, are close to the detection limit of 1 ppb (Thompson and Howarth, 1976). Consequently, in order to evaluate whether a high value is worth following up or not, its spatial location with respect to other anomalies, geological setting and reproducibility should all be considered.

Transport distance of anomalous concentrations of gold in till

In the Grew Creek area, where at least two mineralized zones are known, detailed till sampling was conducted to determine the distance of transport of anomalous concentrations of gold from the source of mineralization (Fig. 9). Assuming that the dispersal train depicted in Figure 9 is derived from a unique source, i.e. the Main Zone, a single sample collected 250 m from the mineralization would have been recognized as anomalous (above the 90th percentile or 7 ppb) compared to the samples within the entire area. Furthermore, if the 75th percentile is declared anomalous (5 ppb), mineralization could be recognized as far away as 500 m. From these data, it is concluded that mineralization similar to Grew Creek might remain undetected with the sample interval of 2 km employed along the Campbell Highway. Any serious Au prospecting for epithermal deposits similar to Grew Creek along the Tintina Fault requires a till sample interval ≤ 500 m measured parallel to ice flow direction. More work is required in order to define the width of the gold dispersal train at Grew Creek. This would help define a reliable sampling interval measured perpendicular to ice flow direction.

Au geochemical map

A geochemical map for gold in the silt plus clay size fraction is depicted in Figure 10. High gold values are concentrated in the northwestern part of the study area between Ketza River and Grew Creek. The Grew Creek gold-silver deposit is well reflected in this size fraction of till, as indicated by a series of anomalies directly over and northwest of the Tarn and Main Zones (Fig. 9). Anomalies were also detected near gold occurrences reported by Kindle (1946; p.24) (MINFILE 105F 044,045) along the Lapie River. Abundant high values occur over and in proximity to Tertiary felsic and intermediate volcanic bedrock mapped by Tempelman-Kluit (1977) along the Tintina Fault Zone (MINFILE 105F 062,075,076). They represent a good prospecting target for buried hydrothermal systems similar to

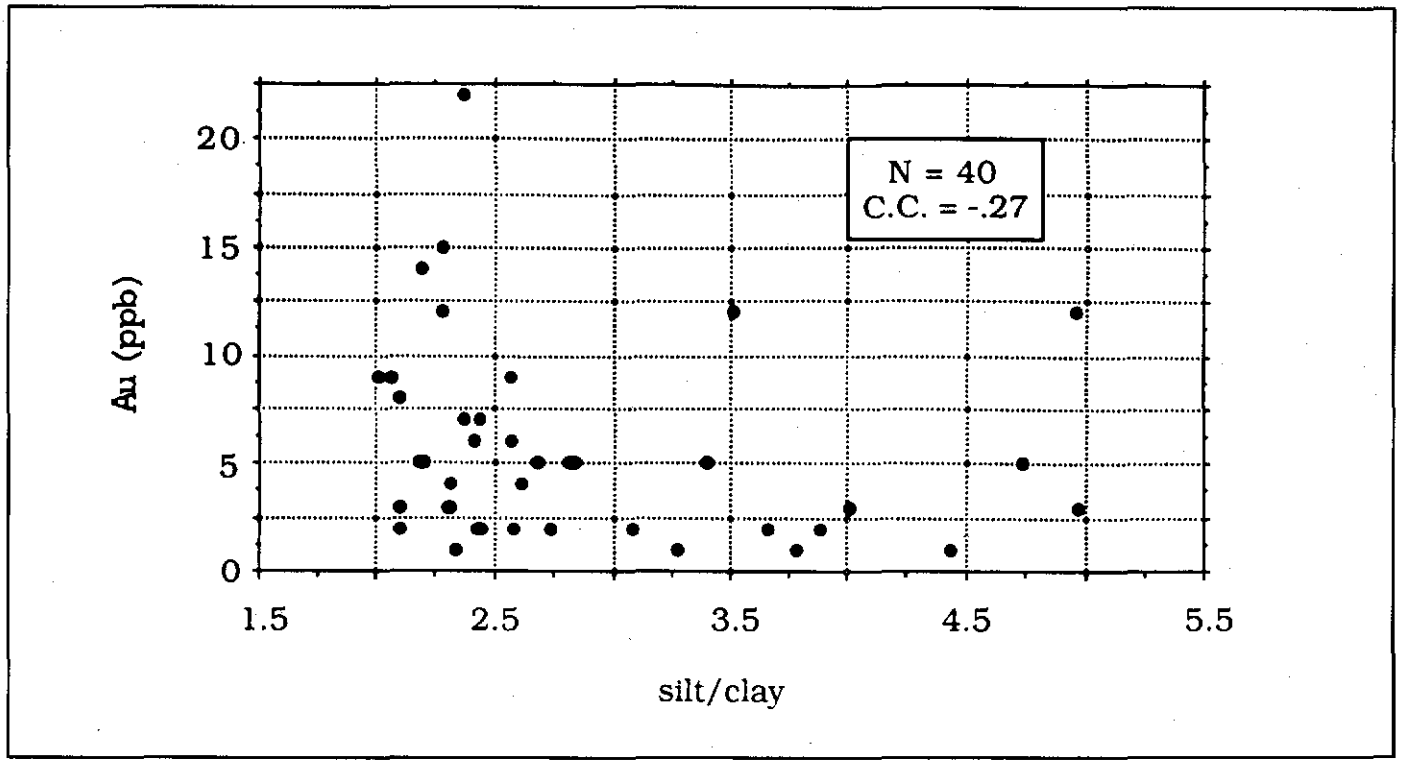

Figure 7. Correlation graph of Au content and silt/clay ratio of the silt plus clay size fraction of till (C.C.= correlation coefficient).

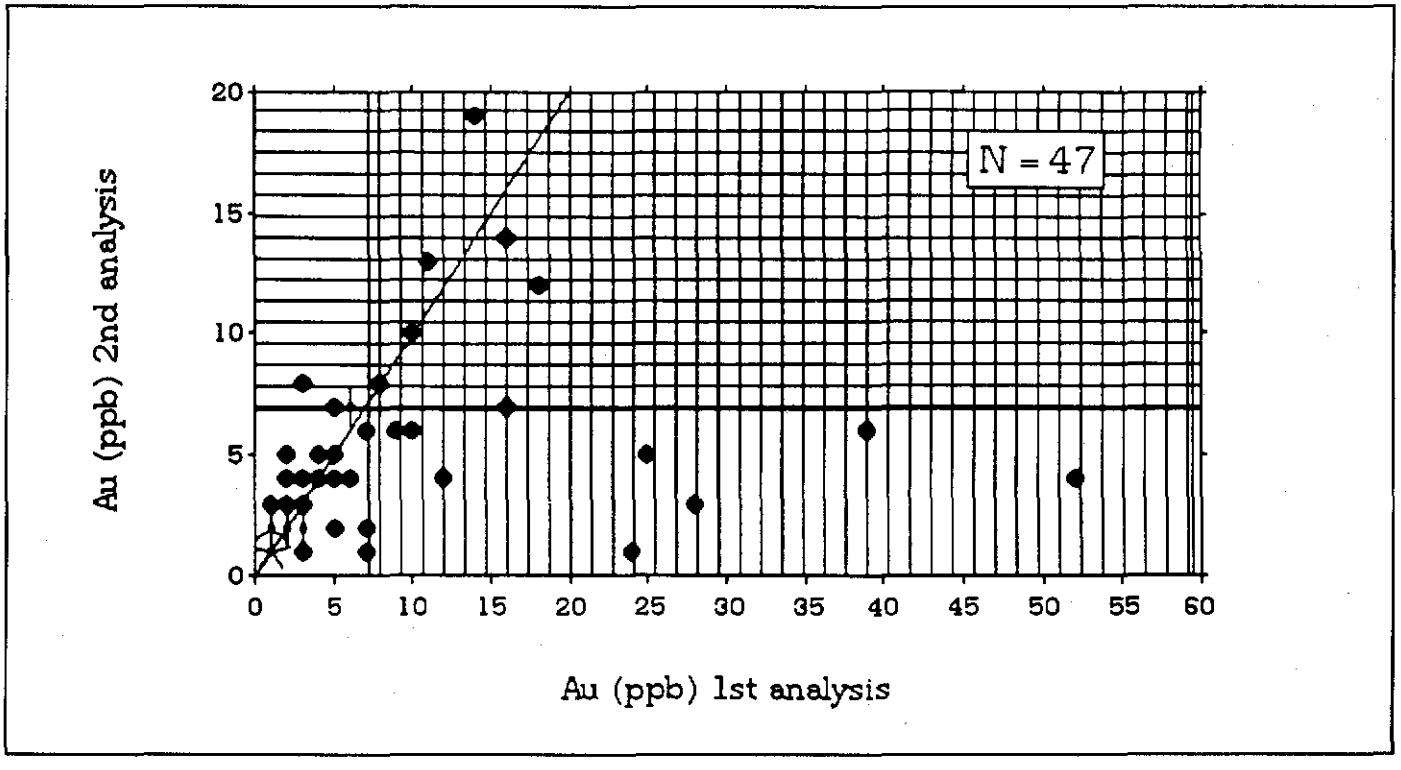

Figure 8. Graph showing results of duplicate analyses (using a graphic technique modified from Shilts (1975).

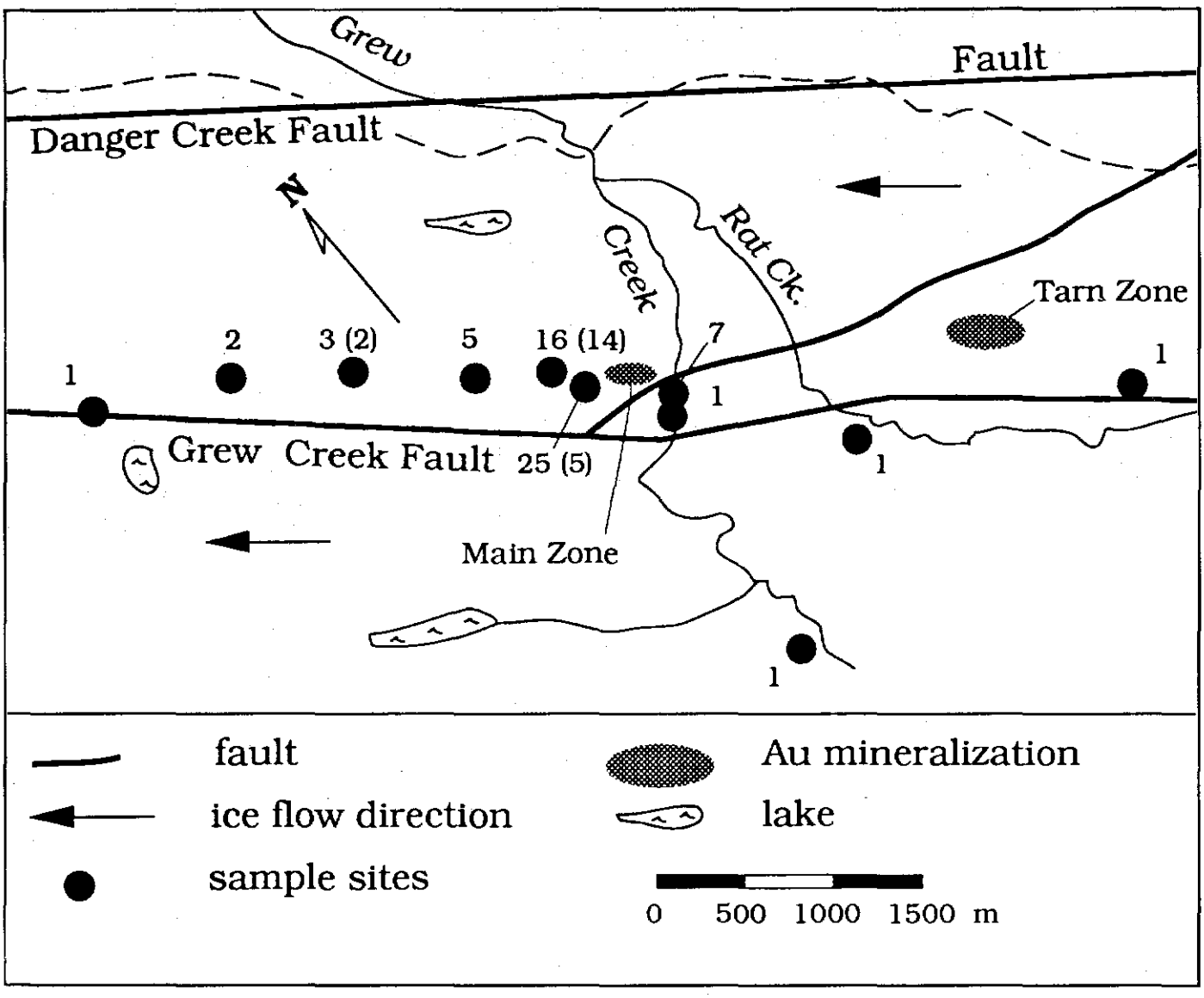

Figure 9. Detailed view of glacial dispersal of gold in the silt plus clay size fraction of till near the Grew Creek mineralization. Concentrations are in ppb, and values in parentheses represent duplicate analyses. Location of mineralized zones and faults from Duke and Godwin (1986).

the Grew Creek mineralization. Follow-up work on the anomalies near the Lapie River valley should be undertaken with special care because of the more complex ice flow patterns presented in the first part of this paper.

Jackson et al. (1986) suggested a link between Paleogene volcanism and the source of placer gold in the area. Values above the 75th percentile over and northwest of some of these volcanic bodies (Ketza River (105F 062), Starr Creek (105G 103,106) and northeast of Ross River) support this hypothesis (Fig. 10). To verify this hypothesis, more till sampling in closer proximity to these volcanic bodies is needed, since the transport distance of anomalous gold concentrations in till was found to be fairly short, in the order of 250 to 500 m. Follow-up of any of these anomalies should be undertaken with special care and as a first step, an attempt should be made to reproduce the results presented here.

Gold Pathfinders

Four common gold pathfinders were analysed to determine their possible use for drift prospecting in the study area. They are Ag, As, Hg and Sb. Correlation coefficients calculated for these elements and for gold are depicted in Table 2. Correlation of gold with each of these elements is very low, hence the use of these gold pathfinders in till exploration is not recommended in this area. This poor correlation reflects the bedrock geochemistry of Grew Creek, where at shallow depths (outcrop level), gold mineralization is

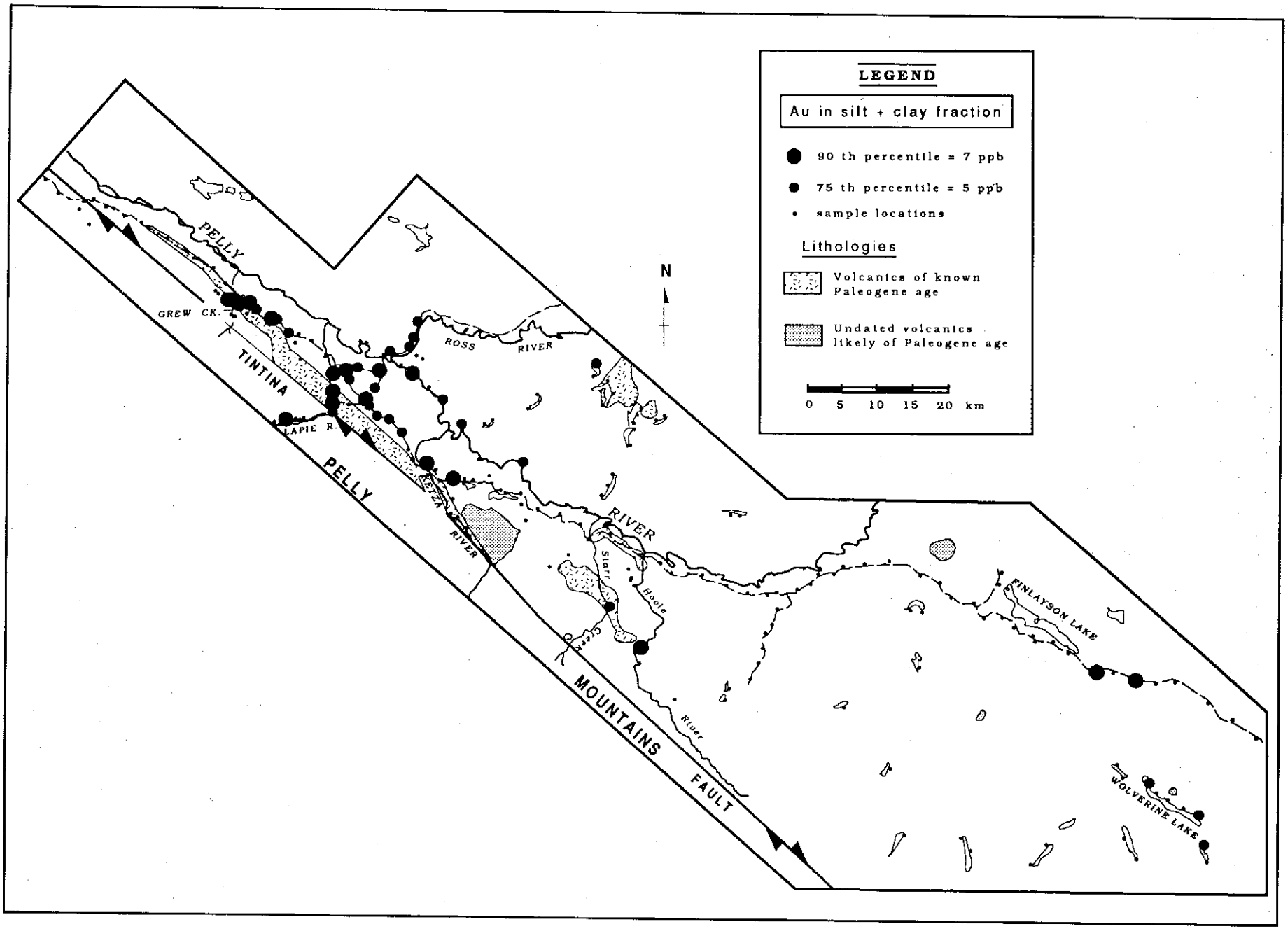

Figure 10. Gold abundance in silt plus clay size fraction of till.

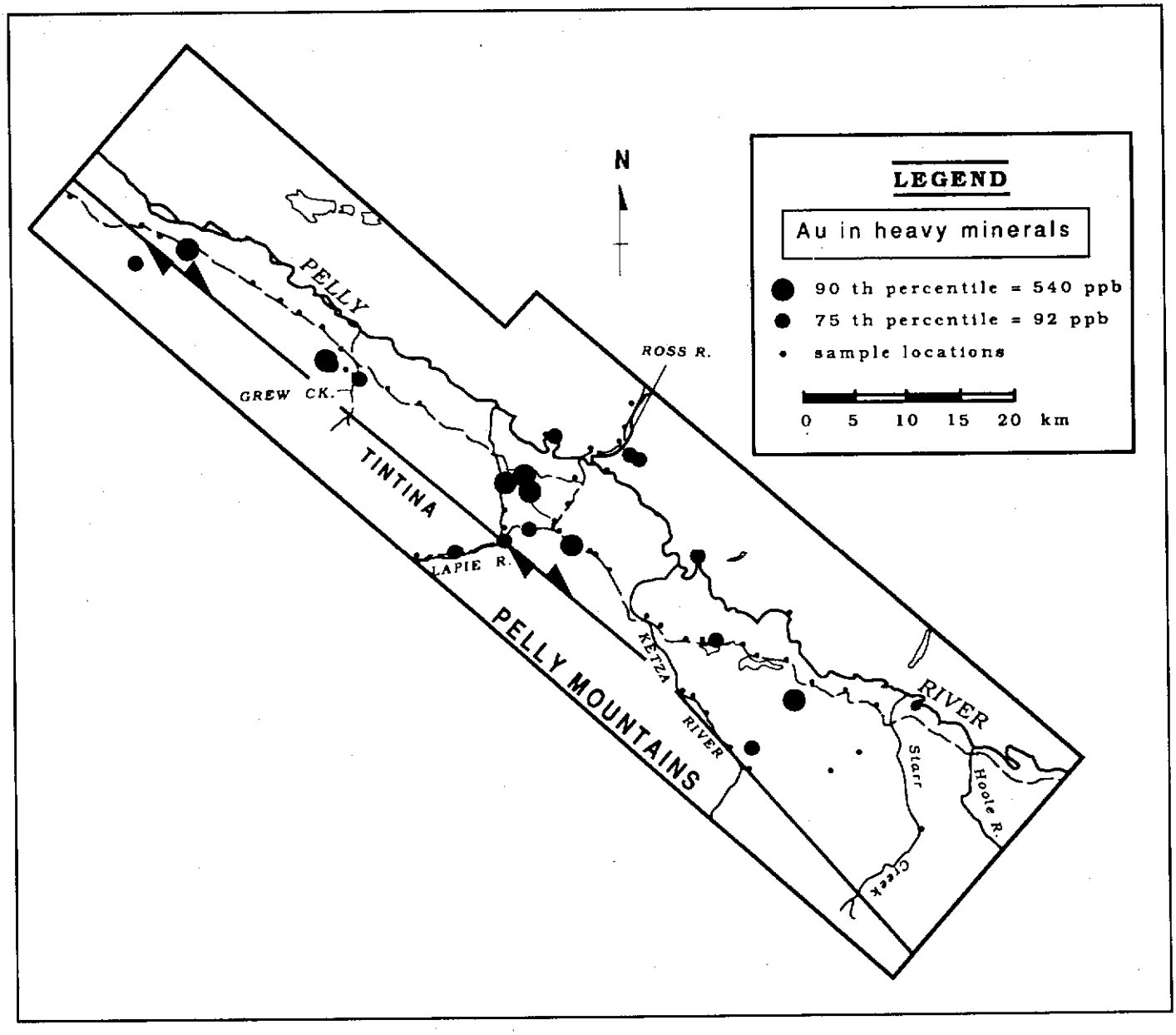

Figure 11. Gold abundance in heavy mineral concentrate from till in the northwest part of the study area.

not associated with high As, Ag, Hg or Sb concentrations (T. Christie, oral presentation, Whitehorse Geoscience Forum, 1988). Geochemical maps showing the distribution of Ag, As, Hg and Sb concentrations over the area are presented in Plouffe (1989).

Use of heavy minerals for gold exploration

The use of heavy mineral concentrates in drift prospecting for gold was originally thought to be useful in the Tintina Trench, but with certain site specific limitations[1]. Two examples of site specific limitations are the following: (1) most of the gold at Grew Creek is attached to quartz with a minor amount bound in pyrite (Duke and Godwin, 1986; Duke, 1986); gold in quartz is not recovered in the heavy mineral concentrate, and (2) surficial samples, as collected in reconnaissance surveys, are oxidized (except for certain areas where samples are collected in sections). Thus, gold in sulphides can be released, and reprecipitated or fixed in finer size fractions. In both cases, gold would go undetected in heavy mineral concentrates.

Heavy mineral separations, (s.g. $\geq$ 3.3) on the 125 to 250 μm size fraction, were done only for samples of the northwestern region to test the reliability of this fraction for gold exploration in the Tintina Trench. No visible gold grains were seen in heavy mineral concentrates under a binocular microscope. However, as shown in Figure 11, the Grew Creek deposit is reflected in the gold content of heavy mineral

Fabric	V1	V2	V3	S1	S2	S3
F-032-1	072 01	162 18	339 72	0.802	0.147	0.051
F-038-1	057 01	147 15	323 75	0.701	0.192	0.107
F-038-2	262 01	172 22	354 68	0.714	0.164	0.123
F-038-3	307 04	217 01	116 86	0.703	0.206	0.090
F-044-1	286 03	017 11	179 79	0.544	0.390	0.066
F-044-2	112 12	017 23	227 64	0.518	0.374	0.108
F-044-3	080 16	347 11	224 70	0.667	0.222	0.110
F-044-4	098 20	188-02	282 70	0.591	0.317	0.092
F-076-1	116 06	207 13	002 75	0.686	0.268	0.047
F-076-2	090 03	181 03	315 85	0.507	0.387	0.106

Table 1. Eigenvalues and eigenvectors of till fabrics calculated with the stereonet program (v. 3.6 by R.W. Allmendinger), following Mark (1973) eigenvalue method. Note that these values should be interpreted with care since as presented by Woodcock (1977), bimodal and multimodal data (which is the case for the till fabrics presented here) can result in the eigenvectors falling between modes. V1, V2 and V3 represent the trend and plunge of the eigenvectors; V1 being the direction of maximum clustering, and V3 that of normal clustering. S1, S2 and S3 are the respective normalized eigenvalues.

concentrates from McConnell till, in a few samples down-ice from the known mineralization. Likewise, heavy minerals show patterns of gold enrichment similar to those observed in the silt plus clay size fraction along the Campbell Highway close to the Lapie River (Fig. 10) (MINFILE 105F 044,045). Dispersed anomalous gold values (above the 90th percentile), not associated with known mineralization, occur throughout the area (Fig. 11). Some of these anomalies lie close to documented MINFILE occurrences (105F 050,051,060).

Most of the bedrock in the study area is not particularly enriched in heavy minerals. Consequently, till derived from it has the same characteristics. That explains why several till samples yielded only small amounts of heavy minerals. In some instances, like certain samples down-ice from the Grew Creek mineralization, not enough heavy minerals were recovered for geochemical assays. In order to obtain a representative amount of heavy minerals for geochemical analysis (>5 g), much larger till samples would have to be taken. This can represent a practical problem in a reconnaissance survey where numerous samples have to be collected over wide areas and have to be carried long distances by the sampler.

Correlation coefficients

	Au	Ag	As	Sb	Hg
Au	1				
Ag	-.04	1			
As	-.071	.283	1		
Sb	-.105	.2	.357	1	
Hg	.14	.445	.295	.232	1

Table 2. Correlation coefficients of gold with arsenic, antimony, mercury, and silver.

Based on these observations, it can be concluded that heavy minerals could be used for reconnaissance-level gold exploration in the Tintina Trench, if sample size does not represent a practical problem. In follow-up surveys, where samples are recovered from below the zone of oxidation (from sections or overburden drill cores), heavy minerals may be particularly efficient in detecting mineralization.

CONCLUSIONS

Based on till lithologies and till fabrics, glacier ice flowed west to northwest over the area during McConnell and pre-McConnell glaciations. However, at the onset of McConnell glaciation, a valley glacier might have flowed initially out of the Lapie River valley. More field information is needed to further verify this hypothesis. At the end of McConnell glaciation, an ice tongue flowed up gradient into the Lapie River valley.Within the study area, the silt plus clay size fraction of till is reliable for gold exploration since it reflects known gold mineralization at Grew Creek and is not influenced by textural parameters. On the other hand, reproducibility of gold analyses of the <63 μm size fraction is very low because of the heterogeneity of the samples and the fact that gold levels in this size fraction are low, i.e. close to detection limit, where precision is low. The problem of poor reproducibility can be solved in part by duplicate analyses.

High gold values in the silt plus clay size fraction of till in proximity to Tertiary volcanics support the hypothesis that these rocks could be a source of placer gold as proposed by Jackson et al. (1986). However, since the transport distance of anomalous gold in till was found to be fairly short (250 to 500 m), more detailed sampling close to these volcanic bodies would be needed to detect any gold mineralization. The use of Ag, As, Hg and Sb as pathfinder elements for gold exploration is not recommended because their correlation with gold is very poor in surficial samples. Heavy minerals could

be used for reconnaissance-level gold exploration in the Tintina Trench with certain site specific limitations.

ACKNOWLEDGEMENTS

Much of this paper was extracted from a M.Sc. thesis (Plouffe, 1989). Dr W.W. Shilts and Dr F.A. Michel are acknowledged for supervising the thesis and for useful discussions of the material presented here. I. Poliquin provided cheerful field assistance. Noranda Exploration Co. Ltd financed the geochemical analyses and heavy mineral separations. Field work was funded by Indian and Northern Affairs Canada, and by a grant from the Northern Research Group of the Ottawa-Carlton Geoscience Centre.

REFERENCES

AMARK, M., 1986. Glacial tectonics and deposition of stratified drift during formation of tills beneath an active glacier - examples from Skane, southern Sweden. Boreas, Vol. 15, p. 155-171.

BOSTOCK, H.S., 1966. Notes on glaciation in Central Yukon Territory. Geological Survey of Canada, Paper 65-36, 18 p.

BOSTOCK, H.S., 1934. The mining industry of Yukon 1933 and notes on the geology of Carmacks map area. Geological Survey of Canada, Summary Report 1933, Part A, p. 6-8.

BOULTON, G.S., 1970. On the origin and transport of englacial debris in Svalbard Glaciers. Journal of Glaciology, Vol. 9, p. 213-229.

BOYLE, R.W., 1979. The geochemistry of gold and its deposits. Geological Survey of Canada, Bulletin 280, 585 p.

BOYLE, R.W., ALEXANDER, W.M. and ASLIN, G.E.M., 1975. Some observations on the solubility of gold. Geological Survey of Canada, Paper 75-24, 6 p.

CAMPBELL, R.B., 1967. Glenlyon map area, Yukon Territory. Geological Survey of Canada, Memoir 352.

DILABIO, R.N.W., 1985. Gold abundances vs. grain size in weathered and unweathered till. In: Current Research, Part A; Geological Survey of Canada, Paper 85-1A, p. 117-122.

DUKE, J.L., 1986. The geology and alteration of an epithermal gold-silver prospect at Grew Creek, south-central Yukon Territory. Unpublished B.Sc. thesis, University of British Columbia.

DUKE, J.L. and GODWIN, C.I., 1986. Geology and alteration of the Grew Creek epithermal gold-silver prospect, south-central Yukon. In: Yukon Geology, Volume 1; Exploration and Geological Services Division, Yukon, Indian and Northern Affairs Canada, p. 72-82.

DUKE-RODKIN, A., JACKSON, L.E. Jr. and RODKIN, O., 1986. A composite profile of the Cordilleran Ice Sheet during McConnell Glaciation, Glenlyon and Tay River map areas, Yukon Territory. In: Current Research, Part B; Geological Survey of Canada, Paper 86-18, p. 257-262.

FOLK, R.L., 1968. Petrology of sedimentary rocks. Hempill's, University of Texas, 170 p.

GORDEY, S.P., 1988. The South Fork Volcanics: mid-Cretaceous caldera fill tuffs in east-central Yukon. In: Current Research, Part E; Geological Survey of Canada, Paper 88-1E, p. 13-18.

HUGHES, O.L., 1987. Quaternary Geology. In: Morison, S.R. and Smith, C.A.S. (eds), Guidebook to Quaternary Research in Yukon, INQUA Congress, Ottawa, Canada, National Research Council of Canada, Ottawa, p. 12-16.

HUGHES, O.L., CAMPBELL, R.B., MULLER, J.E. and WHEELER, J.O., 1969. Glacial limits and flow patterns, Yukon Territory, south of 65 degrees latitude. Geological Survey of Canada, Paper 68-34, 9 p.

JACKSON, L.E. Jr., 1989. Paleoglaciology of the Selwyn Lobe of the Cordilleran Ice Sheet and Quaternary stratigraphy of east central Yukon. In: Late Cenozoic history of the Interior Basins of Alaska and the Yukon. Carter, L.D., Hamilton, T.D. and Galloway, J.P. (eds.); United States Geological Survey, Circular 1026, p. 46-48.

JACKSON, L.E. Jr., 1987. Terrain Inventory Quiet Lake map area (105F). Geological Survey of Canada, Open File 1536.

JACKSON, L.E. Jr., 1986a. Terrain Inventory Finlayson Lake map area (105G). Geological Survey of Canada, Open File 1379.

JACKSON, L.E. Jr., 1986b. Terrain Inventory Tay River map area (105K). Geological Survey of Canada, Open File 1380.

JACKSON, L.E. Jr., GORDEY, S.P., ARMSTRONG, R.L. and HARAKAL, J.E., 1986. Bimodal Paleogene volcanics near Tintina Fault, east-central Yukon, and their possible relationship to placer gold. In: Yukon Geology, Volume 1; Exploration and Geological Services Division, Yukon, Indian and Northern Affairs, Canada, p. 139-147.

JACKSON, L.E. Jr., MACDONALD, G.M. and WILSON, M.C., 1982. Paraglacial origin for terraced river sediments in Bow Valley, Alberta. Canadian Journal of Earth Sciences, Vol. 19, p. 2219-2231.

KINDLE, E.D., 1946. Geological reconnaissance along the Canol Road, from Teslin River to Macmillan Pass, Yukon. Geological Survey of Canada, Paper 45-21, 29 p.

LERBEKMO, J.R., WEETGATE, J.A., SMITH, D.G.W. and DENTON, G., 1975. New data on the character and history of the White River volcanic eruption. In: Quaternary studies, Suggate, R.P. and Creswall, M.M. (eds); The Royal Society of New Zealand Bulletin, Vol. 13, p. 203-209.

MARK, D.M., 1973. Analysis of axial orientation data, including till fabrics. Geological Society of America Bulletin, Vol. 84, p. 1369-1374.

PLOUFFE, A., 1989. Drift prospecting and till geochemistry in Tintina Trench, southeastern Yukon. Carleton University and Ottawa Carleton Geoscience Centre, Ottawa, unpublished M.Sc. thesis, 111 p.

ROSE, A.W., HAWKES, H.E., WEBB, J.S., 1979. Geochemistry in mineral exploration. Academic Press, London, 657 p.

SHILTS, W.W., 1984. Till geochemistry in Finland and Canada. Journal of Geochemical Exploration, Vol. 21, p. 95-117.

SHILTS, W.W., 1978. Detailed sedimentological study of till sheets in a stratigraphic section, Samson River, Quebec. Geological Survey of Canada, Bulletin 285, 30 p.

SHILTS, W.W., 1975. Principles of geochemical exploration for sulphide deposits using shallow samples of glacial drift. Canadian Institute of Mining and Metallurgy, Bulletin 68, p. 73-80.

SINCLAIR, A.J., 1974. Selection of threshold values in geochemical data using probability graphs. Journal of Geochemical Exploration, Vol. 3, p. 129-149.

TEMPELMAN-KLUIT, D.J., 1977. Quiet Lake (105F) and Finlayson Lake (105G) map areas, Yukon. Geological Survey of Canada, Open File 486, (3 sheets), scale 1:250,000.

THOMPSON, M., and HOWARTH, R.J., 1976. Duplicate analysis in geochemical practice, part 1: theoretical approach and estimation of analytical reproducibility. The Analyst, Vol. 101, p. 690-698.

WARD, B., 1989. Quaternary stratigraphy along Pelly River in Glenlyon and Carmacks map areas, Yukon Territory. In: Current Research, Part E, Geological Survey of Canada, Paper 89-1E, p. 257-264.

WOODCOCK, N.H., 1977. Specification of fabric shapes using an eigenvalue method. Geological Society of America Bulletin, Vol. 88, p. 1231-1236.

1.'site specific limitations' is used in the sense of Shilts (1978).

APPLICATION OF LANDSAT TM THERMAL IMAGERY TO STRUCTURAL INTERPRETATIONS OF THE TINTINA TRENCH IN WEST-CENTRAL YUKON

J.K. Mortensen
Geological Survey of Canada
601 Booth St
Ottawa, Ontario
K1A 0E8

P. Von Gaza
Imperial Metals Corporation
800-601 West Hastings St
Vancouver, B.C.
V6B 5A6

MORTENSEN, J.M., and VON GAZA, P., 1992. Application of Landsat TM thermal imagery to structural interpretations of the Tintina Trench in West-Central Yukon Territory. In: Yukon Geology, Vol. 3; Exploration and Geological Services Division, Yukon, Indian and Northern Affairs Canada, p.214-222

ABSTRACT

The structure of the Tintina Fault Zone (TFZ) within the Tintina Trench in west-central Yukon is almost completely unknown, due largely to very poor exposure, and thick overburden cover. In this study, we have used digitally enhanced Landsat Thematic Mapper thermal imagery as a basis for a preliminary structural interpretation of the Tintina Trench in the Dawson-McQuesten area. Linear features visible on the enhanced images are divided into first order (obvious, long strike-length), second order (less obvious, shorter strike-length), and third order (subtle, very short strike-length) lineaments. The images show major, NW-SE trending first and second order lineaments within the Trench which we interpret to be separate strands of the TFZ. Sag ponds and fresh fault scarps in glacial drift along these lineaments attest to relatively recent fault activity. NE-SW trending first and second order lineaments that cut obliquely across the Trench are considered to be late faults and fracture zones which formed after major strike-slip displacement on the TFZ. Third order lineaments show strong preferred orientations over large portions of the image area, and are thought to reflect overall structural grain (bedding or foliation trends and/or regionally-developed joint patterns).

RÉSUMÉ

La structure de la zone faillé de Tintina (ZFT) à l'intérieur du sillon de Tintina dans la partie centrale ouest du Yukon est presque totalement inconnue, principalement parce que très mal mise à nu ainsi qu'en raison de la présence d'épais morts-terrains. Dans le cadre de cette étude nous avons utilisé l'imagerie thermique numériquement améliorée de l'appareil de cartographie thématique du Landsat pour effectuer une interprétation structurale préliminaire du sillon de Tintina dans la région de Dawson-Mcquesten. Les entités linéaires visibles sur les images accentuées se répartissent en linéaments de premier ordre (évidents; longs dans l'axe), de deuxième ordre (moins évidents, plus courts, dans l'axe) et de troisième ordre (ténus, très courts, dans l'axe). Les images montrent des linéaments majeurs des premier et deuxième ordres orientés NW-SE que nous interprétons comme étant deux branches distinctes de la ZFT. Des étangs occupant des dépressions et des escarpements de failles récents dans le drift glaciaire le long de ces linéaments témoignent d'une activité relativement récente le long de ces failles. Les linéaments des premier et deuxième ordres orientés NE-SW qui recoupent obliquement le sillon sont considérés comme étant des failles et des zones de fracture tardives qui se sont formées après le décrochement majeur le long de la ZFT. Les linéaments de troisième ordre présentent des orientations préférentielles marquées dans de grandes parties de la région imagée et l'on pense qu'ils reflètent le grain structural général (tendances de la stratification ou de la schistosité et configurations des diaclases régionales, ou les deux).

INTRODUCTION

The Tintina Trench is an elongated topographic depression which follows the trace of the Tintina Fault Zone (TFZ) for much of its length in Yukon. The TFZ is a major zone of Late Cretaceous and/or Early Tertiary dextral displacement. It separates two very different crustal blocks: to the northeast are strata of the North American miogeocline, and to the southwest lies an assemblage of crystalline rocks belonging to the Yukon-Tanana Terrane (e.g. Monger and Berg, 1987; Wheeler et al., 1988). In west-central Yukon there is almost no outcrop in the Tintina Trench and little is known about the detailed structure of the TFZ.

The Tintina Trench is of economic interest for two main reasons. First, several small lignite-grade coal deposits, some of which have been mined on a limited scale (MINFILE 116B 005,030,031), occur within faulted Paleocene-Eocene sediments in the Tintina Trench in the Dawson area (e.g. Mortensen, 1988a) and near Ross River (MINFILE 105F 048)(Hughes and Long, 1980)(Fig. 1). Second, epithermal precious metal mineralization associated with Eocene volcanic and sedimentary rocks has recently been discovered in the Grew Creek area within the Tintina Trench in east-central Yukon (Fig.1)(e.g. Duke and Godwin, 1986; Jackson et al., 1986)(MINFILE 105K 009). The suggestion that these Eocene volcanic rocks may be genetically related to the TFZ (e.g. Mortensen, 1988c) has focused attention on the mineral potential of the Tintina Trench elsewhere in western Yukon and eastern Alaska. An understanding of the overall structure of the TFZ will be critical to evaluating this potential.

The Tintina Trench in western Yukon approximately coincides with the southwest extent of Pleistocene glaciation. The region northeast of the Tintina Trench was glaciated and displays rugged relief and excellent bedrock exposure, whereas the area southwest of the Trench escaped glaciation, and generally shows low relief, very poor exposure and deep surface weathering. Much of the Tintina Trench in this area is mantled by glacial drift shed from the Ogilvie Mountains to the northeast. These factors complicate recognition and interpretation of surface features in the area.

This paper is an outgrowth of geological studies of the Klondike District and southwest Dawson map area (Fig. 1) by JKM (Mortensen, 1988a, b; 1990) and remote sensing studies of this and other areas of Yukon by PVG (e.g. Von Gaza and Eyton, 1988; Von Gaza, 1989). In this contribution we present a preliminary interpretation of the structure of the TFZ in west-central Yukon based on analysis of Landsat TM imagery. We hope that this work will both shed new light on the geology of this complex region and focus attention on some structural features in the area which may be of economic importance. The study also provides an example of how remote sensing may be applied to geological interpretation in areas of poor exposure in the northern Cordillera.

GEOLOGY OF THE TINTINA TRENCH IN THE DAWSON-MCQUESTEN AREA

The Tintina Trench in the Dawson-McQuesten area is a region of low relief ranging from 5 to nearly 20 km wide. In several places it is bounded on one or both sides by steep slopes that may represent eroded fault scarps. The bottom of the Tintina Trench is generally covered by glaciofluvial deposits and till (including the "Flat Creek Beds" and "Klondike Gravels" of McConnell, 1905, 1907) or by recent alluvial deposits (e.g. Hughes, 1987). Locally the unconsolidated deposits reach 200 m in thickness (Hughes, 1987). Rare bedrock exposures within Tintina Trench in this area consist of immature clastic sediments, including pebble conglomerate, sandstone, siltstone and mudstone. Seams of lignite grade coal occur in a number of localities (Fig. 1), and Paleocene to Eocene palynomorphs have been recovered from several exposures of coal-bearing clastic strata in this area (Hughes and Long, 1980). In many cases the clastic rocks are very poorly indurated, and decomposed outcrops of the coarser-grained units are commonly difficult to distinquish from glacial outwash gravels. All known outcrops of these Early Tertiary rocks display evidence of strong deformation: fault zones, folds, and locally overturned bedding are well developed (Bostock, 1935-1937 unpublished field notes, 1964; Hughes and Long, 1980; Mortensen, 1988b). Observed faults and fold axes are generally sub-parallel to the Tintina Trench.

The Tintina Trench ends just northwest of Chandindu River (Fig. 1), and between there and the Yukon-Alaska border the trace of the TFZ is marked by almost continuous exposure in outcrop and felsenmeer of the Early Tertiary sediments described above (Green, 1972; Hughes and Long, 1980; Mortensen, 1988a, b, 1990). Granitic and metamorphic rocks exposed along the banks of the Stewart River within the Tintina Trench near McQuesten (Fig. 1) imply that Early Tertiary rocks must be thin or absent in this area. About 50 km farther to the southeast (south of Stewart Crossing; Fig. 1), there is semi-continuous exposure of Mesozoic granite and Paleozoic and older metamorphic and sedimentary wall rocks right across the trace of the TFZ. The Early Tertiary strata apparently do not reappear in Tintina Trench until near the Pelly River, some 80 km farther to the southeast (Fig. 1)(e.g. Gordey and Irwin, 1987; Pride, 1988).

The region southwest of Tintina Trench in west-central Yukon is mainly underlain by low to medium grade metamorphic rocks of the Yukon-Tanana Terrane (e.g. Monger and Berg, 1987; Mortensen, 1988a, b, 1991). Three distinct magmatic events of relatively young age have been recognized in the area southwest of the TFZ (Woodsworth et al., 1989; Mortensen, 1988a, b, 1990). Intermediate to felsic volcanic and plutonic rocks which yield mid-Cretaceous (110-85 Ma) or Late Cretaceous (70-64 Ma) ages are widespread in this area. A suite of bimodal dykes, plugs, and minor subaerial volcanic rocks which yield mid-Eocene ages (59-53 Ma)(Mortensen, 1988a, b, unpublished data), is present in the Klondike District and parts of southwest Dawson map-area (Mortensen, 1988a, 1991) (Fig. 1). This magmatism is

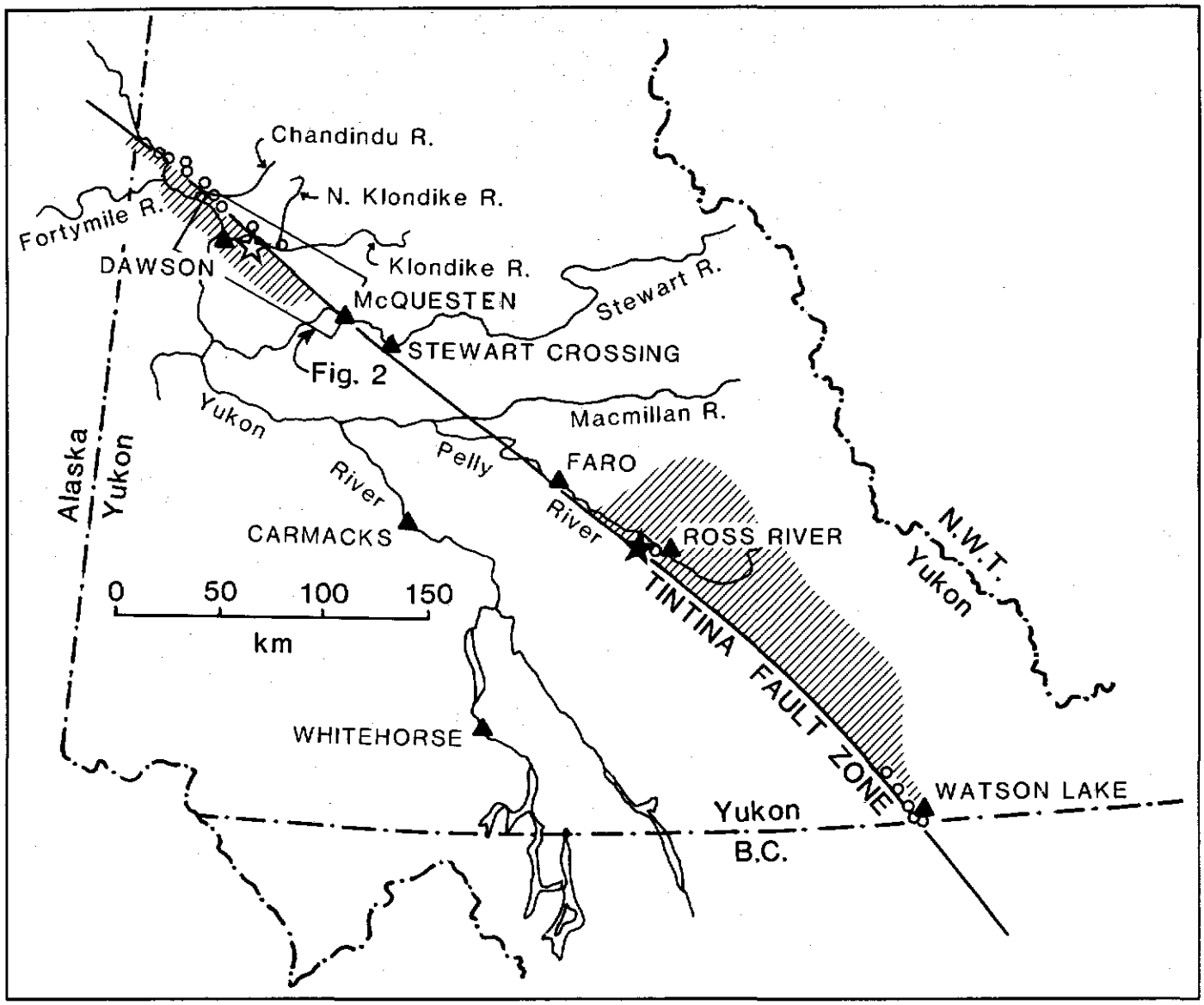

Figure 1. Location of study area (box). Limit of Eocene magmatism adjacent to the Tintina Trench is hachured. Location of the Grew Creek epithermal Au-Ag occurrence is shown by solid star; location of zone of epithermal-style alteration in the northern Klondike District shown by open star; location of coal occurrences within Tintina Trench is shown by open circles.

spatially and probably genetically related to the TFZ (Mortensen, 1988c). It is also identical in lithological association, composition and age to the igneous suite which hosts the Grew Creek epithermal precious metal deposit. Volcanic members of this suite in the Dawson area interlayered with immature clastic sediments that are indistinguishable from those in the Tintina Trench.

The area northeast of the Tintina Trench is underlain by an almost complete stratigraphic sequence from Proterozoic through Jurassic age (Green, 1972; Thompson and Roots, in preparation). Alkaline plutonic rocks which intrude this sequence in the Ogilvie Mountains (Tombstone Suite, Woodsworth et al., 1989) yield mainly mid-Cretaceous ages (90 ± 10 Ma). Quartz monzonite intrusions which are also mid-Cretaceous in age (85 Ma) occur sporadically throughout the area southeast of the North Klondike River on the north side of the TFZ (Fig. 1). Eocene igneous rocks have not been recognized in this area.

Geological mapping and analysis of conventional aerial photographs show little evidence of linear structures southwest of the Tintina Trench, which is surprising in an area so close to a major fault zone where subsidiary strands might reasonably be expected. A possible exception in the area between the Yukon River and Tintina Trench south of Chandindu River is documented by Mortensen (1988b).

Despite relatively good exposure northeast of the trench, geological mapping has yielded little evidence for strands of the TFZ outside of the Tintina Trench itself (e.g. Green, 1972; Thompson et al., in preparation).

STRUCTURAL INTERPRETATION OF THE TINTINA TRENCH USING LANDSAT TM IMAGERY

The use of Landsat Thematic Mapper (TM) imagery for structural interpretation has three main advantages. First, individual images cover a much larger area than conventional aerial photographs (a full TM scene represents 180 km E-W by 175 km N-S) allowing easier recognition of regional-scale patterns and large individual features. Second, a typical Landsat image is evenly illuminated across the entire scene, using a low sun angle which can enhance important structural features which have a topographic expression. In contrast, mosaics of aerial photographs usually show a variety of illumination patterns that can make interpretation difficult. Third, the TM imagery is acquired in seven spectral bands consisting of three visible bands, three near-infrared bands (reflected solar radiation), and a thermal infrared band (emitted terrestrial radiation). Using simple processing techniques these bands can be enhanced and viewed individually or in combination with other bands. The multispectral capability is valuable for enhancing lineaments where subtle changes in surface material such as soil or vegetation reflect underlying geology but the difference in image contrast is very low.

However, remote sensing techniques can be abused, by failure to recognize that some features may be artefacts, features produced during data acquisition and/or subsequent data manipulation. Ground checking of the satellite image-based interpretation is critically important.

Application

The digital image data set used for this study was captured by the TM multispectral scanner onboard the Landsat 4 satellite on June 14, 1986, at approximately 9:30 a.m. (path 63; row 15). A half to a full Landsat scene (two quadrants), with a footprint of approximately 85 km by 180 km, was obtained from the Canada Centre for Remote Sensing (CCRS) satellite receiving station located in Prince Albert, Saskatchewan.

We selected the segment of Tintina Trench between Chandindu River and McQuesten (Fig. 1) as a test area because of poor bedrock exposure and because known epithermal-type alteration occurs in Eocene volcanic and sedimentary rocks on the southwest margin of the Trench in the Dawson area (Fig. 1), and related mineralization may occur within the Trench.

The thermal band was the most successful in penetrating the thick vegetation cover of this unglaciated, geomorphically mature area. Thermal band data has a spatial resolution of 120 metres and is centred on a portion of the electromagnetic spectrum (11 μm) which detects changes in topography (sunlit slopes are "hot" and shadowed slopes are "cold") and gross changes in vegetation. This band does not appear to be significantly affected by subtle changes in the type of surface cover. The visible and reflected infrared bands, however, are affected by the "spectral clutter" of the regional vegetation response which masks subtle topographic changes.

Most of the interpretation that follows is based on analysis of the thermal band data. Each linear feature was assigned to one of three groups which reflect the degree of confidence placed on the interpretation. The classification is based on criteria such as length and/or clarity of the linear feature, supporting geological evidence, and whether the feature can also be recognized on other spectral bands or conventional aerial photographs.

First order lineaments are prominent on the thermal band without enhancement, and portions of these features can also be detected on other spectral bands. On the thermal image, first order lineaments can generally be followed continuously for more than 10 km along strike. Segments of first order features generally coincide with obvious topographic features such as aligned drainages, and are also usually visible on conventional aerial photographs. We believe that first order lineaments correspond to major through-going faults or fracture zones. Second order lineaments are somewhat more subtle, but can generally be recognized with minimal enhancement of the imagery. Second order features cannot always be recognized on other spectral bands. They also usually have shorter strike lengths, and are thought to represent minor faults and fracture zones.

Third order lineaments are subtle features that were only distinguished using a non-topographic hillshading technique (Von Gaza, 1989). This technique treats the digital image data as an actual topography, which is artificially illuminated by a single light source using a computer-assisted cartographic hillshading procedure. The shading of the digital image data provides an added depth clue that greatly improves the interpreter's ability to perceive subtle details in the image data. Various user-defined solar azimuths and solar elevations were used to identify third order lineaments.

To check the possibility that these third order features might represent artefacts produced by the enhancement technique, a digital lineament mask produced by the enhancement technique was overlaid on the contrast-stretched raw thermal image. In all cases, third order features were found to correspond with specific topographic features, usually short drainage segments, breaks in slope, or segments of ridge crests.

A variety of other lineaments that appear on the satellite image were examined on conventional aerial photographs and proved to be man-made features or natural surface features such as fluvial channels and levees or edges of old forest fire burns. These lineaments have been excluded from further discussion.

Figure 2 shows an enhanced thermal image of the study area, as well as a line sketch of the same area identifying the main first and second order linear features. Some of these features have been named where they coincide with named topographic features (e.g. Gravel Creek lineament, Barlow Lake lineament, etc.).

Two main orientations of first and second order lineaments are evident, generally trending to the NW-SE or NE-SW. The NW-SE trending lineaments occur only within

Figure 2a. NW area. Linearly contrast-stretched image of the TM Band 6 (thermal) data for the study area.

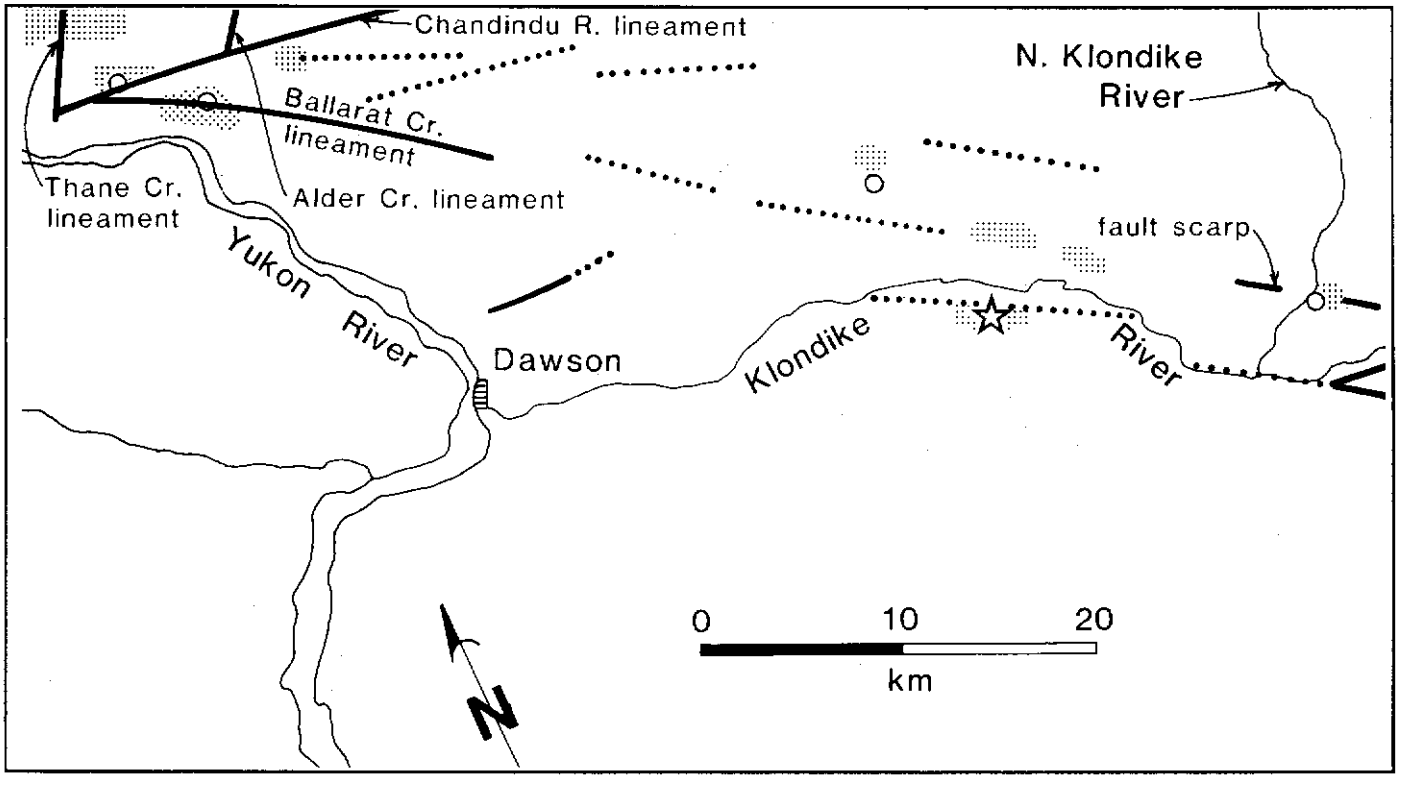

Figure 2b. NW area. Line sketch of the same area (same scale) showing the major first order (solid lines) and second order (dotted lines) lineaments identified in this study. Open star shows location of the zone of epithermal-style alteration; open circles show locations of coal occurrences. Areas of light stipple show outcrops of Eocene sedimentary rocks.

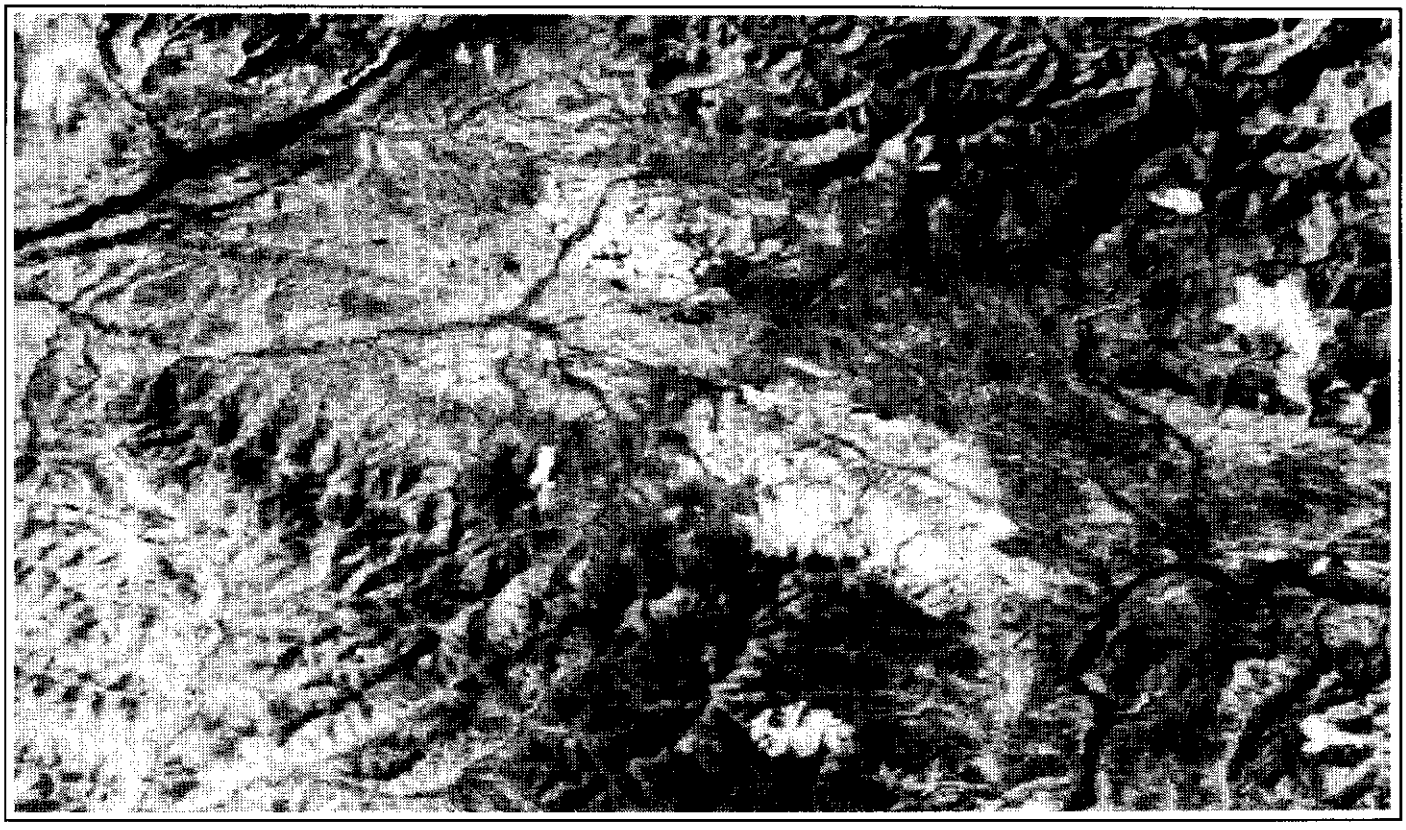

Figure 2a. SE area. Linearly contrast-stretched image of the TM Band 6 (thermal) data for the study area.

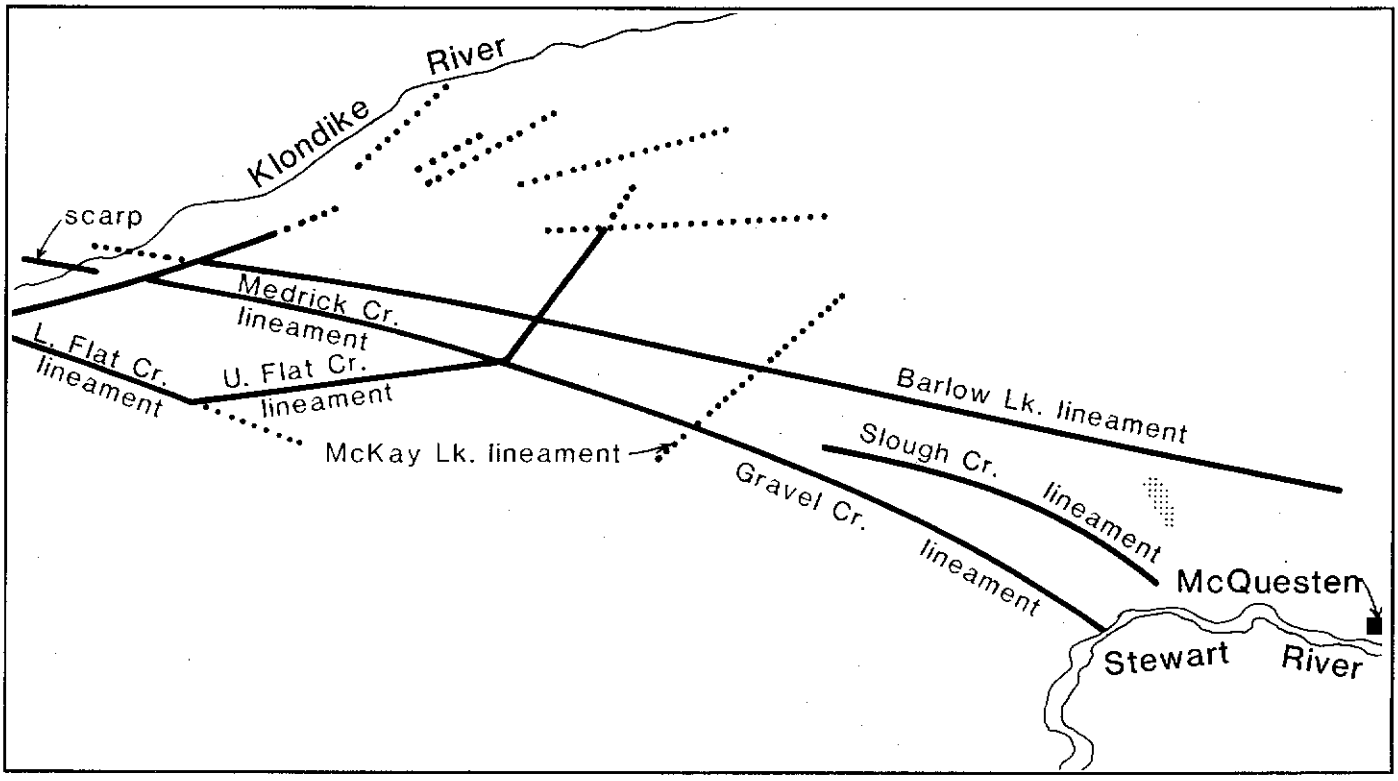

Figure 2b. SE area. Line sketch of the same area (same scale) showing the major first order (solid lines) and second order (dotted lines) lineaments identified in this study. Open star shows location of the zone of epithermal-style alteration; open circles show locations of coal occurrences. Areas of light stipple show outcrops of Eocene sedimentary rocks.

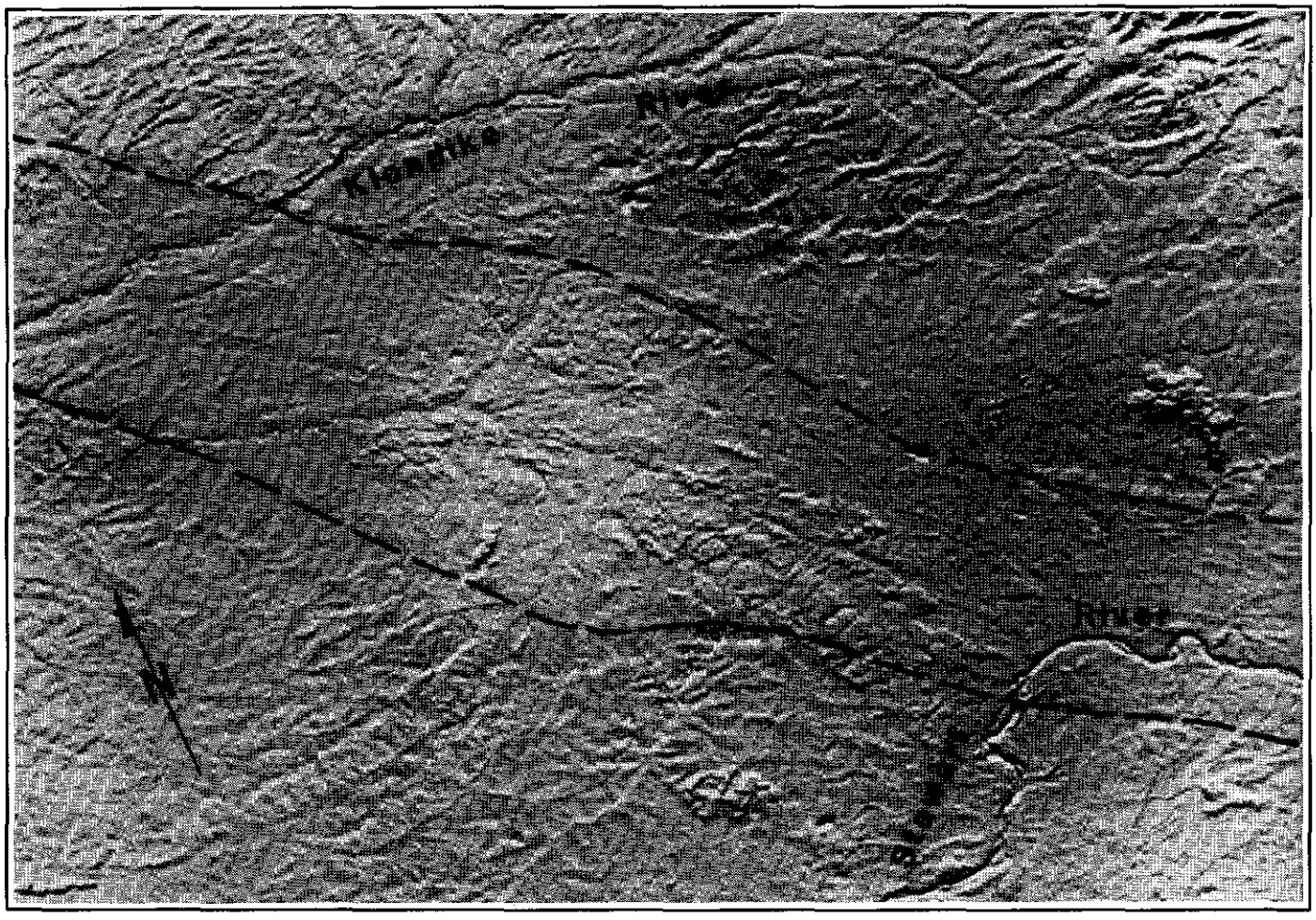

Figure 3. A non-topographically hillshaded image of TM Band 6 data for the southeast half of the study area, using sun angle = 0° and sun azimuth = 30°. The third order linear "fabric" is visible oriented at aproximately N-S and E-W in the north and southwest portions of the image area. Dashed lines show the approximate limits of the Tintina Trench.

or immediately adjacent to the Tintina Trench. The Barlow Lake lineament (Fig. 2) is one of the most obvious of these. At the southeast edge of the image, the lineament coincides with a prominent escarpment which forms the northeast edge of the Tintina Trench, and is probably an eroded fault scarp. A series of aligned, shallow lakes (including Barlow, Gravel, Lenore, and Strickland lakes) marks the northwest extension of the Barlow Lake lineament. These aligned lakes resemble "sag ponds" developed over small pull-apart zones in major strike-slip fault zones elsewhere in the world (e.g. Sylvester, 1988).

The Slough Creek, lower Flat Creek, and Gravel Creek-Medrick Creek lineaments are mainly marked by aligned drainages; however, clusters of small ponds which may also represent sag ponds are present along both of these features. Firm evidence that the Medrick Creek lineament is at least partially related to faulting is found at its northwest end, where the lineament crosses a small area of bedrock exposed during construction of the South Klondike ditch. The outcrop consists of strongly sheared and contorted Eocene sedimentary rocks. Shear planes generally parallel the Tintina Trench and dip vertically. Approximately 3 km farther to the northwest, immediately northwest of the Dempster Highway, a prominent scarp marks the trace of a normal fault down thrown at least 3 m to the south. The fault scarp can be traced for over 1 km along strike and is easily visible on aerial photographs (No. A37497:51-52). A similar but less obvious fault trace can be followed from the exposure of sheared Eocene sediments southeast to the Klondike River, a distance of 3 km (Fig. 2).

Some strong oblique lineaments are also evident. These are oriented at a moderate to high angle to the trend of the Tintina Trench. Some of the oblique lineaments, such as the upper Flat Creek lineament (Fig. 2), are confined to the Trench, and appear to connect pairs of the main NW-SE trending lineaments. Other features such as the McKay lineament (Fig. 2), however, cut right across the Trench and extend into topographically higher areas either side of the Trench. There is no evidence that the NW-SE trending features in the Trench are offset by this second set of lineaments, or vice versa.

Lineaments are less evident in the area northwest of the North Klondike River. Short segments of second order

lineaments were identified crossing upper Rock Creek and Coal Creek. The Ballarat Creek, lower Chandindu River, and Alder Creek lineaments are all prominent features, and there is good field evidence at least along lower Ballarat Creek for significant normal fault offset (Mortensen, 1988b).

Two sets of third order lineaments showing approximate north-south and east-west trends are visible in large parts of the study area but appear to be poorly developed or absent within the Tintina Trench. These lineaments are visible on a non-topographically hillshaded thermal image (Fig. 3). They define an almost pervasive "fabric" across most of the area northeast of the Trench and parts of the region to the southwest. This fabric is defined by the preferred orientation of a great number of relatively short topographic lineaments which are not visible on conventional aerial photographs.

All of the first and second order lineaments identified on Figure 2 are interpreted as fault or fracture zones cutting bedrock. The NW-SE trending lineaments are believed to be individual strands of the main TFZ, and mark zones of substantial strike-slip displacement. Some of the oblique features such as the upper Flat Creek lineament may also represent anastomosing strike-slip faults or "step-over zones" between main strands of the fault zone. Because the lineaments which cut all the way across the Trench do not appear to offset the NW-SE lineaments, they must represent relatively young faults or fractures, with little or no strike-slip displacement.

Third order lineaments are probably an expression of the main structural fabric of large bodies of bedrock (such as bedding, foliation planes and joint sets). This may explain why they do not appear to be developed in the unconsolidated material within Tintina Trench itself.

The development of sag ponds and apparently very young fault scarps in unconsolidated Plio-Pleistocene glacial deposits within the Tintina Trench attests to recent fault activity in this area. Maps of recent earthquake activity in Yukon show a concentration of epicentres which roughly coincides with the TFZ, indicating that the zone is still seismically active.

DISCUSSION AND CONCLUSIONS

This study shows there is evidence for a variety of structures within the Tintina Trench in the Dawson-McQuesten area. Most of these are interpreted as steep faults and fracture zones cutting bedrock. The most prominent structures are outlined on the Landsat thermal image by first and second order lineaments which are sub-parallel to the TFZ. These features are almost entirely confined to the Tintina Trench, and probably represent individual strike-slip strands of the TFZ itself, some of which have apparently experienced late normal offset. First and second order lineaments which cut obliquely across the Trench do not appear to be offset by the Trench-parallel lineaments, and probably represent younger faults or fracture zones which post-date the major strike-slip movement. Third order lineaments are thought to reflect the overall structural "grain" of underlying bedrock.

This study demonstrates that enhanced Landsat TM thermal imagery can yield important structural information even in heavily vegetated areas of with thick overburden. Some of the lineaments identified in this study may represent possible loci for structurally controlled epithermal precious metal mineralization. The evidence of recent fault activity in the Tintina Trench may also have significance for geological hazard assessment in west-central Yukon.

ACKNOWLEDGEMENTS

The Landsat images used in this study were made available through the Exploration and Geological Services Division, Indian and Northern Affairs Canada, Whitehorse, Yukon, in support of PVG's M.Sc. thesis project. We thank Owen Hughes for directing our attention to some recent fault scarps in the study area, and Mike Power for discussions on recent seismicity in Yukon. R. Parrish provided a critical review of the manuscript. This is Geological Survey of Canada contribution 13090.

REFERENCES

BOSTOCK, H.S., 1964. Geology, McQuesten, Yukon Territory. Geological Survey of Canada, Map 1143A.

DRURY, S.A., 1987. Image interpretation in geology. Allen and Unwin, 243 p.

DUKE, J.L. and GODWIN, C.I., 1986. The geology and alteration of an epithermal gold and silver prospect at Grew Creek, south central Yukon; in Yukon Geology, Vol. 1. Exploration and Geological Services Division, Yukon, Indian and Northern Affairs Canada, p. 72-82.

GORDEY, S.P., and IRWIN, S.E.B., 1987. Geology of Sheldon Lake (105 J) and Tay River (105 K) map areas, east-central Yukon. Geological Survey of Canada, Preliminary Map 19-1987.

GREEN, L.H., 1972. Geology of Nash Creek, Larsen Creek and Dawson map-areas, Yukon Territory. Geological Survey of Canada, Memoir 364.

HUGHES, J.D., and LONG, D.G.F., 1980. Geology and coal resources potential of Early Tertiary strata along Tintina Trench, Yukon Territory. Geological Survey of Canada, Paper 79-32, 21 p.

HUGHES, O.L., 1987. Flat Creek Hill section. In: Guidebook to Quaternary Research in Yukon, S.R. Morison and C.A.S. Smith (eds); XII INQUA Congress, Ottawa, Canada; National Research Council of Canada, Ottawa, p. 61.

JACKSON, L.E., GORDEY, S.P., ARMSTRONG, R.L., and HARAKAL, J.E., 1986. Bimodal Paleogene volcanics near Tintina Fault, east-central Yukon Territory, and their possible relationship to placer gold. In: Yukon Geology, Vol. 1; Exploration and Geological Services Division, Yukon, Indian and Northern Affairs Canada, p. 139-147.

McCONNELL, R.G., 1905. Report on the Klondike gold fields. Geological Survey of Canada, Annual Report, Vol. 14, 1901, p. 25-36.

McCONNELL, R.G., 1907. Report on gold values in the Klondike high level gravels. Geological Survey of Canada Publication No. 979, 34 p.

MONGER, J.W.H. and BERG, H.C., 1987. Lithotectonic terrane map of western Canada and southeastern Alaska. U.S. Geological Survey, Miscellaneous Field Studies Map 1847-B.

MORTENSEN, J.K., 1988a. Geology of southwestern Dawson map area, Yukon Territory (NTS 116 B&C). In: Current Research, Part E, Geological Survey of Canada, Paper 88-1E, p. 73-78.

MORTENSEN, J.K., 1988b. Geology of southwestern Dawson map area (NTS 116 B&C). Geological Survey of Canada, Open File 1927.

MORTENSEN, J.K., 1988c. Eocene magmatism associated with the Tintina Fault Zone in Yukon Territory: new contraints on timing and magnitude of strike-slip displacement. Paper presented at 1988 Geoscience Forum, Nov. 30, 1988, Whitehorse, Yukon.

MORTENSEN, J.K., 1990. Geology and U-Pb geochronology of the Klondike District, west-central Yukon Territory. Canadian Journal of Earth Sciences, Vol. 27, p. 903-914.

PRIDE, M.J., 1988. Bimodal volcanism along the Tintina Trench, near Faro and Ross River. In: Yukon Geology, Vol. 2, Exploration and Geological Services Division, Yukon, Indian and Northern Affairs Canada, p. 69-80.

SABINS, F.F.Jr., 1987. Remote sensing principles and techniques. W.H. Freeman and Company, 449 p.

SYLVESTER, A.G., 1988. Strike-slip faults; Geological Society of America Bulletin, Vol. 100, p. 1666-1703.

VON GAZA, P., 1989. Image enhancements for mineral exploration. Unpublished M.Sc. thesis, University of Alberta, Edmonton, Alberta.

VON GAZA, P. and EYTON, J.R., 1988. Enhanced Landsat Thematic Mapper imagery for exploration geology in the Wheaton River District, southern Yukon. In: Yukon Geology, Vol. 2; Exploration and Geological Services Division, Yukon, Indian and Northern Affairs Canada, p. 99-107.

WOODSWORTH, G.J., ANDERSON, R.G. and ARMSTRONG, R.J., 1989. Plutonic regimes in the Canadian Cordillera. Geological Survey of Canada, Open File 1983.

GREW CREEK EPITHERMAL GOLD-SILVER DEPOSIT, TINTINA TRENCH, YUKON, (105K/2)

Anthony B. Christie,
DSIR Geology and Geophysics
P.O. Box 30-368,
Lower Hutt, New Zealand

Jesse L. Duke,
Noranda Exploration Company Limited,
Suite 203-107 Main Street,
Whitehorse, Yukon,
Y1A 2A7

and

Ralph Rushton,
Department of Geology,
University of Alberta,
Edmonton, Alberta
T6G 2E3

CHRISTIE, A.R., 1992. Grew Creek epithermal gold-silver deposit, Tintina Trench, Yukon. In: Yukon Geology, Vol. 3; Exploration and Geological Services Division, Yukon, Indian and Northern Affairs, Canada, p.223-259

ABSTRACT

The Grew Creek epithermal gold-silver deposit in southeast Yukon (MINFILE 105K 009) is hosted by Eocene volcanic and sedimentary rocks deposited in a pull-apart basin within the Tintina Fault Zone. Flow rhyolites forming a dome in the Tarn Zone area, 1.5 km east of Grew Creek, pass westward into a succession of rhyolitic ignimbrites and air fall tuffs, exposed along Grew Creek and in the Main Zone, 500 m west of Grew Creek. These rhyolitic rocks are faulted against fluvial sediments to the north, along the W-E Fault, and basaltic rocks to the west. In the Main Zone, the volcanics, sediments, and the W-E Fault all dip steeply to the north.

The gold-silver mineralization forms an elongate tabular zone within the rhyolitic tuffs. The zone strikes parallel to the W-E Fault and dips vertically or steeply to the north. The eastern end of the mineralized zone is defined by a decrease in grade, whereas the western end is faulted off against the basaltic rocks. Within the zone, stockwork veins and hydrothermal breccias contain assemblages which include quartz, adularia, carbonates, quartz pseudomorphous after calcite, pyrite, marcasite, and traces of arsenopyrite, chalcopyrite, acanthite, electrum, silver selenides, galena, and sphalerite.

There is good correlation between gold and silver in drill core assays, with a gold:silver ratio of around 1:4 for the ore grade mineralization. The mineralization is strongly anomalous in arsenic and mercury, but there is only a weak correlation of mercury with gold and silver, with most high values for mercury lying above the gold-silver zone and associated with the W-E Fault. Arsenic concentrations are elevated over much of the area but there is no statistical correlation with the locally high concentrations of gold or silver.

Outcropping rhyolitic rocks are hydrothermally altered to intermediate argillic and advanced argillic assemblages, whereas subsurface rhyolitic rocks are altered to quartz-adularia or illite-quartz assemblages adjacent to veins, and to illite-quartz-adularia ± carbonate elsewhere. Advanced illite-quartz-adularia ± carbonate alteration is accompanied by an increase in Na_2O and decreases in TiO_2, CaO and Al_2O_3. Basalts are altered to carbonate-chlorite (propylitic) assemblages, accompanied at an advanced stage by a slight increase in CaO, and decreases in K_2O, Na_2O, SiO_2, and Al_2O_3.

Mineralization postdated tilting of the host pyroclastic and sedimentary rocks. Episodic fault movements in the Tintina Fault Zone structurally focused the hydrothermal fluids by providing locally high secondary permeability, whereas the high primary permeability of the rhyolitic tuffs promoted the development of stockwork veins and breccias. The absence of significant alteration and mineralization in the sediments suggests that a partly welded and intensely altered tuff unit, along the footwall of the W-E Fault, acted as an aquiclude, confining the hydrothermal fluid within the rhyolitic tuffs. Intense pyritic alteration of this unit and high concentrations of mercury in the vicinity of the W-E Fault form pyrite and mercury zones north of the mineralization.

RÉSUMÉ

Le gisement épithermal d'or et d'argent Grew Creek, au sud-est du Yukon, se trouve dans des roches volcaniques et sédimentaires de l'Éocène déposées dans un bassin d'extension situé à l'intérieur de la zone faillée de Tintina. Des coulées de rhyolites provenant d'un dôme dans la région de la zone Tarn, à 1,5 km à l'est du ruisseau Grew passent vers l'ouest à une succession d'ignimbrites et de projections de tufs rhyolitiques qui sont mis à nu le long du ruisseau Grew et dans la zone Main, à 500 m à l'ouest du ruisseau Grew. Ces roches rhyolitiques sont faillées et reposent contre des sédiments fluviaux au nord, le long de la faille W-E, et contre des roches basaltiques à l'ouest. Dans la zone Main, les roches volcaniques et sédimentaires et la faille W-E présentent un fort pendage en direction du nord.

La minéralisation en or et en argent forme une zone tabulaire à l'intérieur des tufs rhyolitiques. La zone est orientée parallèlement à la faille W-E et présente un pendage vertical ou abrupt en direction du nord. L'extrémité orientale de la zone minéralisée est définie par une diminution des teneurs alors qu'à son extrimité occidentale elle est séparée des roches basaltiques par une faille. À l'intérieur de la zone, un réseau de veines minéralisées et des brèches hydrothermales renferment des assemblages englobant du quartz, de l'adulaire, des carbonates, du quartz pseudomorphe de la calcite, de la pyrite, de la marcasite et des traces d'arsénopyrite, de chalcopyrite, d'acanthite, d'electrum, de séléniures d'argent, de galène et de sphalérite.

Il existe une bonne corrélation entre les déterminations des teneurs en or et en argent dans des carottes de forages et le rapport or sur argent est d'environ 1:4 pour la minéralisation à teneur commerciale. La minéralisation présente des concentrations fortement anormales en arsenic et en mercure, mais le mercure ne présente qu'une faible corrélation avec l'or et l'argent. La plupart des concentrations élevées en mercure ont été relevées au-dessus de la zone aurifère et argentifère et sont associées à la faille W-E. Les concentrations en arsenic sont élevées sur une bonne partie de la région, mais ne présentent aucune corrélation statistique avec les concentrations élevées par endroits en or et en argent.

Les roches rhyolitiques affleurantes ont été hydrothermalement altérées en assemblages argilliques intermédiaires à avancés, alors que les roches rhyolitiques subsuperfricielles sont altérées en assemblages de quartz-adulaire ou de quartz-illite près des veines et en illite-quartz-adulaire ± carbonate ailleurs. Une altération poussée en illite-quartz-adulaire ± carbonate s'accompagne d'accroissements des concentrations en Na_2O et de diminutions des concentrations en TiO_2, en CaO et en Al_2O_3. Les basaltes sont altérés en assemblages de carbonate et chlorite (propylitiques) avec un léger accroissement de la concentration en CaO et des diminutions des concentrations en K_2O, en Na_2O, en SiO_2 et en Al_2O_3.

La minéralisation est postérieure à l'inclinaison des roches pyroclastiques et sédimentaires hôtes. Des déplacements épisodiques le long des failles dans la zone faillée de Tintina ont concentré les fluides hydrothermaux en fournissant des perméabilités secondaires élevées par endroits alors que la perméabilité primaire élevée des tufs rhyolitiques favorisait la formation du réseau de veines et des brèches. L'absence d'une altération importante et d'une minéralisation dans les sédiments suggère qu'une unité partiellement soudée de tuf ayant subi une intense altération, le long de la lèvre inférieure de la faille W-E, a agi comme une aquiclude confinant les fluides hydrothermaux aux tufs rhyolitiques. Une intense altération pyriteuse de l'unité de tuf rhyolitique et des concentrations élevées en mercure sont observées aux environs de la faille E-W au nord de la minéralisation.

INTRODUCTION

The Grew Creek prospect (MINFILE 105K 009) is a volcanic-associated epithermal gold-silver deposit located about one kilometre south of the Robert Campbell Highway, half way between Faro and Ross River, in south-east Yukon (Fig. 1A; NTS 105 K/2 115815; Latitude 62°03'N and Longitude 132°50'W). The prospect has been of considerable interest to the exploration industry because it was the first reported showing of epithermal mineralization in the Tintina Trench. Lesser showings have since been discovered near Dawson (Mortensen, 1988) and Glenlyon (Pride, 1988). We commenced this study in 1988 with the aims of characterizing the geology of the deposit and determining its genesis, building on previous descriptions of the deposit by Duke (1986), and Duke and Godwin (1986), but using a much larger database of drillhole information. This paper reports preliminary results of our work. Oxygen isotope analyses of vein and wall rock samples, and petrographic work, are continuing.

EXPLORATION HISTORY

Mineralization was discovered in outcrop, 600 m west of Grew Creek, by prospector Al Carlos in 1983 while exploring for a possible source of the previously known placer gold in Grew Creek. He reported an assay of 10 grams gold/tonne (g/t Au) across the discovery outcrop. Hudson Bay Exploration and Development Company Limited (Hudson Bay) optioned the property in November 1983 and carried out geological, geophysical and geochemical surveys, trenching, 1,732 m of diamond drilling in 13 holes, and 1,660 m of rotary drilling in 19 holes (Anon, 1985; Stroshein, 1986a, 1986b). An area of gold-silver mineralization, named the Main Zone, was defined around the discovery outcrop (10062E/9945N on the Noranda grid, see below) and centred approximately 500 m west of Grew Creek. An area of extensive hydrothermal alteration and anomalous geochemistry centred approximately 1.5 km east of Grew Creek, was named the Tarn Zone (Figs 1C and 2). Hudson Bay dropped its option in January 1987, and a new option agreement was taken up by Noranda Exploration Company Limited (Noranda) in June 1987. Golden Nevada Resources Incorporated (Goldnev) and Brenda Mines farmed into the property in June 1987, by funding the subsequent exploration program operated by Noranda. During 1987 and 1988 Noranda carried out geological mapping, as well as ground based magnetometer, induced polarization (IP)/resistivity and soil geochemistry surveys, an airborne electromagnetic survey, 235 m of trenching, 19,173 m of diamond drilling in 77 holes, and 1,651 m of reverse circulation drilling in 13 holes (Copland, 1988a, 1988b; Duke, 1988). Noranda defined the Main Zone mineralization as an east-west orientated body up to 550 m long, 110 m wide and 150 m deep. No significant mineralization was encountered in the Tarn Zone but additional drill targets near the Main Zone were identified. Subsequently, Goldnev became operator and, during 1989, drilled 10 diamond drillholes totalling 1,164.5 m in the Main Zone, to further define the ore reserves (Seto and Crowe, 1989).

The airborne geophysical surveys proved useful as an aid to interpreting regional structure and geology, and the IP/resistivity anomalies defined depth of overburden. However, the thick cover of till appears to have masked the detailed trends of the mineralization. On a regional scale, the mineralization is characterized by anomalous arsenic and mercury soil (till) geochemistry, but these anomalies are broad and failed to define drill targets in the mineralized zone.

ORE RESERVES

Orcan Mineral Associates estimated geological reserves of 852,100 short tons (773,012 tonnes) grading 0.260 oz/ton Au (8.9 g/t Au) and 0.98 oz/ton Ag (33.6 g/t Ag) at a cut-off grade of 0.058 oz/ton (0.2 g/t), and containing a higher grade reserve of 203,870 short tons (184,947 tonnes) grading 0.354 oz/ton Au (12.1 g/t Au) (Goldnev news release, December 4, 1989).

PREVIOUS RESEARCH WORK

Duke (1986) and Duke and Godwin (1986) mapped and sampled Grew Creek, the discovery outcrop, and several of Hudson Bay's exploration trenches, and carried out mineralogical, geochemical, oxygen isotopic, and K-Ar age analyses and petrographic work. They demonstrated that the mineralization consisted of gold, electrum, pyrite, and silver selenide minerals in quartz and K-feldspar veins hosted by rhyolitic tuffs. Silicic, acid sulphate, and argillic acid sulphate hydrothermal alteration types were identified in trenches and surface outcrops, and found to be overprinted by "surficial alteration" weathering. K-Ar ages on least altered basalts (51.4 and 50.7 m.a. B.P.) and palynological ages on mudstones (age range representing 56 to 46 m.a. B.P.) associated with the rhyolitic tuffs indicated a mid Eocene age for the host rocks, whereas three K-Ar ages on hydrothermally altered tuffs (51.5, 47.0 and 36.0 m.a. B.P.) suggested a mid to late Eocene age for the mineralization. A deep magmatic source for the mineralization was postulated based on the degree of heavy oxygen isotope enrichment.

Jackson et al. (1986) and Pride (1988) described the basalt and rhyolite associated with the Tintina Fault, including those at Grew Creek, and reported XRF analyses and several whole rock K-Ar ages. Jackson et al. (1986) concluded that the volcanic rock suite was strongly bimodal, with calc-alkaline to transitional tholeiitic basalts and high potassic subaluminous rhyolites. The basalts were dated as Eocene (5 K-Ar ages ranging from 55.4 to 46.4 m.a. B.P.) and the rhyolites as Paleocene to Eocene (4 K-Ar ages ranging from 58.2 to 51.5 Ma).

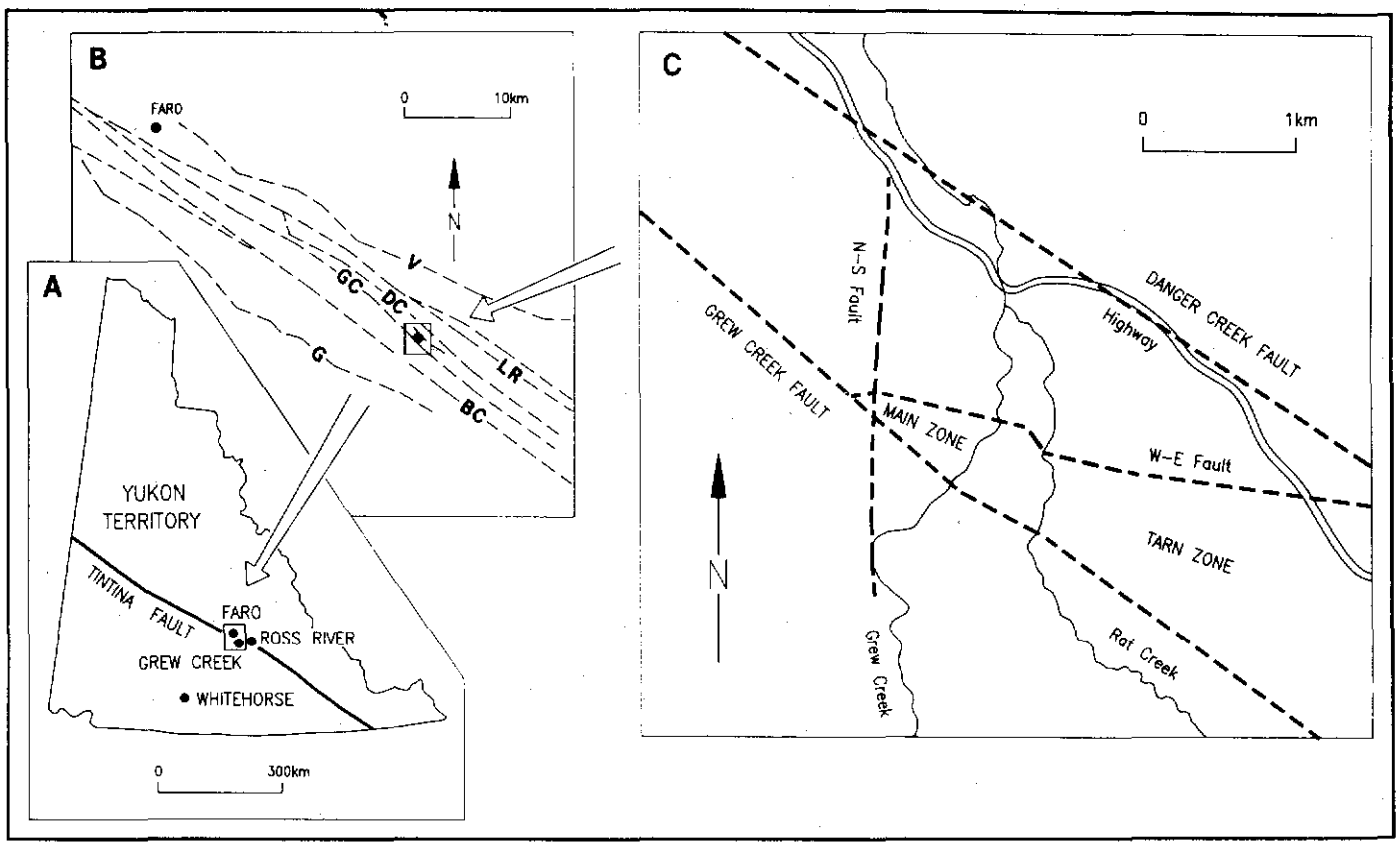

Figure 1. Maps showing the location of the Grew Creek gold-silver deposit on the Tintina Fault Zone in south-eastern Yukon Territory (Figure 1A), the component faults of the Tintina Fault Zone in the Grew Creek area (Figure 1B), and the location of the deposit within the fault zone (Figure 1C). In Figure 1B, BC = Buttle Creek Fault, DC = Danger Creek Fault, G = Glenlyon Fault, GC = Grew Creek Fault, LR = Lapie River Fault and V = Vangorda Fault.

METHODOLOGY

Field work for this study was carried out during the 1988 summer. Duke was the Noranda Project Geologist at Grew Creek, whereas Christie made a one week visit in May to define the project and a six week visit with Rushton, during July and August, to relog drill core, and map and collect surface samples from outcrop. Thirty nine of the total of 90 diamond drillholes (in 1988) were relogged using a scheme that emphasized descriptive features that were considered helpful in correlating the pyroclastic units (e.g. quantity, grain size and texture of the crystal, lithic, pumice and matrix components). These logs were used, in conjunction with Noranda drill logs, to construct 1:500 scale vertical cross-sections (listed by coordinates in Fig. 3) and a longitudinal stratigraphic section through the Main Zone. Samples representative of the different lithological units were collected and 70 were later examined in thin section. Forty-eight samples were analysed for mineralogy, and major and trace elements, using XRD, XRF and ICP techniques respectively (Appendix).

Drillhole descriptive logs, downhole assay data, drill sections, maps and geophysical results were made available by Noranda. The Noranda drillhole descriptive logs were used to prepare hand plotted cross-sections, individually showing veins, visually estimated percent pyrite concentration, and intensity and type of hydrothermal alteration, for eight cross-sections through the Main Zone (listed by coordinates in Fig. 3).

GEOLOGIC AND STRUCTURAL SETTING

The Grew Creek deposit occurs in the Tintina Fault Zone, a transcurrent fault more than 1000 km long which crosses Yukon Territory (Fig. 1), and extends into Alaska to join the Kaltag Fault, and into British Columbia to join the Rocky Mountain Trench Fault. Displacement, crushing and erosion of rocks along the Tintina Fault Zone have formed a major linear physiographic depression termed the Tintina Trench. Dextral displacement of rock units either side of the fault zone indicates transcurrent movement of more than 500 km, mostly during the Late Cretaceous and Tertiary. In the Grew Creek area, rocks of the Pelly-Cassiar Platform to the southwest are juxtaposed against rocks of the Anvil Allochthon to the northeast. Pull-apart basins were formed along the fault zone where it expanded into braided sections, and these were the locus of sedimentation and bimodal basaltic-rhyolitic volcanism

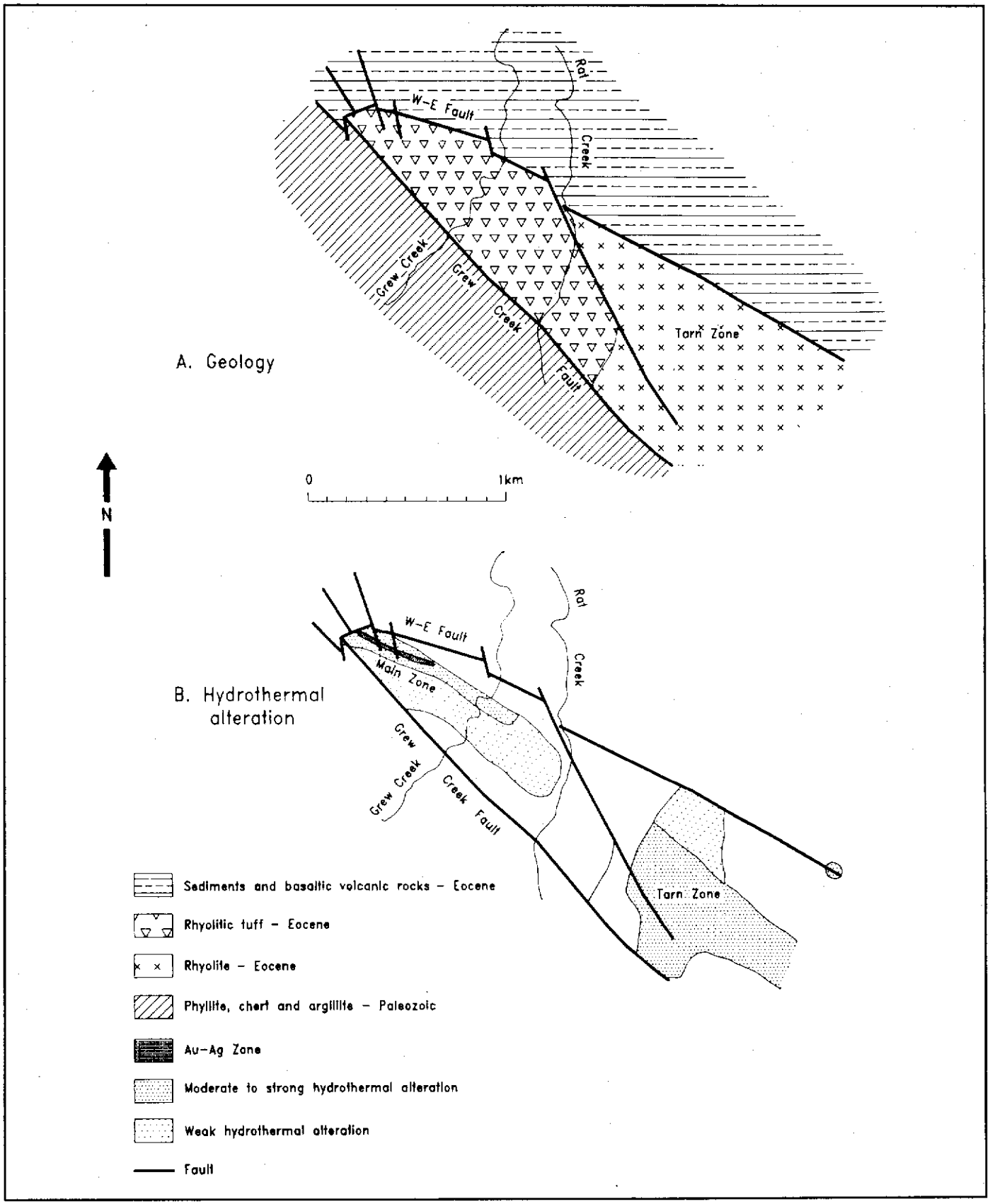

Figure 2. Grew Creek prospect geology (Figure 2A) and hydrothermal alteration (Figure 2B) maps (modified after Duke, 1988).

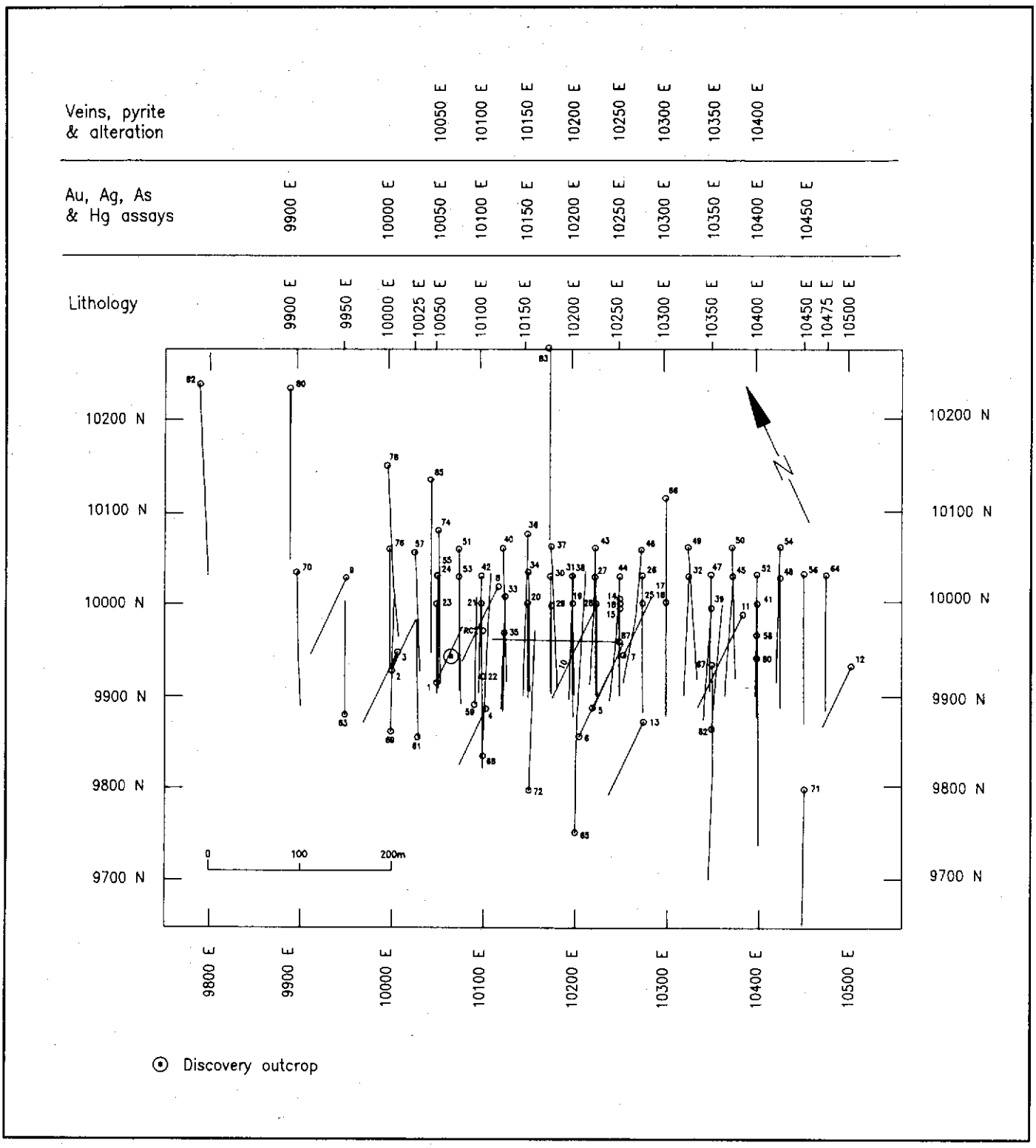

Figure 3. Map of drillhole locations on the Noranda exploration grid in the Main Zone. The grid is orientated at 019°/109°. All drillholes shown are angled diamond drillholes (generally 45° or 55° dip). The rows of section numbers above the diagram note the sections on which the following work was carried out: 1. veins, pyrite and alteration row = sections on each grid line were hand plotted from information in Noranda's descriptive drill logs, to show veins, visually estimated percent pyrite concentration, and intensity and type of hydrothermal alteration, 2. Au, Ag, As & Hg assays row = assay sections were computer plotted and examined, and 3. Lithology row = drillholes in these sections were relogged.

during the Eocene (Christie and Gordey, 1989; Pride, 1988; c.f. Hughes and Long, 1980). Subsequent differential uplift and erosion has exposed some of these Eocene rocks, preserved in graben within the Tintina Trench.

In the Grew Creek area, the Tintina Fault Zone includes at least six major faults; namely, from north to south: Vangorda, Lapie River, Danger Creek, Grew Creek, Buttle Creek, and Glenlyon (Fig. 1B). The Grew Creek prospect lies on the northern side of the Grew Creek Fault, on the south side of the Tintina Trench. Duke (1988) considered that the Main Zone is located where the Grew Creek Fault is intersected by a north-south extensional fault (N-S Fault in Fig. 1C), defined by a physiographic linear feature.

The Grew Creek area is covered with Quaternary glacial till, typically 50 m thick, which limits bedrock exposures to the creeks and rare exposures elsewhere, such as the discovery outcrop. The northwest striking Danger Creek and Grew Creek faults enclose a 1.5 km wide graben (Canyon Graben; Stroshein 1986b) of Eocene sedimentary and volcanic rocks. The faults separate the graben from Triassic metabasalt and limestone to the north, and from Paleozoic phyllite, argillite and chert to the south. A west-northwest striking fault (hereafter termed the W-E Fault) subdivides the Eocene rocks into a northern sequence of fluvial sedimentary rocks intercalated with basaltic pyroclastic and epiclastic rocks, and a southern sequence of rhyolitic volcanic rocks (Fig. 2A). To the east, the rhyolitic rocks consist predominantly of dome facies rhyolite flows and quartz feldspar porphyries, which pass westward into a succession of rhyolitic pyroclastic rocks exposed along and west of Grew Creek. Basalt and rhyolite dykes intrude both the volcanic and sedimentary sequences. From the Main Zone northwards, the tuffs, sediments, and intervening W-E Fault all dip about 80° to the north (Fig. 4A) so that a plan view transect (Fig. 2A) approximates a stratigraphic section.

PROSPECT STRUCTURE

In the Main Zone, drillhole intersections of the Grew Creek Fault define a more than 10 m wide zone of unconsolidated gouge and rock fragments. The W-E Fault is represented by shearing along the sedimentary-volcanic rock contact, sometimes with fault gouge developed. Many other faults have been intersected in the Main Zone drillholes, some with wide clay gouge zones and others represented by tectonic breccias. Duke (1988) correlated some of these intersections with air photo lineaments, and magnetic and IP/resistivity anomalies. He postulated the presence of six north to northwest-striking extensional faults, and several small northeast striking faults within the Main Zone, to account for displacements in the stratigraphy and jogs in the W-E and Grew Creek faults (Figs 2 and 5).

Severely broken core in mineralized vein and breccia zones indicates that many of the mineralized structures have been tectonically reactivated since cessation of mineralization.

DETAILED PROSPECT GEOLOGY

We constructed a stratigraphic column for each of the drillhole cross-sections by assuming that dip was a constant 80°, and by correlating and projecting the drillhole information onto a plane dipping 10° south and passing through a pivot on the 9950N grid line at an elevation of 700 m (equivalent to a depth of 90-145 m). These columns were assembled to produce a stratigraphic section for the Main Zone at 1:500 scale, simplified and reproduced here at smaller scale in Fig. 5. This section illustrates the relationships of the rhyolitic and basaltic volcanic rock, and fluvial sedimentary rock sequences, and subdivides the rhyolitic sequence into a number of composite pyroclastic units. Lateral variations in thickness and pinching of units in the rhyolitic sequence, and the jagged trace of the W-E Fault, may be caused by changes in dip along the section (not compensated for) and displacements on several north and northwest striking faults (see Structure section above). Additionally, several primary volcanic facies features may also contribute to the lateral variations, including: (a) rapid thickening and thinning caused by draping over existing topography, and valley filling, (b) erosion and production of epiclastites, and (c) overlapping volcanic centres.

Rock types

(a) Rhyolite and felsic porphyries

Coarse grained "quartz eye" porphyritic rhyolite outcrops along a prominent ridge from Rat Creek southeast to Danger Creek. Porphyritic rhyolites, including quartz-feldspar, quartz-eye, and feldspar "porphyries", are the main lithologies in the Tarn Zone drillholes and occur elsewhere in the sedimentary and volcanic sequences as dykes. Many of the dykes in the Main Zone logged by Noranda geologists as rhyolite and quartz feldspar porphyry proved to be hydrothermally altered basalt ("rhyolite"), vitric ash tuff ("rhyolite"), or partly welded lapilli tuff ("quartz feldspar porphyry") when examined in thin section. In the Main Zone there is a semi-continuum of textures from "quartz feldspar porphyry" to partly welded, crystal vitric lapilli ash tuff with pseudo quartz-feldspar porphyry macro-texture but containing some welded shards and pumice. These pseudo-porphyries may have been formed by melting and remobilization of basal pyroclastic units.

Samples of Tarn Zone rhyolite from DDH 90 contain about 40% phenocrysts, up to 4 mm in diameter, of plagioclase (euhedral), sanidine, quartz and a mafic mineral, in a groundmass recrystallized to quartz, K-feldspar and illite. Flow banding and spherulitic textures are developed locally. Quartz-feldspar porphyry is similar to rhyolite but with larger phenocrysts and well developed flow banding. Large quartz "eyes" are prominent in altered examples.

(b) Rhyolitic pyroclastites

Rhyolitic tuffs are the most important lithology in economic terms, as they host the Main Zone mineralization.

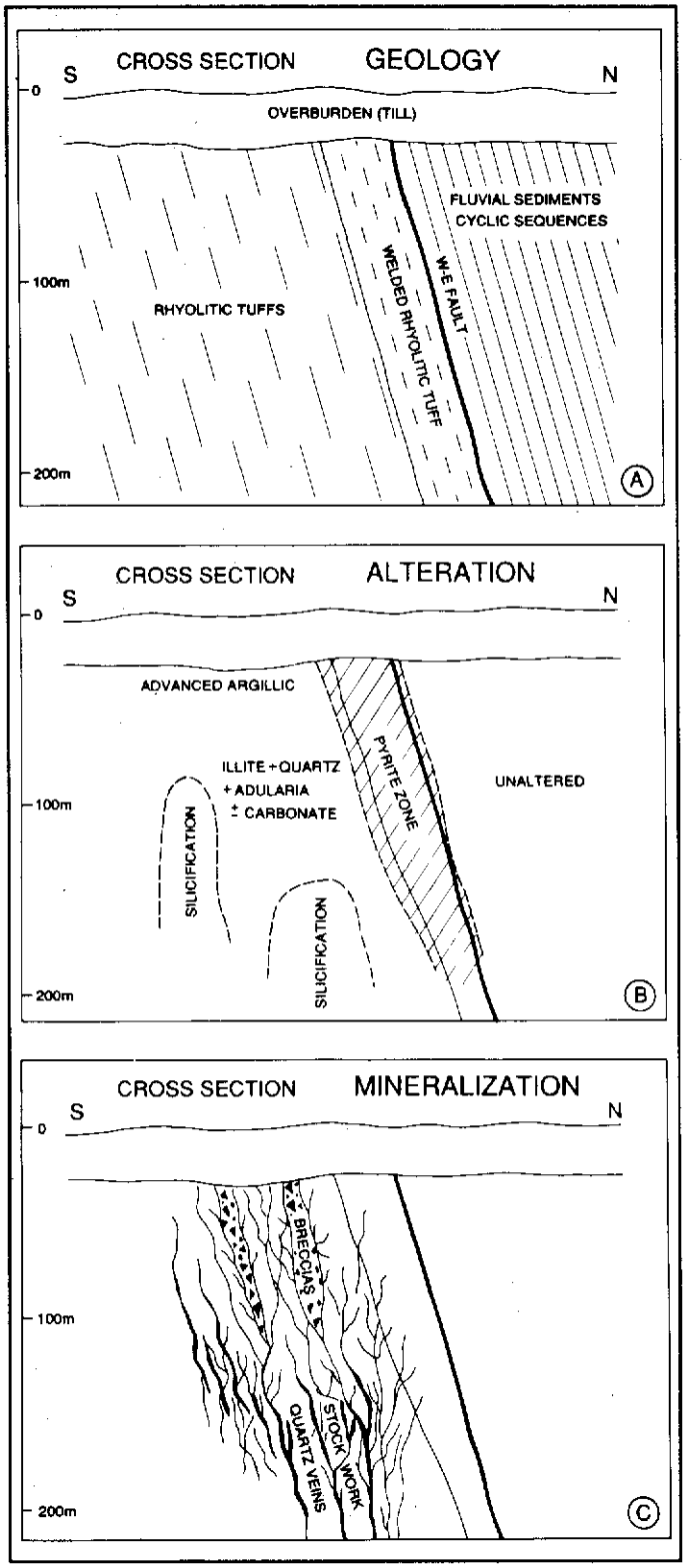

Figure 4. Diagrammatic cross-sections through the main zone illustrating geology (Figure 4A), hydrothermal alteration (Figure 4B), and mineralization (Figure 4C).

They are exposed in the creeks and were intersected by the Main Zone drillholes, south of the W-E Fault (Figs 2A, 4A and 5), and can be grouped into the following three major types, based on grain size and composition (Table 1 and Fig. 6):

1. S&P (salt & pepper) tuff: S&P tuff comprises "crystal- and lithic-rich" mixed coarse ash tuff, lapilli-ash tuff and lapilli tuff with a distinctive, well sorted granular "salt & pepper" appearance (Fig. 7). These are the crystal lithic tuffs described by Duke and Godwin (1986) from exposures along Grew Creek. They mapped six depositional units based on cyclic increases in grain size northward down the creek (up the stratigraphic sequence). We have identified more than 12 units of S&P tuff in the eastern drillholes of the Main Zone with contacts marked by major changes in grain size or tuff type (e.g. interbedded thin units of VA tuff or CLP tuff, see below). Each unit is internally homogeneous and no sedimentary structures were observed. The upper part of the S&P sequence contains only "fine" grained S&P units (crystals and lithics average about 1.5 mm), whereas several coarse grained S&P units (crystals and lithics averaging 3 mm) are present in the lower part.

2. CLP (crystal lithic pumice) tuff: CLP tuffs are "glass-rich" coarse ash tuff and lapilli-ash tuff (Figs 8 and 9) which occur mostly in the upper part of the rhyolitic sequence and dominate the western end of the section (Fig. 5). Three major types are identified: (a) non-welded coarse ash tuff, (b) non-welded lapilli-ash tuff, and (c) welded or partly welded lapilli ash tuff (logged by Noranda as quartz-feldspar porphyry). Two units of non-welded CLP tuff on section 1000E are separated by a 40 cm thick unit of trough cross bedding (Fig. 10), representing either a basal surge layer or an epiclastite.

3. VA (vitric ash) tuff: VA tuff (Figs 11 and 12) is characterized by having more than 75% glass ash matrix and pumice fragments. It generally occurs as thin units separating units of S&P tuff and/or CLP tuff.

In all three types of tuff, the crystal fragments are mainly quartz and lesser feldspar (mostly sanidine), whereas the lithics are mostly fragments of rhyolitic tuff and rhyolite flows, and lesser basalt, shale, phyllite, and diabase (dolerite). The lithics generally have a coarser average grainsize than the crystals, and in some samples there is a bimodal grain size distribution of crystals with the finer population predominating. Pumice exhibits a considerable range in grain size, averaging 3-5 mm in diameter, but commonly around 1 cm, with rare blocks up to 25 cm in diameter (Fig. 8). The glass matrix is generally too fine grained, hydrothermally altered and/or recrystallized to identify components, but good examples of glass shard textures are present in some samples (e.g. 8/34.1m, 10/81.1m, 18/159.6m, 47/100.8m, 59/99.65m, 60/271m 65/346.5m, and 85/333.4m; Fig. 12). Some CLP and VA tuffs are welded (e.g. 47/79.95m, 60/271m, 65/346.5m, RR19, and TR1) with flattening of pumice

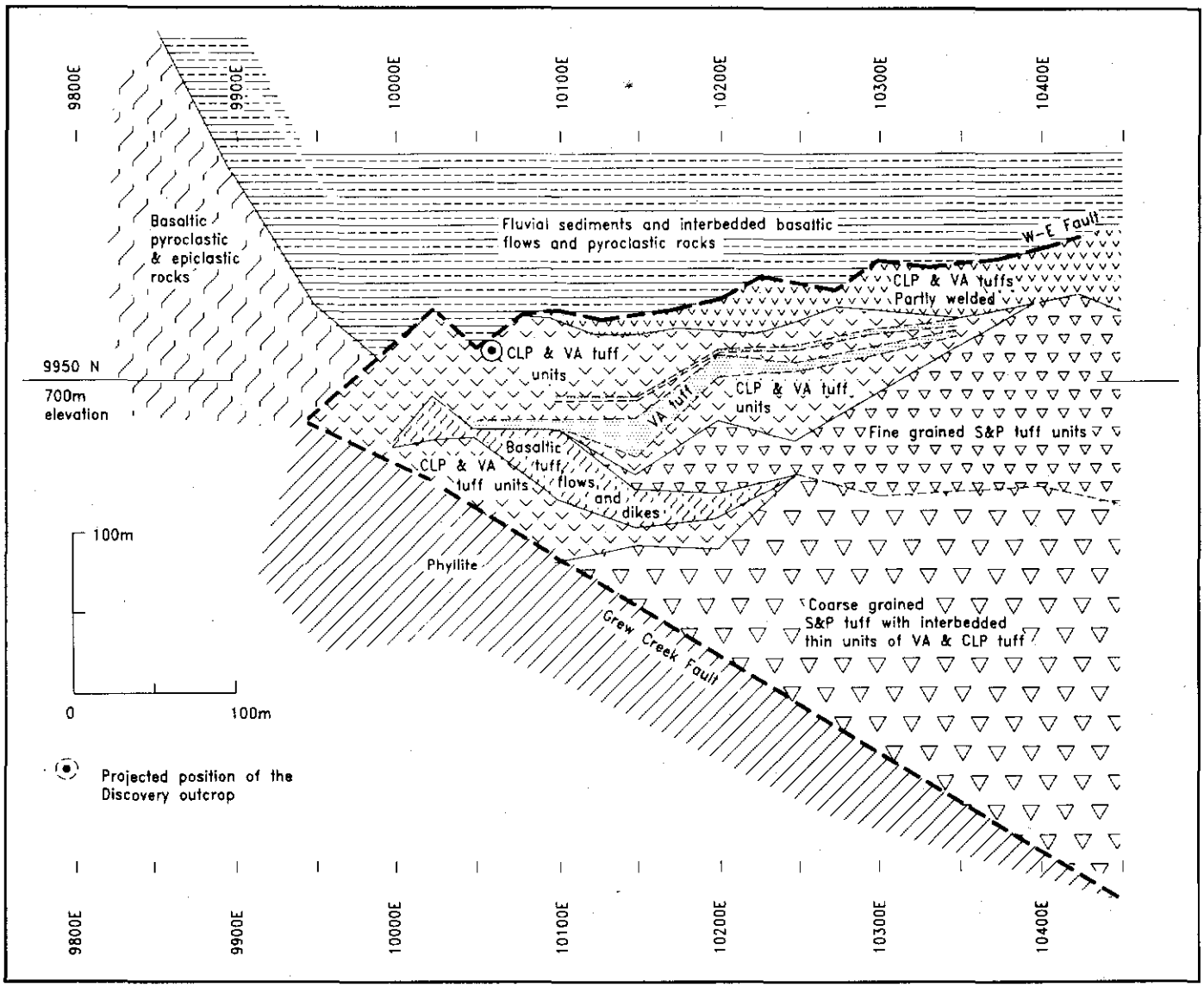

Figure 5. Stratigraphic section through the Main Zone constructed on a plane dipping 10° southward and passing through section 9950N (Figure 2) at an elevation of 700 m. See Table 1 for definitions and descriptions of CLP, S&P and VA tuffs.

fragments and glass shards, and the development of a eutaxitic texture in the glass (+shard) groundmass. Welding and hydrothermal alteration of some CLP tuff units has produced an appearance similar to quartz feldspar porphyry and led to the misidentification of these units as dykes, particularly the "quartz feldspar porphyry" noted on the footwall of the W-E Fault by Duke (1988), Christie and Gordey (1989), Christie et al. (1989), which in reality is the uppermost CLP tuff unit (Fig. 5).

(c) Fluvial sediments

Clastic sedimentary rocks ranging from conglomerates to claystones occur north of the W-E Fault. They are exposed in Grew Creek, northeast of the Tarn Zone, and in a small quarry north of the Highway, and were intersected in many of the drillholes (Figs 2, 4 and 5). The sediments generally dip steeply north but are folded in Grew Creek and the quarry area, near the Robert Campbell Highway (e.g. see Fig. 12 of Pride 1988). Bedding is marked by changes in grain size, whereas a lamination is defined by alternating pale low density mineral and dark higher density mineral bands in some of the sandstones and finer sediments. The coarser beds contain logs and twigs, and beds of coal are associated with some fine grained units.

The conglomerates are clast supported, polymictic, and moderately to poorly sorted. The clasts are typically about 4 cm in diameter, up to a maximum of 15 cm in diameter, and set in a coarse sandy matrix. Clast lithologies include schist, quartz vein material, felsic and mafic volcanic rocks, chert, and quartzite.

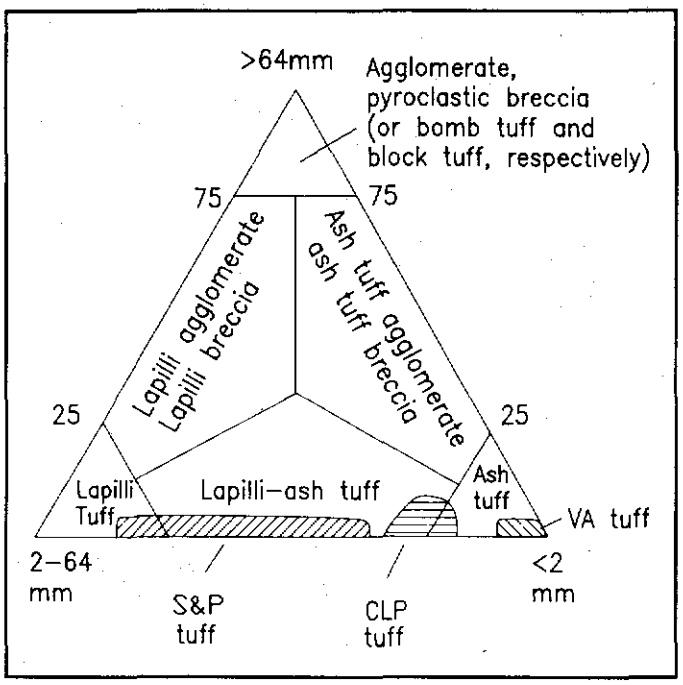

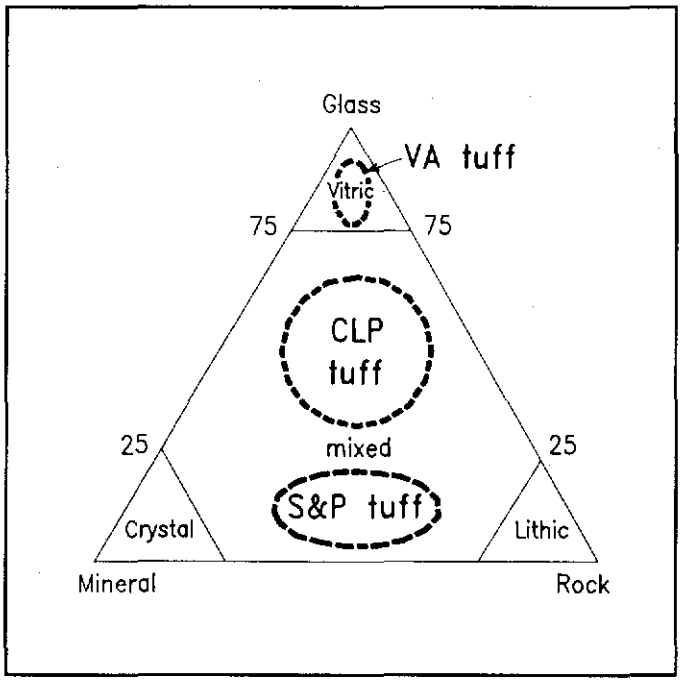

Figure 6. Relative compositions of the S&P, CLP, and VA rhyolitic tuffs (Table 1) plotted on pyroclastic rock classification ternary diagrams from Dietrich & Skinner (1979).

Drillhole sections through the sediments in the Main Zone typically exhibit fining upward cycles from conglomerate, through pebbly sandstone, sandstone, siltstone and claystone, to coal beds, although many of the cycles are only partially preserved and are usually missing the fine grained units. Thicknesses vary considerably. Forty two measurements of the fining upward cycles average 4.2 m thick (corrected for a dip of 80° northward) with a standard deviation of 3.6 and maximum value of 19.3 m, whereas 260 measurements of individual units of conglomerate, sandstone, etc., average 1.4 m with a standard deviation of 1.5 and maximum value of 8.1 m (pebbly sandstone).

(d) Basaltic pyroclastites and epiclastites

Duke and Godwin (1986) described basaltic breccias, and ash to block tuff from exposures in Grew Creek. Some of the exposures are bedded.

A more than 250 m thick continuous sequence of basaltic ash tuffs, lapilli tuffs, and epiclastites is present in the drillholes at the western end of the Main Zone area and crops out northwest of the Main Zone. Units have considerable variability in thickness, up to a maximum of 37 m for lapilli tuff in section 9900E. Cyclic fining upward sequences are locally present, mostly in the epiclastites (see below), where the cycles resemble those in the fluvial sediments but are composed almost entirely of basaltic material.

The tuffs mostly consist of lapilli sized fragments (rare examples up to about 10 cm in diameter) and fine grained crystals (averaging 0.6 mm in diameter) of plagioclase and accessory quartz, in a fine grained ash matrix (Fig. 13). The lapilli are mostly basaltic, consisting of fine (0.3 mm) subhedral laths of plagioclase feldspar and lesser mafic minerals, and lithic fragments in a submicroscopic ash matrix (about 50%). Lapilli of a few units have been altered to pale hues of yellow, brown, green and red within the same rock, thus forming distinctive multicolored units compared to the pale green colour of most other altered rocks. A group of multicolored tuffs interbedded with basalt (flows?) forms a major marker unit in the western and central part of the Main Zone rhyolitic sequence (Fig. 5). Another set of units (not shown in Fig. 5) is present in the lower part of the eastern section, too low to be correlated with the upper unit, and is assumed to pinch out westward on the Grew Creek Fault.

(e) Basalt flows and dykes

Basalt flows and dykes are exposed in Grew and Rat creeks, and west of the Main Zone, and are intersected in the Main Zone drillholes (mostly logged by Noranda geologists as andesite).

In the Main Zone, the flows and dykes range from 0.1 to 38.7 m and average 4.5 m in intersection width downhole (the dips of the dykes are unknown). They are generally porphyritic with 5-30% phenocrysts (averaging 1-2 mm long but up to 10 mm) set in a microcrystalline (typically 0.5 mm) groundmass with some glass (0-20% but 40% in one sample). Weak glomeroporphyritic and variolitic textures are present in many samples, some are amygdaloidal (e.g. 72/135.3m) and one exhibits trachytic texture (83/62.5m).

Labradorite, some with oscillatory zoning, is the dominant phenocryst and microcrystalline phase, followed by clinopyroxene (zoned pale green diopsidic core to purplish titaniferous augite rim in sample 39/149.8m), opaques, and

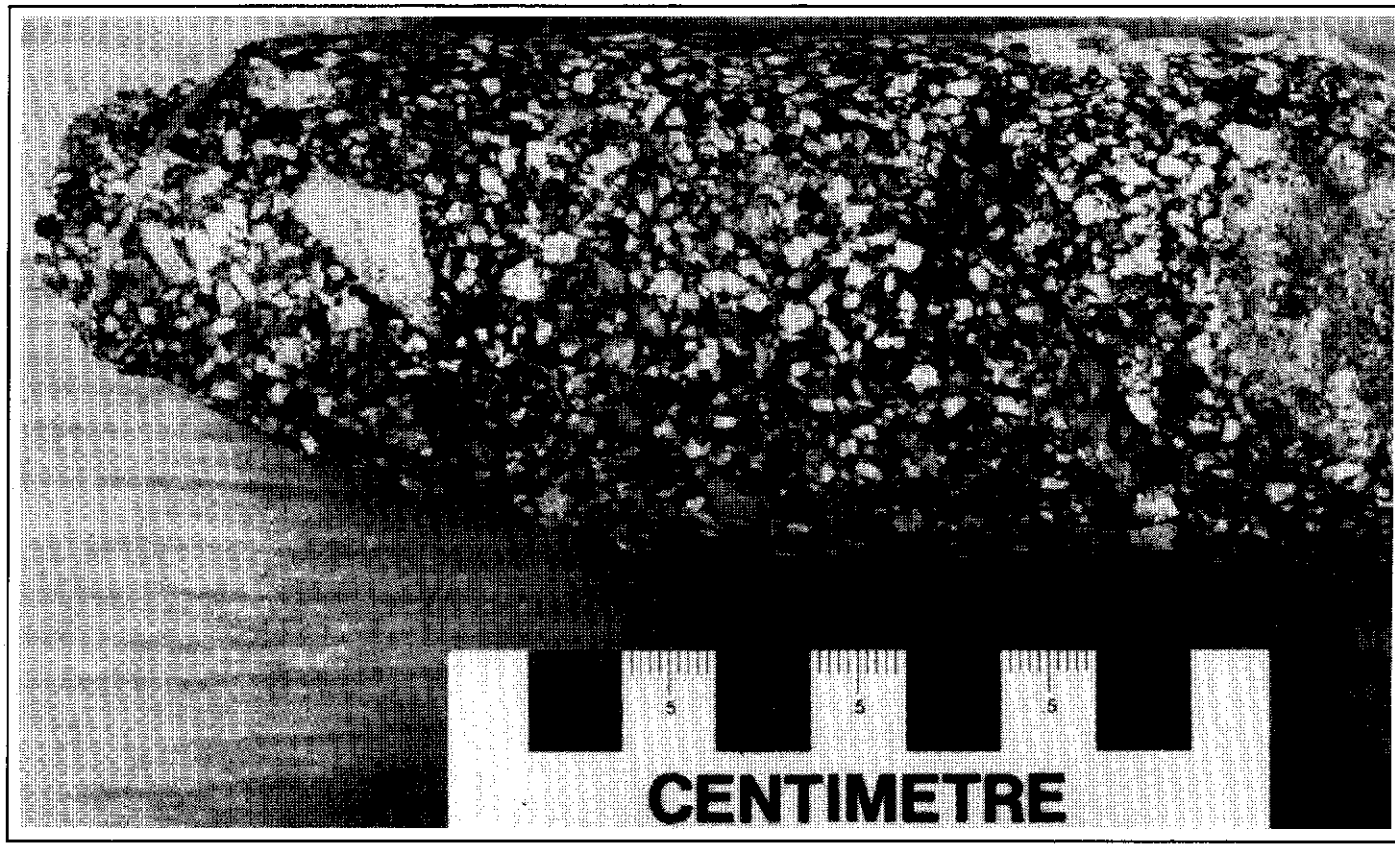

Figure 7. Drill core of S&P tuff from a downhole depth of 200.4 m in DDH 60.

Figure 8. Drill core of CLP tuff with 18 cm long pumice block (immediately above scale) at a downhole depth of about 72 m in DDH 72.

Figure 9. Thin section of CLP tuff (DDH 66 at 181.5 m downhole depth) under plane polarized light, showing quartz (white) and hydrothermally altered feldspar and rock fragments (mottled grey), pumice lower left) and pyrite (black).

Figure 10 Drill core of CLP tuff units (top and bottom) separated by a 40 cm thick (stratigraphic) trough cross bedded unit between 228.75 and 229.15 m downhole in DDH 69. At least three cross sets are present and may represent the basal surge layer of an ignimbrite sheet.

Figure 11. Drill core of welded vitric ash tuff from 123.3 m downhole in DDH 65. Mild eutaxitic texture is marked by partial flattening of pumice fragments (white).

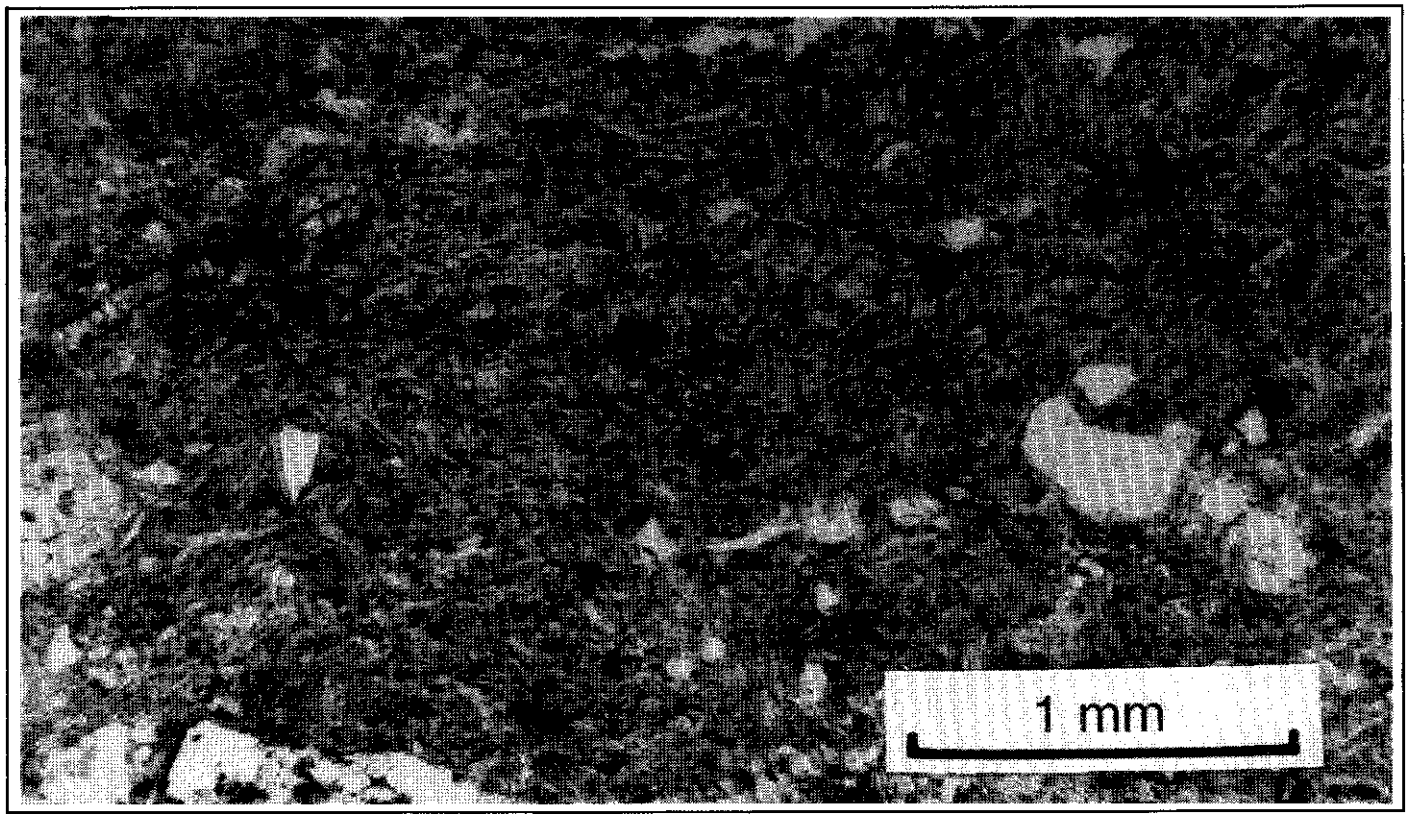

Figure 12. Thin section of vitric ash tuff (DDH 65 at 346.3 m downhole depth) showing sparse quartz fragments in a matrix dominated by glass shards (vitroclastic texture). Mild welding is marked by a preferred orientation of the shards.

Figure 13. Drill core of basaltic lapilli tuff from a downhole depth of 307 m in DDH 82.

Figure 14. Thin section of a medium grained diabase dike ("bird's foot porphyry") sampled at a downhole depth of 353.78 m in DDH 67. The rock consists of coarse subhedral plagioclase laths (altered to albite) with interstitial anhedral mafic (altered to carbonate and chlorite) and acicular opaque minerals.

olivine. Some labradorite and olivine phenocrysts have reaction and/or resorbed rims.

(f) Diabase (dolerite) dykes

Medium to coarse grained mafic dykes are exposed in Grew Creek and intersected in the drillholes in the Main and Tarn zones. Two rock types are identified:

1. Porphyritic rocks (e.g. 39/149.8m and 90/58.85m), which are essentially coarse grained basalts, with 10-30% plagioclase phenocrysts averaging 2-3 mm but commonly up to 7 mm long, and 5-10% mafic phenocrysts averaging 1 mm, clustered (glomeroporphyritic texture) or scattered in a 0.3-0.5 mm feldspar and mafic mineral groundmass. Needles of an opaque mineral (dendritic ilmenite?), averaging 0.3 mm long, make up about 5% of the rock.

2. Medium to coarse grained equigranular rocks (e.g. 67/353.78m and 90/44.7m; Fig. 14) which consist of 60-70% 1-1.5 mm (but up to 4 mm) plagioclase laths and 25-35% 0.5 mm mafic minerals. Needles of an opaque mineral, averaging 0.3 mm long, make up about 5% of the rock. We named these rocks "bird's foot porphyry" in hand specimen because of their variolitic texture. In thin section they are sub-ophitic and weakly variolitic. The original plagioclase composition could not be determined because of hydrothermal alteration to albite, illite and calcite but these rocks have almost identical chemical compositions to the basalts (see XRF geochemistry section below) and we therefore considered that they were diabase (dolerite). A similar but coarser grained rock (microgabbro) occurs as a dike crossing Grew Creek, near the camp.

HYDROTHERMAL ALTERATION

Introduction

Hudson Bay and Noranda geologists mapped hydrothermal alteration in the volcanic rocks south of the W-E Fault over a three kilometre strike length, including the Main and Tarn zones (Fig. 2B). The sedimentary rocks north of the fault are little altered apart from a few metres immediately adjacent to the fault in the Main Zone and north east of the Tarn Zone (Figs 2B and 4B). Alteration in the rhyolitic rocks is pervasive although there is some structural control on the intensity and type. The specific types of alteration present are listed below and in Table 2, and results of XRD analyses are listed in the Appendix:

1. Illite-quartz-adularia ± carbonate alteration is the predominant alteration type in the subsurface rhyolitic rocks. Other minerals which may be present include pyrite, interlayered illite/smectite, and albite. In the groundmass, felsic volcanic lithic fragments and pumice are generally altered to a finely crystallized mosaic of quartz and adularia. In moderate to strongly altered rocks, the lithics and groundmass textures merge into a recrystallized mass, and feldspar crystals are alterated to quartz, adularia, illite and carbonate.

2. Quartz-adularia alteration (silicification) occurs adjacent to some quartz veins and breccias including the discovery outcrop. It is gradational to illite-quartz-adularia ± carbonate alteration, representing an increase in the proportion of quartz and adularia.

3. Illite-quartz (sericitic or phyllic) alteration is represented by clay rich zones in the drillcore, particularly adjacent to veins, and brecciated, fractured or sheared zones. This alteration was logged by Noranda as argillic because of the presence of clays in hand specimen. The primary clays are predominantly illite, with lesser interlayered illite/smectite and smectite, overprinted with secondary kaolinite and therefore we prefer to classify this alteration as illite-quartz and not argillic. Illite-quartz alteration is gradational with illite-quartz-adularia ± carbonate alteration, representing an increase in the proportion of illite and quartz.

4. Carbonate-chlorite (propylitic) alteration is the dominant alteration type in basaltic rocks. Other minerals that may be present include albite, illite, quartz, pyrite, adularia, interlayered illite/smectite, and interlayered chlorite/clay (-illite?). The alteration of mafic minerals, and to a lesser extent feldspars, is dominated by the development of the carbonates calcite, siderite and dolomite, which form pseudomorphs of the original minerals and fill voids and vesicles. Alteration of feldspars has also produced illite, K-feldspar and quartz, whereas chlorite and pyrite have replaced the mafic minerals. XRD analyses also indicate the presence of minor smectite, interlayered illite/smectite and chlorite/smectite (Appendix). Epidote was noted in one hand specimen of drill core. Amygdules are filled with calcite, sometimes with a chalcedonic quartz core.

5. Intermediate argillic alteration was mapped by Duke and Godwin (1986) in the rhyolitic rocks exposed in surface trenches within the Main Zone and it is also present, particularly as an overprint clay assemblage, in some subsurface zones. It is characterized by abundant smectite and may also contain kaolinite, pyrite, interlayered illite/smectite, quartz and relict carbonate, illite and K-feldspar. The relict minerals in some of the trench material indicate that alteration of this material may have been primarily illite-quartz-adularia ± carbonate type, later overprinted by argillic alteration.

6. Advanced argillic (acid sulphate) alteration is clay alteration characterized by the presence of alunite and/or abundant kaolinite, and was identified by Duke and Godwin (1986) in rhyolitic rocks in the trenches in the Main Zone. Other minerals which may be present include smectite, quartz, pyrite, and relict carbonate and interlayered illite/smectite.

7. Weathering: Much of the strong "argillic" clay alteration, in both the illite-quartz-adularia+/-carbonate and propylitic alteration zones, may result from supergene alteration by surface weathering and/or acidified (from the oxidation of pyrite) groundwater. Duke and Godwin (1986) noted a deep weathering profile with a clay-carbonate mineral assemblage at Grew Creek. We were impressed at the rapid rate that rocks in exposed trenches and drill core decomposed to clay. Post-drilling weathering and resultant clay alteration was particularly noticeable in drill core when a complete hole was laid out. In many of the early holes, we noted that every tenth core box was extensively clay altered. This was because the core trays had been stacked in open racks, ten trays high and the rock in the exposed top tray was weathering more quickly than that in the other trays. The core tray racks were roofed subsequent to our work. Strong clay alteration elsewhere was generally concentrated near faults or sheared and crushed zones, and could be attributed to either late hydrothermal or supergene processes.

Alteration trends

We plotted hydrothermal alteration and visually estimated pyrite concentrations from the Noranda lithological drill logs for several cross-sections (listed as coordinates in Fig. 3), and correlated this data with our logs and analytical results to determine the alteration pattern and trends.

The hydrothermal alteration forms an envelope around the mineralized zone. The complete drill tested width of the Main Zone (about 300 m) is altered, but medium to high intensity alteration is concentrated within a width of about 100 m. Basaltic rocks within the rhyolitic sequence are altered to carbonate-chlorite (propylitic) assemblages, whereas those to the west, faulted against the rhyolitic sequence, are little altered (although green in hand specimen). At the time of alteration, they may have been remote from the centre of hydrothermal activity, but later, may have moved close to the mineralization along the intervening fault. Illite-quartz-adularia+/-carbonate alteration is the most common type of alteration in the rhyolitic sequence. This grades into illite-quartz, argillic (overprint?), or quartz-adularia alteration around major veins and other fracture structures. Quartz-adularia is the highest rank of alteration present and is usually associated with zones of quartz veining but not necessarily vice versa. Although quartz-adularia alteration is present up to the highest level in some drillhole cross-sections, in many others it passes upward into illite-quartz and illite-quartz-adularia$\pm$carbonate alteration with similar (and sometimes greater) frequency of quartz veining (Fig. 4B). Illite-quartz and argillic clay zones associated with structural features range in thickness from a few centimetres to several metres. This clay alteration is considered the primary reason for poor recovery in mineralized intersections (c.f. Duke, 1988; Seto and Crowe, 1989).

Welded and partly welded CLP units present at various horizons are consistently moderately to intensely altered to illite-quartz-adularia and illite-quartz assemblages, suggesting that this lithology was highly permeable and thus more susceptible to alteration. As a highly competent rock, it would have developed good fracture controlled permeability. Following alteration, the permeability would have been greatly decreased, thus causing the uppermost partly welded CLP unit adjacent to the W-E Fault to act as an aquiclude to hydrothermal fluid flow. Where this unit is present, the fluvial sediments across the W-E Fault are little altered, whereas where it is absent, the sedimentary rocks exhibit much greater alteration, extending more than 100 m into the sedimentary sequence on section 10050E.

Intermediate argillic and advanced argillic alteration are the main types of alteration in the upper parts of the system mostly as an overprint on earlier illite-quartz-adularia$\pm$carbonate alteration.

The concentration of pyrite shows poor correlation with intensity of alteration, veining, and mineralization but exhibits a strong increase in concentration in the vicinity of the W-E Fault, and particularly in the adjacent partly welded CLP unit (Fig. 15). This results in a pyrite zone adjacent to and north of the mineralization.

MINERALIZATION

Gold and silver mineralization of the Main Zone occurs in stockwork quartz veins and hydrothermal breccias. The quartz veins are mostly 2-10 cm but possibly up to 1 m thick, and the hydrothermal breccias are a few centimetres to 1 or 2 m thick. Many of the quartz veins are banded on a millimetre scale and some consist of, or contain bands of, brecciated and recemented vein material. The larger veins and breccias are poorly preserved in the drill core because of their broken nature and resultant poor core recovery (Noranda drill logs). Rubbly vein and breccia material, logged up to maxima of about 5 m and 10 m of apparent drill core length respectively, are not considered true representations of original widths of the veins and breccias because part of these drill lengths would have been occupied originally by clay altered wall rocks that have been flushed away during drilling.

Plots for some drill cross-sections showing veins noted in the Noranda drill logs (Fig. 3) indicate that veining is mostly confined to a steeply northward dipping zone, 40 m to 80 m wide. The veins die out below the 650 m elevation on most sections but extend down to at least the 550 m elevation on sections 10150E and 10200E (the intervening 10175E section was not plotted), suggesting a funnelling down in this area. The greatest density of veins per unit distance occurs at intermediate depths.

Stroshein (1986a) considered that the discovery outcrop was a hydrothermal vent breccia. This outcrop is severely weathered and although it exhibits clast textures, we consider it is more likely to be quartz-adularia altered coarse CLP tuff, part of which projects to this surface position on the stratigraphic section (Fig. 5).

The main non-metallic phases in veins and hydrothermal breccias are quartz, adularia, carbonates, clays (mostly illite), and quartz pseudomorphous after calcite. Additionally,

fluorite occurs in the Tarn Zone veins. The quartz is mostly chalcedonic and rarely finely crystalline. Crystal lined vugs are very rare.

McNeal (in Duke, 1988) noted that pyrite and marcasite are the main metallic minerals but there are also traces of arsenopyrite, chalcopyrite, sphalerite, galena, electrum, acanthite, naumannite, aguilarite, and silver amalgam. The electrum averages 7.5 μm in diameter, with a maximum diameter of 60 μm. Eleven analyses range in fineness from 640 to 160 and average 360 fine (64 to 16 and 36 weight percent Au respectively).

GEOCHEMISTRY

XRF and ICP analyses

Whole-rock XRF (X-ray fluorescence) and ICP (Inductively Coupled Plasma Spectroscopy) analyses of samples of basaltic and rhyolitic rocks are presented in the Appendix. When normalized free of water and carbon dioxide (Table 3), the analyses of basalt and rhyolite are similar to those from Grew Creek and nearby occurrences previously reported by Duke and Godwin (1986), Jackson et al. (1986), and Pride (1988). Jackson et al. (1986) concluded that the basalts were calc-alkaline to transitional tholeiites, whereas the rhyolites were a high potassic subaluminous type.

Measurements of rock density were made and the analyses converted to units of kg/m^3 to reduce the apparent enrichment and depletion effects caused by changes in rock density during hydrothermal alteration. Densities were measured with a Walkers Steelyard beam balance and used in the following formula:

$$\frac{Wt\%}{\sum -H_2O-CO_2} \times \rho = \frac{kg}{m^3}$$

Where Wt% = weight percent of oxide = ppm x 10^{-4}

ppm = parts per million of element

Σ = total of analysis (Wt%)

H_2O = water loss on drying (Wt%)

CO_2 = carbon dioxide (Wt%) determined by wet chemical methods

ρ = density in kg/m^3

Binary plots of oxides and elements versus silica, presented in Figs 16 and 17, were constructed using the density corrected data in the computer program IGPET-II from Terra Soft Incorporated, New Jersey. Even though hydrothermally altered, the different rock types form distinct trends and groupings on these plots, generally with the tuffs lying between basalt and rhyolite end members in the order: basalt, basaltic tuff, S&P tuff, CLP tuff, VT tuff, and rhyolite. The intermediate composition of the tuffs reflects the presence of both basalt and rhyolite pyroclastic fragments. Separation of the various rock types is particularly good in binary and ternary plots (not shown) using Cr, Co, Cu, Ni, Y, La, and Pb.

Basaltic rocks: All of the basalt samples are propylitically altered, with intensities of alteration ranging from mild (55/30.7m) to strong (72/117.6m and 66-115.2m). This is reflected in their high loss on ignition (H_2O, CO_2 and S) in comparison to average analyses of basalts from exposures in Grew Creek and other nearby occurrences reported by previous authors (Table 3). Also, our hydrothermally altered basalts exhibit a marked K_2O enrichment, and are slightly enriched in Al_2O_3 and Na_2O (probably secondary illite, K-feldspar and albite), in addition to carbonate. In contrast, within our suite of analyses, trends exhibited with increasing intensity of alteration are generally in reverse to those mentioned, although at subdued levels: there are small decreases in K_2O, Na_2O, SiO_2, and Al_2O_3, a small increase in CaO, and possibly a slight increase in MgO (probably reflecting an increasing importance of secondary carbonate and chlorite).

Rhyolitic rocks: The rhyolites analysed are all similarly moderately altered to illite-quartz-adularia$\pm$carbonate assemblages, although sample 90/98.6m is more strongly altered and close to an illite-quartz assemblage. This sample is distinguished from the others by having greater Na_2O and less TiO_2, CaO and Al_2O_3. However, in comparison to less altered rhyolites reported from other nearby occurrences by previous authors, the Grew Creek rhyolites are depleted in Na_2O (Table 3). An initial assessment of the suite of tuff samples indicates that the markedly different chemistry of the individual tuff types (S&P, CLP, and VA tuffs) may mask the alteration effects, but further work is in progress.

Drill core assays

Noranda sampled a half split of the drill core over intervals of 1.5 m in holes DDH 19 to DDH 90 but used a smaller sampling interval (e.g. 0.5 m or 0.75 m) over all or parts of DDH 14 to DDH 18. Similarly, Hudson Bay sampled DDH 1 - DDH 13 using varying intervals (mostly between 0.5 m to 1.5 m). All Hudson Bay core samples were analysed for gold by fire assay, silver by hot HCl-HNO_3 extraction and atomic absorption, arsenic by perchloric-HNO_3 extraction and colorimetry, and mercury by flameless atomic absorption. Noranda core samples were analysed for gold and silver by fire assay, iron and arsenic by hot HCl-HNO_3 extraction and ICP, and mercury by flameless atomic absorption. Composite 5 m samples of holes 29 and 30 were analysed for a suite of 30 elements by hot acid extraction and ICP (Table 4). The composite sample ICP analyses are useful for comparative purposes, however they may underestimate the real concentrations of many elements by about 50% - 75% (c.f. Sketchley, 1985), because of only partial leaching of the

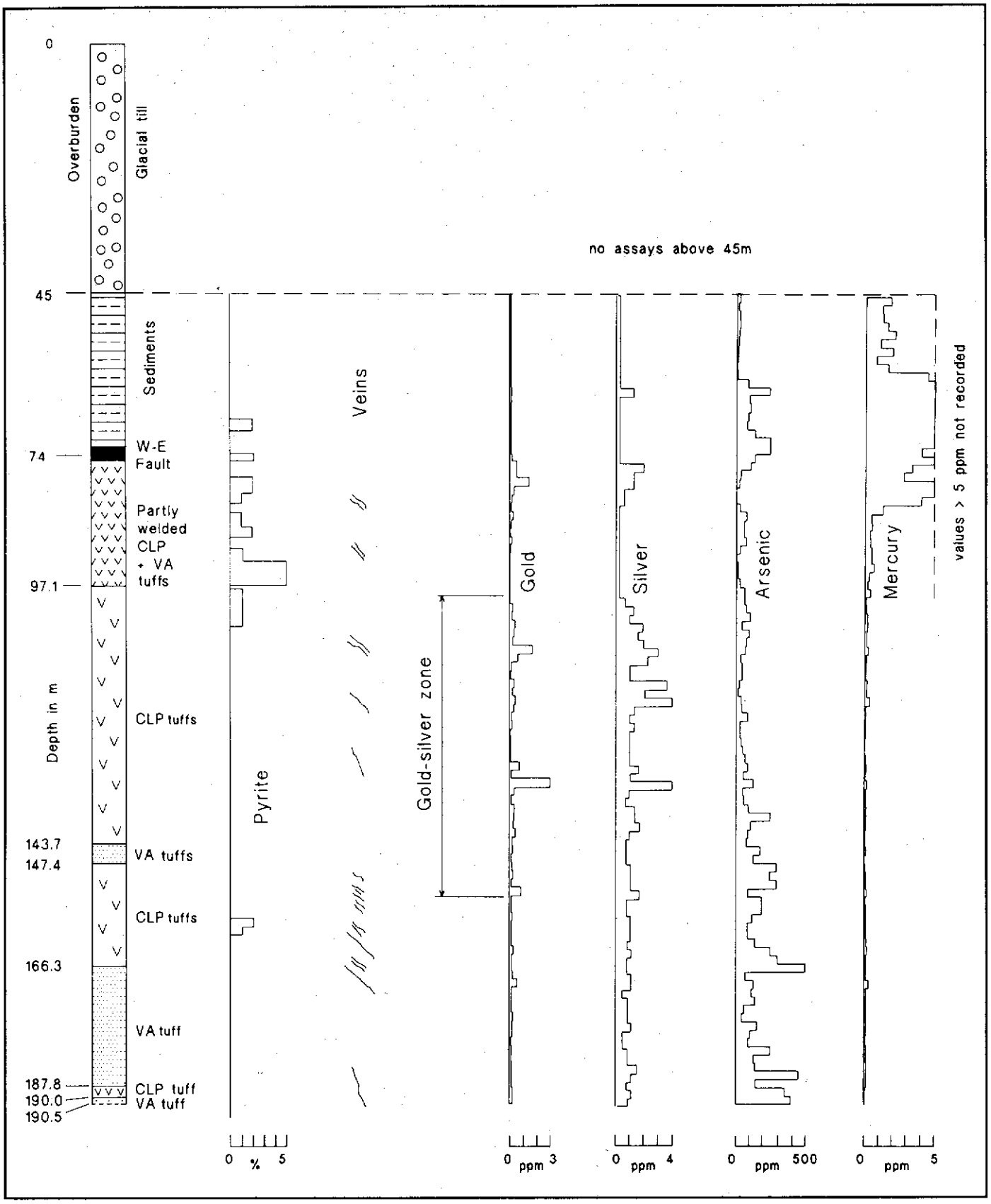

Figure 15. Down hole trends in DDH 34 (190.5 m diamond drillhole, section 10150E, bearing 199°, and dipping 45°; see Figure 3).

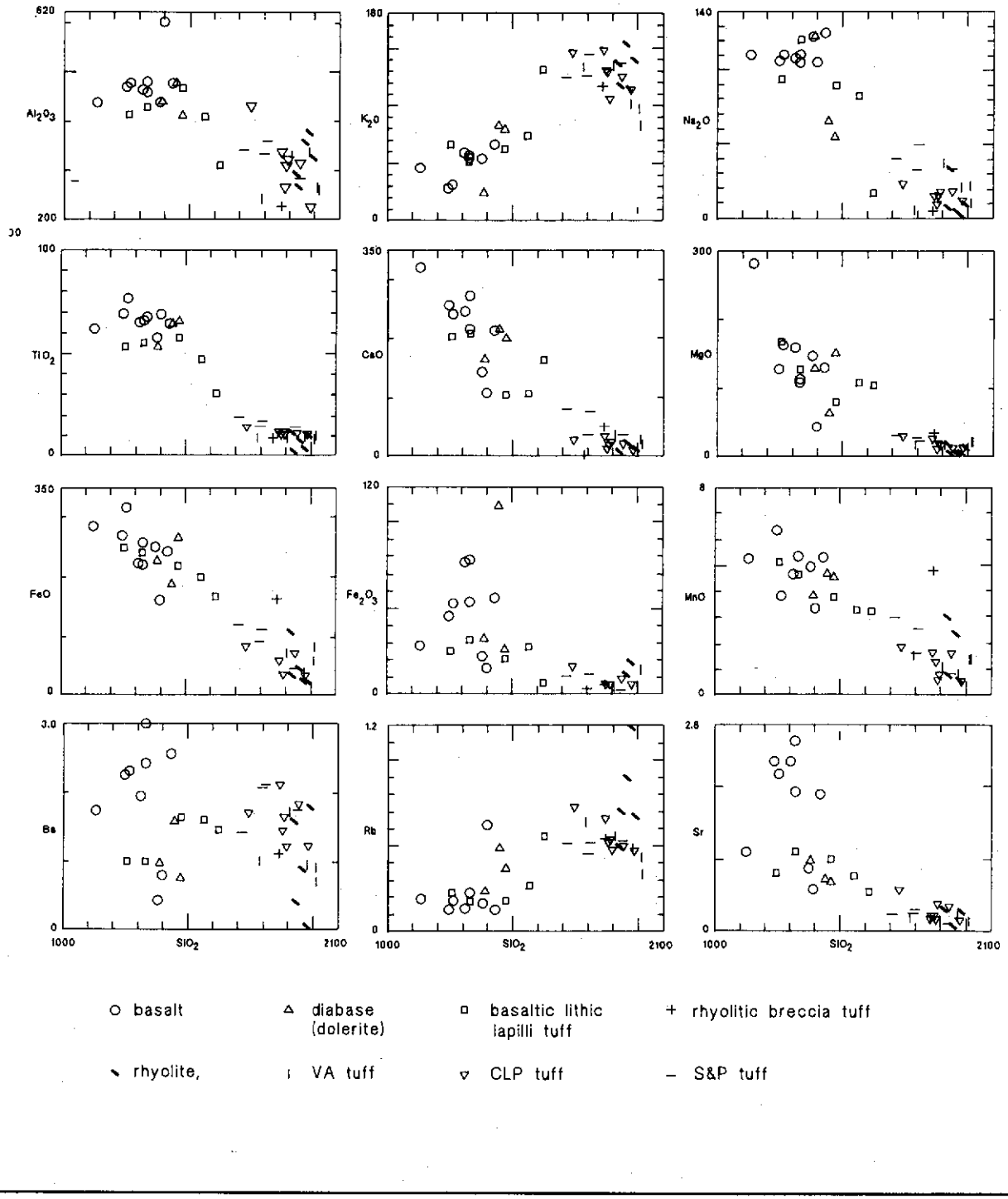

Figure 16. Binary plots for whole-rock XRF and ICP analyses against SiO_2 corrected for density. Units are kg/m^3. The analyses show positive variations of K_2O and Rb and negative variations of all other oxides and elements except Ba which exhibits an almost buckshot pattern.

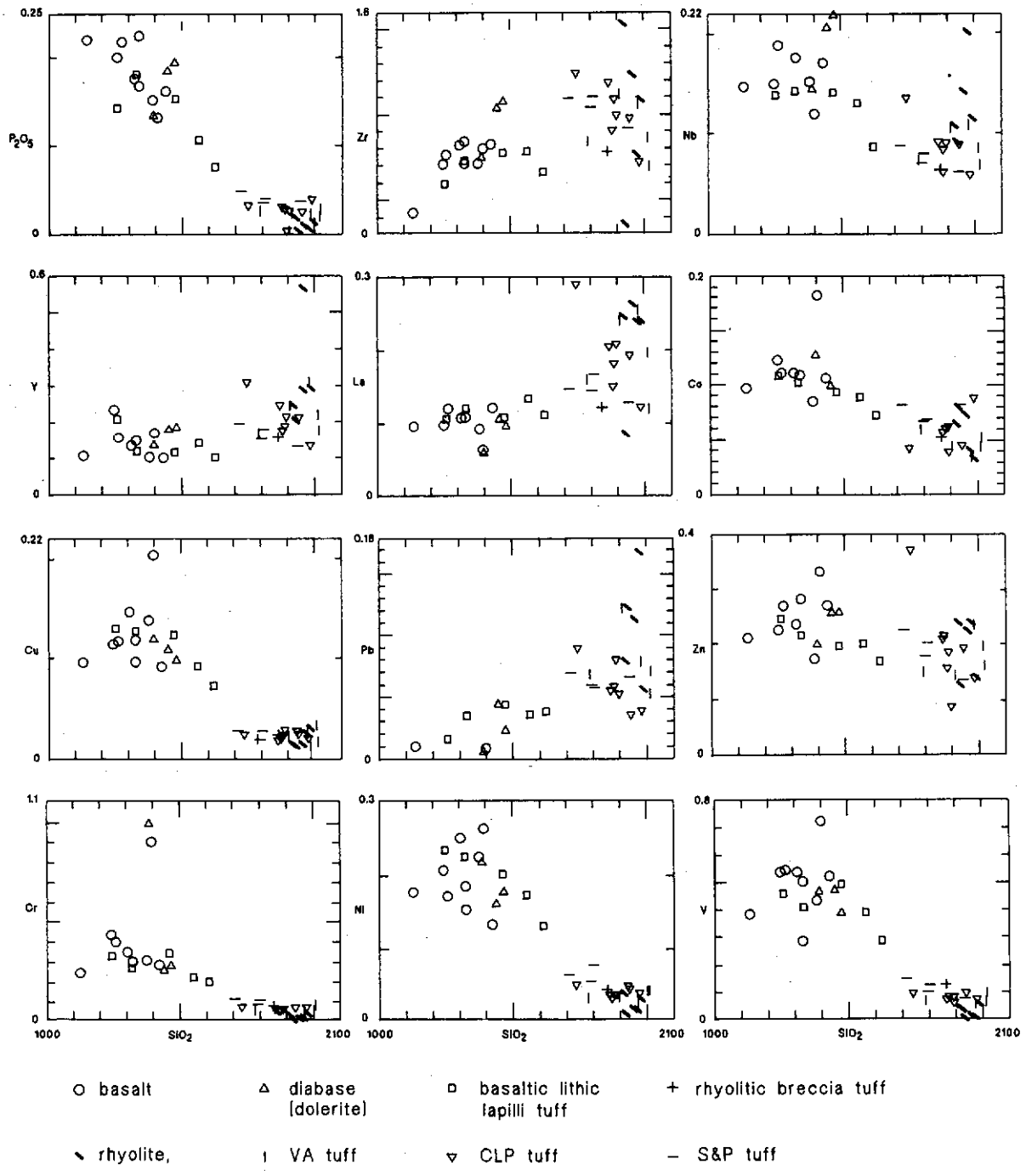

Figure 17. Binary plots for whole-rock XRF and ICP analyses corrected for density. Units are kg/m^3. The analyses form positive (Zr, Y, La, and Pb) and negative (all others) variation trends with SiO_2.

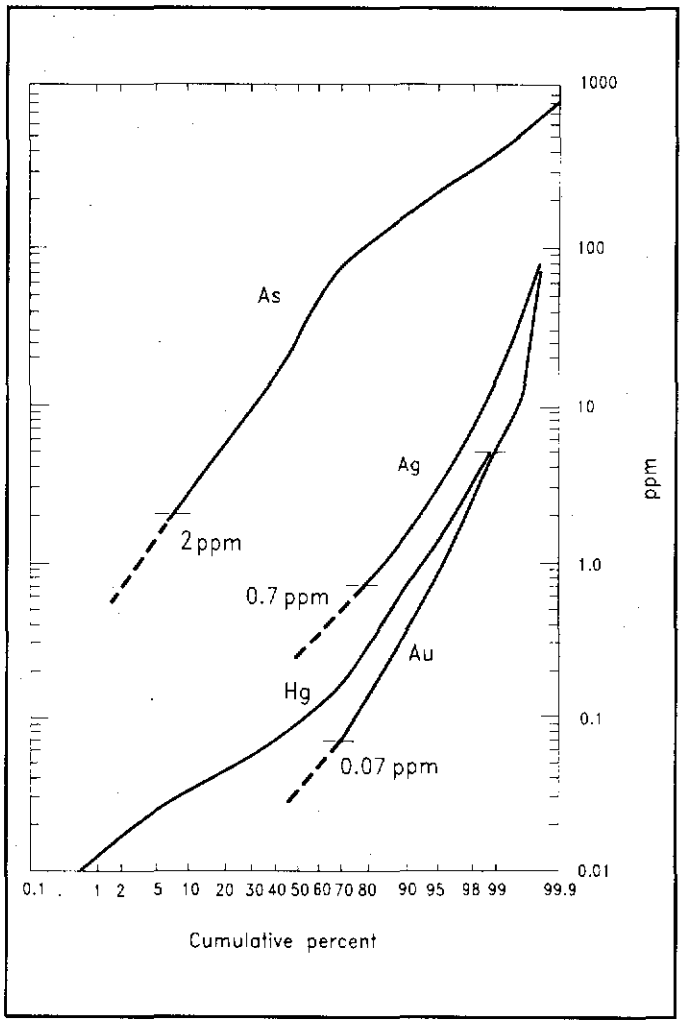

Figure 18. Cumulative probability curves of As, Ag, Hg, and Au for 11,416 samples from DDH 1 to DDH 90 but excluding holes DDH 17 and DDH 65 (analyses not available). As, Ag and Au are truncated at their lower ends by detection limits of 2 ppm, 0.7 ppm and 0.07 ppm respectively. Hg is truncated at the upper end by a maximum recorded assay level of 5 ppm for some Hg-rich samples. Statistical parameters are listed in Table 5.

elements during extraction. Nevertheless, concentrations for silver determined by the two different analytical techniques showed good agreement, although many of the low concentration values are below the ICP detection limit and the high concentration values generally have higher peak values in the ICP analyses.

The various analyses show that, in addition to gold and silver, the mineralization exhibits strongly anomalous arsenic and mercury concentrations, but low concentrations of copper, lead, zinc, antimony and barium, and very low concentrations of molybdenum, nickel, cobalt and tungsten (some shown in Table 4 and Fig. 15). Uranium and thorium were below their analytical detection limits.

Cumulative probability plots for 11,416 drillhole assays of gold, silver, arsenic and mercury are shown in Fig. 18 and some statistics generated using the MINITAB computer program (MINITAB Incorporated, Pennsylvania State University) are listed in Table 5. About 70 % of gold and 80% of silver values are below the detection limits for these elements (0.07 ppm for Au and 0.7 ppm for Ag). At 1 ppm gold (96th percentile), equivalent concentrations of other elements are: 3.4 ppm silver, 235 ppm arsenic and 1.54 ppm (1540 ppb) mercury.

Regression lines and R-squared values for correlation between gold, silver, arsenic, and mercury assays were calculated using MINITAB and are shown in Fig. 19; the regression equations are listed in Table 6. The arsenic-mercury pair was calculated using assays for all 11,416 samples, whereas gold-silver, gold-arsenic, gold-mercury, silver-arsenic, and silver-mercury pairs were calculated using assays of a subset of 2,771 samples with gold greater than 0.07 ppm and silver greater than 0.7 ppm (i.e. above their detection limits). There is relatively good correlation between gold and silver (R-sq = 50.6%), weak correlation of silver and mercury (R-sq = 18.0%) and gold and mercury (R-sq = 14.6%), and little correlation between mercury and arsenic (R-sq = 2.4%). There is no correlation between gold and arsenic or silver and arsenic (R-sq = 0.1% each). The gold-silver regression line shows a decreasing gold:silver ratio with increasing concentration, e.g. 1:3 at 1 ppm gold and 1:6 at 3 ppm gold.

Visual examination of computer plotted drill sections, showing downhole assays as histograms, for 12 cross-sections (listed as coordinates in Fig. 3) confirms the statistical analysis. Gold and silver show strong correlation and their enrichment in many of the sections defines a steeply northward-dipping gold-silver mineralized zone (termed the Gold-silver Zone) within the rhyolitic tuffs, southward and below the W-E Fault and upper welded CLP unit (Figs 2A, 4C, 15, and 20). In contrast, mercury exhibits a strong enrichment above and north of the Gold-silver Zone in the vicinity of the W-E Fault, with enrichment in the adjacent rhyolitic tuffs and fluvial sediments, defining a mercury zone partly coincident with the pyrite zone (Fig. 15). In some holes, a second order enrichment of mercury associated with the Gold-silver Zone, has caused the weak correlation with gold and silver suggested by the statistical analysis. A local third order enrichment of mercury is associated with some breccia zones, faults other than the W-E Fault, and lithological contacts in a few holes. Arsenic shows elevated concentrations throughout large sections of the drillholes, and exhibits some local correlations with elevated gold and silver and/or mercury, but there is no consistent trend (e.g. Fig. 15).

Down hole trends in the southward angled holes 29 and 30 are illustrated in Fig. 20, from analyses listed in Table 4. There are coincident high concentrations of gold and silver representing the Gold-silver Zone, half to two thirds of the way down the holes. Lead and zinc are depressed around the

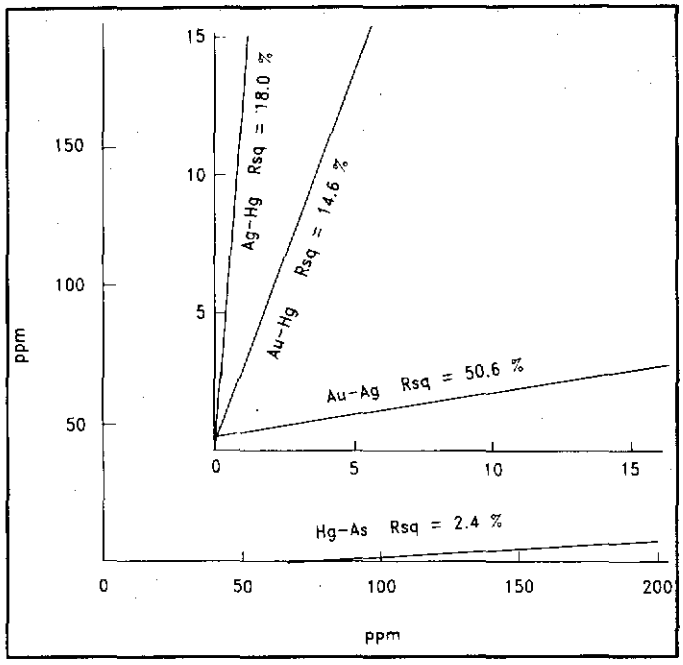

Figure 19. Plots of regression lines determined for drill core assay data (see Table 6). The vertical axis scale relates to the first element listed in each element pair, whereas the horizontal scale relates to the second element.

Gold-silver Zone and show strongest concentrations higher in the holes (north of the Gold-silver Zone). Copper values are high in the Gold-silver Zone and similar copper values occur uphole with lead and zinc in DDH 30. Antimony values are highest near the top of the holes but also show a lesser concentration in the Gold-silver Zone. Cobalt and nickel generally follow iron with concentrations in the upper parts of the hole, above the Gold-silver Zone, and a narrow peak near the bottom of each hole. Manganese also generally follows iron but has an irregular pattern in the upper part of DDH 30. Arsenic has an irregular distribution, but shows small peaks in the Gold-silver Zone.

The Gold-silver Zone occurs in the shape of an elongated wedge, widening upwards, and has approximate maximum dimensions of 550 m long, 110 m wide and 150 m deep. The east end of the zone is defined by a marked decrease in grade, whereas the western end is faulted off against the basaltic rocks. The highest gold values lie between the vertical cross-sections 10150E and 10350E, and above the 700 m level horizontal section, with a rapid decrease in gold grade away from this zone. Grade in the Gold-silver Zone appears to increase upward to the point where the zone is truncated by erosion. The only high level part of the system which is preserved is the discovery outcrop, which assays fairly low levels of gold and silver. However, this does not necessarily indicate an overall fall-off of Au-Ag at this level because the outcrop is about 100 m to the west of the high grade zone. A feeder zone may be present near section 10200E where high assays extend down to a level of almost 700 m and quartz veining also appears to funnel down (see Mineralization section). In other sections, drillholes below the high grade zone return low gold assays. The possible extension of high grade gold values below 700 m in section 10200E was not drill tested.

DISCUSSION

Volcanic environment

Contemporaneous basaltic and rhyolitic volcanism is indicated by: (1) interbedded basaltic tuffs and flows in the rhyolitic sequence, (2) fragments of basalt in the rhyolitic tuffs, and (3) abundant quartz xenocrysts in some of the basaltic tuffs. The Tarn Zone rhyolites are considered to represent a rhyolite dome which, by reason of proximity, was probably the source of the rhyolitic pyroclastic rocks in the Grew Creek area, although there are other potential source rhyolite domes within a few kilometres distance (see Gordey and Irwin, 1987).

A basaltic eruptive centre west of the Main Zone is suggested by the predominance of basaltic rocks at the western end of the Main Zone, and strong magnetic anomalies extending to the west.

The CLP and VA tuff units are considered to have been erupted as a series of ignimbrites (ash flow tuffs). The high crystal and lithic fragment content and degree of sorting of the S&P tuffs suggests a high degree of initial fragmentation of a crystal rich magma and/or efficient sorting processes during eruption and transport (see review of possible origins of crystal rich tuffs by Cas, 1983). Crystal-lithic rich ignimbrites similar to the S&P tuffs have been described elsewhere, for example Victoria, Australia (Birch, 1978; Clemens and Wall, 1984) and Colorado (Lipman, 1975), and therefore an ignimbritic origin is also possible for the S&P tuffs. The individual S&P units are generally homogeneous and lack sedimentary structures or other features which might help further determine their origin.

Sedimentary environment

Hughes and Long (1980) and Long (1981) described Tertiary age, coal bearing fresh water clastic sediments from many localities within the Tintina Trench and suggested that they resulted from sedimentation within separate orinterconnected fault controlled basins. Cyclic fining upward sequences at a few locations were considered to indicate deposition in river, deltaic (fine sequences) and alluvial fan (e.g. coarse sequences at Lapie River and Watson Lake) environments. The Grew Creek cyclic fining upward sequences are similar to point bar deposits formed by meandering streams, but the abundance of conglomerates suggests that an alluvial fan environment may have been more likely. During tectonically active episodes, alluvial fans would be common within the Tintina Trench, receiving detritus from the rapidly eroding marginal fault scarps.

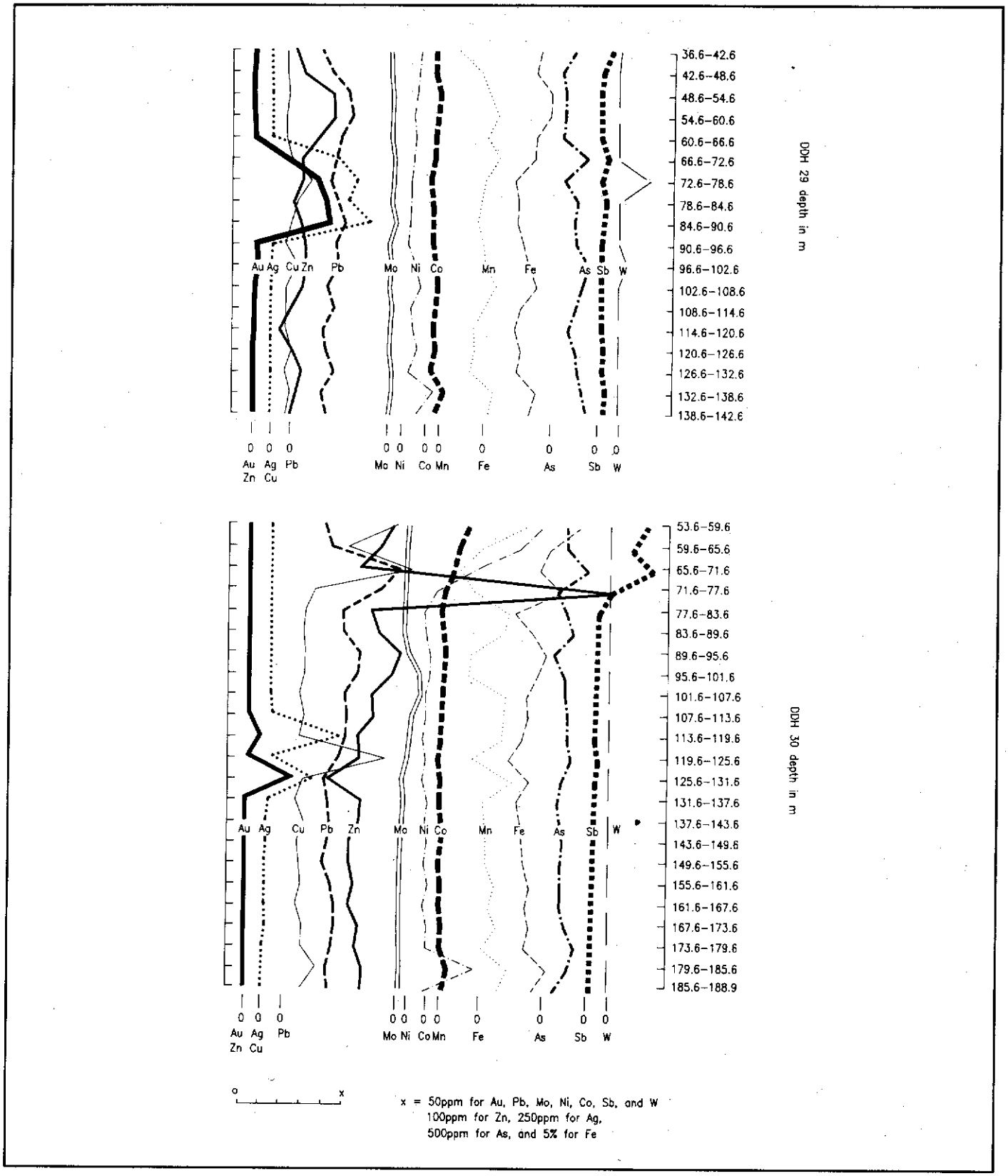

Figure 20. Downhole trends for concentrations of several elements determined by ICP analyses of 6 m composite samples (Table 4), together with Au and Ag curves based on averages of fire assays for 1.5 m samples. Au and Ag exhibit strong concentrations half way (DDH 29) to two thirds (DDH 30) downhole depth, defining the Gold-silver Zone, whereas Pb and Zn exhibit concentration peaks higher in the holes. Cu peaks in both zones in DDH 30.

Hydrothermal environment

The Grew Creek hydrothermal system exhibits many of the well documented features of volcanic hosted, low sulphur, quartz-adularia, epithermal and geothermal systems (see Berger and Eimon, 1983; Bonham, 1986; Hayba et al., 1986; Henley, 1986). The widespread illite-quartz-adularia alteration in the permeable tuffs, and propylitic alteration of the basaltic rocks, are typical of equilibration with near neutral pH alkali chloride water. The presence of illite and trace epidote suggests temperatures of $>220° <250°$ C. The quartz-adularia alteration results from high permeability in the tuffs and adjacent structurally controlled channelways (now veins and breccia zones), accompanied by higher fluid temperatures, and a more alkaline pH, probably produced by boiling. Cyclic sealing of channelways by mineral deposition and subsequent rupture by overpressure and hydraulic fracturing produced the hydrothermal breccias and ruptured veins. Intermediate argillic and advanced argillic alteration of the near surface rocks resulted from equilibration with acid sulphate water, evolved from the alkali chloride water by oxidation of contained sulphide to sulphate, or condensation in near surface waters of H_2S and CO_2 evolved from boiling.

Structural and stratigraphic control of mineralization

The mineralization is structurally controlled on all scales. The deposit occurs along splinter faults of the Tintina Fault Zone, and is localized where these are intersected by the second order, northerly striking N-S Fault. These features were probably the control for focusing deep fluid upflow at Grew Creek. Nearer surface, high permeability was provided by the rhyolitic tuffs (primary permeability) and numerous small scale tensional faults and fractures, now represented by veins and breccia zones (secondary permeability). The high primary permeability of the rhyolitic tuffs was probably a key factor in the development of the stockwork vein and breccia style of mineralization. Alteration and sealing of the upper welded CLP unit, accompanied by strong pyrite enrichment, prevented flow of hydrothermal fluid into the clastic sediments and confined the mineralization mostly in the non-welded CLP units. Mercury was concentrated along the W-E Fault possibly sometime after mineralization.

Tectonic style

The Grew Creek area records several local changes of tectonic style within a short period. Bimodal basalt-rhyolite volcanism, by analogy with similar occurrences elsewhere, was probably associated with regional extension. The mineralization occurs in approximate original orientation (near vertical veining), whereas the host rocks dip steeply, indicating that most of their tilting, as a result of a compressional tectonic regime, was pre-mineralization. Subsequently, mineralization was probably associated with extension because quartz veins are generally dilatant structures. However, the Grew Creek stockwork vein and breccia structures were generated by the hydrothermal system itself, i.e. by hydrofracture mechanisms, which could develop in either a compressional or extensional environment.

Sequence of events

The sequence of events at Grew Creek is considered to be as follows:

1. Around 60-50 Ma, a local tensional tectonic regime within the Tintina Fault Zone caused the formation of a pull-apart basin and associated bimodal basalt-rhyolite volcanism. Clastic sediments were also deposited within the basin.

2. A period of local compressional tectonics caused major deformation of the rocks including tilting and folding.

3. Around 50 Ma, a hydrothermal system developed, probably within a local extensional tectonic environment. Deep fluid upflow was localised at the intersection of the Grew Creek, North-South, and West-East faults. Near the surface, the hydrothermal fluid flowed into and through the permeable nonwelded ignimbrites, causing hydrothermal alteration and mineral deposition in these and adjacent units, including the formation of the pyrite zone. This was followed by the development of a hot springs style epithermal deposit with cyclic sealing and rupture resulting in quartz veining and hydrothermal breccias.

4. Cessation of hydrothermal activity was followed by additional faulting with considerable crushing and breaking of the veins and immediately adjacent wall rocks. This provided good secondary permeability for penetration and circulation of groundwater through the deposit, causing substantial supergene clay alteration. Considerable movement along some faults is demonstrated by the juxtaposition of the moderately to strongly altered rocks of the Main Zone against the little altered basaltic rocks in the west.

SUMMARY AND CONCLUSIONS

1. The Grew Creek prospect is a volcanic-associated epithermal gold-silver deposit of the low sulphur, quartz-adularia type.

2. The "Main Zone" deposit is hosted by rhyolitic tuffs, grouped into: (1) "crystal-lithic rich" mixed coarse ash tuff, lapilli-ash tuff, and lapilli tuff, (2) "glass rich" mixed coarse ash tuff and lapilli-ash tuff, and (3) vitric ash tuff. Welding and hydrothermal alteration have given some tuff units a pseudo rhyolite or quartz-feldspar porphyry appearance in hand specimen, causing previous misidentification of these rocks. The tuffs were most probably erupted as a series of ignimbrite (ash flow tuff) sheets associated with a rhyolite dome in the "Tarn Zone", 4 km to the east-southeast. The rhyolitic rocks are faulted against basaltic pyroclastic rocks

and flows to the west and fluvial sediments to the north.

3. An alkali chloride-type hydrothermal fluid altered the rhyolitic rocks adjacent to the veins to quartz-adularia and illite-quartz assemblages, and elsewhere to illite-quartz-adularia ± carbonate assemblages. Basaltic rocks are altered to carbonate-chlorite assemblages. Acid sulphate fluid formed intermediate argillic and advanced argillic alteration in the near surface environment. Hydrothermal alteration of the sediments is limited to a zone adjacent to the W-E Fault.

4. Gold and silver mineralization occurs in stockwork veins and hydrothermal breccias. The major minerals are electrum and acanthite, with associated pyrite, marcasite, and traces of arsenopyrite, chalcopyrite, sphalerite, galena, naumannite, aguilarite, and silver amalgam, in a gangue of quartz, adularia, carbonates, clays (mostly illite), and quartz pseudomorphous after calcite. A localized concentration of pyrite above and north of the mineralization forms a pyrite zone.

5. The mineralization occurs in a zone shaped like an elongate wedge, widening upwards, approximately 550 m long, 110 m wide and 150 m deep. The eastern end of the zone is defined by a marked decrease in grade, whereas the western end is faulted off against the basaltic rocks. Within the zone, the highest gold and silver assays occupy a level lying above the most intense quartz veining. Gold concentrations vary proportionally with silver, generally in a 1:4 ratio in the ore grade mineralization. A zone of anomalous mercury geochemistry is associated with the W-E Fault and coincides with the pyrite zone. Arsenic is present in anomalous concentrations but there is no statistical correlation with gold and silver when viewed in detail.

6. Hydrothermal activity and mineralization were intimately linked with the tectonic environment of the Tintina Fault and suggest a major period of activity along the fault in the mid Eocene. The deposit is hosted by volcanic rocks formed during extension in a pull-apart basin along the Tintina Fault Zone. Episodic fault movements structurally prepared the Grew Creek area by providing locally high secondary permeability for the focus of upflowing hydrothermal fluids.

7. The high primary permeability of the rhyolitic tuffs resulted in the development of mineralization structures by hydrofracture type mechanisms, producing the stockwork vein and breccia style of mineralization.

8. The absence of significant mineralization and hydrothermal alteration in the clastic sediments is attributed to damming of the hydrothermal fluids by the partly welded tuffs along the footwall of the W-E Fault.

9. Mineralization postdated tilting of the sedimentary and pyroclastic sequences.

10. Post-mineralization movements along the Tintina Fault Zone have disrupted the deposit, with displacements along several parallel and oblique faults, and crushing of vein material and adjacent wall rocks.

ACKNOWLEDGEMENTS

Christie carried out research on this project while on study leave from New Zealand Geological Survey (now DSIR Geology and Geophysics), and was hosted by Geological Survey of Canada in affiliation with the Department of Geological Sciences, University of British Columbia. These organizations are thanked for their support. Ken Dawson and Jim Morin suggested the topic. Fieldwork by Christie and Rushton, and some direct project costs were funded by a research grant from Indian and Northern Affairs Canada and supported by Noranda and Golden Nevada. Steve Morison, Bill Lebarge, and other staff of Indian and Northern Affairs Canada, provided advice and logistical support.

Confidential proprietary data, generated by many company geologists, was supplied by Noranda, Goldnev, and Prime Explorations Ltd. We thank these companies for permission to publish their data in this paper.

Many Noranda staff and their contractors provided assistance during the study, and special thanks are due to Managers Bill Mercer (Vancouver) and Hugh Copland (Whitehorse), and the geologists who worked at Grew Creek: Heather Brown, Dennis Bull, Louise Gagnon, Ken Galambos, Jan Helsen, Sheila Reid, and Chris Wild. Alison Star produced plans, sections and data from the Grew Creek computerized database in Noranda's Vancouver office.

XRD, XRF and some ICP analyses were supplied by the laboratories at Geological Survey of Canada, Ottawa. In particular we thank Jeanne Percival, Ruth Winter, and Gina Lechaminant for XRD -, Gerry LaChance for XRF -, and Ian Jonasson for coordinating - analytical work. Colin Tinker and Andy Tulloch of DSIR Geology & Geophysics assisted with the use of the MINITAB and IGPET computer programs respectively.

Bob Brathwaite, Andy Tulloch and David Skinner reviewed the manuscript and provided constructive comments which have measurably improved the paper. The figures were drafted by Jeff Lyall and the manuscript was typed by Sue Nepe.

REFERENCES

ANON., 1985. Canyon project, Yukon Territory, 1984 - 1985 summary. Unpublished report, Hudson Bay Exploration and Development Company Limited.

BERGER, B.R., and EIMON, P., 1983. Conceptual Models of Epithermal Precious-metal Deposits. In: Cameron Volume on Unconventional Mineral Deposits, W.C. Shanks (ed.), Society of Mining Engineers of the American Institute of Mining, Metallurgical, and Petroleum Engineers, Inc., New York, p. 191-205.

BIRCH, W.D., 1978. Petrogenesis of some Palaeozoic rhyolites in Victoria. Journal of the Geological Society of Australia, Vol. 25, No. 2, p. 75-87.

BONHAM, H.F. Jr., 1986. Models for volcanic-hosted epithermal precious metal deposits; a review. Proceedings of Symposium 5: Volcanism, Hydrothermal Systems and Related Mineralization, International Volcanological Congress, February 1986, p. 13-17.

CAS, R.A.F., 1983. Submarine 'crystal tuffs': their origin using a Lower Devonian example from southeast Australia. Geological Magazine, Vol. 120, No. 5, p. 471-486.

CHRISTIE, A.B., and GORDEY, S.P., 1989. The Tintina Fault and gold: Grew Creek, Yukon. Program and Abstracts for Contributions of the Geological Survey of Canada, Cordilleran Geology and Exploration Roundup, February 7-10, 1989, Hotel Vancouver, Vancouver. Energy Mines and Resources Canada.

CHRISTIE, A.B., DUKE, J. and RUSHTON, R., 1989. Grew Creek gold deposit, Tintina Trench, Yukon. Program and Abstracts for Contributions of the Geological Survey of Canada, Cordilleran Geology and Exploration Roundup, February 7-10, 1989, Hotel Vancouver, Vancouver. Energy Mines and Resources Canada.

CLEMENS, J.D. and WALL, V.J., 1984. Origin and evolution of a peraluminous silicic ignimbrite suite: the Violet Town Volcanics. Contributions to Mineralogy and Petrology, Vol. 88, p. 354-371.

COPLAND, H., 1988a. Geochemical and geophysical report on the Canyon 37-96, 218-222, 301-347, and Grand 1-136, 138-162 claims. Unpublished report, Noranda Exploration Company Limited for the Grew Creek Development Project.

COPLAND, H., 1988b. Geochemical and geophysical report on the Canyon 7-16 and 33-36 claims. Unpublished report, Noranda Exploration Company Limited for the Grew Creek Development Project.

DIETRICH, R.V. and SKINNER, B.J., 1979. Rocks and rock minerals; John Wiley & Sons, New York, 319 p.

DUKE, J.L., 1986. The geology and alteration of the Grew Creek epithermal gold-silver occurrence in south-central Yukon Territory (105 K 2). Unpublished BSc thesis, The University of British Columbia, 65 p.

DUKE, J.L., 1988. Report on 1988 exploration activities on the Canyon and Grand claims, NTS 105 K/2, Whitehorse Mining District, latitude 62 03" N longitude 132 50" W. Unpublished report, Noranda Exploration Company Limited for the Grew Creek Development Project.

DUKE, J.L. and GODWIN, C.I., 1986. Geology and alteration of the Grew Creek epithermal gold-silver prospect, south-central Yukon. In: Yukon Geology, Vol. 1. Exploration and Geological Services Division, Yukon, Indian and Northern Affairs Canada, p. 72-82.

GORDEY, S.P. and IRWIN, S.E.B., 1987. Geology, Sheldon Lake and Tay River map areas, Yukon Territory. Geological Survey of Canada, Map 19-1987 (3 sheets), scale 1:250 000.

HAYBA, D.O., BETHKE, P.M., HEALD, P. and FOLEY, N.K., 1986. Geologic, mineralogic, and geochemical characteristics of volcanic-hosted epithermal precious-metal deposits. In: Berger, B.R., and Bethke, P.M. (eds), Geology and Geochemistry of Epithermal Systems, Society of Economic Geologists, Reviews in Economic Geology, Vol. 2, p. 129-167.

HENLEY, R.W., 1986. The geothermal framework of epithermal deposits. In: Berger, B.R., and Bethke, P.M. (eds), Geology and Geochemistry of Epithermal Systems, Society of Economic Geologists, Reviews in Economic Geology, Vol. 2, p. 1-24.

HUGHES, J.D. and LONG, D.G.F., 1980. Geology and coal resource potential of Early Tertiary strata along the Tintina Trench, Yukon Territory. Geological Survey of Canada, Paper 79-32, 21 p.

JACKSON, L.E., GORDEY, S.P., ARMSTRONG, R.L. and HARAKAL, J.E., 1986. Bimodal Paleogene volcanics near Tintina Fault, east-central Yukon, and their possible relationship to placer gold. In: Yukon Geology, Vol. 1. Exploration and Geological Services Division, Yukon, Indian and Northern Affairs Canada, p. 139-147.

LIPMAN, P.W., 1975. Evolution of the Platoro Caldera Complex and related volcanic rocks, southeastern San Juan Mountains, Colorado. United States Geological Survey Professional Paper 852.

LONG, D.G.F., 1981. Dextral strike slip faults in the Canadian Cordillera and depositional environments of related fresh-water intermontane coal basins. Geological Association of Canada Special Paper 23, p. 154-186.

MORTENSEN, J.E., 1988. Eocene magmatism in central Yukon - tectonic and metallogenic implications. Oral presentation at the Yukon Geoscience Forum, November 27-29, 1988, Whitehorse, Yukon.

PRIDE, M.J., 1988. Bimodal volcanism along the Tintina Trench, near Faro and Ross River. In: Yukon Geology, Vol. 2; Exploration and Geological Services Division, Yukon, Indian and Northern Affairs Canada, p. 69-80.

SETO, S., and CROWE, G.C., 1989. Diamond drilling report on the Grew Creek property, Grand and Canyon claims, Whitehorse Mining District, Yukon Territory. Unpublished report by Azimuth Geological Incorporated for Goldnev Resources Inc.

SKETCHLEY, D.A., 1985. Application of mineralogical and geochemical characteristics of carbonate alteration envelopes to exploration for auriferous white quartz veins at the Erickson gold mine, Cassiar, North-Central British Columbia. Proceedings of "Alteration with special reference to precious metal deposits" conference, Department of Geological Sciences, University of British Columbia, December 9, 1985, p. 1-15.

STROSHEIN, R., 1986a. The gold mineralization, geology and exploration potential at Grew Creek, Yukon Teritory. Unpublished report, Hudson Bay Exploration and Development Company Limited, January 1986.

STROSHEIN, R., 1986b. The 1986 exploration program on the Canyon project. Unpublished report, Hudson Bay Exploration and Development Company Limited, November 1986.

TABLE 1: Textural and compositional features of the three groups of rhyolitic tuffs.

NAME			COL-OUR	UNIT THICKNESS	COMPONENTS % (rounded to nearest 5%)				TEXTURE AND FABRIC					
												Average Grain Size mm		
Acro-nym	Components	Size		Avg. Maximum (section)	Crys-tal	Li-thic	Pum-ice	Ma-trix	Sorting (crystals & lithics)	Shards in matrix	Welding	Crys-tals	Lith-ics	Pum-ice
S&P	mixed crystal, lithic & vitric	coarse ash tuff, lapilli ash tuff, & lapilli tuff	Pale grey	15 54 (10300E)	40	20	10	30	moderately - well sorted	rare - absent	absent	1.5	2.5	5
CLP	mixed crystal, lithic, & vitric	coarse ash tuff & lapilli ash tuff	Med. grey	7 35 (10400 E)	20	15	15	50	moderately - poorly sorted	present	absent - moderate	1	2.5	3
VAT	vitric	ash tuff	Dark grey	1 20 (10150 E)	10	5	10	75	moderately - poorly sorted	abun-dant	absent - moderate	1	1	3

Table 2: Hydrothermal alteration types and constituent mineral assemblages

(A = abundant, M = moderate, T = trace, ± = present or absent, and Opr = overprint)

	Illite-quartz-adularia ± carbonate	Quartz-adularia	Illite-quartz	Carbonate-chlorite	Intermediate argillic	Advanced argillic
Quartz	M-A	A	A	±	M	T-M
Carbonate	T-A		±	A	relict	relict
Illite	M-A	±	Tr-M	±	relict	
Adularia	T-A	M-A	A	±	relict	
Albite	±	±	±	±		
Chlorite	±			±		
Epidote				T		
Smectite	Opr		Opr	Opr	A	±
Illite/smectite	Tr	±	±	±	±	relict
Chlorite/smectite				±		
Kaolinite	Opr		Opr	Opr	T-M	M-A
Alunite						T-M
Pyrite	T-M	T-M	T-M	T-M	T-M	T-M

TABLE 5: Diamond drill hole assay statistics

	Au	Ag	As	Hg*[2]
Number of assays	11,416	11,416	11,416	11,416
Mean (average) ppm	0.35	1.45	62.2	0.32
50th percentile (median) ppm	<0.07*[1]	<0.7*[1]	25	0.09
90th percentile ppm	0.35	1.4	115	0.68
96th percentile ppm	1.0	3.4	235	1.5
Maximum value ppm	183.5	907.2	1262.0	12.8*[2]
Standard deviation ppm	-	-	88.70	0.75
Detection limit ppm	0.07	0.7	2	0.01

Analyses from DDH1-DDH90 but excluding DDH17 and DDH65. Statistical analysis calculated using MINITAB on Digital Equipment Corp. VAX mainframe computer

*[1] Below detection limits. Extrapolation of cumulative frequency curves (Fig. 18) suggest means of approximately 0.03 ppm for Au and 0.25 ppm for Ag.

*[2] Most analyses of >5 ppm Hg samples were recorded as 5 ppm and therefore samples more concentrated than the 12.8 ppm maximum value may be present.

TABLE 6: Regression analyses of drillhole assay data

Element pair	Number of Assays	Regression equation	R-sq*
Au-Ag	2,771	Au= 0.521 + 0.158 Ag	50.6%
Ag-Hg	2,771	Ag= - 1.00 + 13.5 Hg	18.0%
Au-Hg	2,771	Au= 0.125 + 2.68 Hg	14.6%
As-Hg	11,416	As= 56.6 + 18.4 Hg	2.4%
Au-As	2,771	Au= 1.53 - 0.00185 As	0.1%
Ag-As	2,771	Ag= 5.62 - 0.00633 As	0.1%

Regression analyses carried out using MINITAB on Digital Equipment Corp. VAX mainframe computer

* R-sq is a measure of how well the regression equation fits the data, with 100% indicating a perfect fit.

R-sq = R- squared = $\frac{100 \text{ (sum of squares due to regression)}}{\text{(sum of squares total)}}$

Table 3: Average whole rock analyses of Eocene basalts and rhyolites (calculated free of water and carbon dioxide but LOI noted to give indication of alteration).

	B A S A L T S									R H Y O L I T E S				
Location	Grew Ck.	Grew Ck.	Grew Ck.	Glenlyon	Ketza R.	Weasel Ck.	Hoole R.	Pillow Mt	L.Starr Ck.	Grew Ck.	Glenlyon[1]*	Glenlyon[2]*	Riddle R.	Tay R.
Source**	1	2	3	3	3	4	4	4	4	1	3	3	4	4
Number of analyses	9	2	3	19	3	1	1	1	1	6	8	5	1	1
LOI***	12.45	3.45	1.44	5.45	1.98	1.38	3.18	3.21	2.82	3.38	1.34	1.85	0.7	1.6
S_iO_2	48.36	49.32	50.30	49.77	50.89	49.77	51.79	50.65	51.83	77.93	75.01	72.06	75.33	76.32
TiO_2	2.43	2.42	2.34	2.15	2.62	1.84	2.41	2.25	2.14	0.25	0.03	0.29	0.07	0.13
Al_2O_3	17.61	16.70	15.95	16.50	14.65	15.63	16.04	15.07	16.50	12.65	11.93	12.90	13.40	12.09
Cr_2O_3	0.02													
Fe_2O_3T	11.74		11.72	11.38	12.40					2.26	0.16	2.81		
Fe_2O_3	1.75	4.01				2.18	4.38	3.66	4.42	0.19			1.00	1.00
FeO	9.01	6.57				8.52	5.67	7.50	5.72	1.88			1.00	0.90
MnO	0.18	0.51	0.21	0.18	0.19	0.16	0.17	0.21	0.14	0.05	1.34	0.07	0.02	0.02
MgO	5.13	4.64	5.26	5.18	4.91	8.06	4.50	5.26	4.51	0.33	0.41	0.17	0.04	0.12
CaO	8.18	7.98	8.02	9.03	8.62	8.74	8.96	8.67	9.02	0.94	3.12	0.66	0.90	0.36
Na_2O	4.15	3.74	3.67	2.83	2.88	2.72	3.14	2.51	3.00	0.45	5.21	2.88	3.79	2.03
K_2O	2.32	1.69	1.53	1.33	1.43	1.02	1.43	1.57	1.29	4.95	0.18	5.80	5.45	5.08
P_2O_5	0.66	0.60	0.42	0.70	0.85	0.44	0.84	0.71	0.58	0.03	0.04	0.04	0.02	0.04
Ba	708		923	810	788	401	733	553	581	333	620	660	10	41
Nb	58		47	34	44					52	84	58		

Rb	79		68	45	51					295	356	290		
Sr	647		599	580	374	283	385	329	326	58	50	39		
Y	51									123				
Zr	270		241	260	384					400	550	598		
Be	4.5					0.5	1.0	0.5	0.5	4.2			8.7	6.6
Co	42		36	34	22	29	23	23	22	25	1	2	3	3
Cr	144		148	154	166	210	164	156	122	8	30	28	6	6
Cu	46		29	20	19	38	49	37	43	8	3	2	18	11
La	38									90			57	63
Ni	72		61	53	24	67	41	38	42	9	2	2	7	9
Pb	1					1	1	1	1	42			63	30
V	190					140	140	146	159	7			11	3
Yb	2.54									9.4			11.0	2.8
Zn	90					86	86	97	86	81			121	84
Ag						0.6	0.2	0.2	0.2				1.0	1.0

* Glenlyon 1 = low K rhyolites, Glenlyon 2 = high K rhyolites

** Source: 1 = this study, 2 = Duke and Godwin (1986), 3 = Pride (1988), and 4 = Jackson et al. (1986)

*** LOI = loss on ignition (H_2O + CO_2 + S)

Table 4: Multi-element assays for DDH 29 and DDH 30

DDH29[a]

DEPTH m	Au ppm (FA)*3	Ag ppm (FA)*3	Ag ppm (ICP)*4	Cu ppm	Pb ppm	Zn ppm	Mo ppm	Ni ppm	Co ppm	Mn ppm	Fe %	As ppm	Sb ppm	Bi ppm	W ppm
36.6-42.6	0.81	1.03	1.2	8	13	65	1	9	4	151	2.48	101	7	2	2
42.6-48.6	0.22	0.53	0.3	8	18	72	1	8	4	375	2.23	45	3	2	1
48.6-54.6	0.06	0.35	0.1	9	26	100	2	7	6	427	2.96	56	2	2	1
54.6-60.6	0.19	0.35	0.1	8	28	101	2	6	5	518	2.93	54	2	2	1
60.6-66.6	0.1	0.35	0.2	8	23	86	2	7	4	439	2.23	47	2	2	1
66.6-72.6	15.43	159.4	163.1	10	21	71	4	6	4	553	2.21	164	5	2	1
72.6-78.6	30.48	218	274.4	20	18	71	3	5	2	412	1.25	55	2	2	16
78.6-84.6	34.72	175.4	191.8	13	21	63	2	5	3	378	1.44	114	4	2	1
84.6-90.6	36.78	237.5	272.4	11	25	70	4	5	3	340	1.35	100	3	2	1
90.6-96.6	1.96	3.6	2.3	8	21	74	1	4	3	382	1.61	110	2	2	1
96.6-102.6	2.12	3.4	2.7	13	22	74	2	7	4	411	1.86	171	2	2	4
102.6-108.6	0.95	2.1	1.9	8	17	71	1	9	5	510	2.23	133	2	2	1
108.6-114.6	0.59	1.5	1.6	8	20	62	2	5	4	388	1.53	110	2	2	1
114.6-120.6	0.7	2.1	2.2	8	15	50	1	6	3	301	1.25	73	2	2	1
120.6-126.6	0.37	1.2	1.4	11	16	62	1	8	4	309	1.47	105	3	2	1
126.6-132.6	0.33	3.1	0.9	8	20	70	2	4	2	275	1.31	115	2	3	1
132.6-138.6	0.28	0.78	0.8	10	14	66	2	16	8	488	2.25	138	4	3	1
138.6-142.6	0.46	1.1	1	8	16	61	1	8	4	448	1.94	154	3	2	1

Table 4 (contd)

DDH30[*2]

DEPTH m	Au ppm (FA)[*3]	Ag ppm (FA)[*3]	Ag ppm (ICP)[*4]	Cu ppm	Pb ppm	Zn ppm	Mo ppm	Ni ppm	Co ppm	Mn ppm	Fe %	As ppm	Sb ppm	Bi ppm	W ppm
53.6-59.6	0.03	0.35	0.1	50	16	97	2	60	15	731	4.21	65	24	4	1
59.6-65.6	0.04	0.35	0.2	27	19	85	1	50	11	326	2.81	70	18	2	1
65.6-71.6	0.56	0.61	0.5	58	52	67	1	27	8	132	2.45	170	27	2	1
71.6-77.6	0.04	0.35	0.1	12	43	205	1	10	6	267	3.47	27	7	2	1
77.6-83.6	0.45	0.43	0.1	8	25	78	1	5	3	602	1.27	75	2	2	1
83.6-89.6	0.21	0.35	0.1	7	26	85	1	6	4	567	2.11	103	2	2	1
89.6-95.6	0.03	0.35	0.1	8	34	107	3	8	5	242	2.73	17	2	2	1
95.6-101.6	0.07	0.35	0.1	8	33	99	8	8	5	228	2.37	69	2	2	1
101.6-107.6	0.14	0.63	0.4	6	27	80	9	6	4	581	1.92	71	2	2	1
107.6-113.6	0.47	2.93	2.7	8	28	82	5	6	4	576	1.94	88	2	2	1
113.6-119.6	7.3	34.63	35.7	6	28	67	4	5	4	558	1.72	84	2	3	1
119.6-125.6	1.2	2.58	2.7	47	25	70	3	7	3	288	1.17	108	3	2	1
125.6-131.6	22.04	22.78	29.6	8	18	40	1	6	4	670	2.06	64	2	2	1
131.6-137.6	0.57	1.98	1.1	5	20	71	2	8	4	393	1.52	45	2	2	1
137.6-143.6	0.09	0.7	0.6	9	21	70	2	7	5	408	1.78	62	2	2	1
143.6-149.6	0.16	0.7	0.4	6	20	62	1	8	5	423	1.85	75	2	2	1
149.6-155.6	0.15	0.7	0.6	7	18	62	1	7	4	439	1.96	70	2	2	1
155.6-161.6	0.16	0.7	0.5	8	22	66	1	9	5	508	2.27	73	2	2	1
161.6-167.6	0.25	0.88	0.7	6	24	62	1	7	5	470	2.03	70	2	2	1
167.6-173.6	0.11	1.13	0.9	9	24	72	1	9	6	554	2.26	99	2	2	1
173.6-179.6	0.13	0.68	0.6	9	23	70	1	9	6	409	2.04	147	2	2	1
179.6-185.6	0.04	0.35	0.1	16	21	77	2	22	9	673	3.18	113	2	2	1
185.6-188.9	0.03	0.35	0.1	9	22	76	2	9	7	576	2.54	48	2	2	1

*DDN29: Section 10175E (Fig. 3), length 142.65m, bearing 199° and dip 45°.

*2DDN30: Section 10175E (Fig. 3), length 188.98 m, bearing 199° and dip 45°.

*3FA = fire assay

*4ICP = ICP analyses by Acme Analytical Laboratories Ltd, Vancouver. 0.5 grams of sample were digested with 3 ml 3-1-2 HCl-HN03-$H_2$0 at 95°C for one hour and diluted with 10 ml of $H_2$0.

APPENDIX: XRF and XRD analyses of Grew Creek samples

Rock Type	Basalt									Diabase (diorite)		
Sample No. DL	39-149.8	55-30.7	57-58.8	66-96.1	66-115.2	72-117.2	71-135.3	83-58.7	83-62.5	67-355.8	90-44.7	90-58.85
Density (kg/m³)	2700	2830	2680	2770	2740	2740	2740	2740	2770	2610	2760	2740
Lab. No.	63	1,67,68	2,72,73,74	3,82,83	84	84	4,90,91	5,94,95	6,96	86	43	44
No. of analyses	1	3	4	3	1	1	3	3	2	1	1	1

WHOLE ROCK XRF ANALYSES

SiO_2 %	0.40**	46.60	46.13	44.88	42.30	32.60	44.80	42.60	41.43	39.75	47.20	45.30	46.20
TiO_2 %	0.02	2.31	2.08	2.21	2.10	1.77	1.87	2.11	2.30	2.40	1.94	2.01	2.05
Al_2O_3 %	0.40	20.10	15.40	15.50	15.27	12.60	14.20	15.07	15.60	15.00	15.00	12.70	15.30
Cr_2O_3 %	0.02	0.04	0.01	0.01	0.01	0.01	0.01	0.02	0.02	0.02	0.06	0.01	0.01
Fe_2O_3T %	0.10	6.40	10.33	10.88	10.80	9.90	9.70	10.47	11.37	12.65	9.70	9.90	10.20
Fe_2O_3 %		0.50	1.80	2.63	1.70	0.80	0.70	2.47	1.50	1.65	1.10	0.80	3.50
FeO %	0.20	5.30	7.77	7.43	8.20	8.20	8.10	7.20	8.90	9.90	7.70	8.20	6.00
MnO %	0.01	0.11	0.17	0.18	0.17	0.15	0.16	0.15	0.21	0.12	0.13	0.14	0.15
MgO %	0.10	1.45	4.19	3.77	3.51	8.20	4.77	5.21	4.23	5.12	4.39	4.66	2.05
CaO %	0.10	3.62	6.92	7.27	8.70	9.22	4.61	7.99	8.55	7.58	5.61	6.17	6.86
Na_2O %	0.50	3.50	4.03	3.88	3.53	3.20	4.00	3.50	3.53	3.50	4.20	1.70	2.10
K_2O %	0.05	5.56	2.16	1.91	1.72	1.32	1.78	1.92	0.94	0.99	0.83	2.48	2.66
H_2OT %	0.10	2.50	0.43	2.05	1.30	1.80	1.90	2.37	1.93	2.35	1.70	2.00	2.80
CO_2T %	0.05	6.50	8.30	7.98	10.53	20.10	12.10	9.00	10.43	10.50	10.00	13.80	9.80
P_2O_5 %	0.02	0.43	0.52	0.56	0.71	0.63	0.49	0.57	0.64	0.68	0.46	0.60	0.59
S %	0.04	0.49	0.03	0.06	0.05	0.04	0.08	0.07	0.08	0.20	0.03	0.04	0.00
Ba ppm		268	824	819	954	500	139	631	727	725	334	232	510
Nb ppm		40	55	59	52	42	49	56	48	59	49	67	66
Rb ppm		208	40	54	71	54	54	43	41	57	81	114	157
Sr ppm		201	608	645	829	320	289	757	748	680	335	214	230
Y ppm		56	32	41	46	30	32	43	74	49	46	56	57
Zr ppm		265	265	284	227	121	229	267	226	240	253	329	330
TOTAL		99.00	100.12	100.51	100.02	100.80	99.70	100.43	100.48	99.94	100.40	100.80	100.20

WHOLE ROCK ICP ANALYSES

Be ppm	0.50	14.0	2.0	2.3	2.6	2.5	5.9	2.3	1.8	1.7	1.3	6.3	3.4
Co ppm	5	61	35	34	35	28	28	36	40	35	44	29	32
Cr ppm	10	300	92	101	91	71	100	115	140	125	340	88	84
Cu ppm	10	68	30	33	38	28	45	48	37	37	41	32	36
La ppm	10	21	39	40	35	28	30	35	32	38	20	30	34
Ni ppm	10	88	43	52	59	51	73	82	67	54	75	55	52
Pb ppm	20	3				3	0				2	7	14
Sr ppm		200	610	650	850	320	290	765	755	680	340	210	230
V ppm	5	240	167	170	153	110	140	173	173	170	160	120	150
Yb ppm	0.50	4.20	2.40	2.30	2.00	1.50	1.50	2.00	1.90	2.20	2.60	3.00	3.20
Zn ppm	5	110	87	95	69	61	56	76	72	85	68	79	82

WHOLE ROCK XRD ANALYSES

		PLAG	K-FELD	PLAG	PLAG	PLAG	PLAG	plag	PLAG	PLAG	PLAG	qtz	qtz
		K-FELD	PLAG	K-FELD	K-FELD	K-FELD	qtz	K-feld	sid	sid	K-FELD	plag	plag
		ca	sid	(qtz)	sid	DOL	sid	sid	dol	(qtz)	qtz	sid	ca
		sid	(qtz?)	(ca)	(qtz)	sid	dol	(qtz)	(qtz?)	(ca)	sid	dol	sid
		(mica)	(py?)	(sid)	(ca)	(qtz)	(ca)	(ca)	(ca?)	chl/clay	dol	chl/clay	(mica)
							chl/clay?	(dol?)	chl/clay				

CLAY SEPARATE XRD ANALYSES

		ILL	SID	CHL	SM	ILL	ILL	CHL	CHL	CHL	ILL	ILL	ILL
		(ill/sm)	PLAG	PLAG	ch	PLAG	PLAG	chl/sm	plag	plag	CHL	KFELD	plag
			qtz	sid	sid	K-FELD	chl	ill	sid	ill	K-feld		ca
			(dol?)	qtz	plag	(ill/sm)	(qtz)	ca	(qtz)	sid	sid		kaol
				ca	(ca)	anatase?	(py)	qtz	(py)	ca	qtz		qtz
				chl/sm	(qtz)		(ill/sm)	sid	(ill/sm)	(qtz)			(py)
					(py)				(dol?)	(ill/sm)			

Rock Type	Basaltic tuffs					Rhyolite					
Sample No.	63-66.2	82-307	55-188.3	61-99.15	63-67.1	17-347.1	50-104.3	90-83.3	90-98.6	90-142.1	90-218.3
Density (kg/m³)	2.65	2600	2570	2550	2630	2570	2530		2390	2520	2550
Lab No.	77	93	70	76	78	53	66	45	46	47	48
No. of Analyses	1	1	1	1	1	1	1	1	1	1	1

WHOLE ROCK XRF ANALYSES

SiO_2 %	42.90	51.00	55.70	41.40	52.90	70.70	76.20	75.30	79.20	76.20	74.20
TiO_2 %	1.77	2.00	1.03	1.76	1.48	0.40	0.36	0.23	0.08	0.13	0.25
Al_2O_3 %	13.80	16.20	10.70	13.60	13.90	10.80	12.50	10.80	11.10	14.50	13.60
Cr_2O_3 %	0.01	0.02	0.01	0.02	0.01	0.00	0.00	0.00	0.00	0.00	0.00
Fe$_2$O$_3$T %	9.50	9.20	6.50	10.00	8.30	4.50	1.00	2.30	1.40	1.70	2.20
Fe_2O_3 %	1.00	0.70	0.20	0.80	0.90	0.00	0.00	0.00	0.00	0.70	0.40
FeO %	7.70	7.60	5.70	8.20	6.70	4.00	0.90	2.10	1.30	0.90	1.70
MnO %	0.15	0.13	0.11	0.17	0.11	0.11	0.00	0.03	0.03	0.02	0.09
MgO %	4.92	2.74	3.52	5.47	3.64	0.64	0.43	0.33	0.17	0.18	0.16
CaO %	6.67	3.59	5.59	6.71	3.57	1.18	0.44	2.24	0.16	0.59	0.85
Na_2O %	3.90	3.10	0.60	3.10	2.80	0.30	0.40	0.20	1.40	0.10	0.20
K_2O %	1.64	2.17	4.51	2.18	2.48	5.07	5.39	3.12	4.86	4.40	5.85
H_2OT %	2.20	3.60	1.30	2.20	2.30	1.40	2.20	1.60	0.90	2.00	1.40
CO_2T %	12.80	6.90	10.90	14.40	9.00	3.90	0.70	3.00	0.90	0.60	1.70
P_2O_5 %	0.58	0.53	0.26	0.47	0.36	0.06	0.05	0.03	0.01	0.02	0.03
S %	0.36	0.14	0.13	0.20	0.18	0.09	0.02	0.02	0.03	0.18	0.03
Ba ppm	320	574	449	330	543	587	687	122	171	24	340
Nb ppm	46	49	30	46	44	40	44	48	38	78	54
Rb ppm	54	62	188	73	89	184	259	184	288	457	340
Sr ppm	357	350	187	274	266	120	111	66	0	0	37
Y ppm	38	40	38	68	47	88	111	108	82	218	108
Zr ppm	234	268	228	195	265	567	416	428	146	295	466
TOTAL	**100.50**	**100.60**	**100.40**	**100.80**	**100.40**	**99.70**	**99.70**	**99.10**	**100.20**	**100.70**	**100.50**

WHOLE ROCK ICP ANALYSES

Be ppm	6.3	4.1	10.0	7.9	6.5	3.0	5.8	3.8	2.1	6.1	3.9
Co ppm	33	33	25	36	30	24	13	29	33	16	28
Cr ppm	87	120	69	110	76	13	16	8	6	7	8
Cu ppm	41	43	25	43	31	6	12	7	6	10	6
La ppm	39	37	38	35	45	91	92	110	35	92	100
Ni ppm	73	70	45	78	59	14	12	9	5	6	7
Pb ppm	11	15	13	5	12	29	22	37	50	65	43
Sr ppm	360	350	190	270	270	120	110	66	0	0	37
V ppm	130	170	96	150	130	12	18	5	1	2	3
Yb ppm	2.00	2.50	2.80	1.90	2.70	6.40	7.70	8.30	7.20	17.00	8.10
Zn ppm	69	68	58	81	68	88	54	100	52	92	85

WHOLE ROCK XRD ANALYSES

	PLAG	plag	qtz	dol	NA-FELD	qtz	QTZ	QTZ	QTZ	QTZ	QTZ
	sid	qtz	sid	plag	qtz	K-feld	K-feld	mica	K-feld	K-MICA	mica
	dol	(ca)	dol	sid	sid	(mica)	(mica)	sid	plag		K-feld
	(qtz)	(sid)	(feld)	(qtz)	(mica)	(ca)		(ca)	(sid)		
	(mica)	chl/clay?	(mica)	(mica)	(ca)				(mica?)		
	(ca)		(ca)		chl/clay?						
	chl/clay?				(dol?)						

CLAY SEPARATE XRD ANALYSES

	PLAG	CHL	ILL	ILL	ILL	ILL	ILL	ILL	ILL	ILL	ILL
	ILL	ILL	K-FELD	PLAG	K-FELD	K-FELD	K-FELD	(qtz)	plag	QTZ	K-FELD
	CHL	PLAG	sid	chl	PLAG	qtz	qtz	(ca)	qtz	plag	qtz
	K-feld	K-feld	qtz	(sid)	chl	sid	(ill/sm)	(sid)	(ill/sm?)		ca
	sid	qtz	(ill/sm)	(qtz)	sid	(ill/sm)		(ill/sm?)			(ill/sm)
	dol	sid		(dol)	qtz						(sm)
	ca	(ca)		(ill/sm)	(ill/sm)						
	qtz	(ill/sm)		(py)							
	(ill/sm)										
	(hem or py)										

Rock Type	VA tuff						CLP tuff					
Sample No.	18-	23-106.8	72-172.8	85-33.4	29-84.3	65-123.3	17-113.7	18-159.6	28-97.7	35-36.5	38-143.6	40-193.8
Density (kg/m³)	311.9	2380	2510	2540		2510	2540	2380	2400			
Lab. No.		57	92	42	59	81	49	54	58	60	61	64
No. of analyses	52	1	1	1	1	1	1	1	1	1	1	1
	1											

WHOLE ROCK XRF ANALYSES

SiO_2 %	76.30	72.80	75.90	71.70	80.50	74.70	72.60	76.30	80.80	79.80	80.50	74.40
TiO_2 %	0.38	0.32	0.28	0.31	0.27	0.33	0.42	0.40	0.41	0.38	0.22	0.26
Al_2O_3 %	9.90	10.00	10.10	12.50	10.10	12.80	11.90	10.80	9.20	9.00	7.30	8.20
Cr_2O_3 %	0.00	0.00	0.00	0.00	0.00	0.00	0.00	0.00	0.00	0.00	0.00	0.00
Fe2O3T %	4.00	3.60	2.30	3.10	0.90	1.50	3.70	2.80	1.50	2.00	3.10	3.10
Fe_2O_3 %	0.50		0.00	0.10	0.00	0.00		0.20	0.20	0.20	0.00	
FeO %	3.10		2.20	2.70	1.00	1.50		2.30	1.20	1.60	2.90	
MnO %	0.05	0.06	0.05	0.04	0.02	0.02	0.02	0.05	0.02	0.03	0.07	0.08
MgO %	0.74	0.67	0.75	0.65	0.29	0.52	0.64	0.40	0.43	0.36	0.52	0.95
CaO %	0.62	0.27	1.02	1.18	0.13	0.26	0.62	0.31	0.30	0.21	0.21	2.81
Na_2O %	0.40	0.20	0.80	1.40	0.20	0.80	0.60	0.40	0.50	0.20	0.20	0.20
K_2O %	3.11	5.42	3.66	5.05	5.53	3.84	4.98	5.30	4.61	6.14	3.52	5.20
H2OT %	1.70		1.70	1.40	1.10	2.50		1.40	1.20	0.80	1.10	
CO2T %	2.80	1.70	3.60	3.00	0.70	2.60	0.80	1.80	0.80	1.30	2.30	4.10
P_2O_5 %	0.10	0.10	0.07	0.08	0.07	0.08	0.12	0.11	0.15	0.10	0.07	0.07
S %	0.41	1.01	0.01	0.29	0.25	0.01	2.78	0.40	0.47	0.32	0.24	1.16
Ba ppm	267	410	345	653	399	355	633	589	496	426	296	325
Nb ppm	26	30	32	40	37	41	32	25	24	24	29	24
Rb ppm	156	261	163	211	290	183	207	212	190	328	177	248
Sr ppm	57	76	31	67	44	84	64	88	60	46	35	90
Y ppm	66	69	83	93	83	116	71	71	53	52	71	50
Zr ppm	264	341	326	421	364	398	420	368	293	338	259	279
TOTAL	**100.10**	**96.20**	**100.10**	**100.60**	**100.30**	**100.10**	**99.20**	**100.30**	**100.40**	**100.50**	**99.30**	**100.60**

WHOLE ROCK ICP ANALYSES

Be ppm	3.5	6.8	5.2	4.6	7.8	7.6	6.0	5.7	7.3	6.7	8.0	5.5
Co ppm	20	25	17	17	32	13	24	25	36	31	32	16
Cr ppm	32	21	17	15	13	17	22	23	24	21	18	17
Cu ppm	7	8	13	9	6	10	9	8	8	6	8	6
La ppm	46	65	74	91	75	97	69	60	49	50	64	45
Ni ppm	16	13	16	13	9	10	14	13	15	11	13	13
Pb ppm	27	28	20	46	27	30	31	24	16	20	25	21
Sr ppm	57	76	31	67	44	84	64	88	60	46	35	90
V ppm	36	27	26	20	14	21	28	30	26	27	22	18
Yb ppm	4.30	5.10	6.40	6.60	5.90	8.20	5.40	4.90	3.70	4.00	5.30	3.80
Zn ppm	61	60	74	54	74	88	70	63	56	57	59	63

WHOLE ROCK XRD ANALYSES

	QTZ	QTZ	QTZ	QTZ	QTZ	QTZ	QTZ	QTZ	QTZ	QTZ	QTZ	QTZ
	K-feld	K-FELD	(mica)	K-FELD	K-FELD	mica	K-feld	K-FELD	K-FELD	K-FELD	K-FELD	K-feld
	sid	(sid?)	(plag)	PLAG		(plag)	(mica)	(mica)	(mica?)			dol/ank
	(mica)			(mica)		(K-feld)						(ca)
	(ca)			(sid?)		(sid)						

CLAY SEPARATE XRD ANALYSES

	ILL	ILL	ILL	ILL	K-FELD	ILL	K-FELD	ILL	ILL	K-FELD	K-FELD	K-FELD
	KFELD	K-FELD	K-FELD	PLAG	ILL	QTZ	ILL	K-FELD	K-FELD	ILL	ILL	ILL
	qtz	qtz	qtz	qtz	qtz	K-FELD	qtz	qtz	qtz	qtz	qtz	qtz
	sid	(ill/sm)	plag	sm	(ill/sm)	ill/sm	sid	sid	(ill/sm)	(ill/sm2)	sid	(ill/sm)
	(ill/sm)		(sid)	(ill/sm)			ca	(ill/sm)		(sid?)	(ill/sm)	(dol?)
			(ill/sm)				(ill/sm)					

Appendix (continued): XRD and XRF analyses of Grew Creek samples

Rock Type	CLP tuff (continued)				S & P tuff					Hydro-thermal	-breccia	Quartz vein
Sample No.	64-57.9	64-68.2	66-165.4	68-262.4	17-221.5	17-291.9	39-90	56-264.4	60-200.4	55-183.8	21-61.7	29-74.90
Density (kg/m³)	2.44	2500	2500	2500	2510	2470		2480	2600	2490		
Lab. No.	79	80	85	87	50	51	62	71	75	69	56	(27)
No. of analyses	1	1	1	1	1	1	1	1	1	1	1	1

WHOLE ROCK XRF ANALYSES

SiO_2 %	74.60	66.10	74.50	71.80	74.80	68.90	74.60	64.00	65.10	70.10	76.30	79.60
TiO_2 %	0.40	0.52	0.41	0.44	0.52	0.55	0.48	0.70	0.60	0.35	0.30	0.01
Al_2O_3 %	12.70	16.40	12.10	13.00	11.00	12.80	10.80	12.80	13.00	8.60	8.00	7.30
Cr_2O_3 %	0.00	0.00	0.00	0.00	0.00	0.00	0.00	0.00	0.00	0.00	0.00	0.00
Fe_2O_3T %	1.70	3.90	3.30	1.40	2.00	4.00	2.10	5.20	4.80	7.00	4.20	1.10
Fe_2O_3 %	0.20	0.60	0.30		0.10	0.10		0.40	0.40	0.20		
FeO %	1.30	3.00	2.70		1.70	3.50		4.40	4.00	6.10		
MnO %	0.03	0.07	0.06	0.06	0.03	0.06	0.01	0.11	0.09	0.18	0.11	0.07
MgO %	0.58	1.04	0.04	0.70	0.44	1.01	0.49	1.10	0.82	1.22	0.85	1.11
CaO %	0.81	0.86	0.66	1.19	1.34	1.31	0.52	2.98	2.69	1.53	0.84	2.32
Na_2O %	0.70	0.90	0.70	0.60	1.30	1.30	0.40	1.50	1.80	0.20	0.10	0.10
K_2O %	4.18	5.55	4.77	5.68	5.34	4.86	5.20	4.71	5.23	4.31	5.25	5.67
H_2OT %	2.30	2.30	1.70	1.80	0.90	1.60		1.40	1.20	1.10		0.30
CO_2T %	1.50	2.80	2.20	2.00	2.10	3.80	0.70	5.70	5.10	5.60	2.30	3.40
P_2O_5 %	0.10	0.12	0.09	0.11	0.14	0.13	0.12	0.17	0.14	0.11	0.07	0.00
S %	0.25	0.13	0.19	0.66	0.39	0.04	1.22	0.07	0.02	0.48	1.78	0.02
Ba ppm	485	646	704	811	678	802	576	530	761	420	375	124
Nb ppm	35	51	34	35	24	27	27	33	29	24	24	0
Rb ppm	186	275	191	253	205	176	219	192	187	204	286	326
Sr ppm	148	220	131	83	50	96	102	88	113	71	69	58
Y ppm	83	115	80	93	50	58	56	72	64	59	51	14
Zr ppm	392	469	376	455	355	399	387	407	397	295	267	38
TOTAL	**99.70**	**100.60**	**100.90**	**99.60**	**110.20**	**100.10**	**96.70**	**100.20**	**100.40**	**100.30**	**100.30**	**101.00**

WHOLE ROCK ICP ANALYSES

Be ppm	5.3	8.1	5.0	7.0	4.4	2.9	5.7	3.4	3.9	65.0	15.0	24
Co ppm	15	16	17	22	32	26	76	31	25	20	44	2
Cr ppm	21	26	23	22	25	34	31	43	40	31	24	11
Cu ppm	11	9	10	7	11	8	10	11	10	9	9	16
La ppm	81	110	73	78	49	55	58	55	59	47	52	0
Ni ppm	14	19	17	14	19	21	18	24	28	17	16	6
Pb ppm	21	34	14	21	26	23	25	26	21	21	24	
Sr ppm	150	220	130	83	50	96	100	88	110	71	69	
V ppm	21	35	34	25	29	38	24	53	45	47	22	3
Yb ppm	6.30	8.60	5.70	6.10	3.50	3.90	4.00	4.60	4.40	4.10	3.60	0.90
Zn ppm	33	140	73	82	53	68	67	84	73	78	60	11

WHOLE ROCK XRD ANALYSES

	QTZ	qtz	QTZ	QTZ	QTZ	QTZ	QTZ	qtz	K-FELD	QTZ	QTZ	
	(mica)	mica	mica	K-feld	K-FELD	K-FELD	K-FELD	K-feld	ca	K-feld	K-FELD	
	(plag)	plag	plag	(mica)	PLAG	PLAG	(mica?)	plag	qtz	sid	(py)	
	(K-feld)	K-feld	(sid)	(dol)	(mica)	sid		ca	sid	(mica?)		
	(dol)	(sid)		(py)		(mica)		sid				
						(ca)		(mica)				

CLAY SEPARATE XRD ANALYSES

	ILL	ILL	ILL	ILL	K-FELD	ILL	ILL	ILL	ILL	ILL	ILL	
	K-FELD	qtz	K-FELD	K-FELD	ILL	K-FELD	K-FELD	sid	plag	K-FELD	K-FELD	
	qtz	(ill/sm)	QTZ	qtz	qtz	qtz	qtz	ca	qtz	sid	qtz	
	(ill/sm)		sid	(ill/sm)	plag	(ill/sm)	(ill/sm)	qtz	sm	qtz	(ill/sm)	
			(ill/sm2)		(m-lay)			(ill/sm)	ca	(ill/sm)		
									(ill/sm)			

All analyses by Geological Survey of Canada laboratories, Ottawa. XRF analyses on fused disks except FeO, H_2OT, CO_2T, and S by wet chemical techniques.

Fe_2O_3 is calculated using: $Fe_2O_3 = Fe_2O_3T$ (XRF) - 1.11134 X FeO (volumetric) ICP analyses are Geological Survey of Canada's ICP-TR1 group obtained on 1.0 gram of sample (acid + fusion of residue) dissolved in 10% HCl and diluted to 100 ml. Interpretation of XRD diffractograms was by J.B. Percival of Geological Survey of Canada. For clay separates, analyses were made of untreated, heated and glycolated samples to aid interpretation of the clay minerals present.

XRD quantitative estimates: ILL = abundant, ill = minor, (ill) = trace, and (ill?) = trace, tentative identification

XRD abbreviations: ank = ankerite, ca = calcite, chl = chlorite, dol = dolomite, feld = feldspar, ill = illite, kaol = kaolinite, plag = plagioclase, py = pyrite, qtz = quartz, sid = siderite, and sm = smectite

* Column of analytical detection limits

PRELIMINARY OBSERVATIONS ON THE GEOLOGY AND GEOCHEMISTRY OF QUARTZ VEINS IN THE KLONDIKE DISTRICT, WEST-CENTRAL YUKON

J.K. Mortensen
Geological Survey of Canada
601 Booth St
Ottawa, Ontario
K1A 0E8

and

B.E. Nesbitt and R. Rushton
Department of Geology
University of Alberta
Edmonton, Alberta
T6G 2E3

MORTENSEN, J.K., NESBITT, B.E., and RUSHTON, R., 1992. Preliminary observations on the geology and geochemistry of quartz veins in the Klondike District, West-Central Yukon. In: Yukon Geology, Vol. 3; Exploration and Geological Services Division, Indian and Northern Affairs Canada, p.260-270

ABSTRACT

Four main styles of quartz veining are recognized in the Klondike District. These include foliaform and discordant mesothermal quartz veins in schistose metamorphic rocks, quartz-carbonate veins in altered ultramafic rocks and greenstones, epithermal chalcedony veins cutting Eocene igneous and sedimentary rocks, and low-temperature epithermal veins associated with intensely altered Plio-Pleistocene White Channel Gravel deposits. Foliaform mesothermal quartz veins are invariably barren; however discordant mesothermal veins locally contain visible gold. Both styles of epithermal veins in the Klondike contain at least geochemically anomalous levels of gold. The complex history of hydrothermal activity in the Klondike has led to considerable confusion about the nature of veining in this area. The results of this study provide a preliminary framework within which to evaluate the various prevailing theories regarding the major sources of gold in the Klondike placer deposits.

RÉSUMÉ

Quatre principaux types de veines de quartz sont reconnus dans le district du Klondike; ce sont des veines de quartz mésothermal foliiformes et discordantes dans les roches métamorphiques schisteuses, des veines de quartz et carbonate dans les roches ultramafiques altérées et les roches vertes, des veines de calcédoine épithermale recoupant des roches ignées et sédimentaires de l'Éocène et enfin des veines épithermales formées à basse température associées aux dépôts plio-pléistocènes de graviers de White Channel intensément altérés. Les veines de quartz mésothermal foliiformes sont invariablement stériles; cependant les veines mésothermales discortantes renferment par endroits de l'or visible. Au klondike, les deux types de veines épithermales renferment au moins des concentrations géochimiquement anormales d'or. L'histoire complexe de l'activité hydrothermale au Klondike a suscité une confusion considérable quant à la nature de la formation des veines dans cette région. Les résultats de cette étude assurent un cadre préliminaire pour l'évaluation des diverses théories prédominantes concernant les sources majeures d'or dans des dépôts alluvionnaires au Klondike.

INTRODUCTION

Exploration for lode gold mineralization in the Klondike District began immediately after the discovery of rich placer gold deposits in the area in 1896. Although many quartz veins, some containing visible gold, were discovered early in the development of the Klondike District (e.g. McConnell, 1905), they have received little detailed study. In this paper we summarize preliminary results of an on-going investigation of the field relationships, genesis and composition of the different vein systems, and discuss the implications of this work for the origin of placer gold deposits in the area.

GEOLOGY OF THE KLONDIKE DISTRICT

The bedrock geology of the Klondike District is shown in Figure 1 (from Mortensen, 1990). Bedrock units can be divided into four main groups; (1) schistose metamorphic rocks, (2) greenstones and ultramafic rocks, (3) undeformed intrusive rocks, and (4) young volcanic and sedimentary rocks. The schistose metamorphic rocks include a variety of metaplutonic, metavolcanic, and metasedimentary rocks which range in age from pre-Late Devonian to mid-Permian. These rocks display a penetrative foliation which generally parallels compositional layering, and formed during the first main deformation event in the area (F1). Metamorphism associated with the F1 event was at middle greenschist facies (chlorite-biotite grade) throughout most of the area, but reached garnet grade along the southwest margin of the study area, and sillimanite grade along lower Dominion Creek adjacent to the granitic orthogneiss which underlies Mt Burnham (Fig. 1).

A younger deformation event (F2) produced macroscopic scale folds in the Bonanza Creek and Eldorado Creek areas, and one or more crenulation cleavages over much of the Klondike area. Metamorphism associated with F2 was at lower greenschist facies, and is usually seen only as a retrogression of F1 mineral assemblages.

The schistose metamorphic rocks in the Klondike have been imbricated by regional scale thrust faults along which bodies of massive greenstone and altered ultramafic rocks (including serpentinized harzburgite, serpentinite, and quartz-carbonate-Cr mica rocks) were emplaced. The greenstones and ultramafic rocks were not affected by F1 deformation, and field observations suggest that the F2 event approximately coincided with the thrust faulting (Mortensen, 1990).

K-Ar and Rb-Sr ages for metamorphic muscovite and hornblende in the Klondike range from Middle Jurassic to earliest Cretaceous, probably reflecting very prolonged cooling after the F1 event.

Two distinct suites of undeformed and unmetamorphosed intrusive rocks which post-date thrust faulting have been recognized in the Klondike. These are: (1) hornblende-biotite granodiorite which forms a small plug along middle Hunker Creek (Fig. 1) and yields a latest Cretaceous K-Ar hornblende age (R.L. Debicki, pers. comm., 1984), and (2) a widespread bimodal suite of quartz-feldspar porphyry and diabase and plagioclase-phyric mafic porphyry which occur as dykes and as a large stock between lower Hunker Creek and the Klondike River (Eocene K-Ar whole-rock age, R.L. Debicki, pers. comm., 1984; Mortensen, 1990) (Fig. 1).

Unmetamorphosed andesite flows which are interlayered with clastic sediments along Last Chance Creek (Fig. 1) are undated, but closely resemble similar sequences south of Indian River that have given latest Cretaceous isotopic ages (Lowey et al., 1986). An undated sequence of felsic lapilli tuff and volcanic breccia interlayered with immature clastic rocks near the mouth of Germaine Creek (Fig. 1) is composed of quartz-feldspar porphyry identical to the Eocene felsic porphyry intrusions and is considered to be their extrusive equivalent.

Despite the close promixity of the Klondike District to the Tintina Fault, there is surprisingly little evidence for large-scale steep faults in the area (Mortensen, 1990).

The Klondike District is unglaciated and three main unconsolidated units in the area are known to contain gold. These are: (1) White Channel Gravels of Plio-Pleistocene age that rest on high level terraces, (2) gravels that occupy the beds of present streams, and (3) colluvium which mantles hillslopes (e.g. McConnell, 1905; Morison, 1987).

VEIN SYSTEMS IN KLONDIKE DISTRICT

Four main styles of veining are recognized in the Klondike District. These are: (1) mesothermal quartz veins in schistose metamorphic rocks; (2) quartz-carbonate veins cutting greenstones and ultramafic rocks; (3) Fluorite and chalcedony veins cutting igneous and sedimentary rocks of Eocene age; and (4) Quaternary, low-temperature epithermal veins.

Veins of the first type are by far the most widespread and abundant, and form the main focus of this paper.

MESOTHERMAL VEINS IN SCHISTOSE METAMORPHIC ROCKS

Quartz vein material makes up a significant proportion of the schists and gneisses that underlie most of the Klondike District. Two main types of veins can be distinguished based mainly on their structural setting. Foliaform veins form typically lensoid bodies oriented along F1 foliation planes. Discordant veins form tabular bodies that crosscut the main foliation in the wall rocks. The main characteristics of these two types of veins are briefly summarized below.

Foliaform veins.

These veins range up to 3 m in thickness, but are typically discontinuous. They are present in all metamorphic rock units in the area, and are particularly abundant in the mica-rich lithologies (i.e. felsic schist, chloritic schist, and carbonaceous schist), where they locally comprise up to 10% of the rock volume. Structurally, the foliaform veins have been little affected by the F2 deformation, but locally occupy F2 fold hinges (see description of the PORTLAND occurrence

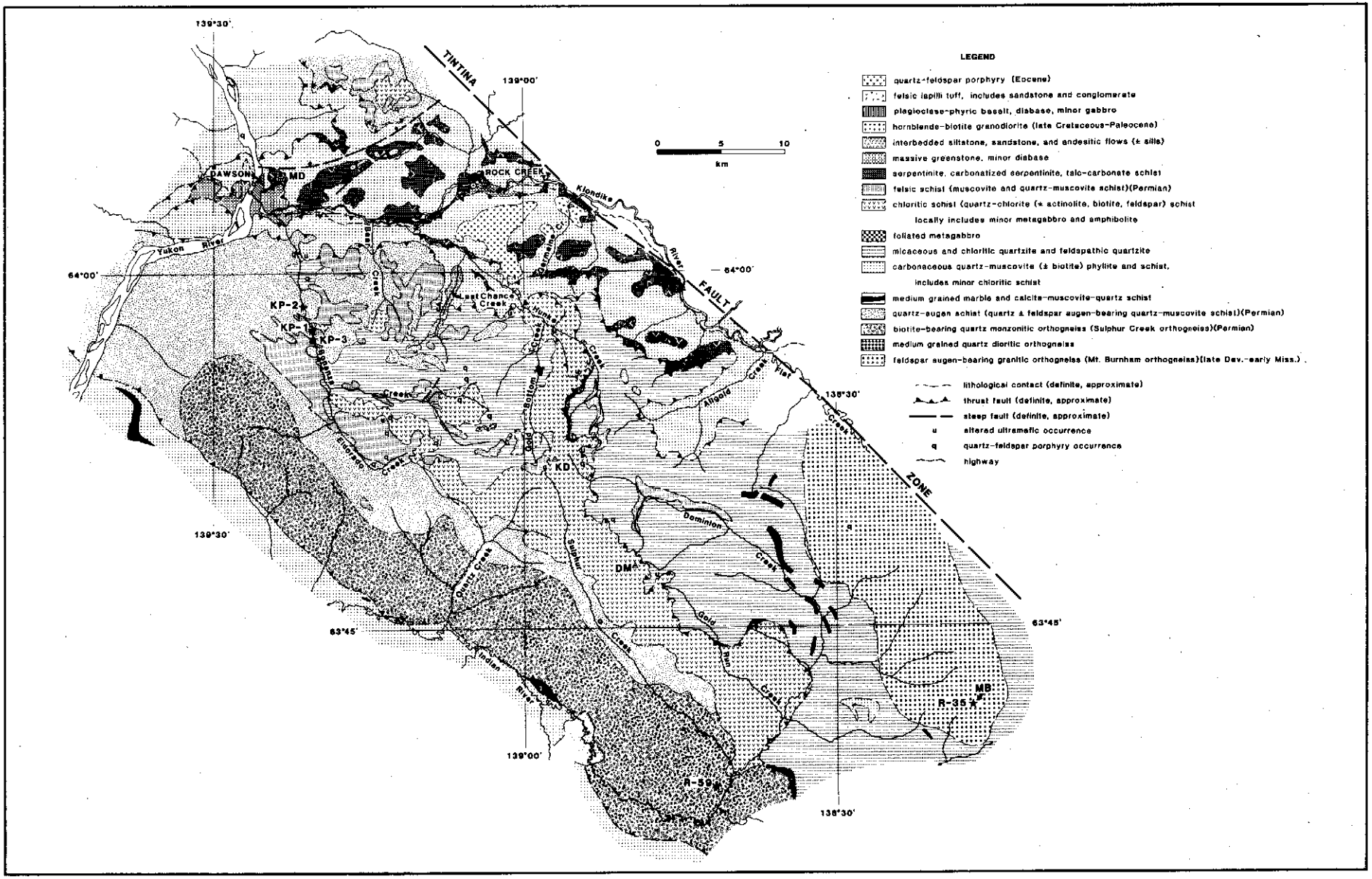

Figure 1. Geological map of Klondike District. Solid stars show locations for geochronological samples discussed by Mortensen (1990). MD = Midnight Dome; KD = King Solomon Dome; DM = Dominion Mountain; MB = Mt Burnham.

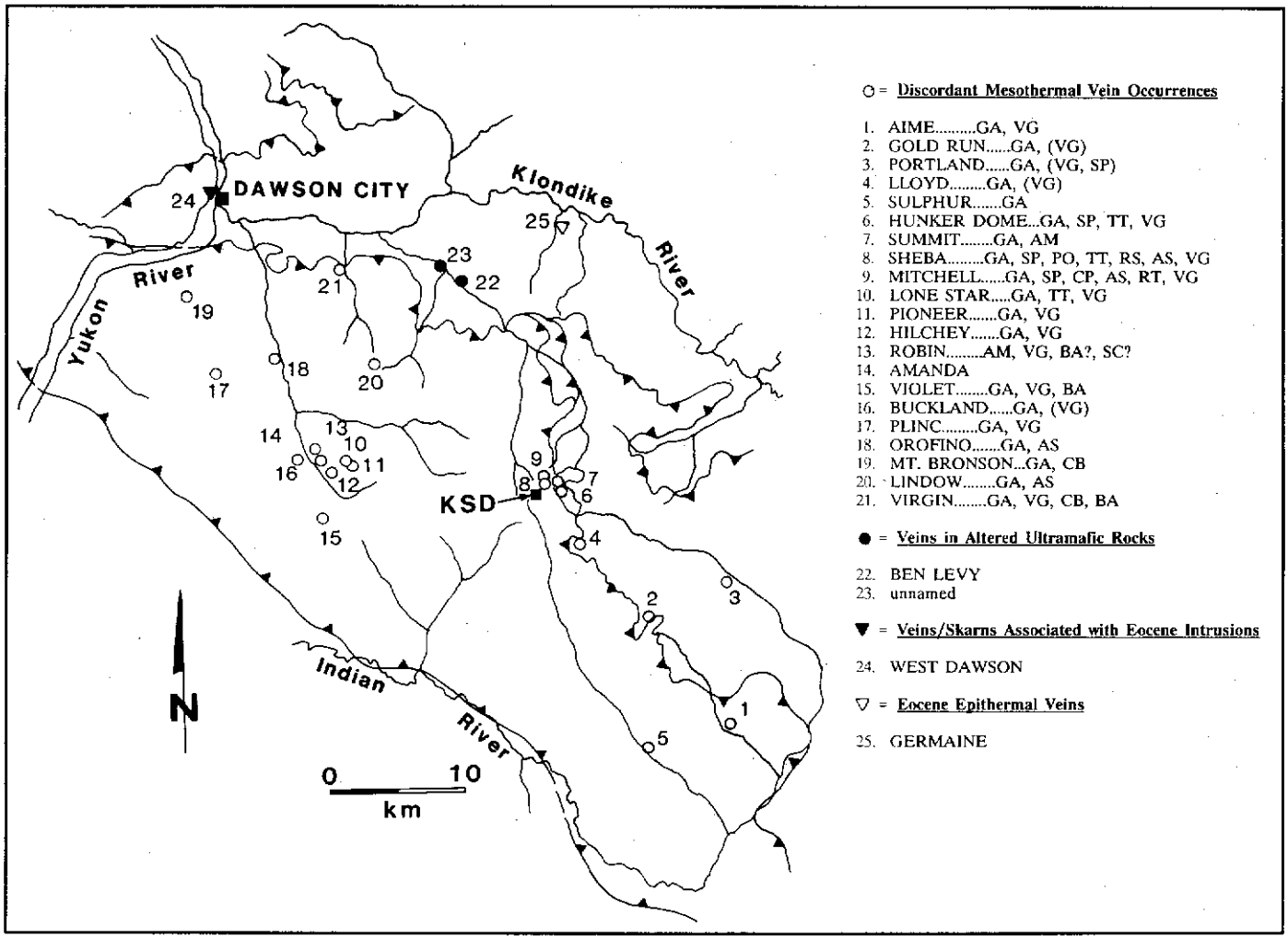

Figure 2. Sketch map of the Klondike District showing locations of the mineralized discordant vein occurrences as well as other occurrences referred to in the text. Also shown are the occurrence name (in capital letters) and minerals present other than quartz and pyrite (minerals in parentheses reported to be present but not confirmed). GA = galena, SP = sphalerite, AS = arsenopyrite, PO= pyrrhotite, TT = tetrahedrite, VG = visible gold, RS = pyrargyrite, AM = amethyst, CB = carbonate, BA = barite, SC = scheelite, RT = rutile. Includes data from Debicki (1984), Friedrich and Hoymann (1989), and Yukon Minfile (1991). KSD refers to King Solomon's Dome.

(MINFILE 115O 064) in Maclean, 1914, p. 101-102 for an example), suggesting formation late in the F2 event.

Foliaform veins consist almost entirely of milky to clear, coarse grained quartz with locally abundant calcic to ferroan carbonate. Small masses of muscovite and/or chlorite are present in some of the foliaform veins, but it is uncertain whether these minerals form part of the vein assemblage or are small screens of mica-rich wall rock. Pink K-feldspar occurs in small amounts in foliaform veins within the quartz-augen schist unit and the Sulphur Creek orthogneiss, both along Bear Creek and in areas of somewhat higher metamorphic grade in the southwestern part of the district. Vuggy cavities appear locally in the foliaform veins.

The foliaform veins appear to contain no visible sulphides or gold and no evidence of alteration is visible in adjacent wallrocks.

Discordant veins.

Discordant veins occur sporadically throughout the Klondike, although they are most abundant in the central and southern parts of the district. The abundance of discordant veins appears to decrease rapidly north of the Klondike River, northeast of Hunker and Dominion Creeks, and south of Indian River. The locations of some of the better known and explored veins and vein sets are shown in Figure 2. Discordant veins are usually less than 1 m thick; however examples up to 3 m thick are present at some localities (e.g. AMANDA occurrence on Eldorado Creek, (MINFILE 115O 051). In some instances single veins can be traced up to 800 m along strike. Most of the veins occupy steeply dipping extensional structures, which locally appear to form en echelon arrays. An example of such an array includes the

MITCHELL-SHEBA-HUNKER DOME occurrences (MINFILE 115O 068 and 1150 067) north and east of King Solomon Dome, where the largest and most continuous veins present form a north-south trending, left-stepping en echelon array. There is no obvious geometric relationship, however, between the orientation of these veins and any of the presently recognized regional deformation events.

Discordant veins crosscut, and are therefore younger than, foliaform veins at a number of localities in the Klondike District. In two instances, however, clearly discordant quartz veins appear to merge with foliaform veins, suggesting a possible partial overlap in age between the two types of veins.

Small vuggy cavities lined by clear quartz (and rare carbonate) crystals are abundant in some discordant veins. Ribboned veins are very rare; most veins appear to represent simple, single-stage, open space filling. Ribboned vein material appears in float at the south end of the vein system at the HUNKER DOME occurrence (MINFILE 115O 067), and on the dump at the AIME occurrence (MINFILE 115O 061)(Fig. 2). Angular wall rock fragments to 25 cm in longest dimension appear in discordant veins at the LLOYD (MINFILE 115O 066) and SHEBA (MINFILE 115O 068b) occurrences (Fig. 2). There is no evidence for faulting synchronous with vein formation, although post-vein faults produce minor (up to several metres) offset on veins in the Lone Star mine area (MINFILE 115O 072) and zones of crush breccia along vein margins at the MITCHELL-SHEBA occurrence (MINFILE 115O 068)(Fig. 2).

Like the foliaform veins, discordant veins consist mainly of milky white to locally clear, coarse grained quartz. Coarse grained amethyst crystals line a vuggy cavity in a discordant vein near the north end of the HUNKER DOME occurrence (Fig. 2). A greater range of vein minerals is generally present in the discordant veins than in the foliaform veins. Barite, calcite, ferroan carbonate and rare rutile and feldspar occur locally as gangue in some of the veins. Scheelite appears in placer concentrates from most drainages in the Klondike (Gleeson, 1970), and coarse scheelite and barite grains have also been recovered from colluvial deposits in an area with abundant discordant veins near the ROBIN occurrence (MINFILE 115O 148) on Oro Grande Gulch (Fig. 2). Although scheelite has not been found in outcrop, it is most likely derived mainly from the discordant veins.

The discordant veins typically display very low sulphide concentrations. Pyrite is usually present in at least trace amounts, mainly as discontinuous selvages along vein walls or as irregular disseminations in vein interiors. Galena also commonly occurs in trace amounts, typically as disseminated grains and grain aggregates associated with pyrite in vein interiors. In relatively sulphide-rich portions of the discordant veins, other sulphides and sulphosalts including sphalerite, chalcopyrite, tetrahedrite, and rare pyrrhotite, arsenopyrite and pyrargyrite have also been noted.

Visible gold is present in a number of discordant veins in the Klondike District (Fig. 2). It is typically associated with sulphide (especially pyrite) concentrations, and occurs both in pyritic selvages and as disseminations in vein interiors. The gold occurs as flakes and irregular inclusions up to 5 mm in diameter in pyrite (and in masses of limonite after pyrite) and as free grains of similar size in quartz. Crystalline gold has been reported from discordant veins at the LONE STAR occurrence (Tyrrell, 1912). Zones of relatively high gold grades appear locally in some veins; for example, assays of up to 857 g/t (25 opt) have been reported for handpicked specimens of vein material from the HUNKER DOME occurrence (Fig. 2) (Yukon Minfile, 1991). Pyrite-rich discordant veins in the vicinity of the Lone Star mine locally contain abundant visible gold. Such veins include narrow, shallowly dipping quartz-pyrite and pyrite veins and stringers in the open cut at the Lone Star mine itself (Fig. 2) and a very pyrite-rich vein (now largely altered to limonite) near the ROBIN occurrence on Oro Grande Gulch (Fig. 2). There appears to be an empirical correlation between the gold and pyrite contents of discordant veins, although it is also possible that the pyrite-rich veins described above represent a different (possibly younger) discordant vein event.

Mineralized discordant vein systems in the Klondike District produce irregular zones of weakly to moderately anomalous gold and arsenic values in soil which are locally associated with sporadic anomalous Pb, Zn and Cu values (Yukon Minfile, 1991).

The nature and extent of alteration around discordant veins is controlled to some extent by the mineralogy and bulk composition of the wall rocks. Felsic wall rocks are generally visually unaltered, but the more mafic lithologies, especially the chloritic schist unit, commonly display discernible alteration up to 3 m from the margins of discordant veins. The alteration consists mainly of introduction of ferroan carbonate into the wall rocks where it imparts a distinctive brownish weathering character to the otherwise green-weathering chloritic schist. The carbonate alteration is particularly well developed in an area of bulldozer trenching along the MITCHELL vein (MINFILE 115O 068)(Fig. 2). Pyritization and sericitization also occur locally in narrow zones adjacent to discordant veins in the chloritic schist. At the MITCHELL occurrence (MINFILE 115O 068)(Fig. 2), narrow zones of fine to coarse euhedral pyrite grains locally comprise up to 40 % of the wall rock by volume within 1-4 cm of the vein walls. At least some of the pyrite is formed from the sulphidization of magnetite porphyroblasts that are abundant in some bands in the chloritic schist unit in this area. The remainder of the schist in these zones is strongly bleached and altered to a muscovite-quartz assemblage. R.J. Cathro reported that samples of pyritic bleached schist adjacent to the MITCHELL vein assayed between 3.4 and 39.7 g/t gold (Yukon Minfile, 1991). The gold content of the alteration halo significantly increases the potential for proving up mineable tonnages of ore from relatively narrow discordant vein systems.

VEINS IN GREENSTONES AND ULTRAMAFIC ROCKS

Quartz and quartz-carbonate veins occur in massive greenstone and altered serpentinite in the northern and central

parts of the Klondike District. Greenstone-hosted veins are exposed in new road cuts on the Midnight Dome access road and along the Klondike Highway east of Rock Creek (Fig. 1). They are typically quartz-rich, and are superficially similar to the discordant veins described above, but contain no sulphides and tend to be more irregular and discontinuous than the discordant veins in schistose wall rocks. Ferroan carbonate-rich veins occur within silica-carbonate altered serpentinite ("listwanite") in two areas on lower Hunker Creek. These include the BEN LEVY occurrence (MINFILE 116B 157) and a new occurrence exposed by bulldozer stripping approximately 2.5 km to the northwest (MINFILE 116B 167)(Fig. 2). The BEN LEVY occurrence consists of a vein at least 5 m thick which has been explored by limited underground development and by recent reverse circulation and core drilling by United Keno Hill Mines Ltd. It appears to dip moderately northeast and consists of 1-5 mm bands of comb-structured ferroan carbonate with rare interbands of clear fine grained quartz. Vuggy cavities, usually lined by drusy quartz crystals, appear locally, and angular fragments of strongly carbonatized serpentinite (and minor carbonaceous schist) occur within the vein. No sulphides are present in the vein or in adjacent wall rocks, and only trace levels of gold were detected (A.J. McFaull, pers. comm., 1988).

The second occurrence consists of irregular, coarse grained, apparently discontinuous ferroan carbonate-quartz veins and vein breccias up to 0.5 m wide. Disseminated rutile needles and blebs of galena, chalcopyrite, and pyrite are locally present. No assay information is presently available for this occurrence.

VEINS IN EOCENE IGNEOUS AND SEDIMENTARY ROCKS

Two distinct types of veins are included in this category. Medium grained quartz-calcite-epidote-tremolite-sulphide veinlets up to 2.5 cm wide occur in mafic porphyry dykes of inferred Eocene age on the west side of the Yukon River across from Dawson. This occurrence lies less than 300 m west of the WEST DAWSON occurrence (MINFILE 116B 015)(Fig. 2), a Cu-Pb-Ag skarn developed in calcareous bands within the graphitic schist unit. Sulphides present in the veinlets include chalcopyrite, pyrite and galena. Wall rocks appear to be weakly carbonatized. The identical mineralogy and Pb isotopic signature of the veins and skarn mineralization suggest a close genetic relationship.

Veining is also associated with high-level quartz-feldspar porphyry intrusions, felsic tuffs and coarse clastic rocks of Eocene age in the northern and eastern portions of the Klondike District. The felsic igneous rocks typically contain high levels of fluorine (W.D. Sinclair and S.B. Ballantyne, pers. comm., 1988), and fluorite is present as both disseminations and narrow discontinuous stringers at several localities along lower Hunker Creek (MINFILE 116B 006)(Fig. 2). This mineralization was probably produced during late or post-magmatic volatile streaming. Chalcedony veins to 10 cm wide and zones of chalcedonic breccia up to 1 m in diameter cut felsic lapilli tuff, volcanic breccia, and underlying pebble and cobble conglomerate and altered serpentinite between the mouths of Germaine and Goring creeks (MINFILE 116B 004)(Fig. 2). The chalcedonic material includes structureless, medium grey to resinous reddish brown open space fillings, and delicately laminated grey to very pale blue veinlets and crustifications. The veining is associated with intense kaolinization and silicification of wall rocks, and breccia fragments enclosed by veins are similarly altered. No sulphide mineralization has been found immediately adjacent to the chalcedony veins, although clay-altered felsic and mafic dykes of the Eocene suite locally contain up to 2% pyrite elsewhere in the Klondike. The veins and associated alteration are variably anomalous in As, Hg, Sb and Tl, but available analyses indicate only rare anomalous precious metal values (S.B. Ballantyne, pers. comm., 1988). The style of veining and associated alteration, and the nature of its geochemical signature are typical of volcanic-hosted epithermal systems elsewhere in the Cordillera.

QUATERNARY VEINING

Plio-Pleistocene White Channel Gravel deposits have been intensely altered in several areas of the northern Klondike district (e.g. MINFILE 116B 159)(Tempelman-Kluit, 1982; Dufresne, 1986; Dufresne et al., 1986). Narrow quartz-chalcedony veins are observed cutting both metamorphic rocks and diabase dykes of probable Eocene age beneath these altered zones. These veins are generally less than 2-3 cm thick, and range from vuggy, banded and crustiform quartz (plus minor siderite) to thinly banded quartz and chalcedony veins. Both the veins and the associated alteration zones are geochemically anomalous for S, Ba, As, Sb, and Au, and are considered to be the products of an epithermal mineralizing system of Quaternary age (Dufresne, 1986; Dufresne et al., 1986, 1987).

FLUID INCLUSION STUDIES

Doubly polished chips for fluid inclusion studies were prepared from more than 100 samples of vein quartz from the Klondike District in order to define the temperature and salinity of vein fluids, and gain information on the paleopressures under which the veins formed. Data discussed here pertain to primary inclusions which are thought to represent the main phase of each vein formation event.

Epithermal Veins

Ten of the chips represent Eocene epithermal veins in the Germaine Creek area. The samples include chalcedonic vein quartz cutting Eocene quartz-feldspar porphyry, and vuggy quartz veins in the underlying brecciated serpentinite. No useable inclusions were found in these samples.

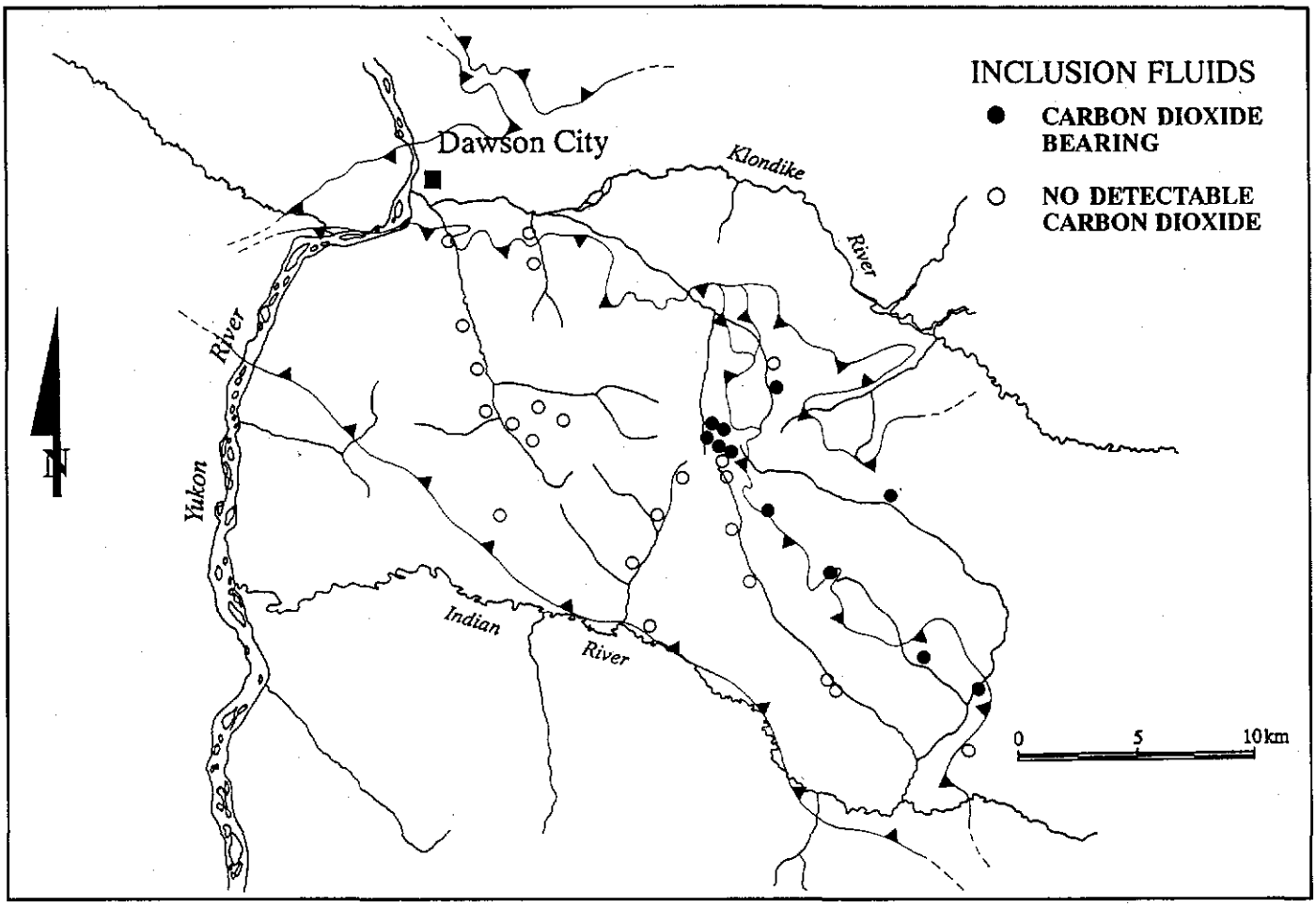

Figure 3. Map showing the distribution of samples analyzed for fluid inclusions and the occurrence of carbon dioxide in inclusion fluids. KSD refers to King Solomon Dome.

Mesothermal Veins

In contrast to the epithermal veins, excellent fluid inclusions were found in nearly all of the 80 chips prepared from mesothermal quartz vein samples. Both foliaform and discordant veins from a number of localities were examined.

Nesbitt et al. (1990) define mesothermal lode gold deposits as those formed at temperatures of 250-350°C and pressures greater than 600 bars. By averaging only those samples which gave results above 250°C, it is evident that the foliaform veins have a higher average homogenization temperature than the discordant population (Table 1). There is a suggestion that homogenization temperatures for both types of veins increase from north to south in the Klondike area, although further data are needed to confirm this.

Inclusion fluid salinities, determined from freezing experiments, are similar for both vein types, although the foliaform veins show a slightly larger range (Table 1). Detectable CO_2 in inclusion fluids is confined to veins in the east-central and southeastern parts of the study area (Fig. 3), and occurs predominantly in discordant veins. CO_2 homogenization temperatures range from approximately 20-29°C and appear to decrease toward the south, possibly indicating an increase in paleopressure in this direction.

The apparent increase in homogenization temperatures toward the south-southeast approximately parallels the increase in metamorphic grade in that direction (Mortensen, 1990). The difference in average homogenization temperatures between the foliaform and discordant veins may reflect the slight difference in their relative ages. If, as field observations suggest, the foliaform veins are older than the discordant veins, they probably formed slightly earlier in the cooling history of the area, and therefore at slightly higher temperatures.

The occurrence of CO_2 in fluid inclusions appears to be confined to veins in the central and southeastern parts of the Klondike. This may also be due to the increase in metamorphic grade. Elevated paleopressures in these regions may have prevented the loss of CO_2 by effervescence from the vein-forming fluid during its passage through the host rocks. The presence of CO_2 in the mineralizing fluids may also explain the common occurrence of wallrock carbonatization around discordant veins in the King Solomon Dome area.

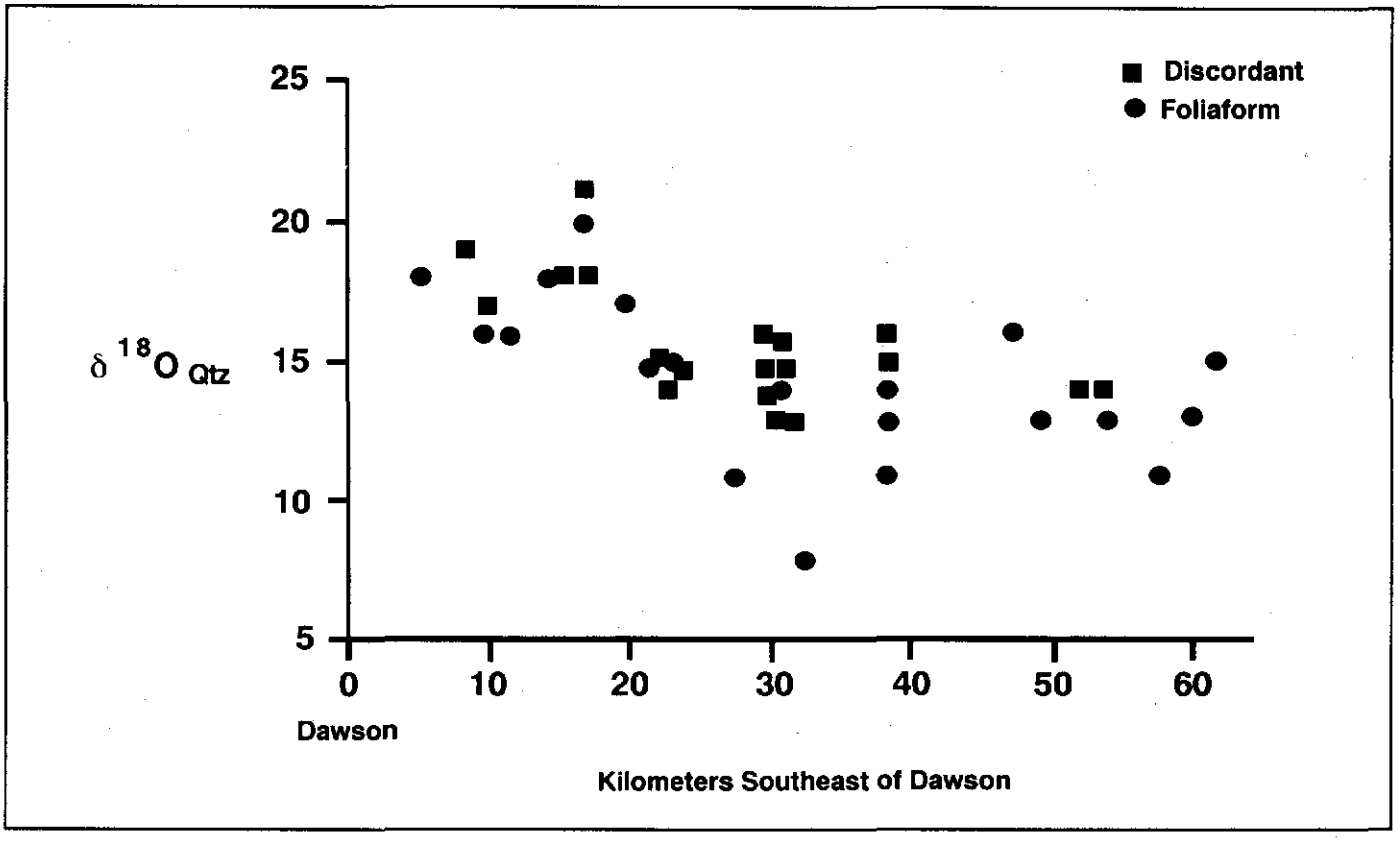

Figure 4. Projection of $\delta^{18}O$ values for discordant and foliaform mesothermal veins to a northwest-southeast reference line through the Klondike District (see Fig. 3).

Quaternary veins

Fluid inclusion studies by Dufresne (1986) and Dufresne et al. (1987) indicate that veins associated with intense alteration of White Channel Gravel deposits in the northern Klondike District formed at relatively low temperatures ($\approx$125°C) and were of low salinity ($\leq$2 wt % NaCl equivalent).

LIGHT STABLE ISOTOPES

The principal objective of light stable isotope studies of the quartz ($\pm$ carbonate) veins in the Klondike District is to document the origin and chemical evolution of fluids responsible for the formation of mineralized and barren mesothermal veins in the area. In addition, these studies are useful for evaluating the relationships between foliaform and discordant vein systems, as well as documenting any regional trends in isotopic patterns which might relate to the distribution of Au-bearing mesothermal veins.

Numerous samples were collected from vein systems which have been reported to yield high gold assay values. A number of samples were also taken from apparently barren veins throughout the Klondike. Quartz and carbonate from the veins were analysed for $^{18}O/^{16}O$ ratios. Carbonate and fluid inclusion CO_2 were analysed for ^{13}C, and δD analyses were conducted on fluids extracted from fluid inclusions.

$\delta^{18}O$ values for mesothermal vein quartz range from +8 to +21‰ with most of the data in the +13 to 17‰ range. Where carbonate coexists with quartz in the mesothermal veins, the carbonate $\delta^{18}O$ is 1 to 4‰ lower than the $\delta^{18}O$ value for the quartz.

In Figure 4, $\delta^{18}O$ values for vein quartz are projected onto a line which runs between Dawson and the Gold Run-Dominion Creek junction. The data show a northwest to southeast regional control on the distribution of $\delta^{18}O$ in vein quartz. Near Dawson, the $\delta^{18}O$ values tend to be enriched in ^{18}O, ranging from +21 to +16‰. To the southeast, the $\delta^{18}O$ values decrease to the +13 to +16‰ range for LONE STAR (MINFILE 115O 072) and LLOYD (MINFILE 115O 066) veins and occurrences in the King Solomon Dome area, to +11 to +15‰ further southeast.

A comparison of $\delta^{18}O$ values for foliaform versus discordant veins (Fig. 4) does not reveal any consistent pattern of enrichment or depletion of ^{18}O between the two morphological types of veins, i.e. based on the stable isotope data the two vein types are indistinguishable. In addition, the results from areas of known mineralization and those from apparently barren veins in the same area are statistically identical.

Only six of the sampled veins contain carbonate. Results of ^{13}C analyses of these vein carbonates vary from -1 to -

11‰. Analyses of CO_2 from fluid inclusions produced a similar large spread of $\delta^{13}C$ values varying from -5 to -17‰. The results from analyses of both inclusion CO_2 and carbonates are too limited at this stage to be of use in defining regional trends or comparisons between discordant or foliaform vein systems.

Approximately 20 samples of inclusion fluids have been analyzed for D/H ratios. The data cover a very wide range of values from -31 to -167‰ and appear to possess a regional zonation pattern similar to that observed in the $\delta^{18}O$ study. Near Dawson, veins typically have relatively low δD values of -15‰ or lower. Areas of known mineralization near King Solomon Dome and at the LONE STAR (MINFILE 115O 072) and LLOYD (MINFILE 115O 066) occurrences typically have values in the -140 to -160‰ range. Farther southeast, δD values increase somewhat and are generally in the range -130 to 100‰. Additional work is needed to verify the apparent trend; however, there is a general indication that vein-forming fluids in the southeast part of the Klondike incorporated significantly higher proportions of D in the fluids. Similar to the results from the $\delta^{18}O$ study there do not appear to be any distinct differences in D/H ratios between foliaform and discordant veins or between mineralized and apparently barren veins.

The results of the $\delta^{18}O$ and δD studies, in addition to geological relationships and fluid inclusion studies, suggest that the depth of erosion in the Klondike increases from northwest to southeast, so that veins exposed in the southeast were formed at deeper levels than those in the northwest. Consequently, the vein systems of the Klondike offer an opportunity to observe the progressive evolution of a mesothermal vein system from deeper (southeast) to shallower (northwest) levels of exposure.

The regional trend recognized in the oxygen isotope results for vein quartz could either reflect increasing temperatures of vein formation toward the southeast or decreasing $\delta^{18}O$ values in the vein-forming fluids. At present neither possibility can be excluded but based on the observation that the metamorphic grade in the Klondike increases to the southeast, it appears likely that the temperature of vein formation is higher in the southeast part of the area. Assuming a temperature of 350°C for vein formation in the southeast part of the region (see Fluid Inclusion section) and an average $\delta^{18}O$ value of 14 ± 2‰ for vein quartz, calculations indicate the vein fluids had a $\delta^{18}O$ value 9 ± 2‰. Farther north the estimated $\delta^{18}O$ value of the vein-forming fluid is 7 ± 2‰. Considering the approximations incorporated into these estimates, these results show there is no significant difference between veins in the two areas in terms of $\delta^{18}O$.

The low δD values obtained from inclusion fluids in quartz veins near Dawson indicate that the major component of the vein-forming fluid was meteoric water. This result coupled with the relatively heavy $\delta^{18}O$ values determined for the fluids indicates the vein-forming fluids consisted of deeply convected, isotopically evolved meteoric water (Nesbitt and Muehlenbachs, 1989). The increased δD values toward the southeast can be explained either as the result of isotopic interaction of meteoric water with the wallrock at very low water/rock ratios (< 0.1) or as a result of mixing meteoric and metamorphic devolatilization fluids with convecting meteoric water. Given the increase in metamorphic grade in the area, the second explanation involving mixing of meteoric and metamorphic fluids seems more likely.

The isotopic results show no significant distinctions between mineralized and unmineralized vein systems. However, in the area of known mineralization around the LONE STAR (MINFILE 115O 072), LLOYD (MINFILE 115O 066), and King Solomon Dome occurrences (MINFILE 115O 067,68), $\delta^{18}O$ values begin to increase. This suggests that gold deposition was influenced by the vertical zonation of the fluid regime and that gold may have been preferentially deposited at a specific level in the system. Gold mineralization in the southeast part of the area may have been lost to erosion and in the northwest part of the area, the mineralized level may not yet be exposed.

Dufresne (1986) and Dufresne et al. (1987) report average $\delta^{18}O$ values of +4‰ for epithermal veins of Quaternary age in the northern Klondike District. These values correspond to a calculated $\delta^{18}O$ of -15‰ for the vein-forming fluids, indicating that these fluids were mainly meteoric water which had not interacted extensively with the host rocks.

LEAD ISOTOPE STUDIES

The lead isotopic composition of sulphide minerals, particularly galena, can provide important information about the ultimate source of metals in vein systems. More than 40 Pb isotopic analyses have been carried out at the Geological Survey of Canada on galena from the Klondike District. Most of these samples are from discordant mesothermal quartz veins. The results for the discordant vein samples fall in a broad range with $^{208}Pb/^{204}Pb$ = 38.8-39.5; $^{207}Pb/^{204}Pb$ = 15.67-15.78; and $^{206}Pb/^{204}Pb$ = 19.0-19.9. These relatively radiogenic compositions appear to preclude derivation of the Pb (and, by inference, the Au) in the veins from altered ultramafic rocks, as was suggested by Mortensen (1984). The data are interpreted to indicate mixing of Pb derived from a number of isotopically diverse sources, and the data therefore cannot be used directly to obtain information on the age of the mineralization.

Galena from veins cutting Eocene diabase dykes near the WEST DAWSON (MINFILE 116B 015) occurrences (Fig. 2) yields exactly the same restricted range of Pb isotopic compositions as Cu-Pb-Ag skarn mineralization in adjacent schist ($^{208}Pb/^{204}Pb$ = 39.3; $^{207}Pb/^{204}Pb$ = 15.7; $^{206}Pb/^{204}Pb$ = 19.3). These compositions indicate that the two styles of mineralization are closely related, and are consistent with an Eocene age for the mineralization.

DISCUSSION

The preliminary results reported here indicate that several very different types of quartz veins occur in the Klondike

District. Both mesothermal and epithermal veins are represented, and at least three distinct ages of veining (middle or late Mesozoic, Eocene, and Quaternary) have been distinguished. Vein-forming fluids included meteoric water, metamorphic fluids, and, for at least some of the Eocene veins, magmatic fluids. This complex history of hydrothermal activity and vein formation has led to considerable confusion about which quartz veins are potentially gold-bearing. For example, much of the early hard-rock surface exploration in the Klondike was focused on foliaform mesothermal veins which can easily be identified in the field, and which are now known to be invariably barren. It is hoped that the results of this study will help constrain future lode gold exploration models for the area.

IMPLICATIONS FOR THE ORIGIN OF PLACER GOLD DEPOSITS

At least three of the styles of quartz vein described in this report contain anomalous levels of gold. Discordant mesothermal veins locally contain visible gold, some of which is quite coarse. Epithermal chalcedony veins of Eocene age yield sporadic anomalous Au values. Finally, Quaternary epithermal veins are moderately to strongly anomalous in Au. An important consideration regarding the source of gold in Klondike placer deposits, however, is that only relatively coarse gold had been recovered by historical (and present) placer mining methods. Gold in either of the two epithermal vein systems is likely to be too fine grained to have been recovered from the placers. Three possible candidates therefore remain for the ultimate source of the placer gold. These are (1) gold-bearing, discordant mesothermal veins, (2) coarse-grained gold originally deposited at a high level in Eocene epithermal vein systems, but now completely removed by erosion, and (3) coarse gold grown which grew within White Channel sediments during Quaternary epithermal activity. Additional investigations are now in progress to attempt to determine from which source (or combination of sources) the bulk of the placer gold was derived.

CONCLUSIONS

Four main styles of quartz veining have been recognized in the Klondike District. Included are mesothermal quartz veins in metamorphic rocks, quartz-carbonate veins in altered ultramafic rocks and greenstones, epithermal chalcedonic quartz veins of Eocene age, and low-temperature epithermal veins of Quaternary age. These vein styles are sufficiently different that they can generally be distinguished in the field. Discordant mesothermal veins and Eocene and Quaternary epithermal veins are all known to contain at least geochemically anomalous levels of gold, although only the discordant mesothermal veins contain visible gold. Further investigations are required to determine the relative importance of these three styles of mineralization as the ultimate source(s) of the Klondike placer gold deposits.

ACKNOWLEDGMENTS

Jim McFaull of United Keno Hill Mines Ltd and Scott Tomlinson of the Hughes-Lang Group are thanked for providing R.R. with much appreciated logistical support during the 1989 field season. Financial and logistical support was also provided by the Boreal Institute for Northern Studies at the University of Alberta and Indian and Northern Affairs Canada in Whitehorse. Analytical expenses for R.R. and B.E.N. were covered by NSERC operating grant A8003 to B.E.N. Scott Tomlinson and Ruth Debicki are also thanked for contributing some of the samples analysed in this study. We also thank Bruce Ballantyne for many useful discussions and for a critical review of an early version of the manuscript. This is G.S.C. contribution number 12990.

REFERENCES

DEBICKI, R.L., 1984. Bedrock geology and mineralization of the Klondike area (west), 115O14,15 and 116B2,3. Exploration and Geological Services Division, Yukon, Indian and Northern Affairs Canada, Open File 1984-3 (1:50 000 scale map with marginal notes).

DUFRESNE, M.B., 1986. Origin of gold in the White Channel sediments of the Klondike region, Yukon Territory. Unpublished M.Sc. thesis, University of Alberta, Edmonton.

DUFRESNE, M.B., MORISON, S.R., and NESBITT, B.E., 1986. Evidence of hydrothermal alteration in White Channel sediments and bedrock of the Klondike area, West-central Yukon. Yukon Geology, Vol. 1; Exploration and Geological Services Division, Indian and Northern Affairs Canada, p. 44-49.

DUFRESNE, M.B., NESBITT, B.E., LONGSTAFFE, F.J., and MORISON, S.R., 1987. Plio-Pleistocene epithermal Au mineralization in the White Channel sediments of the Klondike District, Yukon. Geological Association of Canada, Program with Abstracts, Vol. 12, p. 38.

FRIEDRICH, G. and HOYMANN, K.H., 1989. Lithogeochemistry, ore mineralization and alteration of bedrock and auriferous quartz veins, Hunker Dome, Mitchell vein, and Sheba vein, Klondike area, Yukon Territory, Canada. Institute of Mineralogy and Economic Geology, RWTH Aachen, Federal Republic of

Germany, Preliminary Report.

GLEESON, C.F., 1970. Heavy mineral studies in the Klondike area, Yukon Territory. Geological Survey of Canada, Bulletin 173.

LOWEY, G.W., SINCLAIR, W.D., and HILLS, L.V., 1986. Additional K-Ar dates for the Carmacks Group (Upper Cretaceous), West central Yukon. Canadian Journal of Earth Sciences, Vol. 23, p. 1857-1859.

MACLEAN, T.A., 1914. Lode mining in Yukon: an investigation of quartz deposits in the Klondike Division. Canada, Department of Mines, Mines Branch, Pub. No. 222.

McCONNELL, R.G., 1905. Report on the Klondike gold fields. Geological Survey of Canada, Annual Report, Vol. 14, 1901, Part B, p. 1B-71B.

MORISON, S.R., 1971. White Channel placer deposits in the Klondike area. In: Guidebook to Quaternary Research in Yukon, S.R. Morison and C.A.S. Smith (eds); XII INQUA Congress, Ottawa, Canada. National Research Council of Canada, p. 68-71.

MORISON, S.R. and HEIN, F.J., 1987. Sedimentology of White Channel Gravels, Klondike area, Yukon Territory: fluvial deposits of a confined valley. In: Recent Developments in Fluvial Sedimentology, F.G. Ethridge, R.M. Flores, and M.D. Harvey (eds); Society of Economic Paleontologists and Mineralogists, Special Publication 39, p. 205-216.

MORTENSEN, J.K., 1984. Bedrock geology of the Klondike Placer Gold District, and evidence for structural controls on lode gold mineralization. Geological Association of Canada, Cordilleran Section, Program with Abstracts, p. 27-29.

MORTENSEN, J.K., 1990. Geology and U-Pb geochronology of the Klondike District, west-central Yukon Territory. Canadian Journal of Earth Sciences, Vol. 27, p. 903-914.

NESBITT, B.E. and MUEHLENBACHS, K., 1990. Geology, geochemistry and genesis of mesothermal lode Au deposits of the Canadian Cordillera: evidence for ore formation from evolved meteoric water. In: The Geology of Gold Deposits: The Perspective in 1988. Economic Geology, Monograph 6, p. 553-563.

NESBITT, B.E., MUEHLENBACHS, K., and MUROWCHICK, J.B., 1990. Genetic implications of stable isotope characteristics of mesothermal Au deposits and related Sb and Hg deposits in the Canadian Cordillera; Economic Geology, Vol. 84, p. 1489-1506.

TEMPELMAN-KLUIT, D.J., 1982. White Channel gravel of the Klondike. In: Yukon Exploration and Geology, 1981; Exploration and Geological Services Division, Indian and Northern Affairs Canada, Yukon, p. 74-79.

TYRRELL, J.B., 1912. The gold of the Klondike. Transactions of the Royal Society of Canada, Third Series, Vol. 6, p. 29-59.

YUKON MINFILE, 1991 update. Exploration and Geological Services Division, Yukon, Indian and Northern Affairs Canada.

Table 1. Summary of fluid inclusion homogenization temperature and salinity data for Au-bearing discordant and barren foliaform mesothermal quartz veins.

	Discordant Veins	Foliaform Veins
T_{hom} (°C)	310 ± 30	330 ± 43
Salinity (wt-% NaCl equivalent)	4.3 ± 2.2	4.8 ± 2.9

VOLCANIC-HOSTED EPITHERMAL GOLD-SULPHIDE MINERALIZATION AND ASSOCIATED ENRICHMENT PROCESSES, SIXTYMILE RIVER AREA, YUKON TERRITORY, CANADA

U. Glasmacher
&
G. Friedrich

Institute of Mineralogy and Economic Geology
Aachen University of Technology
Wüllnerstr. 2, 5100 Aachen
Aachen, Germany

GLASMACHER, U., & FRIEDRICH, G., 1992. Volcanic-hosted epithermal gold-sulphide mineralization and associated enrichment processes, Sixtymile River area, Yukon Territory, Canada: in Yukon Geology, Vol. 3; Exploration and Geological Services Division, Yukon, Indian and Northern Affairs Canada, p.271-291

ABSTRACT

The upper Sixtymile River area is located approximately 128 km west of Dawson City, Yukon. Lithology in this area consists of Precambrian to Paleozoic metamorphic rocks, Paleozoic ultramafic rocks, Middle Jurassic pegmatitic and aplitic dykes, Upper Cretaceous porphyritic dykes and volcanic rocks with intercalated sedimentary rocks, Quaternary alkaline basaltic dykes and Quaternary alluvial sediments.

Precious metal occurrences in these volcanic rocks are divided into two types, based on differences in local distribution, petrology and wall rock alteration: a gold-bearing pyrite-arsenopyrite type and a silver-bearing galena-sphalerite type. Both types are characterized by four stages of mineralization.

Epithermal gold mineralization at the mouth of Big Gold Creek (MINFILE 116C 153, GLASMACHER) occurs with disseminated, stockwork and vein-type sulphides related to highly altered Late Cretaceous andesitic volcanic rocks. An early kaolinite-carbonate-quartz-pyrite alteration zone in the volcanic rocks surrounding the precious metal occurrence is overprinted by a late phengite-(adularia)-carbonate-quartz-pyrite alteration zone. Toward the unaltered andesites, a propylitic alteration zone is developed.

The mineral paragenesis of the gold-bearing pyrite-arsenopyrite occurrence is characterized by pyrite with gold inclusions and quartz (stage I), followed by pyrite (stage II) containing inclusions of galena with matildite exsolutions, sphalerite, chalcopyrite, molybdenite, arsenopyrite and gold, as well as quartz. Pyrite with gold and arsenopyrite inclusions, arsenopyrite and quartz are typical of stage III. Stage IV consists of finely banded chalcedony and pyrite. From stage I to stage II, temperature, salinity, pH, oxygen and sulphur activity all increased. Temperature increased from 150 to 280°C, salinity from 2 wt-% NaCl equivalent to oversaturated (salt crystals), log $a(O_2)$ from -54 to -33 and log $a(S_2)$ from -20 to -10. From stage II to stage IV these parameters all decreased (temperature from 280 to 200°C, salinity from oversaturated (salt crystals) to 2.5 wt-% NaCl equivalent, log $a(O_2)$ from -33 to -45 and log $a(S_2)$ from -10 to -16.

Paragenetic studies of the silver-bearing galena-sphalerite occurrence (MINFILE 115N 041, PER) also document four stages of mineralization. Stage I consists of iron-poor sphalerite, galena with matildite exsolutions, and quartz. Stage II consists of iron-rich sphalerite, pyrite, pyrrhotite, arsenopyrite, chalcopyrite, galena with matildite exsolutions, and siderite. Stage III consists of sphalerite with an intermediate iron content, pyrite, marcasite, chalcopyrite, galena, siderite, ankerite, dolomite and calcite. Minerals of Stage IV include sphalerite with low iron content, pyrite, tetrahedrite, polybasite, pearcite, pyrostilpnite, chalcedony, ankerite, dolomite and calcite. From stage I to stage II, the fluid pH and temperature increased (170 to 230°C). Between stage II and stage IV, temperature, oxygen activity and sulphur activity all decreased (temperature from 230 to 190°C, log $a(O_2)$ from -39 to -46 and log $a(S_2)$ from -13 to -15).

The following conclusions can be made about the fluid composition and mineralization process associated with the fossil geothermal system of the Sixtymile River area. The fluids which circulated at shallow depths in the volcanic rocks had a low temperature (about 150°C), low salinity (about 2 wt% NaCl equivalent), and a pH of about 4.6. They might represent hybrid fluids generated by the mixing of steam

and groundwater. Deep seated fluids are characterized by high temperature (280°C), high salinity (salt crystals) and higher pH. These fluids are similar to alkaline chloride fluids of active geothermal systems. The upwelling of these deep seated fluids caused the change in physical and chemical conditions during stage II. Arsenic was transported as H3AsO3°, gold as Au(HS)2⁻ and lead, zinc, iron and copper as MeCl2° complexes.

In the gold-bearing pyrite-arsenopyrite occurrence, mineral precipitation during the first enrichment stage was caused by fluid-wall rock interaction. Gold and sulphide enrichment during stages II and III was controlled by boiling of the alkaline-chloride fluids. The mineralization is classified as volcanic-hosted epithermal mineralization of the low sulphur and adularia-sericite types.

In the silver-bearing galena-sphalerite occurrence, the first stage of mineralization was again caused by fluid-wall rock interaction. Subsequent mineral enrichment was controlled by the mixing of two fluids with different physical and chemical characteristics.

RÉSUMÉ

La région du cours supérieur de la rivière Sixtymile est située approximativement à 128 km à l'ouest de Dawson City au Yukon. La lithologie de cette région consiste en roches métamorphiques précambriennes à paléozoïques, en roches ultramafiques paléozoïques, en dykes pegmatitiques et aplitiques du Jurassique moyen, en dykes porphyriques et roches volcaniques avec roches sédimentaires intercalaires du Crétacé supérieur, en dykes basaltiques alcalins quaternaires et en sédiments alluviaux quaternaires.

Les minéralisations épithermales en or se présentent avec des sulfures disséminés dans des stockwerks et de type filonien associés à des roches volcaniques andésitiques du Crétacé tardif très altérées. Une zone d'altération précoce en kaolinite- carbonate-quartz-pyrite dans les roches volcaniques entourant l'indice minéralisé aurifère porte en surimpression une zone d'altération tardive en phengite-(adulaire)-carbonate-quartz-pyrite entourée par une zone d'altération propylitique. Les indices minéralisés de métaux précieux dans ces roches volcaniques sont répartis en deux types selon des différences de distribution locale, de pétrologie et d'altération de la roche encaissante : des indices minéralisés aurifères avec pyrite-arsénopyrite et des indices minéralisés argentifères avec galène-sphalérite. Les deux types sont caractérisés par quatre stades de minéralisation.

La paragenèse des indices minéralisés aurifères avec pyrite et arsénopyrite est caractérisée par de la pyrite avec des inclusions d'or (stade I), suivie de pyrite (stade II) avec des inclusions de galène avec des exsolutions de matildite, de la sphalérite, de la chalcopyrite, de la molybdénite, de l'arsénopyrite et de l'or ainsi que du quartz. La pyrite avec des inclusions d'or et d'arsénopyrite, l'arsénopyrite et le quartz caractérisent le stade III et le stade IV consiste enfin en calcédoine et pyrite finement rubanées. Du stade I au stade II la température, la salinité, le pH ainsi que l'activité de l'oxygène et du soufre ont tous augmenté. La température est passée de 150 à 280 °C, la salinité de 2 % d'équivalents de NaCl en poids à la sursaturation (cristaux de sel), le log a(O2) de -54 à -33 et le log a(S2) de -20 à -10. Du stade II au stade IV les valeurs de tous ces paramètres ont diminué (la température de 280 à 200 °C, la salinité de la sursaturation (cristaux de sel) à 2,5 % d'équivalents de NaCl en poids, le log a(O2) de -33 à -45 et le log a(S2) de -10 à -16.

Des études de la paragenèse de l'indice minéralisé argentifère avec galène et sphalérite indiquent également quatre stades de minéralisation. Le stade I consiste en sphalérite pauvre en fer, en galène avec exsolutions de matildite et en quartz. Le stade II consiste en sphalérite riche en fer, en pyrite, en pyrrhotine, en arsénopyrite, en chalcopyrite, en galène avec exsolutions de matildite et en sidérite. Le stade III consiste en sphalérite d'une teneur en fer intermédiaire, en pyrite, en tétrahédrite, en polybasite, en pearcite, en pyrostilpnite, en calcédoine, en ankérite, en dolomite et en calcite. Du stade I au stade II le ph et la température des fluides ont augmenté (170 à 230 °C). Entre les stades III et IV, la température, l'activité de l'oxygène et l'activité du soufre ont diminué (la température de 230 à 190 °C, le log a(O2) de -39 à -46 et le log a(S2) de -13 à -15).

L'on peut formuler les conclusions suivantes quant à la composition des fluides et quant au processus de minéralisation dans le réseau géothermal fossile dans la région de la rivière Sixtymile. Les fluides ayant circulé à faible profondeur dans les roches volcaniques présentaient une température peu élevée (environ 150 °C), une faible salinité (environ 2 % d'équivalent de NaCl en poids) et un pH d'environ 4,6. Ils on pu être des fluides hybrides résultant du mélange de vapeur et d'eau souterraine. Les fluides profonds sont caractérisés par des températures élevées (280 °C), une salinité élevée (cristaux de sel) et un pH plus élevé. Ces fluides sont similaires aux chlorures alcalins des réseaux géothermiaux actifs. La remontée de

ces fluides profonds a entraîné une modification des conditions physiques et chimiques pendant le stade III. De l'arsenic a été transporté sous forme de H3AsO3, de l'or sous forme de Au(HS)2⁻ et du plomb, du zinc, du fer ainsi que du cuivre sous forme de complexes de MeCl2.

Dans l'indice minéralisé aurifère avec pyrite et arsénopyrite, la précipitation des minéraux pendant le premier stade d'enrichissement a été causée par l'interaction des fluides avec la roche encaissante. L'enrichissement en or et en sulfures pendant les stades II et III a été déterminé par l'ébullition des chlorures alcalins. La minéralisation est classé comme étant une minéralisation «épithermale» dans les roches volcaniques des types «à faible teneur en soufre» et «adulaire-séricite».

Dans les indices minéralisés argentifères avec galène-sphalérite, le premier stade de minéralisation a également été causé par l'interaction des fluides avec la roche encaissante. Un enrichissement ultérieur en minéraux a été déterminé par le mélange de deux fluides aux caractéristiques physiques et chimiques différentes.

INTRODUCTION

The upper Sixtymile River area (here referred to as Sixtymile River area) is located approximately 128 km (80 miles) west of Dawson City, covering parts of NTS map sheets 116 C 2 and 115 N 15 (Fig. 1). The area comprises four tributaries of the Sixtymile River, and parts of Glacier and Little Gold Creek (Fig. 2).

This paper describes gold-bearing disseminated, stockwork and vein-type sulphide mineralization in Carmacks Group volcanic rocks which outcrop at the confluence of Big Gold Creek and Miller Creek with the Sixtymile River. Gold-bearing quartz-(carbonate)-sulphide veins which are hosted by metamorphic rocks along Miller Creek, Glacier Creek, Little Gold Creek and the south side of Mosquito Creek are described in another paper (Glasmacher and Friedrich, this volume). These papers are the result of petrologic, fluid inclusion and isotope studies which followed fieldwork carried out as part of the Canada/Germany Science and Technology Exchange program.

The paper emphasizes gold and silver enrichment processes in the upper part of the Upper Cretaceous geothermal system which mineralized the volcanic rocks in the Sixtymile area.

An ARL-SEMQ electron microprobe was used to obtain the chemical composition of ore, gangue and alteration minerals. Natural and synthetic sulphides, oxides and silicates were used as standards. Analytical techniques and mineral compositions are fully detailed in Glasmacher (1991). On-line data reduction used a modified Magic IV (Colby, 1968). Names of gangue and alteration minerals were assigned using the classification schemes of Hey (1954), Bayliss (1975), Guidotti (1987), and Deer et al. (1979). Formation temperatures, pH, oxygen and sulphur activities of chlorite were calculated using the chlorite model of Walshe (1986).

Alteration reactions 1,2,3 and 4 are based on mineral compositions revealed by the microprobe. Microthermometric data were obtained using a Chaixmeca (MIM 85) heating/freezing stage. The determination of pH ranges was based on thermodymamic calculations detailed by Henley et al. (1984).

Stability fields of ore minerals in log $a(O_2)$-pH and log $a(S_2)$-log $a(O_2)$ diagrams were calculated for the physical and chemical conditions corresponding to each stage of mineral enrichment, using thermodynamic data from Barton (1969), Barton and Skinner (1979), Craig and Barton (1973), Haas and Robbie (1973), Helgeson (1969, 1979), Henley et al. 1984), King et al. (1973), Rau et al. (1973 a,b), Richardson and Jeffers (1952), Toulmin and Barton (1964) and Schneeberg (1973). By analogy with similar mineralization at Creede, Colorado (Roedder et al., (1963)), Baron et al., (1977)) and active geothermal systems (Henley and Hedenquist, (1986), Mann et al., (1986)), a total sulphur concentration of S=0.02M was assumed.

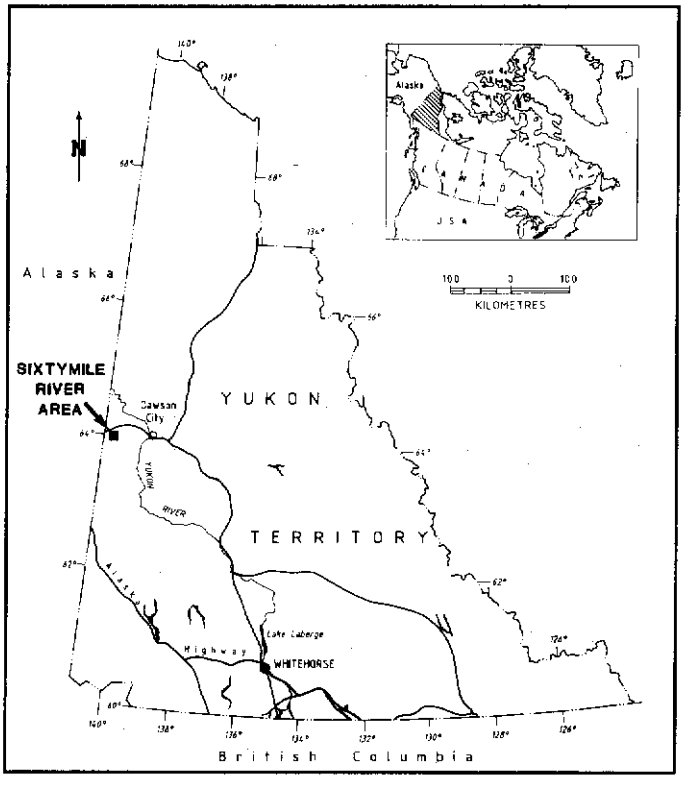

Figure 1. Location of the Sixtymile River Area.

GEOLOGY

The Precambrian to Paleozoic metamorphic basement in the Sixtymile River area is interpreted to be part of the Yukon Tanana Terrane (Monger, 1984; Fig. 3). Based on the

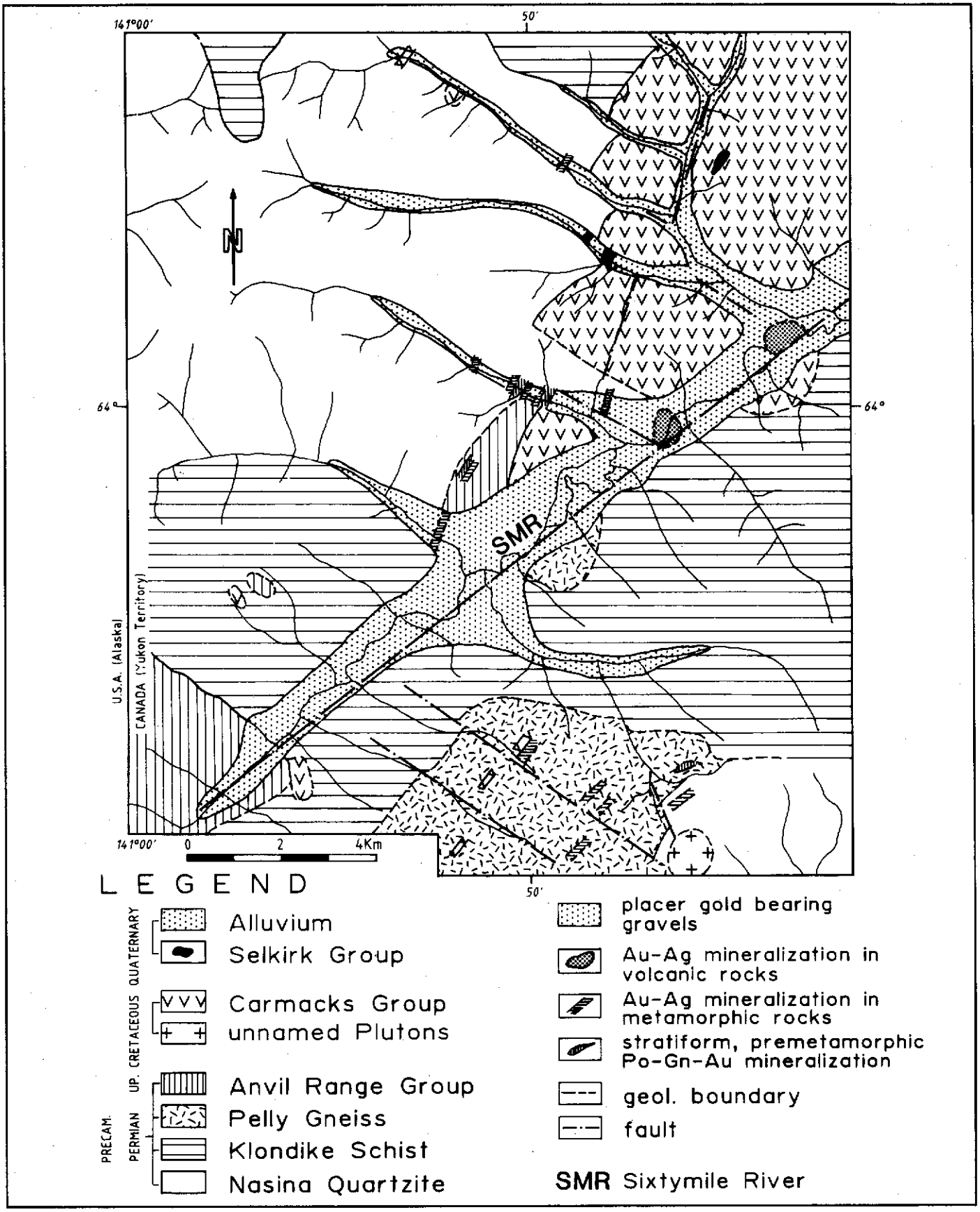

Figure 2. Geological map of the Sixtymile River area (partly compiled after Cockfield, 1921).

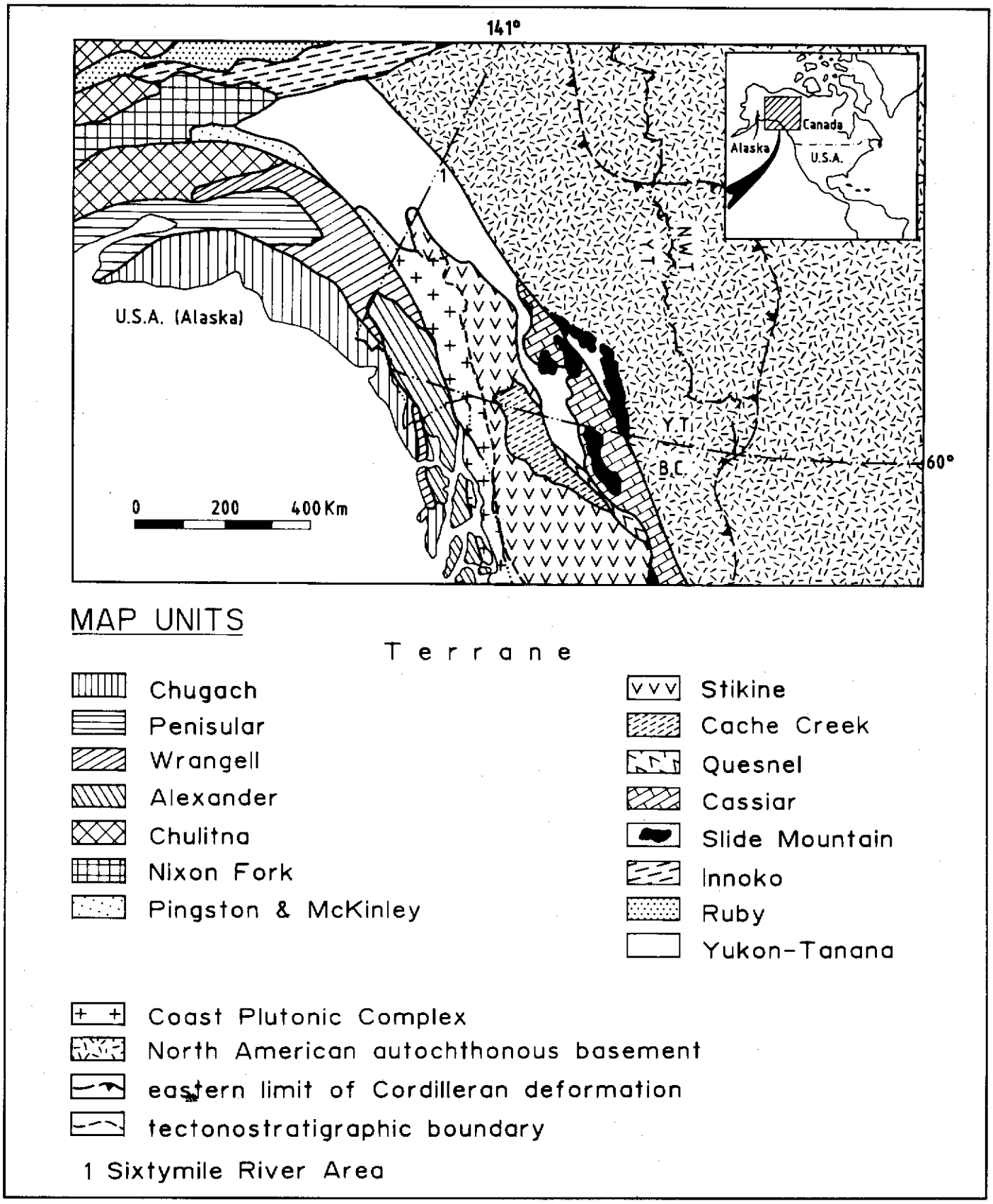

Figure 3. Recent distribution of terranes in the Northern Cordillera and adjacent parts of Alaska (compiled after Coney, 1980; Tempelman-Kluit 1981; Monger, 1984).

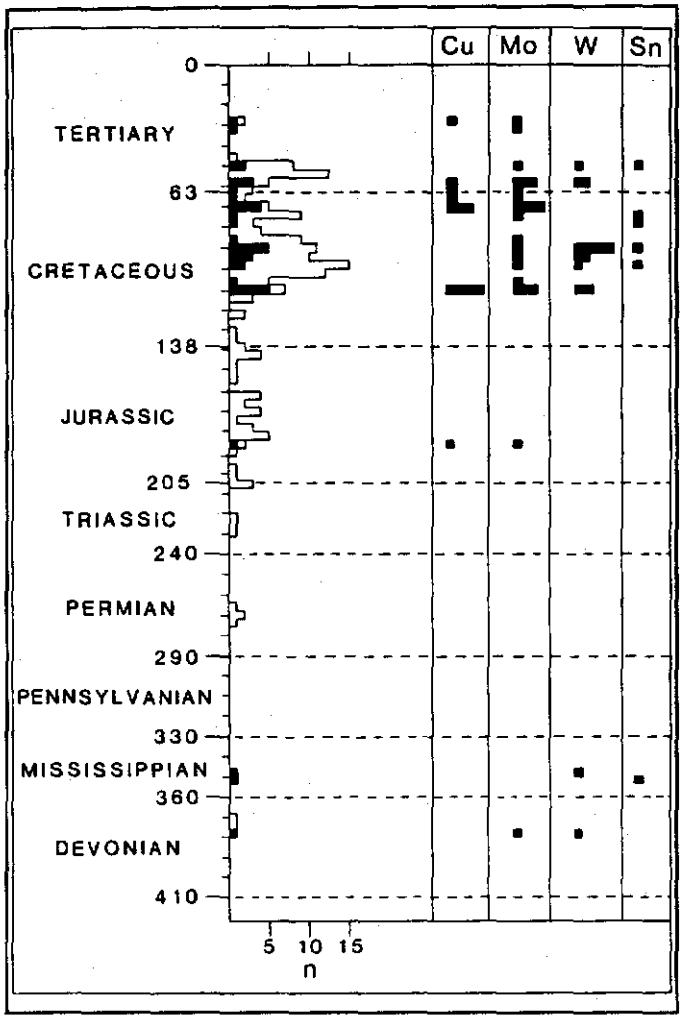

Figure 4. Radiometric ages of granitoid rocks in the Northern Cordillera and adjacent parts of Alaska. Shaded areas represent the ages of intrusions with associated mineral deposits; unshaded areas are ages of intrusions unrelated to any known deposits. The ages of Cu, Mo, W and Sn mineralization are inferred from the ages of associated intrusions (after Sinclair, 1986).

tectonic features of the metamorphic basement south of Tintina Fault, Tempelman-Kluit (1974; 1976; 1979) assigned part of Yukon Tanana Terrane and Stikine Terrane to "Yukon Cataclastic Complex". During Upper Cretaceous and Lower Tertiary, the crustal evolution of the Stikine and Yukon Tanana Terranes was influenced by subduction processes further to the southwest (Monger et al., 1972; Monger et al., 1982). Tholeiitic calcalkaline and shoshonitic magmas were generated above a northeast-dipping subduction zone, (Armstrong, 1988). High local heat flow caused by these magmatic activities initiated the development of hydrothermal systems.

Today, the gold sulphide enrichment in these fossil geothermal systems occurs in mesothermal-type gold bearing quartz-(carbonate)-sulphide veins hosted by metamorphic rocks and gold-bearing skarns (Meinert, 1986) or in gold bearing epithermal-type mineral occurrences hosted by volcanic rocks (Morin and Stroshein, 1987; Sinclair, 1986; Fig. 4). Regionally, most Yukon gold occurrences appear to be located in areas which are underlain by allochthonous terranes (Morin and Downing, 1984).

Due to tectonic and lithostratigraphic differences, the Sixtymile River area has been divided into a northern and a southern part. The boundary is represented by the Sixtymile River fault zone, which strikes east-northeast.

Lithologic units in the northern area comprise Precambrian to Paleozoic metamorphic rocks, Paleozoic ultramafic rocks, Middle Jurassic pegmatitic and aplitic dykes, Upper Cretaceous porphyritic dykes and volcanic rocks with intercalated sedimentary rocks, Quarternary alkaline basaltic dykes and Quarternary alluvial sediments (Glasmacher and Friedrich, 1985, Hughes and Morison, 1986; Fig. 2; Tab 1). Metasedimentary rocks with minor metavolcanic layers are assigned to the Nasina Series, and metavolcanic rocks with minor metasedimentary layers are assigned to the Klondike Schist. Biotite-amphibole orthogneiss of unknown age is discordant to the Nasina Series and Klondike Schist. Serpentinized ultramafic rocks occur along thrust faults (Mortensen, personal communication) and are possibly linked to the Anvil Range Group.

Muscovite from one of the northeast-southwest trending pegmatitic to aplitic dykes yielded a K/Ar age of 180 Ma (Mortensen, 1988), the same age as rocks of the Klotassin Suite. Calcalkaline volcanic rocks of intermediate composition are intruded by a quartz-feldspar porphyry plug dated at 68 $\pm$ 0.3 Ma, (Mortensen, 1988), and are assigned to the Upper Cretaceous Carmacks Group. They are intercalated with sedimentary rocks. Northwest-southeast trending andesitic dykes are possible feeders to the Carmacks Group volcanics. Quaternary alkaline olivine basalts are the youngest igneous rocks in the area and are possibly linked to the Carmacks Group.

Metamorphic rocks in the southern area are similar to those in the northern area with the exception of the Pelly Gneiss (Late Devonian-Early Mississippian; Mortensen, 1988). This stratigraphic unit comprises mainly biotite augen gneisses with minor lenses of quartzite and garnet-mica schist. Magmatic rocks in the southern area include a calcalkaline, I-type biotite granodiorite intrusion and northeast-southwest trending andesite to dacite dykes. These dykes are possibly related to Carmacks Group volcanics in the northern area. Quaternary alluvial sediments occur in all valleys.

MINERALIZATION

Gold and silver occur with disseminated, stockwork and vein-type sulphides in Carmacks Group volcanic rocks which outcrop at the mouths of Miller Creek (MINFILE 115N 041) and Big Gold Creek (MINFILE 116C 153) (Glasmacher (1984). The occurrences are structurally controlled and occur

at the junction of three major fault systems: the ENE-WSW trending Sixtymile River fault zone, a NW-SE trending fault zone and a NE-SW trending fault zone.

Between these two main occurrences, small northeast-southwest trending quartz-(carbonate)-sulphide veinlets crosscut the volcanic rocks in the Sixtymile River valley. These veinlets show alteration patterns and mineral paragenesis similar to the major occurrences.

Recent placer mining activities have covered up outcrops which were uncovered during 1983, 1985 and 1986, leaving only one occurrence exposed. This is located on Granges' placer claims at the mouth of Miller Creek, and has been described in detail.

Two types of mineralization have been identified, based on differences in distribution, petrology and wall rock alteration: a gold-bearing pyrite-arsenopyrite occurrence and a silver-bearing galena-sphalerite occurrence.

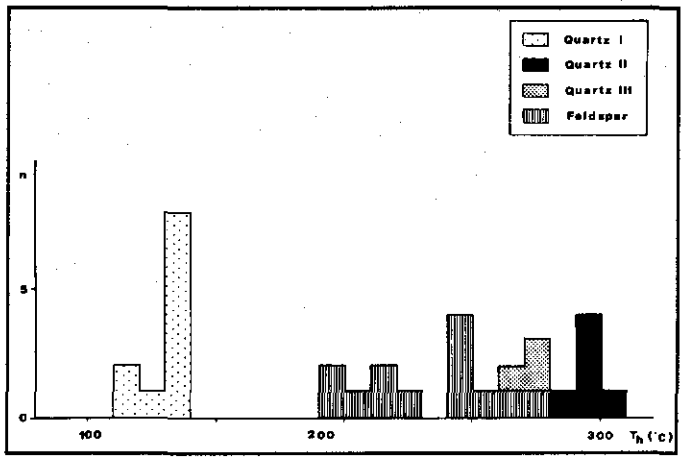

Figure 5. Histogram showing the frequency distribution of homogenization temperatures of fluid inclusions in quartz from the volcanic-hosted, disseminated, stockwork and vein-type gold-bearing pyrite-arsenopyrite occurrence.

Gold-bearing pyrite-arsenopyrite occurrence (MINFILE 116C 153)

Petrology and Mineral Composition

Based on the different textures and intergrowth relationships between the various minerals, the paragenetic sequence was divided into four mineralizing stages.

Stage I is represented by quartz, and pyrite with gold inclusions (Table 2). Stage II is characterized by quartz, and pyrite with inclusions of other minerals including galena with matildite exsolutions, sphalerite, chalcopyrite, molybdenite, arsenopyrite and minor amounts of gold and quartz. Quartz, arsenopyrite and pyrite containing gold and arsenopyrite inclusions precipitated during Stage III. Banded chalcedony and pyrite represent Stage IV.

Pyrite deposited in Stages I, II and III contained no gold above detection limit. Cobalt (<0.08 wt-%) and nickel (<0.06 wt-%) content is similar in all three stages. Stage III pyrite contains up to 9.38 wt-% arsenic. Arsenic values higher than 1 wt-% are inferred to be due to submicroscopic inclusions of arsenopyrite. Arsenopyrite inclusions in Pyrite III contained an average arsenic content of 28.03 at.-%. The trace element content (<0.12 wt-% Co; <0.06 wt-% Ni; <0.03 wt-% Sb) are generally low.

High silver (<9.49 wt-%) and bismuth values (<9.09 wt-%) in Pyrite II galena inclusions are due to matildite exsolutions. Only a few of these inclusions contain antimony, which occurs in amounts less than 0.07 wt-%.

Sphalerite inclusions in pyrite are characterized by low iron (5.31-6.89 mol.-% FeS), manganese (<0.49 wt-%), cadmium (<0.57 wt-%), and copper (<0.22 wt-%).

Gold deposited during Stage II contains a low silver content (4.8 wt-%) compared to gold deposited during Stage I (24.61 wt-% Ag) and Stage III (19.84 wt-% Ag). Except for bismuth (0.18 wt-%) and tellurium (0.11 wt-%), trace elements in gold are below detection limit.

Wall rock alteration and mineral composition

Three zones of hydrothermal alteration are recognized: Zone I (propylitic), Zone II (quartz-carbonate-kaolinite), and Zone III (quartz-phengite).

In general the Mn content of all alteration minerals in these alteration zones increases from low in Stage I to high in Stage III.

In the propylitic zone (Table 3), amphibole and pyroxene are replaced by chlorite (Fe-clinochlore/ripidolite or pycnochlorite) and minor epidote, and plagioclase is replaced by minor sericite, epidote and K-feldspar. Pyrite occurs along small fractures and is intergrown with chlorite.

Alteration zone II is characterized by quartz, kaolinite, ankerite and disseminated pyrite. Stockwork veinlets of chalcedony and pyrite up to 1 cm wide are typical of this zone.

Alteration zone III is characterized by quartz, phengite and pyrite, with minor ankerite, dolomite and calcite.

The transition between zones II and III is frequently brecciated and healed by quartz, chalcedony and pyrite. Zone III ankerite is enriched in manganese, and depleted in iron and magnesium compared to Zone II.

Geochemical surveys reveal a consistent increase in average gold content from 40 ppb Au in zone I, through 57 ppb in zone II to 252 ppb in zone III. The highest gold values (up to 12 ppm) occur in quartz-sulphide samples.

Whereas ankerite of zone II is characterized by lower manganese and higher iron and magnesium content, ankerite of zone III contains higher manganese and lower iron and magnesium.

The transition from plagioclase and chlorite (zone I) to kaolinite, ankerite, quartz and pyrite (zone II) can be described by reaction 1:

$16((Ca_{0.5}Na_{0.5})(Al_{1.5}Si_{2.5}O_8)) + 2(Mg_{2.8}Fe_{1.5}Al_{2.2}Fe_{0.4}Si_{2.9}O_{10}(OH)_8) + 18CO_2 + 2.8H_2S + 13.6H_2 + 7.3O_2 + 8H_+ = 14.2(Al_2Si_2O_5(OH)_4) + 8(Ca(Mg_{0.7}Fe_{0.3})(CO_3)_2) + 17.4SiO_2 + 1.4FeS_2 + 8Na^+$

The change from kaolinite-ankerite-quartz-pyrite (zone II) to phengite-ankerite-dolomite-calcite is represented by reaction 2:

$9.1(Al_2Si_2O_5(OH)_4) + 8(Ca(Mg_{0.7}Fe_{0.3})CO_3)_2) + 3.5SiO_2 + 0.9MnCl_2 + 5.6 KCl + 0.8H_2S = 7(K_{0.8}Al_{1.7}Fe_{0.1}Al_{0.9}O_{10}(OH)_2) + Ca(Mg_{0.8}Fe_{0.1}Mn_{0.1})(CO_3)_2 + 4Ca(Mg_{0.5}Fe_{0.3}Mn_{0.2})(CO_3)_2 + 3CaCO_3 + 0.4FeS_2 + 7.4H_2 + 3.5O_2 + 3CO_2 + 7.4H^+ + 7.4Cl^-$

Microthermometry

Stage I quartz is fractured, healed and surrounded by Stage II quartz. Primary inclusions in Stage I quartz indicate a homogenization temperature of 135°C and a salinity of 2 wt-% NaCl equivalent (Fig. 5). Primary inclusions in Stage II quartz and secondary inclusions in Stage I quartz are characterized by a homogenization temperature of 295°C and up to six daughter crystals including sphalerite, hematite and halite. Stage III quartz crystals surround and are intergrown with Stage II quartz, and yield homogenization temperatures of 200°C and salinities of 2.5 wt-% NaCl equivalent. Stage II and Stage III inclusions in quartz exhibit features characteristic of boiling. Three phase inclusions (gas, liquid and solid) on microfractures which crosscut Stage I, II and III quartz homogenize at 200°C and yield a salinity of 2.5 wt-% NaCl equivalent. These fluids might represent the Stage IV fluids associated with the deposition of chalcedony. Secondary inclusions in feldspar from alteration zone I lie along microfractures showing two distinct orientations. Inclusions from one set microfractures homogenize at a temperature of 200°C, and inclusions from the other set yield a homogenization temperature of 250° and a salinity of 3.4 wt-% NaCl.

Physical and chemical conditions

Matildite exsolutions in Stage II galena indicate a formation temperature above 215 ± 15°C (Craig, 1967). If the Stage II and Stage III fluids were entrapped under boiling conditions, the homogenization temperatures of both stages were higher than the formation temperature. Without pressure data, the formation temperatures of Stage I and IV minerals cannot be determined from fluid inclusions, but the homogenization temperatures give minimum values. The formation temperatures obtained from chlorite in alteration zone I are 260 and 180°C. Secondary fluid inclusions in feldspar in alteration zone I yielded homogenization temperatures of 250 and 200°C.

The mineral assemblage ankerite-dolomite-calcite which occurs in alteration zone III has been found in active hydrothermal systems at temperatures above 195°C (McDowell and Paces, 1985). Dolomite together with calcite is stable between 195°C and about 280°C. Phengite first occurs as an alteration mineral at about 280°C (McDowell and Elders, 1980; Scrodon and Eberl, 1987).

Assuming that the kaolinite and quartz of Stage I were transformed during stages II, III and IV into phengite and quartz via the potassium-muscovite-quartz and muscovite-kaolinite reactions, formation temperature and molarity were used to calculate the pH range. The temperatures used were 150°C for Stage I, 280°C for stage II, 260°C for stage II and 200°C for stage IV.

The calculated pH ranges are:

pyrite-arsenopyrite-quartz veinlets

stage I	$pH_{150°C} \approx 4.6$	neutral $pH_{150°C} = 5.8$
stage IV	$4.2 < pH_{200°C} < 6.0$	neutral $pH_{200°C} = 5.7$

alteration zone I

feldspar	$4.2 < pH_{250°C} < 5.7$	neutral $pH_{250°C} = 5.6$
chlorite	$pH_{260°C} = 5.7$	neutral $pH_{260°C} = 5.6$
chlorite	$pH_{180°C} = 6.4$	neutral $pH_{180°C} = 5.7$

The mineral paragenesis indicates a range of oxygen activity between log $a(O_2) < -43$ and log $a(O_2) > -54$, and a range of sulphur activity between log $a(S_2) = -7$ and log $a(S_2) = -20$ during Stage I mineral enrichment (Figs 6A,B). Based on the presence of early pyrrhotite inclusions in pyrite, followed by crystallization of sphalerite inclusions (6 mol.-% FeS), Stage II is characterized by increasing oxygen activity (from log $a(O_2) = -35$ to log $a(O_2) = -33$) and sulphur activity (from log $a(S_2) = -12$ to log $a(S_2) = -10$)(Figs 6C,D). The mineral paragenesis of stage III indicates oxygen activity of about log $a(O_2) = -30$. Arsenopyrite inclusions in stage III pyrite formed at a sulphur activity of about log $a(S_2) = -12$ (Figs 6E,F). The alteration assemblage suggests that stage IV pyrite formed under conditions of oxygen activity varying from log $a(O_2) < -34$ to log $a(O_2) > -45$ and sulphur activity from log $a(S_2) < -6$ to log $a(S_2) > -16$ (Figs 6G,H).

Chlorites of alteration zone I formed at 260°C, an oxygen activity of log $a(O_2) = -35$ and a sulphur activity of log $a(S_2) \approx -11$, and also at 180°C, log $a(O_2) \approx -45$ and log $a(S_2) \approx -17$.

Argentiferous galena-sphalerite occurrence (MINFILE 115N 041)

Petrology and mineral composition

The first stage of mineralization consists of low-Fe sphalerite, galena with matildite exsolutions and quartz (Table 4). The second stage consists of high Fe sphalerite, pyrite, pyrrhotite, arsenopyrite, chalcopyrite, galena with matildite exsolutions and siderite. The third stage is represented by sphalerite with intermediate iron content, pyrite, marcasite, chalcopyrite, galena, siderite, ankerite, dolomite and calcite. Silver enrichment occurred during the fourth stage. The main silver minerals are tetrahedrite, polybasite, pearcite and pyrostilpnite. Other stage IV minerals include low Fe sphalerite, pyrite, chalcedony, ankerite, dolomite and calcite.

Major and trace element distribution is similar in pyrite from all four stages, with low levels of cobalt (less than 0.06 wt-%) and nickel (less than 0.03 wt-%).

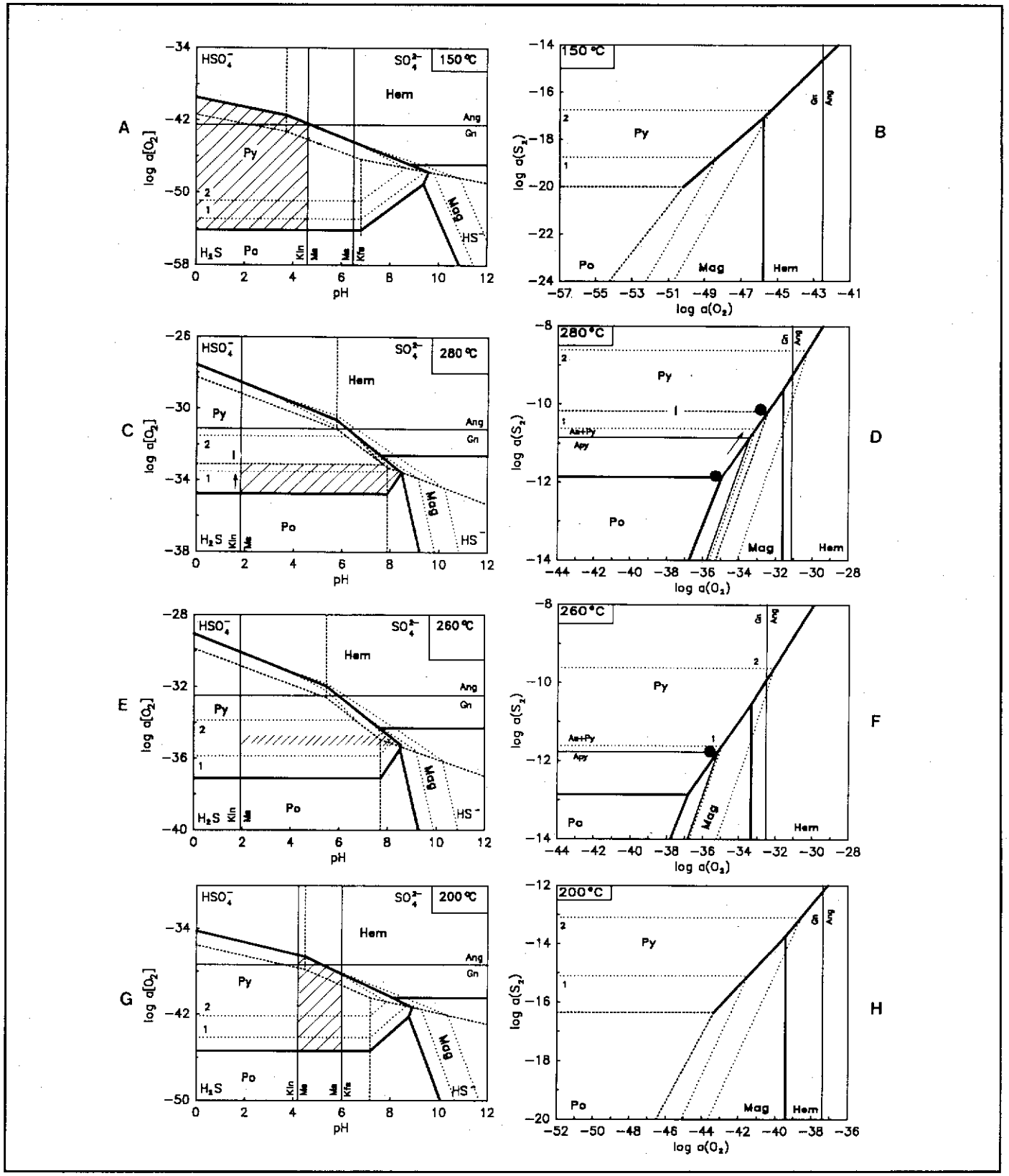

Figure 6. Log $a(O_2)$ - pH and log $a(S_2)$ - log $a(O_2)$ diagrams of the mineralization stages in the volcanic-hosted, disseminated, stockwork and vein-type gold-bearing pyrite-arsenopyrite occurrence (/// = field of enrichment); arrows show direction of increasing physico-chemical conditions; mineral abbreviations after Kretz (1983).

The only exception is stage II pyrite which contains up to 0.96 wt-% arsenic.

The arsenic content of arsenopyrite ranges from 40.42 and 46.31 wt-%, but close to the growth interface between pyrite and arsenopyrite crystals the arsenic content has a more limited range of 40 to 41 wt-%, possibly as a result of equilibrium crystallization of the two minerals.

The high silver (<1.13 wt-%) and bismuth (<2.43 wt-%) contents of stage II galena are caused by matildite exsolutions. Stage III galena is characterized by low silver (<0.64 wt-%), low bismuth (<10.8 wt-%) and low antimony (<0.34 wt-%).

The iron content of sphalerite increases from stage I (0.12-0.39 mol.-% FeS) to stage II (3.99-11.53 mol-% FeS) and decreases in Stage III (6 mol.-% FeS). The transition between stage I sphalerite (core) and stage II sphalerite (rim) in zoned crystals is marked by a small band of sphalerite II with pyrite inclusions. The trend of decreasing iron content, although interrupted by minor retrograde cycles of iron enrichment, continued throughout stage IV, culminating in nearly iron-free sphalerite containing only 0.2 mol.-% FeS.

Wall rock alteration and mineral composition

Three alteration zones resulted from the hydrothermal activity: propylitic (zone I), quartz-carbonate-kaolinite (zone II), and quartz-phengite-adularia (zone III).

In general, the manganese content of all alteration minerals in these zones increases from low in zone I to high in zone III.

In the propylitic zone (I), amphibole and pyroxene are replaced by chlorite (Fe clinochlorite/ripidolite or pycnochlorite) and epidote, and plagioclase is replaced by epidote and calcite (Table 5). Pyrite is intergrown with chlorite and epidote along small fractures. In zone II, quartz, kaolinite, carbonate minerals and pyrite replace chlorite, epidote and sericite. The carbonate minerals are manganese-bearing siderite, ferromagnesite, dolomite, ankerite and calcite. Small fissures of chalcedony, chalcedony-pyrite and quartz-carbonate-sulphides exhibit a stockwork-type distribution pattern. In zone III, adularia and sericite are the main potassium minerals. They are intergrown with quartz, manganese-bearing siderite, ankerite, ferromagnesite, dolomite and calcite.

Epidote in zone I contains 10.04-14.32 wt-% FeO, and 0.24-1.7 wt-% MnO.

Whereas the calcium content of siderite decreases from zone I toward the quartz-carbonate-sulphide veinlets, the manganese content increases. Like calcium, the magnesium content decreases from zone I to zone III, but is significantly higher in siderite gangue of the quartz-carbonate-sulphide veinlets.

Adularia in alteration zone III is characterized by a low albite content (3.7-7.0 % Ab) and a low barium content (0.17-1.33 wt-% BaO).

The change from the zone I alteration assemblage plagioclase, chlorite, epidote, ankerite, siderite, ferromagnesite and calcite to the zone II assemblage kaolinite, ankerite, siderite, ferromagnesite, dolomite, calcite and quartz can be described by reaction 3:

$$4((Ca_{0.5}Na_{0.5})Al_{1.5}Si_{2.5}O_8) + 2(Mg_{2.5}Fe_{1.8}Al_{2.3}Fe_{0.4}Si_{2.9}O_{10}(OH)_8) + 2(Ca_2(Al_{2.2}Fe)_{0.8})(SiO_4)(Si_2O_7)O(OH)) + 4(CaMg_{0.6}Fe_{0.4})(CO_3)_2 + (Fe_{0.8}Mn_{0.1}Ca_{0.1})CO_3 + (Fe_{0.5}Mg_{0.4}Ca_{0.1})CO_3 + CaCO_3 + 3.8H_2 + 1.75O_2 + 16.4CO_2 + 1.2H_2S + 2H^+ = 7.5(Al_2Si_2O_5(OH)_4) + 4(Ca_{0.9}Mg_{0.6}Fe_{0.5})CO_3)_2) + (Fe_{0.8}Mn_{0.1}Ca_{0.1})CO_3 + 11(Fe_{0.5}Mg_{0.4}Ca_{0.1})CO_3) + CaMg(CO_3)_2 + 5.4CaCO_3 + 6.8SiO_2 + 0.6FeS_2 + 2Na^+$$

The change from the zone II alteration assemblage kaolinite-ankerite-siderite-ferromagnesite-dolomite-calcite-quartz to the zone III alteration assemblage phengite-adularia-ankerite-siderite-ferromagnesite-dolomite-calcite-pyrite can be represented by reaction 4:

$$7(Al_2Si_2O_5(OH)_4) + 4(Ca_{0.9}Mg_{0.6}Fe_{0.5})(CO_3)_2 + 20(Fe_{0.8}Mn_{0.1}Ca_{0.1})CO_3 + 5(Fe_{0.5}Mg_{0.3}Ca_{0.2})CO_3 + CaMg(CO_3)_2 + CaCO_3 + 6.5SiO_2 + 5.5KCl + 18.6H_2S = 5(K_{0.8}Al_{1.7}Fe_{0.2}Si_{3.2}Al_{0.8}O_{10}(OH)_2) + 1.5(KAlSi_3O_8) + 2(Ca_{0.7}Mg_{0.7}Fe_{0.6})(CO_3)_2) + 10(Fe_{0.8}Mn_{0.2})CO_3 + 2.5((Mg_{0.4}Fe_{0.4}Ca_{0.2})CO_3) + CaMg(CO_3)_2 + 3CaCO_3 + 9.3FeS_2 + 15.8H_2 + 7.9O_2 + 11.8CO_2 + 5.5H^+ + 5.5Cl^-$$

Microthermometry

Primary fluid inclusions were studied in sphalerite, siderite and quartz, and the same sphalerite and siderite crystals were analysed by microprobe. Secondary fluid inclusions occur along microfractures in euhedral quartz which is surrounded by chalcedony. All fluid inclusions consist of two phases at room temperature.

Primary fluid inclusions in stage I (low Fe) sphalerite show a homogenization temperature of 165°C (Figs 7,8). The increased iron in stage II sphalerite is accompanied by increased homogenization temperatures up to 220°C and salinity up to 8.6 wt-% NaCl equivalent. The general decrease in iron in stage III and stage IV sphalerite is interrupted by retrograde zones of increasing iron content. These fluctuations correspond to inclusions which have a narrow range of homogenization temperatures close to 185°C.

Primary fluid inclusions in stage II siderite are characterized by a homogenization temperature of 225°C and a salinity of 8.6 wt-% NaCl equivalent.

Primary fluid inclusions in idomorphic quartz homogenize at 275°C. Homogenization temperatures of secondary fluid inclusions in this quartz range from 170°C to 240°C.

Physical and chemical conditions

Matildite exsolutions in galena indicate a formation temperature above 215 $\pm$ 15°C. Stage I sphalerite formed at a minimum temperature of 165°C, stage II sphalerite formed at 215°C and stage III and IV sphalerite formed at 185°C. Stage II siderite indicates a homogenization temperature of 225°C. Due to the unknown pressure conditions during stages I and IV, the homogenization temperatures for stage I and IV minerals are lower than the formation temperatures.

In alteration zone I, chlorite formed at 260°C and 230°C. Phengite first appears as an alteration mineral in active hydrothermal systems at temperatures above 280°C

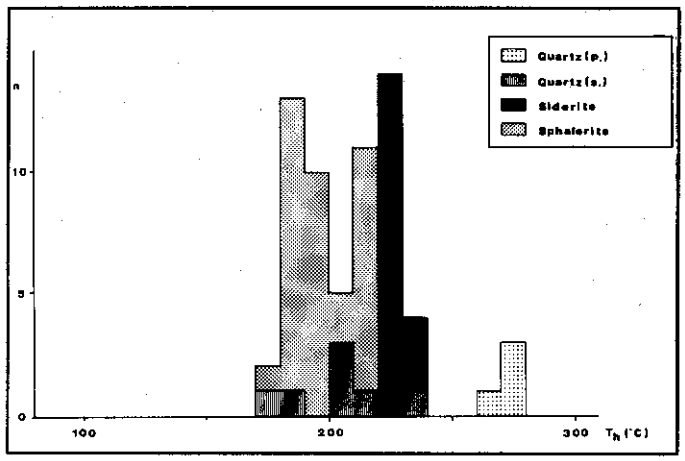

Figure 7. Histogram showing the frequency distribution of homogenization temperatures of fluid inclusions in quartz of the volcanic-hosted, disseminated, stockwork and vein-type silver-bearing galena-sphalerite occurrence.

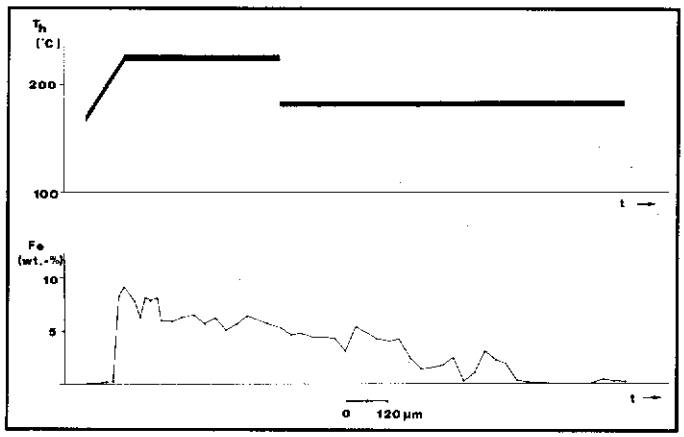

Figure 8. Distribution of iron content in sphalerite relative to homogenization temperature of fluid inclusions in the same sphalerite. (Volcanic-hosted, disseminated, stockwork and vein-type silver-bearing galena-sphalerite occurrence).

(McDowell and Elders, 1980; Scrodon and Eberl 1987).

Based on the information above, temperatures of 170°C for stage I, 230°C for stage II, and 190°C for stages III and IV were used to calculate pH, log $a(O_2)$ and log $a(S_2)$ for each of the mineral enrichment stages.

The pH range was calculated using the potassium-muscovite-quartz and muscovite-kaolinite reactions, as well as the formation temperature and molarity and alteration mineral paragenesis:

(galena-sphalerite-silver-carbonate-quartz veinlets)

stage II	$pH_{230°C} = 5.5$	neutral $pH_{230°C} = 5.6$
alt. zone I	$pH_{230°C} = 5.8$	neutral $pH_{230°C} = 5.6$

Assuming that the iron concentration of the hydrothermal fluid was constant during stages II, III and IV, the change in iron content of sphalerite (4 mol-% to 12 mol-% to 0.2 mol-% FeS) indicates a decrease of oxygen and sulphur activity during stage II (Figs 9A,B) and an increase of oxygen and sulphur activity during stages III and IV (Figs 9C,D), summarized below:

stage	Fe content mol.-% FeS	oxygen activity log $a(O_2)$	sulphur activity log $a(S_2)$
II	4-12	-39 to -40	-13 to -14
III	6	-46	-15
IV	6 to 0.2	-46 to -43	-15 to -12

Some of the chlorite formed in alteration zone I formed at a temperature of 260°C, an oxygen activity of log $a(O_2)$ = -37 and a sulphur activity of log $a(S_2)$ = -13; the remainder formed under conditions of T = 230°C, log $a(O_2)$ = -40 and log $a(S_2)$ = -14.

MINERAL ENRICHMENT PROCESS

The differences in mineral paragenesis, petrology and wall rock alteration between the gold-bearing pyrite-arsenopyrite and the silver-bearing galena-sphalerite occurrence reflect different enrichment processes. The physical and chemical conditions accompanying the formation of the gold-pyrite-arsenopyrite occurrence were influenced by boiling, whereas the silver-bearing galena-sphalerite occurrence is attributed to mixing of fluids with different physical and chemical characteristics.

Seward (1976), Henley et al. (1984), Seward (1984) and Henley and Brown (1985) described the transport of iron, lead, zinc, copper and silver in active hydrothermal systems as metal-chloride complex reaction 5:

$$MeCl_2^\circ + H_2S^\circ = MeS + 2H^+ + 2Cl^-$$

In active hydrothermal systems with similar physico-chemical conditions, gold is transported as a gold-thio complex ($Au(HS)_2^-$) up to about 300°C (Seward, 1973, 1982; Henley et al. 1984; Henley and Brown 1985)(reaction 6):

$$2Au(HS)_2^- + 2H^+ + H_2O = 2Au^\circ + 4H_2S^\circ + 0.5O_2$$

Under the physical and chemical conditions of most active hydrothermal systems, arsenic is transported as the H_3AsO_3 complex (Heinrich and Eadington, 1986; Ballantyne and Moore 1988)(reaction 7):

$$2H_3AsO_3^\circ + 6FeCl_2 + 9H_2S^\circ = 2FeAsS + 3\,FeS_2 + FeS + 12\,Cl^- + 6H_2 + 3O_2 + 12H^+$$

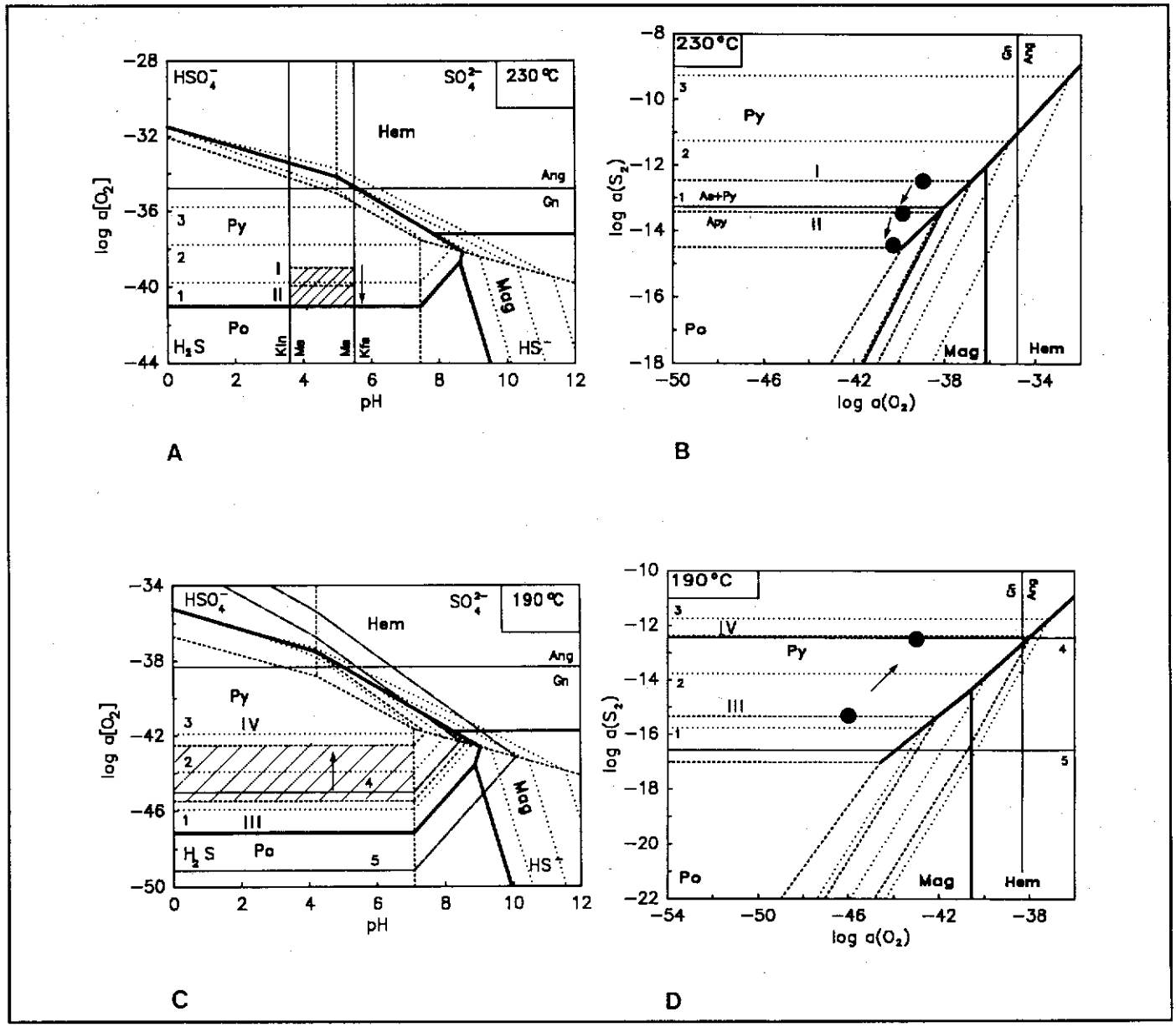

Figure 9. Log $a(O_2)$ - pH and log $a(S_2)$ - log $a(O_2)$ diagrams for the different stages of mineralization at the silver-bearing galena-sphalerite occurrence. Legend as described in Fig. 6; I = sphalerite containing 4 mol.-% FeS; II = sphalerite containing 12 mol.-% FeS; III = sphalerite containing 6 mol-% FeS; IV = sphalerite containing 0.2 mol-% FeS. Mineral abbreviations after Kretz (1983).

Gold-bearing pyrite-arsenopyrite occurrence (MINFILE 116C 153)

Wall rock alteration (reaction 1), along with salinity and fluid inclusion homogenization temperatures indicate a low temperature (about 150°C) low-salinity (2 wt-% NaCl equivalent) low-pH (4.6) stage I fluid. By analogy with the fluid chemistry in active hydrothermal systems the fluid of Stage I might represent a hybrid fluid generated by the mixing of steam (H_2S, CO_2 etc) and groundwater. The steam could have separated during boiling of deeper alkaline chloride fluids. Reaction 1 shows that fluid-wall rock interaction will increase the pH as well as decrease the sulphur and oxygen activity of the fluids. Reaction 5 shows that increasing the pH will cause the deposition of pyrite in quartz-sulphide veinlets. Decreasing sulphur and oxygen activity will initiate the precipitation of gold by reaction 6.

The increase in temperature (280°C), salinity (indicated by salt crystals) and the change in wall rock alteration indicate high-temperature, high salinity, alkali-rich fluids caused the stage II mineralization. The fracturing and healing of sulphide and gangue minerals suggests that the deep alkaline chloride

fluids ascended fast, causing boiling to occur as a result of local pressure drops. Mineralization was concentrated during stages II and III due to the removal of H_2S and CO_2 by boiling (reactions 5,6,7).

Fluids present during stages III and IV are chemically similar to stage I fluids, suggesting a stronger influence of shallow groundwater. Declining temperature and salinity during these stages suggest that stage II corresponds to a single pulse of deep-seated alkaline chloride fluid.

An analogous situation in an active hydrothermal system occurs at "Phlegrean Fields", Italy, where two contemporaneous fluids with different physical and chemical characteristics are isolated in separate stockwork systems. This is described by Belkin et al. (1986).

Silver-bearing galena-sphalerite occurrence (MINFILE 115N 041)

Based on the similarity of wallrock alteration at both showings, it seems that similar physical and chemical conditions might have prevailed during stage I mineralization at both the silver-bearing galena-sphalerite occurrence and the gold-bearing pyrite-arsenopyrite occurrence. However, at the galena-sphalerite showing, there is no evidence for boiling during the main stage II to stage IV mineralizing events, and the mineral precipitation may result from mixing deep-seated alkaline chloride fluid and shallow groundwater. Reaction 5 shows that mixing two contrasting fluids would decrease Cl^- activity and increase precipitation of metal sulphides.

Reaction 6 shows that if gold were transported as $Au(HS)_2^-$, a decrease in sulphur activity would cause precipitation. Because no gold has been found (gold is below the 5 ppb detection limit), either the gold concentration in the hydrothermal fluid was very low and it stayed in solution, or the pH decrease resulting from fluid mixing (reactions 4 and 5) and the increased oxygen activity resulting from both fluid mixing and the wall rock alteration (reaction 4) counteracted the precipitation of gold. The change in iron content of sphalerite between stage III and stage IV happened at constant temperature and may have been caused by an increase in oxygen and sulphur activity.

A distinct event between stages I and II similar to that seen in the gold-pyrite-arsenopyrite enriched area was not observed at this showing, but appears to be possible based on the higher chlorite formation temperature, the difference in wall rock alteration, and the major change in ore mineralogy from stage I to stage II.

CONCLUSIONS

Both the gold-bearing pyrite arsenopyrite (MINFILE 116C 153) and the silver-bearing galena-sphalerite occurrence (MINFILE 115N 041) are believed to have formed in the upper parts of the same fossil geothermal system, which appears to be closely associated with Late Cretaceous magmatism.

The following conclusions are drawn about the fluid composition and mineral enrichment processes which formed the two showings:

(1) The near-surface fluids which circulated in the volcanic rocks during stage I had a low temperature (150°C), low salinity (about 2 wt-% NaCl equivalent) and a pH of about 4.6. They may be hybrid fluids generated by mixing steam and groundwater.

(2) The deep-seated fluids which caused a sudden change in physical and chemical conditions during stage II are characterized by high temperature (280°C), high salinity (salt crystals) and higher pH. These fluids are similar to alkaline chloride fluids of active geothermal systems.

(3) Arsenic was transported as $H_3AsO_3^{\circ-}$, gold as $Au(HS)_2^-$ and lead, zinc, copper and iron as $MeCl_2^\circ$ complexes.

(4) The first stage of mineral enrichment was caused by fluid-wall rock interaction. The volcanic rocks were argillically altered and pyrite with gold inclusions and quartz were deposited at the pyrite-arsenopyrite-gold occurrence, while low-iron sphalerite, galena with matildite exsolutions and quartz were deposited at the silver-bearing galena-sphalerite occurrence.

(5) Stage II and III gold and sulphide enrichment at the pyrite-arsenopyrite-gold occurrence is believed to be due to the boiling of alkaline-chloride fluids.

(6) Stage II, III and IV silver enrichment at the galena-sphalerite showing is believed to result from the mixing of two fluids with different physical and chemical characteristics.

Based on the wall rock alteration, mineral paragenesis and fluid chemistry, and the calculated physical and chemical characteristics of the fluid, the showings can be classified as gold-bearing epithermal volcanic-hosted occurrences of the adularia-sericite type (Hayba et al., 1985, Heald et al., 1987), or the low-sulphur type of Bonham (1986). This kind of mineralization is typical of areas with calcalkaline volcanic rocks of andesitic to dacitic composition (Heald et al. 1987, Henley, 1985).

ACKNOWLEDGEMENTS

This research project was supported by the Deutsche Forschungsgemeinschaft (Grant FR 240/44). The study was also part of the Canada/Germany Science and Technology Exchange Agreement organized by the Geological Survey of Canada and the Federal Institute for Geosciences and Mineral Resources (BGR). Financial support was granted by the German Ministry of Research and Technology and by the Exploration and Geological Services Division of Indian and

Northern Affairs Canada, Whitehorse. We are particularly indebted to the mining companies for allowing access to their properties in the Sixtymile River area. We greatly appreciate discussions with J. Morin, J. Mortensen, G. Lynch, P. Möller, R. Walter, P. Sänger v. Oepen and L. Stroink.

REFERENCES

ARMSTRONG, R.L., 1988. Mesozoic and early Cenozoic magmatic evolution of the Canadian Cordillera. Geological Society of America, Special Paper 218, p. 55-91.

BALLANTYNE, J.M., and MOORE, J.N., 1988. Arsenic geochemistry in geothermal systems. Geochimica et Cosmochimica Acta, Vol. 52, p. 475-483.

BARTON Jr., P.B., 1969. Thermochemical study of the system Fe-As-S. Geochimica et Cosmochimica Acta, Vol. 33, p. 841-857.

BARTON Jr., P.B., and SKINNER, J.B., 1979. Sulphide mineral stabilities. In: Geochemistry of Hydrothermal Ore Deposits, H.L. Barnes, ed., 2nd Edition, Pennsylvania State University, p. 278-404.

BARTON Jr., P.B., BETHKE, P.M., and ROEDDER, E., 1977. Environment of ore deposition in the Creede Mining District, San Juan Mountains, Colorado: Part III. Progress toward interpretation of the chemistry of the ore-forming fluid for the OH vein. Bulletin of the Society of Economic Geologists, Vol. 72, p. 1-24.

BAYLISS, P., 1975. Nomenclature of the trioctahedral chlorites. Canadian Mineralogist, Vol. 13, p. 178-180.

BELKIN, H.E., CHELINI, B. DE VIVO and LATTANZI, P., 1986. Fluid inclusions in hydrothermal minerals from Mofete 2, Mofete 5 and San Vito 3 geothermal wells, Phlegrean Fields, Campania, Italy. International Volcanological Congress, Proceedings of Symposium 5.

BONHAM, H.F., Jr., 1986. Models for volcanic-hosted epithermal precious metal deposits; a review. International Volcanological Congress, Proceedings of Symposium 5, p. 13-17.

COCKFIELD, W.E., 1921. Sixtymile and Ladue Rivers area, Yukon. Geological Survey of Canada, Memoir 123.

COLBY, J.W., 1968. Advances in X-Ray Analyses, Vol. 11, p. 287-305.

CONEY, P.J., 1982. Cordilleran tectonics and plate motions. American Journal of Science, Vol. 272, p. 603-628.

CRAIG, J.R., 1967. Phase relations and mineral assemblages in the Ag-Bi-Pb-S system. Mineralium Deposita, Vol. 1, p. 278-306.

CRAIG, J.R., and BARTON, Jr., P.B., 1973. Thermochemical approximations for sulfosalts. Economic Geology, Vol. 68, p. 493-506.

DEER, W.A., HOWIE, R.A., and ZUSSMAN, J., 1977. An Introduction to the Rock Forming Minerals. Longmans, 528 p.

GLASMACHER, U., 1984. Geologie, petrographie und mineralization im Gebiet des "Sixty Mile River", Yukon Territorium, Canada. RWTH Aachen, unveröff. Diplomarbeit, 205 p.

GLASMACHER, U., and FRIEDRICH, G., 1985. Placer gold in the Sixtymile River Area, Yukon Territory, Canada. Proceedings of the Seventh Annual conference on Alaskan Placer Mining, Fairbanks, p. 53-57.

GLASMACHER, U., 1991. Petrogenetische und metallogenetische Entwicklung ausgewählter Gebiete im "Yukon-Tanana Terrane" und "Stikine Terrane", (Yukon Territorium, Kanada) während der oberkreide und des Alltertiärs. Diss., Aachen University of Technology, 435 p.

GLASMACHER, U., and Friedrich, G. 1992. Gold-sulphide enrichment process in mesothermal veins of the Sixtymile River area, Yukon Territory, Canada. In Yukon Geology, Volume 3, Exploration and Geological Services Division, Yukon, Indian and Northern Affairs Canada, this volume.

GUIDOTTI, C.V., 1987. Micas in metamorphic rocks. In: Micas, S.W. Bailey ed., Reviews in Mineralogy, Mineralogical Society of America, Vol. 13, p. 357-467.

HAAS, Jr., J.L., and ROBIE, R.A., 1973. Thermodynamic data for wüstite, $Fe_{0.947}O$, magnetite, Fe_3O_4, and hematite, Fe_2O_3 (abstract). Transactions of the American Geophysical Union, Vol. 54, p. 438.

HAYBA, D.O., BETHKE, P.M., HEALD, P., and FOLEY, N.K.; 1985. Geologic, mineralogic and geochemical characteristics of volcanic-hosted epithermal precious metal deposits. In: Geology and Geochemistry of Epithermal Systems, Berger, B.R., and Bethke, P.M., eds, Reviews in Economic Geology, Vol. 2, p. 129-169.

HEALD, P., FOLEY, N.K., and HAYBA, D.O., 1987. Comparative anatomy of volcanic-hosted epithermal deposits: acid sulfate and adularia-sericite types. Economic Geology, Vol. 82, p. 1-26.

HEINRICH, C.A., and EADINGTON, P.J., 1986. Thermodynamic predictions of the hydrothermal chemistry of arsenic, and their significance for the paragenetic sequence of some cassiterite-arsenopyrite base metal deposits. Economic Geology, Vol. 81, p. 511-529.

HELGESON, H.C., 1969. Thermodynamics of hydrothermal systems at elevated temperatures and pressures. American Journal of Science, Vol. 267, p. 729-804.

HELGESON, H.C., 1979. Mass transfer among minerals and hydrothermal solutions. In: Geochemistry of Hydrothermal Ore Deposits, H.L. Barnes, ed., 2nd Edition, Pennsylvania State University, p. 568-610.

HENLEY, R.W., 1985. The geothermal framework for epithermal deposits. In: Geology and Geochemistry of Epithermal Systems, Berger, B.R., and Bethke, P.M., eds, Reviews in Economic Geology, Vol. 2, p. 129-169.

HENLEY, R.W., TRUESDELL, A.H., BARTON Jr., P.B. and WHITNEY, J.A., 1984. Fluid-mineral Equilibria in Hydrothermal Systems. Society of Economic Geologists, Vol. 1, 267 p.

HENLEY, R.W., and BROWN, K.L., 1985. A practical guide to the thermodynamics of geothermal fluids and hydrothermal ore deposits. In: Geology and Geochemistry of Epithermal Systems, Berger, B.R., and Bethke, P.M., eds, Reviews in Economic Geology, Vol. 2, p. 129-169.

HENLEY, R.W., and HEDENQUIST, J.W., 1986. Introduction to the geochemistry of active and fossil geothermal systems. In: Guide to the Active Epithermal (Geothermal) Systems and Precious Metal Deposits of New Zealand. Monograph Series on Mineral Deposits, G. Friedrich (chief ed.), Vol. 26, p. 1-22.

HEY, M.H., 1954. A review of the chlorites. Mineralogical Magazine, Vol. XXX, No. 24.

HUGHES, R.L., and MORISON, S.R., 1986. Placer Gravels of Miller Creek, Sixtymile River Area, 116 B,C. In: Yukon Geology, Volume 1, Exploration and Geological Services Division, Yukon, Indian and Northern Affairs Canada, p. 50-55.

KING, L.G., MAH, A.D., and PANKRATZ, L.B., 1973. Thermodynamic properties of copper and its inorganic compounds. INCRA Monograph II on the Metallurgy of Copper, International Copper Research Association.

KRETZ, R., 1983. Symbols for rock-forming minerals. American Mineralogist, Vol. 68, p. 277-279.

MANN, A.W., FARDY, J.J., and HEDENQUIST, J.W., 1986. Major and trace element concentrations in some New Zealand geothermal waters. International Volcanological Congress, Proceedings of Symposium 5, p. 61-80.

McDOWELL, S.D., and ELDERS, W.A.., 1980. Authigenic layer silicate minerals in borehole Elmore I, Salton Sea geothermal field, California, U.S.A. Contributions to Mineralogy and Petrology, Vol. 74, p. 293-310.

McDOWELL, S.D., and PACES, J.B., 1985. Carbonate alteration minerals in the Salton Sea geothermal system, California, U.S.A. Mineralogical Magazine, Vol. 49, p. 469-479.

MEINERT, L.D., 1986. Gold in skarns of the Whitehorse Copper Belt. In: Yukon Geology, Volume 1, Exploration and Geological Services Division, Yukon, Indian and Northern Affairs Canada, p. 19-43.

MONGER, J.W.H., 1984. Cordilleran tectonics: a Canadian perspective. Bulletin of the Geological Society of France, Vol. 7, p. 255-278.

MONGER, J.W.H., SOUTHER, J.G., and GABRIELSE, H., 1972. Evolution of the Canadian Cordillera: a plate tectonic model. American Journal of Science, Vol. 272, p. 577-602.

MONGER, J.W.H., PRICE, R.A., and TEMPELMAN-KLUIT, D.J., 1982. Tectonic accretion and the origin of the two major metamorphic and plutonic belts in the Canadian Cordillera. Geology, Vol. 10, p. 70-75.

MORIN, J.A. and DOWNING, D.A., 1984. Gold-silver deposits and occurrences in Yukon Territory 1:2,000,000 scale map, list of occurrences. Exploration and Geological Services Division, Yukon, Indian and Northern Affairs Canada Open File 1984-2.

MORIN, J.A. and STROSHEIN, R., 1987. Disseminated precious metal exploration targets in Yukon. Geological Society of Nevada Symposium: Bulk Mineable Precious Metal Deposits of the Western United States, Reno, Nevada.

MORTENSEN, J.K., 1988. Geology of southwestern Dawson Map Area, Yukon. Geological Survey of Canada Open File 1927.

RAU, H., KUTTY, T.R.N. and GUEDES de CARVALHO, J.R.F., 1973a. High temperature saturated vapour pressure of sulfur and the estimation of its critical quantities. Journal of Chemical Thermodynamics, Vol. 5, p. 291-302.

RAU, H., KUTTY, T.R.N. and GUEDES de CARVALHO, J.R.F., 1973b. Thermodynamics of sulfur vapor. Journal of Chemical Thermodynamics, Vol. 5, p. 833-844.

ROEDDER, E., RINGIAM, B. and HALL, W.E., 1963. Studies of fluid inclusions III: Extraction and quantitative analyses of inclusions in the milligram range. Economic Geology, Vol. 58, p. 353-374.

SCHNEEBERG, E.P., 1973. Sulfur fugacity measurements with the electrochemical cell $Ag,AgI,Ag_{2+x}S,fs$. Economic Geology, Vol. 68, p. 507-517.

SEWARD, T.M., 1976. Stability of chloride complexes of silver in hydrothermal solutions up to 350°C. Geochimica et Cosmochimica Acta, Vol. 40, p. 1329-1341.

SEWARD, T.M., 1982. The transport and deposition of gold in hydrothermal systems. In: Gold '82: The Geology, Geochemistry and Genesis of Gold Deposits, R.P. Foster (ed.); Geological Society of Zimbabwe, 1.

SEWARD, T.M., 1984. The formation of lead II chloride complexes to 300°C. Spectrophotometric study, Geochimica et Cosmochimica Acta, Vol. 48, p. 121-134.

SINCLAIR, W.D., 1986. Molybdenum, tungsten and tin deposits and associated granitoid intrusions in the Northern Canadian Cordillera and adjacent parts of Alaska. In: J.A. Morin (ed.): Mineral deposits of Northern Cordillera; Canadian Institute of Mining and Metallurgy, Vol. 37, p. 216-234.

SCRODEN, J., and EBERL, D.D., 1987. Illite. In: Micas, S.W. Bailey (ed)., Reviews in Mineralogy, Mineralogical Society of America, Vol. 13, p. 357-467.

TEMPELMAN-KLUIT, D.J., 1974. Reconnaissance geology of Aishihik Lake, Snag and part of Stewart River Map Areas, West-Central Yukon. Geological Survey of Canada, Paper 73-41.

TEMPELMAN-KLUIT, D.J., 1976. The Yukon Crystalline Terrane: Enigma in the Canadian Cordillera. Geological Society of America Bulletin 87, p. 1343-1357.

TEMPELMAN-KLUIT, D.J., 1979. Transported cataclasite, ophiolite and granodiorite in Yukon: Evidence of Arc-Continent Collision. Geological Survey of Canada, Paper 79-14.

TEMPELMAN-KLUIT, D.J., 1981. Geology and mineral deposits of southern Yukon. In: Yukon Exploration and Geology 1979-1980, Exploration and Geological Services Division, Indian and Northern Affairs Canada, p. 7-31.

TOULMIN, P. and BARTON, P.B., 1964. A thermodynamic study of pyrite and pyrrhotite. Geochimica et Cosmochimica Acta, Vol. 28, p. 641-671.

WALSHE, J.L., 1986. A six component chlorite solid solution model and the conditions of chlorite formation in hydrothermal and geothermal systems. Economic Geology, Vol. 81, p. 681-703.

Table 1. Lithostratigraphic units of Sixtymile River area.

SYSTEM	FORMATION	LITHOLOGY NW Area	LITHOLOGY SE Area
QUATERNARY		alluvial sediments	alluvial sediments
	Selkirk Group	alkaline-olivine basalt	
LATE CRETACEOUS	Carmacks Group	andesite, dacite, andesite-dacite dykes, pyroclastic rocks, fluvial sediments	andesite and dacite dykes
	Unnamed plutons		biotite granodiorite
MIDDLE JURASSIC	Klotassin Suite	pegmatite, aplite	
PERMIAN	?	orthogneiss	
	Anvil Range Gp	ultramafic rocks	
	Pelly Gneiss		augen gneiss garnet-mica schist, gneiss
	Klondike Schist	chlorite schist, mica schist	chlorite schist mica schist
PRE-PERMIAN (DEVONO-MISSISSIPPIAN AND ? OLDER)	Nasina Series	paragneiss, quartzite, quartz-mica schist, mica schist, graphite schist, marble	quartzite, quartz-mica schist, mica schist

Table 2. Paragenetic sequence and physico-chemical conditions of volcanic hosted, disseminated, stockwork and vein-type gold bearing pyrite-arsenopyrite occurrences.

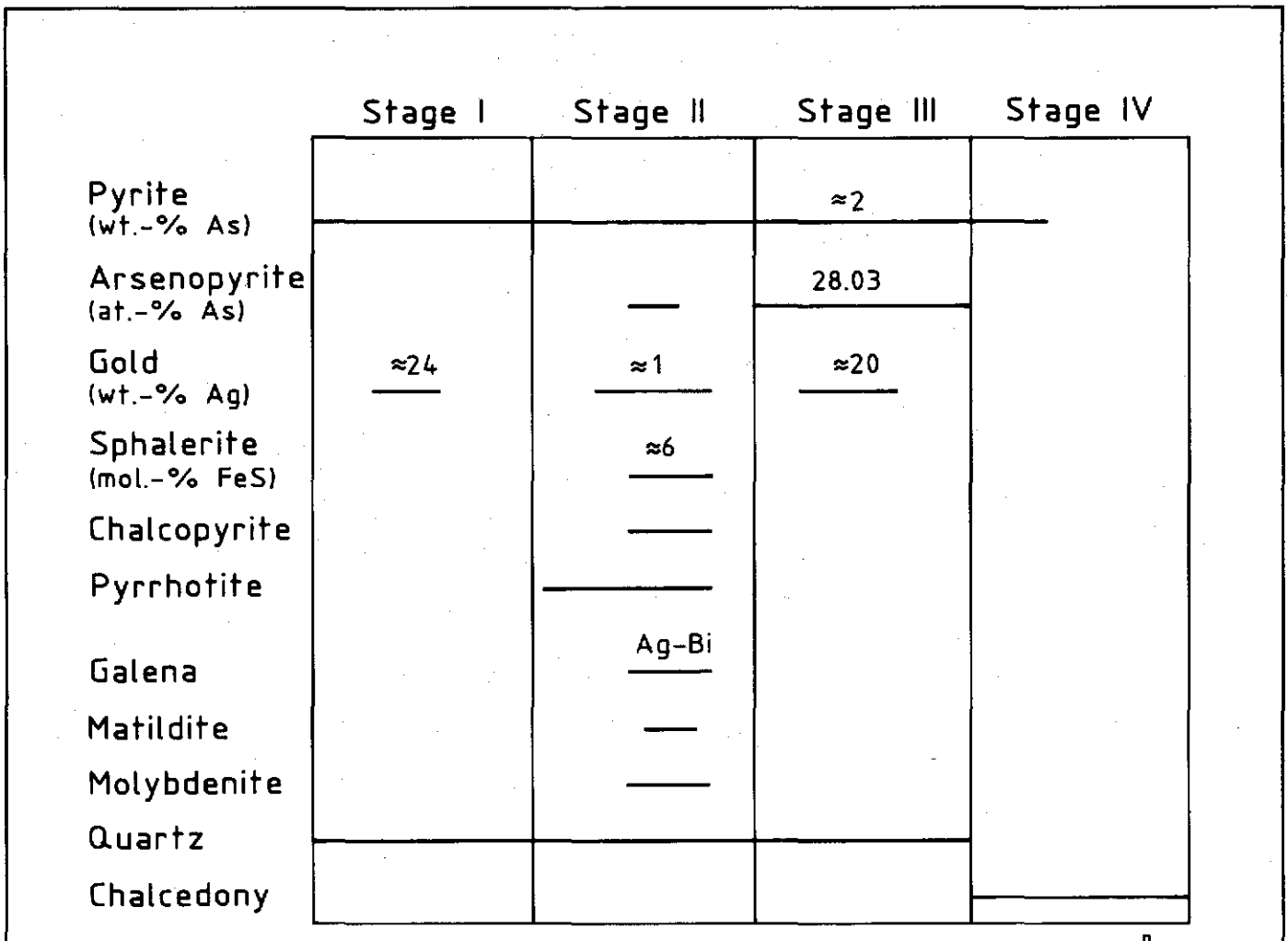

Table 3. Mineral paragenesis and physico-chemical conditions of the sulphide veinlets and the alteration zones encasing the volcanic hosted, disseminated, stockwork and vein-type gold bearing pyrite-arsenopyrite occurrence.

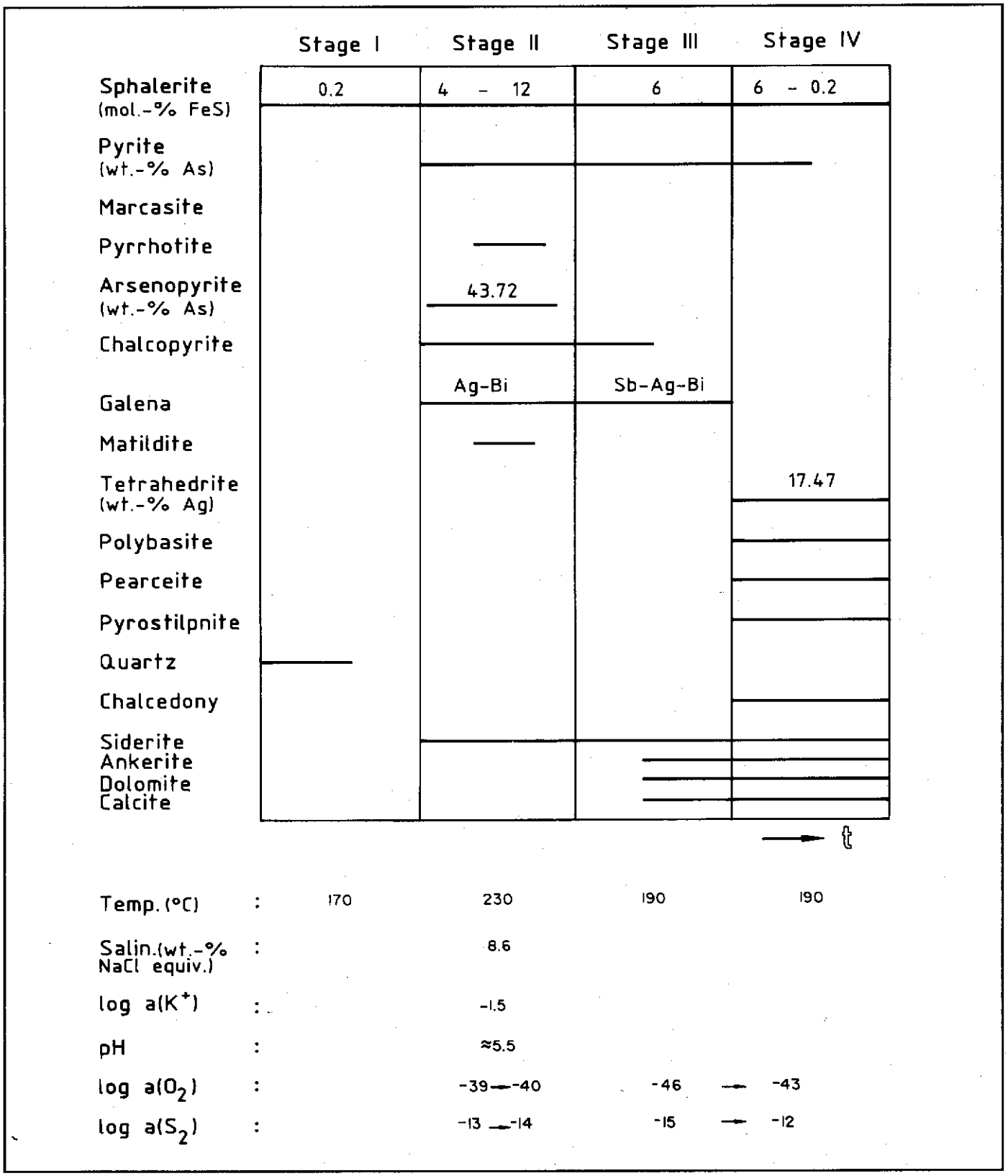

Table 4. Paragenetic sequence and physico-chemical conditions of volcanic hosted, disseminated, stockwork and vein-type silver bearing galena-sphalerite occurrences.

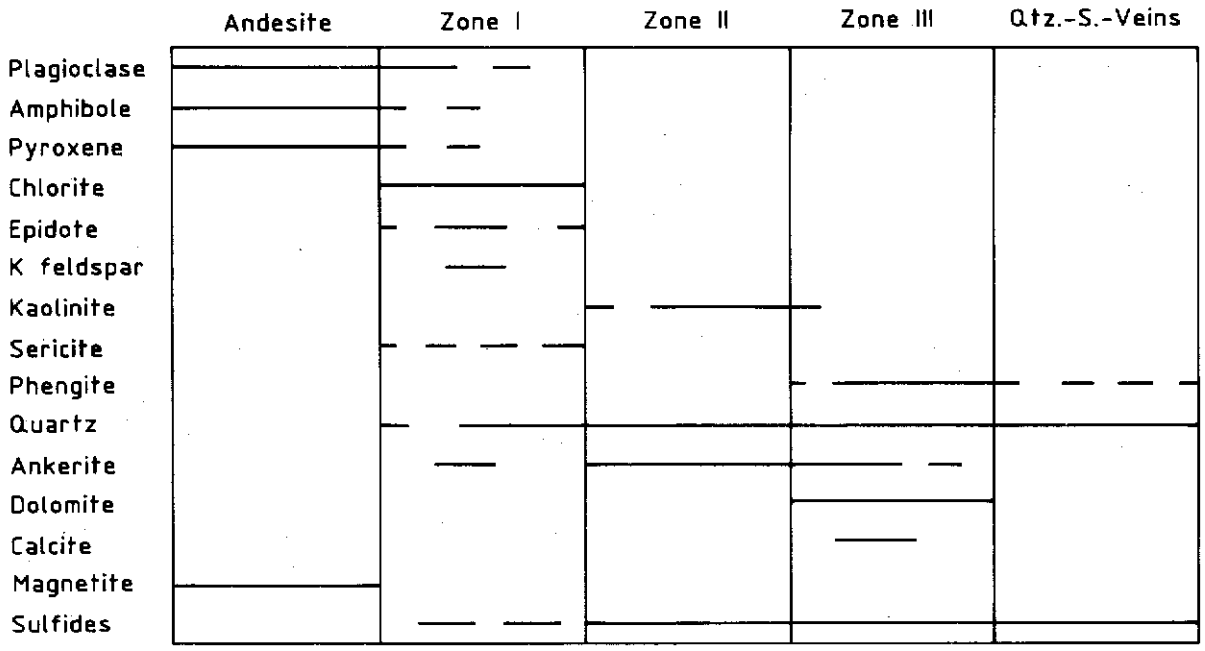

Geothermometer	Chl	Fl/Fsp	Phengite	F.I./Qtz
Temp.(°C)				
Stage I				135
Stage II	260	250	≈280	295
Stage III				275
Stage IV	180	200		200
Salin.(wt.-% NaCl equiv.)				
Stage I		3.4		2
Stage II				salt crystals
Stage III				
Stage IV				2.5
pH				
Stage I				≈4.6
Stage II	5.7	>4.2 ≈≤5.7		
Stage III				
Stage IV	6.4			>4.2 ≈<6.0
log a(O_2)				
Stage I				<-43 ≈>-54
Stage II	-35			-35 ⟷ -33
Stage III				≈-35
Stage IV	-45			<-34 ≈>-45
log a(S_2)				
Stage I				<-7 ≈>-20
Stage II	-11			-12 ⟷ -10
Stage III				≈-12
Stage IV	-17			<-6 ≈>-16

Table 5. Mineral paragenesis of the sulphide veinlets and the alteration zones encasing the volcanic hosted, disseminated, stockwork and vein-type silver bearing galena-sphalerite occurrences.

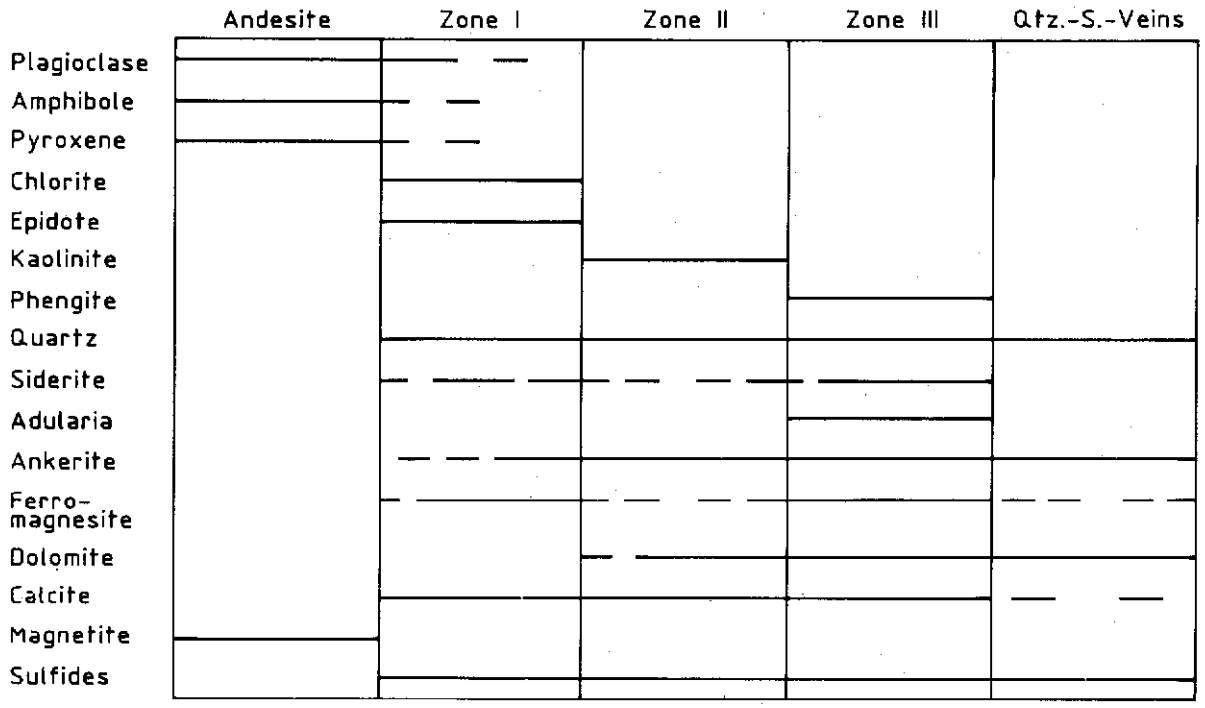

Geothermometer	Chl	Phengite	F.I.Qtz
Temp.(°C)			
Stage I			165
!Stage ?	260	≈280	275
Stage III	230		225
Stage III + IV			185
Salin.(wt.-% NaCl equiv.)			
Stage I			
!Stage ?			8.6
Stage III			
Stage III + IV			
pH			
Stage I			
!Stage ?			
Stage III	5.8		5.5
Stage III + IV			
log a(O_2)			
Stage I			
!Stage ?	-37		
Stage III	-40		-39 — -41
Stage III + IV			-46 — -43
log a(S_2)			
Stage I			
!Stage ?	-13		
Stage III	-14		-13 — -14
Stage III + IV			-15 — -12

GOLD-SULPHIDE ENRICHMENT PROCESSES IN MESOTHERMAL VEINS OF THE SIXTYMILE RIVER AREA, YUKON TERRITORY, CANADA

U. Glasmacher
&
G. Friedrich

Institute of Mineralogy and Economic Geology
Aachen University of Technology
Wüllnerstr. 2, 5100 Aachen
Aachen, Germany

GLASMACHER, U. & FRIEDRICH, G., 1992. Gold-sulphide enrichment processes in mesothermal veins of the Sixtymile River area, Yukon Territory, Canada. In: Yukon Geology, Vol. 3; Exploration and Geological Services Division, Yukon, Indian and Northern Affairs, Canada, p.292-311

ABSTRACT

The upper Sixtymile River area is located approximately 128 km west of Dawson City, Yukon. Lithology in this area consists of Precambrian to Paleozoic metamorphic rocks, Paleozoic ultramafic rocks, Middle Jurassic pegmatite and aplite dykes, Late Cretaceous porphyritic dykes and volcanic rocks with intercalated sedimentary rocks, Quaternary alkaline basaltic dykes and Quaternary alluvial sediments.

Gold bearing, mesothermal quartz-(carbonate)-sulphide veins which trend NNE-SSW are hosted by metamorphic rocks north and south of Sixtymile River.

The mesothermal quartz-(carbonate)-sulphide veins are surrounded by successive envelopes of sericitic, K-feldspar and propylitic alteration. Two stages of vein mineralization are recognized in the northern part of the area, and three stages are recognized in the south part.

In the northern veins, pyrite, arsenopyrite, pyrrhotite and quartz are intergrown and formed first. These minerals are fractured and healed by second stage minerals, which include galena, sphalerite, chalcopyrite, pyrite, carbonate and minor quartz.

Stage I mineralization in the southern veins is represented by quartz, and pyrite containing inclusions of other sulphides. Stage II is the main stage of precious metal enrichment, represented by arsenopyrite and galena which contain tetrahedrite, miagyrite and polybasite exsolutions. Stage I and II minerals are tectonically fractured, and healed by pyrite, sphalerite, chalcopyrite, freibergite and quartz of stage III. In both vein systems, gold enrichment is associated with arsenopyrite and silver enrichment is associated with galena. The evolution of hydrothermal fluids in the northern area is characterized by decreasing temperature (330°C to 280°C), salinity (12.8% wt.-% to 6 wt.-% NaCl equiv.), oxygen activity (log $a(O_2)$ = -30 to log $a(O_2)$ = -35), and sulphur activity (log $a(S_2)$ = -10 to log $a(S_2)$ = -12), as well as a slight increase in pH range (from >3.1 - <5.2 to >3.3 - <5.4).

In the southern vein system the fluid evolution characterized by a decrease in temperature (330°C to 150°C), salinity (18.3 wt.-% to 10 wt.-% NaCl equiv.), oxygen activity (log $a(O_2)$ = -29 to log a (O_2) = -52), and sulphur activity (log $a(S_2)$ = -9 to log $a(S_2)$ = -18, as well as a slight increase in pH range (>3.2 - <5.3 to >4.1 - <5.9).

The following conclusions can be drawn about the fluid composition and mineral enrichment process in the fossil geothermal system of the Sixtymile River area. Deep seated fluids which circulated in the metamorphic rocks were characterized by high temperatures (above 300°C), high salinities (about 18 wt.-% NaCl equiv.) and pH values between 3.1 and 5.2. These fluids are similar to alkaline chloride fluids of active geothermal systems. Arsenic was transported as H_3AsO_3°-, gold as $Au(HS)_2^-$ - and lead, zinc, iron, copper as $MeCl_2$° complexes. The first stage mineralization resulted from reaction of these deep-seated fluid with the wall rock. Second and third stage mineralization is believed to result from the mixing of two fluids with different physico-chemical characteristics.

RÉSUMÉ

La région du cours supérieur de la rivière Sixtymile est située approximativement à 128 km à l'ouest de Dawson City au Yukon. La lithologie de cette région consiste en roches métamorphiques précambriennes à paléozoïques, en roches ultramafiques paléozoïques, en dykes pegmatitiques et aplitiques du Jurassique moyen, en dykes porphyriques et roches volcaniques avec roches sédimentaires intercalaires du Crétacé supérieur, en dykes basaltiques alcalins quaternaires et en sédiments alluviaux quaternaires.

Les filons aurifères «mésothermaux» avec quartz-(carbonate)-sulfures qui sont orientées NNE-SSW se trouvent dans les roches métamorphiques au nord et au sud de la rivière Sixtymile.

Les filons «mésothermaux» avec quartz-(carbonate)-sulfures sont entourés d'enveloppes successives d'altération séricitique, feldspatho-potassique et propylitique. Deux stades de minralisation filonienne sont reconnus dans la partie septentrionale de la région et trois stades sont reconnus dans la partie méridionale.

Dans les filons septentrionaux, la pyrite, l'arsénopyrite, la pyrrhotine et le quartz sont enchevêtrés et se sont formés les premiers. Ces minéraux sont fracturés et ont été soudés les uns aux autres par les minéraux du deuxième stade incluant la galène, la sphalérite, la chalcopyrite, la pyrite, le carbonate et des quantités mineures de quartz.

Le premier stade de minéralisation des filons méridionaux est caractérisé par le quartz et la pyrite qui renferment des inclusions d'autres sulfures. Le deuxième stade est le principal stade d'enrichissement en arsénopyrite et en galène avec exsolutions de tétrahédrite, de miagyrite et de polybasite. En raison de mouvements tectoniques, les minéraux du minerai et de la gaugue des stades I et II sont fracturés et ont été de nouveaux soudés les uns aux autres par de la pyrite, de la sphalérite, de la chalcopyrite, de la freibergite et du quartz du stade III. Dans les deux réseaux de filons l'enrichissement en arsénopyrite coincide avec l'enrichissement en or et l'enrichissement en galène avec celui en argent.

L'évolution des fluides hydrothermaux dans la région septentrionale est caractérisée par une température (de 330 à 280 °C), une salinité (12,8 % à 6 % d'équivalent de NaCl en poids) une activité de l'oxygène (log $a(O^2)$ = -30 à log a (O^2) = -35) et une activité du soufre (log $a(S^2)$ = -10 à log $a(S^2)$ = -12) à la baisse ainsi que par une légère augmentation de la plage des pH (de > 3,1 - < 5,2 à > 3,3 - < 5,4).

Dans le réseau méridional de filons, l'évolution des fluides hydrothermaux en fonction du temps est caractérisée par une température (de 330 à 150 °C), une salinité (18,3 % à 10 % d'équivalent de NaCl en poids) une activité de l'oxygène (log $a(O^2)$ = -29 à log a (O^2) = -52) et une activité du soufre (log $a(S^2)$ = -9 à log $a(S^2)$ = -18) à la baisse ainsi que par une légère augmentation de la plage des pH (de > 3,2 - < 5,3 à > 4,1 - < 5,9).

L'on peut formuler les conclusions suivantes quant à la composition des fluides et quant au processus denrichissement en minéraux dans le réseau géothermal fossile dans la région de la rivière Sixtymile. Les fluides profonds sont caractérisés par des températures élevées (supérieures à 300 °C), une salinité élevée (environ 18 % d'équivalent de NaCl en poids) et des valeurs du pH comprises entre 3,1 et 5,2. Ces fluides sont similaires aux chlorures alcalins des réseaux géothermaux actifs. De l'arsenic a été transporté sous forme de H_3AsO_3, de l'or sous forme de $Au(HS)_2^-$ et du plomb, du zinc, du fer ainsi que du cuivre sous forme de complexes $MeCl_2$.

La précipitation des minéraux pendant le premier stade d'enrichissement a été causée par l'interaction des fluides avec la roche encaissante. Le processus d'enrichissement qui a suivi le premier stade de minéralisation dans les filons aurifères avec quartz-(carbonate)-sulfures de type «mésothermal» été déterminé par le mélange de deux fluides aux caractéristiques physiques et chimiques différentes.

INTRODUCTION

The upper Sixtymile River area (here referred to as Sixtymile River area) is located approximately 128 km (80 miles) west of Dawson City, Yukon, at an average latitude 64°00'N and longitude 141°45'W on N.T.S. map sheets 116C/2 and 115N/15 (Fig. 1). The area encompasses four tributaries of the Sixtymile River, as well as parts of Glacier and Little Gold Creek (Fig. 2). From southwest to northeast, the tributaries are Bedrock Creek, Mosquito Creek (south side), Miller Creek and Big Gold Creek.

At Miller Creek, Glacier Creek, Little Gold Creek and south of Mosquito Creek, NNE-SSW trending gold bearing quartz-(carbonate)-sulphide veins (MINFILE 116C 082, 116C 146, 116C 166 and 116N 39) are hosted by metamorphic rocks. At the mouth of Big Gold Creek and Miller Creek in the Sixtymile River valley, gold-bearing disseminated, stockwork and vein-type sulphide mineralization occurs in Carmacks Group volcanics (MINFILE 116C 153, 115N 041)(Glasmacher and Friedrich, 1985).

The occurrence of two types of gold-bearing mineralization in the area prompted a detailed study of the

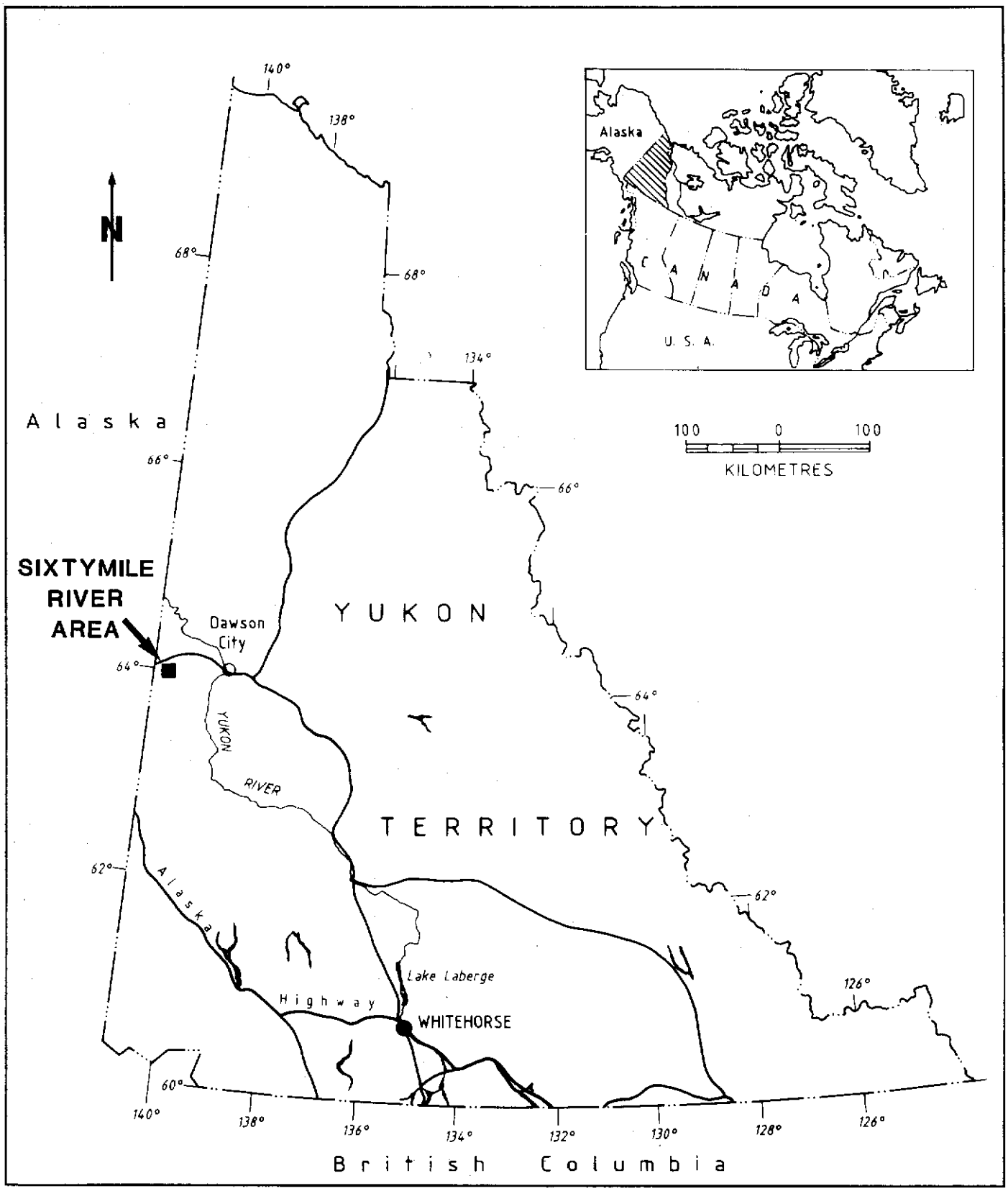

Figure 1. Location of the Sixtymile River area.

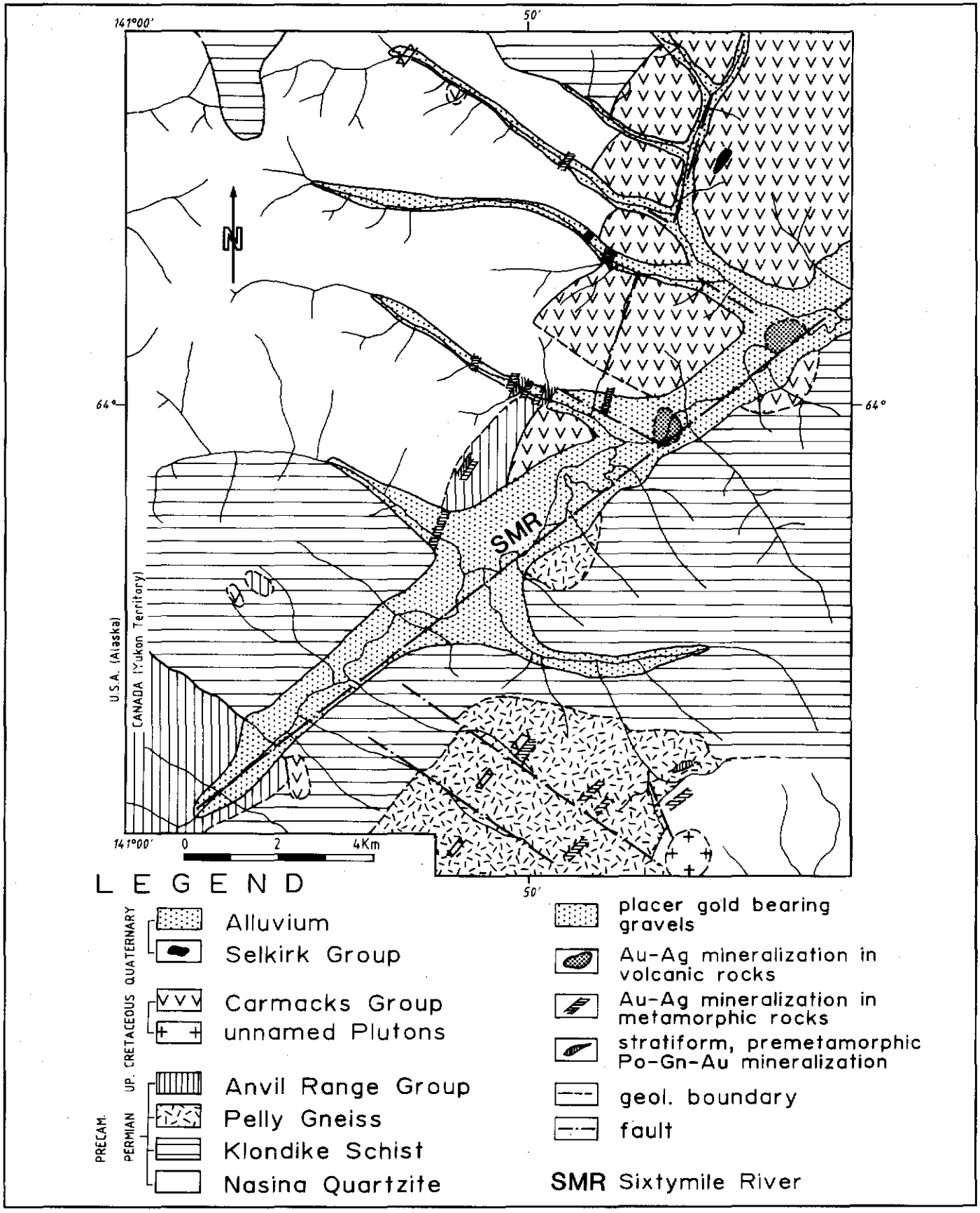

Figure 2. Geological map of the Sixtymile River area (partly compiled after Cockfield, 1921).

enrichment processes, using ore petrology, fluid inclusion and isotope studies. The field work was carried out as part of the Canada/Germany Science and Technology Exchange Program.

The chemical compositions of ore, gangue and alteration minerals were obtained by using an ARL-SEMQ electron microprobe. Natural and synthetic sulphides, oxides and silicates were used as standards. Full details of the analytical technique are given in Glasmacher (1991). On-line data reduction used a modified Magic IV (Colby, 1968). Detailed mineral compositions are reported in Glasmacher (1991). Names of gangue and alteration minerals follow the classification scheme of Deer et al. (1979).

Microthermometric data was obtained using a Chaixmeca (MIM 85) heating/freezing stage. The determination of pH ranges is based on thermodynamic calculations presented in Henley et al. (1984).

Stability fields of ore minerals in log $a(O_2)$ - pH and log $a(S_2)$ - log $a(O_2)$ diagrams were calculated for the physico-chemical conditions of the different enrichment stages. Thermodynamic data bases are described in Barton (1969), Barton and Skinner (1979), Craig and Barton (1973), Haas and Robbie (1973), Helgeson (1969, 1979), Henley et al. (1984), King et al. (1973), Rau et al. (1973a, 1973b), Richardson and Jeffers (1952), Toulmin and Barton (1964), and Schneeberg (1973). By analogy with similar hydrothermal mineralization (Creede, Colorado, Roedder et al., 1963, Baron et al., 1977) and active geothermal systems (Henley and Hedenquist, 1986, Mann et al., 1986) a total sulphur concentration of $\Sigma S = 0.02M$ was assumed.

GEOLOGY

The Precambrian to Paleozoic metamorphic basement in the Sixtymile River area is interpreted as part of the Yukon Tanana Terrane (Monger, 1984; Fig. 3). Based on the tectonic features of the metamorphic basement south of Tintina Fault, Tempelman-Kluit (1974; 1976; 1979) assigned part of Yukon Tanana Terrane and Stikine Terrane to "Yukon Cataclastic Complex". During Upper Cretaceous and Lower Tertiary, the crustal evolution of the Stikine and Yukon Tanana Terranes was influenced by subduction processes further to the southwest (Monger et al., 1972; Monger et al., 1982). Tholeiitic calcalkaline and shoshonitic magmas were generated above a northeast-dipping subduction zone, (Armstrong, 1988). High local heat flow caused by these magmatic activities initiated the development of hydrothermal systems.

Today, gold and sulphides precipitated from these fossil geothermal systems occurs in mesothermal gold-bearing quartz-(carbonate)-sulphide veins hosted by metamorphic rocks and gold-bearing skarns (Meinert, 1986) or in gold-bearing epithermal mineral occurrences hosted by volcanic rocks (Morin and Stroshein, 1987; Sinclair, 1986; Fig. 4). Regionally, most Yukon gold occurrences appear to be located in areas which are underlain by allochthonous terranes (Morin and Downing, 1984).

Due to tectonic and lithostratigraphic differences, the Sixtymile River area has been divided into a northern and a southern part. The boundary is represented by the Sixtymile River fault zone, which strikes east-northeast.

Lithologic units in the northern area comprise Precambrian to Paleozoic metamorphic rocks, Paleozoic ultramafic rocks, Middle Jurassic pegmatitic and aplitic dykes, Upper Cretaceous porphyry dykes and volcanic rocks with intercalated sedimentary rocks, Quarternary alkaline basaltic dykes and Quarternary alluvial sediments (Glasmacher and Friedrich, 1985, Hughes and Morison, 1986; Fig. 2; Table 1). Metasedimentary rocks with minor metavolcanic layers are assigned to the Nasina Series, and metavolcanic rocks with minor metasedimentary layers are assigned to the Klondike Schist. Biotite-amphibole orthogneiss of unknown age is discordant to the Nasina Series and Klondike Schist. Serpentinized ultramafic rocks occur along thrust faults (Mortensen, personal communication) and are possibly linked to the Anvil Range Group.

Muscovite from one of the northeast-southwest trending pegmatitic to aplitic dykes yielded a K/Ar age of 180 Ma (Mortensen, 1988), the same age as rocks of the Klotassin Suite. Calcalkaline volcanic rocks of intermediate composition are intruded by a quartz-feldspar porphyry plug dated at 68 ± 0.3 Ma, (Mortensen, 1988), and are assigned to the Upper Cretaceous Carmacks Group. They are intercalated with sedimentary rocks. Northwest-southeast trending andesitic dykes are possible feeders to the Carmacks Group volcanics. Quaternary alkaline olivine basalts are the youngest igneous rocks in the area.

Metamorphic rocks in the southern area are similar to those in the northern area with the exception of the Pelly Gneiss (Late Devonian-Early Mississippian; Mortensen, 1988). This stratigraphic unit comprises mainly biotite augen gneiss with minor lenses of quartzite and garnet-mica schist. Magmatic rocks in the southern area include a calcalkaline, I-type biotite granodiorite intrusion and northeast-southwest trending andesite to dacite dykes. These dykes are possibly related to Carmacks Group volcanics in the northern area. Quaternary alluvial sediments occur in all valleys.

MINERALIZATION

Northern Area

Gold bearing quartz-carbonate veins in the northern area are hosted by metamorphic rocks and occur along north-northeast trending faults. The veins are lensoid, average 50 cm thick, and are often discontinuous. In the underground placer mine on Miller Creek, quartz-carbonate veins occur along the same structures as the Late Cretaceous volcanic rocks.

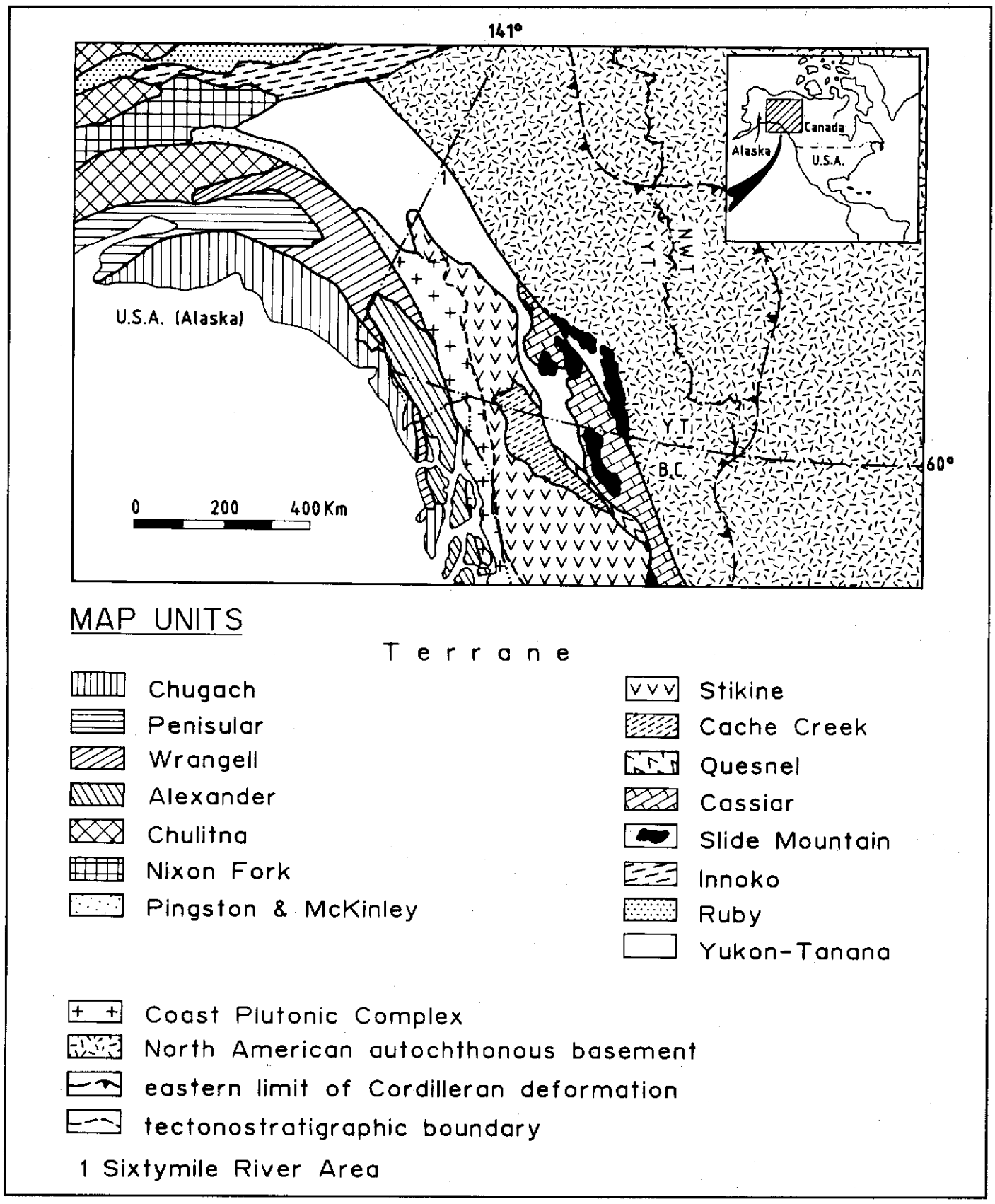

Figure 3. Recent distribution of terranes in the northern Cordillera and adjacent parts of Alaska (compiled after Coney, 1980; Tempelman-Kluit, 1981; Monger, 1984).

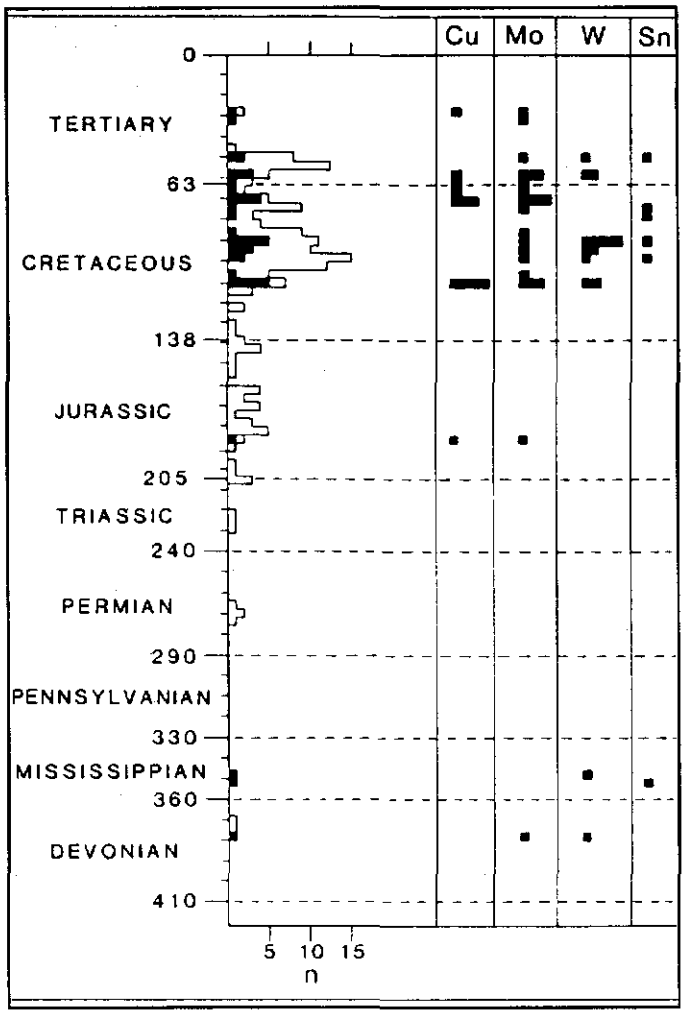

Figure 4. Radiometric ages of granitoid rocks in the northern Cordillera and adjacent parts of Alaska. Shaded areas represent the ages of intrusions with associated mineral deposits; unshaded areas are ages of intrusions unrelated to any known deposits. The ages of Cu, Mo, W and Sn mineralization are inferred from the ages of associated intrusions (after Sinclair, 1986).

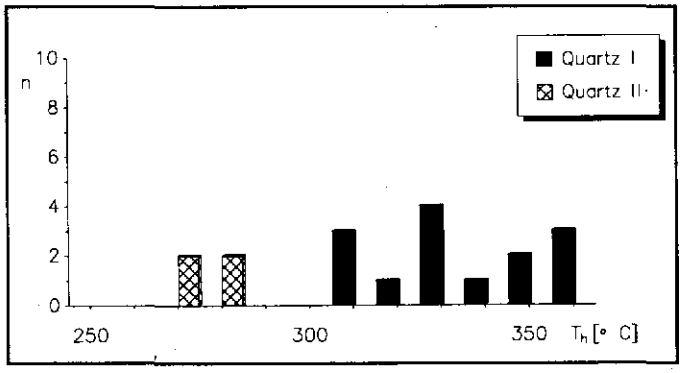

Figure 5. Histogram showing the frequency distribution of homogenization temperatures of fluid inclusions in quartz (gold bearing quartz-carbonate-sulphide veins in the northern area).

Petrology and mineral composition

Based on structural features of and intergrowth relationships of the vein minerals, the paragenetic sequence has been subdivided into two enrichment stages (Table 2). Intergrown pyrite, arsenopyrite, pyrrhotite and quartz formed during the first stage. Stage I minerals are fractured and healed by Stage II galena, sphalerite, chalcopyrite, pyrite and carbonate and minor quartz. Stage I pyrite replaces magnetite in the wall rock and is surrounded by Stage II pyrite. Gold is detectable only by geochemistry and is confined to stage I. High gold content is related to high arsenic content in quartz-carbonate-sulphide samples.

Pyrite in both the veins and in the wall rock contained no gold above detection limit (DL = 0.06 wt.-%). Pyrite of Stage I is enriched in cobalt (0.15-0.64 wt.-%) and nickel (0.08 - 0.16 wt.-%) relative to the wall rock, and is intergrown with arsenopyrite. It contains up to as 0.50 wt.-% As.

The average arsenic content of arsenopyrite is 30.25 at.-% As. The proportions of cobalt (<0.08 wt.-%) and nickel (<0.06 wt.-%) are low. Microprobe analyses along a traverse across arsenopyrite grains did not reveal any distinct zonation. Arsenic ranges from 29.45 to 31.20 at.-% and cobalt and nickel range from 0.03 to 0.05 at.-%. Work by Kretschmar and Scott (1976) suggests that a local fluctuation in sulphur and arsenic activity or disequilibrium between arsenopyrite, pyrite and pyrrhotite during their growth can cause this type of variation.

In galena, bismuth (0.16 to 1.3 wt.-%) and silver (0.07 to 0.54 wt.-%) are the only trace elements above detection limit (0.03 wt.-% Sb).

Sphalerite is characterized by high FeS (21.71 - 23.46 mol.-%) and manganese (0.46 - 0.85 wt.-%) as well as low cadmium content (0.17 - 0.35 wt.-%). Erratic copper distribution is caused by small chalcopyrite inclusions.

Siderite, magnesio-siderite, ferromagnesite and ankerite are the main gangue minerals of stage II. The trace element content of ankerite shows a distinct variation which depends on the galena/sphalerite ratio in the veins. Where galena is the main sulphide component, ankerite contains an average of 1.29 wt.-% PbO and a 1.25 wt.-% MnO. ZnO and SrO are below detection limit. Where sphalerite is the major mineral, the ankerite has a lower lead and manganese content (<0.05 wt.-% PbO; avg: 0.81 wt.-% MnO) a higher zinc and strontium content: (up to 0.43 wt.-% ZnO; avg: 0.12 wt.-% ZnO and up to 0.15 wt.-% SrO). Because the Stage II minerals crystallized simultaneously, these results suggest that manganese has a stronger affinity for sphalerite and/or siderite (which may contain up to 11 wt.-% MnO) than for ankerite.

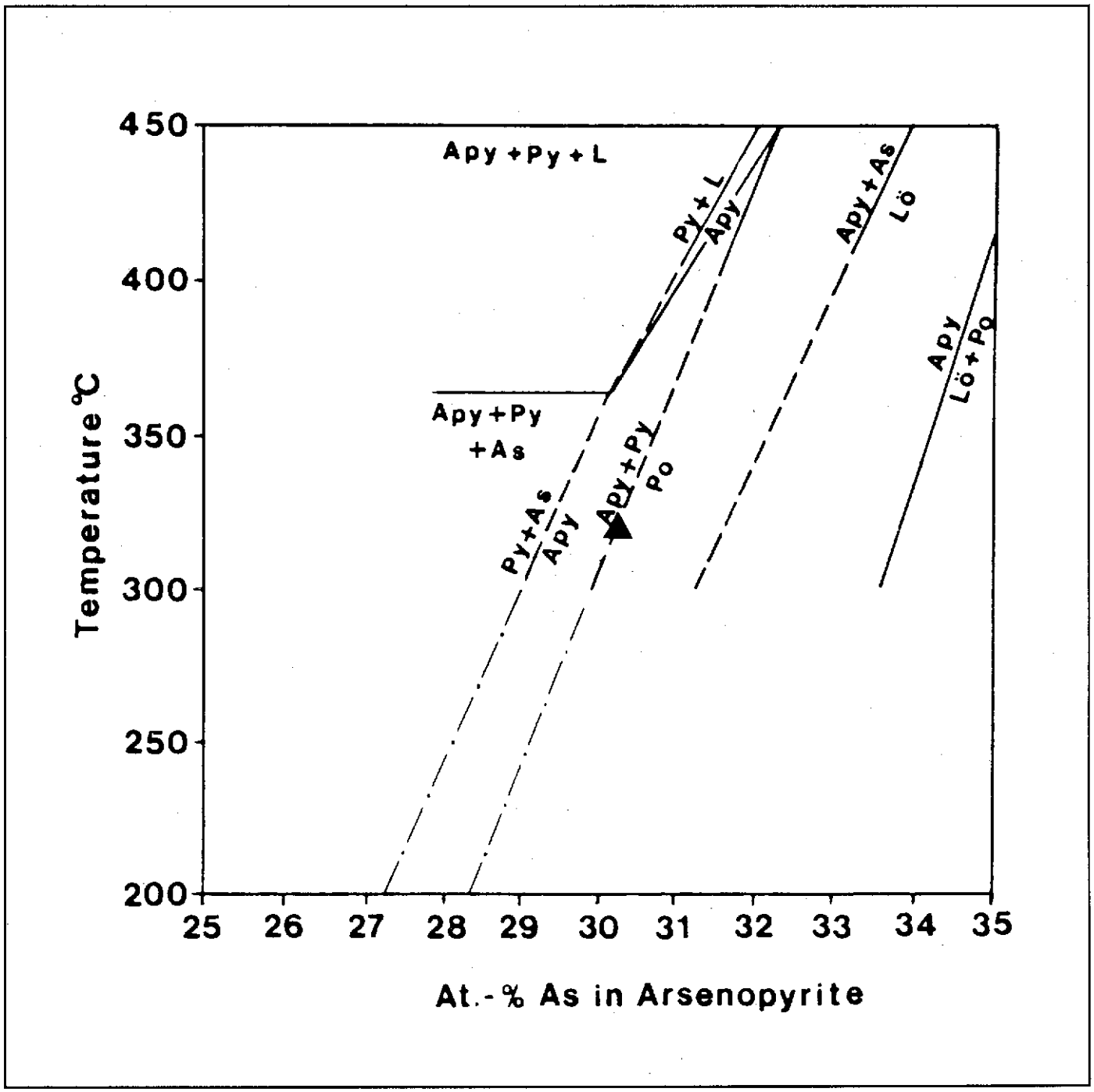

Figure 6. Arsenopyrite composition as a function of temperature and bulk composition (▲ arsenopyrite of the gold bearing quartz-carbonate-sulphide veins in the northern area; stability fields after Kretschmar and Scott, 1976).

Wall rock alteration and mineral composition

Each quartz-carbonate-sulphide vein is surrounded by an irregular zone of sericitic alteration which grades outwards into an alteration zone dominated by K-feldspar (Table 3). In the sericitic alteration zone, pyrite replaces magnetite, and sericite and quartz replace K-feldspar. In the K-feldspar zone, sericite, quartz and minor K-feldspar replace epidote and chlorite. An outer propylitic zone, which is also irregular in shape, is characterized by pyrite and chlorite replacement of biotite, epidote and sericite replacement of plagioclase, and as epidote and chlorite replacement of amphibole.

Microthermometry

Microthermometric studies were carried out on fluid inclusions in quartz crystals of both enrichment stages. Stage I quartz contains both primary and secondary inclusions,

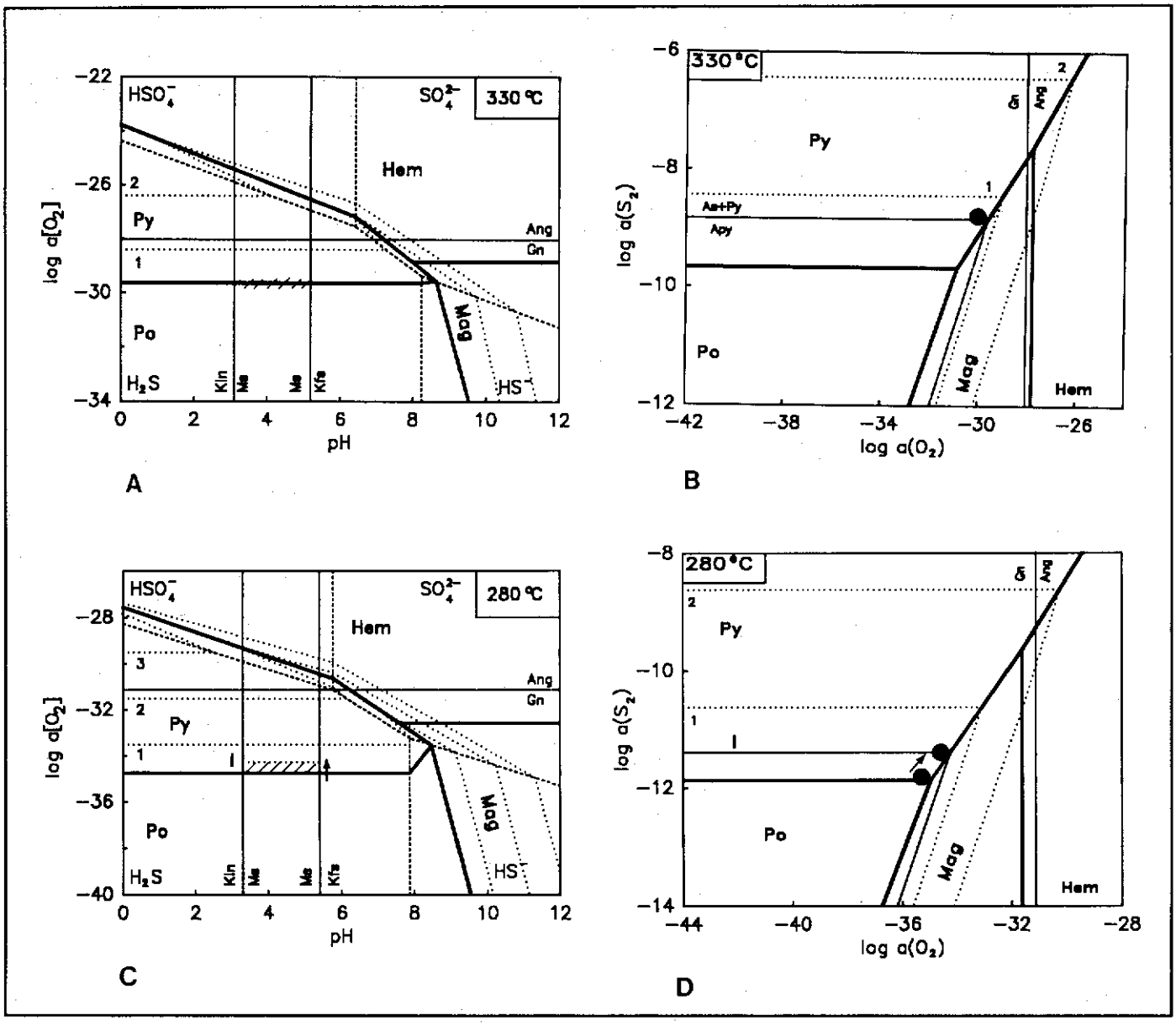

Figure 7. Log $a(O_2)$-pH and log $a(S_2)$-log $a(O_2)$ diagrams of the mineralization stages in the gold bearing quartz-carbonate-sulphide veins in the northern area (//// field of enrichment; ----> direction of change in physico-chemical conditions, I = sphalerite containing 24 mol.-% FeS; Mineral abbreviations follow Kretz, 1983).

whereas Stage II quartz contains only primary inclusions. Stage I inclusions gave homogenization temperatures between 308°C and 353°C with a maximum at 325°C and a salinity of 12.8 wt.-% NaCl-equivalent (Fig. 5). Fluid inclusions along microfractures in Stage I quartz yielded homogenization temperatures similar to fluid inclusions in Stage II quartz, which homogenize between 270°C and 280°C and have a salinity of 6 wt.-% NaCl equivalent.

Physical and chemical conditions

Based on the mineral paragenesis arsenopyrite-pyrite-pyrrhotite (stage I) and the arsenopyrite thermometer of Kretschmar and Scott (1976), the arsenic content (30.25 at.-%) of arsenopyrite indicates an average temperature of 320°C (Fig. 6). This temperature is close to the homogenization temperature (325°C) of primary fluid inclusions in Stage I quartz. Calculations of pH, log $a(O_2)$ and log $a(S_2)$ conditions during Stage I are based on an assumed formation temperature of 330°C, although the actual temperature may have been higher. Because of the tectonic fracturing between Stage I and Stage II it is possible that the fluid pressure during stage II was hydrostatic rather than lithostatic. If so, only a small pressure correction would be necessary to calculate the true formation temperature. Based on this assumption, and the measured homogenization temperatures of fluid inclusions in Stage II quartz (270°C - 280°C), the physico-chemical

conditions during the second stage were calculated assuming a formation temperature of 280°C.

Using the equilibrium between K-feldspar and muscovite, and also between muscovite and kaolinite, the formation temperature, molarity and the mineral paragenesis of alteration zone III the pH range was calculated as:

Stage I	$3.1 < pH_{330°C} < 5.2$	neutral $pH_{330°C} = 5.7$
Stage II	$3.3 < pH_{280°C} < 5.4$	neutral $pH_{280°C} = 5.6$

The mineral paragenesis of Stage I is consistent with an oxygen activity of log $a(O_2) \approx -30$ and a sulphur activity of about log $a(S_2) \approx -10$ (Fig. 7A; Fig. 7B). The Stage II mineral paragenesis indicates that oxygen activity during stage II decreased from log $a(O_2) = -35$ to log $a(O_2) = -34$ and sulphur activity decreased from log $a(S_2) = -12$ to log $a(S_2) = -11$ (Fig. 7C; Fig. 7D).

Southern area

Gold bearing mesothermal quartz veins in the southern area are hosted by metamorphic rocks of the Pelly Gneiss unit and occur along north-northeast trending faults. These veins are often discontinuous and lenticular in shape and have an average thickness of about 70 cm. Some characteristic features of the veins include alternating quartz-sulphide bands, open-space fillings and idiomorphic zoned quartz crystals intergrown with sulphide minerals. Some of the veins show evidence of several phases of mineralization.

Petrology and mineral composition

Three stages of mineral enrichment have been distinguished (Table 4). Stage I minerals include quartz and pyrite with inclusions of bornite, galena with matildite exsolutions, chalcopyrite with mackinawite ex-solutions, cubanite, native bismuth, pyrrhotite, sphalerite, tetrahedrite and quartz.

Stage II coincides with the main enrichment of arsenopyrite and galena with tetrahedrite, miagyrite and polybasite exsolutions. Quartz, and pyrite containing arsenopyrite and galena inclusions (with matildite exsolutions) occur in subordinate amounts. Gold enrichment is associated with the arsenopyrite, and silver enrichment is associated with the galenat. Both the Stage I and Stage II minerals are fractured as a result of tectonic movements which preceded Stage III mineralization. The fractures are healed by Stage III pyrite, zoned sphalerite (iron poor core - iron rich rim), chalcopyrite, freibergite and quartz.

Gold was not detected in pyrite in any of the three stages (detection limit 0.06 wt.-% Au), but Stage II pyrite contains more arsenic (up to 2 wt.-%) than pyrite of stage I or stage III.

Arsenopyrite inclusions, which occur only in pyrite II, contain 27.66 at.-% arsenic, and return low trace element values (0.04 wt.-% Co, Ni, Sb; <0.11 wt.-% Cu; <0.04 wt.-% Ag). Arsenopyrite II, which is intergrown with pyrite and pyrrhotite, contains an average 29.03 at.-% As and a higher trace element content (<0.43 wt.-% Co; 0.09 wt.-% Ni; <0.34 wt.-% Cu; <0.50 wt.-% Sb).

High bismuth (<7.86 wt.-%) and silver (4.35 wt.-%) values in galena inclusions in pyrite I and II are caused by matildite exsolutions. In addition to the matildite ex-solutions, galena inclusions in pyrite II are characterized by high arsenic content (<1.21 wt.-%). Trace element variations (<0.49 wt.-% Bi; <0.78 wt.-% Ag; <1.79 wt.-% Sb) of galena II are caused by tetrahedrite, miagyrite and polybasite exsolutions.

From Stage I to Stage III there was a decrease in the iron content of sphalerite, from 20.22 mol.-% to 3.46 mol.-% FeS, and a decrease in manganese content from 0.20 wt.-% to 0.04 wt.-%. The iron content increased slightly to 5.77 mol.-% FeS during stage III. Cadmium content increased, from 0.34 wt.-% to 0.84 wt.-% between Stage I and Stage III, but decreased slightly to 0.66 wt-% at the end of Stage III. Whereas the copper content of sphalerite I and II is below detection limit (0.04 wt.-%) sphalerite III contains significant copper (up to 0.42 wt.-%).

Wall rock alteration and mineral composition

Veins showing evidence of one, two or three mineral enrichment stages are surrounded by similar envelopes of wall rock alteration. Adjacent to the quartz-sulphide veins is a zone of sericitic alteration, where quartz is recrystallized, and K-feldspar is replaced by sericite and quartz (Table 5). Between the sericite alteration zone and the unaltered biotite augen gneiss is a zone of quartz-K feldspar-sericite alteration, followed by a zone of propylitic alteration. The quartz-K feldspar-sericite zone is characterized by the replacement of plagioclase and chlorite by sericite and quartz. In the propylitic zone, pyrite and rutile replace magnetite, biotite and muscovite replace chlorite and sericite replaces plagioclase.

Microthermometry

The cores of idiomorphic and zoned quartz crystals consist of Stage I quartz I, and the rims consist of Stage II quartz. Quartz of stages I and II is fractured, and healed by Stage III quartz. Primary fluid inclusions in Stage I quartz homogenize at about 275°C and indicate a salinity of 18.3 wt.-% NaCl equivalent (Fig. 8). Homogenization temperatures of primary fluid inclusions in Stage II quartz are about 205°C and the salinity of the fluid is 12 wt.-% NaCl equivalent. Primary inclusions in Stage III quartz and secondary inclusions in Stage I and II quartz return homogenization temperatures of about 145°C and salinity values of about 10 wt.-% NaCl equivalent.

Physico-chemical conditions

Based on studies done by Kojima and Sugaki (1985), Sugaki et al. (1982) and Yund and Kullerud (1966), the presence of chalcopyrite-pyrrhotite, cubanite-pyrrhotite and cubanite-chalcopyrite-pyrrhotite as inclusions in pyrite of stage I are consistent with formation temperatures above 325°C and 334 ± 17°C, respectively. The difference between this

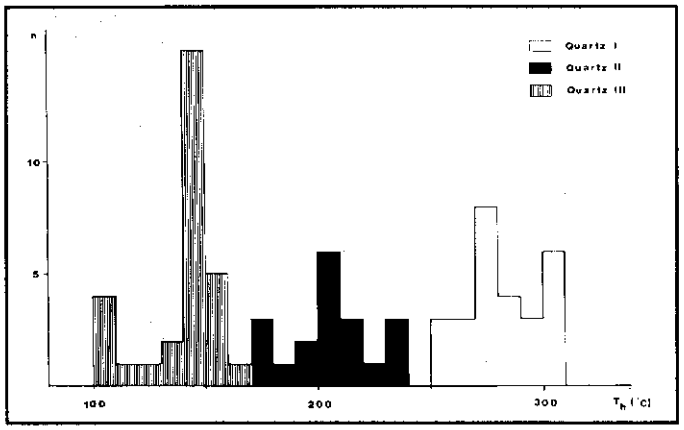

Figure 8. Histogram showing the frequency distribution of homogenization temperatures of fluid inclusions in quartz of the gold bearing quartz-sulphide veins in the southern area.

mineral formation temperature and the 275°C homogenization temperature of Stage I inclusions suggests a minimum fluid pressure of about 500 bar, based on the work of Potter (1977).

According to the studies of Scott and Barnes (1971), Scott and Kissin (1973) and Browne and Lovering (1973), the iron content (15 mol.-% FeS) of sphalerite II intergrown with pyrite indicates a formation temperature above 248°-260°C for the second stage mineralization. Following the same reasoning as the paragraph above, the minimum pressure for hydrothermal fluids of stage II is also about 500 bar. Evidence of tectonic fracturing between stage II and stage III suggests that the fluid pressure may have been hydrostatic at some point.

Using temperatures of 330°C for stage I, 280°C for stage II and 150°C for stage III, and with the additional assumption that the same mineral alteration occurred during each stage of mineralization, pH, log $a(O_2)$ and log $a(S_2)$ of mineral enrichment were calculated. The following pH ranges were obtained:

stage I	$3.2 < pH_{330°C} < 5.3$	neutral $pH_{330°C} = 5.7$
stage II	$3.2 < pH_{280°C} < 5.2$	neutral $pH_{280°C} = 5.6$
stage III	$4.1 < pH_{150°C} < 5.9$	neutral $pH_{150°C} = 5.8$

The change in mineral paragenesis during stage I from sphalerite (21 mol.-% FeS)-pyrrhotite-pyrite to native bismuth-pyrrhotite-pyrite indicates a decrease in oxygen activity from log $a(O_2) = -29$ to log $a(O_2) = -30$ and a decrease in sulphur activity from log $a(S_2) = -9$ to log $a(S_2) = -10$ (Fig. 9A; Fig. 9B).

Oxygen and sulphur activity continued to decrease during stage II. Early arsenic-bearing pyrite with arsenopyrite and galena inclusions was followed by the crystallization of sphalerite (15 mol.-% FeS)-pyrite-pyrrhotite and pyrite-pyrrhotite, indicating a change from log $a(O_2) = -31$ to log $a(O_2) = -35$ and log $a(S_2) = -11$ to log $a(S_2) = -12$ (Fig. 9C; Fig. 9D).

The mineral paragenesis sphalerite (6 mol.-% FeS)-pyrite of stage III is consistent with an oxygen activity of log $a(O_2) = -53$ and a sulphur activity of log $a(S_2) = -18$ (Fig. 9E; Fig. 9F).

MINERAL ENRICHMENT PROCESS

Northern area

Although the physical and chemical conditions of both mineral enrichment stages lie within the stability fields of arsenopyrite, galena and sphalerite, arsenopyrite and gold enrichment occurred during stage I and galena, sphalerite and silver were deposited during stage II. Either the hydrothermal fluids of stage I were depleted in lead, zinc and silver, and the fluids of stage II in arsenic and gold, or these elements were transported as complexes with different stability conditions.

Heinrich and Eadington (1986) and Ballantyne and Moore (1988) described the transport of arsenic in hydrothermal solutions in terms of hydroxide ($H_3AsO_3°$ and/ or $H_3AsO_4°$) or bisulphide ($HAsS_2°$) complexes. Due to the physico-chemical conditions prevalent in most active hydrothermal systems, arsenic is transported as the $H_3AsO_3°$-complex. Transport of arsenic as a bisulphide complex is only possible at sulphur concentrations above $\Sigma S = 0.1$m. At very low pH and high salinities, arsenic is transported as a chloride complex.

Based on the assumptions above, an equilibrium reaction can be written which describes the coprecipitation of arsenopyrite, pyrite and pyrrhotite (**reaction 1**):

$$2H_3AsO_3° + 6FeCl_2 + 9H_2S° = 2FeAsS + 3FeS_2 + FeS + 12Cl^- + 6H_2 + 3O_2 + 12H^+$$

The solubility of arsenopyrite at a particular temperature depends on the oxygen and sulphur activity and pH (Fig. 10). Decreased oxygen activity, or increased pH and sulphur activity, cause precipitation of arsenopyrite.

In active hydrothermal systems under similar physico-chemical conditions, gold is transported as a gold-thio complex ($Au(HS)_2^-$) up to a temperature of about 300°C (Seward, 1973; Seward, 1982; Henley et al., 1984; Henley and Brown, 1985). Above this temperature, the gold-chloride complex predominates (Henley, 1973). An equilibrium reaction describing the precipitation of gold can be written as follows (**reaction 2**):

$$2Au(HS)_2^- + 2H^+ + H_2O = 2Au° + 4H_2S° + 0.5O_2$$

As this reaction shows, the solubility of gold as a gold-thio complex increases with increasing pH and oxygen activity.

Seward (1976), Barnes (1979), Henley et al. (1984), Seward (1984), and Henley and Brown (1985), have described the transport of lead, zinc, copper and silver in active hydrothermal systems as a metal-chloride complex

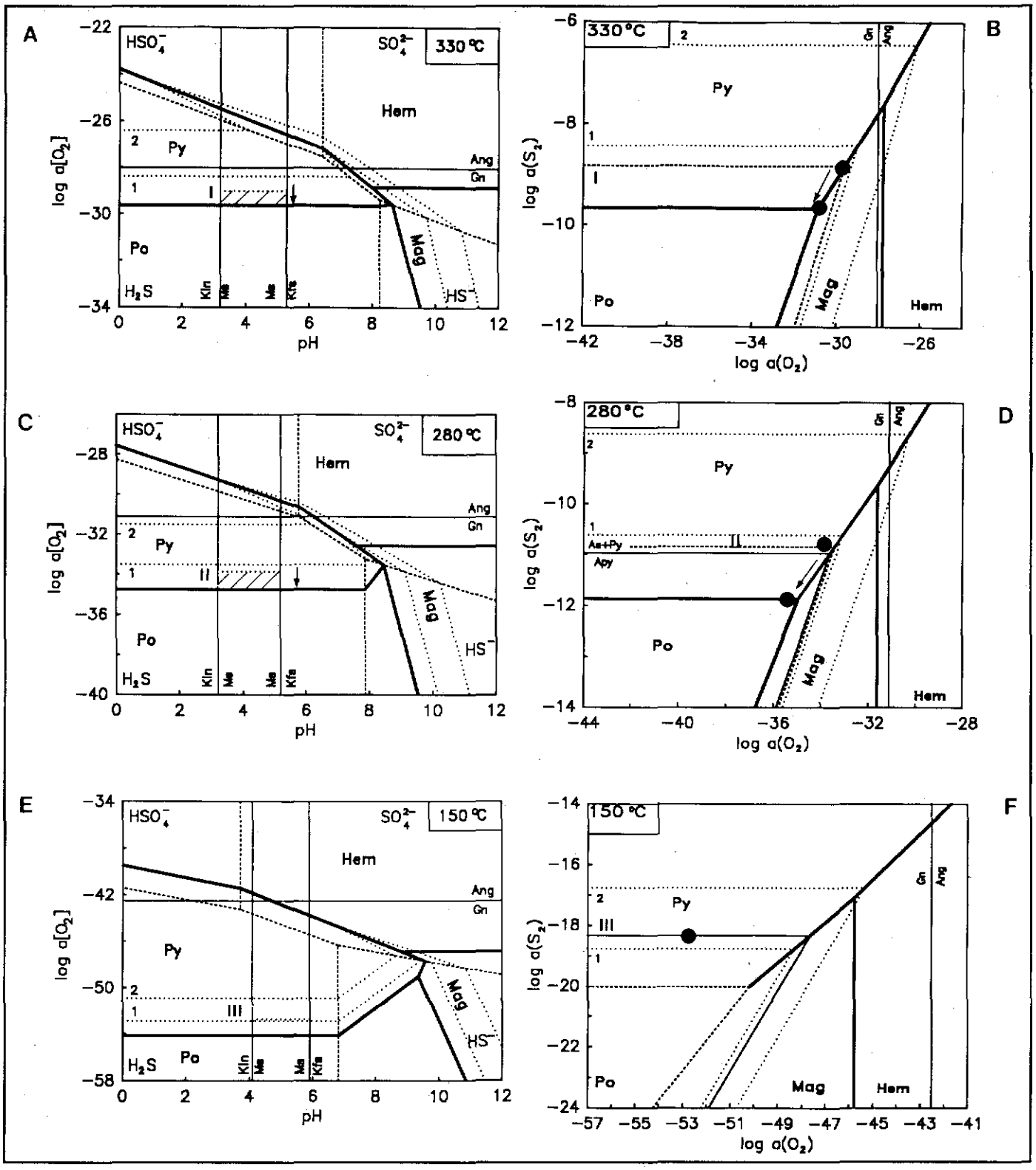

Figure 9. Log $a(O_2)$-pH and log $a(S_2)$-log $a(O_2)$ diagrams of the mineralization stages in the gold bearing quartz-sulfide veins in the southern area (legend as described in Figure 7; I = sphalerite containing 21 mol.-% FeS; II = sphalerite containing 15 mol.-% FeS; III = sphalerite containing 6 mol.-% FeS; Mineral abbreviations after Kretz, 1983).

(reaction 3):

$$MeCl_2^\circ + H_2S^\circ = MeS + 2H^+ + 2Cl^-$$

Above 200°C, these metal-chloride complexes are the prevalent transport mechanism. Increasing the sulphur activity and pH, or decreasing the activity of chlorine, causes the precipitation of sulphides.

In the Sixtymile area, fluid-wall rock interaction during the first stage of mineralization caused the replacement of K-feldspar by muscovite (reaction 4):

$$1.5[KAlSi_3O_8] + H^+ = 0.5[KAl_3Si_3O_{10}(OH)_2] + 3[SiO_2] + K^+$$

This alteration reaction would have increased the pH of the hydrothermal solutions during the first enrichment stage, probably causing the precipitation of arsenopyrite, pyrite and pyrrhotite by reaction 1. The crystallization of arsenopyrite, pyrite and pyrrhotite causes a decrease in pH and sulphur activity, and an increase in oxygen activity. The decrease in pH and sulphur activity as a result of reaction 1 predominates over the change in oxygen activity and probably control the precipitation of gold by reaction 2. On the other hand, an increase in Cl^- activity as a result of reaction 1 would favour the formation of metal-chloride complexes (reaction 3) and may have suppressed the formation of lead, zinc and copper sulphides during stage I.

The decrease in both temperature and salinity from stage I to stage II suggests mixing of two fluids with different physical and chemical characteristics. Decreased Cl^- activity can cause the precipitation of galena, sphalerite, chalcopyrite and silver as a result of reaction 3. The mixing of two fluids with contrasting oxygen activities would increase the oxygen activity of the initial fluid and counteract the deposition of arsenopyrite and gold and possibly dissolve arsenopyrite. The replacement of arsenopyrite I by galena of stage II might have been caused by this process.

Southern area

Physical and chemical conditions of hydrothermal fluids during the three stages of mineralization were within the stability field of galena and arsenopyrite, but whereas galena formed during both Stage I and Stage II, arsenopyrite enrichment is confined to Stage II. Assuming that fluid-wall rock interaction during Stage I caused the alteration of K-feldspar to muscovite by reaction 4, the pH of the fluids must have increased. Depending on the element saturation of the hydrothermal fluids, this pH increase could cause minerals to precipitate as a result of reaction 3. If the arsenic concentration in the fluid were low the change in pH would not cause a precipitation of arsenopyrite by reaction 1.

The decrease in temperature and salinity from Stage I to Stage III suggests mixing of two hydrothermal fluids with different physical and chemical characteristics. Assuming that the element transport and enrichment during stage II occurred as described by reactions 1 to 4, the precipitation of minerals could have been caused by decreasing temperature, Cl^- and oxygen activity between stage I and II.

The absence of arsenopyrite and galena during stage III is indicative of low concentrations of arsenic and lead in the Stage III hydrothermal fluid.

CONCLUSIONS

Gold-bearing, mesothermal quartz-(carbonate)-sulphide veins in the northern and southern areas are believed to have formed in the deeper parts of the same fossil geothermal system, and are probably related to a Late Cretaceous magmatic event. The following conclusions about the fluid composition and mineral enrichment process can be made:

(1) The fluids which circulated at depth in the metamorphic rocks are characterized by high temperatures (above 300°C), high salinities (about 18 wt.-% NaCl equiv.) and pH values in the range 3.1 to 5.2. These fluids are similar to alkaline chloride fluids of active geothermal systems.

(2) Arsenic was transported as a $H_3AsO_3^\circ$ complex, gold as $Au(HS)_2^-$ and lead, zinc, copper and iron as $MeCl_2^\circ$ complexes.

(3) Stage I mineralization resulted directly from fluid-wall rock interaction.

(4) Subsequent (second and third stage) mineralization resulted from the mixing of two fluids with different physical and chemical characteristics.

ACKNOWLEDGEMENTS

This research project was supported by the Deutsche Forschungsgemeinschaft (Grant FR 240/44). The study was also part of the Canada/Germany Science and Technology Exchange Agreement organized by the Geological Survey of Canada and the Federal Institute for Geosciences and Mineral Resources (BGR). Financial support was granted by the German Ministry of Research and Technology and by Exploration and Geological Services Division of the Department of Indian and Northern Affairs, Whitehorse, Yukon. We are particularly indebted to the mining companies for permitting access to their properties in the Sixtymile River area. We greatly appreciate the discussions with J. Morin, J. Mortensen, G. Lynch, P. Möller, R. Walter, P. Sänger v. Oepen and L. Stroink.

REFERENCES

ARMSTRONG, R.L., 1988. Mesozoic and early Cenozoic magmatic evolution of the Canadian Cordillera. Geological Society of America, Special Paper 218, p. 55-91.

BALLANTYNE, J.M. and MOORE, J.N., 1988. Arsenic geochemistry in geothermal systems. Geochimica et Cosmochimica Acta 52, p. 475-483.

BARTON, Jr., P.B., 1969. Thermochemical study of the system Fe-As-S. Geochimica et Cosmochimica Acta 33, p. 841-857.

BARTON, Jr., P.B. and SKINNER, J.B., 1979. Sulfide mineral stabilities. In: Geochemistry of hydrothermal ore deposits, H.L. Barnes (ed.), Pennsylvania State University, p. 278-404.

BARTON, Jr., P.B., BETHKE, P.M. and ROEDDER, E., 1977. Environment of ore deposition in the Creede Mining District, San Juan Mountains, Colorado: Part III. Progress toward interpretation of the chemistry of the ore-forming fluid for the OH vein. Bulletin of the Society of Economic Geologists, Vol. 72, p. 1-24.

BROWNE, P.R.L. and LOWERING, J.F., 1973. Composition of sphalerites from the Broadlands Geothermal Field and their significance to sphalerite geothermometry and geobarometry. Economic Geology, Vol. 68, p. 381-387.

COCKFIELD, W.E., 1921. Sixtymile River and Ladue River area, Yukon. Geological Survey of Canada, Memoir 123.

COLBY, J.W., 1968. Advances in X-Ray Analyses, Vol. 11, p. 287-305.

CONEY, P.J., 1982. Cordilleran tectonics and North American plate motions. American Journal of Science vol. 272, p. 603-628.

CRAIG, J.R. and BARTON Jr., P.B. 1973. Thermochemical approximations for sulfosalts. Economic Geology, Vol. 68, p. 493-506.

DEER, W.A., HOWIE, R.A. and ZUSSMAN, J., 1977. An introduction to the rock-forming minerals.

GLASMACHER, U., and FRIEDRICH, G., 1985. Placer gold in the Sixtymile River Area, Yukon Territory, Canada. Proceedings of the Seventh Annual conference on Alaskan Placer Mining, Fairbanks, p. 53-57.

GLASMACHER, U., 1991. Petrogenetische und metallogenetische Entwicklung ausgewählter Gebiete im "Yukon-Tanana Terrane" und "Stikine Terrane", (Yukon Territorium, Kanada) während der oberkreide und des Alltertiärs. Diss., Aachen University of Technology, 435 p.

GLASMACHER, U. and FRIEDRICH, G., 1992. Volcanic hosted, epithermal gold-sulphide mineralization, Sixtymile River area, Yukon Territory, Canada. In: Yukon Geology, Vol. 3; Exploration and Geological Services Division, Yukon, Indian and Northern Affairs, Canada (this volume).

HAAS Jr., J.L. and ROBIE, R.A., 1973. Thermodynamic data for wüstite, $Fe_{0.947}O$, magnetite, Fe_3O_4, and hematite, Fe_2O_3 (abstract). Transactions of the American Geophysical Union, Vol. 54, p. 438.

HEINRICH, C.A. and EADINGTON, P.J., 1986. Thermodynamic predictions of the hydrothermal chemistry of arsenic, and their significance for the paragenetic sequence of some cassiterite-arsenopyrite-base metal sulfide deposits. Economic Geology, Vol. 81, p. 511-529.

HELGESON, H.C., 1969. Thermodynamics of hydrothermal systems at elevated temperatures and pressures. American Journal of Science, p. 729-804.

HELGESON, H.C., 1979. Mass transfer among minerals and hydrothermal solutions. In: Geochemistry of hydrothermal ore deposits, 2nd. Ed, H.L Barnes (ed.); Pennsylvania State University, p. 568-610.

HENLEY, R.W., 1973. Solubility of gold in hydrothermal chloride solutions. Chem. Geol. Vol. 11, p. 73-87.

HENLEY, R.W., TRUESDELL, A.H., BARTON Jr.,, P.B. and WHITNEY, J.A., 1984. Fluid-mineral equilibria in hydrothermal systems. Society of Economic Geologists, Vol. 1.

HENLEY, R.W. and BROWN, K.L., 1985. A practical guide to the thermodynamics of geothermal fluids and hydrothermal ore deposits. In: Geology and Geochemistry of epithermal systems, B.R. Berger and P.M. Bethke (eds); Reviews in Economic Geology, Vol. 2, p. 25-44.

HENLEY, R.W. and HEDENQUIST, J.W., 1986. Introduction to the geochemistry of active and fossil geothermal systems. In: Guide to the active epithermal (geothermal) systems and precious metal deposits of New Zealand, G. Freidrich (chief ed.); Monograph 26, p.1-22.

HUGHES, R.L. and MORISON, S.R., 1986. Placer gravels of Miller Creek, Sixtymile River area, 116B,C: in Yukon Geology Vol. 1; Exploration and Geological Services Division, Yukon, Indian and Northern Affairs Canada, p. 50-55.

KING, L.G., MAH, A.D. and PANKRATZ, L.B., 1973. Thermodynamic properties of copper and its inorganic compounds. INCRA Monograph II on the Metallurgy of Copper, International Copper Research Association.

KRETSCHMAR, U. and SCOTT, S.D., 1976. Phase relations involving arsenopyrite in the system Fe-As-S and their application. Canadian Mineralogist, Vol. 14, p. 364-386.

KRETZ, R., 1983. Symbols for rock-forming minerals. American Mineralogist, Vol. 68, p. 277-279.

KOJIMA, S. and SUGAKI, A., 1985. Phase relations in the Cu-Fe-Zn-S system between 500°C and 300°C under hydrothermal conditions. Economic Geology, Vol. 80, p. 158-171.

MANN, A.W., FARDY, J.J. and HEDENQUIST, J.W., 1986. Major and trace element concentration in some New Zealand geothermal waters. International Volcanological Congress, Proceedings of Symposium 5, p. 61-80.

MEINERT, L.D., 1986. Gold in skarns of the Whitehorse Copper Belt. In: Yukon Geology, Vol. 1; Exploration and Geological Services Division, Indian and Northern Affairs Canada, p.19-43.

MONGER, J.W.H., 1984. Cordilleran tectonics: a Canadian perspective. Bulletin of the Geological Society of France, Vol. 7, p. 255-278.

MONGER, J.W.H., SOUTHER, J.G. and GABRIELSE, H., 1972. Evolution of the Canadian Cordillera: A plate-tectonic model. American Journal of Science, Vol. 272, p. 577-602.

MONGER, J.W.H., PRICE, R.A. and TEMPELMAN-KLUIT, D.J., 1982. Tectonic accretion and the origin of the two major metamorphic and plutonic belts in the Canadian Cordillera. Geology, Vol. 10, p.70-75.

MORIN, J.A. and DOWNING, D.A., 1984. Gold-silver deposits and occurrences in Yukon Territory. 1:2,000,000 scale map, list of occurrences. Exploration and Geological Services Division, Yukon, Indian and Northern Affairs Canada Open File 1984-2.

MORIN, J.A. and STROSHEIN, R., 1987. Disseminated precious metal exploration targets in Yukon. Geological Society of Nevada Symposium: Bulk Mineable Precious Metal Deposits of the Western United States, Reno, Nevada.

MORTENSEN, J.K., 1988. Geology of southwestern Dawson Map Area, Yukon. Geological Survey of Canada, Open File 1927.

RAU, H., KUTTY, T.R.N. and GUEDES DE CARVALHO, J.R.F., 1973a. High temperature saturated vapour pressure of sulfur and the estimation of its critical quantities. Journal of Chemical Thermodynamics, Vol. 5, p. 291-302.

RAU, H., KUTTY, T.R.N. and GUEDES DE CARVALHO, J.R.F., 1973b. Thermodynamics of sulfur vapor. Journal of Chemical Thermodynamics, Vol. 5, p. 833-844.

ROEDDER, E., RINGIAM, B. and HALL, W.E., 1963. Studies of fluid inclusions III: Extraction and quantitative analyses of inclusions in the milligram range. Economic Geology, Vol. 58, p. 353-374.

SCHNEEBERG, E.P., 1973. Sulfur fugacity measurements with the electrochemical cell Ag AgI $Ag_{2+x}S$ fs. Economic Geology, Vol. 68, p. 507-517.

SCOTT, S.D. and BARNES, H.L., 1971. Sphalerite geothermometry and geobarometry. Economic Geology, Vol. 66, p. 653-669.

SCOTT, S.D. and KISSIN, S.A., 1973. Sphalerite composition in the Zn-Fe-S system below 300°C. Economic Geology, Vol. 68, p. 475-479.

SEWARD, T.M., 1976. Stability of chloride complexes of silver in hydrothermal solutions up to 350°C. Geochimica et Cosmochimica Acta, Vol. 40, p. 1329-1341.

SEWARD, T.M., 1982. The transport and deposition of gold in hydrothermal systems. In: Gold '82: The Geology, Geochemistry and Genesis of Gold Deposits, R.P. Foster (ed.); Geological Society of Zimbabwe, Vol. 1.

SEWARD, T.M., 1984. The formation of lead II chloride complexes to 300°C: a spectrophotometric study. Geochimica et Cosmochimica Acta, Vol. 48, p. 121-134.

SINCLAIR, W.D., 1986. Molybdenum, tungsten and tin deposits and associated granitoid intrusions in the Northern Canadian Cordillera and adjacent parts of Alaska. In: Mineral deposits of Northern Cordillera, J.A. Morin (ed.); Canadian Institute of Mining and Metallurgy, Vol. 37, p. 216-234.

SUGAKI, A., KITAKAZE, A. and UENO, T., 1982. Hydrothermal syntheses of minerals in the system Cu-Fe-S and their phase equilibrium at 400°C and 500°C. Japan. Assoc. Min. Petrol. Econ. Geol., Vol. 3, p. 257-269.

TEMPELMAN-KLUIT, D.J., 1974. Reconnaissance geology of Aishihik Lake, Snag and part of Stewart River Map Areas, West-Central Yukon. Geological Survey of Canada Paper 73-41.

TEMPELMAN-KLUIT, D.J., 1976. The Yukon Crystalline Terrane:' Enigma in the Canadian Cordillera. Geological Society of America, Bulletin 87, p. 1343-1357.

TEMPELMAN-KLUIT, D.J., 1979. Transported cataclasite, ophiolite and granodiorite in Yukon: evidence of arc-continent Collision. Geological Survey of Canada, Paper 79-14.

TEMPELMAN-KLUIT, D.J., 1981. Geology and mineral deposits of southern Yukon. In: Yukon Exploration and Geology 1979-1980; Exploration and Geological Services Division, Indian and Northern Affairs Canada, p. 7-31.

TOULMIN, P. and BARTON, P.B., 1964. A thermodynamic study of pyrite and pyrrhotite. Geochimica et Cosmochimica Acta, vol. 28, p.641-671.

YUND, R.A. and KULLERUD, G., 1966. Thermal stability of assemblages in the Cu-Fe-S system. Journal of Petrology, Vol. 7, p. 454-488.

Table 1. Lithostratigraphic units of Sixtymile River area.

SYSTEM	FORMATION	LITHOLOGY NW Area	LITHOLOGY SE Area
QUATERNARY		alluvial sediments	alluvial sediments
	Selkirk Group	alkaline-olivine basalt	
LATE CRETACEOUS	Carmacks Group	andesite, dacite, andesite-dacite dykes, pyroclastic rocks, fluvial sediments	andesite and dacite dykes
	Unnamed plutons		biotite granodiorite
MIDDLE JURASSIC	Klotassin Suite	pegmatite, aplite	
PERMIAN	?	orthogneiss	
	Anvil Range Group	ultramafic rocks	
	Pelly Gneiss		augen gneiss garnet-mica schist, gneiss
	Klondike Schist	chlorite schist, mica schist	chlorite schist mica schist
PRE-PERMIAN (DEVONO-MISSISSIPPIAN AND ? OLDER)	Nasina Series	paragneiss, quartzite, quartz-mica schist, mica schist, graphite schist, marble	quartzite, quartz-mica schist, mica schist

Table 2. Paragenetic sequence and physico-chemical conditions of the gold-bearing mesothermal quartz-carbonate-sulphide veins in the northern area.

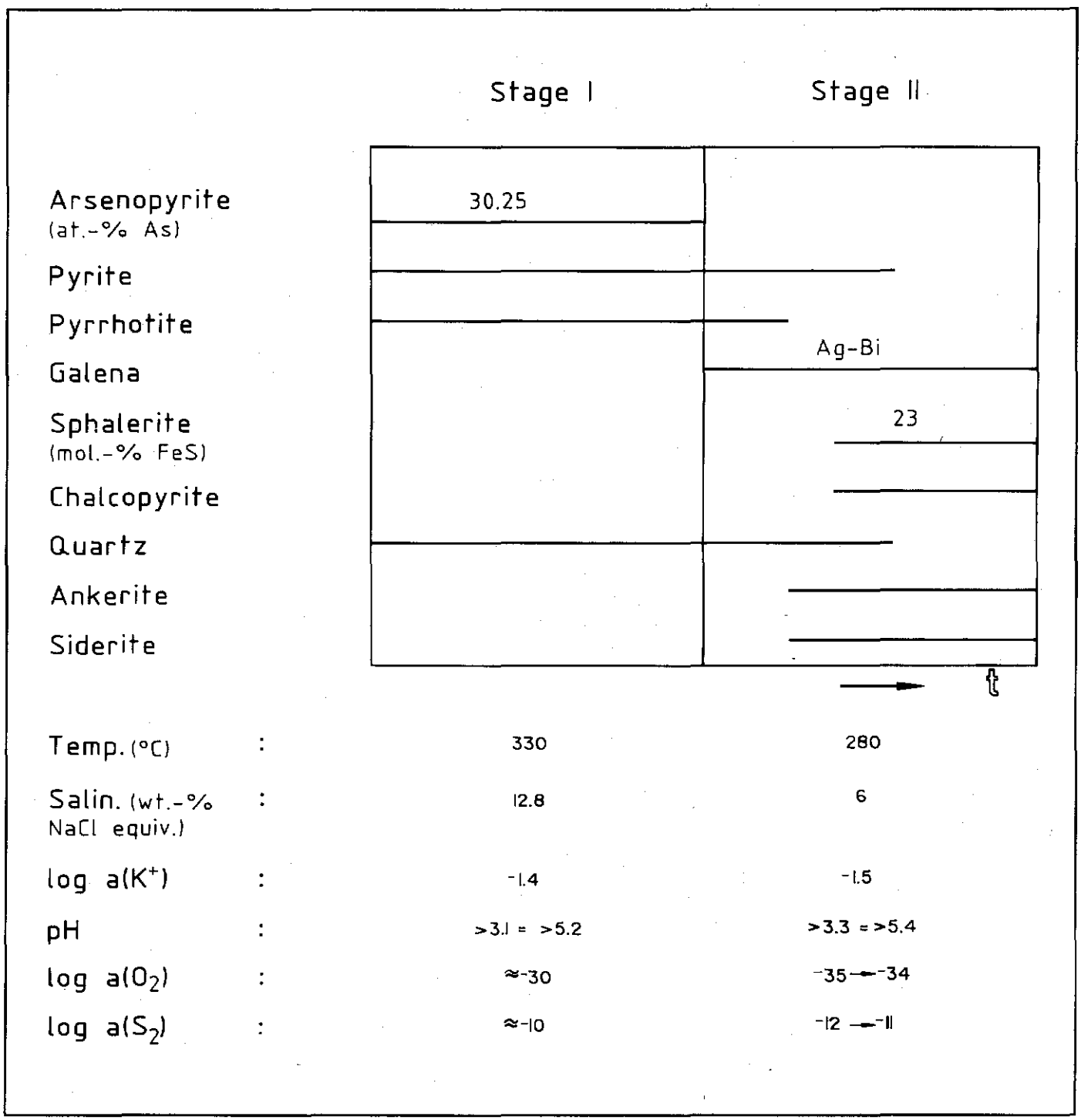

Table 3. Mineral paragenesis of the quartz veins and the alteration zones encasing the gold-bearing mesothermal quartz-carbonate-sulphide veins in the northern area.

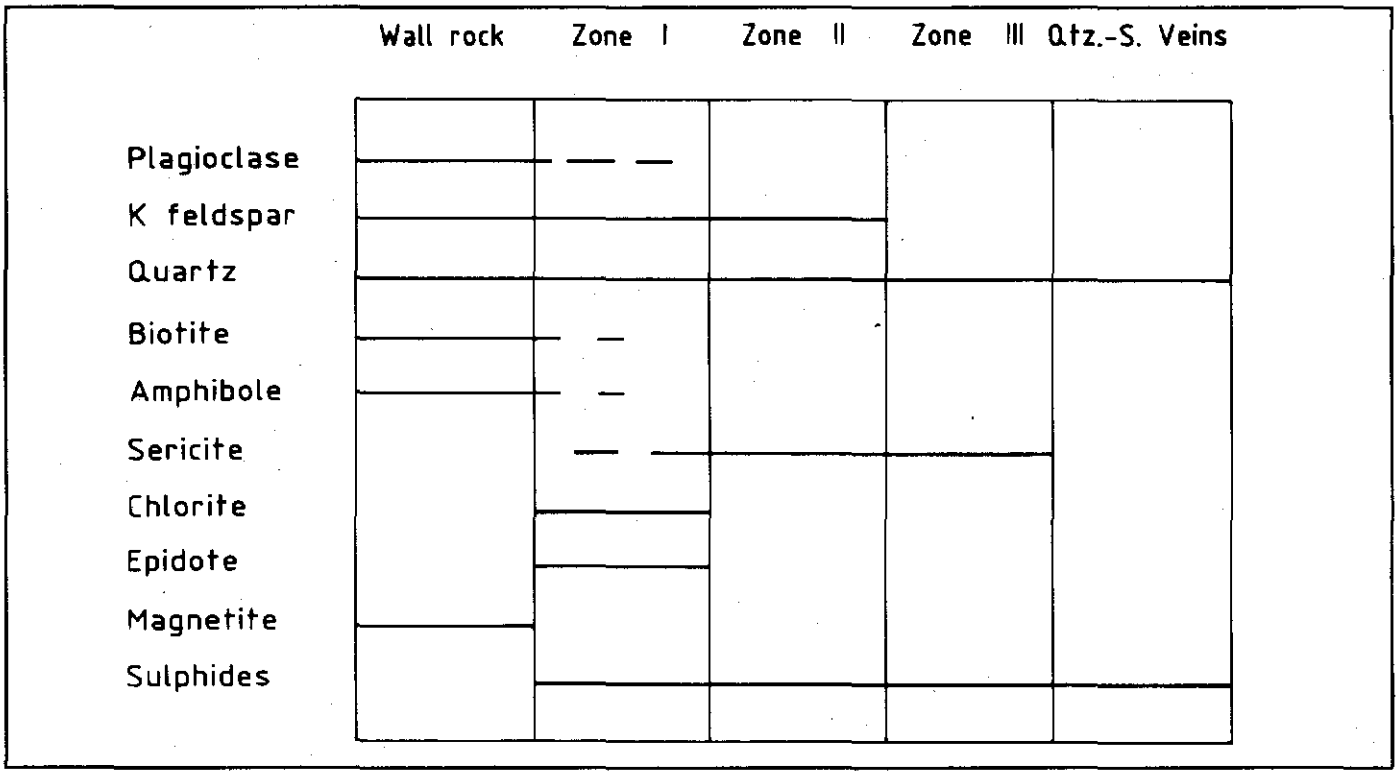

Table 5. Mineral paragenesis of the sulphide veinlets and the alteration zones encasing the gold-bearing mesothermal quartz-carbonate-sulphide veins in the southern area.

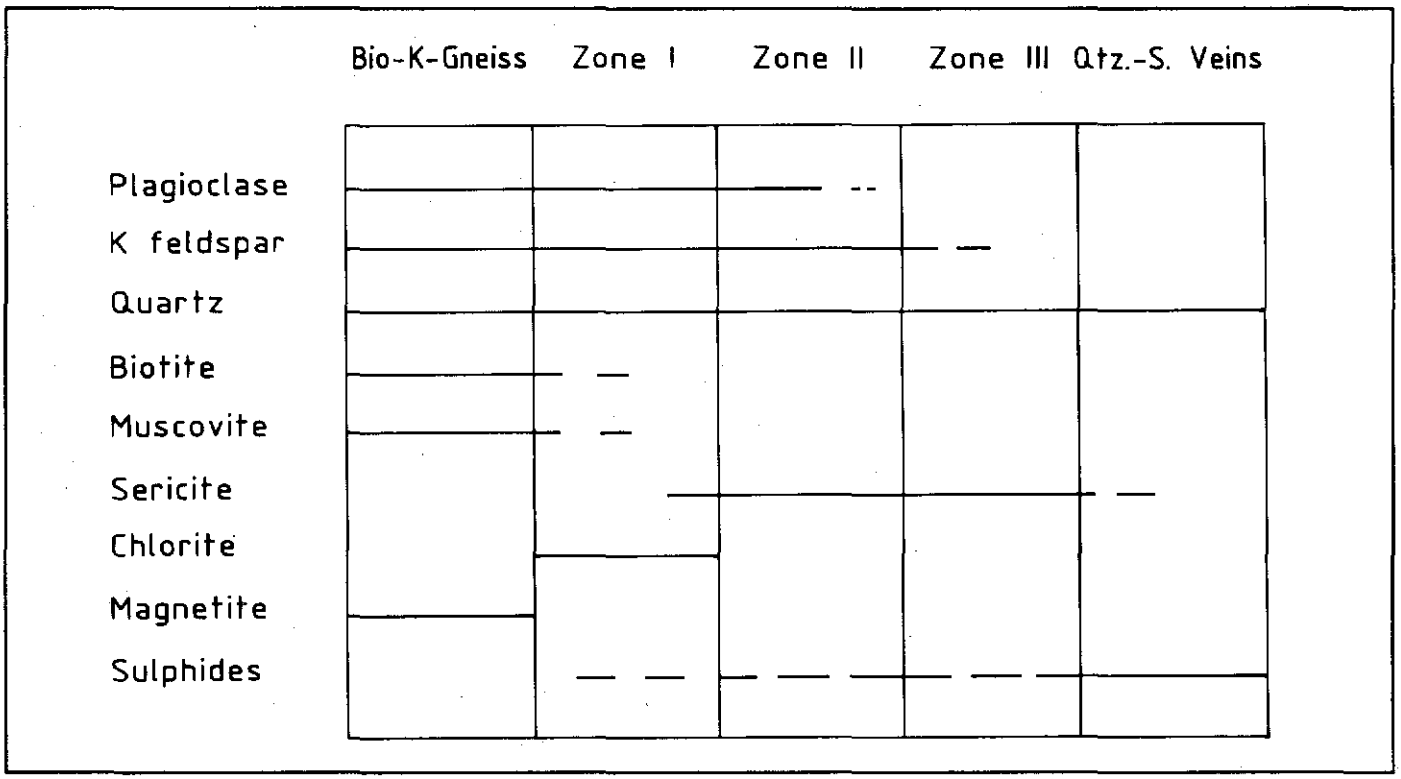

Table 4. Paragenetic sequence and physico-chemical conditions of the gold-bearing mesothermal quartz-carbonate-sulphide veins in the southern area.

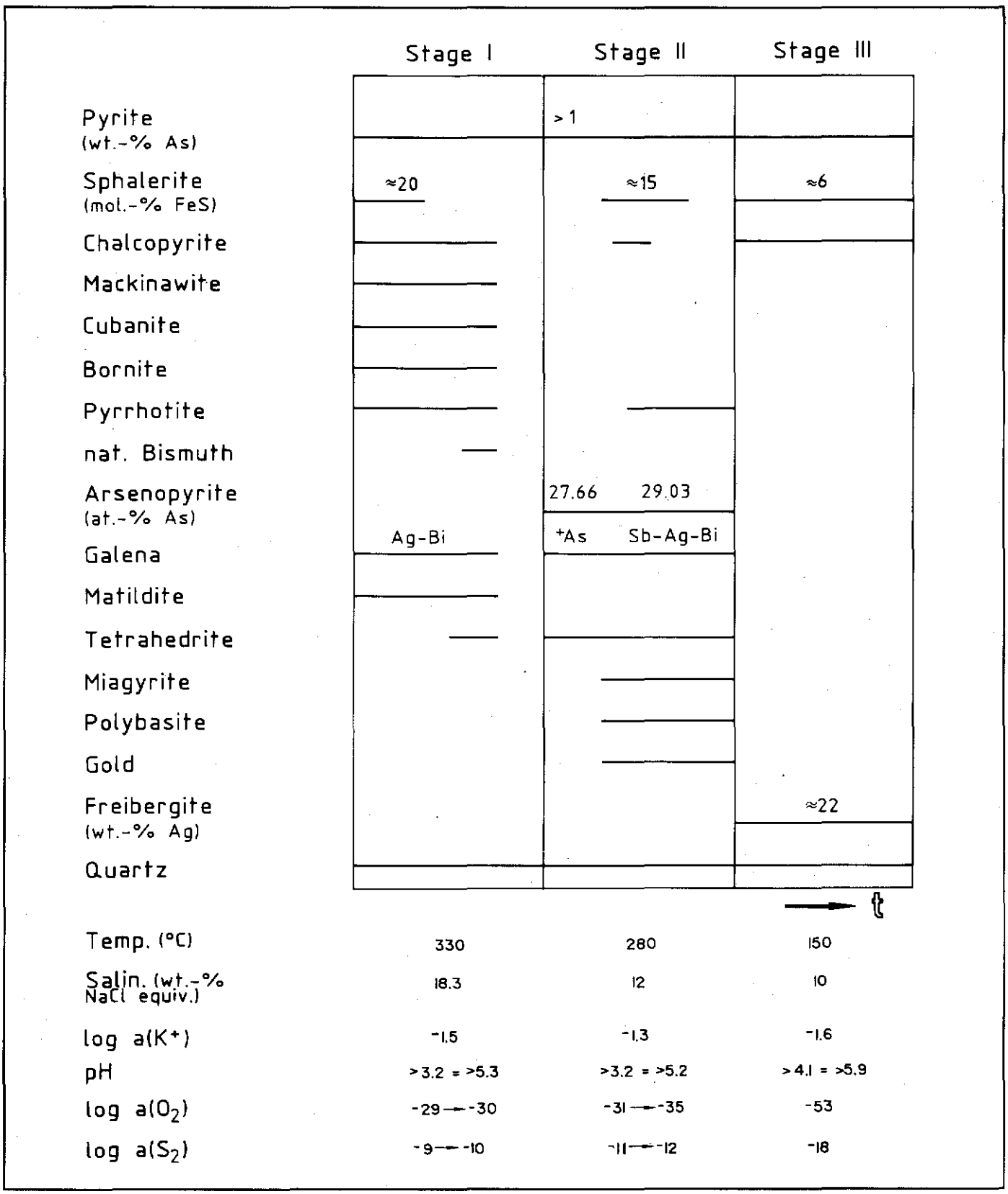

GOLD AND SULPHIDE MINERALIZATION IN THE HUNKER CREEK AREA, YUKON TERRITORY, CANADA

K.-H. Hoymann
&
G. Friedrich

Institute of Mineralogy and Economic Geology
Aachen University of Technology
Wüllnerstr. 2, 5100 Aachen
Aachen, Germany

HOYMANN, K.-H. and FRIEDRICH, G., 1990. Gold and sulphide mineralization in the Hunker Creek area, Yukon Territory, Canada. In Yukon Geology, Vol. 3; Exploration and Geological Services Division, Yukon, Indian and Northern Affairs Canada, p.312-326

ABSTRACT

The Hunker Creek area is located 30 km southeast of Dawson City, Yukon. Gold and sulphide-bearing quartz veins (MINFILE 115O 067,068) crosscut metamorphic rocks of the Klondike Schist. The veins are enclosed by envelopes of sericitic (inner) and propylitic (outer) alteration. Locally, carbonatization occurs between propylitized and sericitized rocks. Three stages of vein mineralization can be distinguished: (I) quartz, carbonates, gold, arsenopyrite, pyrite, pyrrhotite, chalcopyrite, and galena; (II) quartz, carbonates, chalcopyrite, sphalerite, tetrahedrite, freibergite, polybasite, 'polyargyrite', argentite, pyrostilbnite and galena; (III) quartz and gold.

Fluid inclusion data indicate that stage I minerals precipitated from hydrothermal solutions containing CO_2. Homogenization temperatures range from 260° to 390°C. Stage II aqueous fluid inclusions homogenize between 190° and 260°C. Stage III inclusions homogenize between 120° and 210°C. Salinities of the three stages range from 0 to 7.2 wt-% NaCl equiv. and show no significant changes with time.

It is suggested that stage I mineralization was initiated by unmixing of an original single-phase H_2O and CO_2 bearing fluid, and that subsequent hydrothermal evolution was controlled mainly by decreasing temperature.

RÉSUMÉ

La région du ruisseau Hunker est située à 30 km au sud-est de Dawson City (Yukon). Des veines renfermant de l'or et du quartz recoupent le schiste métamorphique de Klondike. Les veines sont entourées d'enveloppes d'altération séricitique (intérieure) et propylitique (extérieure). Par endroits, il y a carbonatation entre les roches séricitisées et les roches propylitisées. Trois stades de minéralisation peuvent être distingués : I) quartz, carbonates, or, arsénopyrite, pyrite, pyrrhotine, chalcopyrite et galène, II) quartz, carbonates, chalcopyrite, sphalérite, tétrahédrite, freibergite, polybasite, «polyargyrite», argentite, pyrostilbnite et galène, III) quartz et or.

Les données sur les inclusions fluides indiquent que les minéraux du stade III ont précipité à partir de solutions hydrothermales renfermant du CO_2. Les températures d'homogénéisation varient de 260 à 390 °C. Les inclusions de fluide aqueux du stade II sont homogénéisées à des températures variant entre 120 et 210 °C. Pour les trois stades les salinités varient entre 0 et 7,2 % d'équivalent de NaCl en poids et ne présentent aucune variation importante en fonction du temps.

Il est suggéré que la minéralisation de stade I a été amorcée par séparation d'un fluide original à une seule phase renfermant H_2O et CO_2 et que l'évolution hydrothermale ultérieure a été principalement déterminée par une température à la baisse.

INTRODUCTION

The Hunker Creek area, located 30 km southeast of Dawson City, is part of the Klondike District (Fig. 1). Gold was discovered here in the late 19th century. The bulk of the gold production was derived from placer deposits. A relatively small amount of exploration was directed toward finding lode sources for the placer gold.

The purpose of this paper is to describe the mineralogy of three gold quartz veins (Mitchell Vein (MINFILE 115O 068a), Sheba Vein, (115O 068b) and Hunker Dome (115O 067) and to present a genetic model for the mineralizing events. The study is based on thin, polished and thick section microscopy, microprobe data, and fluid inclusion investigations.

GEOLOGY

The Hunker Creek area is underlain by metamorphic rocks of the Nasina Series, Klondike Schist, and the Moosehide Assemblage. The three units belong to the Yukon Cataclastic Complex (Tab. 1, Fig. 2). The Nasina Series consists of graphitic schist, graphitic quartzite, siliceous marble, and minor chlorite and muscovite schist. The Klondike Schist is represented by quartz-augen schist, quartz-chlorite-muscovite schist and muscovite schist. The metamorphic grade of the rocks ranges from upper greenschist to middle amphibolite facies (Mortensen, 1990). Mylonitic serpentinite, amphibolite, and chlorite and talc schist of the Moosehide Assemblage overlie the Klondike Schist. Tempelman-Kluit (1979, 1981) correlated this unit with the Anvil Allochthonous Assemblage, a sheared ophiolite sequence. Shear zones are developed between the Nasina Series, Klondike Schist and Moosehide Assemblage (Metcalfe and Clarke, 1983; Mortensen, 1990).

Younger intermediate andesites and their equivalents occur in outcrops along Last Chance Creek. They do not show any indications of major tectonic deformation. According to Debicki (1984, 1985), these volcanic rocks can be correlated with the Carmacks Group volcanic suite. Felsic tuffs, monolithic and heterolithic felsic breccias (Skukum Group), and miarolitic quartz-feldspar porphyry (Nisling Range Alaskite) are of Eocene age (Debicki, 1984). The bedrock is covered by Pleistocene alluvial gravels.

MINERALIZATION

The steeply dipping, northwest striking Mitchell Vein (MINFILE 115O 068A) has an exposed length of about 100 m, an average thickness of 30 cm and an explored depth of about 25 m. The Sheba Vein, (MINFILE 115O 068b) is up to 1 m thick in surface exposures. It is located 850 m south of the Michell Vein and dips steeply to the northeast. At Hunker Dome (MINFILE 115O 067), quartz veins are highly variable in thickness to a maximum of 60 cm. The veins dip steeply to the east or west. Tectonic relationships indicate that the three veins formed during the same mineralizing event.

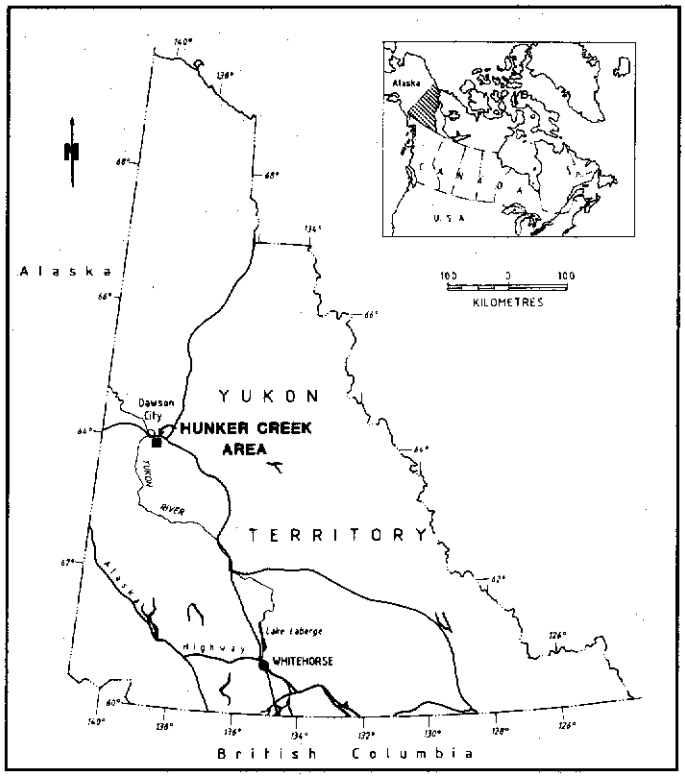

Figure 1. Location map of the Hunker Creek area.

Gold

Three different types of gold have been observed: (1) Inclusions of gold (<0.01mm) with a mean silver content of 17.58 wt-% occur in pyrite from Mitchell Vein (Fig. 3, Tab. 2). (2) Macroscopic visible gold containing small pyrite inclusions was found in quartz from Hunker Dome vein (Fig. 4). This type of gold has mean silver and tellurium contents of 12.74 wt-% and 0.08 wt-%, respectively. (3) Gold intergrown with galena from a Hunker Dome quartz vein (Fig. 5) contains high silver, averaging 22.07 wt-% (Tab. 2).

Silver

Silver-bearing minerals include tetrahedrite-tennantite group minerals, sulphosalts and galena.

Tetrahedrite-tennantite group minerals found in the Hunker Creek area are freibergite, arsenic-bearing freibergite, and arsenic-bearing tetrahedrite. Freibergite and tetrahedrite are characterized by highly variable iron, zinc and cadmium contents (Fig. 6). Freibergite and tetrahedrite intergrown with sphalerite have low zinc and cadmium (Fig. 7). Except for arsenic-bearing freibergite, there is a strong positive correlation between antimony and silver in freibergite and tetrahedrite (Fig. 8).

Freibergite inclusions are often myrmekitically intergrown with galena. This feature indicates dissolution processes along grain boundaries as described by Ramdohr (1980). Freibergite is also intergrown with pyrite, chalcopyrite, sphalerite,

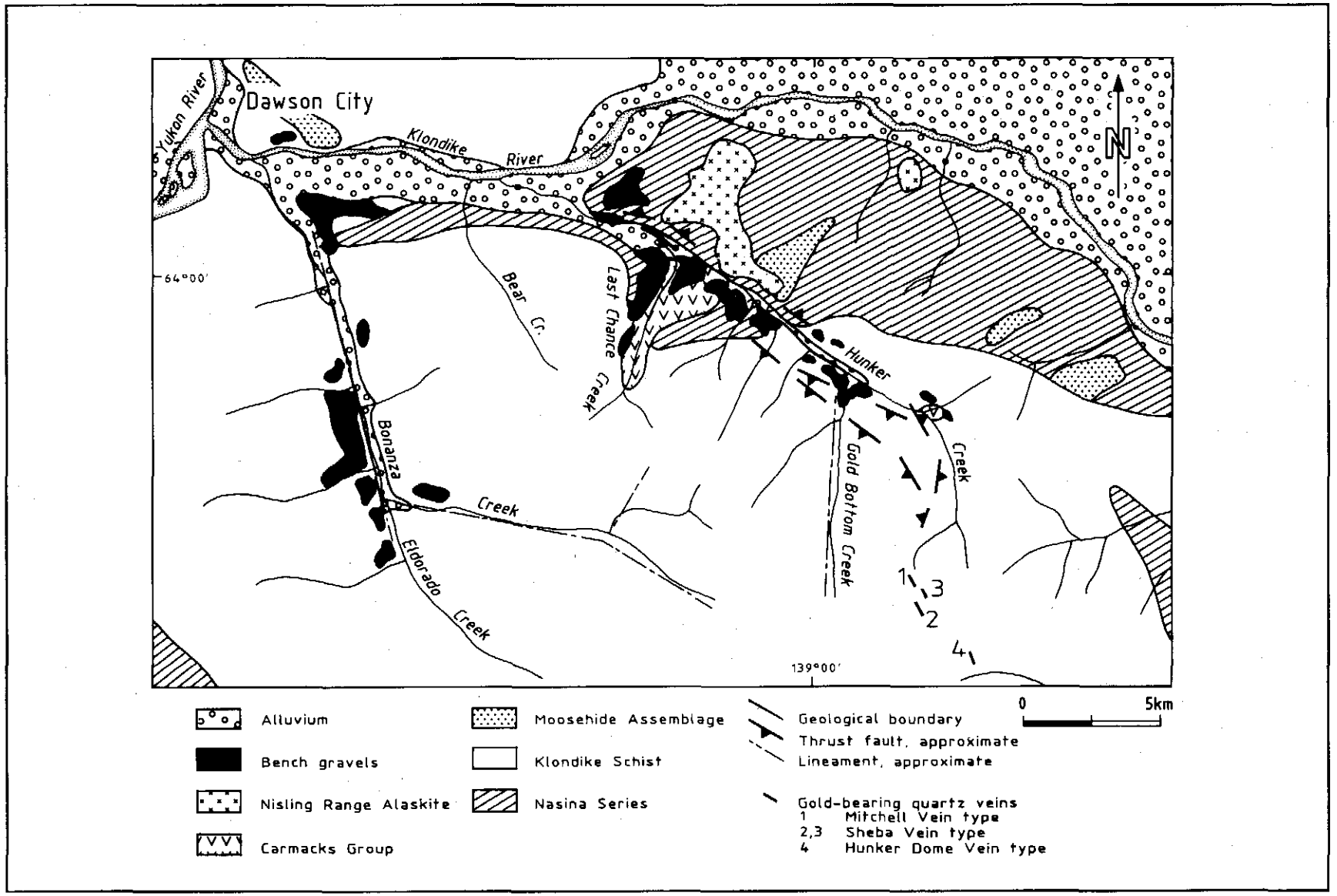

Figure 2. Bedrock geology of the Klondike area (modified after Bostock, 1942; Boyle, 1979, 1987; Debicki, 1984 and 1985, and Dufresne, 1987).

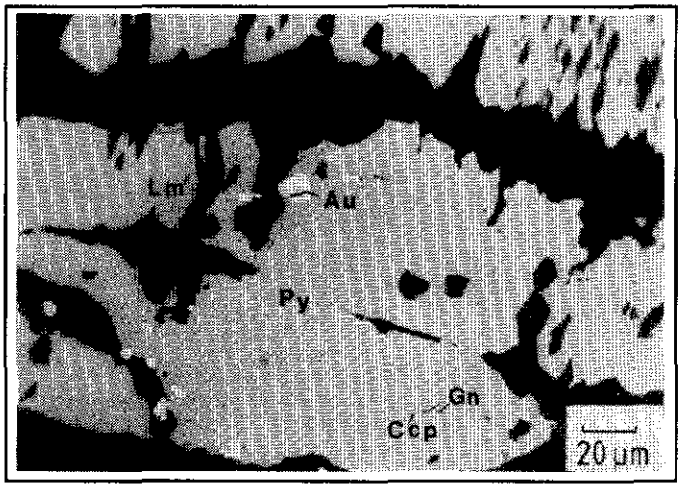

Figure 3. Minute anhedral chalcopyrite (Ccp), galena (Gn) and gold (Au) inclusions within pyrite (Py) which is partly replaced by limonite (Lm): Mitchell Vein.

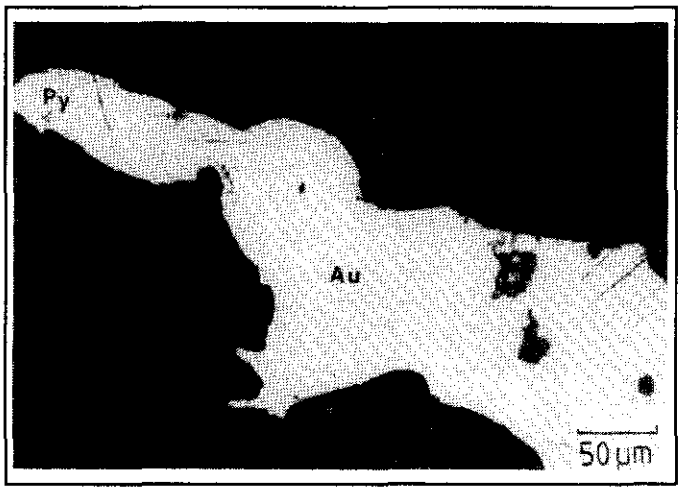

Figure 4. Irregular-shaped gold grain (Au) with anhedral pyrite (Py) inclusions in quartz matrix: Hunker Dome.

polybasite, argentite and 'polyargyrite' and contains rounded inclusions of galena and argentite (Fig. 9). Fractures within euhedral pyrite are partly healed by freibergite which is coated by galena. Freibergite contains high amounts of copper, silver, antimony and cadmium (Tab. 3).

Arsenic-bearing freibergite (<0.03mm) is often intergrown with chalcopyrite and sphalerite and also occurs in galena. Its chemical composition as shown in Table 3 differs from the above-mentioned freibergite: the average arsenic content is 3.68 wt%, the copper, sulphur, iron and zinc contents are higher, and silver and antimony are lower.

Arsenic-bearing tetrahedrite (<3mm) was found only as inclusions in galena from Vein 3 of the Sheba Vein system. It is intergrown with chalcopyrite, sphalerite and subhedral arsenopyrite (Fig. 10), and contains more copper and arsenic,

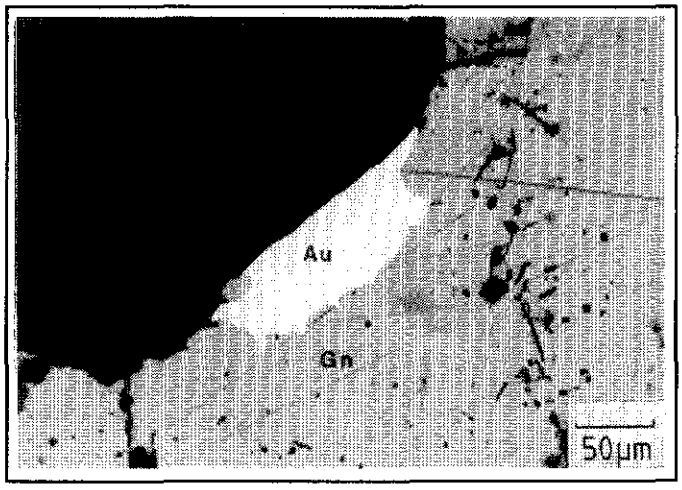

Figure 5. Anhedral gold (Au) intergrown with galena (Gn) in quartz (black): Hunker Dome.

and less silver than the freibergites (Tab. 3).

Sulphosalts like polybasite, 'polyargyrite', pyrostilbnite, and argentite are intimately intergrown with and occur as tiny inclusions in galena. Intergrowths with freibergite (Fig. 9), pyrite, coarse-grained chalcopyrite and sphalerite have also been observed. The term 'polyargyrite' is used in the sense of Dana and Dana (1946) and Strunz (1977) who describe 'polyargyrite' as a submicrosopic intergrowth between pyrargyrite and polybasite or argentite and tetrahedrite.

Galena from the Mitchell Vein is intergrown with pyrrhotite and chalcopyrite. All three sulphides form inclusions in pyrite. The small galena inclusions contain an average of 0.5 weight per cent silver. Coarse-grained, euhedral to anhedral galena occurs at Sheba Vein, Vein 3, and at Hunker Dome. It contains euhedral pyrite and arsenopyrite, anhedral chalcopyrite, sphalerite, freibergite, tetrahedrite, polybasite, 'polyargyrite', argentite, and pyrostilbnite. The mean silver content is 0.2 wt-%.

Arsenopyrite occurs as subhedral inclusions (<0.03mm) in pyrite and as cataclastic single grains (<0.08mm) intergrown with coarse-grained chalcopyrite, arsenic-bearing tetrahedrite, and galena. Cataclastic arsenopyrite is partly replaced by chalcopyrite, sphalerite, and galena.

Euhedral pyrite from veins contains rounded inclusions of anhedral gold, pyrrhotite, chalcopyrite, galena, and arsenopyrite. Pyrite from wall rock has inclusions of pyrrhotite, chalcopyrite, galena, quartz, anhedral rutile, and carbonate. Microprobe analyses do not reveal any differences between pyrite from vein quartz or wall rock. Pyrite from Sheba Vein and Hunker Dome is fractured and healed by chalcopyrite, sphalerite, tetrahedrite, freibergite, galena, and quartz.

Chalcopyrite occurs intergrown with pyrrhotite and galena as inclusions in pyrite. Coarse-grained chalcopyrite contains grains of euhedral pyrite (<0.08mm), arsenopyrite and anhedral arsenic-bearing tetrahedrite, and is intergrown with galena, sphalerite and freibergite. Chalcopyrite also occurs in

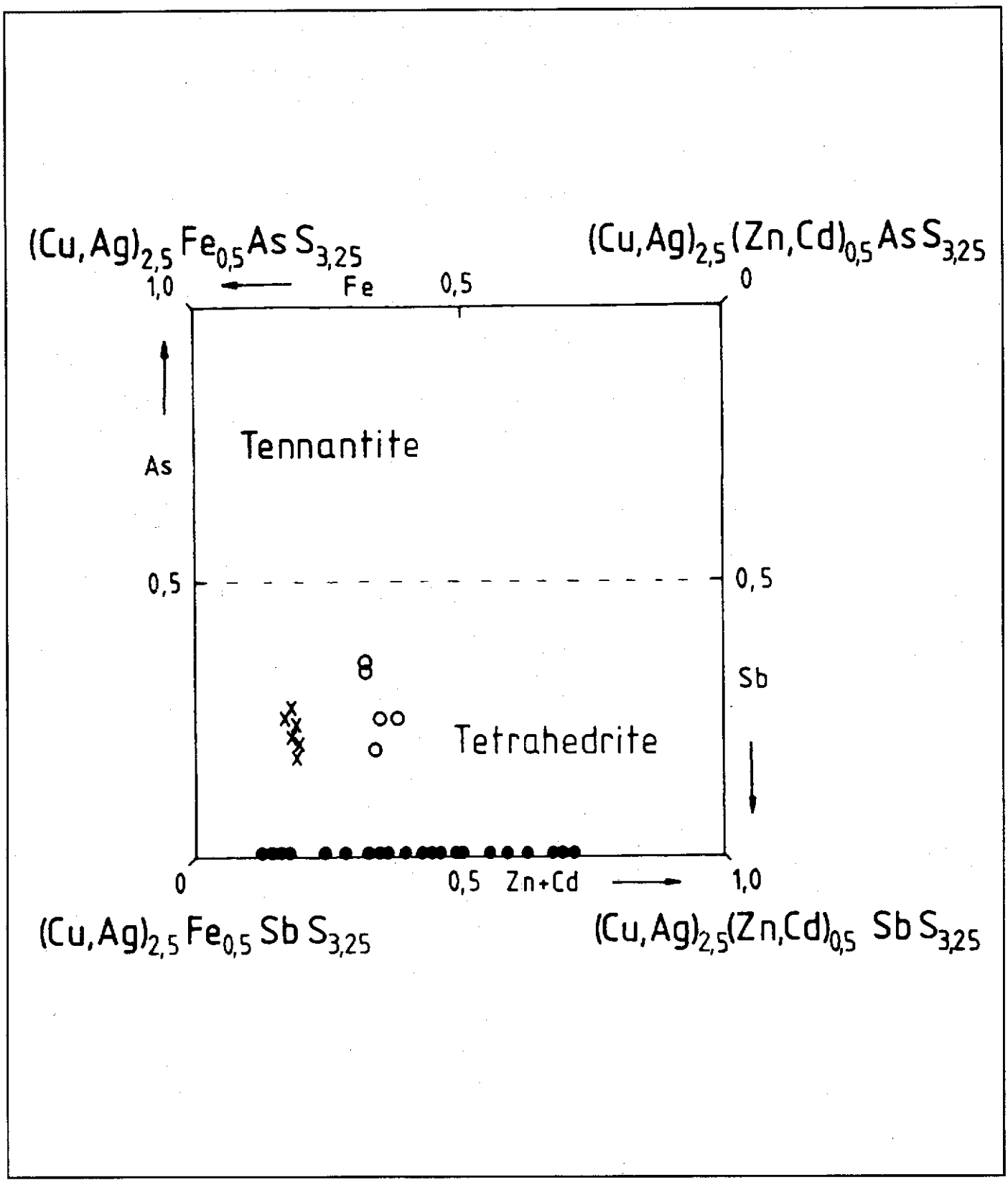

Figure 6. Composition of tetrahedrite-tennantite group minerals from Hunker Dome and Sheba Vein; freibergite = solid circles, arsenic-bearing freibergite = crosses, arsenic-bearing tetrahedrite = open circles (tennantite-tetrahedrite diagram, modified after Springer, 1969).

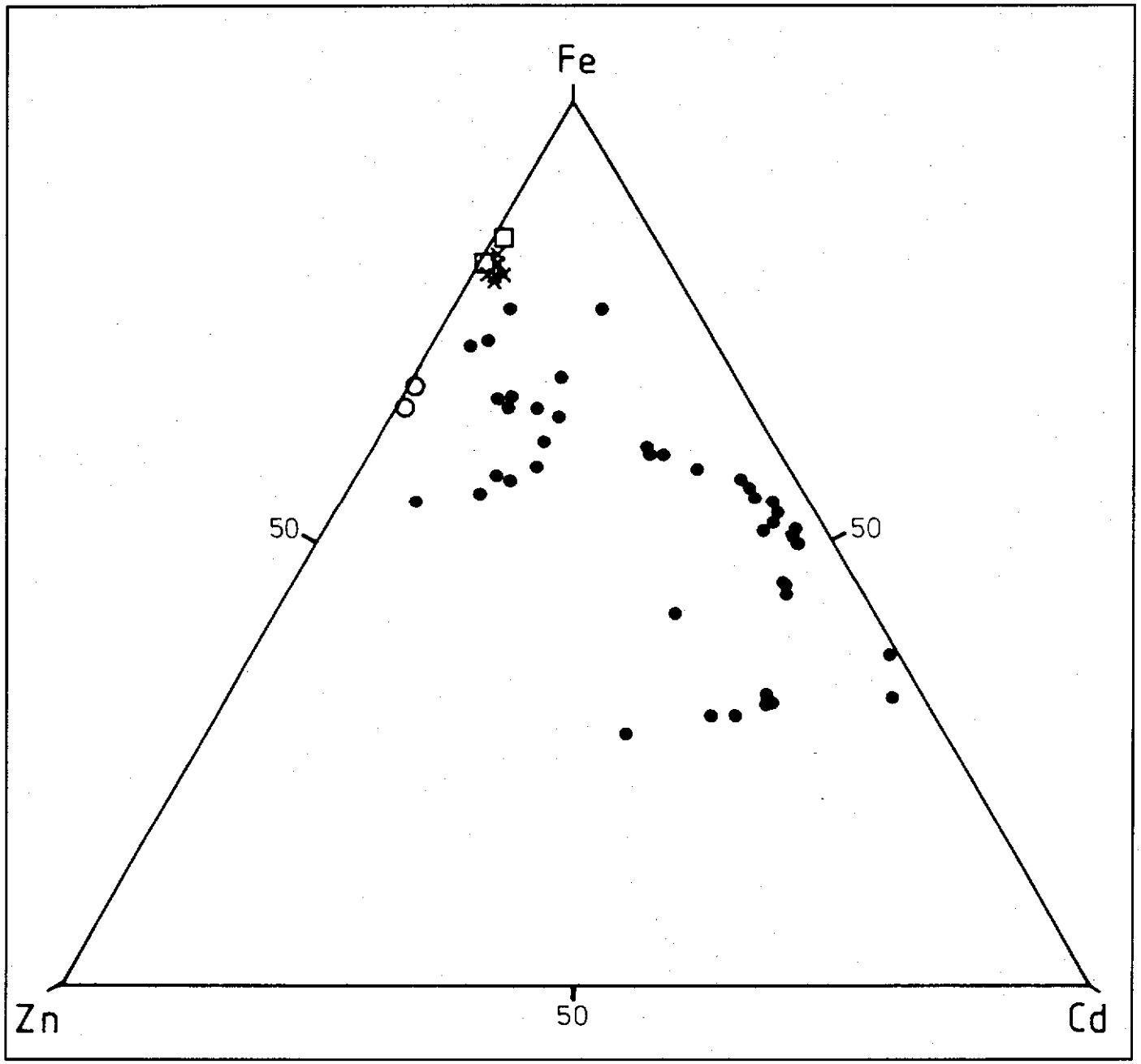

Figure 7. Relative portions of iron, zinc and cadmium (at-%) in tetrahedrite-tennantite group minerals from Hunker Dome and Sheba Vein; solid circles = freibergite not intergrown with sphalerite, open squares = freibergite intergrown with sphalerite, crosses = arsenic-bearing freibergite intergrown with sphalerite, and open circles = arsenic-bearing tetrahedrite intergrown with sphalerite.

galena as coatings on subhedral pyrite and euhedral arsenopyrite crystals. Microprobe analyses indicate no differences between the trace element content of coarse-grained chalcopyrite and the rounded chalcopyrite inclusions in pyrite.

Sphalerite (<3mm) is generally intergrown with arsenopyrite, freibergite, chalcopyrite, and tetrahedrite. Sometimes sphalerite contains drop-shaped chalcopyrite inclusions, and has grown onto subhedral pyrite crystals enclosed by galena. Rounded chalcopyrite inclusions in sphalerite are interpreted as 'chalcopyrite disease' in the sense of Barton (1978).

Limonite, which formed from pyrite as a result of supergene processes, partly contains relict gold grains. Cerussite and finely disseminated covellite occur along fractures in galena. Covellite replacing chalcopyrite, freibergite and tetrahedrite contains up to 0.5 wt-% Ag.

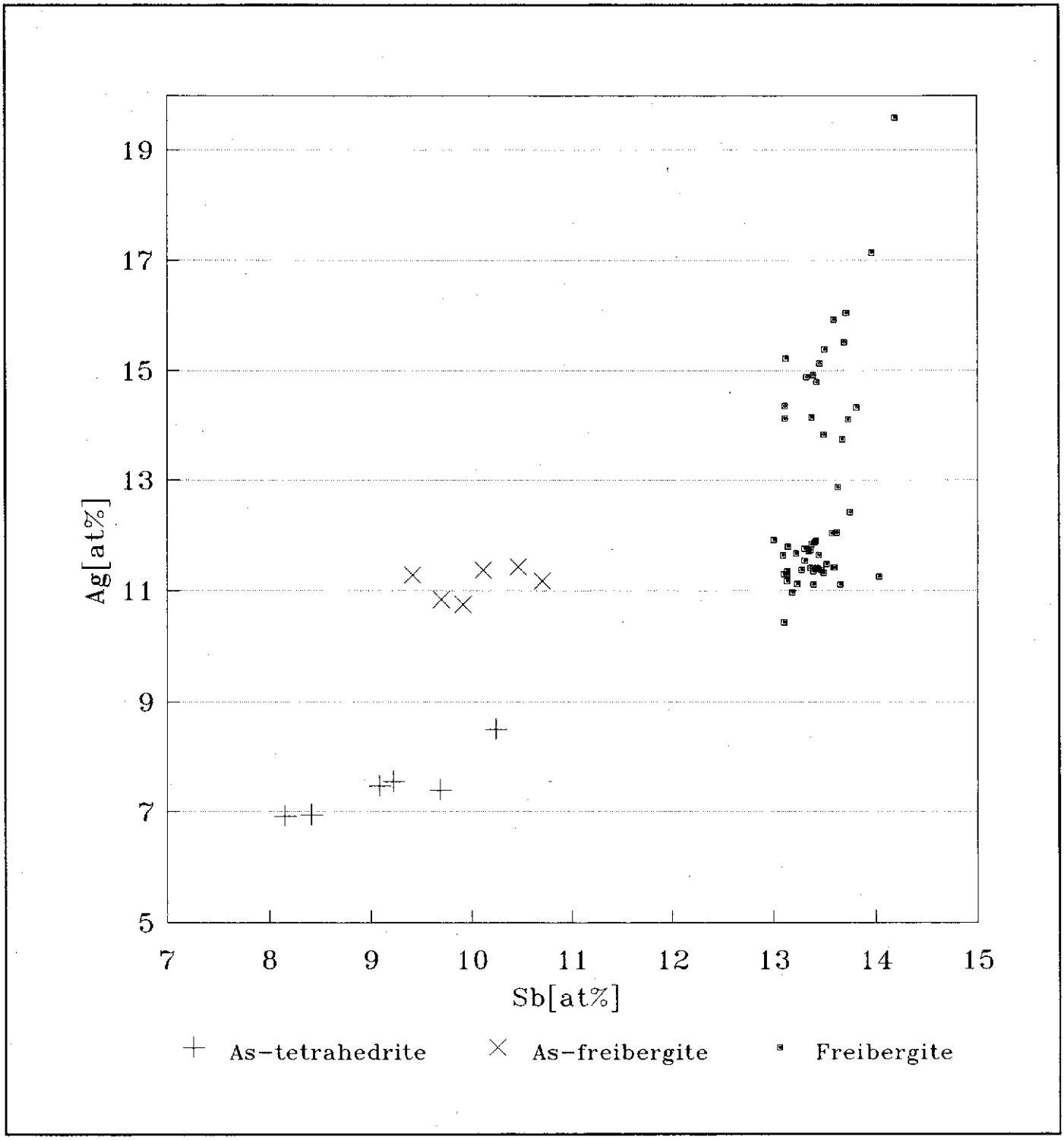

Figure 8. Relationship between silver and antimony (at-%) in tetrahedrite and freibergite from gold-bearing quartz veins; Hunker Dome and Sheba veins.

PARAGENETIC SEQUENCE

Three stages of mineralization are recognized (Fig. 11). Stage I was observed in the Mitchell, Sheba and Hunker Dome veins, and is characterized by the precipitation of arsenopyrite, pyrite, pyrrhotite, chalcopyrite, galena, and gold. Rutile and carbonate form inclusions in pyrite of the wall rock.

Stage II mineralization is developed in the Sheba Vein and at Hunker Dome. The paragenesis consists of chalcopyrite,

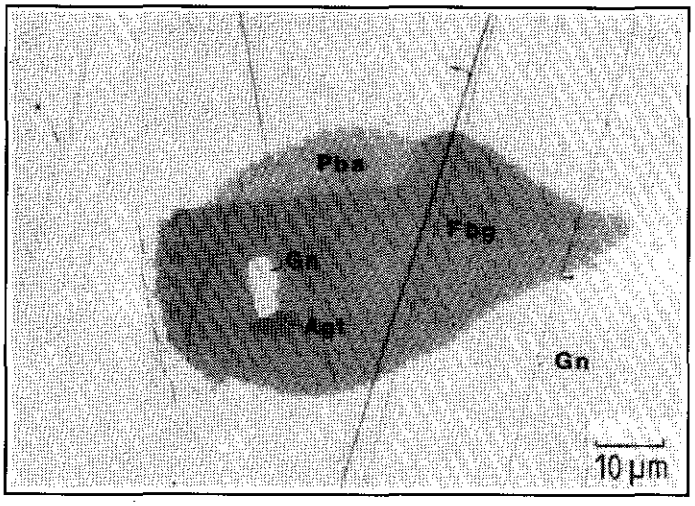

Figure 9. Sheba Vein: anhedral freibergite (Fbg) and polybasite (Pba) with inclusions of galena (Gn), and argentite (Agt) surrounded by galena.

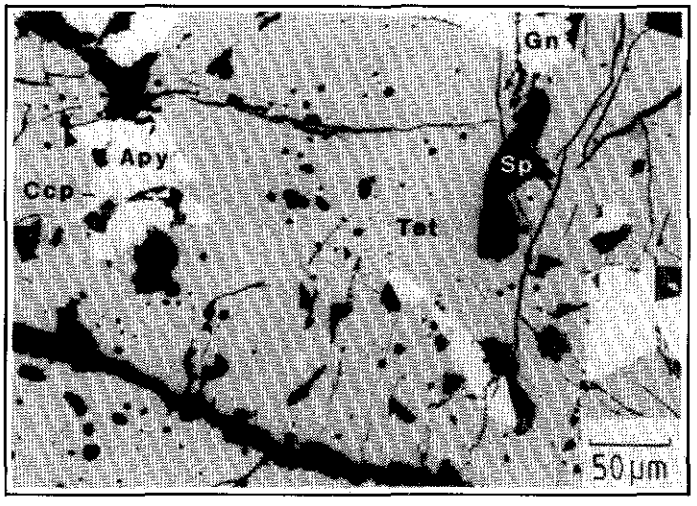

Figure 10. Coarse-grained, arsenic-bearing tetrahedrite (Tet) containing subhedral arsenopyrite (Apy), anhedral chalcopyrite (Ccp), and sphalerite (Sp). Galena (Gn) is the host of this mineral assemblage: Vein (3).

sphalerite, tetrahedrite, freibergite, polybasite, 'polyargyrite', argentite, pyrostilbnite, and galena. Coarse-grained sphalerite, tetrahedrite, chalcopyrite and freibergite of stage II replace pyrite and arsenopyrite of stage I. Coarse-grained chalcopyrite, sphalerite, and arsenic-bearing tetrahedrite are rimmed and partly enclosed by freibergite, polybasite, 'polyargyrite', and argentite. Remaining voids are filled by galena, the youngest mineral phase of stage II.

During Stage III, which was observed only in a quartz vein at Hunker Dome, silver-rich gold intergrown with galena was formed. Quartz is abundant in all three stages.

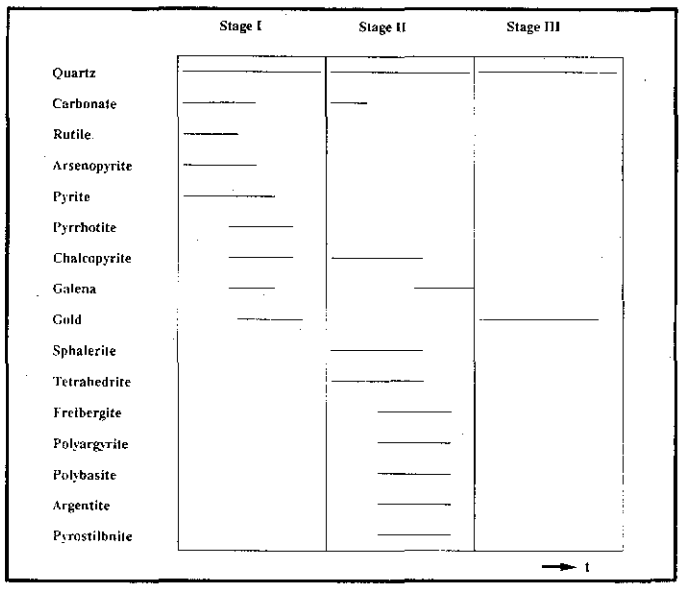

Figure 11. Paragenetic sequence of gold-sulphide mineralization: Mitchell Vein, Sheba Vein and Hunker Dome.

WALL ROCK ALTERATION

Gold-bearing quartz veins are surrounded by a distinct alteration envelope, consisting of an inner zone of sericitization which grades outward into a propylitic zone. A more intensive carbonatization is occasionally developed between the outer propylitic and inner sericitic zone. The alteration envelope ranges up to about 2 m in thickness. The inner zone is characterized by sericite/phengite, quartz and minor amounts of euhedral to subhedral pyrite which contains inclusions of mica, chlorite and quartz. Sericite/phengite micas replace plagioclase, muscovite and chlorite. The propylitic zone contains mainly chlorite, epidote and plagioclase. Muscovite, secondary quartz, and carbonates like calcite/dolomite, occur in smaller amounts. In the carbonate zone, secondary quartz and carbonates replace plagioclase, muscovite and chlorite.

MICROTHERMOMETRIC STUDY

Fluid inclusion studies were carried out in order to relate the paragenetic sequence to the evolution of the hydrothermal fluids. Investigations focused on vein quartz with several different habits: clear and euhedral, milky and brittle, cataclastic, and late stage quartz. Fluid inclusion data confirmed the three stages of mineralization established by microscopic observations.

Stage I: Two phase H_20-bearing fluid inclusions, as well as three phase H_20 and $C0_2$-bearing inclusions, were identified to be of primary origin due to their spatial distrubution in quartz grains. Homogenization temperatures range from 260° to 390° C with a maximum at about 300° ± 40°C (Fig. 12). Melting of frozen $C0_2$ occurs between -60.2° and -56.6° C.

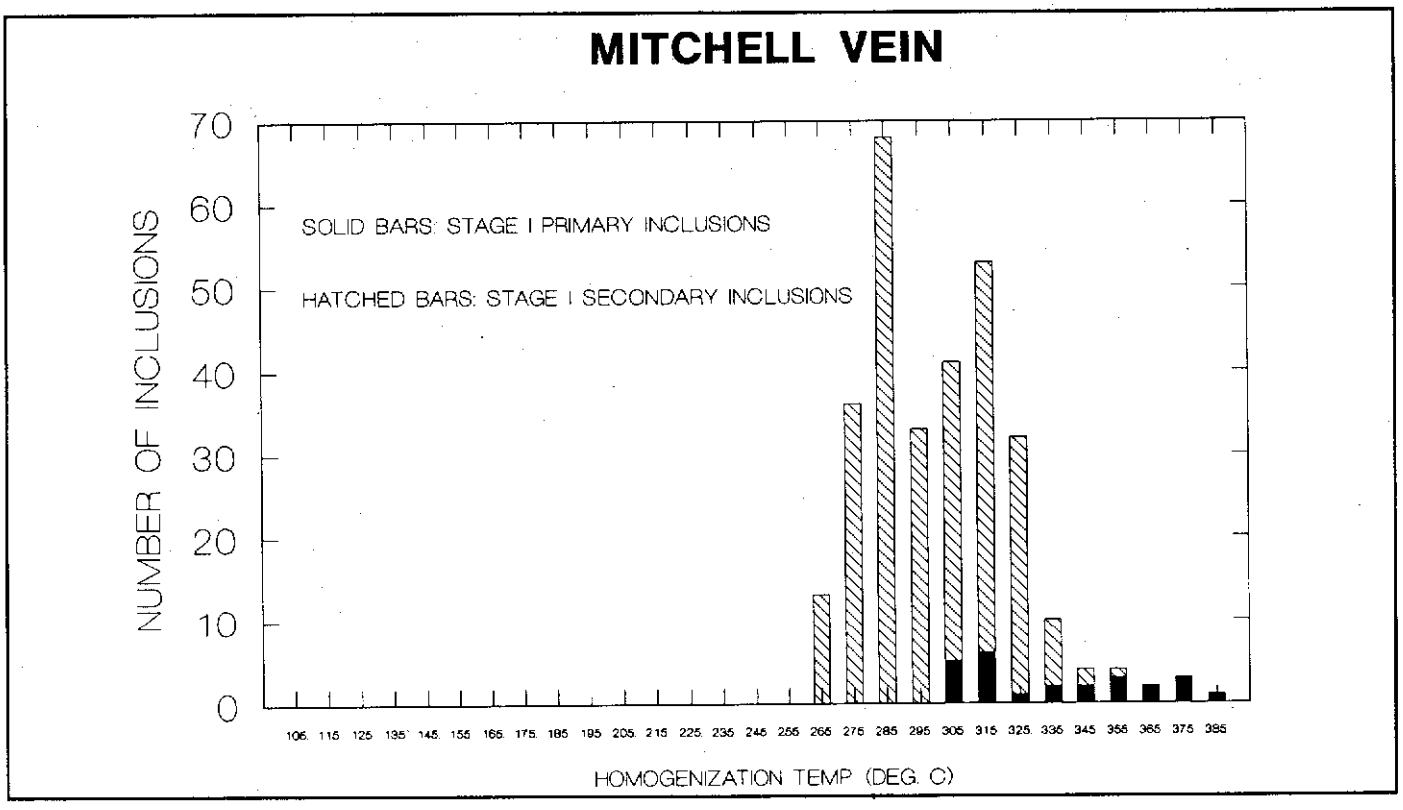

Figure 12. Histogram showing frequency distribution of homogenization temperatures for stage I inclusions in quartz: Mitchell Vein.

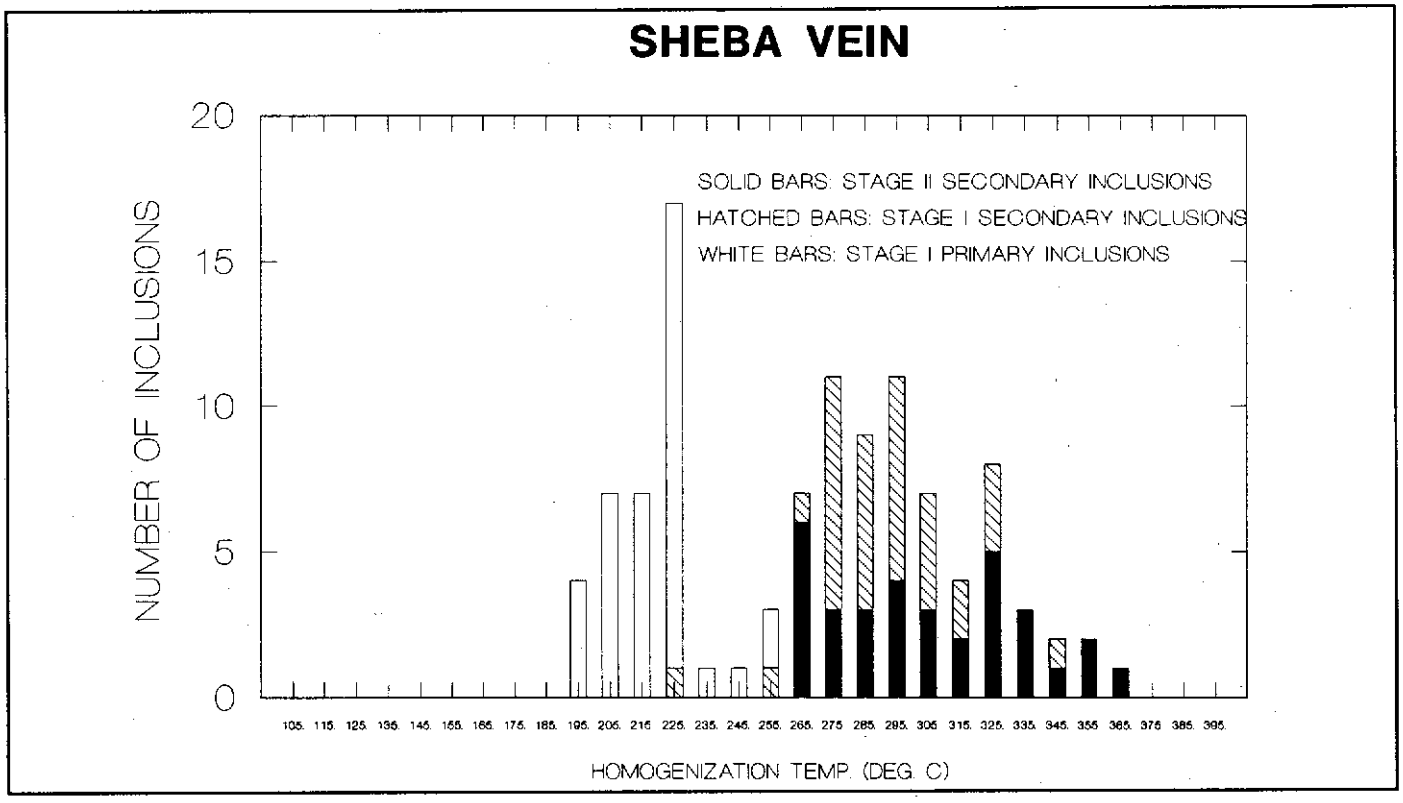

Figure 13. Histogram showing frequency distribution of homogenization temperatures for stage I and II inclusions in quartz: Sheba Vein.

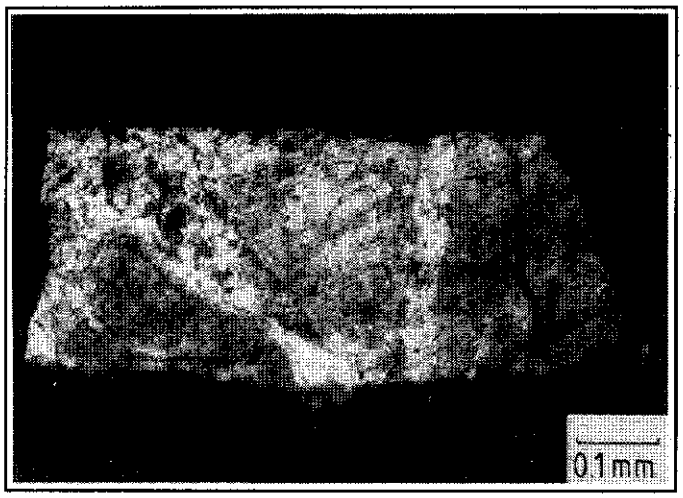

Figure 14. Earlier cataclastic quartz relics (medium to dark grey) healed by late, fine-grained quartz (white): Hunker Dome.

The deviation from the melting point of pure $C0_2$ (-56.6°C) is evidence of the presence of gases like CH_4 or H_2S (Hollister and Crawford, 1981). Melting point measurements of the aqueous phase show salinities ranging from 0 to 7.2 wt-% NaCl equivalent. Secondary fluid inclusions of stage I occurring along microfractures are similar to primary inclusions with respect to their phase relationships and fluid characteristics. Stage I primary and secondary inclusions are observed in all veins.

Stage II: Another type of secondary, H_20-bearing fluid inclusion was identified in quartz from Sheba Vein (Fig. 13). Homogenization temperatures are significantly lower than for stage I fluid inclusions and vary from 190° to 260° C. Indicated salinity values are scattered between 1.5 and 5.7 wt-% NaCl equivalent.

Stage III: Aqueous fluid inclusions of stage III were observed only in late stage quartz at Hunker Dome. While fluid inclusions representing all stages of mineralization are present in quartz clasts, stage III inclusions occur only in quartz cement healing cataclastic vein quartz (Fig. 14). Homogenization temperatures of stage III inclusions range from 120° to 210°C with a maximum at about 170°C (Fig. 15). Last melting of ice occurs between -0.2° and -2.5°C corresponding to salinities between 0.4 and 4.2 wt-% NaCl equivalent.

Eutectic melting of ice was observed between -28° and -38°C in inclusions representing all three stages. This can be explained by the presence of a variety of dissolved salts, among which NaCl, KCl, $MgCl_2$, Na_2C0_3, and $NaHC0_3$ are the most important (Shepherd et al., 1985; Leeder et al., 1987).

SUMMARY AND CONCLUSIONS

The gold-bearing quartz vein system in the Hunker Creek area is an excellent example of the relationship between mineralizing events and changes in the evolution of hydrothermal fluids. Three stages of mineralization recognized in the Mitchell (Stage I only), Sheba (stages I & II) and Hunker Dome (Stages I, II and III) veins are related to three generations of fluid inclusions (Fig. 16).

During stage I (gold, arsenopyrite, pyrite, pyrrhotite, chalcopyrite, rutile, quartz and minor carbonates), H_20-rich and aqueous $C0_2$-bearing fluids with homogenization temperatures of 300° ± 40°C and salinities between 0 to 7.2 wt-% NaCl equiv. were involved.

Stage II mineralization consists of chalcopyrite, sphalerite, tetrahedrite, freibergite, 'polyargyrite', argentite, pyrostilbnite, galena, quartz, and accessory carbonate. Fluid homogenization temperatures are 230 ± 40°C and salinities range from 1.5 to 5.7 wt-% NaCl equivalent.

Fluid inclusions formed during late stage III mineralization homogenize at 170° ± 40°C. Salinities of hydrothermal fluids range from 0.4 to 4.2 wt-% NaCl equivalent.

The sericite/phengite alteration around the gold-sulphide-quartz veins indicates slightly acid conditions (pH = 5 ± 1) during the mineralizing events (Hayba et al., 1985; Henley et al., 1984). The sulphide-sulphosalt mineral paragenesis suggests that reduced sulphur was abundant in the hydrothermal fluids. The abundance of sulphur, reducing conditions during gold deposition, and homogenization temperatures (minimum formation temperatures), at and far below 300°C imply that gold was been transported either as a bisulphide (Henley, 1973; Seward, 1973; Huston and Large, 1989) or as a sulpharsenide complex (Boyle, 1979).

The following model of the mineralization process is consistent with the petrographic and fluid inclusion data: gold deposition was initiated by unmixing of an original one phase H_20 and $C0_2$- bearing fluid accompanying a drop in pressure and temperature. The loss of $C0_2$ caused an increase in pH and a decrease in the bisulphide concentration in the aqueous phase, favouring the formation of sulphides and the precipitation of gold. Subsequent mineralization processes were mainly influenced by decreasing temperature of the hydrothermal fluid.

ACKNOWLEDGEMENTS

This study results from the Canada/Germany Science and Technology Exchange Agreement organized by the Geological Survey of Canada and the Federal Institute for Geosciences and Mineral Resources (BGR) in Germany. Financial support was granted by the German Ministry of Research and Technology and by the Exploration and Geological Services Division of the Department of Indian and Northern Affairs, Whitehorse, Yukon. We also acknowledge cooperation and support from United Keno Hill Mines Limited, particularly D. Prince and J. McFaull. Thanks are extended to H. Liedtke and J. Erikson for the permission to visit their prospects. The cooperation of J. Morin, G. Abbott and U. Glasmacher is greatly appreciated. This paper greatly benefited from discussions with P. Sänger von Oepen and P. Herzig.

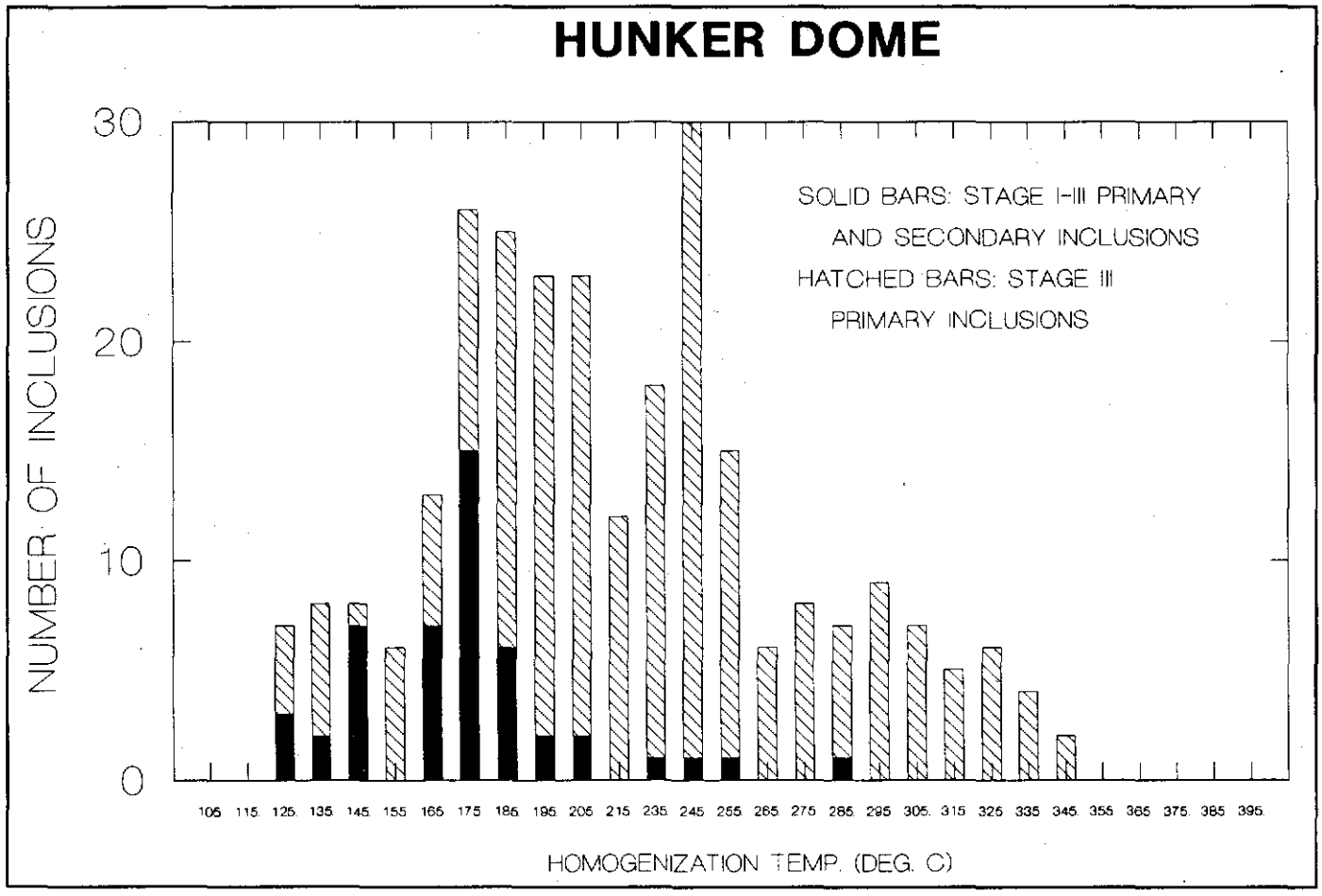

Figure 15. Histogram showing frequency distribution of homogenization temperatures for stage I, II and III inclusions in quartz: Hunker Dome.

	Stage I	Stage II	Stage III
Homog. Temp.(°C):	260-390	190-360	120-210
Salinity (wt% NaCl eq.):	0-7.2	1.5-5.7	0.4-4.2
Mitchell Vein	———		
Sheba Vein	———	———	
Hunker Dome	———	———	———
			Increasing Temperature →

Figure 16. Mineralization stages and fluid inclusion data for gold-sulphide mineralization: Mitchell, Sheba and Hunker Dome veins.

REFERENCES

ARMSTRONG, R.L., 1988. Mesozoic and early Cenozoic magmatic evolution of the Canadian Cordillera. Geological Society of America, Special Paper 218, p. 55-91.

BARTON, P.B., Jr., 1978. Some ore textures involving sphalerite from the Furutobe mine, Akita Prefecture, Japan. Mining Geology, Vol. 28, p. 293-300.

BOSTOCK, H.S., 1942. Ogilvie Map-Sheet. Geological Survey of Canada, Map 711 A.

BOYLE, R.W., 1979. The geochemistry of gold and its deposits. Geological Survey of Canada, Bulletin 280, p. 584.

BOYLE, R.W., 1987. Gold; History and Genesis of Deposits. Van Nostrand Reinhold Company, New York, p. 676.

DANA, J.D., and DANA, E.S., 1946. The System of Mineralogy. 7th ed., Vol.1, John Wiley and Sons, Inc., London, p. 834.

DEBICKI, R.L., 1984. Bedrock geology and mineralization of the Klondike area (west); 115 O/14, 15 and 116 B/2,3. 1:50 000 scale map with marginal notes. Exploration and Geological Services Division, Yukon, Indian and Northern Affairs Canada, Open File 1984-3.

DEBICKI, R.L., 1985. Bedrock geology and mineralization of the Klondike area (east); 115 O/9,10,11,14,15,16 and 116 B/2. 1:50 000 scale map with marginal notes. Exploration and Geological Services Division, Yukon, Indian and Northern Affairs Canada, Open File 1985-1.

DUFRESNE, M.B., 1987. Origin of gold in the white channel sediments of the Klondike Region, Yukon Territory. Unpublished M.Sc. thesis, University of Alberta, Edmonton, p. 181.

GREEN, L.H., and RODDICK, J.A., 1962. Dawson, Larsen Creek and Nash Creek map areas, Yukon Territory. Geological Survey of Canada, Paper 62-7, p. 19.

HAYBA, D.O., BETHKE, P.M., HEALD, P., FOLEY, N.K., (1985). Geologic, mineralogic, and geochemical characteristics of volcanic hosted epithermal precious-metal deposits. In: Geology and Geochemistry of Epithermal Systems, Berger, B.R. and Bethke, P.M.(eds.); Society of Economic Geologists, Reviews in Economic Geology, Vol.2, p. 129-167.

HENLEY, R.W., 1973. Solubility of gold in hydrothermal chloride solutions. Chemical Geology, Vol. 11, p. 73-87.

HENLEY, R.W., TRUESDELL, A.H., BARTON, Jr., P.B., 1984p. Fluid-mineral equilibria in hydrothermal systems. Reviews in Economic geology, Vol.1, p. 267.

HOLLISTER, L.S. and CRAWFORD, M.L., 1981. Fluid inclusions; applications to petrography. Mineral Association of Canada, Short Course Handbook, Vol. 6, p. 304.

HTOON, M., 1979. Geology of the Clinton Creek asbestos deposit, Yukon Territory. Unpublished M.Sc. thesis, University of British Columbia, Vancouver, p. 194.

HUSTON, D.L., LARGE, R.R., 1989. A chemical model for the concentration of gold in volcanogenic massive sulphide deposits. Ore Geology Reviews, Vol. 4, p. 171-200.

LEEDER, D., THOMAS, R., and KLEMM, W., 1987. Einschlusse in Mineralien. VEB Deutscher Verlag für Grundstoffindustrie, Leipzig, p. 180.

METCALFE, P. and CLARK, G.S., 1983. Rb-Sr whole-rock age of the Klondike Schist, Yukon Territory. Canadian Journal of Earth Sciences, Vol. 20, p. 886-891.

MORTENSEN, J., 1990. Bedrock Geology and U-Pb Geochronology of the Klondike District, West-Central Yukon Territory. Canadian Journal of Earth Sciences, Vol. 27, p. 903-914.

RAMDOHR, P., 1980. The ore minerals and their intergrowths. 2nd edition, Pergamon Press, Oxford, p. 1205.

SEWARD, T.M., 1973. Thio-complexes of gold and the transport of gold in hydrothermal ore solutions. Geochimica et Cosmochimica Acta, Vol. 37, p. 379-399.

SHEPHERD, T.J., RANKIN, A.H., and ALDERTON, D.H.M., 1985. A practical guide to fluid inclusion studiesp. Blackie & Son Ltd, Glasgow, p. 239.

SPRINGER, G., 1969. Electron probe analyses of tetrahedrite. Neues Jahrbuch der Mineralogie, p. 24-32.

STRUNZ, H., 1977. Mineralogische Tabellen. Akademische Verlagsgesellschaft, Leipzig, p. 621.

TEMPELMAN-KLUIT, D.J., 1977. Stratigraphic and structural relations between Selwyn Basin, Pelly-Cassiar Platform and Yukon Crystalline Terrain in the Pelly Mountains, Yukon. In: Report of Activities, Part A; Geological Survey of Canada, Paper 77-1A, p. 223-227.

TEMPELMAN-KLUIT, D.J., 1979. Transported cataclasite, ophiolite and granodiorite in Yukon: evidence of arc-continent collision. Geological Survey of Canada, Paper 79-14, p. 27.

TEMPELMAN-KLUIT, D.J., 1981. Geology and mineral deposits of southern Yukon. In: Yukon Geology and Exploration; Exploration and Geological Services Division, Yukon, Indian and Northern Affairs Canada, p. 7-31.

Table 1: Lithostratigraphy of the Klondike area (compiled from Green, 1972; Tempelman-Kluit, 1977; Htoon, 1979, Debicki, 1984 - 1985; and Dufresne, 1987. Formation names of magmatic rocks are used in the sense of Armstrong, 1988).

PERIOD	FORMATION	LITHOLOGY
LATE PLEISTOCENE	low level gravels	alluvial sediments
EARLY PLEISTOCENE, PLIOCENE	gravels at intermediate levels; high level bench gravel	alluvial sediments
EARLY TERTIARY	Skukum Group	felsic tuff, felsic breccia
	Nisling Range Alaskite	rhyolite porphyry
LATE CRETACEOUS	Carmacks Group	andesite, dacite and tuff
PERMIAN?	Moosehide Assemblage	serpentinite, amphibolite
PERMIAN	Klondike Schist	quartz-feldspar-muscovite schist, quartz-feldspar-biotite gneiss
DEVONIAN AND MISSISSIPPIAN	Nasina Series	graphite - muscovite schist, quartz-muscovite schist, limestone

TABLE 2. Chemical composition (in wt-%) of gold in quartz sulphide veins from the Hunker Creek area; ϕ = mean value, σ = standard deviation, DL = detection limit

		Au	Ag	Te	Fe*	S*	Total
Hunker Dome							
gold in quartz	min.	85.96	12.48	0.04	-	-	99.00
n = 16	max.	87.26	13.15	0.11	-	0.02	100.40
	ϕ	86.57	12.74	0.08		0.01	99.40
	σ	0.39	0.20	0.02	-	0.01	0.45
	DL	0.15	0.12	0.06	0.03	0.02	
Mitchell Vein	min.	77.13	16.77	-	0.91	0.06	95.90
gold in pyrite	max.	79.38	18.06	0.15	1.89	0.12	99.25
n = 6	ϕ	78.61	17.58	0.05	1.37	0.08	97.69
	σ	0.81	0.50	0.06	0.45	0.02	1.30
	DL	0.18	0.29	0.16	0.06	0.03	
Hunker Dome	min.	71.20	20.37	0.02	-	-	96.25
gold intergrown	max.	77.34	24.84	0.12	-	0.03	98.28
with galena	ϕ	74.77	22.07	0.07	-	0.02	96.93
n = 11	σ	1.78	1.38	0.04	-	0.02	0.61
	DL	0.15	0.12	0.06	0.03	0.02	

* Fe- and S- contents are probably due to pyrite influencing the microprobe measurements.

Table 3. Chemical composition (in wt-%) of freibergite and tetrahedrite in quartz sulphide veins from the Hunker Creek area; ϕ = mean value, σ = standard deviation, DL = detection limit

		Cu	Ag	Fe	Zn	Cd	Sb	As	S	Total
	min.	15.68	18.48	1.44	0.04	-	24.74	-	20.30	98.16
	max.	25.97	31.52	5.57	2.60	7.29	26.69	0.01	23.80	101.47
1.	ϕ	22.27	21.82	3.46	1.01	2.93	25.63	-	22.44	99.56
	σ	2.33	3.22	1.17	0.59	2.29	0.36	0.01	0.61	0.71
	DL	0.04	0.10	0.03	0.05	0.30	0.10	0.50	0.03	
	min.	24.42	19.34	4.72	1.15	0.19	18.81	2.92	23.38	98.07
	max.	26.17	20.06	5.14	1.23	0.37	21.43	4.30	24.21	99.81
2.	ϕ	25.26	19.75	4.88	1.19	0.25	20.12	3.68	23.79	98.91
	σ	0.69	0.32	0.14	0.04	0.07	0.90	0.52	0.29	0.76
	DL	0.04	0.10	0.03	0.05	0.30	0.10	0.50	0.03	
	min.	28.99	12.64	4.02	2.33	-	16.94	3.02	23.39	98.00
	max.	31.87	15.22	4.41	2.72	-	20.70	5.76	24.57	98.42
3.	ϕ	30.68	13.61	4.15	2.45	-	18.82	4.42	24.05	98.17
	σ	1.03	0.93	0.16	0.14	-	1.33	1.05	0.54	0.15
	DL	0.04	0.10	0.03	0.05	0.30	0.10	0.50	0.03	

1. Freibergite from Sheba Vein and Hunker Dome (n = 54):
$(Cu_{0.63}Ag_{0.37})_{2.59}(Fe_{0.60}Zn_{0.15}Cd_{0.25})_{0.49}Sb_{0.97}S_{3.24}$

2. Arsenic-bearing freibergite of Sheba Vein and Hunker Dome (n = 6):
$(Cu_{0.68}Ag_{0.32})_{2.58}(Fe_{0.83}Zn_{0.17})_{0.49}(Sb_{0.77}As_{0.23})_{0.98}S_{3.25}$

3. Arsenic-bearing tetrahedrite of Vein 3 (n = 6):
$(Cu_{0.79}Ag_{0.21})_{2.62}(Fe_{0.67}Zn_{0.33})_{0.48}(Sb_{0.73}As_{0.27})_{0.96}S_{3.23}$